NNT/NL : 2022AIXM0316/029ED251

THÈSE DE DOCTORAT

Présentée pour obtenir le grade universitaire de
Docteur de l'Université d'Aix-Marseille

Discipline : Sciences de l'environnement

Spécialité : Géosciences

École doctorale : ED 251 – Sciences de l'environnement

Nazim SEMMANI

Étude des archives paléogéographiques et paléoclimatiques dans le système sédimentaire Paléogène du bassin continental de la Vistrenque (Camargue, SE France)

Soutenue à Marseille le 19 septembre 2022

Devant le jury composé de :

Rapporteur :	Pr. Emmanuelle VENNIN	Université de Bourgogne
Rapporteur :	Pr. Christian GORINI	Sorbonne Université
Examinateur :	Dr. Mathieu SCHUSTER	Université de Strasbourg
Examinateur :	Dr. Alexis LICHT	Université d'Aix-Marseille
Invité :	Dr. Jean-Pierre SUC	Sorbonne Université
Invité :	Dr. Michel SÉRANNE	Université de Montpellier
Invité :	Dr. Séverine FAUQUETTE	Université de Montpellier
Invité :	Dr. Pierre MASSE	TotalEnergies
Invité :	Dr. Christophe NUSSBAUMER	TotalEnergies
Directeur de thèse :	Dr. François FOURNIER	Université d'Aix-Marseille
Co-directeur de thèse :	Pr. Jean BORGOMANO	Université d'Aix-Marseille

Résumé

Les remplissages sédimentaires des bassins continentaux constituent des archives précieuses de l'évolution des paramètres environnementaux à diverses échelles de temps. Ces paramètres environnementaux comme la topographie du bassin et la salinité sont influencés par la tectonique et le climat. Dans le Sud-est de la France, plusieurs bassins continentaux se sont formés durant l'intervalle Priabonien-Rupélien dans le contexte du changement du régime tectonique compressif lié à l'orogenèse pyrénéo-provençale au régime extensif associé au rift ouest-européen et de la dégradation climatique majeure de la fin de l'Éocène. L'expression de cette dégradation climatique en milieu continental ainsi que l'origine de la salinité des systèmes lacustres du Sud-est de la France sont encore mal comprises. Le bassin de la Vistrenque situé en Camargue, le plus profond dépôt-centre cénozoïque du Sud-est de la France, est constitué de plus de 3200 m de dépôts paléogènes carbonatés, silicoclastiques et évaporitiques. Cette succession très dilatée représente une archive exceptionnelle pour documenter les conséquences environnementales des changements climatiques liés à la transition Éocène-Oligocène et reconstituer la paléogéographie du Sud-est de la France au Paléogène. La méthodologie adoptée dans ce travail repose sur l'analyse sédimentologique, stratigraphique, micropaléontologique et géochimique des données d'affleurements et de forages (carottes, cuttings, diagraphies).

L'étude des affleurements situés au nord du bassin permet de reconstituer une marge carbonatée d'un lac salin caractérisée par un fort développement de corps oolithiques au Priabonien. L'analyse stratigraphique met en évidence des connexions avec les masses d'eaux salées voisines du Languedoc et de la Vallée du Rhône pendant les transgressions lacustres. Dans le dépôt-centre, les datations obtenues dans ce travail ont permis de construire un cadre chronostratigraphique robuste des séries étudiées qui s'échelonnent de l'Éocène supérieur à l'Oligocène supérieur. Cette thèse apporte des preuves d'incursions au moins épisodiques d'eaux influencées par la mer dans les fossés continentaux camarguais et languedociens durant le Priabonien, le Rupélien inférieur et le Chattien. La salinisation de ces bassins provient de la mer alpine au Priabonien et au Rupélien inférieur et deux couloirs d'incursion marine peuvent être envisagés : 1) la haute vallée du Rhône via le seuil de Crest, 2) la basse vallée du Rhône via les synclinaux pyrénéens du Haut-Var. Au Chattien, les incursions marines dans la Vistrenque proviennent du sud à la faveur de l'ouverture de la Méditerranée occidentale et la formation de la marge du golfe du Lion à la place des reliefs pyrénéens continus qui formaient une barrière topographique méridionale au Priabonien et au Rupélien inférieur.

Quatre séquences de dépôts ont été définies pour documenter l'évolution du bassin de la Vistrenque entre Priabonien - Rupélien basal et le Chattien inférieur. La première séquence est constituée de : 1) un hémicycle transgressif (Priabonien à Rupélien basal) marqué par une sédimentation lacustre profonde gravitaire terrigène dans le centre du bassin et une sédimentation carbonatée sur la marge nord ; 2) un hémicycle de régression forcée du lac (Rupélien inférieur) marqué par une réduction des flux terrigènes et la formation locale d'évaporites. La précipitation des évaporites est conséquente de l'aridification continentale en lien avec le refroidissement global à la transition Éocène-Oligocène. Les trois séquences suivantes dont l'ensemble présente une tendance régressive sur le long terme (régression normale) traduisent l'évolution pendant le Rupélien du système sédimentaire d'un lac profond à un lac peu profond à sédimentation deltaïque et littorale et le développement final d'une plaine d'inondation à partir du Chattien. Le comblement ultime du bassin serait favorisé par la fin de fonctionnement d'un bassin en décrochement contrôlé par la faille de Nîmes.

Mots-clés : Bassin continental, sédimentation lacustre, paléogéographie, paléoclimat, Éocène-Oligocène, Camargue.

Abstract

Sedimentary infills of continental basins constitute valuable archives of the evolution of environmental parameters at different time scales. These environmental parameters such as basin topography and salinity are influenced by tectonics and climate. In South-east France, several continental basins were formed during the Priabonian-Rupelian interval in a context of change from the compressive tectonic regime linked to the Pyreneo-Provençal orogeny to the extensive regime associated with the European Cenozoic Rift System and the fundamental climatic change at the end of the Eocene. The manifestation of this climatic deterioration in continental areas as well as the origin of the salinity of the lacustrine systems of South-east France are still poorly understood. The Vistrenque Basin located in the Camargue, the deepest Cenozoic depocentre in South-east France, is made up of more than 3200 m of Paleogene carbonate, siliciclastic and evaporite deposits. This highly expanded succession represents an exceptional archive to document the environmental impact of the climatic changes related to the Eocene-Oligocene transition and to reconstruct the palaeogeography of South-east France during the Paleogene. The methodology adopted in this work is based on the sedimentological, stratigraphic, micropalaeontological and geochemical analyses of outcrops and borehole data (cores, cuttings, logs).

The study of the outcrops located in the northern part of the basin allows to reconstruct a carbonate margin of a saline lake characterized by significant development of oolitic bodies during the Priabonian. Stratigraphic analysis reveals the existence of lake water connections with neighbouring saline waterbodies located in Languedoc and Rhône Valley during lacustrine transgressions. In the depocentre, the ages obtained in this work have allowed to construct a strong chronostratigraphic framework for the investigated sedimentary series, whose ages range from the Upper Eocene to the Upper Oligocene. This thesis provides evidence for, at least transient, incursions of sea-influenced waters into the Camargue and Languedoc continental troughs during the Priabonian, Lower Rupelian and Chattian. The salinization of these basins derived from the Alpine Sea during the Priabonian and Lower Rupelian times and two potential pathways can be considered: 1) the upper Rhône Valley via the Crest Sill, 2) the lower Rhône valley via the Pyrenean synclines of the Haut-Var area. During the Chattian, marine incursions into the Vistrenque derived from the south thanks to the opening of the western Mediterranean and the formation of the Gulf of Lion margin in place of the continuous Pyrenean reliefs that constituted a southern topographic barrier during the Priabonian and Lower Rupelian.

Four depositional sequences have been defined to document the evolution of the Vistrenque Basin during the Priabonian-Lowermost Rupelian to Early Chattian times. The first sequence consists of: 1) a transgressive hemicycle (Priabonian-earliest Rupelian) characterized by gravity-driven terrigenous sedimentation in deep lake setting in the centre of the basin and carbonate sedimentation on the northern margin; 2) a hemicycle of forced lake regression (early Rupelian) marked by a reduction in terrigenous fluxes and local formation of evaporites. The precipitation of evaporites is a consequence of the continental aridification associated with the global cooling at the Eocene-Oligocene transition. The following three sequences, which together show a long-term regressive trend (normal regression), reflect the evolution of the sedimentary system during the Rupelian from a deep lake to a shallow lake with deltaic and littoral sedimentation and the final development of a floodplain as early as the Chattian. This ultimate filling of the basin would be favoured by the end of the functioning of a strike-slip basin controlled by the Nîmes Fault.

Keywords: Continental basin, lacustrine sedimentation, palaeogeography, palaeoclimate, Eocene-Oligocene, Camargue

Avant-propos

Cette thèse a été réalisée au Centre Européen de Recherche en Géosciences de l'Environnement (CEREGE, Aix-Marseille Université) et a été financée par le ministère de l'Enseignement supérieur et de la Recherche du Gouvernement français. Elle a bénéficié du soutien financier du laboratoire CEREGE sous forme d'APIC et de la chaire industrielle Carb3E TotalEnergies-AMIDEX détenue par **Jean Borgomano** (Aix-Marseille université).

Le projet a été initié par **François Fournier** (Aix-Marseille Université) en 2018 et s'inscrit dans la continuité des travaux de thèse de **A. Lettéron** (2018) sur le système lacustre du bassin d'Alès (SE France) qui proposent des perspectives d'études dans la Camargue pour répondre aux questions paléogéographiques du Sud-est de la France à la transition Éocène-Oligocène.

Cette thèse repose en grande partie sur l'étude géologique de subsurface et des partenariats ont été noués entre l'université d'Aix-Marseille et les entreprises TotalEnergies et Kemone pour la mise à disposition gracieuse des données de recherche.

Remerciements

Après les trois années et quelques mois de ce parcours doctoral, il m'est agréable d'adresser mes remerciements aux nombreuses personnes qui m'ont aidé à réaliser ce travail de thèse.

Je tiens à exprimer toute ma gratitude à **François Fournier** (Aix-Marseille Université) qui a cru en moi depuis le début, qui m'a encadré tout au long de cette thèse et m'a fait partager depuis le master sa passion pour la géologie sédimentaire, et m'a fait bénéficier de ses larges connaissances sur les bassins continentaux du Sud-est de la France. Qu'il trouve ici l'expression de ma reconnaissance pour sa gentillesse, sa grande disponibilité, son enthousiasme, ses encouragements et pour tout ce qu'il m'a appris durant toutes ces années. Encore merci pour la correction du manuscrit et les critiques constructives.

Je remercie **Jean Borgomano** (Aix-Marseille Université) pour la confiance qu'il a placée en moi en acceptant de codiriger cette thèse et pour avoir fourni un soutien financier à ce projet avec la chaire Carb3E TotalEnergies-AMIDEX. Je le remercie pour avoir veillé au déroulement du projet, pour sa disponibilité et pour ses précieux conseils sur la *méthodologie scientifique*.

Je remercie le laboratoire CEREGE pour m'avoir accueilli pour réaliser ces travaux de thèse et pour la mise à disposition des moyens techniques et financiers. Je remercie également TotalEnergies, en particulier **J. Hennuy**, **P. Masse** et **C. Nussbaumer** pour l'aide à passer le contrat de partage des données, pour la mise à disposition des lames minces qui ont été nécessaires à la réalisation de ce travail, et pour l'autorisation à publier ces données. **C. Nussbaumer** est également remercié pour ses commentaires et suggestions pour améliorer ce manuscrit. Merci à **M. Valette** (Kemone Vauvert) pour son accueil dans l'entreprise Kemone, pour le partage des données et des carottes des forages de Parrapon et pour l'autorisation à assister à la réalisation d'un forage près de la saline de Vauvert et à l'échantillonner.

Je tiens à remercier les différentes personnes qui ont collaboré scientifiquement à ce projet : **P. Léonide** (Aix-Marseille Université) pour avoir participé aux missions de terrains et pour son aide durant cette thèse ; **J-P Suc** (Sorbonne Université) pour les analyses des assemblages polliniques de cette thèse et pour sa grande implication dans le projet, et son épouse **S-M. Popescu** pour avoir réalisé les préparations de pollen et pour sa gentillesse et son accueil chez elle lors de la visite de GeoBioStratData ; **S. Fauquette** (Université de Montpellier) pour la réalisation des quantifications climatiques ; **M. Feist** (Université de Montpellier) pour les déterminations des gyrogonites ; **N. Godeau** et **A. Guihou** (CEREGE) pour avoir réalisé les datations U/Pb ; **C. Thomazo** (Université de Bourgogne) pour la réalisation des analyses des isotopes du soufre et de l'oxygène des sulfates ; **M. Séranne** (Université de Montpellier) et **Y. Donnadieu** (CEREGE) qui ont fait partie du comité de suivi de cette thèse pour avoir veillé à son bon déroulement et pour leurs orientations et recommandations.

J'adresse mes sincères remerciements à **Emmanuelle Vennin** (Université de Bourgogne) et à **Christian Gorini** (Sorbonne Université) de l'honneur qu'ils m'ont fait en acceptant d'être rapporteurs de cette thèse. Je remercie particulièrement **Emmanuelle Vennin** d'avoir relu le manuscrit de l'article en cours de publication dans la revue **BSGF-Earth Science Bulletin** et pour ses suggestions à améliorer la qualité du travail. Je remercie également **M. Schuster** (Université de Strasbourg) et **A. Licht** (Aix-Marseille Université) qui ont bien voulu être examinateurs de cette thèse.

Merci à **G. Graffin** (Carothèque STC de Boussens) pour l'autorisation à échantillonner les carottes. Merci à **L. Marié** (CEREGE) pour la réalisation d'une partie des lames minces étudiées dans cette thèse.

Un grand merci à l'équipe du CEREGE Saint-Charles pour leurs nombreuses aides pour mener à bien ces travaux de thèse et pour leur confiance durant les trois années de monitorat que j'ai passées à leur cotés : merci à **J. Lamarche**, **G. Conesa**, **B. Suchéras-Marx**, **A. Ribaud**, **B. Martin-Garin**, **S. Viseur**, **P. Henry**, **A. Nutz** et **B. Arfib**, merci également à **J. Turiello** pour sa gentillesse et son assistance administrative.

Je remercie les anciens doctorants et post-doctorants pour leurs conseils aux débuts de cette thèse et pour la bonne humeur de tous les jours : **Christophe**, **Vincenzo**, **Anthony**, **Thomas**, **Irène**, **Thibaut**, **Alexandre**, **Justine**, **Quentin** et **Jean**. Merci également aux nouveaux doctorants : **Stanislas**, **Paul**, **Eduardo** et **Hugo**.

Un grand merci à tous mes amis de Tizi-Ouzou, Boumerdès, Marseille et d'ailleurs, en particulier **Nabil**, **Amazigh**, **Zimou**, **Mourad**, **Ali** et **Tassadit** qui m'ont été d'un grand soutien.

Merci aux personnes dont j'ai oublié de mentionner les noms ici et qui ont m'aidé de près ou de loin.

Merci à mes chers parents pour tout ce qu'ils m'ont donné. Merci pour votre confiance, votre patience, votre soutien… et pour tous leurs sacrifices.

Merci à ma chère sœur.

A ma famille à qui j'ai manqué toutes ces années et dont le soutien, la générosité et les encouragements ont été essentiels pour faire de longues études, je leur dédie ce modeste travail.

Table des matières

1. INTRODUCTION GÉNÉRALE

1. Introduction générale

1.1. Problématique

1.1.1. Etat de l'art

Les bassins sédimentaires continentaux formés en contexte tectonique actif, en particulier ceux associés aux systèmes de rift, sont occupés par des lacs. Les remplissages sédimentaires de ces systèmes lacustres constituent des archives potentielles pour documenter l'enregistrement des processus géodynamiques et l'évolution des paramètres environnementaux de surface à diverses échelles de temps. Formés à l'interaction de l'atmosphère, l'hydrosphère, la lithosphère et de la biosphère, les sédiments continentaux se sont révélés très sensibles aux changements climatiques car ils résultent de processus physiques ou biologiques se déroulant dans des zones proches ou en contact direct avec l'atmosphère (p.ex., Fabre et Mainguet, 1991 ; Nutz et al., 2019). Les bassins continentaux sont également très étudiés puisqu'ils constituent d'importants réservoirs de ressources énergétiques, minières et hydriques.

Malgré les très nombreuses études et leurs intérêt et enjeux sociétaux, les bassins continentaux, en particulier les systèmes lacustres, demeurent mal compris. Ces systèmes sont uniques et selon leurs caractéristiques propres (taille, morphologie, contexte géographique et histoire tectonique), ils répondent distinctement aux changements climatiques et hydrologiques. Ces bassins occupent des aires géographiques variables et peuvent se former aussi bien au pied des reliefs en érosion qu'en domaine margino-littoral. La chimie des eaux lacustres est influencée par, entre autres, la nature du substratum rocheux drainé. La salinité peut être contrôlée par les bilans apports d'eau-évaporation, les arrivées des flux d'eau drainant des évaporites, et par la connexion avec des masses d'eaux salées continentales voisines et avec le domaine marin (p.ex., Emre and Truc, 1978 ; Talbot, 1990 ; Lettéron et al., 2017).

Plusieurs bassins continentaux cénozoïques se sont formés dans le Sud-est de la France pendant l'extension liée au système de rift ouest-européen (ROE) actif au Priabonien (Éocène supérieur) et au Rupélien (Oligocène inférieur) (ECRIS : *European Cenozoic Rift System* ; Ziegler, 1992 ; Dèzes et al., 2004) (**Fig. 1.1**). Ces bassins sont caractérisés par une épaisse succession sédimentaire silicoclastique, carbonatée et évaporitique (p.ex., Alès-Saint-Chaptes-Issirac (système ASCI), Lettéron et al., 2017, 2018, 2021 ; Mormoiron, Triat & Truc, 1974 ; Apt-Manosque Forcalquier, Lesueur, 1991 ; Rouchy, 1997). Plus tard, la formation de la marge du golfe du Lion qui accompagne le rifting Liguro-Provençal à l'Oligocène supérieur et à l'Aquitanien a également engendré l'ouverture de bassins continentaux (par exemple le bassin de la Vistrenque, Benedicto et al., 1996) (**Fig. 1.2**).

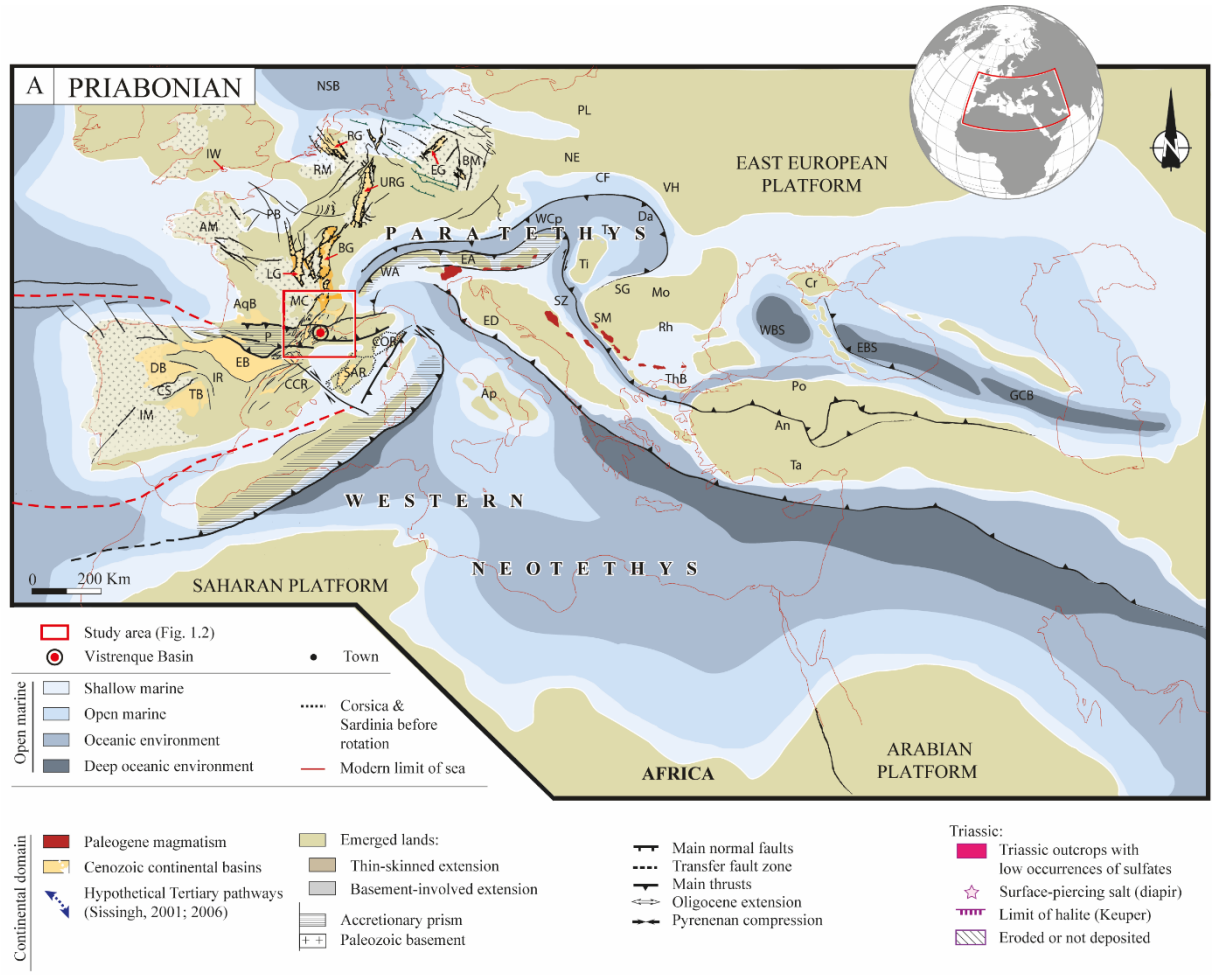

Figure 1.1 : Carte paléogéographique de l'Europe de l'Ouest montrant les différentes structures, les aires de sédimentation et les principaux bassins continentaux cénozoïques (modifié d'après Lettéron et al., 2018).

Dans certains cas, des bassins « polyphasés » ont enregistré les deux phases d'extension (Sanchis and Séranne, 2000). En Languedoc, entre la faille des Cévennes et la faille de Nîmes, les bassins continentaux Priaboniens sont contrôlés par le faisceau de failles décrochantes senestres de direction NNE-SSW et NE-SW qui accommodent durant le Priabonien à la fois la compression N-S encore active dans le segment Languedocien des Pyrénées, aujourd'hui effondré sous le golfe du Lion, et l'extension liée au ROE (Séranne et al., 2021). Plus à l'Est, cette période est caractérisée par des conditions marines dans le bassin d'avant-pays alpin à l'emplacement actuel des Alpes occidentales (Joseph and Lomas, 2004) (**Fig. 1.2**).

Les bassin continentaux paléogènes du Sud-est de la France ont par ailleurs enregistré la transition Éocène-Oligocène (EOT) qui représente la plus importante crise climatique du Cénozoïque. La fin de l'Éocène est marquée par un refroidissement global du climat et consacre le passage de la période *greenhouse* à à la période *icehouse* suite à l'installation du courant circumpolaire antarctique qui engendre la formation de la calotte polaire antarctique (Zachos et al., 2001 ; Liu et al., 2009) ; les prémices de l'installation de ce courant circumpolaire apparaissent au Priabonien (Sarkar et al., 2019).

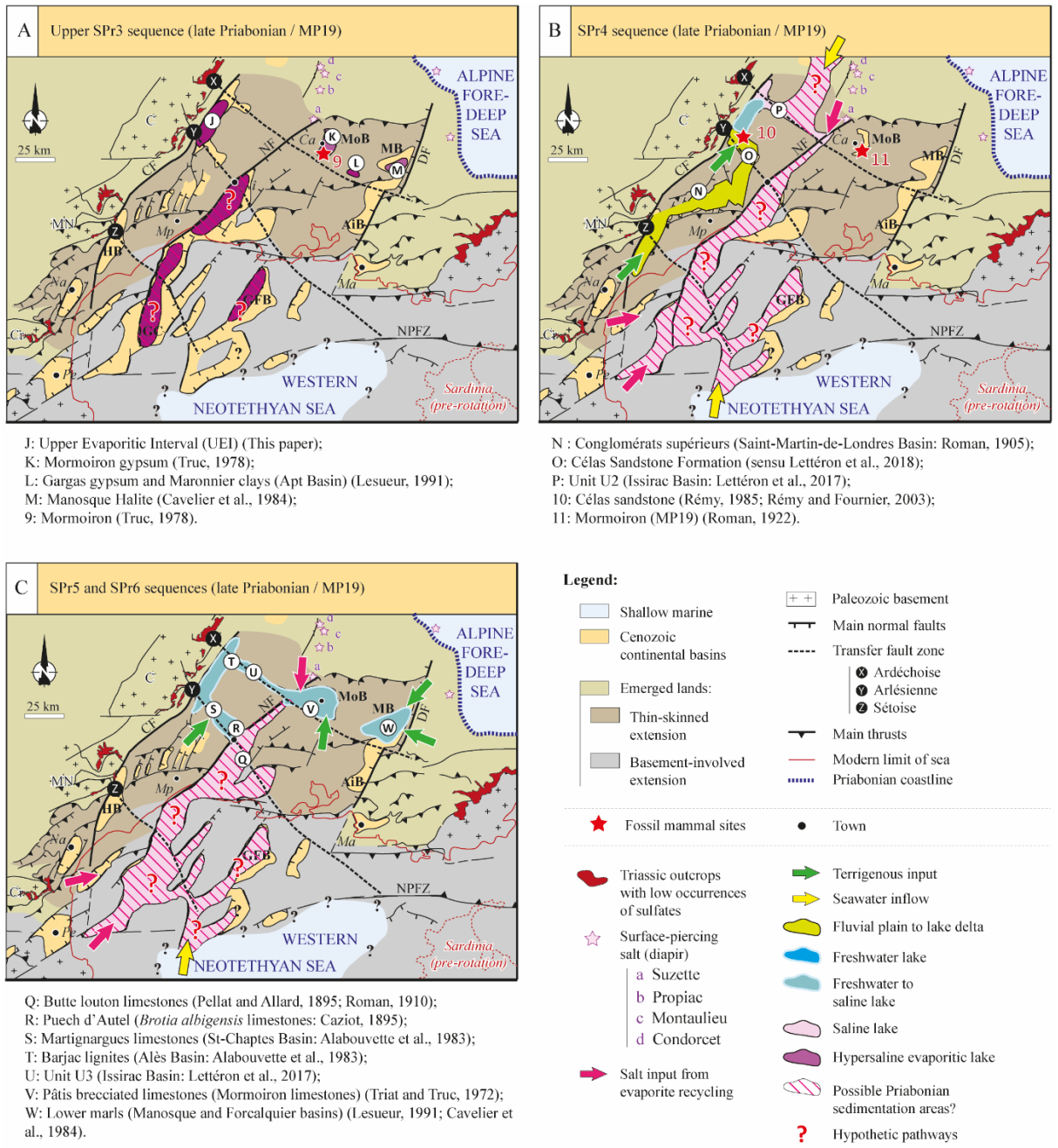

J: Upper Evaporitic Interval (UEI) (This paper);
K: Mormoiron gypsum (Truc, 1978);
L: Gargas gypsum and Maronnier clays (Apt Basin) (Lesueur, 1991);
M: Manosque Halite (Cavelier et al., 1984);
9: Mormoiron (Truc, 1978).

N : Conglomérats supérieurs (Saint-Martin-de-Londres Basin: Roman, 1905);
O: Célas Sandstone Formation (sensu Lettéron et al., 2018);
P: Unit U2 (Issirac Basin: Lettéron et al., 2017);
10: Célas sandstone (Rémy, 1985; Rémy and Fournier, 2003);
11: Mormoiron (MP19) (Roman, 1922).

Q: Butte louton limestones (Pellat and Allard, 1895; Roman, 1910);
R: Puech d'Autel (*Brotia albigensis* limestones: Caziot, 1895);
S: Martignargues limestones (St-Chaptes Basin: Alabouvette et al., 1983);
T: Barjac lignites (Alès Basin: Alabouvette et al., 1983);
U: Unit U3 (Issirac Basin: Lettéron et al., 2017);
V: Pâtis brecciated limestones (Mormoiron limestones) (Triat and Truc, 1972);
W: Lower marls (Manosque and Forcalquier basins) (Lesueur, 1991; Cavelier et al., 1984).

Figure 1.2 : Cartes paléogéographiques du Sud-est de la France pendant le Priabonien supérieur montrant les bassins continentaux cénozoïques, les principales directions d'apports terrigènes et les potentielles voies d'incursions d'eau salées dans les systèmes lacustres, modifiées d'après Lettéron (2018). Le rectangle montre le secteur étudié correspondant au bassin de la Vistrenque en Camargue.

Dans le Sud-est de la France, le climat était subtropical à l'Éocène moyen et au début du Priabonien puis a fluctué entre des configurations subtropicales et tempérées à la fin du Priabonien avec des températures moyennes de 15-20°C (Sittler et al., 1975 ; Schuler, 1990 ; Châteauneuf, 1980 ; Bauer et al., 2016 dans Lettéron, 2018). La dégradation climatique majeure correspondant à la transition Éocène-Oligocène est précédée par des fluctuations enregistrées par des cycles d'aridification et d'humidification documentés dans le bassin d'Alès

(Lettéron, 2018 ; Lettéron et al., 2021). Par la suite, les températures ont diminué de 5°C au début de l'Oligocène (Mosbrugger et al., 2015). Ce refroidissement majeur a engendré des changements drastiques des associations floristiques et faunistiques en milieu terrestre (Châteauneuf, 1980 ; Zhang et al., 2012). L'Oligocène est caractérisé par un climat globalement plus froid et contrasté (Yancey et al., 2003 ; Eldret et al., 2009). L'Oligocene supérieur est marqué par la période de réchauffement '*Late Oligocene warming*' qui précède la glaciation Mi-1 de la fin de l'Oligocène (Zachos et al., 2001).

Les bassins sédimentaires continentaux de l'Éocène supérieur et de l'Oligocène ont été largement documentés dans la littérature dans l'est et le Sud-est de la France (p.ex., Fossé du Rhin supérieur : Blanc-Valleron et Schuler, 1997 ; Fossé de la Bresse : Curial et Moretto, 1997 ; Bassin de Valence : Dromart et Dumas, 1997 ; Bassin d'Apt-Manosque-Forcalquier : Lesueur, 1991 ; Bassin d'Alès-Saint-Chaptes-Issirac : Lettéron et al. 2017, 2018, 2021 ; Bassin de la Vistrenque : Benedicto et al., 1996) et au large du Golfe du Lion (Graben Central, Bassin de Grand Faraman : Séranne et al., 1995) (**Fig. 1.2**). Toutefois, plusieurs questions demeurent non résolues à ce jour. Par exemple, l'origine de la salinité dans les systèmes lacustres évaporitiques paléogènes du Sud-est de la France et les possibilités d'existence d'incursions marines, au moins épisodiques, dans ces lacs sont l'objet d'une controverse qui dure depuis plusieurs décennies (p.ex., Giraud, 1902 ; Fontes et al., 1991 ; Rouchy, 1997 ; Briot and Poidevin, 1998 ; Bodergat et al., 1999 ; Rouchy and Blanc-Valleron, 2009 ; Sissingh, 2001 ; 2006 ; Dèzes et al., 2004 ; Ziegler and Dèzes, 2007; Briot, 2008 ; Lettéron et al., 2017 ; 2018). Récemment, Lettéron et al. (2017 ; 2018 ; 2021) ont considéré deux hypothèses pour rendre compte des accumulations des évaporites: lessivage des évaporites triasiques ou connexions épisodiques avec le domaine marin. Les auteurs ont déplacé le problème paléogéographique salinisation du système Alès– Saint-Chaptes – Issirac vers les bassins camarguais et ceux situés en offshore dans le golfe du Lion (**Fig. 1.2**). Par ailleurs, la proximité du domaine alpin, situé à environ 100 km à l'est, n'interdit pas d'envisager des incursions marines épisodiques provenant cet océan dans la vallée du Rhône et par conséquent en Languedoc (p.ex., Moretto, 1987 ; 1988 dans Lettéron, 2018).

La Camargue par sa position géographique charnière constituerait, à la fin de l'Éocène, un corridor d'eau salée provenant du Sud vers les bassins du Languedoc et de la Vallée du Rhône. La vérification de cette hypothèse passe par l'étude de ces bassins camarguais, notamment le bassin de la Vistrenque. Ce dernier est peu documenté puisque les dépôts paléogènes sont presque entièrement enfouis sous les sédiments du delta du Rhône: aucune étude sédimentologique et stratigraphique de ce bassin n'est publiée d'où les incertitudes qui subsistent également sur les modalités de connexion des masses d'eau salée et le diachronisme des intervalles d'évaporites entre les différents bassins. Par exemple, Lettéron et al. (2018) ont montré que les connexions du système ASCI avec les masses d'eau salines voisines se produisent lors des périodes de haut niveau lacustre. Par ailleurs, dans ce système, les saumures ne résultent pas d'une concentration par évaporation des eaux douces à faiblement salées à la

suite d'un déficit hydrique du lac comme le suggère le modèle classique (p.ex., Rouchy and Blanc-Valleron, 2009). Cela amène à des questionnements sur le contrôle des changements climatiques sur le dépôt des évaporites et l'évolution des systèmes continentaux notamment lors de la transition Éocène-Oligocène (p.ex., Sissingh, 2001 ; Lettéron et al., 2021).

Plusieurs bassins ont été étudiés individuellement ou intégrés dans un ensemble (p.ex., système ASCI, Lettéron et al., 2021 ; Apt-Manosque-Forcalquier, Lesueur, 1991) et des corrélations entre les systèmes lacustres du Sud-est de la France ont été suggérées (p.ex., Lettéron et al., 2021) et l'on montre l'existence d'un diachronisme de fonctionnement entre les bassins au sein d'un même système sédimentaire. A plus grande échelle, le diachronisme entre les segments du rift Ouest-Européen déjà établi (p.ex., Rouchy, 1997) est à l'origine des incertitudes qui demeurent à ce jour dans les reconstructions paléogéographiques à l'échelle de l'Europe de l'Ouest.

1.1.2. Verrous scientifiques

L'absence d'études sédimentologiques et stratigraphiques publiées sur les bassins cénozoïques de la Camargue (bassins de la Vistrenque et du Vaccarès) empêche de trancher sur le rôle de cette région, située en position géographique charnière entre le Languedoc et la Vallée du Rhône mais aussi au nord des Pyrénées en cours de démantèlement, à l'emplacement de l'actuel golfe du Lion, dans la salinisation des lacs évaporitiques continentaux au Priabonien.

Une épaisse accumulation des évaporites est connue dans le bassin de la Vistrenque (Valette and Benedicto, 1995 ; Benedicto et al., 1996) et est attribuée à l'Oligocène supérieur ce qui relie sa formation à la phase du rifting Liguro-Provençal. Dans ces travaux, le bassin de Camargue a toujours été étudié dans le contexte du rifting Oligo-Aquitanien de la marge du golfe du Lion et les auteurs interprètent l'épaisse succession lacustre tertiaire sous-jacente aux évaporites comme des dépôts syn-rift et attribués sans preuve paléontologique à l'Oligocène. Ceci soulève la question du remplissage du bassin à l'Oligocène inférieur et au Priabonien antérieurement à la formation de la marge du Golfe du Lion.

En l'absence de datations des séries paléogènes, aucune étude n'a replacé le bassin de la Vistrenque au sein du système de rift ouest-européen à ce jour même si Cavelier et al. (1984) envisagent le début du fonctionnement de ce bassin à la fin de l'Éocène au même titre que les bassins du Languedoc et de la Vallée du Rhône et suggèrent l'existence d'une aire de sédimentation profonde au Sud à remplissage essentiellement terrigène provenant de l'érosion des Pyrénées à l'opposé de la marge carbonatée connue au Nord sur la butte oolithique d'Iouton située sur le haut de Jonquières (p.ex., Pellat and Allard, 1895) (**Fig. 1.2**). Par ailleurs, le rôle du mouvement décrochant senestre de la faille de Nîmes dans l'accommodation à la fois du raccourcissement pyrénéen et de l'extension ouest-européenne au Priabonien dans les bassins continentaux en Languedoc mis en évidence par Séranne et al. (2021) amène à questionner l'enregistrement de cette phase tectonique priabono-rupélienne à l'est de ce faisceau de failles en Camargue.

Les études tectoniques et structurales de Valette and Benedicto (1995) et de Benedicto et al. (1996) considèrent que le remplissage paléogène du bassin de la Vistrenque est entièrement déposé pendant la phase du rifting de la marge du Golfe du Lion à l'Oligocène qui se poursuit pendant l'Aquitanien. Néanmoins, la suggestion de Cavelier et al. (1984) reste plausible et confortée par les derniers résultats de Séranne et al. (2021) sur le mouvement de décrochement senestre de la faille de Nîmes enregistré au Priabonien. Les séries basales du remplissage paléogène du bassin de la Vistrenque pourraient alors être déposées pendant une phase tectonique précédente probablement durant la fin de l'Éocène et le Rupélien.

Il est donc envisageable de considérer que le bassin Camarguais de la Vistrenque ait commencé à se former à la fin de l'Éocène ou au début du Rupélien au nord des paléo-reliefs pyrénéens en cours de démantèlement et fonctionné de manière contemporaine avec les bassins du Languedoc et de la Vallée du Rhône. Cette hypothèse sera confrontée dans les chapitres suivants avec les nouvelles données d'âge obtenues dans ce travail, notamment l'apport des datations U/Pb et de l'approche climatostratigraphique.

Les paléo-reliefs pyrénéens situés au sud de la Camargue ont été reconstruits par Benedicto et al. (1996) qui leur attribuent une élévation supérieure à 1 Km et par Séranne et al. (2021) qui suggèrent une continuité à travers l'actuel golfe du Lion entre les Pyrénées franco-espagnoles à l'Ouest et la chaîne Pyréno-Provençale à l'est. De plus, Romagny et al. (2020) reconstituent un bloc ibéro-corso-sarde non encore fragmenté à la fin de l'Éocène et attribuent la formation des domaines arrières-arc au début du Rupélien, avant l'ouverture océanique de la méditerranée occidentale au Chattien. Ces reconstitutions paléogéographiques ne laissent pas envisager des connexions avec le domaine marin par le sud au Priabonien à travers cette masse continentale en collision avec l'Europe. D'ailleurs, exceptée la marge carbonatée septentrionale du paléolac salin priabonien de la Camargue (Butte Iouton, Pellat and Allard, 1895 ; Roman, 1910) qui se raccorde facilement aux bassins du Languedoc et de la Vallée du Rhône, aucune étude n'indique la présence de fossés salifères au Priabonien en Camargue et dans le golfe du Lion.

L'hypothèse de l'existence d'un corridor de salinisation par le Sud à travers la Camargue et les bassins offshore du golfe du Lion (p.ex., Grand Faraman, Graben Central, Benedicto, 1996) avancée dans les reconstitutions paléogéographiques de Lettéron (2018) serait par conséquent peu plausible et il faut chercher d'autres voies d'incursions marines dans le Sud-est de la France.

1.1.3. Raison d'être de la thèse

Compte tenu du fait que les bassins paléogènes de la Camargue (bassins de la Vistrenque et du Vaccarès) sont situés dans une position géographique charnière parmi les bassins du sud-est de la France, entre le Languedoc à l'ouest, la Provence à l'est, et la vallée du Rhône au nord, l'étude détaillée du Bassin de la Vistrenque permet de combler les lacunes sur la connaissance de l'évolution géodynamique et structurale du sud-est de la France et des régions du golfe du Lion au cours de l'Éocène supérieur et de l'Oligocène et de fournir de nouveaux éclairages pour

élucider les questions paléogéographiques non résolues à ce jour. *Le manque de données en quantités suffisantes dans le secteur de Vaccarès occupé par la réserve naturelle nationale de Camargue ne permet d'étudier le bassin de Vaccarès.*

De plus, puisque le problème de la salinisation de ces systèmes lacustres a été déplacé en Camargue (p.ex., Lettéron, 2018), la lacune scientifique découlant de l'absence d'études sédimentologiques détaillées sur le Paléogène du Bassin de la Vistrenque constitue un verrou scientifique à lever pour apporter des éléments nouveaux à la discussion des questions relatives à l'origine de la salinité dans lacs paléogènes, les possibles connexions entre les masses d'eau salées et les modalités de transgression lacustre, et l'influence du bilan hydrique et par conséquent du climat régional sur la formation des évaporites. Seule une révision complète et détaillée des aspects chronostratigraphiques, sédimentologiques, stratigraphiques, et géochimiques de la succession sédimentaire paléogène du bassin de la Vistrenque, à la fois sur la marge carbonatée (p.ex., Butte Iouton) et dans le dépôt-centre permet de déterminer les contextes paléogéographiques, paléoclimatiques et paléohydrologiques de formation et de remplissage des bassins de la Camargue et de ses environs à la fin de l'Éocène et pendant le Rupélien et répondre aux questions en suspens.

Cette thèse se révèle nécessaire pour replacer la Camargue au sein des systèmes de rifts cénozoïques du Sud-est de la France et à l'avant-pays des paléo-reliefs Pyrénéens, aujourd'hui effondrés dans le golfe du Lion, du début de leur démantèlement à la fin de l'Éocène aux prémices de l'ouverture de la méditerranée occidentale à l'Oligocène et renseigner sur l'enregistrement en milieu continental de la transition climatique Éocène-Oligocène dans la région.

En plus des implications à l'échelle régionale, l'étude de la succession paléogène du bassin de la Vistrenque est intéressante à l'échelle du bassin sédimentaire puisqu'elle permet de documenter : (1) une marge carbonatée oolithique d'un système lacustre salin, et (2) l'enregistrement d'un système turbiditique dans le dépôt-centre d'un fossé lacustre fortement subsident. Ces cas d'environnements sédimentaires sont décrits ici pour la première fois dans le Paléogène du Sud-est de la France.

Par ailleurs, la succession paléogène très dilatée (>3000 m) du bassin de la Vistrenque représente une archive sédimentaire exceptionnelle pour documenter les changements climatiques ayant affecté les environnements continentaux du Sud-Est de la France pendant l'Éocène supérieur et l'Oligocène, et notamment autour de la transition Éocène-Oligocène qui représente la plus grande crise climatique du Cénozoïque matérialisée par un refroidissement majeur du climat global (Liu et al., 2009 ; Wade et al., 2012). Plusieurs proxies climatiques sont utilisés dans ces travaux de thèse pour documenter les modalités et le calendrier des changements climatiques dans le Sud-est de la France au voisinage de la transition Éocène-Oligocène : 1) enregistrement des changements floristiques par l'analyse qualitative et quantitative des assemblages polliniques, 2) enregistrement des changements de nature des systèmes sédimentaires et modalité de remplissage du bassin sédimentaire et 3) enregistrement

de changements paléohydrologiques régionaux par les signatures isotopiques du carbone et de l'oxygène des carbonates lacustres.

1.2. Objectifs et portée de l'étude

L'étude sédimentologique, stratigraphique et géochimique des séries paléogènes du bassin de la Vistrenque vise à :

- (1) définir un cadre chronostratigraphique contraint de la succession sédimentaire paléogène du bassin de la Vistrenque.
- (2) Reconstituer les paléoenvironnements de dépôt de la marge lacustre carbonatée et du dépôt-centre du bassin de la Vistrenque, et questionner certains concepts de stratigraphie séquentielle des séries lacustres notamment les modalités des transgressions lacustres et l'impact conjugué du volume des masses d'eau connectées et de la subsidence du bassin.
- (3) comprendre le fonctionnement du bassin de la Vistrenque et sa réponse aux changements climatiques à la transition Éocène-Oligocène et à l'évolution tectonique de la région du Sud-est de la France au cours des temps paléogènes.
- (4) apporter des éclairages sur le rôle de la Camargue dans la salinisation des bassins continentaux priaboniens et rupéliens du Sud-est de la France et de leurs connexions avec des masses d'eaux salées et discuter des voies d'incursions marines dans ces systèmes sédimentaires lacustres avec les nouvelles données micropaléontologiques et géochimiques.
- (5) fournir de nouveaux détails pour les reconstitutions paléogéographiques et paléoclimatiques du Sud-est de la France à la fin de l'Éocène et à l'Oligocène.

1.3. Objet d'étude : les séries paléogènes du bassin de la Vistrenque

La Camargue est située dans le Sud-est de la France près de l'embouchure du Rhône dans la mer Méditerranée (**Fig. 1.3A**). Cette région a une forme approximativement triangulaire et est formée de deux bassins sédimentaires principaux séparés par une zone haute (haut d'Albaron) : le bassin de la Vistrenque à l'ouest et le bassin de Vaccarès à l'est (Benedicto et al., 1996). Le bassin de la Vistrenque est limité à l'ouest par la faille majeure de Nîmes et est relayé au nord par le fossé de Pujaut (**Fig. 1.2**). Il est limité au sud par les hauts de Grau-du-Roi et de Saintes-Maries-de-la-Mer couvre une superficie d'environ 50*30 Km². Ce bassin Cénozoïque est le plus profond (~ 5 km) du Sud-est de la France avec plus de 3000 m d'épaisseur de dépôts paléogènes. La succession paléogène est entièrement enfouie à l'exception de quelques affleurements dans la marge carbonatée septentrionale (Roman, 1910 ; Cavelier et al., 1984). Dans le dépôt-centre, l'épaisse succession paléogène est subdivisée en trois formations : « Série

Grise » inférieure d'une épaisseur de plus de 2000 m, « Série Rouge » intermédiaire épaisse d'environ 200 m et « Série Calcaréo-salifère » supérieure pouvant atteindre plusieurs centaines de mètres d'épaisseur (Valette and Benedicto, 1995) (**Fig. 1.3D**).

Cette thèse est la première étude scientifique complète qui analyse cette succession paléogène du bassin de la Vistrenque. Elle concerne les formations sédimentaires antérieures à la phase d'extension du rifting Oligo-Aquitanien de la marge du Golfe du Lion (Valette and Benedicto, 1995 ; Benedicto et al., 1996) c'est-à-dire les formations Série Rouge et sous-jacentes.

Excepté pour la marge septentrionale accessible en affleurement, l'étude de subsurface repose sur la disponibilité et la qualité des données de forages et de sismique qui contraignent le choix des secteurs du bassin à étudier. Deux secteurs du bassin de la Vistrenque sont caractérisés par une densité exceptionnelle des données de subsurface : le secteur de Pierrefeu-Parrapon et le secteur de Gallician (**Fig. 1.3**).

- Le secteur de Parrapon – Pierrefeu est connu notamment par le forage Pierrefeu 1 qui atteint le substratum Mésozoïque à 4920 m de profondeur, forage le plus profond du bassin cénozoïque de la Vistrenque. Dans ce secteur, plus de 40 forages saliniers ont été réalisés dans un périmètre de quelques Km² autour du forage Pierrefeu afin d'exploiter l'épaisse accumulation de sel (Valette and Benedicto, 1995) (**Fig. 1.3C**). Malgré un maillage serré des données de puits et de sismique haute résolution, les forages saliniers de ce secteur ont été arrêtés dans la formation « Série Calcaréo-salifère » et par conséquent ne permettent pas de répondre à la question de recherche sur la Série Rouge et les formations sous-jacentes. Le forage Pierrefeu 1 est le seul étudié dans ce secteur et sera intégré avec les forages du secteur voisin de Gallician.

- Le secteur de Gallician est situé à environ 4 km au sud du secteur de Pierrefeu. Connu par l'exploration du champ pétrolier de Gallician, les forages profonds sont nombreux et traversent les formations paléogènes antérieures à la Série Calcaréo-salifère. Même si aucun forage n'a atteint le substratum Mésozoïque, certains forages de ce secteur ont l'avantage d'être carottés en continu sur des sections de plusieurs dizaines de mètres à quelques centaines de mètres. En plus des carottes, des déblais de forages, des diagraphies et des sections sismiques constituent alors une base de données complète pour l'analyse du remplissage sédimentaire Paléogène du bassin de la Vistrenque. La liste des forages ayant traversé les séries étudiées est fournie en **Annexe A** à la fin de ce manuscrit.

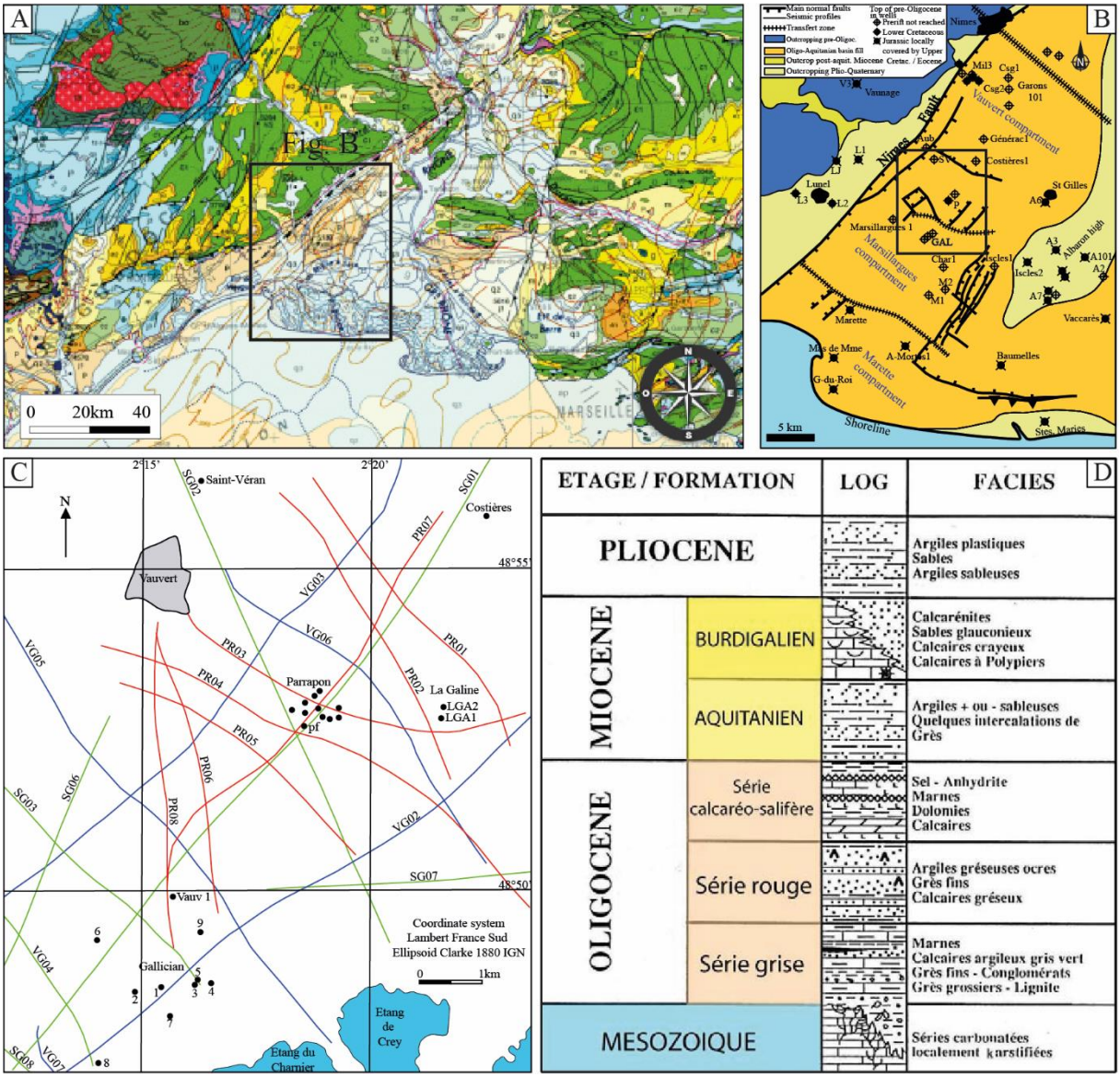

Figure 1.3 : A) Extrait de la carte géologique de la France 1/1000000 montrant la faille majeure de Nîmes orientée NE-SW (ligne en pointillé) qui sépare d'une part les Garrigues de Nîmes constituant le substratum mésozoïque et d'autre part le bassin cénozoïque de la Vistrenque. Le rectangle indique l'aire correspondant au secteur d'étude illustrée dans la Figure B à droite. B) Schéma structural du bassin de la Vistrenque montrant la localisation des forages profonds, modifié d'après Benedicto et al. (1996). (1996). V3 : Vaunage 3 - LJ : La Jasette - L1 : Lunel 1 - L2 : Lunel 2 - L3 : Lunel 3 - Csg : Caissargues - Aub : Aubord 1 - SV : Saint-Véran 1 - P : Pierrefeu 1 - A6 : Albaron 6 - A3 : Albaron 3 - A7 : Albaron 7 - A101 : Albaron 101 - A2 : Albaron 2 - Char 1 : Charnier 1 - GAL : Gallician - M1 : Montcalm 1 - M2 : Montcalm 2 - P : Pierrefeu - SM : Saintes-Maries-de-la-Mer : 101 - Mil 3 : Milhaud 3. t.z. : transfert zone. C) Carte géographique du rectangle en (B) montrant la localisation des données de subsurface (forages, sismique) des secteurs de Gallician et de Pierrefeu, pf=Pierrefeu 1 well, LGA=LaGaline, les numéros 1 à 9 indiquent les forages de Gallician (1 à 9). Les lignes sismiques PR et VG ont été acquises pendant les campagnes 86Parrapon (1986) et 86Vauvert-Gallician (1986), modifiée d'après Valette (1991). D) Synthèse stratigraphique du dépôt-centre du bassin de la Vistrenque compilée à partir des forages par Gorini (1993), d'après Bache, 2008.

1.4. Méthodes et outils analytiques

Cette thèse repose sur une approche multidisciplinaire et intègre des résultats obtenus par différentes méthodes et outils analytiques. La **Figure 1.4** présente l'approche méthodologique intégrée suivie pour atteindre les objectifs scientifiques de ce travail. Les analyses ont été réalisées sur des données d'affleurement provenant de la carrière de la butte Iouton près de Beaucaire (Gard) et sur les données de subsurface (carottes, cuttings, diagraphies) acquises pendant les compagnes d'exploration pétrolière des années 1950-1960 dans les secteurs de Gallician et de Pierrefeu du bassin de la Vistrenque. Sur les 25 forages pétroliers ayant traversé les séries étudiées, seuls sept forages sont considérés dans ce travail et choisis en fonction de la disponibilité des carottes et d'autres ressources (documents, diagraphies, rapports). Les carottes ont été décrites et échantillonnées à la carothèque de Boussens où elles sont stockées.

1.4.1. Biostratigraphie

La carrière de la butte Iouton a fourni des fossiles de mollusques (gastropodes, bivalves) et des gyrogonites de characées. Les gyrogonites ont été identifiés par M. Feist (Université de Montpellier) et les attributions stratigraphiques qu'ils fournissent sont complétées par la révision des assemblages malacologiques afin de contraindre le cadre chronologique de la formation de cette succession carbonatée de la marge nord du bassin de la Vistrenque.

1.4.2. Chronostratigraphie

Pour remédier à la rareté des données biostratigraphiques dans les séries étudiées en subsurface, la construction du cadre chronostratigraphique du bassin de la Vistrenque repose sur l'apport des datations absolues par la méthode U/Pb sur la calcite, l'approche de climatostragraphie utilisant les assemblages polliniques et sur la modélisation géochimique des isotopes du Soufre et du Strontium sur les sulfates.

- **Datations absolues par la méthode U/Pb sur la calcite**

Environ 30 échantillons présentant des phases carbonatées sparitiques (p.ex., ciments vadoses et météoriques précoces, remplissages de fractures) sont sélectionnés sur les carottes et un jeu de lames géologiques minces et épaisses sont réalisées. Les lames minces servent à analyser la séquence diagenétique de la formation des phases sparitiques sous microscopie optique, cathodoluminescence et microscopie confocale. Les phases intéressantes à dater sont sélectionnées (nb de lames=12) à ce stade et les analyses sont réalisées sur les équivalents épais des lames choisies. Les datations U/Pb ont été réalisées par Nicolas Godeau et Abel Guihou (Plateforme A *midex DatCarb, CEREGE, Aix-Marseille université). La méthode repose sur l'ablation laser de plus de 30 cratères d'environ 100µm le long de la phase diagenétique choisie et les rapports isotopiques obtenus sont reportés sur le diagramme de Tera-Wesserburg.

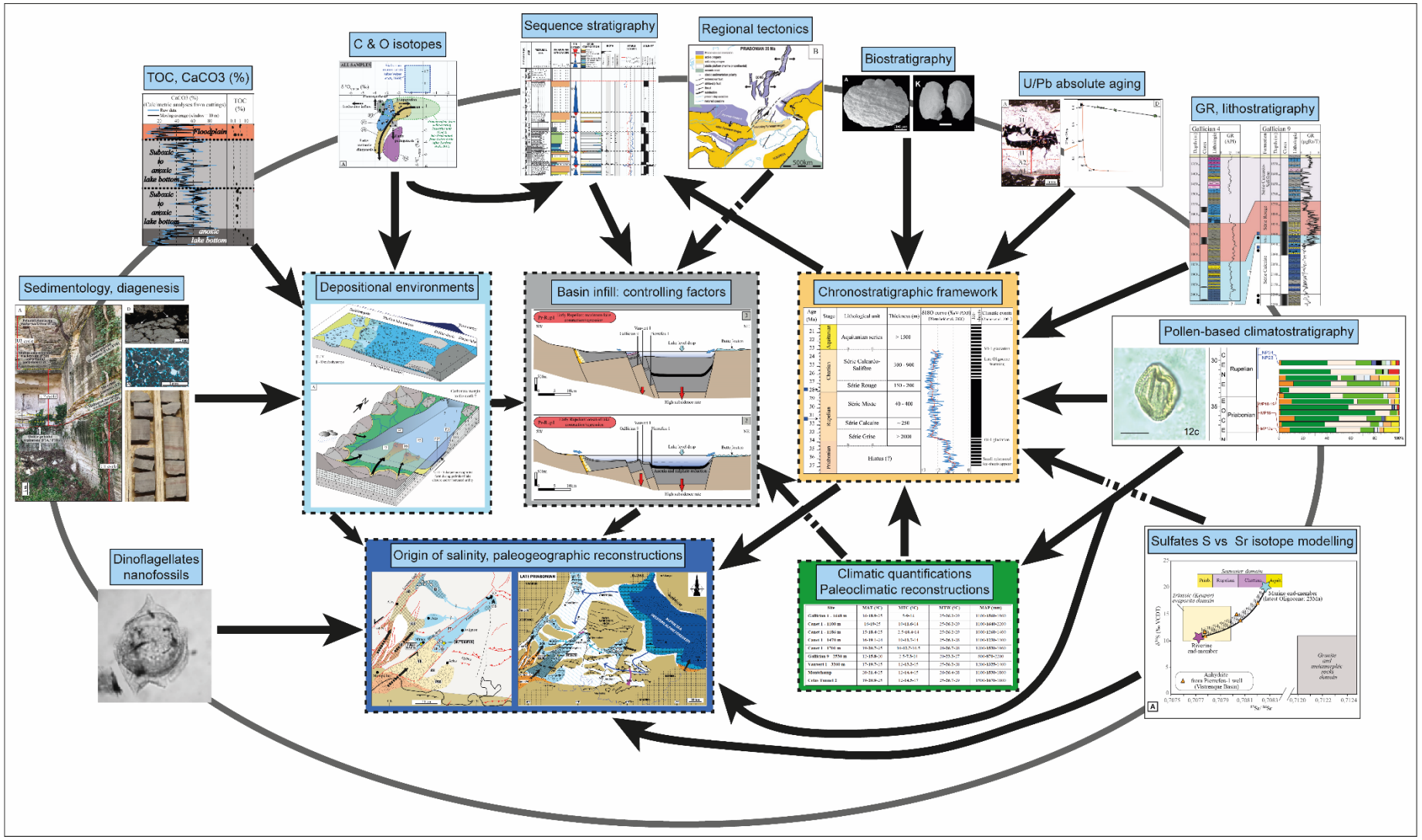

Figure 1.4 : Schéma montrant l'approche méthodologique intégrée (workflow) de la thèse, les différentes disciplines et les outils analytiques utilisés pour atteindre les objectifs de la thèse indiqués dans le centre de la figure.

- **Palyno-climatostratigraphie**

52 échantillons de roches provenant des forages du bassin de la Vistrenque, de Roussillon et d'Alès-Saint-Chaptes-Issirac ainsi que des affleurements de ce dernier ont traités chimiquement pour extraire les grains de pollen à GeoBioStratData.Consulting. Seuls 18 échantillons ont livré des grains de pollen en quantité suffisante. L'observation sous microscope à fort grossissement (X 1000) a été réalisée par J-P. Suc (Sorbonne Université) qui a identifié les grains de pollens. L'analyse statistique des grains de pollen repose sur 150 grains par échantillon en excluant les grains de *Pinus*, ceux des plantes méso-microthermes des moyennes altitudes et ceux des plantes microthermes des hautes altitudes. La diversité taxonomique est prise en considération et les proportions des groupes de plantes par affinité climatique, géographique et altitudinale. Les diagrammes polliniques sont disposés verticalement et l'approche de datation indirecte repose sur la comparaison avec les assemblages connus régionalement, la contrainte avec les repères mammalogiques et le calage sur la courbe des températures globales du Cénozoïque de Westerhold et al. (2020). Les analyses de pollen fournissent en plus les indications sur la végétation dans les environs du lac. En plus de la recherche de plantes halophiles, l'identification des nannofossiles calcaires dans les assemblages polliniques des sédiments lacustres terrigènes permet d'apporter des preuves d'incursions marines en plus de l'identification des pollens de mangroves et de kystes de dinoflagellés.

- **Géochimie des isotopes du soufre et du strontium des sulfates**

Cinq échantillons d'anhydrite ont été sélectionnés sur les évaporites de la Série Calcaréo-salifère du forage de Pierrefeu 1 du bassin de la Vistrenque. Dans le bassin d'Alès, trois échantillons d'anhydrite ont été sélectionnés dans les forages SC-1 et SC-2 qui traversent les séries évaporitiques d'âge Priabonien. Ces huit échantillons ont été analysés pour les isotopes du soufre $\delta^{34}S$ et du strontium $^{87}Sr/^{86}Sr$. Les analyses des isotopes du strontium ont été réalisées au laboratoire SARM-CRPG (Vandœuvre-lès-Nancy, France) et les analyses des isotopes du soufre et de l'oxygène ont été réalisées par Christophe Thomazo à l'université de Bourgogne. La modélisation des compositions isotopiques repose sur la loi des mélanges de Denison et al. (1998) et nécessite un ensemble de points de collecte distribués verticalement sur l'unité évaporitique étudiée. La modélisation permet de déterminer la nature des eaux ayant alimenté le système lacustre salin en solutés (eaux marines, lessivage des roches évaporitiques et des roches métamorphiques) et fournit par conséquent des indications précieuses pour les reconstitutions paléogéographiques. Par ailleurs, lorsque les connexions avec la mer sont établies, les valeurs isotopiques $^{87}Sr/^{86}Sr$ mesurées peuvent être utilisées pour donner des indications directes sur l'âge de précipitation des évaporites (McArthur et al., 2001).

1.4.3. Estimations paléoclimatiques : Méthode d'amplitude climatique

Cette méthode mise en place par Fauquette et al. (1998) repose sur l'abondance relative des taxons de pollen identifiés et le climat pour estimer les températures moyennes annuelles, les températures du mois le plus froid et les températures du mois le plus chaud. Les précipitations

annuelles moyennes sont estimées pour les végétaux de faible altitude. Les estimations pour chaque paramètre ont été réalisées par S. Fauquette (Université de Montpellier) et sont fournies sous forme d'intervalles autour de la valeur la plus probable correspondant à la moyenne pondérée.

1.4.4. Sédimentologie

La description des affleurements et des carottes (carothèque de Boussens) et l'analyse pétrographique des lames minces au laboratoire (>2000, dont une grande partie a été mise à disposition par TotalEnergies) permet de définir les faciès de dépôt qui fournissent les indications pour interpréter les paléoenvironnements de sédimentation. La définition des facies repose sur le contenu biologique, les structures sédimentaires et les figures diagenétiques observées. Les faciès de dépôt carbonatés ont été décrits d'après la classification de Dunham (1962) complétée par Embry and Klovan (1971).

1.4.5. Géochimie du carbone et de l'oxygène des carbonates

Les mesures des compositions isotopiques du carbone et de l'oxygène des carbonates fournissent des indications pour affiner les reconstitutions paléoenvironnementales et des clés pour les reconstitutions paléohydrologiques et paléoclimatiques. Cette thèse intègre 299 mesures réalisées sur des échantillons de roche totale (Butte Iouton =58, Subsurface=241) à l'université Friedrich-Alexander (Erlangen-Nürnberg, Allemagne).

1.4.6. Stratigraphie séquentielle

L'évolution verticales des faciès et des signaux géochimiques des carbonates et les corrélations entre les forages, incluant le Gamma Ray (GR), les calcimétries (% $CaCO_3$) et les mesures de carbone total de la roche (TOC) permettent de documenter les cycles de transgression-régression lacustre. Cette démarche est importante dans les systèmes lacustres salins afin de discuter de l'origine des solutés dans ces milieux et les modalités de leurs connexions avec les masses d'eaux voisines.

1.5. Plan de la thèse

Cette introduction (chapitre 1) ayant présenté la question de recherche, l'objet d'étude choisi, la méthodologie et les hypothèses de travail, le chapitre 2 donnera le contexte géographique du bassin de Camargue et sa position dans le Sud-est de la France, puis présentera l'état de l'art et et les principales études réalisées à ce jour sur le bassin et détaillera le contexte tectonique et structural ainsi son remplissage sédimentaire et la lithostratigraphie détaillées des formations paléogènes qui font l'objet de cette thèse.

Le chapitre 3 repose sur une approche multidisciplinaire pour discuter de la marge nord du bassin lacustre de la Vistrenque au Priabonien (Eocène supérieur). Cette marge carbonatée est étudiée en intégrant la révision biostratigraphique basée sur la malacologie continentale et des

données inédites de datations de gyrogonites de characées, et l'analyse sédimentologique, diagénétique, et géochimique de la succession carbonatée de la butte Iouton. Ce chapitre, accepté pour publication dans le Bulletin de la Société Géologique de France (**BSGF Earth Science Bulletin)**, propose un modèle de dépôt d'une marge oolitique enregistrant principalement les phases de transgression lacustre et discute des modalités de connexion des masses d'eaux salines au Priabonien au Sud-est de la France.

Le chapitre 4 concerne les séries de subsurface et se concentrera sur la construction du cadre chronologique du remplissage du dépôt-centre du bassin de la Vistrenque au Paléogène. Ce chapitre intégrera des données inédites de datations absolues obtenues par la méthode U/Pb sur la calcite ainsi que des âges interprétés à l'aide de l'approche climatostratigraphique fondée sur les assemblages polliniques et complétées par de la modélisation géochimique des isotopes du soufre et du strontium sur les sulfates. Ce chapitre apporte de nouveaux éléments pour préciser les reconstitutions paléogéographiques et discuter des couloirs de salinisation potentiels des bassins continentaux du Sud-est de la France ainsi que de l'enregistrement floristique en milieu terrestre de la dégradation climatique à la transition Eocène-Oligocène.

Le chapitre 5 concerne l'analyse sédimentologique, stratigraphique et géochimique du remplissage paléogène dans les secteurs de Gallician et de Pierrefeu situés dans le centre du bassin de la Vistrenque. Ce chapitre fournit les interprétations paléoenvironnementales et les modèles de dépôts pour rendre compte de la sédimentation dans le bassin pendant la période qui s'échelonne de la fin de l'Eocène à l'Oligocène supérieur. Le modèle de remplissage du bassin fourni intègre le cadre chronostratigraphique construit dans le chapitre 4. Ce chapitre documente l'enregistrement sédimentaire du refroidissement bref survenu au début du Rupélien et discute de l'influence de la tectonique et du climat sur le remplissage du bassin continental.

La conclusion (chapitre 6) synthétise les nouveaux éclairages apportés par cette étude intégrée et multidisciplinaire sur la géologie de la Camargue en particulier et du Sud-est de la France. Elle propose aussi des perspectives pour affiner la compréhension du remplissage sédimentaire de la série paléogène très épaisse des bassins Camarguais de la Vistrenque et de Vaccarès.

1.6. Références bibliographiques du chapitre 1

Bauer H, Bessin P, Saint-Marc P, Châteauneuf J-J, Bourdillon C, Wyns R, Guillocheau F. 2016. The Cenozoic history of the Armorican Massif : New insights from the deep CD81 borehole (Rennes Basin, France). *Comptes rendus Géosciences* 348, 387-397.

Benedicto A. 1996. Modèles tectono-sédimentaires de bassins en extension et style structural de la marge passive du Golfe du Lion (partie nord), sud-est France. Université de Montpellier II. Thèse de doctorat, 249 pp.

Benedicto A, Labaume P, Séguret M, Séranne M. 1996. Low-angle crustal ramp and basin geometry in the Gulf of Lion passive margin: the Oligocene-Aquitanian Vistrenque graben, SE France. *Tectonics* 15(6): 1192–1212.

Bodergat A.-M, Briot D, Hugueney M, Poidevin J.-L, Picot L, Giraud F, et al. 1999. Incursions marines dans l'environnement lacustre du rift oligocène de Limagne (Massif Central, France): apport des organismes halophiles et des isotopes du strontium, datation par les mammifères. *Bulletin de la Société Géologique de France* 170 : 499-511.

Briot D, Poidevin J. 1998. Stratigraphie 87Sr/86Sr de quelques laminites carbonatées du Rupélien inférieur du fossé de Limagne: incursions marines dans le rift du Massif Central Français? *Comptes Rendus de l'Académie des Sciences de Paris* 236 : 479-483.

Briot D, 2008. Sr isotopes of the shells of the euryhaline gastropod *Potamides lamarcki* from the Oligocene of the French Massif Central and Paris Basin – A clue to its habitats. *Palaeogeography, Palaeoclimatology, Palaeoecology* 268 : 116-122.

Cavelier C, Alabouvette G, Amberger J.P, Cautru J.-P, Charollais J, Châteauneuf J.-J, et al. 1984. Paléogène. In : Debrand-Passard ed., Synthèse géologique du Sud-Est de la France. *Mémoire du BRGM* 125 : pp. 389-468.

Châteauneuf J.-J. 1980. Paléostratigraphie et paléoclimatologie de l'Éocène supérieur et de l'Oligocène du bassin de Paris. *Mémoires du Bureau de Recherches géologiques et Minières* 116: 357 pp.

Denison, R.E., Kirkland, D.W., Evans, R., 1998. Using Strontium Isotopes to Determine the Age and Origin of Gypsum and Anhydrite Beds. *Journal of Geology*, 106, 1-17.

Dèzes P, Schmid S.M, Ziegler P.A. 2004. Evolution of the European Cenozoic Rift System: interaction of the Alpine and Pyrenean orogens with their foreland lithosphere. *Tectonophysics* 389: 1–33.

Dunham R.J. 1962. Classification of Carbonate Rocks According to Depositional Texture. In: Ham, W.E., Ed., Classification of Carbonate Rocks, AAPG, Tulsa, 108-121.

Embry A.F, Klovan J.E. 1971. A Late Devonian Reef Tract on Northeasterm Banks Island. *Canadian Petroleum Geology* 19: 730-781.

Emre T, Truc, G. 1978. Mise en évidence d'un contact discordant Oligocène-Trias dans le Massif de Suzette. Implications tectoniques et conséquences sur l'origine des évaporites ludiennes du bassin de Mormoiron (Vaucluse). Géologie Alpine 57 : 17-23.

Fabre J, Mainguet M. 1991. Continental sedimentation and palaeoclimates in Africa during the Gondwanian Era (Cambrian to Lower Cretaceous): the importance of wind action. *Journal of African Earth Sciences* 12 (1-2): 107-115.

Fauquette S, Guiot J, Suc J.-P. 1998. A method for climatic reconstruction of the Mediterranean Pliocene using pollen data. *Palaeogeography, Palaeoclimatology, Palaeoecology* 144: 183–201.

Fontes J.-C, Filly A, Gaudant J, Duringer P. 1991. Origine continentale des évaporites paléogènes de Haute Alsace : arguments paléoécologiques, sédimentologiques et isotopiques. *Bulletin de la Société Géologique de France* 162: 725–737.

Giraud J. 1902. Études géologiques sur la Limagne. *Bulletin du Service de la Carte Géologique de France* 13(87): 410 p.

Fontes J-C, Filly A, Gaudant J, Duringer P. 1991. Origine continentale des évaporites paléogènes de Haute Alsace: arguments paléoécologiques, sédimentologiques et isotopiques. *Bulletin de la Société Géologique de France* 162: 725-737

Joseph P, and Lomas S. 2004. Deep-water sedimentation in the Alpine Foreland Basin of SE France: new perspectives on the grès d'Annot and related systems - An introduction. Dans P. Joseph, & S. Lomas (Éds.), Deep-water sedimentation in the Alpine Foreland Basin of SE France: new perspectives on the grès d'Annot and related systems (Vol. 1, pp. 1-16). *The Geological Society of London, Special Publications*.

Lesueur J.-L. 1991. Etude sédimentologique et stratigraphique du Bassin Paléogène d'Apt–Manosque–Forcalquier (Alpes de Haute Provence). Modalités de la transition Burdigalienne. Ph.D. thesis, University M. de Montaigne, Bordeaux III, France : 407 pp.

Lettéron A, Fournier F, Hamon Y, Villier L, Margerel J.-P, Bouche A, Feist M, Joseph P. 2017. Multi-proxy paleoenvironmental reconstruction of saline lake carbonates: paleoclimatic and paleogeographic implications (Priabonian-Rupelian, Issirac Basin, SE France). *Sedimentary Geology* 358: 97–120.

Lettéron, A. 2018. Caractérisation sédimentologique, stratigraphique et paléoenvironnementale du système carbonaté lacustre à salinité variable du bassin d'Alès et des régions limitrophes (Priabonien, SE France) : implications paléoclimatiques et paléogéographiques. PhD thesis, Aix-Marseille University : 344 pp.

Lettéron A, Hamon Y, Fournier F, Séranne M, Pellenard P, Joseph P. 2018. Reconstruction of a saline, lacustrine carbonate system (Priabonian, St-Chaptes Basin, SE France): depositional models, paleogeographic and paleoclimatic implications. *Sedimentary Geology* 367: 20–47.

Lettéron A, Hamoun Y, Fournier F, Demory F, Séranne M, Joseph P. 2021. Stratigraphic architecture of a saline lake system: From lake depocenter (Alès Basin) to margins (Saint-Chaptes and Issirac basins), Eocene-Oligocene transition, south-east France. *Sedimentology, Blackwell Publishing, in press*, ⟨DOI: 10.1111/sed.12920⟩, ⟨hal-03406458⟩.

Liu Z, Pagani M, Zinniker D, DeConto R, Huber M, Brinkhuis H, Shah S.R, Leckie R.M, Pearson A. 2009. Global cooling during the Eocene-Oligocene climate transition: *Science* 323 : 1187-1190.

McArthur J.M, Howarth R.J, Bailey T.R. 2001. Strontium Isotope Stratigraphy: LOWESS Version 3: best fit to the marine Sr-isotope curve for 0-509 Ma and Accompanying look-up table for deriving numerical ages. *The Journal of Geology*, 109(2) 155-170 https://doi.org/10.1086/319243

Moretto R. 1987. Etude sédimentologique et géochimique des dépôts de la série salifère paléogène du basin de Bourg-en-Bresse (France). (PhD thesis). Université de Nancy I, France (252pp).

Moretto R. 1988. Observations on the incorporation of trace elements in halite in Oligocene salt beds, Bourg-en-Bresse Basin, France. *Geochemistry Cosmochimica Acta* 52: 2809-2814.

Mosbrugger V, Utescher T, Dilcher D.L. 2005. Cenozoic continental climatic evolution of Central Europe. *PNAS* 102 (42): 14964-14969.

Nutz A, Kwiecien O, Breitenbach S, Cai Y, Della Porta G, Danisch J, Kabiri L, Bodin S. 2019. Fluvio-lacustrine sedimentation in the Agadir-Tissint Feija (Anti-Atlas, Morocco): A promising palaeoclimate archive for the last glacial cycle in northwest Africa. *Depositional Record* 5(2): 362-387. ⟨10.1002/dep2.65⟩. ⟨hal-02468873⟩

Pellat E, Allard M. 1895. Dépôts lacustres de la Butte Iouton entre Comps et Beaucaire (Gard). *Bulletin de la Société Géologique de France* 23 : 434-436.

Roman F. 1910. Faune saumâtre du sannoisien du Gard. *Bulletin de la Société Géologique de France (4ème série)* 10 : 927–955.

Romagny A, Jolivet L, Menant A, Bessière E, Maillard A, Canva A, Gorini C, Augier R. 2020. Detailed tectonic reconstructions of the Western Mediterranean region for the last 35 Ma, insights on driving mechanisms, *BSGF - Earth Sciences Bulletin* 191 : 37

Rouchy J.-M. 1997. Paleogene continental rift system ofWestern Europe: locations of basins, paleogeographic and structural framework, and the distribution of evaporites. In: Busson, G., Schreiber, B.C. eds., Sedimentary Deposition in Rift and Foreland Basins in France and Spain. Columbia Univ. Press, New York: pp. 45–94.

Rouchy J.-M, Blanc-Valleron M.-M. 2009. Les évaporites matériaux singuliers, milieux extrêmes. Vuibert, Paris, 184 pp.

Sanchis E, Séranne M. 2000. Structural style and tectonic evolution of a polyphase extensional basin of the Gulf of Lion passive margin: the Tertiary Alès Basin, southern France. *Tectonophysics* 322: 243–264.

Sarkar S, Basak C, Frank M. et al. 2019. Late Eocene onset of the Proto-Antarctic Circumpolar Current. *Scientific Reports* 9, 10125. https://doi.org/10.1038/s41598-019-46253-1

Schuler M. 1990. Environnements et paléoclimats paléogènes. Palynologie et biostratigraphie de l'Éocène et de l'Oligocène supérieur dans les fossés rhénan, rhodanien et de Hesse. *Document du Bureau de Recherches Géologiques et Minières*, 190, Orléans (503 pp).

Séranne M, Couëffé R, Husson E, Baral C, Villard J. 2021. The transition from Pyrenean shortening to Gulf of Lion rifting in Languedoc (South France) –A tectonic-sedimentation analysis. *BSGF - Earth Sciences Bulletin* 192, 27.

Sittler C, Schuler M, Caratini C, Châteauneuf J-J, Gruas-Cavagnetto C, Jardine S, Ollivier M.F, Roche E, Tissot C. 1975. Extension stratigraphique, répartition géographique et écologie de deux genres polliniques paléogènes observes en Europe occidentale : *Aglaoreidia* et *Boehlensispollis*. *Bulletin de la Société Géologique de France* 122, sup 1, 231-245.

Sissingh W. 2001. Tectonostratigraphy of the West Alpine Foreland: correlation of Tertiary sedimentary sequences, changes in eustatic sea-level and stress regimes. *Tectonophysics*: 333, 361–400.

Sissingh W. 2006. Synkinematic paleogeographic evolution of the West European Platform: correlation with Alpine plate collision and foreland deformation. *Géologie en Mijnbouw, Nehterlands Journal of Geosciences* 85(2):131-180.

Talbot MR. 1990. A review of the palaeohydrological interpretation of carbon and oxygen 1121 isotopic ratios in primary lacustrine carbonates. *Chemical Geology* 80: 261–279.

Triat J.M, Truc G. 1974. Evaporites paléogènes du domaine rhodanien. *Revue de Géographie Physique et de Géologie Dynamique* 16: 235–262.

Valette M. 1991. Etude structurale du gisement salifère Oligocène de Vauvert (Gard), *Thèse de doctorat*, Univ. Montpellier II, 229 pp.

Valette M, Benedicto A. 1995. Chevauchements gravitaires halotectoniques dans le bassin distensif de Camargue (marge du golfe du Lion, SE de la France). *Bulletin de la Société Géologique de France* 166(2): 137-147.

Wade, B. S., Houben, A. J. P. Quaijtaal, W. Schouten, S. Rosenthal, Y. Miller, K. G., Katz, M. E., Wright, J. D. , Brinkhuis, H., 2012. Multiproxy record of abrupt sea-surface cooling across the Eocene-Oligocene transition in the Gulf of Mexico. Geology, 40, 2, 159-162.

Westerhold T, Marwan N, Drury A.J, Liebrand D, Agnini C, Anagnostou E, Barnet J.S.K, Bohaty S.M, De Vleeschouwer D, Florin D, Lauretano V, Littler K, Lourens L.J, Lyle M, Pälike

H, Röhl U, Tian J, Wilkens R.H, Wilson P.A, Zachos J.C. 2020. An astronomically dated record of Earth's climate and its predictability over the last 66 million years. *Science* 369: 1383–1387.

Zachos J, Pagani M, Sloan L, Thomas E, Billups K, 2001. Trends, rythms and aberrations in global climate 65 Ma to present. *Science* 292, 686-693.

Zhang R, Kravchinsky V.A, Yue L. 2012. Link between global cooling and mammalian transformation across the Eocene–Oligocene boundary in the continental interior of Asia. *Int J Earth Sci (Geol Rundsch)* 101: 2193–2200. https://doi.org/10.1007/s00531-012-0776-1.

Ziegler P.A. 1992. European Cenozoic rift system. In: Ziegler, P.A. (Ed.), Geodynamics of Rifting, Volume I, Case History Studies on Rifts: Europe and Asia. *Tectonophysics* 208: 91–111.

Ziegler P.A, Dèzes P. 2007. Cenozoic Uplift of Variscan Massifs in the Alpine Foreland: Timing and Controlling Mechanisms. *Global Planetary Change* 58: 237-269.

2. CONTEXTE GÉOLOGIQUE

2. Contexte géologique et stratigraphie du bassin de la Vistrenque

2.1. Cadre géographique

La zone d'étude est située dans le Sud-Est de la France et s'étend sur les régions naturelles des Costières, de la Petite Camargue et de la Camargue. Délimitée au Nord-Ouest par la région des Garrigues et au Sud par le Golfe du Lion, elle couvre un triangle équilatéral, d'environ 60 Km de côté, qui relie les villes de La Grande-Motte, Nîmes et Remoulins le long de la faille de Nîmes, et les villes de Beaucaire et Port-Saint-Louis-du-Rhône le long du fleuve du Rhône et est bordée au Sud par la mer Méditerranée.

Sous les formations détritiques des Costières et les limons et les alluvions des vallées du Rhône et du Gardon d'âges Plio-Quaternaire à Holocène est enfoui un système sédimentaire Cénozoïque appelé « bassin de Camargue » (**Fig. 2.1A**). Le *bassin de Camargue* est structuré en un système de horsts et grabens et est constitué de deux « *sous-bassins* » principaux : le fossé de la Vistrenque *sensu stricto* situé à l'ouest et bordé au Nord-Ouest par la faille de Nîmes ; et le fossé de Vaccarès à l'est qui se prolonge en mer où il prend la dénomination de « graben de Petite Camargue » (Séranne et al., 1995 ; Benedicto, 1996) (**Fig. 2.1B**). Les données gravimétriques montrent que les deux fossés sont séparés par une zone haute appelée « horst d'Albaron » (Trauth, 1984 dans Cavelier et al., 1984 ; Chauvin and Follin-Arbelet, 1985 ; Benedicto, 1996). Au Sud, Le bassin de Camargue est limité par les horsts du Grau-du-Roi et des Saintes-Maries-de-la-Mer (**Fig. 2.1B**).

Le fossé de Vaccarès est peu étudié en raison de la protection dont bénéficie le périmètre géographique sur lequel est situé le parc naturel régional de Camargue. Quelques puits profonds (Vaccarès 1, Sainte-Cécile 1, Villeneuve 1) forés au nord de l'étang de Vaccarès montrent l'existence d'un fossé tertiaire à l'est du haut d'Albaron (**Fig. 2.1C**). Le bassin de Vaccarès est désigné par la dénomination « bassin de Camargue orientale » tandis que le fossé de la Vistrenque est dénommé « Camargue occidentale ». Pour ce dernier, on trouve parfois dans la littérature la dénomination de « fossé de Nîmes » donnée par Rouchy (1997) en raison du rôle de la faille de Nîmes dans la structuration du bassin. Par souci de simplification, la Camargue désignera dans ce travail l'aire géographique tandis que « **bassin de la Vistrenque** » désignera l'objet géologique étudié.

Le bassin de la Vistrenque est orienté approximativement NE-SW et s'étend sur environ 50*30 Km². Il a été mis en évidence par les études de subsurface et s'est révélé comme le plus profond dépôt-centre tertiaire de la marge du golfe du Lion (Benedicto, 1996). Contrairement aux bassins cénozoïques voisins d'Alès, Mormoiron, Sommières, les affleurements paléogènes du bassin de la Vistrenque sont rares : on peut citer la présence de quelques lambeaux tertiaires sur la terminaison Nord du bassin près de Baucaire à la Butte Iouton (rocher de Triple Levée ;

Pellat and Allard, 1895 ; Roman, 1903 ; 1910 ; **Fig. 1D**) et du Puech du Teil à l'ouest, près de la ville de Nîmes (Caziot, 1896).

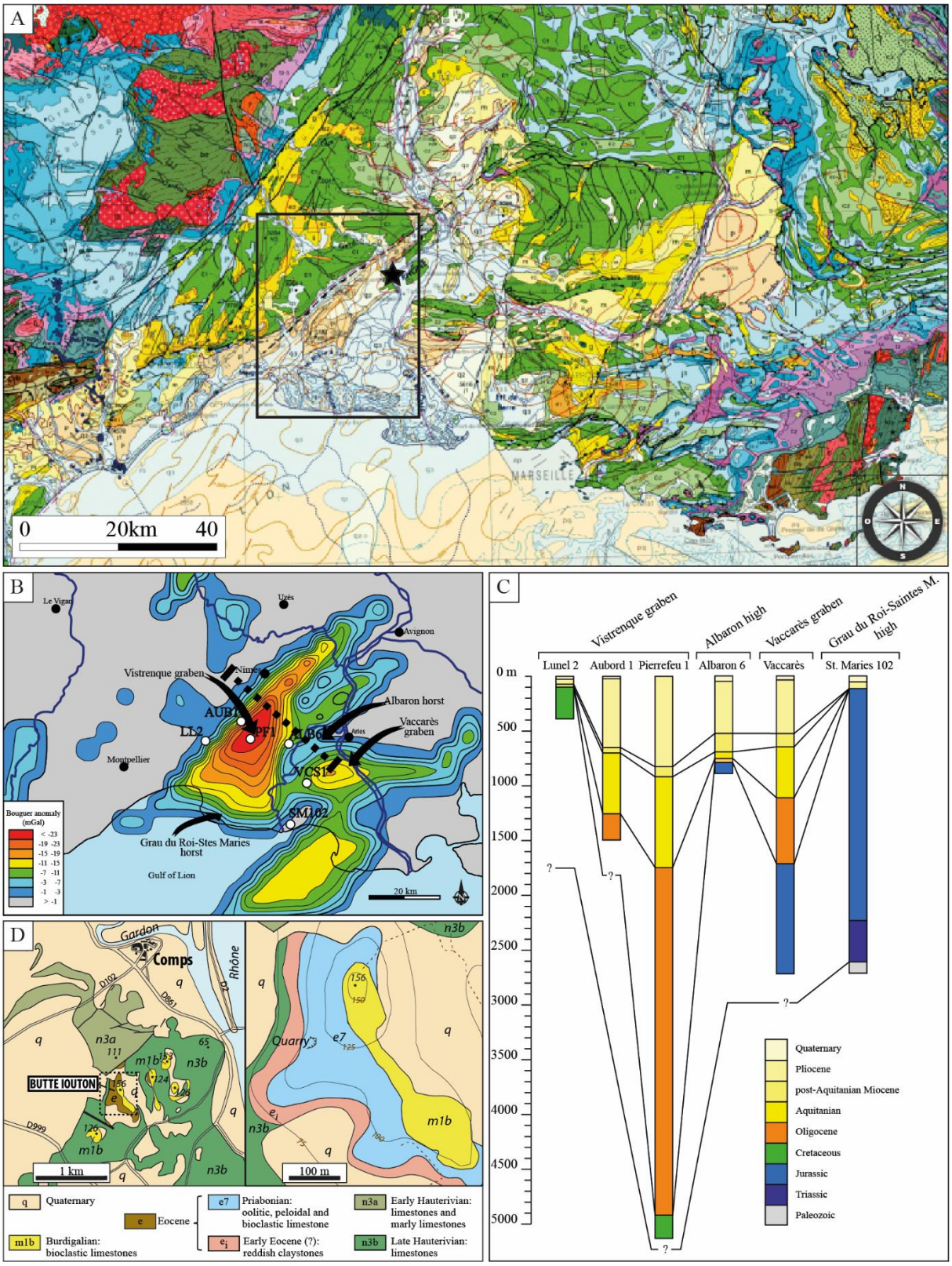

Figure 2.1 : Présentation du secteur d'étude. A) Extrait de la carte géologique de la France 1/1 000000 montrant la faille majeure de Nîmes orientée NE-SW (ligne en pointillé) qui sépare d'une part les Garrigues de Nîmes constituant le substratum mésozoïque et d'autre part le bassin cénozoïque de la Vistrenque. Le rectangle indique

l'aire correspondant au secteur d'étude et l'étoile indique la position de la succession paléogène affleurant au nord du Bassin près de Beaucaire (Butte Iouton, Pellat and Allard, 1895, Chapitre 3 de ce mémoire). B) Carte de l'anomalie gravimétrique de Bouguer, modifiée d'après Chauvin and Follin-Arbelet (1985). C) Corrélations lithostratigraphiques de quelques puits traversant les deux fossés Camarguais : le Bassin de la Vistrenque et le Bassin de Vaccarès. Ces deux bassins sont séparés par le haut structural d'Albaron et sont limités au sud par le haut du Grau-du-Roi-Saintes-Maries, modifié d'après Benedicto (1996). LL2 : Lunel 2, AUB1 : Aubord 1, PF1 : Pierrefeu 1, ALB6 : Albaron 6, VCS1 : Vaccarès 1, SM102 : Saintes-Maries-de-la-Mer 102, voir localisation des forages dans (B). D) A gauche, extrait de la carte géologique 1/50000 montrant le secteur de Comps et de la butte Iouton (modifié d'après carte géologique du BRGM, feuille de Nîmes 1/50000 (Ménillet, 1973), la carte montre les affleurements d'âge Éocène à Miocène et leur substratum Crétacé inférieur. A gauche, détails sur le secteur de la butte Iouton indiqué par le rectangle dans l'extrait à gauche.

Les bordures mésozoïques constituées des plateaux calcaires des Garrigues nîmoises à l'Ouest et de la chaîne des Alpilles au Nord marquent le paysage contrastant avec les Costières et la plaine camarguaise, et déterminent les limites géographiques de la Camargue. La faille majeure de Nîmes qui borde la Camargue à l'ouest est orientée NE-SW et souligne ce contraste géographique entre le substratum mésozoïque et le bassin cénozoïque de la Vistrenque. La formation des bassins cénozoiques du Sud-est, et de la Camargue en particulier, est accompagnée d'un amincissement crustal indiqué par la remontée du Moho (Ménard, 1980 dans Valette, 1991) et qui se traduit également par la forte anomalie gravimétrique à l'aplomb des fossés cénozoïques (Arthaud et al., 1981 ; Chauvin and Follin-Arbelet, 1985) (**Fig. 2.1B**).

Cette étude concerne uniquement le bassin de la Vistrenque situé dans la partie occidentale de la Camargue et les affleurements paléogènes qui le bordent au nord, en particulier la butte Iouton près de Beaucaire (voir localisation dans **Fig. 2.1A**, **2.1D**).

2.2. Travaux antérieurs et état de l'art sur le bassin de la Vistrenque

Plusieurs travaux scientifiques et industriels ont été réalisés sur le bassin de la Vistrenque. Connu au 19ème siècle par quelques affleurements isolés de sa bordure septentrionale (p.ex., Butte Iouton), le bassin de la Vistrenque sera l'objet d'une exploration pétrolière durant les années 1940-1950, puis de l'exploitation minière souterraine de sel par lixiviation avec des forages profonds de plus de 2000 m depuis les années 1970 à ce jour. Parallèlement, la Camargue est étudiée depuis les années 1970-1980 du point de vue tectonique et structural pour comprendre le système ECRIS (Ziegler, 1992), la marge du golfe du Lion (Benedicto, 1996), et le Languedoc (p.ex., Séranne et al., 2021).

La revue de la littérature sur le bassin de la Vistrenque présentée ci-après n'est pas exhaustive tant les études antérieures, en grande partie des documents internes industriels, sont nombreuses. Les notes industrielles proviennent des différentes compagnies ayant été incorporées au groupe TotalEnergies au cours des dernières décennies ainsi que de ses partenaires pour les travaux pétroliers d'une part, et de Kemone qui exploite le sel en

subsurface dans la saline de Vauvert d'autre part. Les références aux travaux cités dans cette section sont fournies dans la liste bibliographique à la fin de ce chapitre.

Les premiers travaux scientifiques sur la géologie du bassin de Camargue datent de la deuxième moitié du 19ème siècle et du début du 20ème siècle et étaient limités aux affleurements, peu nombreux, des bordures près de Beaucaire et de Nîmes. Les études portaient essentiellement sur la stratigraphie et la description des faunes malacologiques saumâtres et considéraient les affleurements des calcaires lacustres comme faisant partie tantôt du bassin d'Alès (orthographié anciennement *Alais*) tantôt des bassins de la Vallée du Rhône (p.ex., Pellat and Allard, 1895 ; Roman, 1910).

Contrairement aux autres bassins cénozoïques du Sud-Est de la France qui étaient connus grâce à la présence d'affleurements nombreux et à la faveur de l'exploitation des ressources minérales et énergétiques (par exemple les bitumes et le lignite d'Alès, Dumas, 1876), l'existence des bassins paléogènes profonds en Camargue n'a été révélée que tardivement. Les indices d'hydrocarbures de surface de Milhaud, près de la faille de Nîmes (p.ex., Maugy and Fisches, 1949), ont attiré l'attention des géologues pétroliers et les premiers forages ont été réalisés dans les années 1949-1951 dans le secteur des gradins de la faille de Nîmes mais également plus à l'est et au sud sur les hauts mésozoïques d'Albaron et du Grau-du-Roi-Saintes-Maries-de-la-Mer (**Fig. 2.1B**, **2.1C**). L'acquisition de données géophysiques (sismique réflexion, gravimétrie) a permis de confirmer l'existence des deux bassins cénozoïques voisins de la Vistrenque et de Vaccarès enfouis sous les formations plio-quaternaires des Costières et du delta du Rhône.

Lors d'une deuxième phase d'exploration (1951-1953), la structure du bassin et ses limites ont été ébauchées rapidement et un champ de pétrole a été exploité brièvement dans le secteur de Gallician situé dans le centre du bassin (voir localisation dans **Fig. 2.4B**). Les nombreux forages et les données géophysiques de ce secteur ont constitué une importante quantité de données et permis de réaliser des études détaillées par les compagnies pétrolières sous forme de rapports internes non publiés (par exemple : rapports géologiques des forages, études micropaléontologiques et notes stratigraphiques).

Plus tard, une importante accumulation d'évaporites est traversée par le forage Pierrefeu 1 (Valette and Benedicto, 1995) dans le secteur de Pierrefeu-Parrapon en 1963. Depuis les années 1970 à ce jour, ce secteur est le siège d'une saline qui exploite le sel par lixiviation. Toujours dans ce secteur, la densité des forages et des nouvelles données géophysiques, dont une étude microsismique haute résolution, ont fourni le matériel d'étude pour des travaux détaillés de géologie structurale du secteur de Pierrefeu-Parrapon et du bassin de la Vistrenque dans le cadre de la formation de la marge du Golfe du Lion (Valette, 1991 ; Valette and Benedicto, 1995 ; Benedicto, 1996 ; Benedicto et al., 1996).

Dans les années 1980-1990, de nouveaux efforts d'exploration ont concerné le champ de Gallician avec l'acquisition de nouvelles données sismiques, la réalisation de quelques

sondages supplémentaires (p.ex., Baumelles 1, Cros-de-Lagnon 1), l'acquisition de nouvelles données palynologiques (p.ex., Jan du Chene, 1989 ; Biteau et al., 1993) et la révision des données pétrolières héritées des années 1950-1960. Ces travaux ont donné lieu à des synthèses géologiques industrielles non publiées sur le champ de Gallician.

Grâce aux données géophysiques de subsurface acquises lors de grands programmes de recherche (ECORS, compagnes sismiques diverses), plusieurs études tectoniques et structurales concernant la Camargue et les bassins cénozoïques voisins ainsi que le golfe du Lion ont été réalisées entre les années 1970 et 2000 (Lefevre, 1980 ; Arthaud et al., 1981 ; Arthaud and Séguret 1981 ; Valette, 1991 ; Gorini, 1993 ; Valette and Benedicto 1995 ; Séranne et al., 1995 ; Benedicto, 1996 ; Benedicto et al., 1996 ; Mauffret and Gorini 1996 ; Séranne, 1999). Tout au long de ces travaux, on peut suivre l'évolution des idées sur la géodynamique, la structure profonde et la géophysique des formations sédimentaires mésozoïques et cénozoïques du Sud-est de la France et du golfe du Lion.

Comme indiqué précédemment, les quelques études publiées sur le bassin de la Vistrenque (p.ex., Valette, 1991 ; Valette and Benedicto 1995 ; Benedicto, 1996 ; Benedicto et al., 1996) concernent essentiellement l'analyse de la structure profonde du bassin et son contexte géodynamique dans le cadre du rifting de la marge du golfe du Lion à l'Oligo-Miocène. Le rifting Ouest-Européen (Ziegler, 1992) ainsi que la dynamique décrochante en Languedoc (Séranne et al., 2021) sont bien documentés dans les bassins paléogènes continentaux voisins de la Vallée du Rhône et du Languedoc mais les modalités d'expression de ces phases tectoniques demeurent à ce jour non décrites en Camargue.

Par ailleurs, les études les plus récentes en géologie structurale (Séranne et al., 2021) et en sédimentologie (Lettéron et al., 2018 ; 2021) soulèvent des questions de calendrier de fonctionnement des bassins cénozoïques et les relations entre les systèmes sédimentaires lacustres associés à ces bassins notamment avec le bassin de la Vistrenque situé en position géographique charnière au Sud de ces fossés paléogènes et présentant une importante succession sédimentaire paléogène dépassant 3000 m d'épaisseur.

2.2.1. Géologie structurale et analyse du bassin de la Vistrenque

Les premiers travaux scientifiques qui concernent le style structural du bassin de la Vistrenque s'inscrivent dans des études à grande échelle et portent sur la marge du golfe du Lion : elles proposent une structuration en horsts et grabens de la marge par des failles à fort pendage (p.ex., Arthaud et al., 1981 ; Lefevre, 1981 ; Arthaud and Séguret 1981 ; Bessis, 1986 ; Bessis and Burrus 1986). Les failles majeures de direction NNE-SSW et NE-SW (p.ex., Faille des Cévennes, Faille de Nîmes ; **Fig. 2.1A**, **2.4A**) qui bordent les aires de sédimentation cénozoïque sont considérées comme le résultat de la réactivation des accidents anciens hérités de la structuration varisque. Par ailleurs, Bessis (1986) et Bessis and Burrus (1986) ont contraint

le cadre chronostratigraphique de la phase du rifting de la marge du golfe du Lion pendant laquelle le bassin de la Vistrenque a fonctionné. En considérant une structuration en horsts et grabens bordés par des failles à fort pendage, les auteurs ont défini deux phases d'affaissement du bassin : une subsidence tectonique à l'Oligocène-Aquitanien inférieur et une subsidence thermique entre l'Aquitanien moyen et le Pliocène (Bessis and Burrus, 1986 ; Valette, 1991).

Le modèle structural en horsts et grabens adopté jusqu'alors est tombé en désuétude après l'interprétation des données de sismique très profonde (ECORS : Etude des Continents et des Océans par Réflexion Sismique) acquises à la fin des années 1980 (Gorini, 1993). L'exploitation de l'ensemble des données pétrolières (sismique, données de forages) et l'intégration des profils ECORS ont permis de proposer des modèles tectono-sédimentaires et de décrire les styles structuraux des bassins tertiaires de la marge (Gorini, 1993 ; Séranne et al., 1995 ; Benedicto et al., 1996).

Benedicto et al. (1996) ont réalisé la première interprétation structurale détaillée du bassin de la Vistrenque et ont décrit la géométrie de son remplissage sédimentaire en proposant un modèle de géométrie à faible pendage pour la faille de Nîmes. Parallèlement, grâce à l'exceptionnelle densité des données sismiques et des forages du secteur de la saline de Vauvert, Valette (1991) et Valette and Benedicto (1995) ont décrit le style structural et analysé les déformations halotectoniques du remplissage sédimentaire évaporitique Oligocène-Aquitanien du secteur de Pierrefeu-Parrapon situé au nord du graben de la Vistrenque.

A l'échelle de la marge du golfe du Lion, Gorini et al. (1994) ont réalisé la première synthèse sur la structure de la marge qui assimile les bassins tertiaires à des structures en demi-grabens contrôlées par des failles listriques. Plus tard, Séranne et al. (1995) et Benedicto (1996) ont analysé les bassins de la partie de la marge située à terre et décrit le style d'extension de la marge en distinguant deux domaines avec différents styles structuraux séparés par la faille de Nîmes : un domaine de décollement de la couverture mésozoïque au Nord-ouest entre la faille des Cévennes et la faille de Nîmes, et un domaine de décollement de socle au Sud-est de la faille de Nîmes.

Les grabens Oligo-aquitaniens de la marge du golfe du Lion orientés NE-SW se sont formés à la faveur de l'ouverture du bassin Liguro-provençal et sont à distinguer des structures NNE-WSW formées à l'Éocène supérieur-Oligocène dont le moteur d'extension est à chercher dans le rifting ouest européen (Ziegler, 1992 ; Mauffret et al., 1995).

Ces travaux d'interprétation structurale qui ont porté sur la marge du Golfe du Lion et sur le bassin de la Vistrenque en particulier ont intégré les données de forage issues essentiellement de l'industrie pétrolière des années 1950 et adopté avec réserves la nomenclature stratigraphique des formations géologiques traversées en l'absence de nouvelles datations. Ainsi, le bassin de la Vistrenque a toujours été étudié dans le contexte du rifting Oligo-Aquitanien de la marge du golfe du Lion et les premiers dépôts sédimentaires de son remplissage ont été attribuées à l'Oligocène (Benedicto et al., 1996).

Aucune étude structurale n'a raccordé le bassin de la Vistrenque à l'extension liée au système du Rift Ouest-européen (Ziegler, 1992) et aux décrochements senestres Languedociens (Séranne et al., 2021) qui ont pourtant joué un rôle majeur dans la formation des bassins voisins (p.ex., Alès, Mormoiron, Apt-Manosque-Forcalquier) pendant le Priabonien.

2.2.2. Stratigraphie et datations

A - Les affleurements de la terminaison nord du bassin

Les premières recherches sur le Paléogène en Camargue étaient limitées à l'étude des affleurements des bordures où les calcaires qui les constituent étaient considérés tantôt comme faisant partie des bassins gardois tantôt de la vallée du Rhône (Pellat and Allard, 1895 ; Roman, 1910). Abordées d'une manière succincte par Dumas (1876) dans son ouvrage sur la géologie du département du Gard, les formations paléogènes affleurantes ont par la suite fait l'objet de plusieurs notes dans lesquelles sont données les coupes sédimentologiques, les associations faunistiques et les attributions stratigraphiques (Fontannes, 1885 ; Pellat and Allard, 1895 ; Caziot, 1896 ; Roman, 1905). Une révision de la faune malacologique saumâtre est entreprise par Roman (1910) qui rapporte les formations de la Butte Iouton et du Puech du Teil au Sannoisien (Priabonien ; *Ludien* dans Alabouvette et al., 1983). Cette succession paléogène est recouverte en discordance dans le secteur de la butte Iouton par des dépôts marins transgressifs constitués de calcaires à algues rouges d'âge Burdigalien (Pellat and Allard ; Roman, 1903).

B – La subsurface (dépôt-centre du bassin)

Concernant les formations de subsurface traversées par les forages dans le bassin de la Vistrenque, les attributions stratigraphiques sont robustes lorsque les analyses micropaléontologiques ont été réalisées (p.ex., dans le Néogène et le Quaternaire) mais sont plutôt approximatives dans le Paléogène en raison de la rareté des marqueurs biostratigraphiques et découlent des analogies des lithologies et des styles de remplissage avec les bassins voisins (p.ex., Cavelier et al., 1984 ; Benedicto et al., 1996). Dans l'optique de la révision stratigraphique du bassin de la Vistrenque, de nouvelles données palynologiques ont été acquises récemment (Jan du Chene, 1989 ; Biteau et al., 1993). Toutefois, la valeur des marqueurs utilisés est discutable et ces analyses n'ont fait l'objet d'aucune publication scientifique.

Dans le forage Pierrefeu 1, le seul à atteindre le substratum mésozoïque à 4920 m de profondeur, les séries anté-aquitaniennes ont une épaisseur dépassant 3000 m dont une accumulation de près de 700 m de sel à leur sommet. Dans la terminologie pétrolière reprise par Benedicto (1996), trois unités lithologiques d'épaisseurs hectométriques à kilométriques ont été définies et sont de bas en haut : la « Série Grise », la « Série Rouge », et la « Série Calcaréo-salifère ». Ces formations ont été attribuées à l'Oligocène sans preuve paléontologique. Le Néogène de la Vistrenque est composé des séries aquitaniennes à mio-pliocènes datées à l'aide des foraminifères (Valette and Benedicto, 1995).

2.2.3. Sédimentologie et paléoenvironnements

a- Les affleurements de la terminaison nord du bassin

Les premières études géologiques sur le Tertiaire de la Camargue ont porté sur les buttes de Beaucaire et sur le Puech du Teil près de Nîmes. La butte Iouton est connue comme une carrière de pierre au Moyen Âge (Dumas, 1876), le caractère lacustre de la succession carbonatée qui y affleure a été reconnu par Pellat and Allard (1895) qui en décrivent les niveaux fossilifères. Cette succession carbonatée oolithique a été documentée plus tard par Roman (1910) qui décrit les faunes de mollusques et qui fournit une stratigraphie détaillée au niveau de la carrière de la butte Iouton. Parallèlement, le lambeau du Puech du Teil situé près de Nîmes est décrit par Fontannes (1885) puis par Caziot (1896) qui a effectué l'examen des fossiles de mollusques et la descrption de la stratigraphie de la succession carbonatée.

b – La subsurface (dépôt-centre du bassin)

Les études sédimentologiques et stratigraphiques internes aux entreprises ayant exploité le bassin de la Vistrenque sont nombreuses mais ne sont pas publiées. On peut citer en particulier les travaux de Vincent (1956a ; 1956b ; 1957), Bellon (1959 ; 1961 ; 1964), et Magné and Malmoustier (1960). Ces notes de recherches concernent la révision stratigraphique et proposent des corrélations lithostratigraphiques en particulier pour les unités supérieures du Paléogène traversées par de nombreux forages dans le secteur de Gallician, à savoir la Série Calcaréo-salifère et la Série Rouge. Ces résultats d'analyses lithologiques et pétrographiques n'ont pas fait l'objet d'interprétations paléoenvironnementales et nécessitent une révision complète.

2.3. Histoire tectonique et contexte géodynamique

L'histoire tectonique et la structure de la marge du golfe du Lion ont été étudiées en détails dans plusieurs travaux (p.ex., Séranne et al., 1995 ; Benedicto 1996 ; Bache, 2008). Les grands traits structuraux de la marge du Golfe du Lion sont hérités de la fin du Paléozoïque. La chaîne varisque est formée au Dévonien et au Carbonifère inférieur et l'orogène sera affecté par l'extension tardi-orogénique au Permien (Arthaud and Matte, 1975). Les accidents majeurs résultant de cette extension vont structurer le Sud-est de la France durant toute son histoire méso-cénozoïque. Le bassin du Sud-est se forme au Mésozoïque sur le socle paléozoïque (Baudrimont and Dubois, 1977). La sédimentation est d'abord marneuse et évaporitique au Trias avant le rifting Téthysien au Jurassique (Lias-Dogger) pendant lequel le bassin du Sud-est se forme sur la marge ouest de l'océan Téthys (Lemoine and Graciansky, 1988 ; Ziegler, 1992). Les accidents NE-SW et NNE-SSW (p.ex., Faille des Cévennes, Faille de la Durance) hérités de la fin du Paléozoïque structurent le bassin du Sud-est jusqu'au Crétacé et l'épaisseur totale des sédiments marins déposés peut atteindre 12 km (Ménard, 1980).

Au Crétacé inférieur, l'ouverture du golfe de Gascogne est accompagnée par la dérive du bloc ibéro-corso-sarde le long de la faille nord-pyrénéenne (Choukroune and Mattauer, 1978).

Elle est suivie par la phase de compression pyrénéenne qui résulte de la convergence de ce bloc vers l'Europe (Mascle et al., 1994). Pendant cette phase de compression qui s'étend du Crétacé supérieur à l'Éocène (**Fig. 2.2A**), les aires de sédimentation marine se réduisent et l'essentiel du bassin du Sud-est est émergé avec une sédimentation qui devient exclusivement continentale. Toujours pendant cette phase, les anciennes structures normales E-W, NE-SW, NNE-SSW sont réutilisées en chevauchements à vergence nord et en décrochement senestres (Arthaud and Séguret 1981 ; Arthaud et al., 1981). Au Priabonien (Éocène supérieur), les décrochements senestres languedociens accommodent la compression pyrénéo-provençale et l'extension intracontinentale ouest-européenne (Séranne et al., 2021) (**Fig. 2.2B**).

Le rift Ouest-Européen (ECRIS ; Ziegler, 1992) a été actif durant le Priabonien et le Rupélien et a engendré un système de fossés continentaux à l'échelle de l'Europe de l'Ouest (**Fig. 2.3**). Ces bassins continentaux sont organisés selon des segments répartis entre le Sud-est de la France et la mer du Nord (**Fig. 2.2B**, **2.2C**).

Plus tard, dans le contexte général de la convergence Afrique-Europe (Auzende et al., 1973 ; Biju-Duval, 1979), la subduction de la plaque Africaine sous l'ensemble Europe-Ibérie résulte en l'extension arrière-arc engendrant l'ouverture du bassin Liguro-provençal à l'Oligocène-Aquitanien et la rotation du bloc corso-sarde (**Fig. 2.2D**, **2.2E**) (Olivet et al., 1984 ; Bois, 1993 ; Romagny et al. 2020). Selon Romagny et al. (2020), l'extension arrière-arc en Méditerranée a commencé plutôt à l'Oligocène inférieur dans les zones de subduction sous le bloc ibéro-corso-sarde. A l'échelle du Sud-est de la France, cette extension est à l'origine de la formation de la marge du golfe du Lion (**Fig. 2.2C**, **2.2D**, **2.2.E**).

La marge du Golfe du Lion est limitée au nord-ouest par la faille des Cévennes et au sud-est par la faille Catalane tandis que la zone de transfert de l'Arlésienne marque la limite avec le domaine de la vallée du Rhône (**Fig. 2.4A** ; Gorini, 1993). La marge est structurée par la faille listrique de Nîmes néoformée durant cette phase d'extension (Séranne et al., 1995) et qui individualise deux zones de décollement : une zone de décollement de la couverture mésozoïque « *thin-skinned* » entre la faille des Cévennes et la faille de Nîmes et une zone de décollement du socle « *thick-skinned* » dans la partie externe de la marge (**Fig. 2.4C**). Dans la partie terrestre de la marge, les bassins Oligo-Aquitaniens reposent sur une couverture mésozoïque à Éocène tandis que les bassins situés en mer recoupent pour la plupart le socle Paléozoïque constituant le segment pyrénéen aujourd'hui effondré dans le golfe du Lion (p.ex., Benedicto, 1996).

Les zones de transfert jouent un rôle important dans la structuration des bassins dans le Sud-est de la France. Par exemple, à l'Oligo-Aquitanien, la zone de transfert de l'Arlésienne (orientée NW-SE) traversant le bassin de la Vistrenque sépare à l'échelle du Sud-est de la France deux domaines ayant deux histoire géodynamiques différentes : à l'ouest le domaine du golfe du Lion qui correspond à la marge actuelle de l'océan liguro-provençal, et à l'est le domaine de la vallée du Rhône qui est resté au stade de rift avorté (**Fig. 2.4A** ; Gorini, 1993 ; Benedicto, 1996).

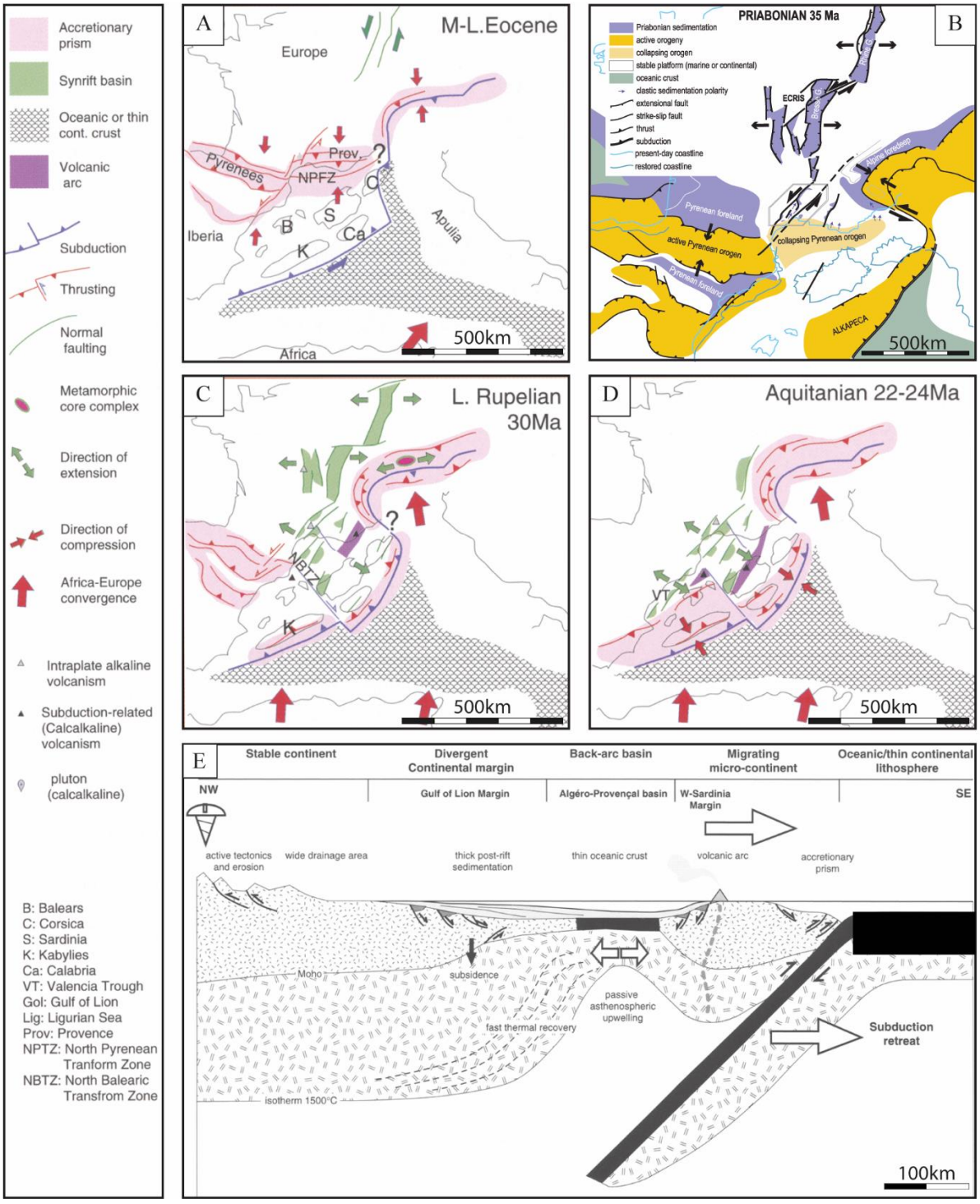

Figure 2.2 : Géodynamique et systèmes cénozoïques de l'Europe de l'Ouest et de la Méditerranée occidentale. A) à D) Schémas structuraux montrant l'évolution de l'Europe de l'Ouest et de la Méditerranée occidentale entre l'Éocène moyen-supérieur et l'Aquitanien. Les cartes A), B) et D) ont été modifiées d'après Séranne, 1999 ; le schéma structural en C) provient de Séranne et al., 2021. E) Coupe lithosphérique à travers la Méditerranée occidentale montrant l'ouverture de bassin Provençal avec le style de bassin arrière-arc et le retrait du slab au niveau de la zone de subduction au Miocène, d'après Séranne, 1999.

La marge du golfe du Lion se prolonge en mer par une croûte océanique qui commence à se former à la fin du rifting Liguro-Provençal au Burdigalien (**Fig. 2.2E**). La sédimentation post-rift commence par la transgression burdigalienne et se poursuit jusqu'à la fin du Miocène.

Durant le Miocène, les bassins continentaux du Sud-est de la France ont été inversé dans le cadre de la compression alpine (p.ex., Roure et al., 1992). A la fin du Miocène, une importante érosion affecte les dépôts cénozoïques de la marge à la suite de l'incision de vallées résultant de la crise de la salinité messinienne (Beaufort, 1954). Les canyons creusés seront comblés durant le Pliocène et la sédimentation se poursuit jusque durant le Quaternaire (**Fig. 2.4C**, **2.5A**).

Bien qu'ils soient formés durant la même phase d'extension, les différents bassins continentaux du Sud-est de la France présentent chacun des caractéristiques morphostructurales distinctes et une histoire géologique propre (**Fig. 2.3**). A plus grande échelle, par exemple, Rouchy (1997) souligne le diachronisme de la formation des bassins du système ECRIS entre le Nord de l'Europe (p.ex., Bassin du Rhin supérieur : Éocène moyen) et le Sud (p.ex., Bassin de Marseille : Oligocène).

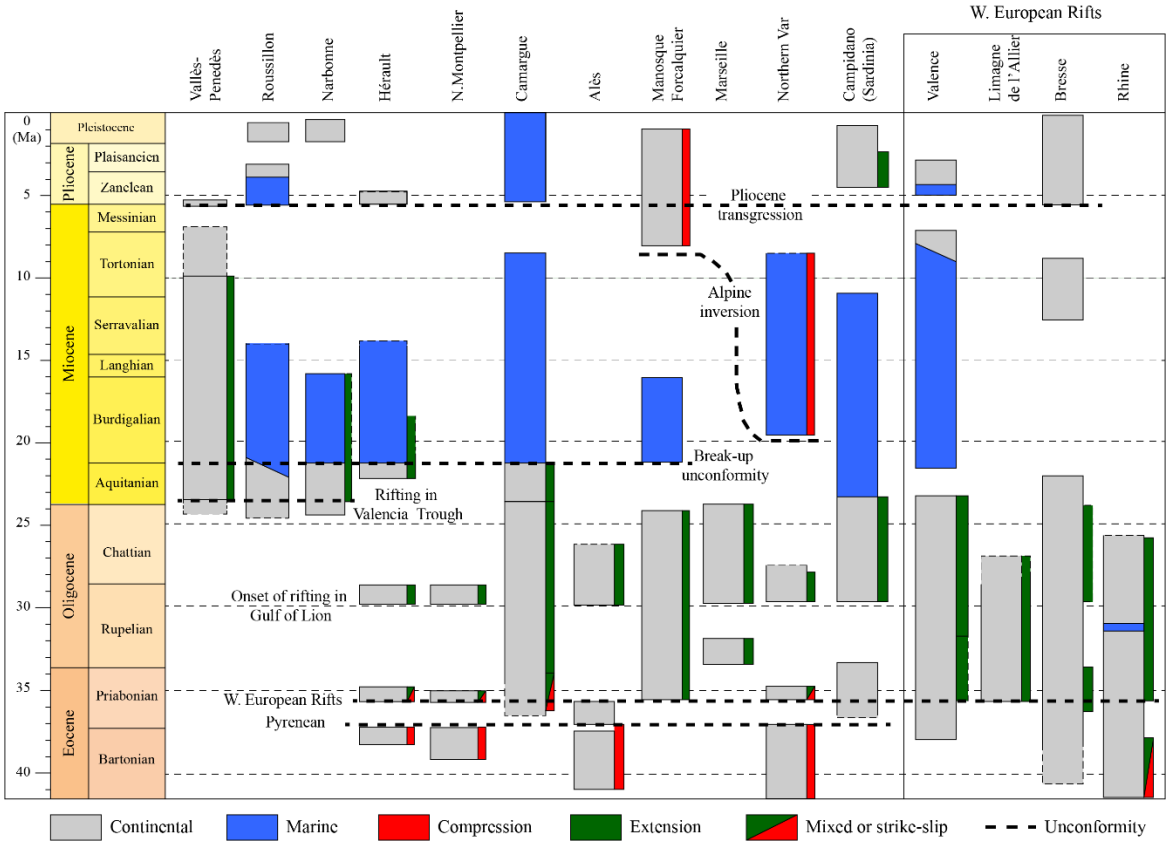

Figure 2.3 : Charte montrant la stratigraphie et les contextes tectoniques de remplissage des bassins continentaux cénozoïques de l'Est et du Sud-est de la France, modifiée d'après Séranne (1999) et Lettéron et al. (2021).

2.4. Structure du bassin de la Vistrenque

La structure profonde du bassin de la Vistrenque a fait l'objet d'une analyse détaillée dans Benedicto et al. (1996) et Benedicto (1996). Sur la base des données sismiques (p.ex., **Fig. 2.8B**) et des forages profonds, les auteurs ont proposé un modèle de géométrie à faible pendage en profondeur pour la faille de Nîmes (**Fig. 2.5A**)**.** La faille de Nîmes de direction NE-SW ayant

un pendage SE à faible angle en profondeur (25°) avant de s'enraciner dans le socle joue un rôle majeur dans la structuration de la marge du golfe du Lion (**Fig. 2.4C**). Cette rampe crustale néoformée à l'Oligocène pendant l'extension Oligo-Aquitanienne liée au rifting de la marge du Golfe du Lion (Séranne et al., 1995) est différente de la partie plus ancienne (mésozoïque) de la faille de Nîmes (**Fig. 2.5A**). Les études les plus récentes ont mis en évidence des mouvements de décrochements senestres qui ont affecté pendant le Priabonien (Éocène supérieur) un faisceau de failles dans le couloir situé entre la faille des Cévennes et la faille de Nîmes (Séranne et al., 2021).

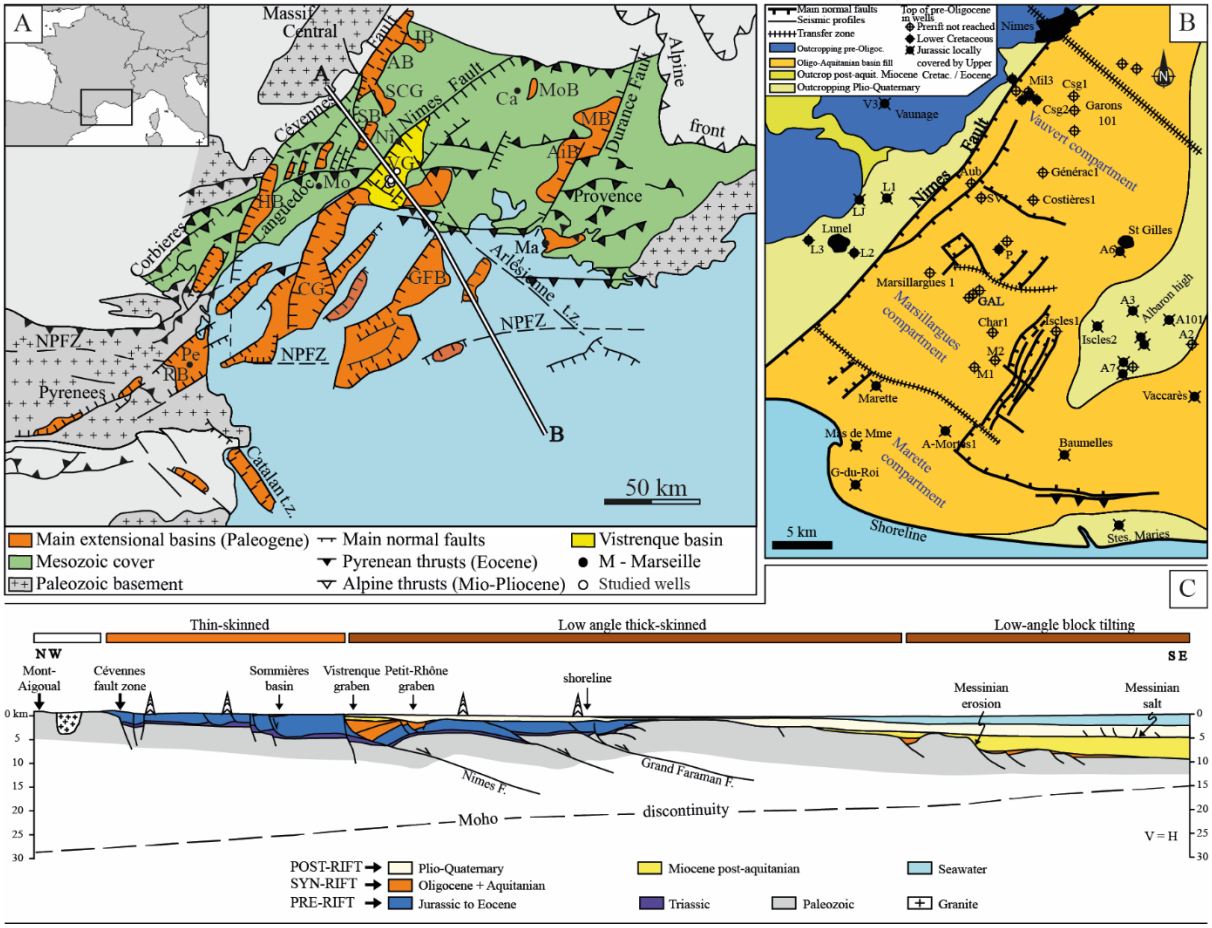

Figure 2.4 : A) Schéma structural du Sud-est de la France et localisation du bassin de la Vistrenque Basin et des bassins continentaux cénozoïques (modifiée d'après Benedicto, 1996). AB : Bassin d'Alès, AiB : Bassin d'Aix, Ca : Carpentras, CG : Graben Central, GFB : Bassin du Grand Faraman, HB : Bassin de l'Hérault, IB : Bassin d'Issirac, Ma : Marseille, Mo : Montpellier, MB : Bassin de Manosque, MoB : Bassin de Mormoiron, Nî : Nîmes, NPFZ : Zone des failles Nord-Pyrénéennes, Pe : Perpignan, RB : Bassin du Roussillon, SB : Bassin de Sommières, SCG : Graben de Saint-Chaptes, t.z. : zone de transfert, VG : Bassin de la Vistrenque. B) Schéma structural du bassin de la Vistrenque montrant la localisation des forages profonds, modifié d'après Benedicto et al. (1996). (1996). V3 : Vaunage 3 - LJ : La Jasette - L1 : Lunel 1 - L2 : Lunel 2 - L3 : Lunel 3 - Csg : Caissargues – Aub : Aubord 1 – SV : Saint-Véran 1 – P : Pierrefeu 1 - A6 : Albaron 6 - A3 : Albaron 3 - A7 : Albaron 7 - A101 : Albaron 101 - A2 : Albaron 2 - Char 1 : Charnier 1 – GAL : Gallician – M1 : Montcalm 1 - M2 : Montcalm 2 – P : Pierrefeu – SM : Saintes-Maries-de-la-Mer : 101 - Mil 3 : Milhaud 3. t.z. : transfert zone. C) Coupe géologique à travers la marge du Golfe du Lion (modifiée d'après Benedicto, 1996).

Le moteur du régime distensif évoqué pour la néoformation de la rampe crustale de Nîmes est la fragilisation de la croûte par son épaississement lors de l'orogenèse pyrénéenne (Benedicto et al., 1996). De plus, le rôle précurseur de la faille mésozoïque de Nîmes est évoqué dans la localisation de la zone de l'émergence de la rampe crustale néoformée.

Contrairement aux bassins limitrophes (p.ex., Alès-Saint-Chaptes-Issirac, Mormoiron, Apt-Manosque-Forcalquier), aucune étude ne montre l'enregistrement de l'épisode extensif du rifting ouest européen et des décrochements senestres languedociens en Camargue. L'épaisse accumulation sédimentaire déposée pendant le Paléogène et l'Aquitanien dans bassin de la Vistrenque est entièrement attribuée à l'extension du rifting Oligocène-Aquitanien par plusieurs auteurs (p.ex., Valette and Benedicto, 1995 ; Benedicto, 1996). Toutefois, des analyses palynologiques sur les forages récents laissent envisager la présence de dépôts sédimentaires d'âge Éocène à la base des séries paléogènes, et par conséquent antérieurs à la phase de rifting oligo-aquitanienne (Forage de Baumelles1, Jan du Chene, 1989, **Fig. 6B**).

Le bassin paléogène de la Vistrenque s'est formé au nord d'un relief pyrénéen dont les reconstructions pré-rifting Oligo-Aquitanien suggèrent une altitude supérieure à 1 km (Séranne et al., 1995 ; Benedicto et al., 1996 ; Benedicto, 1996) (**Fig. 2.5B**). Par ailleurs, Séranne et al. (2021) ont montré que le démantèlement de ce segment pyrénéen a commencé au Priabonien au sud du Languedoc.

L'architecture des séries paléogènes du bassin de la Vistrenque est contrôlée par la structure en profondeur de la faille de Nîmes. Benedicto et al. (1996) ont identifié deux zones de transfert qui individualisent trois compartiments dont le remplissage syn-rifting Oligo-Aquitanien présente des géométries différentes (**Fig. 2.4B**, **2.6**). Cette compartimentalisation est due à l'héritage structural de l'extension mésozoïque et aux chevauchements pyrénéens qui ont déterminé la position de la faille de Nîmes et des zones de transfert (Benedicto et al., 1996). La zone de transfert de Gallician sépare le compartiment de Vauvert au nord et le compartiment de Marsillargues au sud (**Fig. 2.4B**). Le compartiment de Vauvert dans lequel est réalisé le forage Pierrefeu 1, présente une géométrie en graben de compensation (**Fig. 2.6A**). Le compartiment de Marsillargues (**Fig. 2.6B**), dans lequel se situe le secteur de Gallician et ses forages ainsi que le compartiment de Marette, situé plus au sud (**Fig. 2.6C**), montrent au contraire une structuration en demi-graben.

2.4.1. Structure du secteur de Pierrefeu-Parrapon

Le secteur de Pierrefeu-Parrapon situé dans le compartiment de Vauvert est le plus profond connu à ce jour dans le bassin de la Vistrenque. Ce compartiment est limité à l'est par la faille de Nîmes et à l'ouest par le haut d'Albaron et le sous-bassin de Pierrefeu est séparé du sous-bassin de Gallician par une zone haute correspondant à la zone de transfert de Gallician (Valette, 1991 ; Benedicto et al., 1996) (**Fig. 2.4B**). Ce secteur est caractérisé par une épaisse accumulation d'évaporites dans la Série Calcaréo-salifère.

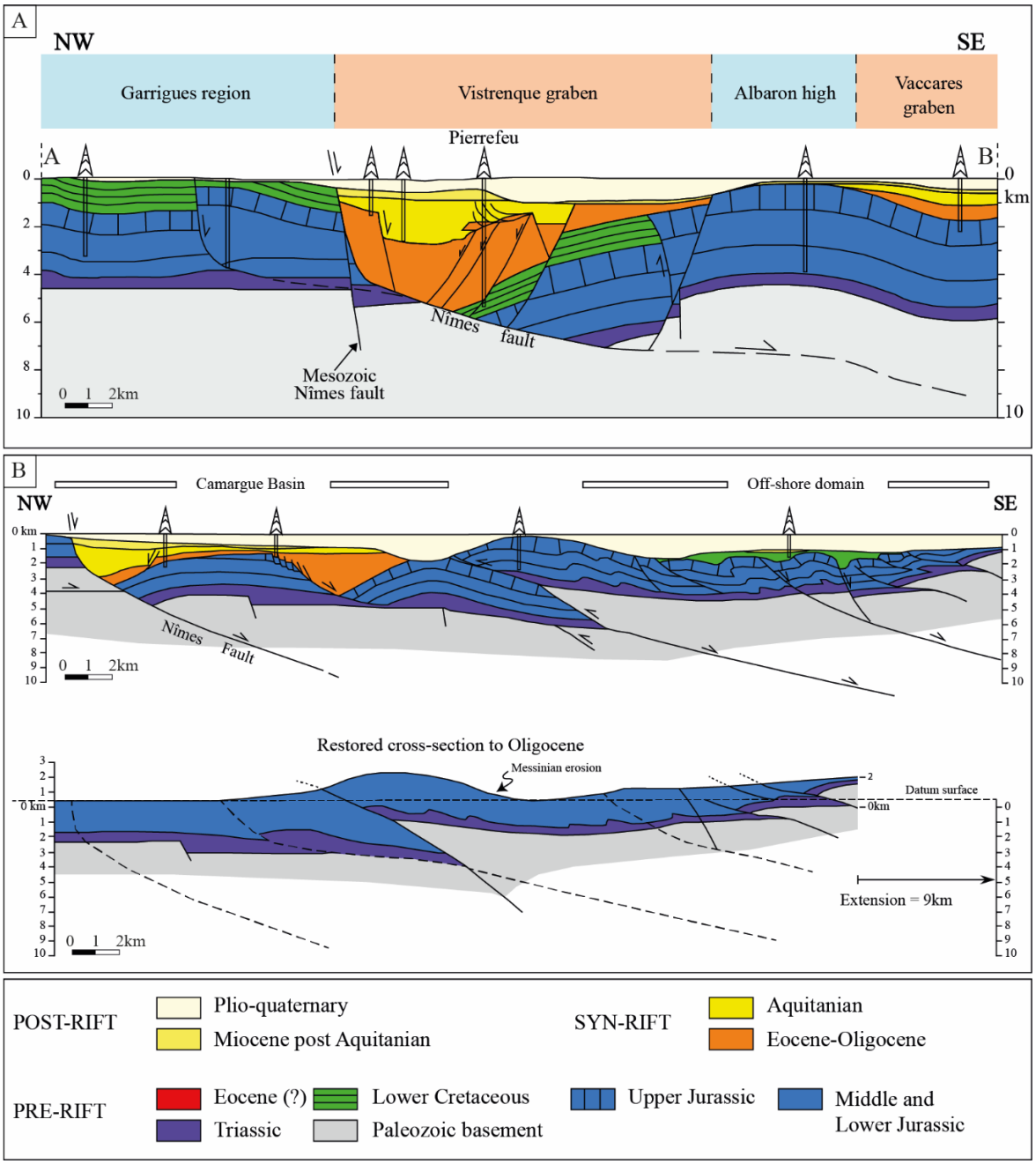

Figure 2.5 : Structure du bassin de la Vistrenque. A) Coupe géologique NW-SE à travers le bassin de Vistrenque dans sa partie Nord (compartiment de Vauvert, voir localisation des compartiments dans la **Figure 2.4B**), d'après Benedicto et al., 1996. B) Coupe géologique à travers les bassins de la Vistrenque et de Vaccarès (panneau supérieur) et coupe restaurée dans la position pré-rift à l'Oligocène (panneau inférieur).

L'épaisseur de la Série Calcaréo-salifère est particulièrement importante (~ 900m) dans le secteur de Pierrefeu-Parrapon par rapport au secteur voisin de Gallician (~ 300 m). Cette anomalie résulte d'une superposition des couches évaporitiques à la faveur de chevauchements gravitaires halotectoniques pendant l'extension générale du bassin de la Vistrenque à l'Oligocène-Aquitanien (Valette and Benedicto, 1995). Les auteurs ont montré que les failles normales et listriques à l'origine de cette tectonique sont synchrones à la sédimentation évaporitique (**Fig. 2.7A**). Valette (1991) a fourni un découpage structural de la Série Calcaréo-

salifère et a distingué les évaporites autochtones déposées *in situ* des évaporites allochtones déplacées par les chevauchements gravitaires.

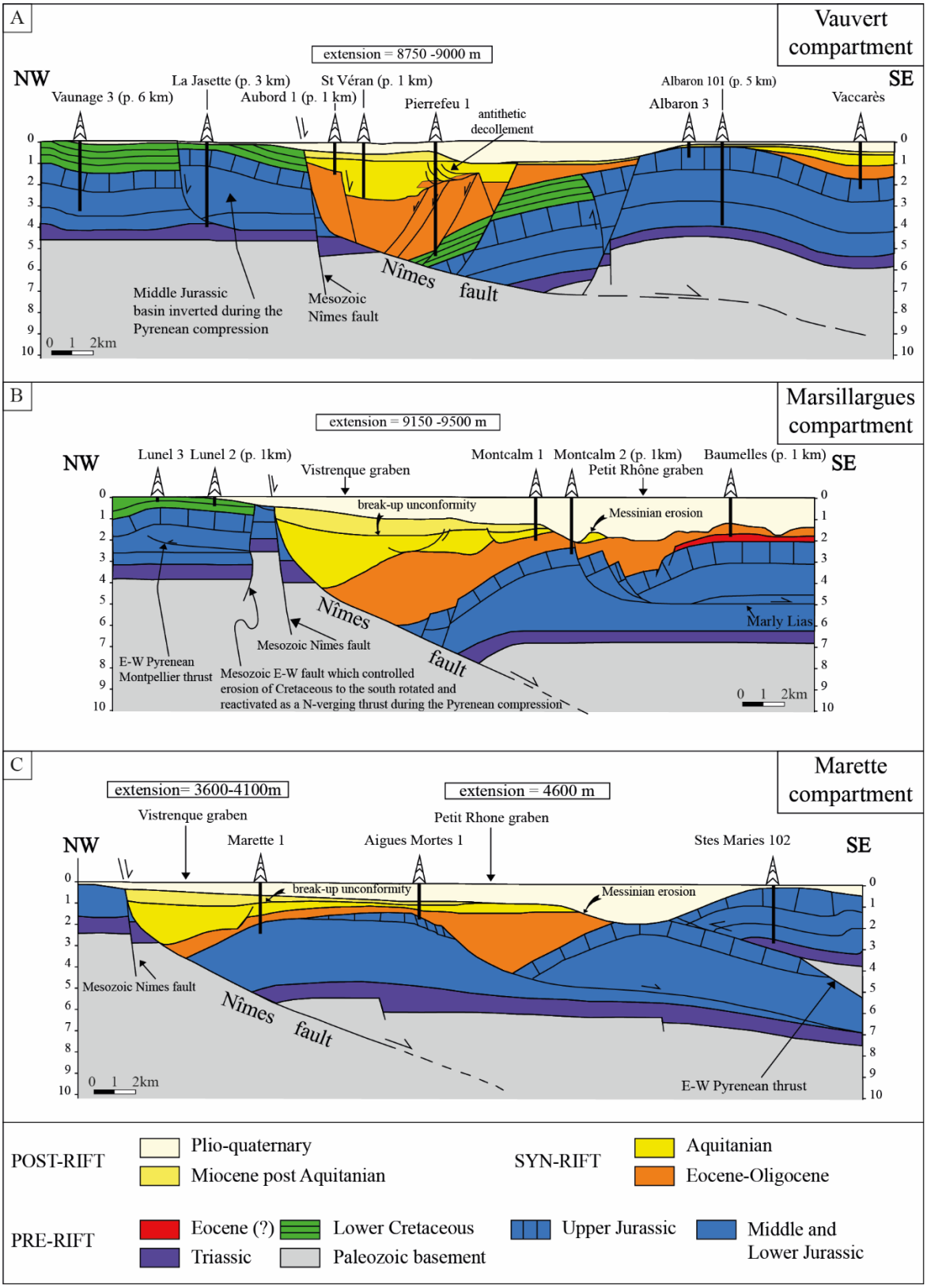

Figure 2.6 : Coupes géologiques à travers le bassin de la Vistrenque montrant les différentes structures profondes selon les compartiments séparés par des zones de transfert (voir localisation des zones de transfert dans la **Figure 2.4B**), modifiées d'après Benedicto et al. (1996). Les compartiments de Vauvert, Marsillargues et de

Marette se situent au nord, au centre et au sud du bassin respectivement. Les secteurs d'étude (Pierrefeu et Gallician) sont localisés dans les compartiments de Vauvert et de Marsillargues respectivement.

La chronologie de mise en place des évaporites autochtones et leur recouvrement par deux unités allochtones (inférieure et supérieure) ainsi que les accidents listriques et les surfaces de décollement à l'origine de ce salifère multicouches ont été reconstitués par Valette and Benedicto (1995) (**Fig. 2.7**).

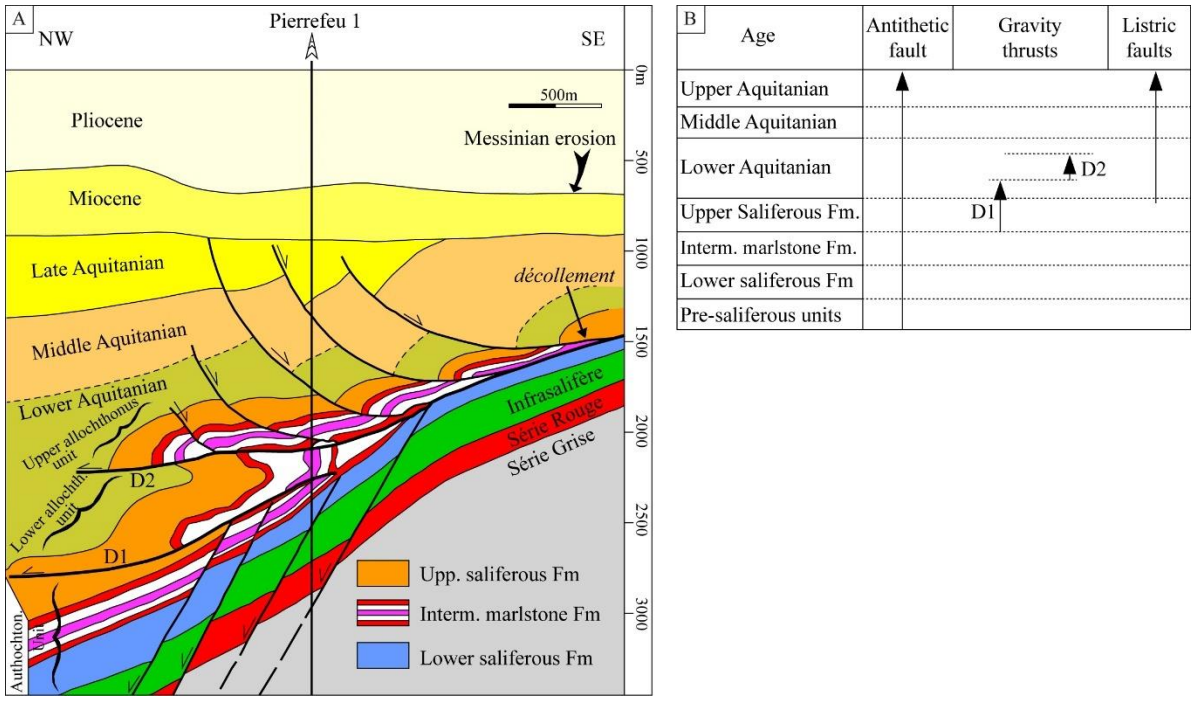

Figure 2.7 : A) Coupe géologique à travers le secteur de Pierrefeu-Parrapon montrant les chevauchements gravitaires halotectoniques ; B) Tableau montrant le calendrier de la formation des différentes structures (failles antithétiques à la faille majeure de Nîmes, Chevauchements gravitaires et failles listriques), modifiés d'après Valette and Benedicto, 1995. Fm : formation, D1-D2 : chevauchements gravitaires halotectoniques. Les unités Série Grise à Série Calcaréo-salifère (Upper saliferous Fm.) sont attribuées par les auteurs à l'Oligocène.

2.4.2. Structure de la terminaison Nord du bassin :

Les quelques buttes situées près de Beaucaire (p.ex., butte Iouton) et le lambeau du Puech du Teil près de Nîmes constituent la partie affleurante de la terminaison Nord du bassin de la Vistrenque (**Fig. 2.1.A**, **2.1D**). Les terrains paléogènes de la butte Iouton sont constitués d'une succession carbonatée oolithique d'âge Éocène supérieur qui repose sur le substratum Crétacé inférieur par l'intermédiaire d'un intervalle d'argiles bariolées attribuées à l'Éocène moyen (Pellat and Allard, 1895). Ils sont surmontés de dépôts marins transgressifs attribués au Burdigalien (Roman, 1910). Trauth (1984 dans Cavelier et al.,1984) suggère l'existence d'une polarité de sédimentation silicoclastique-carbonatée à travers la Vistrenque. En d'autres termes, il est admis qu'à l'opposé de cette marge carbonatée située dans le domaine des buttes septentrionales, le domaine méridional du bassin de la Vistrenque serait soumis dès l'Éocène supérieur à des décharges détritiques importantes provenant du Sud.

2.5. Lithostratigraphie

La succession sédimentaire cénozoïque du bassin de la Vistrenque comprend les terrains paléogènes, attribués à l'Oligocène, reposant sur un substratum d'âge Crétacé à Éocène et surmontés d'une épaisse succession de dépôts néogènes et quaternaires (**Fig. 2.8**).

2.5.1. Le substratum Mésozoïque à Éocène

Dans le Sud-est de la France, les bassins cénozoïques forment des structures superposées sur le substratum mésozoïque, lui-même reposant sur le socle paléozoïque. Sur les roches plissées et métamorphiques du paléozoïque, une sédimentation détritique et évaporitique a lieu au Trias et suivie d'une sédimentation marine carbonatée durant le Jurassique et le Crétacé inférieur (**Fig. 2.8D**). Le domaine nord-provençal de la plateforme carbonatée est émergé à la fin du Crétacé inférieur durant le Bombement Durancien conduisant à la formation d'importantes accumulations de bauxite ; le moteur de cette inversion tectonique est encore débattu (Guyonnet-Benaize et al., 2010). La sédimentation marine se poursuit sur des aires de dépôt individualisées au Crétacé supérieur et la sédimentation devient de plus en plus continentale (Baudrimont and Dubois, 1977 in Valette, 1991). Les principaux fossés d'effondrement cénozoïques du Sud-est de la France se sont formés durant l'Éocène supérieur et l'Oligocène (p.ex., Rouchy, 1997 ; Séranne, 1999).

Le substratum mésozoïque du bassin de la Vistrenque affleure sur ses bordures nord-ouest et nord-est (**Fig. 2.8A**) et est constitué essentiellement des carbonates marins d'âges Crétacé inférieur à Jurassique (**Fig. 2.8B-C**). Par exemple, dans les garrigues nîmoises, à l'ouest de la faille de Nîmes, le substratum est d'âge Hauterivien à Barrémien.Plus au Sud, la Vaunage est formée de terrains d'âge Valanginien inférieur et sépare la Camargue du bassin voisin de Sommières. Dans la terminaison nord et nord-est du bassin de la Vistrenque, le substratum Crétacé affleure à la butte Iouton près de Beaucaire et constitue l'essentiel de la chaîne des Alpilles situées plus à l'est (**Fig. 2.1A, 2.8A**). En subsurface, lorsque les forages traversent le substratum anté-Paléogène, la nature de celui-ci varie entre les secteurs du bassin de la Vistrenque. Ainsi, au Nord-Ouest, il est constitué par des carbonates marins d'âge Crétacé inférieur tandis qu'au Sud le substratum est d'âge Jurassique qui peut être surmonté par des séries continentales fluviatiles fini-crétacées, par exemple le sondage de Marette 1, ou parfois continentales carbonatées d'âge Éocène « probable » dans le sondage de Baumelles 1 (Benedicto et al., 1996) (**Fig. 2.6**).

Plusieurs forages ont rencontré les terrains mésozoïques dans le bassin de la Vistrenque et ses bordures (**Fig. 2.6**). Dans le centre du bassin, seul le forage Pierrefeu 1 a retrouvé à 4920 m de profondeur des calcaires attribués au Valanginien (**Fig. 2.1C**, **2.6C**). A l'est et au sud, les forages réalisés dans les hauts d'Albaron et de Saintes-Maries-de-la-Mer ont rencontré le Jurassique. En Camargue, le Paléozoïque n'a pas été rencontré en forage et est connu seulement dans les forages des bassins situés en mer dans le golfe de Lion (Arthaud and Séguret, 1981).

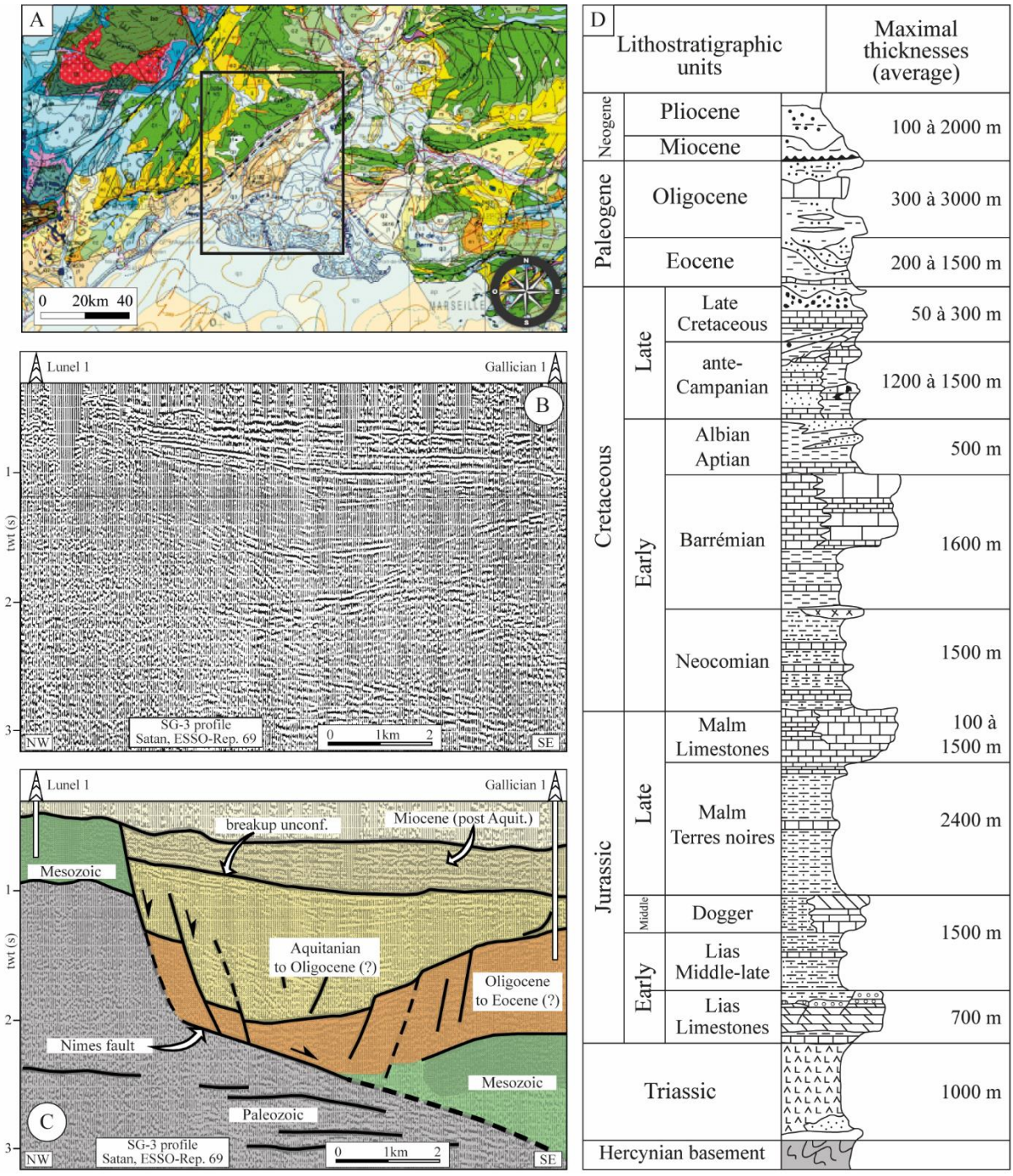

Figure 2.8 : A) Extrait de la carte géologique de la France 1/1 000000 montrant la faille majeure de Nîmes orientée NE-SW (ligne en pointillé) qui sépare d'une part les Garrigues de Nîmes constituant le substratum mésozoïque et d'autre part le bassin cénozoïque de la Vistrenque. Le rectangle indique l'aire correspondant au secteur d'étude. B) Profil sismique SG3 orienté NW-SE non migré et interprété (C) dans le compartiment de Vauvert, d'après Benedicto (1996) (voir localisation dans **Figure 2.1B**). D) Colonne lithostratigraphique synthétique du bassin du Sud-est, modifiée d'après Valette (1991) et Baudrimont and Dubois (1977).

2.5.2. Le remplissage sédimentaire du bassin de la Vistrenque

2.5.2.1. Chronostratigraphie des séries paléogènes

Les affleurements paléogènes des bordures du bassin de la Vistrenque ont été revus dans la synthèse de Cavelier et al. (1984) sur le Paléogène du Sud-est de la France. Les attributions stratigraphiques à l'Éocène supérieur de ces terrains sont basées sur la faune malacologique et des corrélations avec les autres bassins du Sud-est (p.ex., bassin d'Alès) ont été proposées (Pellat and Allard, 1895 ; Roman 1910).

Les séries du dépôt-centre de la Vistrenque sont connues par des forages profonds et la chronologie des formations traversées est peu précise en raison de l'absence de marqueurs stratigraphiques. Les attributions stratigraphiques varient entre les forages et sont révisées à chaque acquisition de nouvelles données de subsurface. L'utilisation des données anciennes parfois désuètes (Rapports de SNPLM et CEP, ancêtres de TotalEnergies) rend difficile toute démarche visant à établir des corrélations entre les puits profonds de la Vistrenque d'autant que les échelles stratigraphiques utilisées ont beaucoup évolué depuis. En revanche, des corrélations lithostratigraphiques précises ont été réalisées au sein d'un même sous-bassin (par exemple Gallician) et demeurent assez fiables. Nous considérons avec précaution les interprétations stratigraphiques et les âges attribués sans preuves paléontologiques et radiochronologiques. Par ailleurs, cette thèse comprend un travail de révision stratigraphique tant sur la marge que dans le dépôt-centre du bassin et les résultats sont présentés dans les chapitres **3** et **4**.

2.5.2.2. Lithostratigraphie et nature des séries paléogènes du bassin de la Vistrenque

Le forage Pierrefeu 1 situé dans le dépôt-centre du bassin traverse 4920 m de dépôts cénozoïques. Il permet de restituer la colonne stratigraphique du dépôt-centre du bassin de la Vistrenque (**Fig 2.9**).

a. Le remplissage Paléogène du bassin de la Vistrenque

Près des bordures du fossé, les séries tertiaires anté-aquitaniennes ont été traversées par de nombreux forages implantés près de la faille de Nîmes (p.ex., Milhaud 3, Aubord 1) ainsi que les forages situés près du haut d'Albaron (p.ex., Albaron 6) (**Fig. 2.4B**). Ces sondages ont rencontré des intervalles de puissances décamétriques constitués de dépôts grossiers et conglomératiques remaniant les bordures crétacées et jurassiques ainsi que de marnes et de grès rouges. Ces intervalles sont attribués à l'Oligocène et reposent sur le substratum mésozoïque.

C'est dans les secteurs de Gallician et de Pierrefeu-Parrapon situés dans le dépôt-centre du bassin que la densité des forages permet d'établir des coupes détaillées et assez complètes du Paléogène de la Vistrenque (**Fig. 2.10**). Dans le secteur de Gallician, les séries paléogènes sont subdivisées en cinq formations, de bas en haut : Série Grise, Série Calcaire, Série Rouge, Série

Mixte, et Série Calcaréo-salifère. Bien que la succession sédimentaire soit plus dilatée dans le secteur de Pierrefeu, la Série Calcaire et la Série Mixte n'y ont pas été reconnues et y sont probablement confondues avec la partie supérieure de la Série Grise et la base de la Série Rouge par variation latérale des faciès. Certains intervalles stratigraphiques peuvent toutefois manquer par faille dans ce bassin fortement structuré.

Dans ce travail, le terme « Série », hérité des travaux antérieurs et repris comme tel, désigne un ensemble sédimentaire d'une épaisseur de quelques dizaines de mètres à plusieurs centaines de mètres caractérisé par une certaine association lithologique permettant de le différencier des ensembles sous-jacents et sus-jacents. Le terme « Série » utilisé ici est donc synonyme de « formation ».

b. Description des unités lithologiques du dépôt-centre du bassin de la Vistrenque

❖ La « Série Grise » et la « Série Calcaire »

Ces ensembles ont été traversés dans leur partie supérieure par plusieurs sondage dans le secteur de Gallician (p.ex., Gallician 9, Iscles 1, Charnier 1, Montcalm 2, Marette 1). La partie inférieure de la Série Grise est connue à seulement à Pierrefeu 1. Dans ce forage, la Série Grise (2060 m) est subdivisée par Valette (1991) en 03 « méso-séquences » pluri-hectométriques non datées. Elle est caractérisée à sa base par des dépôts détritiques fins à moyens (argiles et grès) parfois intercalés de lignite qui évoluent vers le sommet à des alternances de marnes et calcaires argileux avec des niveaux de grès et de conglomérats (**Fig. 2.9B**). Ces deux ensembles sont surmontés par des calcaires argileux et des marnes entrecoupées de bancs conglomératiques (Valette, 1991). Les dépôts fins du fond de ce forage évoluent au sud, par exemple dans les forages Gallician 9, Montcalm 2 et Charnier 1 vers des dépôts plus grossiers.

Dans le sondage de Vauvert 1, les faciès sédimentaires sont voisins de ceux traversés par la Série Grise de Pierrefeu 1 mais cette unité est appelée ici Série Calcaire. Par ailleurs, dans le forage Gallician 9, la partie supérieure (251 m) de la série grise est également appelée Série Calcaire mais la lithologie des dépôts est similaire à celle trouvée dans la Série Grise excepté une tendance à l'enrichissement en carbonates d'où l'utilisation de terminologies différentes pouvant parfois prêter à confusion.

Plusieurs découpages stratigraphiques ont été réalisés dans les études sédimentologiques et stratigraphiques internes aux compagnies pétrolières. Ces travaux utilisent des nomenclatures qui varient selon les auteurs et selon les secteurs d'étude et les limites adoptées ne sont pas précises (p.ex., Vincent (1956a ; 1956b ; 1957) ; Bellon (1959 ; 1961 ; 1964) ; Magné and Malmoustier, 1960). La monotonie lithologique dans les formations « Série Grise » et « Série Calcaire » et l'absence d'un contrôle biostratigraphique ne permettent pas de proposer des unités de temps cohérentes.

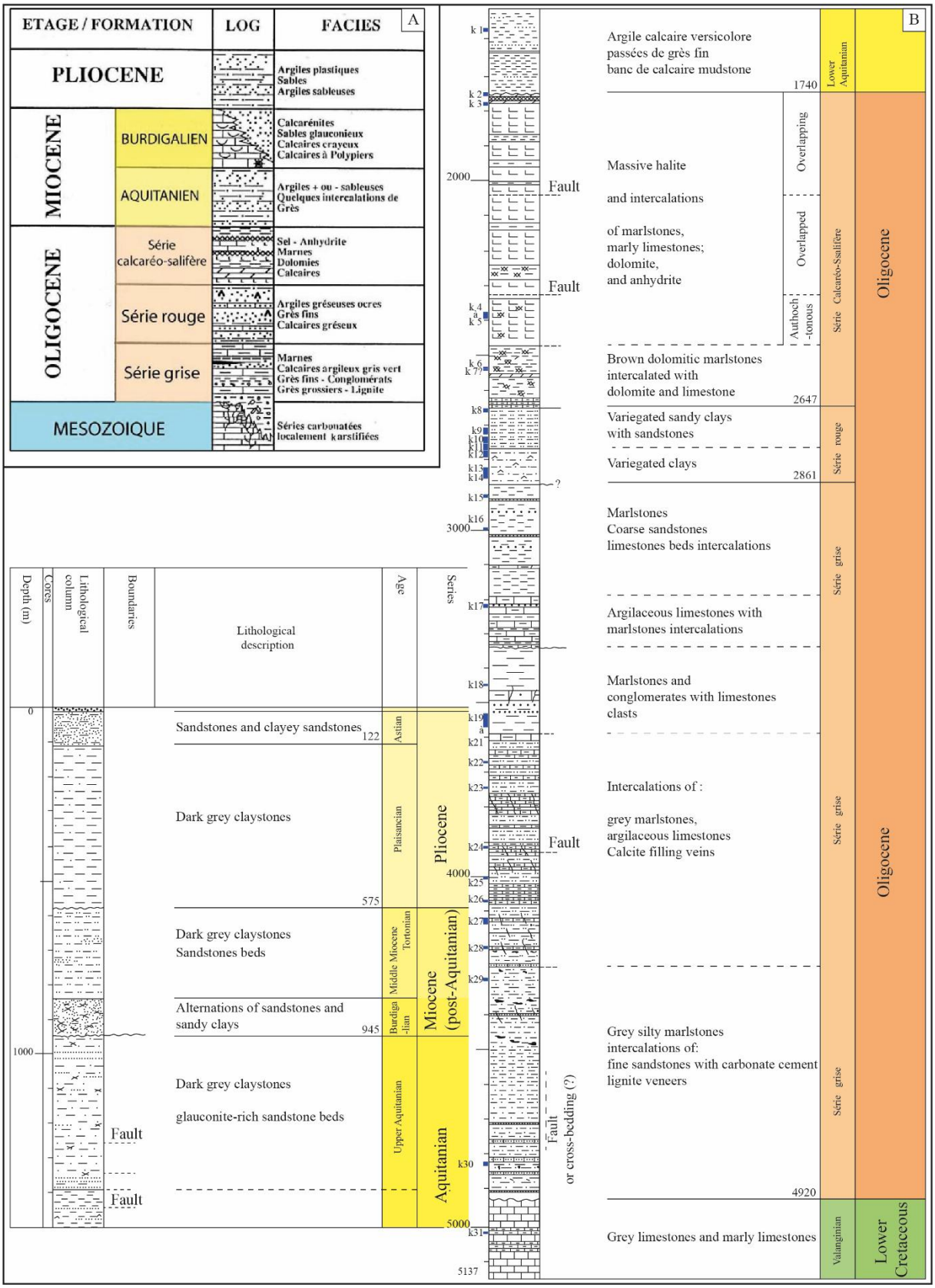

Figure 2.9 : A) Synthèse stratigraphique du dépôt-centre du bassin de la Vistrenque compilée à partir des forages par Gorini (1993), modifiée d'après Bache, 2008. B) Colonne Lithologique du bassin de la Vistrenque dans le secteur de Pierrefeu/Parrapon montrant les unités lithologiques (formations) paléogènes et les unités structurales de la Série Calcaréo-salifère, modifiée d'après Valette, 1991.

❖ La Série Mixte

Elle est intercalée entre la Série Calcaire sous-jacente et la Série Rouge sus-jacente avec lesquelles elle présente des ressemblances lithologiques. Le caractère distinctif de la Série Mixte est la présence de nombreux bancs de calcaires pseudo-bréchiques et vacuolaires intercalés dans la dépôts détritiques constitués de grès et de conglomérats polygéniques à éléments cristallins. Dans certains forages qui la traversent, elle est constituée d'une répétition de séquences sédimentaires métriques à plurimétriques allant des conglomérats polygéniques au calcaires en passant par des grès et siltites. En raison de l'absence des caractéristiques lithologiques qui la distinguent de la Série Rouge (voir définition ci-après), la série Mixte n'est pas reconnue dans le forage Pierrefeu 1. Dans le secteur de Gallician, la majorité des forages ont été arrêtés dans la partie supérieure de cette formation, seul le forage Gallician 9 la traverse entièrement sur une épaisseur d'environ 41 m (**Fig. 2.10A**).

❖ La Série Rouge

Repère lithologique et diagraphique à travers le bassin de la Vistrenque, les nombreux forages qui ont traversé la Série Rouge montrent que celle-ci a une épaisseur relativement homogène, environ 200 m, dans tous les secteurs du bassin de la Vistrenque (Valette, 1991). Lithologiquement, cette formation est constituée d'argiles silteuses bariolées à intercalations de grès fins à grossiers et de quelques conglomérats à la base. Dans le secteur de Gallician, la Série rouge est subdivisée en deux sous-unités : la séquence rouge proprement dite (R1) et la séquence terminale rouge bariolée (R2) (**Fig. 2.10B**).

❖ La Série Calcaréo-salifère

La Série Calcaréo-salifère ne sera pas étudiée en détail dans ce travail : seuls les grands traits de la sédimentation sont présentés. La Série Rouge constitue donc l'intervalle supérieur des séries paléogènes analysées dans cette étude.

Située immédiatement sous le Néogène, la Série Calcaréo-salifère est d'épaisseur pluri-hectométrique et présente des développements variables selon les secteurs (300 à 900 m d'épaisseur) (**Fig. 2.10A**). Elle est constituée d'alternances de calcaires, grès, marnes et d'évaporites. Traversée par de nombreux forages, cette formation présente des variations lithologiques entre les secteurs en raison d'une importante structuration du bassin par des failles de transfert (Benedicto et al., 1996) (**Fig. 2.4B)** et des chevauchements gravitaires halotectoniques dans le secteur de Pierrefeu-Parrapon (Valette and Benedicto, 1995).

Dans le secteur de Gallician, l'épaisseur maximale de la série est de 328 m au sondage Gallician 4. Les nombreux forages ont permis aux géologues pétroliers de découper la Série Calcaréo-salifère en quatre unités lithologiques (**Fig. 2.10B**). La base, épaisse d'environ 25 m, est constituée de calcaires crayeux, de marno-calcaires imprégnés et de lignite, et est appelée « ***Zone de polyfaciès ou Sx*** ».

Cette zone de polyfaciès est surmontée par la séquence des ***marnes papyracées « S3 »*** qui est constituée de marno-calcaires finement feuilletés à intercalations de grès à la base et de calcaire crayeux blancs à silex au sommet. Leur contenu fossilifère comprend des gastéropodes, notamment des *Potamides Laurae* et de *Melania sp.* signalés dans le forage Vauvert 1. *Potamides laurae* est connue dans les calcaires en plaquettes de l'Estaque du bassin de Marseille datés du Stampien supérieur (Nury, 1977). Ensuite, la série se complète par deux séquences, ***la séquence inférieure S2*** et ***la séquence supérieure S1*** respectivement, montrant une évolution d'une sédimentation *marno-gréseuse* à la base à *calcaréo-marneuse* au milieu puis à *calcaréo-évaporitique* contenant de l'anhydrite et parfois du sel au sommet (**Fig. 2.10B**).

Dans le secteur de Pierrefeu-Parrapon, Valette (1991) a étudié la tectonique gravitaire à l'origine de l'épaisse accumulation des évaporites (**Fig. 2.7**, **2.9**, **2.10A**). Par exemple, dans le forage Pierrefeu 1, la série Calcaréo-salifère atteint une puissance de 900 m. Les carbonates dominent dans les 100 mètres inférieurs de la formation tandis que les évaporites deviennent dominantes vers le sommet. L'intervalle évaporitique, d'environ 700 m d'épaisseur, est constitué de dépôts rythmés de marnes, anhydrite et d'halite.

A environ 2km à l'est du secteur de Pierrefeu-Parrapon, les forages du secteur de La Galine (cf. localisation dans **Fig. 2.10C**) traversent une Série Calcaréo-salifère non affectée par les mouvements halotectoniques et permettent d'établir une coupe lithologique affranchie des redoublements des unités. Valette (1991) et Valette and Benedicto (1995) suggèrent de découper la Série Calcaréo-salifère du secteur de La Galine en quatre unités sédimentaires (**Fig. 2.7**). Reposant sur la Série Rouge, l'unité **«** Infrasalifère **»** est épaisse d'environ 180 m et est constituée de marnes et grès intercalés de dolomies et d'anhydrites. Comparable en faciès et en puissance à la partie inférieure, incluant ***Sx***, ***S3*** et la base de ***S2***, de la Série Calcaréo-salifère de Gallician, elle indique des conditions de sédimentation « pré-évaporatoires » (Busson, 1997). Surmontant cette unité, l'unité « Salifère Inférieure **»**, l'unité « Marneuse Intermédiaire **»** et l'unité « Salifère Supérieure **»** totalisent plusieurs centaines de mètres d'épaisseur et sont constituées d'alternances d'anhydrite et d'halite avec des proportions variables de marnes et dolomies.

2.5.3. Stratigraphie sismique du bassin de la Vistrenque

Selon Valette and Benedicto (1995) et Benedicto et al. (1996), la Série Calcaréo-salifère et les formations sous-jacentes (Série Rouge à Série Grise) sont mal datées (attribuées à l'Oligocène sans preuve) et forment avec la succession aquitanienne le remplissage sédimentaire syn-tectonique du bassin de la Vistrenque lié au rifting de la marge du golfe du Lion. La fin du rifting (*break-up unconformity*) est attribuée par Valette (1991) à la base de la transgression burdigalienne. La disposition en discordance des réflecteurs burdigaliens sur l'Aquitanien indique que ceux-ci sont postérieurs à la phase du rifting (**Fig. 2.8B-C**). Les séries miocènes post-Aquitanien à plio-quaternaires constituent les dépôts post-rift.

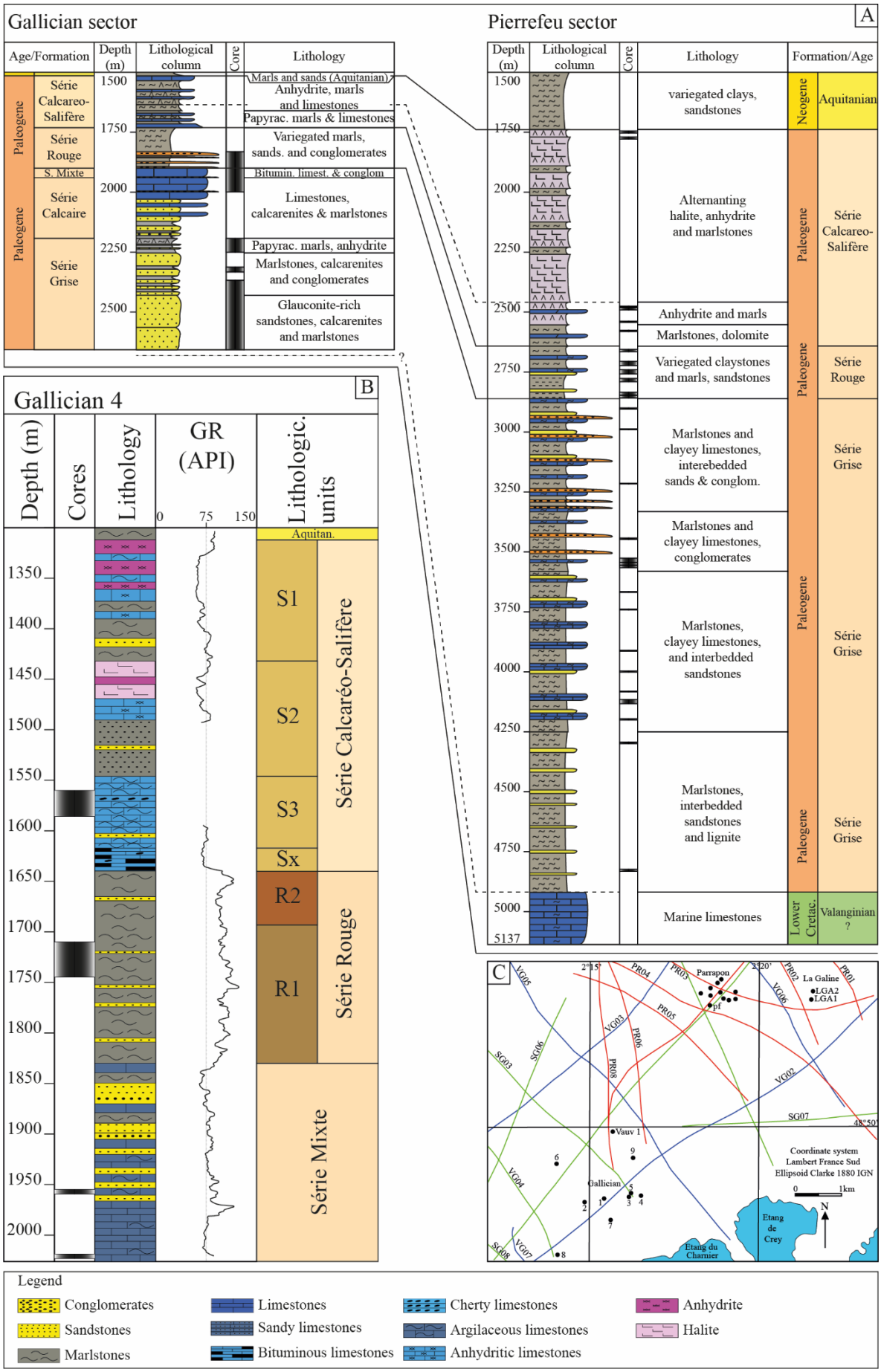
Gallician sector
Pierrefeu sector
A
Age/Formation
Depth (m)
Lithological column
Core
Lithology
Formation/Age
Paleogene
Série Calcareo-Salifère
Série Rouge
S. Mixte
Série Calcaire
Série Grise
Marls and sands (Aquitanian)
Anhydrite, marls and limestones
Papyrac. marls & limestones
Variegated marls, sands. and conglomerates
Bitumin. limest. & conglom
Limestones, calcarenites & marlstones
Papyrac. marls, anhydrite
Marlstones, calcarenites and conglomerates
Glauconite-rich sandstones, calcarenites and marlstones
variegated clays, sandstones
Neogene
Aquitanian
Alternanting halite, anhydrite and marlstones
Anhydrite and marls
Marlstones, dolomite
Variegated claystones and marls, sandstones
Marlstones and clayey limestones, interebedded sands & conglom.
Marlstones and clayey limestones, conglomerates
Marlstones, clayey limestones, and interbedded sandstones
Marlstones, interbedded sandstones and lignite
Marine limestones
Lower Cretac.
Valanginian ?
Gallician 4
B
Depth (m)
Cores
Lithology
GR (API)
Lithologic. units
Aquitan.
S1
S2
S3
Sx
R2
R1
Série Calcaréo-Salifère
Série Rouge
Série Mixte
C
Parrapon
La Galine
LGA2
LGA1
Vauv 1
Gallician
Etang du Charnier
Etang de Crey
Coordinate system
Lambert France Sud
Ellipsoid Clarke 1880 IGN
Legend
Conglomerates
Sandstones
Marlstones
Limestones
Sandy limestones
Bituminous limestones
Cherty limestones
Argilaceous limestones
Anhydritic limestones
Anhydrite
Halite

Figure 2.10 : A) Colonnes lithologiques et corrélations des forages Gallician 9 et Pierrefeu 1 situés dans les secteurs de Gallician et de Pierrefeu respectivement. La colonne lithologique du secteur de Gallician a été compilée à partir des rapports internes de SNPLM. La colonne lithologique de Pierrefeu est modifiée d'après Valette (1991) B) Colonne lithologique du forage Gallician 4 montrant les différentes sous-unités des séries Calcaréo-salifère et Rouge, d'après rapport interne SNPLM, modifiée d'après le log de fin de sondage. C) Carte géographique montrant la localisation des données de subsurface (forages, profils sismiques) des secteurs de Gallician et de Pierrefeu, pf=Pierrefeu 1 well, LGA=LaGaline, les numéros 1 à 9 indiquent les forages de Gallician (1 à 9), modifiée d'après Valette (1991). Noter que le découpage lithologique dans le secteur de Gallician diffère de celui du secteur de Pierrefeu (Fig. 2.9B, *cf* texte pour plus de détails).

Le calage des forages de Parrapon sur les profils sismiques a toutefois permis à Valette (1991, pages 134-138) de distinguer les séquences paléogènes antérieures au rifting Oligo-Aquitanien des séries déposées pendant cette phase d'extension. Les réflecteurs des parties intermédiaire et supérieure de la Série Calcaréo-salifère et de l'Aquitanien sus-jacent (épaisseur : 800 - 1500 m) sont divergents et montrent des discordances progressives révélant le caractère syn-tectonique du dépôt de ces séries. Ce n'est pas le cas pour la partie basale de la Série Calcaréo-salifère qui est concordante avec la Série Rouge et la Série Grise sous-jacentes. Les réflecteurs de ces dernières formations sont disposés parallèlement et sont par conséquent *attribuables* au pré-rift. Par ailleurs, Valette and Benedicto (1995) montrent que ces formations, c'est-à-dire la Série Rouge et la Série Grise, sont solidaires et affectées dans leur ensemble par les failles antithétiques à la faille majeure de Nîmes dans le secteur de Pierrefeu (**Fig. 2.7**). Ainsi, une discordance peut être suggérée à la base des évaporites de la série Calcaréo-salifère marquant le début du rifting de la marge du Golfe du Lion.

2.6. Références bibliographiques du chapitre 2 :

Alabouvette B, Chedhomme J, Fredet J.M, Lartaud, et al. Inventaire des ressources nationales de Charbon. Lignites du Fossé d'Alès-Barjac. *Rapport BRGM*, 83 SGN 519/GEO/LRO, 105 pp.

Arthaud F, Matte P. 1975. Les décrochements tardi-hercyniens du Sud-Ouest de l'Europe. Géométrie et essai de reconstruction des conditions de déformation. *Tectonophysics* 25: 139-171.

Arthaud F, Ogier M, Séguret M. 1981. Géologie et géophysique du Golfe du Lion et de sa bordure nord. *Bulletin du BRGM* 1(3): 175–193.

Arthaud F, Séguret M. 1981. Les structures pyrénéennes du Languedoc et du golfe du Lion (Sud de la France). *Bulletin de la Société Géologique de France* 7(23) : 51-63.

Auzende J.M, Bonnin J, Olivet J.L. The origin of the Western Mediterranean Basin. *J. Geol. Soc. London* 129 :607-620.

Bache F. 2008. Evolution Oligo Miocène des marges du micro océan Liguro-Provençal. Université de Bretagne-occidentale, Brest. Thèse de doctorat, 329 pp.

Baudrimont A, Dubois P. 1977. Un Bassin mésogéen du domaine péri-alpin : le Sud-est de la France. *Bull. Centres Rech. Explor.-Prod. Elf-Aquitaine* 1(1) : 261-308.

Beaufort L, Bruneau J, Crepin A, Julian Y. 1954. Ampleur de l'érosion pontienne et du comblement Pliocène en Camargue. *Bulletin de la Société Géologique de France* 6(4) : 157-184.

Bellon J. 1959. Renseignements stratigraphiques concernant la série de Camargue. Révisions des microfaciès des sondages de Vauvert 1 – Gallician 9 – Charnier 1 et Montcalm 2 dans les formations sous-jacentes à la série rouge. *Document interne CEP*, 18pp.

Bellon J. 1961. Renseignements stratigraphiques concernant le sondage Marette 1. Note n°1 : Etude de l'ensemble de la Série stratigraphique. *Document interne CEP*, 6pp.

Bellon J. 1964. Renseignements stratigraphiques concernant le sondage Pierrefeu 1. Note n° 1 : Etude de microfaciès. *Document interne CEP*, 9pp.

Benedicto A. 1996. Modèles tectono-sédimentaires de bassins en extension et style structural de la marge passive du Golfe du Lion (partie nord), sud-est France. Thèse de doctorat. Université de Montpellier II, Montpellier, 249pp.

Benedicto A, Labaume P, Séguret M, Séranne M. 1996. Low-angle crustal ramp and basin geometry in the Gulf of Lion passive margin: the Oligocene-Aquitanian Vistrenque graben, SE France. *Tectonics* 15(6): 1192–1212.

Bessis F. 1986. Some remarks on the study of subsidence in sedimentary basins. Application to the Gulf of Lions margin (Western Mediterranean). *Marine and Petroleum Geology* 3 :37-63.

Bessis F, & Burrus J. (1986). Etude de la subsidence de la marge du Golfe du Lion (Méditerranée occidentale). *Bulletin des Centres de recherche, Exploration et Production de Elf Aquitaine* 10(1) : 123-141.

Biju-Duval B, Letouzey J, Montardet L. 1979. Variety of margins and deep basins in the Mediterranean, *AAPG Bulletin* 293-317.

Biteau, Morash, Mervoyer, Canard, Buisson. 1993. Permis Vauvert-Gallician – « Farm out » Coparex. Compte rendu de visite chez Coparex. Synthèse sur le secteur de Gallician. *Elf Aquitaine Production, Document interne*. 27 pp.

Bois C. 1993. Initiation and evolution of the Oligo-Miocene rift basins of southwestern Europe: contribution of deep seismic profiling. *Tectonophysics* 226 : 227-252.

Busson G, Schreiber B. 1997. Sedimentary deposition in rift and foreland basins in France and Spain (Paleogene and lower Neogene). New York: Columbia University Press.

Caline B. 1983. Le bassin occidental de Camargue et le gisement salifère de Vauvert, *Rapport ENSPM*.

Cavelier C, Alabouvette G, Amberger J.P, Cautru J.-P, Charollais J, Châteauneuf J.-J, et al. 1984. Paléogène. In : Debrand-Passard ed., Synthèse géologique du Sud-Est de la France. *Mémoire du BRGM* 125 : pp. 389-468.

Caziot M. 1896. Sur le Tertiaire inférieur des environs de Nîmes. *Bulletin de la Société Géologique de France* 24: 1–32.

Chauvin A, Follin-Arbelet. 1985. Apport de la gravimétrie à l'étude des structures ante-triasiques sous le Languedoc et la Camargue. Université de Montpellier II. Mémoire DEA.

Choukroune P, Mattauer M. 1978. Tectonique des plaques et Pyrénées : sur le fonctionnement de la faille transformante nord-pyrénéenne, comparaison avec des modèles actuels. *Bulletin de la Société Géologique de France* 20 : 689-700.

Dumas E. 1876. Statistique Géologique, Minéralogique, Métallurgique et Paléontologiques du Département du Gard. Arthus Bertrand ed. 735 pp.

Fontannes, F. 1885. Etudes stratigraphiques et paléontologiques pour servir à l'histoire de la période Tertiaire dans le bassin du Rhône, *Société Géologique de France*, Paris (195pp).

Gorini C, Le Marrec A, Mauffret A. 1993. Contribution to the structural and sedimentary history of the Gulf of Lions (western Mediterranean), from the ECORS profiles, industrial seismic profiles and well data. *Bulletin de la Société géologique de France* 164(3): 353–363.

Guyonnet-Benaize C, Lamarche J, Masse J-P., Villeneuve M, Viseur S. 2010. 3D structural modelling of small-deformations in poly-phase faults pattern. Application to the Mid-Cretaceous Durance uplift, Provence (SE France). *Journal of Geodynamics* 50 : 81–93. https://doi.org/10.1016/j.jog.2010.1003.1003.

Jan du Chene R. 1989. Etude Palynologique du Sondage Eurafrep (Camargue) : BAM 1. In Buisson A. Rapport de fin de sondages Baumelles 1. *Document interne Eurafrep* : 29-36.

Lefevre D. 1980. Evolution morphologique et structurale du Golfe du Lion. Essai de traitement statistique des données (PhD Thesis). Université Paris-VI, 163pp.

Lemoine M, Graciansky P.C. 1988. Marge continentale téthysienne dans les Alpes occidentales. *C.R. Acad. Sci. Paris* 8(4)485 : 597-797

Lettéron A, Hamon Y, Fournier F, Séranne M, Pellenard P, Joseph P. 2018. Reconstruction of a saline, lacustrine carbonate system (Priabonian, St-Chaptes Basin, SE France): depositional models, paleogeographic and paleoclimatic implications. *Sedimentary Geology* 367: 20–47.

Lettéron A, Hamon Y, Fournier F, Demory F, Séranne M, Joseph P. 2021. Stratigraphic architecture of a saline lake system: From lake depocenter (Alès Basin) to margins (Saint-Chaptes and Issirac basins), Eocene-Oligocene transition, south-east France. *Sedimentology, Blackwell Publishing, in press,* ⟨DOI: 10.1111/sed.12920⟩, ⟨hal-03406458⟩.

Magne J, Malmoustier G. 1960. Révision et essai de corrélation de trois forages de Camargue: Vauvert 1, Gallician 9 et Montcalm 2. *ESSO REP*, Département Géologie 13 pp.

Mascle A, Jacquart G, Deville E. 1994. The Corbières transverse zone of the Pyrenee-Provence thrust belt (south France) – Tectonic history and petroleum plays. *6th Conference, European Association of Petroleum Geoscientists & Engineers*, Extended Abstract, P556, Vienna, 1994.

Mauffret A, Pascal G, Maillard A, Gorini C. 1995. Tectonics and deep structure of the north-western Mediterranean Basin. *Marine and Petroleum Geology* 12(6): 645-666.

Mauffret A, Gorini C. 1996. Structural style and geodynamic evolution of Camargue and Western Provencal basin, southeastern France. *Tectonophysics* 15(2): 356-375.

Mauguy V, Fischer P. 1949. L'indice de Milhaud. Document interne SNPL, 12pp.

Ménard, G. 1980. Profondeur du Socle anté-triassique dans le Sud-Est de la France. *Comptes Rendus de l'Académie des Sciences de Paris*, 299-302.

Ménillet F. 1973. Carte géologique 1/50000 de la France au 1/50000 : feuille de Nîmes n° 965. *BRGM.*

Nury D. 1977. Le bassin oligocène de Marseille : stratigraphie, évolution paléogéographique. *Géologie méditerranéenne* 4(1) : 25-35.

Olivet J.L, Beuzard P, Auzende J.M, Bonnin J. 1984. Cinématique de l'Atlantique Nord et Central. *Publ. Cent. Nat. de la Rech. Sci.* 54, 1-107.

Pellat E, Allard M. 1895. Dépôts lacustres de la Butte Iouton entre Comps et Beaucaire (Gard). *Bulletin de la Société Géologique de France* 23: 434-436.

Roman F. 1903. Contributions à l'étude des Bassins lacustres de l'Éocène et de l'Oligocène du Languedoc. *Bulletin de la Société Géologique de France (4ème série)* 3 : 546-616.

Roman, F. (1905). La géologie des environs de Nîmes. Mémoire, *Bulletin de la Société d'étude des Sciences Naturelles de Nîmes*.

Roman F. 1910. Faune saumâtre du sannoisien du Gard. *Bulletin de la Société Géologique de France (4ème série)* 10: 927–955.

Romagny A, Jolivet L, Menant A, Bessière E, Maillard A, Canva A, Gorini C, Augier R. 2020. Detailed tectonic reconstructions of the Western Mediterranean region for the last 35 Ma, insights on driving mechanisms, *BSGF - Earth Sciences Bulletin* 191: 37

Rouchy J.-M. 1997. Paleogene continental rift system of Western Europe: locations of basins, paleogeographic and structural framework, and the distribution of evaporites. In: Busson, G., Schreiber, B.C. eds., Sedimentary Deposition in Rift and Foreland Basins in France and Spain. Columbia Univ. Press, New York: pp. 45–94.

Roure F, Brun J.P, Colletta B, Van den Driessche J. 1992. Geometry and kinematics of extensional structures in the Alpine Foreland Basin of southeastern France. *J. Struct. Geol.* 4 : 503-519.

Séranne M, Benedicto A, Truffert C, Pascal G, Labaume P. 1995. Structural style and evolution of the Gulf of Lion Oligo-Miocene rifting: Role of the Pyrenean orogeny. *Marine and Petroleum Geology* 12: 809–820.

Séranne M. 1999. The Gulf of Lion continental margin (NW Mediterranean) revisited by IBS: an overview. In: Durand, B, Jolivet, L, Horváth, F, Séranne, M, eds. The Mediterranean basins: Tertiary extension within the Alpine Orogen. Volume Special Publication, 156. London: *The Geological Society* 15–36.

Séranne M, Couëffé R, Husson E, Baral C, Villard J. 2021. The transition from Pyrenean shortening to Gulf of Lion rifting in Languedoc (South France) –A tectonic-sedimentation analysis. *BSGF - Earth Sciences Bulletin* 192, 27.

Trauth N. 1984. Camargue, In Cavelier et al., Paléogène. In: Synthèse Géologique du Sud-Est de la France - Stratigraphie et Paléogéographie (Eds S. Debrahnd-Passard and S. Courbouleix). BRGM, 125(1) : 433-434.

Valette M. 1991. Etude structurale du gisement salifère Oligocène de Vauvert (Gard). Univ. Montpellier II. Thèse de doctorat. 229 pp.

Valette M, Benedicto A. 1995. Chevauchements gravitaires halotectoniques dans le bassin distensif de Camargue (marge du golfe du Lion, SE de la France). *Bulletin de la Société Géologique de France* 166(2) : 137-147.

Vincent R. 1956a. Etude de la série rouge et de la série mixte de Gallician. *Document interne CEP*, 27pp.

Vincent R. 1956b. Etude de subsurface du champ de Gallician – Etude quantitative de Gallician 9. *Document interne CEP*, 55pp.

Vincent R. 1957. Zone productive de la série calcaire de Gallician 9. *Document interne CEP*, 8pp.

Ziegler, P.A. 1992. European Cenozoic rift system. In: Ziegler, P.A. (Ed.), Geodynamics of Rifting, Volume I, Case History Studies on Rifts: Europe and Asia. *Tectonophysics* 208: 91–111.

3. LA MARGE CARBONATÉE NORD DU BASSIN DE LA VISTRENQUE : ÉTUDE DE LA BUTTE IOUTON

3. La marge carbonatée nord du bassin de la Vistrenque : étude de la butte Iouton

Synthèse

Ce chapitre concerne l'étude intégrée d'une butte-témoin de carbonates lacustres (Butte Iouton) affleurant sur le haut de Jonquières et vise à documenter le fonctionnement de la marge nord du bassin de la Vistrenque (SE France) au Priabonien (Eocène supérieur).

L'approche multidisciplinaire de ce travail repose sur la révision biostratigraphique, l'analyse sédimentologique, diagénétique et géochimique détaillée de la succession carbonatée oolithique. Elle a permis d'établir un modèle de dépôt détaillé d'une marge carbonatée oolithique de lac salin, de mettre en évidence des cycles de transgression-régression et d'apporter de nouveaux éclairages aux reconstitutions paléogéographiques des bassins lacustres priaboniens du sud-est de la France.

Un modèle de rampe carbonatée lacustre a été mis en évidence. Cette rampe présente, du pôle proximal au pôle distal : 1) un domaine interne à laminites microbiennes et wackestones à ostracodes et mollusques, 2) un domaine plus ouvert, d'énergie modérée à sédimentation granulaire péloïdale et 3) un environnement externe de plus haute énergie à accumulation d'ooïdes et de péloïdes. La sédimentation carbonatée de bordure de lac se produit principalement pendant des phases de transgression lacustre contrôlées par la subsidence alors que les surfaces d'émersion marquent des périodes de bilan hydrique déficitaire et d'assèchement du lac (régression forcée). Les signatures isotopiques (carbone et oxygène) des carbonates ainsi que les tendances d'évolution verticale de la salinité estimées par les assemblages de mollusques suggèrent que les transgressions lacustres ne sont pas associées à un bilan hydrologique excédentaire, mais à des connexions avec des masses d'eau salées adjacentes dans un contexte subsident.

Les sédiments carbonatés de la Butte Iouton se sont déposés sur les marges d'un système de lacs salins interconnectés de grande dimension, occupant différents sous-bassins du Languedoc et de la Vallée du Rhône. La marge sud de ce système lacustre était à sédimentation silicoclastique dominante, alimentée depuis le sud par l'érosion des reliefs pyrénéens, alors que la marge nord était carbonatée avec un développement significatif de corps oolithiques.

Ce chapitre est présenté sous forme d'un article scientifique (**Article 1**) *accepté pour publication dans le Bulletin de la Société Géologique de France* (**BSGF Earth Science Bulletin**).

Article 1 – Transgressive-regressive cycles in saline lake margin oolites: paleogeographic implications (Priabonian, Vistrenque basin, SE France)

Nazim SEMMANI, François FOURNIER, Philippe LÉONIDE, Monique FEIST, Sarah BOULARAND, Jean BORGOMANO. « **Transgressive-regressive cycles in saline lake margin oolites: paleogeographic implications (Priabonian, Vistrenque basin, SE France** ». Dans BSGF Earth Sciences Bulletin (sous presse). DOI: https://doi.org/10.1051/bsgf/2022012

Transgressive-regressive cycles in saline lake margin oolites: paleogeographic implications (Priabonian, Vistrenque basin, SE France)

Nazim Semmani[1], François Fournier[1*], Philippe Léonide[1], Monique Feist[2], Sarah Boularand[3], Jean Borgomano[1]

[1]: Aix Marseille Univ, CNRS, IRD, Coll France, CEREGE, 3 Place Victor Hugo, Case 67, 13331, Marseille Cedex 03, France.

[2]: Université de Montpellier, Institut des Sciences de l'Evolution (ISEM), Campus Triolet, CC065, 34095 Montpellier cedex 5, France

[3]: Fédération de Recherche Sciences Chimiques Marseille FR 1739, Pôle PRATIM, 13331 Marseille Cedex 03, France.

[*]Corresponding author: fournier@cerege.fr

Abstract

The integrative analysis of a lacustrine carbonate succession from Butte Iouton hill (Vistrenque basin, SE France) brings new insights into depositional models and stacking patterns of oolitic saline lake margins and provides new details regarding the late Eocene paleogeography of southeast France.

Depositional facies analysis and paleoenvironmental reconstructions allow reconstructing an oolitic lacustrine ramp model, displaying from the proximal to the distal areas: 1) shallow marginal saline lake domain with deposition of planar microbial laminites, and molluscan-ostracodal wackestone, 2) a more distal and open lacustrine environments with low to moderate energy characterized by the deposition of peloidal grainstones and 3) a domain of higher energy with accumulation of ooids mixed with peloids in the vicinity of the area of ooid production. Lake margin carbonate sedimentation dominantly occurred during stages of lake transgression while subaerial exposure surfaces developed during periods of negative inflow-evaporation balance (forced regression). Carbon and oxygen isotopes together with vertical trends in salinity inferred from molluscan associations show that lake transgression does not result from increasingly positive freshwater-evaporation balance volume but from the combination of subsidence and outflow from neighbouring saline waterbodies.

The Butte Iouton carbonate margin is part of a set of interconnected saline lakes, occupying continental basins from Languedoc and Rhodanian region during the Priabonian, with a siliciclastic-dominated sedimentation in the southern margin, sourced by erosion of Pyrenean reliefs, and a carbonate-dominated northern margin with significant oolitic sedimentation in high-energy nearshore area.

Keywords: lacustrine carbonates, oolite, saline lakes, paleogeography, Eocene.

Résumé

Cycles de transgression-régression sur une marge oolithique de lac salin : implications paléogéographiques (Priabonien, Bassin de la Vistrenque, Sud-Est de la France)

L'étude intégrée d'une butte-témoin de carbonates lacustres (Butte Iouton) a permis d'établir un modèle de dépôt détaillé d'une marge carbonatée oolithique de lac salin, de mettre en évidence des cycles de transgression-régression et d'apporter des éléments de reconstitution paléogéographique des bassins lacustres priaboniens du sud-est de la France.

Un modèle de rampe carbonatée lacustre a été mis en évidence, présentant du pôle proximal au pôle distal : 1) un domaine interne à laminites microbiennes et wackestones à ostracodes et mollusques, 2) un domaine plus ouvert, d'énergie modérée à sédimentation granulaire péloïdale et 3) un environnement externe de plus haute énergie à accumulation d'ooïdes et de péloïdes. La sédimentation carbonatée de bordure de lac se produit principalement pendant des phases de transgression lacustre contrôlées par la subsidence alors que les surfaces d'émersion marquent des périodes de bilan hydrique déficitaire et d'assèchement du lac (régression forcée). Les signatures isotopiques (carbone et oxygène) des carbonates ainsi que les tendances d'évolution verticale de la salinité estimées par les assemblages de mollusques suggèrent que les transgressions lacustres ne sont pas associées à un bilan hydrologique excédentaire, mais à des connexions avec des masses d'eau salées adjacentes dans un contexte subsident.

Les sédiments carbonatés de la Butte Iouton se sont déposés sur les marges d'un système de lacs salins interconnectés de grande dimension, occupant différents sous-bassins du Languedoc et de la Vallée du Rhône. La marge sud de ce système lacustre était à sédimentation silicoclastique dominante, alimentée par l'érosion des reliefs pyrénéens, alors que la marge nord était carbonatée avec un développement significatif de corps oolithiques.

Mots-clés : carbonates lacustres, oolithe, lacs salins, paleogéographie, Éocène.

3.1. Introduction

The European Cenozoic Rift System (ECRIS) (Ziegler, 1992; Dèzes et al., 2004) is a NE-SW system of continental lake basins formed during the upper Eocene in the Alpine foreland. These basins are characterized by thick siliciclastic, carbonate and evaporite deposits (e.g. Rouchy, 1997). In southeast France, the onset of saline lakes occurred as early as the early Priabonian in the Saint-Chaptes basin (Lettéron et al., 2018) and then developed on a larger scale during the middle to late Priabonian in the Alès (Lettéron et al., 2018), Issirac (Lettéron et al., 2017), Mormoiron-Carpentras (Triat and Truc, 1974; Truc, 1978), Manosque-Forcalquier (Lesueur, 1991) basins and further north in the Valence graben (Dromart and Dumas, 1997) (**Fig. 3.1A**). Despite detailed studies on individual basins or connected lake systems (e.g. ASCI lake system: Lettéron et al., 2022; Apt-Manosque-Forcalquier lake system: Lesueur, 1991),

there are still unresolved questions, debates and controversies on the paleogeography of western Europe during the late Eocene – lower Oligocene times, the origin of the salinity in the lakes and the connections between the lakes and the oceanic realm (e.g. Fontes et al., 1991; Rouchy, 1997; Briot and Poidevin, 1998; Bodergat et al., 1999; Rouchy and Blanc-Valleron, 2009; Lettéron et al., 2017; 2018). For instance, Lettéron et al. (2017, 2018) found that the ASCI lacustrine system was connected to neighbouring saline water bodies whose location and source of which are not formally established. According to these authors, saline water feeding is presumably from the leaching of northern Triassic diapirs via Mormoiron-Carpentras throughs and/or marine domain through the Vistrenque area. The latter is poorly documented since the Paleogene deposits are almost entirely buried beneath the Rhône delta sediments.

Another major issue for the reconstruction of paleogeographic and tectonic evolution of Paleogene basins from southeast France is the availability and quality of chronostratigraphic constraints (Séranne et al., 2021). East of the Nîmes fault, the Cenozoic Vistrenque graben is known only through subsurface studies and has been assigned to the Oligocene Gulf of Lion margin (Valette and Benedicto, 1995; Benedicto et al., 1996), while Cavelier (1984) suggested that the Vistrenque graben initiated during the Priabonian coevally with the neighbouring Languedoc basins such as the north-Montpellier, Sommières, Saint-Chaptes, Alès and Issirac basins (Séranne et al., 2021; Lettéron et al., 2022). To date, the paucity of chronostratigraphic data from the basal filling of the graben (*Série grise* siliciclastic unit, e.g. Valette and Benedicto, 1995) does not allow this hypothesis to be validated. However, the northern part of the basin offers the possibility to study on outcrops carbonate successions assumed to be upper Eocene in age (Roman, 1910) and thus provides clues to address the question.

In the present work, we carry out a detailed petrographic, sedimentological and geochemical analysis of a carbonate succession which outcrops on a residual hill (Butte Iouton, Beaucaire) located east of the Nîmes fault on the northern margin of the Vistrenque graben and that is characterized by the dominance of oolitic deposits (**Fig. 3.1A**, **3.3A**). The main objectives of this study are 1) to document the existence of a salt lake carbonate sedimentation during the Priabonian in the north of the Vistrenque basin and provide new constraints to the chronostratigraphic framework 2) to reconstruct the depositional environments for a Cenozoic oolitic saline lake margin 3) to discuss the control of tectonics and paleohydrological changes onto the vertical facies stacking pattern and depositional sequence development and 4) to provide new insights into the paleogeography of the southeast France by investigating the possible relationships between the saline lake basins of the ECRIS.

3.2. Geological setting

3.2.1. The Vistrenque Cenozoic basin: regional tectonic setting and stratigraphy

The Vistrenque basin is a NE-SW trending Cenozoic basin located in the western part of the Camargue region (SE France). The basin extends over 50*30 Km² and is assumed to be the deepest Cenozoic basin in the SE of France (Benedicto et al., 1996), it is linked to the Northeast

with the Pujaut trough and is separated from the neighbouring Vaccarès (Petit-Rhône) basin by the Albaron structural high (**Fig. 3.1A**).

The Nîmes fault is a major low angle-ramp that bounds the Vistrenque and Pujaut basins to the NW and was active during the Oligo-Aquitanian rifting of the Gulf of Lion margin that preceded the oceanic accretion in the Liguro-Provençal basin during the Burdigalian (Gorini et al., 1993; Séranne et al., 1995; Valette and Benedicto, 1995; Benedicto et al., 1996).

Prior to the Oligo-Miocene rifting, strike-slip deformation regime led to the development of many continental sedimentary basins (e.g. Alès–Saint-Chaptes–Issirac basin, Lettéron et al., 2022) during the Priabonian (late Eocene) in Languedoc area within a NE trending sinistral strike-slip shear zone, located between the Cévennes and Nîmes faults (Séranne et al., 2021). The Eocene and Oligocene basins of the Languedoc area have well constrained chronostratigraphic frameworks and their depositional and structural settings are well documented (Benedicto et al., 1996; Séranne et al., 2021; Lettéron et al., 2022). The Nîmes and Cévennes sinistral strike-slip faults have accommodated simultaneously the E-W extension of the Western European rifting in the north and the Pyrenean compression from the south (Séranne et al., 2021). In the Camargue region located southern to the Languedoc, Eocene deposits are only known from the Jonquières high (**Fig. 3.1A**), and no evidence can be provided to confirm the presence of upper Eocene deposits in the Camargue basins (e.g. Vistrenque basin) since their chronostratigraphic framework is not constrained (Benedicto et al., 1996).

Stratigraphically, the Eocene (?) to Aquitanian sedimentary succession of the Vistrenque basin exceeds 3000 m in thickness and is subdivided in the depocentre of the basin into three main units, from bottom to top: *Série grise* (more than 2000 m thick), *Série Rouge* (~ 200 m) and *Série Calcaréo-salifère* (900 m) formations (Benedicto, et al., 1996). The lowermost *Série grise* unit consists mainly of deep-lake non-fossiliferous mixed siliciclastic-carbonate detrital sediments and their attribution to the beginning of the Oligo-Miocene gulf of Lion rifting (Benedicto, 1996) or to the late Eocene development of continental basins is an open question. The upper *Série Calcaréo-Salifère* unit is made essentially of evaporite deposits that were assigned to the Upper Oligocene (Valette, 1991).

According to Cavelier (1984), the similarity of the sedimentation pattern between the Languedoc grabens and Vistrenque basin (i.e. dominant siliciclastic sedimentation to south and carbonate lacustrine margin to the north) would suggest that the deposition of the lowermost *Série grise* unit or at least the basal intervals of this unit was coeval with the widespread Priabonian continental sedimentation in the Issirac, Alès, Saint-Chaptes and Sommières basins.

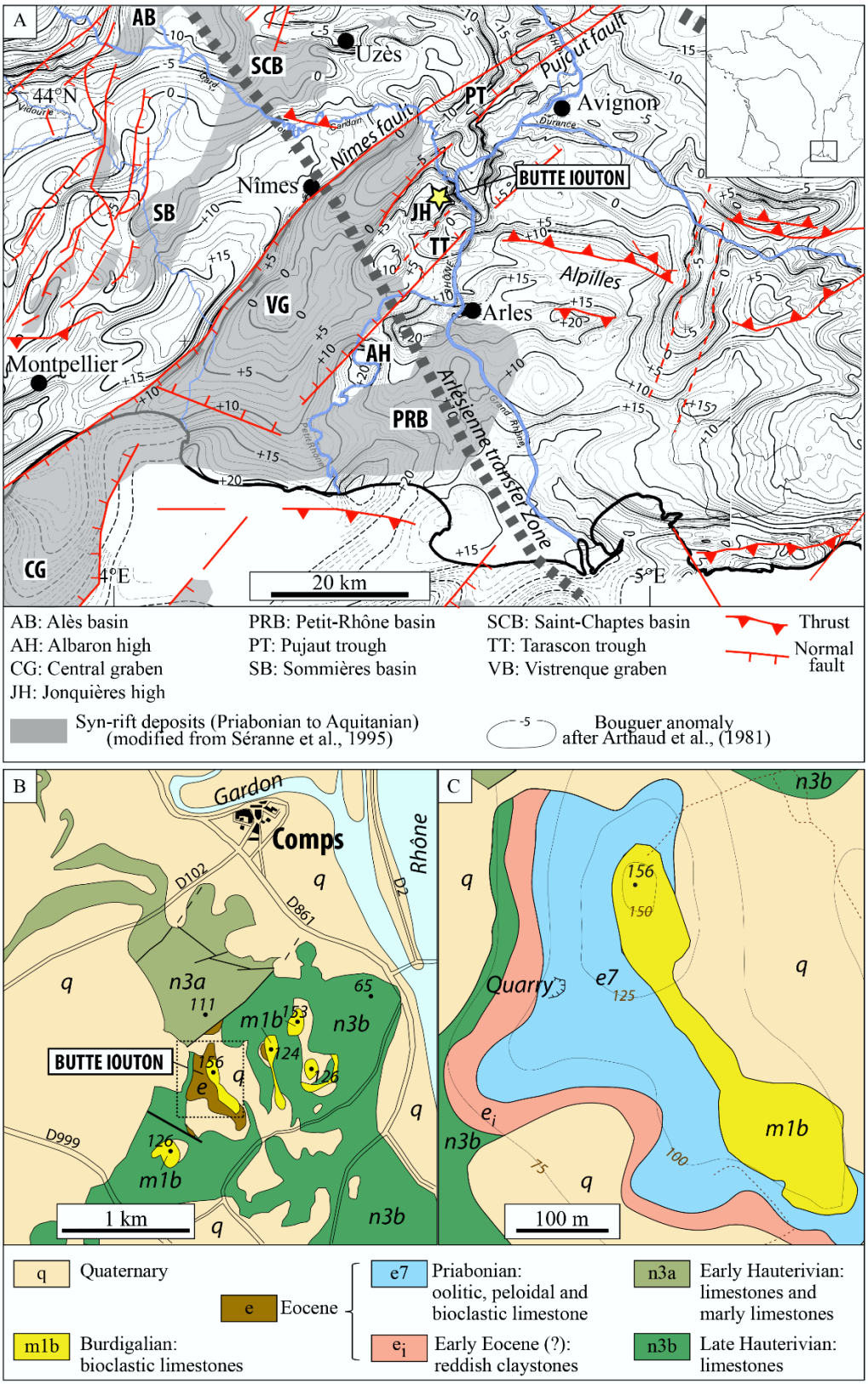

Figure 3.1: A) Simplified structural map of Languedoc and southern Rhône valley (SE France) (after Séranne et al., 2021; Mauffret and Gorini, 1996): the grey shaded areas indicate late Eocene to Aquitanian deposits (after Séranne et al., 1995; Séranne et al., 2021) and the background map displays the Bouguer anomaly (after Arthaud et al., 1980). B) Geological map of the Comps and Butte Iouton area, modified from the BRGM geological map, Nîmes sheet 1/50000 (Ménillet, 1973): the map shows the Eocene to Miocene outcrops and the Cretaceous

substratum of the Jonquières high. C) Detailed geological map displaying the close-up view of the box around the butte Iouton hill in B).

3.2.2. The Jonquières high: stratigraphy of the Priabonian lacustrine margin

The Jonquières high is about 5-6 km wide and represents a NE-SW horst structure bordering the Vistrenque basin to the north and located southeast to the Pujaut through and northwest to the Tarascon trough **(Fig. 3.1A)**. The high is constituted essentially of the Lower Cretaceous substratum; the Eocene to Miocene cover is limited to a few small residual hills between the villages of Comps and Beaucaire **(Fig. 3.1B)**. Resting on the Hauterivian marine limestones and marly limestones, the Eocene deposits from these hills (e.g. butte Iouton) consist essentially of a ~30 m thick lacustrine limestone succession resting on variegated clays and silts (about 20 m thick interval) attributed by Pellat and Allard (1895) to the early Eocene on the basis of regional facies analogy without any paleontological evidence. These Eocene lacustrine limestones are unconformably overlain by Burdigalian (early Miocene) transgressive coralline algal marine limestones (Pellat and Allard, 1895; Roman, 1903) **(Fig. 3.1C)**.

The lacustrine limestones from Butte Iouton include oolithic intervals that have been exploited since the Middle Ages as a statuary stone (Dumas, 1876). They yielded a rich molluscan fauna that has attracted the attention of geologists since the first half of the 19th century (de Roys, 1846). The first detailed section of the Butte Iouton hill was carried out by Pellat and Allard (1895) who identified 9 main fossiliferous carbonate layers and mentioned a preliminary list of fossil molluscs. Roman (1910) took charge of the detailed study of fossil molluscs from the regional “Sannoisian” formations and has drawn up a comprehensive inventory of 30 taxa including eight holotypes (hosted in the collections of the University of Lyon) of gastropod species.

3.3. Material and methods

The 50m-thick Cenozoic succession of the Butte Iouton hill has been mapped (**Fig. 3.1B**). Most of the carbonate section is quarried on the western flank of the hill (see location in **Fig. 3.1C**) thus enabling a continuous and detailed observation of the rock succession. Data on sedimentary structures, depositional textures, biological content, and diagenetic features are compiled in the detailed sedimentary log (**Fig. 3.2**).

3.3.1. Depositional facies and petrographic characterization

A total of 28 thin sections have been prepared to perform detailed microfacies characterization and to determine the petrographic features of the grains using a conventional transmitted polarized light microscope. Carbonate depositional facies have been defined on both macroscopic descriptions and microscopic observations using the Dunham classification of carbonates (Dunham, 1962) expanded by Embry and Klovan (1971).

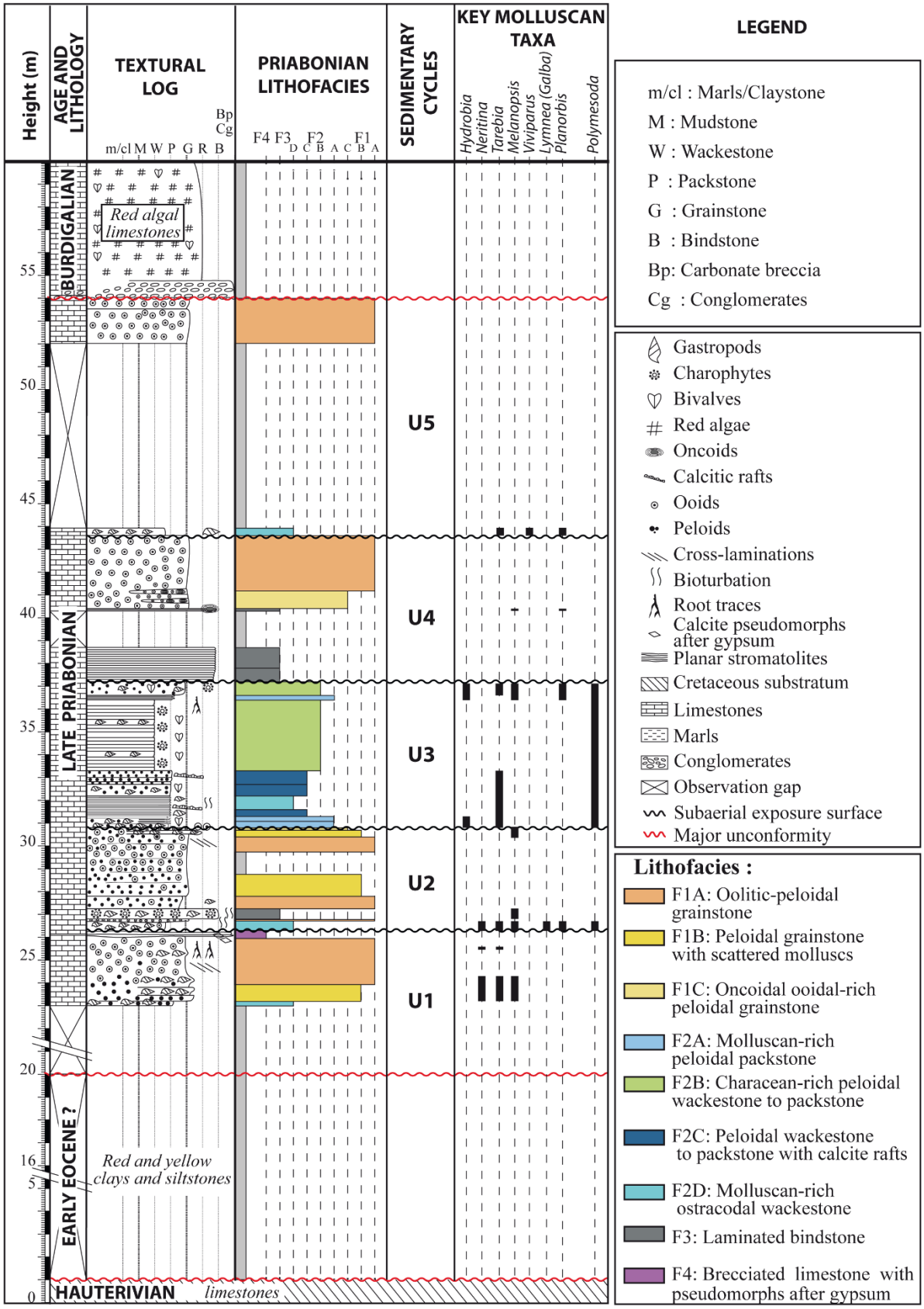

Figure 3.2: Detailed sedimentary log of the butte Iouton succession and main molluscan taxa identified on field. Most of the section is measured on the quarry (see location in Fig. 3.1C). See text for the definition of lithofacies and sedimentary cycles.

Point-counting (300 points) performed with the JMicroVision software allows to quantify the allochem proportions in thin sections (Roduit, 2007). SEM observations conducted at Pôle PRATIM (Plateforme de Recherche Analytique Technologique et Imagerie, Aix-Marseille University, FSCM) using a Philips XL30 ESEM (environmental scanning electron microscope) enable to investigate in more detail the internal microstructure of some carbonate grains.

3.3.2. Biological assemblages and chronostratigraphic framework

Particular attention was paid to the examination of the quarry's fossiliferous layers to determine the fossil assemblages, namely the molluscs (gastropods and bivalves) and the remains of characean algae (**Fig. 3.3**). Molluscan assemblages provide key indications for paleoecological reconstructions (e.g. Lettéron et al., 2017) and contribute to a lesser extent to constrain the chronostratigraphic framework (Cavelier, 1984). Charophyte gyrogonites constitute an essential tool to better constrain the age of the deposition of fresh and brackish water carbonates and will therefore be used for the biostratigraphic review of the studied succession from the butte Iouton hill. Molluscan shells and charophyte gyrogonites are often well preserved and are easily extracted. In few horizons, the shells are totally dissolved and only the external moulds remain. Casts have been made by injecting silicone resin into the moulds and the resulting casts allow a detailed examination of the external ornamentation of the molluscan shell casts. The identification of the molluscan taxa is carried out in accordance with the diagnoses documented in Fontannes (1884) and in Roman (1910). The fossil collection of Pierre de Brun, hosted in the Museum of Paleontology of the Aix-Marseille University, that catalogues most of the molluscs found in the butte Iouton have been also consulted.

The chronostratigraphic framework of the butte Iouton limestones has been therefore established using: (1) characean gyrogonites and (2) key molluscan taxa with significant stratigraphic value.

3.3.3. Carbon and oxygen stable isotopes

A total of 58 powdered samples (average spacing = 50 cm) were extracted from the limestones using a Dremel micro-drill tool. Bulk-rock stable carbon and oxygen isotope analyses were performed at the GeoZentrum Nordbayern department, Friedrich-Alexander-Universität Erlangen-Nürnberg (Germany) in order to detect potential diagenetic overprints (e.g. pedogenesis at exposure surfaces) and/or to provide insights into lake paleohydrology. The analysis technique employed consists in the reaction of the powders with 100% phosphoric acid at 70°C using a Gasbench II connected to a Thermo Fisher Scientific DELTA V Plus mass spectrometer. All values are reported in per mil relative to V-PDB. Reproducibility and accuracy were monitored by replicate analysis of laboratory standards calibrated by assigning $\delta^{13}C$ values of +1.95‰ to NBS19 and -47.3‰ to IAEA-CO9 and $\delta^{18}O$ values of -2.20‰ to NBS19 and -23.2‰ to NBS18. Reproducibility for $\delta^{13}C$ and $\delta^{18}O$ was ±0.04 and ±0.03 (1 standard deviation), respectively.

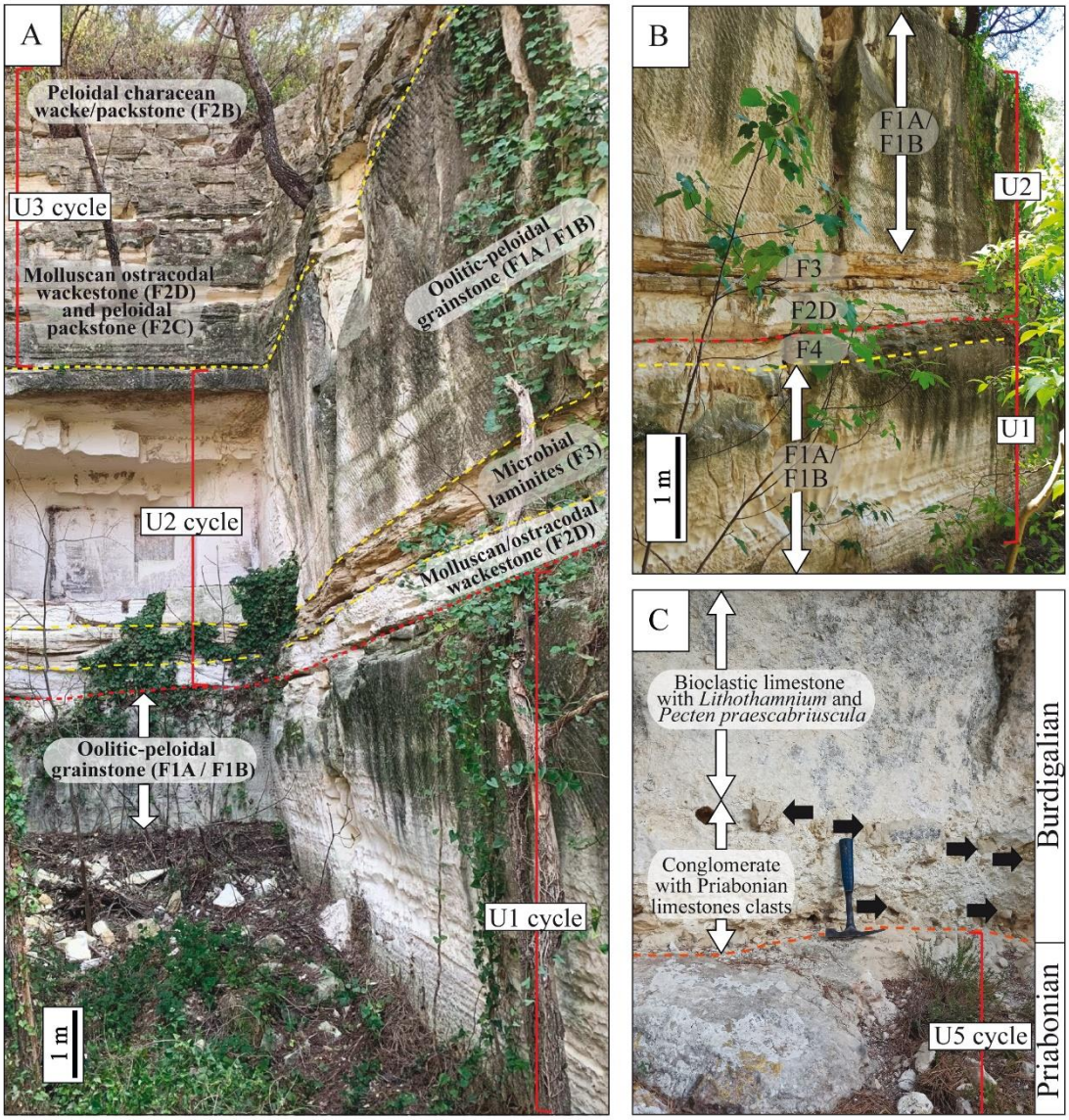

Figure 3.3: Field photographs from the Butte Iouton quarry. A) Stratal succession from U1 to U3 cycles showing the thick and horizontally layered oolitic-peloidal grainstone beds. B) Close view on stratal succession from U1 and U2 cycles C) Erosional contact between Priabonian lacustrine oolitic grainstones and overlying Burdigalian bioclastic limeston.es. Priabonian limestone clasts are reworked within the Burdigalian deposits (black arrows).

3.4. Results and interpretations

3.4.1. Biostratigraphy

The Butte Iouton quarry yields two taxa from the genus *Gyrogona* and some specimens are catalogued in the collections of the University of Montpellier under the number CF.3088.

a. *Gyrogona caelata* Ried and Groves, 1921 **(Fig. 3.4A)**

This species is largely dominant in the charophyte assemblage. The general morphology as well as the dimensions of the examined samples are consistent with the definition given by Grambast and Grambast-Fessard (1981). *G. caelata* is widespread in the European area and

occurs within the charophytes biozones ranging from *Maedleriella embergeri* zone to *Stephanochara vectensis* zone (Riveline et al., 1996). These biozones encompass the upper Lutetian – Priabonian interval.

b. *Gyrogona* aff. *lemani capitata* Grambast and Grambast-Fressard, 1981 (**Fig. 3.4B**)

This species is uncommon in the butte Iouton deposit and only a couple of specimens have been identified. The specimens meet the morphological criteria given by Grambast and Grambast-Fessard (1981) although their dimensions are found to be slightly smaller. This taxon is reported from many areas in Western Europe, such as the Paris Basin, Campbon Basin (southern Brittany), Upper Rhine Basin (Bouxwiller site) and southwestern Languedoc (Causse-et-Veyran site) (Riveline, 1986). *G. lemani capitata* appears, together with the whole species of the genus *Gyrogona*, within the *Maedleriella embergeri* biozone and has a lesser range than *G. caelata* (Riveline et al., 1996). The former extends only up to the *Psilochara repanda* biozone, thus suggesting an age ranging from the Lutetian to the upper Bartonian. The difference in dimensions with the holotype raises uncertainties about the taxonomic attribution of the two specimens to *G. lemani capitata*, hence the insertion of the complement aff. (*species affinis*). The insufficient amount of material makes it difficult any attempt to define a new species. Because of such a taxonomic uncertainty, these two specimens were not considered for constraining biostratigraphic ages.

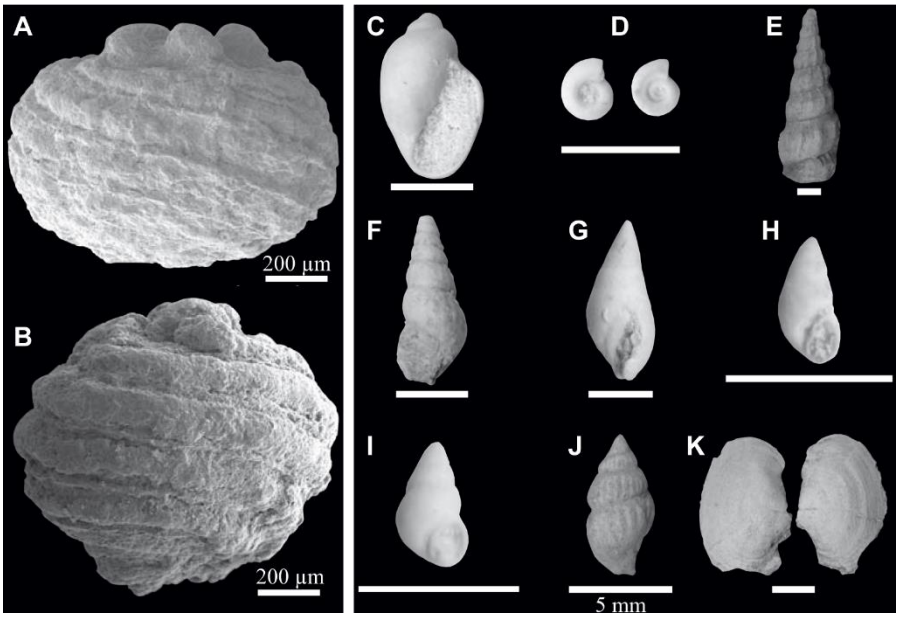

Figure 3.4: Charophyte gyrogonites and key gastropods and bivalves from the butte Iouton limestones. A-B: SEM photographs of characean gyrogonites from the lowermost characean-rich microbial laminites. A: *Gyrogona caelata* (Reid and Groves, 1921), lateral view. B: *Gyrogona* aff. *lemani capitata* (Grambast and Grambast-Fessard, 1981) lateral view. C-K: Common molluscan taxa. C) *Lymnea Ioutensis* (Roman, 1910). D) *Planorbis stenocyclotus* (Fontannes, 1884). E) *Brotia Albigensis* (Noulet, 1854). F) *Tarebia barjacensis* (Fontannes, 1884). G) *Melanopsis acrolepta* (Fontannes,1884). H) *Hydrobia celasensis* (Fontannes, 1884). I) *Assiminea nicolasi* (Roman, 1910). J) *Nystia plicata* (d'Archiac & Verneuil, 1855). K) *Polymesoda dumasi* (M. de Serres, 1827). Scale bar is 5 mm.

The molluscan taxa identified on the butte Iouton outcrops are illustrated in **Figure 3.4** and fall within the list of taxa compiled by Roman (1910) (**Fig. 3.4C-K**). Out of a total of the 30 molluscan taxa described by the same author in this site, 15 species are also documented from the molluscan associations of the middle to upper Priabonian successions from the Alès and Issirac basins (Fontannes, 1884; Lettéron et al., 2017). Among the mollusc taxa of the butte Iouton, some fossils are considered to have a reliable regional stratigraphic value and are therefore used as key-stratigraphic markers in continental settings (Cavelier et al., 1984; Fauré, 2007). For instance, *Nystia plicata* (d'Archiac & Verneuil, 1855) extends from the late Priabonian to the Rupelian while *Viviparus soricinensis* (Noulet) has a much wider range since it is known from middle Priabonian up to Rupelian deposits. However, the bivalve *Polymesoda dumasi* (M. de Serres, 1827) has a narrow range since it occurs only from the middle to upper Priabonian and has never been reported in the Oligocene successions. Along with the previously discussed stratigraphic implications of the charophyte flora, the molluscan assemblage especially the occurrence of the taxa *N. plicata* and *P. dumasi* provides strong evidence to assign a late Priabonian age to the Butte Iouton limestones.

3.4.2. Carbonate petrography and diagenetic features

Petrography and SEM observations of thin sections from the butte Iouton limestones help to identify five grain types, namely ooids, peloids, aggregate grains, reworked sparitic crusts and miscellaneous skeletal grains including molluscans (both bivalves and gastropods) and ostracods, and charophyte remains.

Ooids are the dominant grain type and are generally small, averaging 300 microns in diameter (medium sand) (**Fig. 3.5A, 3.6A-B**). These small ooids display various cortex fabrics: thin cortices are found in superficial ooids while radial fibrous or concentric micritic cortices define radiaxial (**Fig. 3.5A-B**) and micritized ooids (**Fig. 3.5C-D**) respectively. The ooids have either peloid, bioclast or fine quartz grain nuclei and show different stages of micritization obliterating the original microstructure. Other coated grains include coarse ooids and/or oncoids (=coated grains whose cortex is formed by cyanobacterial laminae) (**Fig. 3.6G**), their sizes range between 600 microns and may reach up to 2 mm and most of them display concentric laminae cortices. Peloids are frequent in the butte Iouton limestones and show various shapes and sizes (**Fig. 3.5A-6E-F**). Peloids are in general sub-rounded to elongated, range between 80 and 200 microns in size and display dark and homogeneous micritic internal structure. Aggregate grains from the butte Iouton section are very irregular in shape and are recognized based on the characteristic lobate to rounded outlines **(Fig. 3.6E)**. These aggregate grains have a wide range of sizes from 0.5 mm to several mm and the original separate grains may either be peloids or micritized ooids; their smooth outlines allow to consider them as lumps according to the description provided by Tucker and Wright (1990). Reworked sparitic crusts are flattened and are thin sheets formed by calcite crystals arranged side by side. The sparry crystals are equigranular, dogteeth shaped, and each is between 40 and 50 µm in size (**Fig. 3.7F**). Calcite crystals line up in one or more rows and this may reflect single or multiple generations of crystal

growth from an initial surface, possibly a microbial film and have been reworked and re-deposited without any particular orientation.

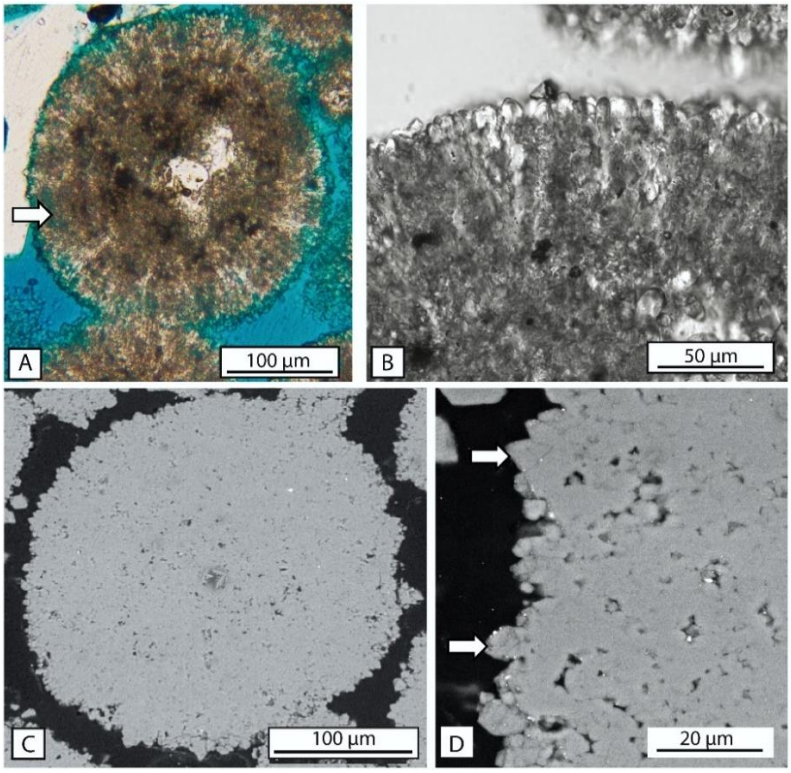

Figure 3.5: Microstructure of ooids. A) Thin-section microphotograph under polarized-light microscopy showing the variably preserved radiaxial microstructure within the cortex and the occurrence of micritized areas (arrows). The inner part of the ooid is pervasively micritized and the nucleus consists of a quartz grain. B) Detail of the radiaxial microstructure of ooid cortex under reflected-light microscopy. C) SEM photograph of a thin-sectionned micritized ooid showing the euhedral to subhedral micrite probably replacing the initially radiaxal microstructure and the presence of significant inter-crystalline microporosity. D) Close-up on the outer cortex of a micritized ooid under SEM showing microrhombic calcite overgrowths (arrow).

The molluscs from the butte Iouton limestones consist mainly of freshwater to oligo-mesohaline taxa. Gastropods and bivalves may be found in the form of entirely micritized calcitic shells (**Fig. 3.6E-F**) or recognized by their external moulds if they are completely dissolved especially in case of formerly aragonitic shells (**Fig. 3.7A**, **3.7D**, **3.7G-H**). Ostracods (**Fig. 3.7G**) and characean gyrogonites (**Fig. 3.8C**) are preserved owing to their original calcite mineralogy.

The main diagenetic processes observed are: a) compaction (ooids, shells, characean remains), b) micritization of molluscan shells and ooid cortices, c) selective mouldic dissolution of aragonite grains (mainly molluscs), d) cementation (calcite spar: **Fig. 3.8E**), e) pedogenesis (soil formation, brecciation), and f) calcite pseudomorphs after gypsum (**Fig. 3.8E**).

Petrographic observations show preferential dissolution of the aragonite shells of molluscs and the preservation of the ooids cortices that may point to different original mineralogies of these grains, while some samples display strong micritization of both molluscan shells and ooids. The original mineralogy of the ooids is difficult to establish since both radiaxial and

micritized layers can coexist and since petrographic observations show evidences of severe neomorphic processes. The mineralogy of ooids and their fabric, in particular those formed in freshwater and extreme environments is still a matter of debate (e.g. Kahle, 1974; Sandberg, 1975, 1980; Swirydczuk and Wilkinson, 1979).

3.4.3. Depositional facies and paleoenvironmental interpretations

Based on depositional texture (Dunham classification), sedimentary structures, biotic composition, and the petrographic character of the allochems, nine depositional facies have been defined and summarized in **Table 3.1**.

F1A. Oolitic-peloidal grainstone

This facies consists of moderately to well-sorted grainstones composed of a mixture of ooids and peloids in variable proportions: ooids (~ 300 microns in size) are dominant and their proportion ranges from 50% (bimodal distribution) to 95% (unimodal distribution) (**Fig. 3.6A-B**). Some ooids exhibit superficial and radiaxial internal structures of their cortices although most of them are strongly micritized. The peloids are predominantly small and have different morphologies, their dimensions range between 100 and 200 microns; other allochems include few aggregate grains (<1%). Molluscan shells and fragments can accumulate in the form of fossiliferous gravelly lenses interbedded with the ooidal-peloidal sand levels (**Fig. 3.6C**). The gravelly lenses are about 10 cm thick and few metres wide, and most of the fossils are complete or slightly broken. The molluscan assemblage is dominated by *Melanopsis*,*Tarebia* and *Neritina*Together with the peloidal grainstones (see description hereinafter), the oolitic-peloidal grainstones form subhorizontal beds with thicknesses varying from 2 m to 3 m (**Fig. 3.3B-3.6C**). Cross-stratifications are seldom visible on outcrop and when observed (e.g. **Fig. 3.6D**) they may form 10-50 cm height sets that are bounded at base and top by planar nearly horizontal surfaces (“planar cross-stratifications”). The scarce apparent paleocurrent directions measured on the quarry faces are toward the south-west.

Interpretation: The moderately to good sorting of these grainstones and the winnowing of the micrite suggest high energy depositional conditions. Though seldom observable, the occurrence of planar cross-stratifications within the oolitic beds may reflect sandwaves or dunes migration related to high energy currents (Dalrymple, 1992). Ooids are generally produced in shallow nearshore shoals subject to high hydrodynamic conditions and form very well sorted sediments. Thus, the mixture of ooids and peloids in F1A facies suggests deposition in the vicinity of these shoals where ooids are remobilized by waves and currents. In lacustrine environments, well sorted oolitic sediments are essentially reported from shallow lake margin shoreface (e.g. Williamson and Picard, 1974; Tänavsuu-Milkeviciene et al., 2017; Gallois et al., 2018; Deschamps et al., 2020) and foreshore settings (Swirydczuk et al., 1980; Milroy and Wright, 2002). The relative scarcity of sedimentary structures in most oolitic beds may result from significant burrowing of a stable substrate in a low to moderate energy environment in backshoal setting as reported from shallow marine environments (Pomar et al., 2015).

Table 3.1: Facies classification of the Butte Iouton limestones: biological contents, sedimentary and diagenetic features, and their paleoenvironmental interpretations.

Code	Facies	Dominant biota	Sedimentary structures	Stratal pattern	Diagenetic features	Paleoenvironmental interpretation
F1A	Oolitic-peloidal grainstone	Gastropods: Melanopsis, *Tarebia*, *Neritina*	Seldom visible cross-up stratification. Good sorting (unimodal) to bimodal distribution	Massive, can form up to 2-3 metres thick units with peloidal rich grainstones (F1B).	- Micritization of shells and ooids cortices -Intragranular microporosity development - Microrhombic micrite overgrowths -Minor compaction features at grain contact	Moderate to high energy, shallow, oligo-mesohaline, perennial lake environments, at the vicinity of oolitic shoals.
F1B	Peloidal grainstone	Gastropods: Melanopsis, *Tarebia*, *Neritina*.	Seldom visible cross-stratifications. Bimodal distribution of the grains.	Massive, can form up to 2-3 metres thick units with oolitic-rich grainstones (F1A)	- Micritization of shells and ooids cortices -Intragranular microporosity development -Minor compaction features at grain contact	Moderate energy, shallow, oligo-mesohaline, perennial lake environments, in backshoal setting.
F1C	Oncoidal-ooidal-peloidal grainstone	Scarce gastropods	Gravel lenses of coarse-sized grains	Centimetre-thick strata	- Micritization of shells and ooids cortices -Intragranular microporosity development -Minor compaction features at grain contact	Moderate to high energy, shallow, oligo-mesohaline, perennial lake environments.
F2A	Mollusk-rich peloidal packstone-grainstone	Bivalves (*Polymesoda*), gastropods (Hydrobids, *Tarebia*), ostracods, scarce charophytes	Structureless	Few centimetres to decimetre tabular beds	- Microsparry and sparry calcite cements - dissolution of molluscan shells	Shallow, oligo-mesohaline lake with low to moderate water energy.

F2B	Characean-rich peloidal wackestone-packstone	Characean gyrogonites and stems, ostracods, mollusks (*Polymesoda*, *Tarebia*, hydrobids)	Structureless	Centimeter-thick tabular to nearly horizontal beds forming up to 4 m thick set of platelets limestones	- Dissolution of aragonitic shells -Microsparry to sparry calcite cements in molds	Shallow, perennial oligo-mesohaline lake with Characean meadows
F2C	Peloidal wackestone to packstone with calcitic rafts	Bivalves (*Polymesoda*), gastropods (*Tarebia*)	Structureless	Decimetre tabular beds	- Dissolution of aragonitic shells	Shallow, perennial oligo-mesohaline lake, within or at vicinity of unpreserved macrophyte meadows
F2D	Molluscan-ostracodal wackestone	Ostracods, gastropods (*Lymnaea*, *Viviparus*, *Planorbis*, *Tarebia*)	Inhomogeneous micrite, burrowing and bioturbation	Decimetre tabular beds to metre beds	- Dissolution of aragonitic shells	Low energy, shallow freshwater to oligohaline pools and sheltered areas of the lake margin.
F3	Planar-laminated bindstone	Characean gyrogonites and stems, ostracods, gastropods (mainly *Melanopsis*)	Alternation of subhorizontal to wavy and crinkled millimeter-thick micritic and microsparitic laminae	Up to 2 m-thick intervals of massive to platy limestones	- Dissolution of aragonitic shells -Microsparry to sparry calcite cements in molds	Low energy, very shallow freshwater to oligohaline lake margin.
F4	Carbonate breccia with pseudo-morphs after gypsum	No preserved biota	Structureless	Decimetre thick tightly cemented and irregularly bedded limestone. Gradual transition with underlying oolitic grainstone	- Circumgranular cracks -Dissolution vug and conduits formations - Root traces - Intrasediment growth of microlenticular gypsum - Calcite pseudomorphs after gypsum - Sparry calcite cements	Paleosoil in evaporitic setting

The molluscan-rich gravelly lenses are also indicative of moderate to high energy at least intermittently to make fossil accumulations possible. Gastropod *Tarebia* is known to thrive preferentially in oligo-mesohaline waters (e.g. Plaziat and Younis, 2005; Esu and Girotti, 2010; Miranda et al., 2010) while *Melanopsis* is mostly indicative of freshwater to oligohaline settings (Velasco et al., 2006). Plaziat and Younis (2005) found that smooth morphologies of *Melanopsis*, such as evidenced in Butte Iouton specimens, prefer brackish-water environments. The oolitic-peloidal grainstones and gravelly lenses are therefore interpreted to form within and/or at the vicinity of shallow nearshore oolitic shoals, in low to moderate salinity (from oligo- to mesohaline) and moderate to intermittently high energy waters.

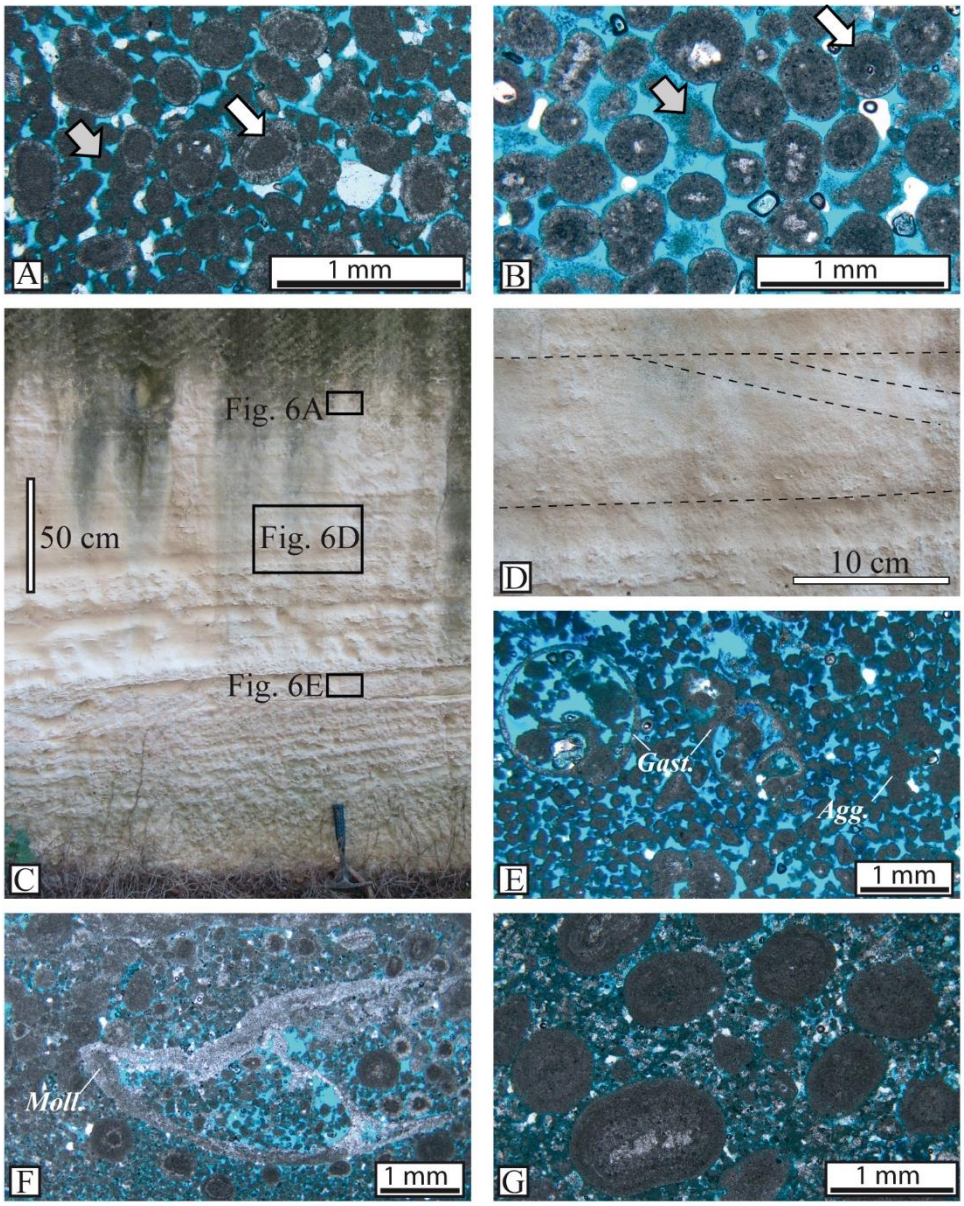

Figure 3.6: Oolitic-peloidal and peloidal grainstones facies (F1). A-B-E-F-G) Thin section microphotographs under plane polarized light; C-D: Field photographs. A) Oolitic-peloidal grainstone (Facies F1A) showing a mixture of ooids (white arrow) and peloids (grey arrow). Note the bimodal distribution of grains: the medium-sized grains include superficial, radiaxial and strongly micritized ooids while the peloids are the finer (around 0.1 – 0.2 mm size) and structureless grains. The nuclei of the ooids are essentially made of peloids. B) Well-sorted

oolitic-peloidal grainstone displays abundant radiaxial ooids (white arrow) and few peloids (grey arrow). The nuclei of the ooids consist of quartz grains or bioclasts. Note the high amount of intergranular porosity and the almost lack of compaction features. C) Field photograph of the southern face of the quarry showing a massive bed of oolitic peloidal grainstones with decimetre-thick, gravelly fossiliferous lenses. Cross-stratifications are seldom visible (see Fig. 3.6D). D) Close-up view of sub-planar cross-stratification from the oolitic-peloidal grainstones indicated by the dotted lines. The cross-beddings heights range between 10 and 50 cm. E) Peloidal grainstones with scattered molluscs (F1B facies) displaying slightly elongated peloids, micritized molluscan shells (mainly gastropods: *Gast.*) and few aggregate grains (*Agg*.). F) Oncoidal-ooidal rich peloidal grainstones (F1C facies) are poorly sorted sands consisting of a mixture of peloids and coarse grains (coated grains and molluscans). Note the strong micritization of the molluscan shells (*Moll.*). G) F1C facies displays bimodal distribution made of millimetric coated grains (ooids and/or oncoids) floating in a peloidal sand matrix: F1C facies occurs generally within few centimetres thick lenses.

F1B: Peloidal grainstone with scattered molluscs

F1B facies consists of a moderately to well-sorted grainstones composed mainly of peloids with proportions ranging between 75% and 90% and molluscan shells (<20%) with few aggregate grains and ooids (**Fig. 3.6E**). The peloids occur in a wide range of morphologies and are between 0.05 and 0.2 mm in size. The aggregate grains (**Fig. 3.6E**) are large with dimensions comprised between 0.5 mm and few millimetres and are often lumps formed by peloids and few micritized ooids bound together by microbial cement. Gastropods are the dominant organisms found in these facies and their association is similar to that described previously from the oolitic-peloidal grainstones, among others *Melanopsis* and *Tarebia*: the shells are found to be entirely micritized. Together with the previously described oolitic-peloidal sands (F1A) and the gravelly fossiliferous lenses, these peloidal grainstones are organized into massive (2-3 m thick) and subhorizontal, structureless beds.

Interpretation: Like in the F1A facies, the lack of mud matrix and the good sorting of the grains suggest that F1B facies are deposited in moderate to high energy settings. In addition, the occurrence of F1B facies together with F1A facies and the presence of minor proportion of ooids in the peloidal sands strongly indicate nearby depositional environments. The good sorting and the low variation in shape of peloids suggest they are likely to be mostly produced by organisms (i.e., faecal pellets) like gastropods and ostracods. Molluscan-rich accumulations probably result from transportation and deposition of molluscan shells during higher energy episodes. Similarly to F1A, the molluscan assemblage indicates oligo-mesohaline shallow waters probably of less than 10 m in depth (e.g. Lettéron et al., 2017 and references therein). Furthermore, the absence of subaerial exposure features within these facies indicates perennial lake conditions. Consequently, F1B facies is interpreted to form in the shallow parts of a perennial lake close to the oolitic shoals with moderate to high energy levels.

F1C: Oncoidal-ooidal rich peloidal grainstone

F1C facies is a peloidal grainstone comprising large proportions of oncoids and coarse ooids, and molluscan shells (**Fig. 3.6F-G**). This facies has been only encountered within centimetre to few centimetres thick lenses, interbedded within F1B peloidal grainstones at top of U2 and in

U4 cycle. Peloids are predominant (50%) and the coated grains (20-40%) consist either of coarse ooids (~ 600-900 microns) or oncoids (up to 2 mm in size), their grain distribution exhibits floating coarse grains in a peloidal matrix. The molluscan shells are less frequent and are strongly micritized.

Interpretation: The scarcity of mud matrix in these grainstones indicates at least intermittent water turbulence allowing the winnowing of fines. In addition, the poor sorting and the presence of coarse coated grains reflect sporadic high energy events such as fluvial floods. The peloids from F1C facies resemble those of F1B facies in which they are intercalated, and therefore may form in the same perennial shallow lake settings with moderate to high water energy. Oncoid-rich grainstones have been found to form as a result of fluvial overbank in lacustrine and floodplain environments (Schäfer and Stapf, 1978; Arenas et al., 2007; Lettéron et al., 2018), but are also common along the shoreline of various modern and ancient lakes (e.g. Plio-Pleistocene from Lake Turkana: Hargrave et al., 2014; Nutz et al., 2020; Lake Geneva: Davaud and Girardclos, 2001). Therefore, the F1C facies is interpreted to form in a shallow nearshore environment of a perennial lake, similar to that of F1B depositional environments, the oncoids perhaps deriving from the shoreline or from a nearby mouth of an oncoid-producing river.

F2A: Molluscan-rich peloidal packstone-grainstone

This facies consists of limestones containing large amounts of small peloids mixed with frequent molluscs, few ostracods and scarce small ooids set in micrite to microspar matrix (**Fig. 3.7A-7D**). The peloids are densely packed, irregular in shape and are very small (80-200 microns in size). The molluscan shells are dissolved, and the organisms are identified only from their external moulds, the biological association comprises mainly *Polymesoda*, *Hydrobia and Tarebia* (**Fig. 3.7B**). These peloidal-dominated packstones are found in the form of decimetre thick beds and are devoid of sedimentary structures (**Fig. 3.7C**).

Interpretation: The occurrence but relative scarcity of micrite matrix suggests relatively calm environments but with transient periods of higher energy. The abundance of peloids in the matrix and their regular shape and comparable size (50-100 µm) may be interpreted as faecal pellets and likely results from the presence of abundant molluscan and crustacean cummunities. The molluscan assemblage dominated by *Polymesoda* and *Hydrobia* and *Tarebia* is indicative of warm, shallow and oligo-mesohaline waters (Daley, 1972; Morton, 1983, Fretter and Graham, 1978, Lettéron et al., 2017). Extant *Polymesoda* bivalves are found in a variety of variable salinity shallow environments (Reichenbacher et al. 2004; Harris et al., 2015) and their optimal depth is lower than 1 m (Tabb and Moore, 1971) even though these may be found at depths of 10 m (Morton, 1983; Lettéron et al., 2017). *Polymesoda* are found both valves connected thus indicating deposition in their living environment. Extant *Hydrobia acuta neglecta* are found in coastal lagoons where salinity ranges between 10 and 24‰ (Fretter and Graham, 1978). Thus, the biological community of F2A facies, particularly through the presence of *Hydrobia*, exhibits the greatest tolerance to salinity elevation compared to the

freshwater to oligo-mesohaline gastropods and charophytes found in the overlying and underlying levels (F2B and F2D facies, see descriptive sections hereinfater). The lack of subaerial exposure features indicates deposition in perennial waters. The facies F2A is therefore interpreted to form in shallow, warm, and brackish lake with low to moderate water energy.

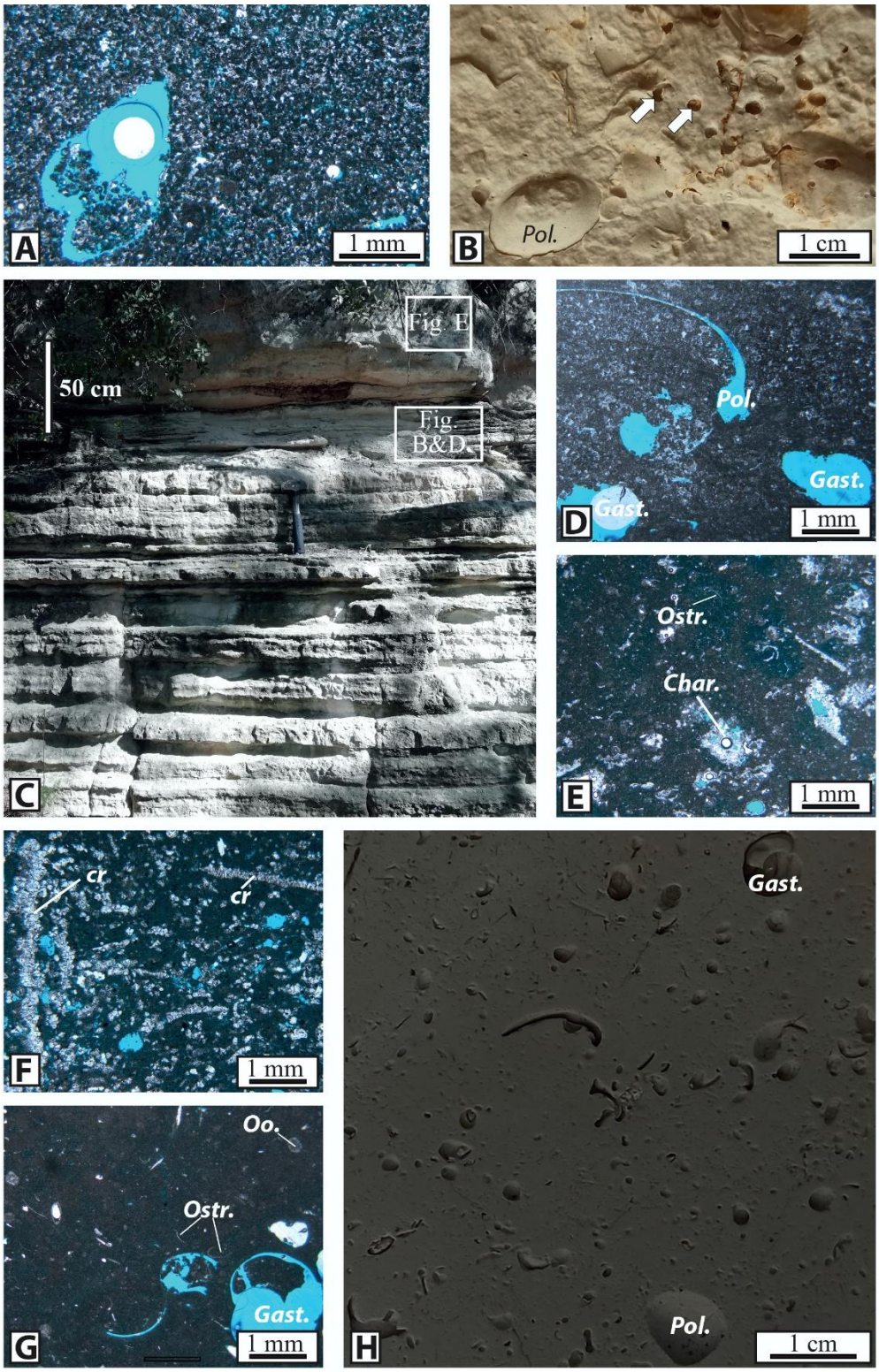

Figure 3.7: Mud-dominated facies F2. A) Molluscan-rich peloidal packstones (F2A facies) The thin section shows dissolution of a gastropod and the abundance of microspar cement (PPL: plane polarized). B) Hand sample

image showing the accumulation of molluscs in the facies F2A. The molluscan assemblage is dominated by *Polymesoda sp.* (*Pol.*) and small hydrobids (white arrow). C) Outcrop photograph showing the decimetre thick tabular beds of the mud-dominated facies (F2). D) Thin section of the facies F2A exhibits a mould after *Polymesoda sp. (Pol.)* in the upper quarters of the picture and small gastropod moulds (*Gast.*) in the lower left and right-hand quarters and abundant microspar cementation (PPL). E) Thin section of Characean-rich peloidal wackestone to packstone (F2B facies) displaying abundant characean cortical cells and stems (*Char.*) and ostracods (*Ostr.*). The matrix is made of densely packed peloids. F) Peloidal wackestone to packstones with reworked calcitic rafts (*cr*) (F2C facies). G) Thin section (under PPL) of the facies F2D showing abundant ostracods (*Ostr.*), molds of gastropods (*Gast.*) and (reworked?) ooids (*Oo.*). The micrite is inhomogeneous suggesting burrowing and bioturbation. H) Hand sample image displaying molluscan-rich ostracod wackestone (F2D facies): the molluscan shells are preserved as moulds. The assemblage is dominated by gastropods (*Gast.*) and by the bivalve *Polymesoda* (*Pol.*).

F2B: Characean-rich peloidal wackestone to packstone

This facies consists of a mixture of densely packed peloids of very small size (50 - 100 microns) with frequent characean cortical cells, stems and gyrogonites, and numerous ostracods, occasional molluscs and few ooids (**Fig. 3.7C-3.7E**). The charophytes remains are preserved and are slightly compacted. Molluscan shells are either entirely leached or completely micritized and their association is dominated by *Polymesoda, Tarebia* and hydrobids. F2B facies occurs in several centimetres to decimetre thick tabular to nearly horizontal beds and form together with F2A peloidal packstones an approximately 4 m high package of platelets limestones (**Fig. 3.7C**).

Interpretation: The mud-supported texture results from the trapping of micrite and peloids and indicates low water energy which limits the winnowing of fine particles. The abundance of characean remains reflects the development of macrophyte meadows in shallow lake margin environments which act like a natural barrier against hydrodynamic energy. Charophytes colonize lacustrine substrates and may cover large areas but are limited by light penetration and their maximum depth does not exceed 12 m (Garcia, 1994; Garcia and Chivas, 2006) thus supporting the shallow water column during the deposition of the F2B facies. Charophytes thrive in freshwater lakes, but some taxa tolerate brackish waters and withstand changes in salinity (Garcia, 1994; Van Den Berg et al., 1998, Lettéron et al., 2017). In addition, the molluscan assemblages found in these wackestones indicate warm, shallow and fresh to oligo-mesohaline waters. Finally, the F2B facies reflects deposition within calcifying and non-calcifying charophyte meadows in shallow, freshwater to oligo-mesohaline lake settings.

F2C: Peloidal wackestone to packstone with calcitic rafts

This facies occurs in decimetre tabular beds formed by densely packed peloids similar to those from facies F2A and F2B and comprises various proportions of crystalline flakes (calcitic rafts), few ostracods and scarce small gastropods and ooids (**Fig. 3.7F**). The peloids are very small (120-200 microns in size) and may be of faecal origin. Calcite rafts, described early as reworked sparitic crusts, are fragmented into pieces of various size (0.1 to 5 mm) or even as individual spar crystal. Gastropod shells are entirely leached. Faunal content is poor and

molluscan assemblage is dominated by *Polymesoda* and *Tarebia*. These facies are found close to the F2A and F2B tabular beds and arranged together within the platelets limestones package.

Interpretation: The abundance of mud matrix in these facies suggests deposition in low-energy areas. However, the breakage of the calcite rafts and the abundance of peloids indicate intermittent hydrodynamic conditions. Features resembling those crystalline flakes are documented in the literature and many hypotheses have been considered to explain their origin. Many authors described these structures in various depositional settings and referred to them as calcite rafts, paper thin rafts and floating mats (see review in Lettéron et al., 2018 and references therein). The abundance of peloids may indicate abundant gastropods and crustacean communities. The presence of small gastropods is indicative of shallow lake conditions probably of less than 10 m while the molluscan assemblage is indicative of brackish water environments. The close occurrence of this facies with F2A and F2B facies indicate nearby depositional settings. Therefore, the peloidal wackestones to packstones with calcite rafts facies reflect deposition in calm waters, supersaturated for $CaCO_3$ at the water-air interface (calcite rafts), with intermittent moderate water energy in the shallow sheltered areas of the lake in the vicinity of non-calcifying macrophyte meadows.

F2D: Molluscan-rich ostracod wackestone

This facies consists of limestones that contain sparse to loosely packed allochems including numerous ostracods and mollusc shells as well as few ooids and peloids (**Fig. 3.7G-H**). These wackestones occur in beds of several centimetres to few tens of centimetres (**Fig. 3.8A**). Ostracods are small (around 0.5 mm) and thin-shelled and their valves may be found either articulated or disarticulated. Gastropods are often leached but their complete external moulds allow easy identification (**Fig. 3.7G**). The molluscan assemblage is widely diversified, and the community comprises essentially terrestrial and freshwater to oligo-mesohaline water taxa, among them *Lymnea (Galba)*, *Planorbis*, *Tarebia*, *Viviparus and Polymesoda*.

Interpretation: The molluscan-rich ostracod wackestones are formed in low energy environments as suggested by the high micrite content of the facies. The matrix of these wackestones consists of inhomogeneous micrite and this likely results from ostracod burrowing and bioturbation. Burrowing and bioturbation indicate intense biological activity in very well oxygenated conditions. In addition, the molluscan assemblage, reflecting various ranges of salinity mostly freshwater for *Lymnea*, *Planorbis* and *Viviparus* and oligo-mesohaline for *Polymesoda*, indicates shallow and variable salinity settings, potentially marginal pools close to emerged wetlands or a saline lake margin at the vicinity of freshwater springs. Charophyte remains are not found thus excluding the development of calcifying meadows although non calcifying subaqueous prairies could have developed. The presence of significant amount of small ooids in F2D wackestones indicates the vicinity of oolitic bodies from which the ooids are sporadically exported into the sheltered areas. Moreover, these molluscan-rich ostracod wakestones are sharply overlain by high energy oolitic deposits (F1A) and this suggests lateral

migration of the oolitic sand bodies. Finally, F2D facies is interpreted to form in low energy and shallow freshwater to brackish pools and sheltered areas of the lake margin.

F3: Planar-laminated bindstones (microbial laminites)

Microbial laminites are made of an alternation of subhorizontal to wavy and crinkled dark clotted and peloidal micrite laminae (100 microns to 1 mm thick) and light thin laminae (0.5 to 1 mm) constituted of the accumulation of crushed charophyte stems and cortical cells with fine calcite spar cement (**Fig. 3.8B-C**). This facies exhibits a bindstone fabric (*sensu* Embry and Klovan, 1971) and is formed by micrite stabilization and binding of various skeletal grains including gastropod and ostracod shells as well as characean gyrogonites (**Fig. 3.8B-C**). The molluscan assemblage is dominated by the gastropod *Melanopsis acrolepta* the shells of which are entirely dissolved (**Fig. 3.8B**). The laminated bindstones show very little fenestral porosity and the presence of small-scale undulations and corrugations in the laminae may point to a microbial origin of the micrite. This facies occurs in centimetre tight beds and may form up to metre intervals of laminated limestones (**Fig. 3.8A**).

Interpretation: Planar laminated stromatolites from Tertiary basins of SE France are interpreted to form in very shallow water lacustrine environments that may experience occasional short-term emersions (e.g. Wattine et al., 2003; Lettéron et al., 2017). The shallow-water conditions prevailing for the deposition of facies F3 are supported by the abundance of characean gyrogonites and stems, and by the bathymetric range of the bound molluscs (*Melanopsis*). The presence of charophyte gyrogonites indicates colonization of the lake substrate by charophyte algae in the nearby areas and suggests freshwater to slightly brackish water conditions. While stromatolites are euryhaline and tolerate a wide range of salinities (e.g. Talbot and Allen, 1996), the biological content points to freshwater to oligohaline conditions. Extant *Melanopsis* are found to live in coastal streams and freshwater to oligohaline lake waters under Mediterranean and semi-arid climates (Plaziat and Younis, 2005; Velasco et al., 2006; Van Damme, 2014). In the Priabonian lacustrine deposits from the Issirac basin (SE France), planar stromatolites are interpreted to form in the shallowest parts of the lake margin while the charophytes are considered to thrive at depths comprised between 0.5 m and 10 m (Lettéron et al., 2017). However, it has been documented that the development of either photosynthetic (e.g. charophytes) or microbial communities is presumably driven by changes in trophic conditions regardless of the depositional depth (Lettéron, 2018). The microbial communities can adapt to trophic changes (oligotrophic conditions) as evidence by the trapping of characean gyrogonites by the microbial binding organisms, the charophyte meadows likely occupying the deeper areas of the lake. Finally, facies F3 is interpreted to form in very shallow lake conditions under freshwater to oligo-mesohaline conditions within perennial lake body.

F4. Carbonate breccia with pseudomorphs after gypsum

The facies F4 is found only in one bed (0.50 m) from the butte Iouton succession (**Fig. 3.8A**). It consists of a carbonate breccia displaying vertical changes in texture and diagenetic features.

The lower part of the bed is made of a fractured, tight oosparite whose ooids appear to be floating within sparry calcite pseudomorphs after gypsum (**Fig. 3.8F-G**). The mechanical contact between ooids argue for subsequent displacement of the grains in the initial grainstone sediment during the formation and growth of gypsum crystals. The upper part of the breccia interval is characterized by the occurrence of 1) Root traces and curved cracks (**Fig. 3.8D**) occluded by microsparite and sparite cements and 2) gypsum crystals, replaced by calcitic micrite, infilling cavities (**Fig. 3.7D-E**). These tight limestones have a total thickness of around 50 cm and are irregularly bedded and capped by an uneven surface. Furthermore, these brecciated limestones are overlain by an interval of few centimetres thick of mottled vivid red clays (**Fig. 3.8A**).

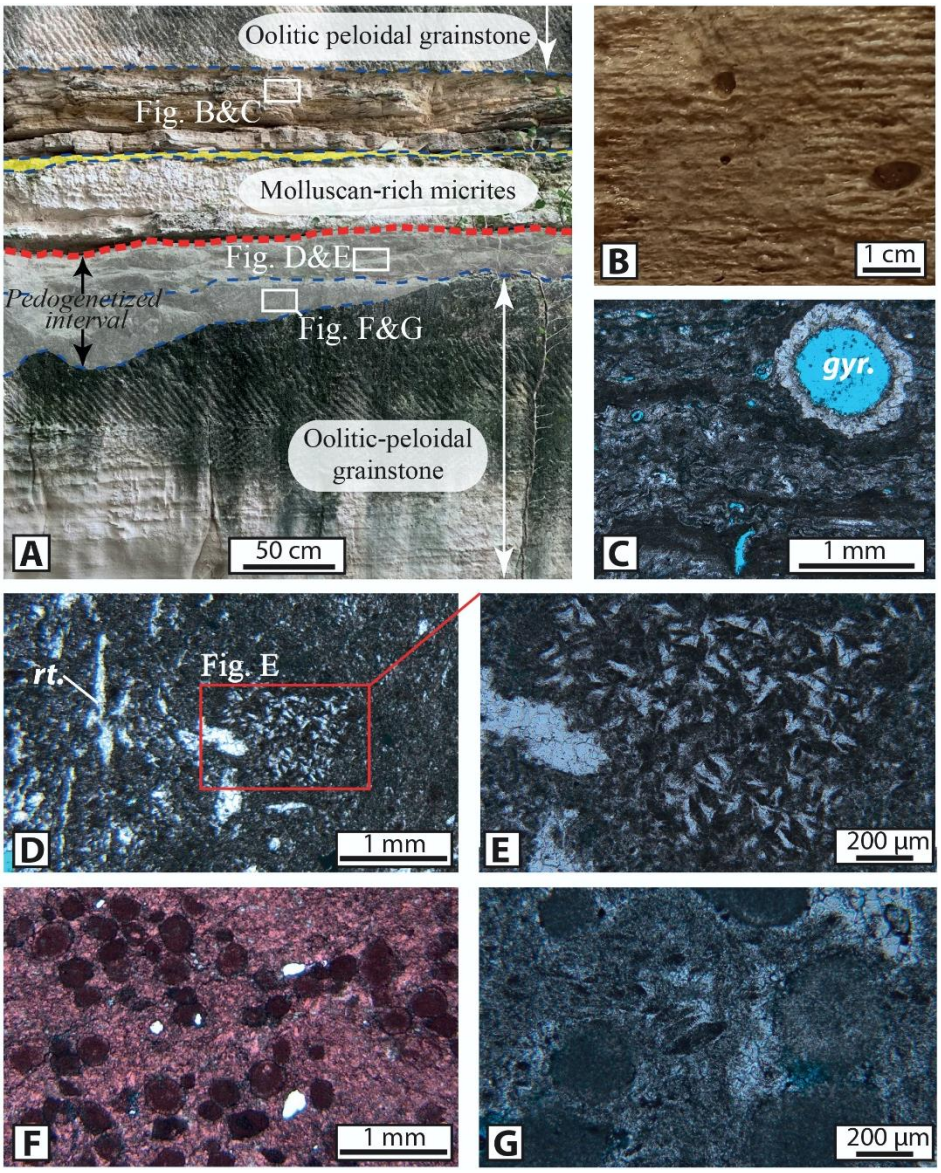

Figure 3.8: Planar-laminated bindstones (F3 facies) and pedogenic carbonate breccia (F4 facies). A) Field photograph of the southern face of the quarry displaying the vertical evolution from the oolitic peloidal grainstones (lower white double arrow) to the brecciated interval (dark double arrow). The red thick dashed line indicates a subaerial exposure surface, and the yellow interval indicates few centimetres-thick oolitic grainstone. The laminated bindstones occur in the upper part of the picture (see Fig. 3.8B and 3.8C). B) Close-up view of the

planar-laminated bindstone. Infra-centimetric pores are moulds after *Melanopsis* gastropod dissolution. C) Thin section under plane polarized light of F3 facies displaying alternations of dark (micrite) and light (accumulation of characean cortical cells fragments and calcite microspar) crinkled to wavy laminae, with characean gyrogonite (*gyr.*). D-E) Microphotographs under plane polarized light of brecciated limestones with pseudomorphs after gypsum. D) Thin section showing vertical and curved cracks (root trace: *rt*) filled with calcite. White box indicates a dissolution vug filled with calcitic pseudomorphs after gypsum. E) Close-up view of the box in B) showing relicts of the tabular to microlenticular gypsum and the replacing calcitic micrite to microspar. F) Thin section showing the intrasediment growth of gypsum within the oolitic-peloidal grainstone. The similarity in petrographic characters with the underlying F1B facies (see Fig. 3.8A) and the grain contact points to post-depositional gypsum growth after lake evaporation. The Alizarine Red staining in red colors indicates calcite mineralogy (plane polarized light). G) close-up view showing calcite pseudomorphs after gypsum that occupy the inter-ooidal space.

Interpretation: the development of curved cracks and root marks affecting the initial oolitic-peloidal grainstones (F1A facies) suggests pedogenic processes during a stage of subaerial exposition (Freytet and Plaziat, 1982; Alonso-Zarza, 2003). Grain displacement during gypsum growth indicate that sulfate precipitation occurred shortly after ooid deposition, before compaction. The presence of calcite pseudomorphs after gypsum would indicate hypersaline conditions within the paleosoil and the enrichment of water in sulphate solutes. Evaporative concentration of solutes and thereby gypsum formation necessarily reflect climate aridity and negative water inflow/evaporation. The F4 succession is therefore interpreted as representing a paleosoil horizon developed during a stage of saline lake drying.

3.4.4. Vertical evolution of facies

The Priabonian carbonate succession from the butte Iouton is approximately 30 m thick and is characterized by the dominance of oolitic and peloidal grainstone facies (F1 facies) organized in the form of massive, horizontally bedded intervals associated with fossiliferous muds (F2 facies) and stromatolite levels (F3 facies) found in the form of platelets limestones (**Fig. 3.3**). Four massive intervals of oolitic grainstones (F1A facies) and peloidal grainstones (F1B facies) have been identified in the sedimentary succession and have a maximum individual thickness of about 3 m. In addition, the succession records episodic high-energy sedimentation as indicated by the regular occurrence of thin gravelly lenses and coarse-sized sands (F1C facies). Such grain-supported massive intervals are interbedded within thinly-layered limestones of wackestone to packstone texture (Facies F2A, F2B, F2C and F2D) or microbial laminites (Facies F3). The alternation of wackestone-packstone and microbial laminites with massive grainstone intervals allows the definition of 5 depositional cycles, U1 to U5, despite large masked parts (**Fig. 3.2**). Within the butte Iouton quarry, the lowermost cycle U1 (3.30 m thick) overlies the lower Eocene variegated clays and silts and displays the transition from thinly layered molluscan-rich ostracod wackestones (F2D facies) to massively bedded peloidal grainstones (F1B facies) and oolitic-peloidal grainstones (F1A facies) with scarce planar cross-stratifications: the base of the massive bed is sharp and contains gravelly-sized fossil shells accumulations (**Fig. 3.3A-3.3B**). The oolitic interval is capped by a subaerial exposure surface as illustrated by the development of brecciated limestones (F4 facies) and overlying paleosol horizon (**Fig. 3.8A**).

Cycle U2 (4.50 m thick) starts with mud-supported facies (**Fig. 3.3A-3.3B**) dominated by freshwater to oligo-mesohaline molluscans (F2D facies) that pass upwards into oolitic grainstones deposits (F1A facies). Above the thin oolitic bed (**Fig. 3.7A**), a 50 cm thick interval of characean-rich laminated bindstones (F3 facies) is overlain by massively bedded peloidal and oolitic grainstones (F1A and F1B facies). These grainstones become coarser and gravelly toward the top and are capped by a thin interval of oncoidal-ooidal grainstone (F1C).

In cycle U3 (6.40 m thick) sediments are dominantly mud-supported (F2 facies) and organized into centimetre to decimeter–thick tabular strata (**Fig. 3.7C**). In the lowermost 2 metres, sedimentation is dominated by molluscan-rich ostracod wackestones (F2D facies) and molluscan-rich peloidal packstone (F2A facies) together with peloidal micrites with calcite rafts (F2C facies). The upper part of the cycle is dominated by the characean-rich peloidal wackestones and packstones (F2B) and molluscan-rich peloidal packstone (F1A). The top of the cycle displays incipient pedogenic modifications (root traces, circumgranular cracks).

The cycle U4 (6.40 m thick) shows at its base lacustrine stromatolites (F3 facies) that pass upwards into a decimetre thick oncoidal rich grainstones (F1C facies) that gives way to a massively bedded oolitic-peloidal grainstones (F1A facies). At the top, the cycle is capped by a sharp and smooth surface. The uppermost U5 cycle (10.40 m thick) begins with a molluscan-rich ostracodal wackestones containing *Viviparus soricensis* gastropods. After an observational gap of few metres, this cycle ends with a thick oolitic and peloidal grainstone interval that is truncated by an erosional surface. This unconformity separates the Priabonian limestones from the unconformably overlying transgressive marine Burdigalian limestones characterized by the coralline red algae *Lithothamnium sp* and marine bivalves *Pecten praescabriusculus* that rest on the basal conglomerates reworking Priabonian lacustrine limestones (**Fig. 3.3C**).

3.4.5. Carbon and oxygen stable isotopes

Prior to the analysis of the geochemical data of whole-rock bulk carbon and oxygen stable isotopes and to extract the primary geochemical signal, it is necessary to take into account the diagenetic overprints undergone by the investigated samples. Samples have been classified as a function of the diagenetic features evidenced from macroscopic, thin-section and SEM observations (**Table 3.A** in *Supplementary data*). Most of the analysed samples are devoid of sparry calcite cements. In addition, in grainstone intervals (F1 facies), ooids are pervasively micritized, display significant microporosity and microrhombic calcite overgrowths (**Fig. 3.5C-D**), while aragonitic shells are converted into calcitic micrite (**Fig. 3.6E-F**). Moderate amounts of calcite microspar cements are present in a few samples of F2A facies while brecciated limestones (F4 facies) have undergone pervasive pedogenesis and pervasive sparry calcite cementation or calcite pseudomorphosis after gypsum (**Fig. 3.8E-G**).

In the whole carbonate succession, samples which are devoid of sparry calcite cement and pedogenetic features exhibit negative values of $\delta^{18}O$ and $\delta^{13}C$ values ranging from -3.99‰ to -1.33‰ PDB and from -4.79‰ to -0.43‰ PDB, respectively (**Fig. 3.10A-B**).

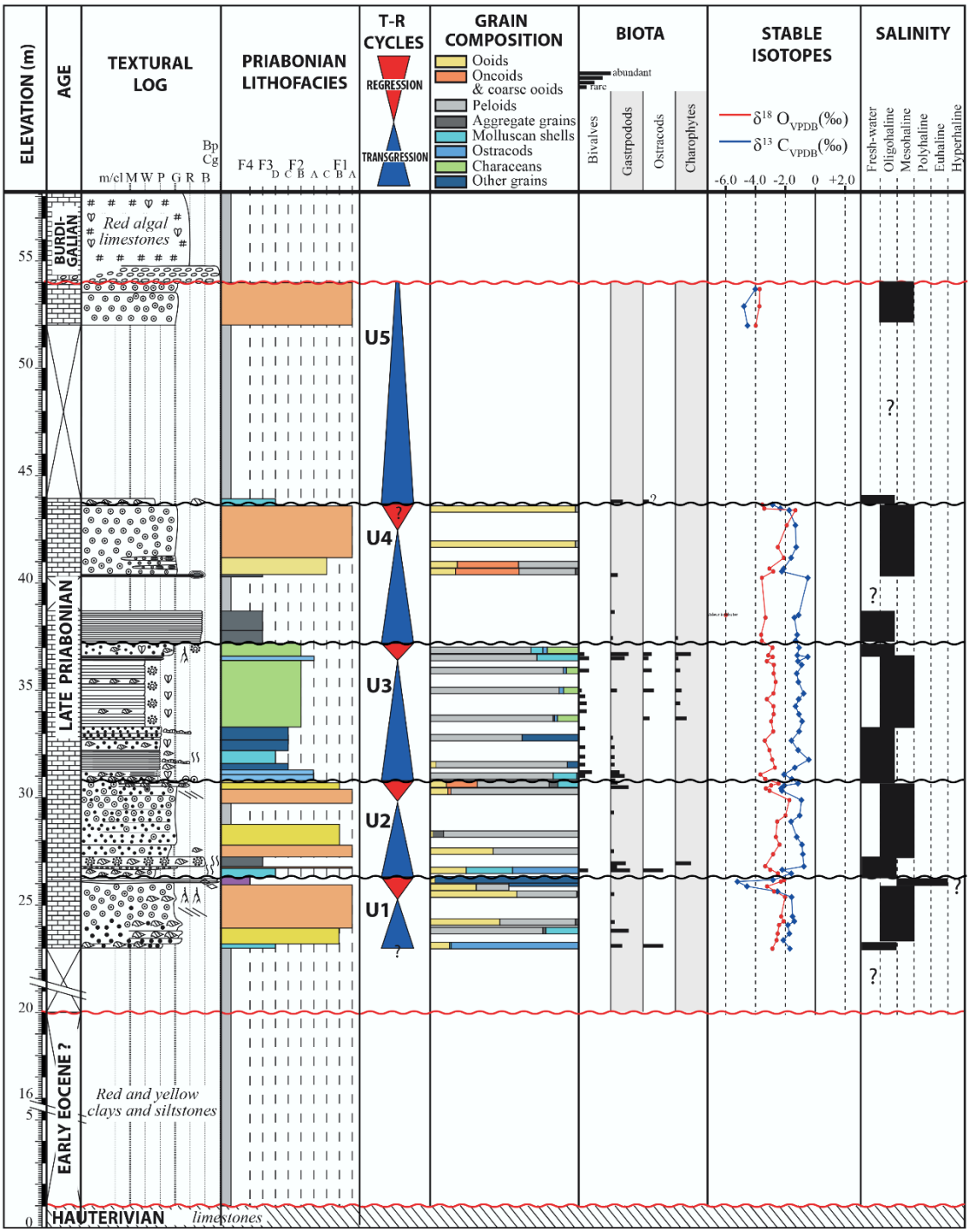

Figure 3.9: Composite log of the butte Iouton succession compiling the depositional textures, the lithofacies stacking pattern, the interpreted transgressive-regressive (T-R) cycles, carbonate grain composition of limestones after point-counting on thin-sections, the relative abundance of selected preserved biota, $\delta^{18}O$ and $\delta^{13}C$ vertical changes and estimated salinity domains. See Figure 3.2 for detailed legend.

Brecciated limestones (F4 facies), which are characterized by pedogenic features and sparry calcite cementation, are strongly ^{13}C-depleted. Grainstone samples (F1 facies) exhibit an inverted-J pattern on $\delta^{18}O$-$\delta^{13}C$ plots (**Fig. 3.10A**).

Measurements from cycle U1 display a very narrow range of $\delta^{13}C$ since values which oscillate between -2.54‰ and -1.40‰ PDB while $\delta^{18}O$ values exhibit a moderately increasing

trend, with values ranging from -2.87‰ to -2.02‰ PDB (**Fig. 3.10B**). At the top of U1, $\delta^{13}C$ is strongly negative with values down to -5.21‰ PDB. A poorly-expressed covariant trend exists between $\delta^{13}C$ and $\delta^{18}O$ within this cycle, especially in the oolitic-peloidal grainstones which corresponds to a part of the inverted-J trend.

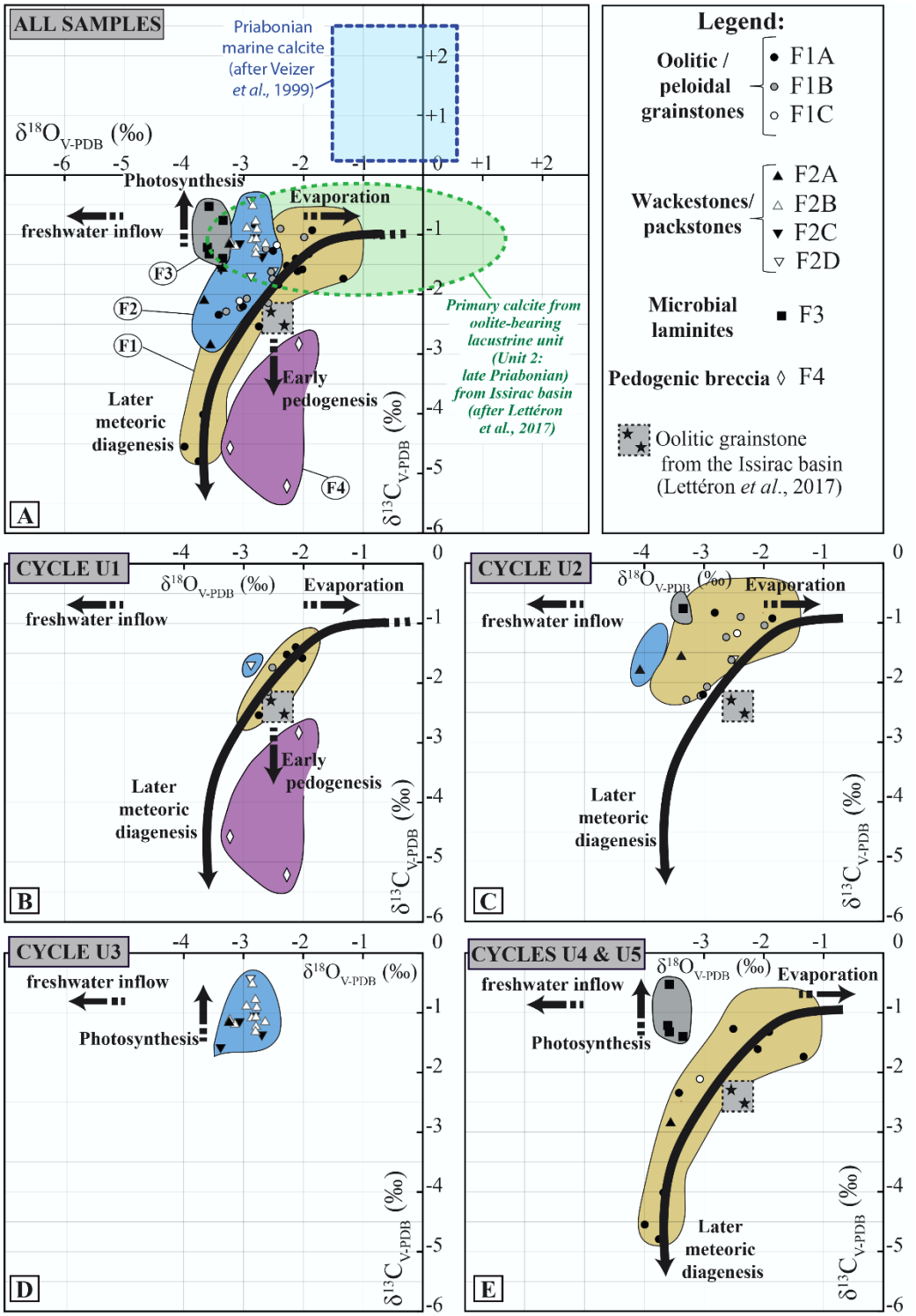

Figure 3.10: Carbone and oxygen stable isotopes results. A) $\delta^{18}O$ – $\delta^{13}C$ cross-plot for all samples (n = 58): the labels refer to the lithofacies (see text for further detail). The Priabonian marine box (Veizer et al., 1999), isotope signatures of lacustrines carbonates from the Issirac basin (Lettéron et al., 2017) as well as interpretations of factors

controlling $\delta^{18}O$ – $\delta^{13}C$ trends are reported. B-C-D) $\delta^{18}O$ – $\delta^{13}C$ cross-plot for cycles U1 (B), U2 (C), U3 (D) and U4-U5 (E) with samples labelled as a function of lithofacies. Isotope values are expressed in per mil (‰) and are relative to V-PDB.

In cycle U2, $\delta^{18}O$ and $\delta^{13}C$ signals have much wider ranges of values (-3.35‰ to -1.86‰ PDB and -2.29‰ to -0.76‰ PDB respectively) and grainstone samples (F1 facies) exhibit a covariant trend similar to that of U1 cycle (**Fig. 3.10C**). In the lower part of cycle U2, stromatolites exhibit the most ^{13}C-enriched and ^{18}O-depleted signatures of the available database. In cycle U3, $\delta^{18}O$ values display little variations and range between -3.66‰ and -2.64‰ PDB whereas $\delta^{13}C$ fluctuates considerably with values ranging from -2.09‰ to -0.43‰ PDB (**Fig. 3.10D**). Within cycles U4 and U5, samples exhibit wide ranges of $\delta^{18}O$ with values ranging from -3.99‰ to -1.33‰ PDB and $\delta^{13}C$ ranging from -4.79‰ to -0.53‰ PDB. Stromatolites (F3) forming the lower part of the cycle display depleted ^{18}O and enriched ^{13}C isotope signature.

3.5. Discussion

3.5.1. Depositional model for an oolitic saline lake margin

The analysis of carbonate microfacies, preserved biota, bedding patterns and sedimentary structures of individual lithofacies as well as the vertical succession of lithofacies enable the reconstruction of depositional models (**Fig. 3.11**) for further interpreting the vertical evolution of paleoenvironments and stages of transgression and regression of the paleolake.

Oolitic cycles (U1, U2, U4 and U5)

The lower intervals of the oolitic-peloidal cycles U1, U2, U4 and U5 are made of molluscan-rich ostracod wackestones (F2D) and laminated bindstones (F3). As suggested by microfacies analysis and preserved biota, such a facies association is indicative of a deposition in a very shallow, sub-emergent, low-energy, freshwater to oligo-mesohaline lake margin. The occurrence of scattered but well preserved ooids within the molluscan-ostracodal wackestones suggests that oolitic sediments formed coevally with the F2D-F3 low-energy lake margin association. In cycles U1, U2, U4 and U5, microbial laminites or molluscan-ostracodal wackestones are sharply overlain by oolitic-peloidal (F1A) or peloidal grainstones (F1B). The high degree of sorting in oolitic-peloidal grainstone, the lack of mud matrix and the occurrence of planar cross laminations suggest an increase in water energy compared with the underlying F2D and F3 facies. The planar cross-bedded oolitic grainstones (F1A) were likely deposited at the outer part of a lacustrine margin, in the vicinity of the main oolitic factory as supported by the dominant proportion of ooids. Indeed, the significant proportion of peloids as well as the variable degree of micritization of ooids suggest that the oolitic fraction of F1A is not produced in situ but likely derives from neighbouring, high-energy, oolitic shoals. Structureless oolitic-peloidal and peloidal grainstones (F1A-F1B) likely represent a slightly calmer area, possibly in back-shoal position. The structureless nature of such carbonate sand blankets has been interpreted, in shallow marine environments, as resulting from significant bioturbation of a

stable substrate in a low to moderate energy back-shoal environments (Pomar et al., 2015). Additionally, peloidal grainstones exhibit significant proportions of peloidal aggregates which are interpreted to form, in modern marine environments, in area with some water circulation allowing the winnowing of fines, followed by periods of stabilization (Wanless, 1981). Finally, the vertical facies transition recorded in cycles U1, U2, U4 and U5 suggests a lake transgression and a lacustrine carbonate ramp model (**Fig. 3.11**) displaying the following facies transition from proximal to distal areas: : 1) a shallow marginal saline lake domain with deposition of planar microbial laminites (F3), and molluscan-ostracodal wackestone (F2D), 2) a more distal and open lacustrine environments with low to moderate energy characterized by the deposition of peloidal grainstones (F1B) and 3) a domain of higher energy with accumulation of ooids mixed with peloids (F1A). The area of ooid production as well as more distal (profundal) components of this lacustrine depositional model have not been captured by the studied outcrops.

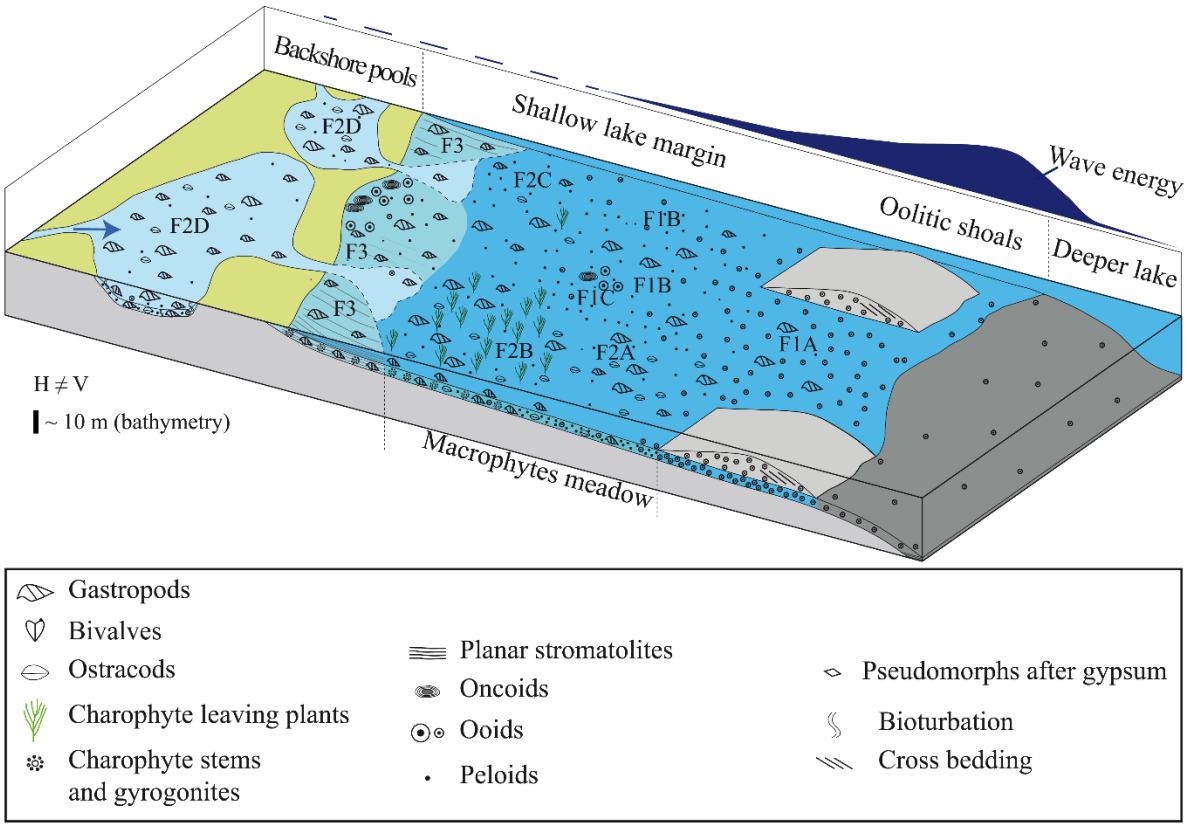

Figure 3.11: Depositional model for the late Priabonian saline lake margin from butte Iouton.

Carbonate ramp models with oolite sand body development in open, shallow lacustrine setting have been documented in modern and ancient lacustrine environments. In the modern Great Salt Lake, similarly to the Butte Iouton lake margin, muddy sediments occupy the coastal area of the lake while oolite sand bodies develop in more open lake setting (Eardley, 1938; Bouton et al., 2019). In the Eocene Green River Formation (Utah), shoreline and protected nearshore carbonate sedimentation is characterized by mud-supported sediments with ostracods, mollusks and ooids, while shallow open lake margin is occupied by oolitic shoals

(Williamson and Picard, 1974; Tänavsuu-Milkeviciene et al., 2017). In the Upper Cretaceous to Paleocene Yacoraite Formation (Argentina), a high gradient carbonate ramp model is proposed with ostracod-rich low energy eulittoral deposits protected by oolitic shoals (Deschamps et al., 2020). In the modern Lake Tanganyika, oolitic sand shoals dominate the open nearshore environment while inner and more protected area are characterized by charophyte-rich calcareous silts (Cohen and Thouin, 1987).

The Butte Iouton lake margin shows major differences with other published depositional models involving oolite formation. In the Pliocene Glenns Ferry Oolite (Swirydczuk et al., 1980), oolite sediments occupy both foreshore and shoreface environments and no mud-rich, low energy, carbonate deposits are documented from this lake margin. In the late Triassic Clevedon lake, shoreline deposits are dominated by oolitic beachrocks while trough cross-stratified oolitic grainstones characterize shoreface sedimentation (Milroy and Wright, 2002).

Mud-dominated cycle (U3)

Cycle U3 exhibits a distinct facies association since ooids are relatively uncommon and sediments have dominantly muddy textures. The lower part of the cycle is characterized by an alternation of molluscan-rich peloidal packstones (F2A), peloidal wackestones to packstones with calcitic rafts (F2C) and molluscan-rich ostracod wackestones (F2D).

Similarly to cycles U1, U2, U4 and U5, the occurrence of F2D wackestones is indicative of very shallow, low energy environments, in the most proximal area of the lake margin. The upper part of the cycle is dominated by F2B characean wackestone which likely represents a slightly deeper (<10 m), low-energy marginal lake environment.

Finally, the facies succession in cycle U3 suggests a shallow, protected, low energy lake margin with extensive development of macrophytes (including charophytes and non-calcifying taxa). The scarce occurrence of ooids within F2D facies suggests the coeval formation of oolitic sediment in more open area of the lake margin. However, the lack of oolitic grainstones indicates that the supersaturation with regards to carbonate minerals required for ooid formation and high energy conditions have been never reached at the outcrop location during the deposition of U3 cycle.

3.5.2. Stable isotope signatures and paleohydrological implications

As evidenced by Hasiuk et al. (2016) and as supported by petrographic evidences (microporosity and microrhombic calcite overgrowths within micritized ooids: **Fig. 3.5C-D**), the inverted-J pattern on δ18O-δ13C plots (**Fig. 3.10A**) evidenced for grainstones from the whole section, likely results from neomorphic processes leading to microporosity development in meteoric environments. According to such an interpretation the $\delta^{18}O$- and $\delta^{13}C$-enriched end-member would represent the less-altered samples and therefore would approximate the primary signature of carbonate grains (ooids and peloids), the ooidal and peloidal grainstone being devoid of carbonate cement. Furthermore, the end-member of least meteoric alteration for grainstone samples (F1) ranges from -2.5‰ to 1.0‰ PDB in δ18O and from -2.0‰ and -0.5‰

PDB in δ13C, which matches with primary signatures measured in late Priabonian ooid-bearing unit (Unit 2 in Letteron et al., 2017) from the Issirac basin (**Fig. 3.10A**). Carbon and oxygen isotope signatures for wackestone-packstones (F2) and microbial laminites (F3) are significantly 18O-depleted compared to the end-member of least meteoric alteration for grainstones (F1). The 18O-depletion of stromatolites likely results from significant freshwater inputs while the 18O-enriched values measured in F1 grainstones may reflect either more evaporative conditions, either mixture with neighbouring saline lake water as suggested by primary isotope signatures from the Issirac basin (**Fig. 3.10A**). The position of the Priabonian marine box (**Fig. 3.10A**, after Veizer et al., 1999) makes also possible a mixture with marine-influenced waters. Additionally, the relative 13C-enrichement could be partly related to a photosynthetic control on the carbon budget of the lake during the deposition of microbial (cyanobacterial) carbonates (Talbot and Kelts, 1990; Andrews et al., 1993; 1997), as particularly evidenced in microbial laminites (F3) from cycles U2, U3, U4 and U5 (**Fig. 3.10 C-E**) and by the vertical trend in the δ13C-δ18O plot from U3.

In cycle U1, a poorly-expressed covariant trend exists between δ13C and δ18O (**Fig. 3.10B**), especially in the oolitic-peloidal grainstones which coincides with a segment of the overall inverted-J trend. Even though such an isotope trend likely largely result from neomorphic processes affecting micrite in meteoric environments (Léonide et al., 2014; Hasiuk et al., 2016) as suggested by petrographic observations, the interpretation of a partial preservation of a primary covariant trend cannot be entirely ruled out. Such primary covariant trends have been reported from a variety of modern lacustrine carbonates and are interpreted to result from hydrologic closure of the lake for long time periods and varying residence time of water and dissolve inorganic carbon (e.g. Talbot, 1990; Li and Ku, 1997).

The strongly negative excursion of δ13C at top of cycle U1 (**Fig. 3.9**) reflects the formation of pedogenic carbonates during a phase of subaerial exposition (e.g. Allan and Matthews, 1982). Negative δ18O and δ13C excursion at top of cycles U2 and U4 suggest that the cycle is capped by a subaerial exposure surface (**Fig. 3.9**) in spite of the lack of petrographic evidence. Finally, the negative δ18O and δ13C excursion at top of U4 (**Fig. 3.9**) suggests that the cycle is capped by an intraformational subaerial exposure surface, while the very negative values at top of U5 are likely to be related to meteoric overprint during the long-duration subaerial exposure preceding the Burdigalian transgression.

3.5.3. Origin of transgressive-regressive cycles

The vertical succession of lithofacies and associated depositional environments, together with stable isotope signatures allows the identification of transgressive-regressive cycles (**Fig. 3.9**) and the reconstruction of lake margin evolution and changes in paleohydrologic setting. In cycles U1, U2, U4 and U5, the upward vertical facies change from mud-supported fabrics (F2 facies) or microbial laminites (F3 facies) from shallow and sheltered lake margin environments to oolitic and peloidal grainstones (F1A-B) deposited in moderate to high energy perennial waterbody records the lake transgression. The maximum flooding stage therefore occurs within

the oolitic grainstone beds (F1A) which represents the most distal facies identified in the section. Pedogenetic features as well as carbon isotope signatures (**Fig. 3.9**) strongly suggest a subaerial exposition on top of these cycles which reflects the stage of maximum regression of the lake.

In the upper part of cycle U1, the abrupt upward vertical change in facies from oolitic-peloidal grainstone F1A to pedogenetized carbonate breccia (F4) together with the occurrence of pseudomorphs after gypsum are indicative of a forced lacustrine regression related to drying of the lake. In other oolitic cycles (U2, U4 and U5), the forced regressive stage is recorded by the subaerial exposure surfaces which sharply truncate the massive oolitic/peloidal grainstone intervals. It seems plausible to consider significant erosion during the forced regressive phase or during the early transgressive phase, as suggested by the lack of marginal/palustrine deposits preserved on top of these cycles. Moreover, it is not excluded that part of grainstone intervals has formed during a stage of normal regression. As an apparent paradox, the stable isotope signatures are indicative of greater freshwater inputs with the wackestone (F2) and microbialitic (F3) beds (lower transgressive hemicycle) than in grainstone intervals (upper transgression to normal regression?) where they suggest either a more negative inflow-evaporation balance, or a mixture with a closed lake water body or even seawater. Similarly, the vertical changes in molluscan assemblages do not indicate a salinity decrease during transgression, but on the contrary the few freshwater taxa identified (e.g. *Viviparus*, *Lymnaea*, *Planorbis*) are mainly present in the wackestone and microbialitic facies from the lower transgressive hemicycles (**Fig. 3.2**). In contrast to other lake basins (e.g. Holocene, Dead Sea: Klinger et al., 2003; Plio-Pleistocene, Lake Turkana: Nutz et al., 2020), lake transgression does not result from an excess balance between freshwater inflow and evaporation. A lack of unequivocal control of paleohydrologic balance on transgressive/regressive cycle development has been regionally evidenced in coeval lake margin carbonate deposits from the Issirac and Saint-Chaptes basins (Letteron et al., 2017, 2018, 2022), but also in other syn-tectonic lake basins (Chen and Hu, 2017).

Such a paradox can be explained by an increasing connexion of the Butte Iouton lake waters with regional salt waterbodies during transgression. This interpretation therefore implies that the lake basin to which the Butte Iouton carbonate margin represented an outflow of neighbouring salt water bodies. The volume of connected lake waters is controlled by a regional inflow-evaporation balance which is strongly dependent on climate conditions. In the case of Priabonian lakes from south-east France, lake closure and saline waters are associated with semi-arid conditions prevailing at regional scale (Letteron et al., 2017, 2018). In contrast, the dominantly transgressive pattern of cycles evidenced in Butte Iouton margin likely results from both 1) local subsidence driven by normal faults in a regional extensional tectonic setting which is known regionally to have started as early as the middle Priabonian (Cavelier et al., 1984; Sanchis and Seranne, 2000) and 2) saline water outflow from neighbouring regional waterbodies. Forced regression stages recorded at top of depositional cycles may result from:

1) periods of increased aridity associated with a fast and significant reduction in connected lake volume, or 2) the formation of an outlet which led to the fast emptying of the lake basin (Garcia-Castellanos, 2006).

In Cycle U3, the upward vertical transition from the F2C and F2D wackestone/packestone indicative of very sheltered and shallow area of the lake margin to characean wackestones (F2B) suggests a transgressive trend. Similarly to oolitic cycles, molluscan assemblages and isotope signatures are indicative of a connexion with a salt waterbody (evaporative or seawater-influenced lake), while the ^{13}C-enrichment is likely to be related to the effect of enhanced photosynthetic activity (e.g. Coletta et al., 2001; Leng and Marshall, 2004), which is consistent with the extensive development of charophytes, cyanobacteria and possibly non-calcifying macrophytes. A subaerial exposition on top of cycle U4 is evidenced from the occurrence of pedogenic features (root-traces).

3.5.4. The Butte Iouton outcrop: a preserved relict of a regional-scale saline lake?

The vertical evolution of depositional environments and lake salinity recorded at Butte Iouton outcrop provide significant insights into the paleogeography of Priabonian paleolakes at a larger regional scale. The lack of decreasing salinity trends within the carbonate cycles, as evidenced from the persistence of oligo-mesohaline mollusks, as well as the carbon and oxygen isotope signatures strongly suggest that the transgressive trends recorded by the vertical facies evolution at Butte Iouton is not related to an increase in lake water volume resulting from an increasing inflow-evaporation balance. The present data rather support the interpretation of a carbonate sedimentation in a subsident lake basin which is fed by the outflow of adjacent saline lakes. The relatively dry conditions evidenced regionally by Priabonian lacustrine sedimentation (Lettéron et al., 2017; 2018; 2022) suggest that salinity may derive, at least partly, from a negative inflow-evaporation balance, but a salinization by recycling evaporites in the drainage area of the lake or within the lake itself is a possible interpretation. Indeed, as evidenced by Emre and Truc (1978), the erosion of the piercing Suzette diapir and subsequent sulfate recycling occurred coevally with the late Priabonian carbonate and evaporite sedimentation of the Mormoiron basin (~50 km north of Butte Iouton: **Fig. 3.12**). Additionally, connections with the Alpine Sea through topographic corridors may represent a possible origin for salinity in regional Priabonian lakes (Sissingh, 2001) even though a continental origin for evaporites from the Valence basin has been inferred from stable isotope and mineralogical analyses (Fontes, et al., 1996).

The Butte Iouton outcrop is located within a 20 km-wide corridor bounded by the Nîmes fault to the NW and structured by set of SW-NE-trending normal faults (**Fig. 3.1A**). To the southeast a thick (>4000m) lacustrine sedimentation occurred in the Vistrenque Basin (Valette and Benedicto, 1995; Benedicto et al., 1996). Although the age of the lowermost syn-rift interval (Série Grise Formation: ~2000 m-thick) is unknown, the similarity in depositional polarity (siliciclatic-dominated the south and carbonate-dominated the north) between the Série Grise Formation and the Célas formation from the Sommières, Saint-Chaptes and Alès basins

may suggest a Priabonian age for the lower part of the syn-rift sedimentation in the Vistrenque basin, as suggested by Cavelier *et al*., (1984). According to this hypothesis, the Butte Iouton outcrop would represent the northern shallow carbonate margin of a lake basin fed in siliciclastics from the southern collapsing Pyrenean reliefs. Additionally, the strike-slip movement of the Nîmes fault during a transitional tectonic phase comprised between the Pyrenean compression and the Gulf of Lion rifting (Séranne et al., 2021) is consistent with the formation of a subsiding strike-slip basin, east of the Nîmes fault, capable to accumulate a thick sedimentary cover as early as the Priabonian times. The Série Grise Formation from the Vistrenque Basin is dominantly made of organic-rich shales interbedded with thin sandstone and conglomerate horizons (Cavelier et al., 1984; Valette and Benedicto, 1995) suggesting profundal lake environments with terrigenous supplies.

On the footwall of the Nîmes fault, a small-sized and isolated lacustrine limestone outcrop was documented by Caziot (1896) at Puech d'Autel, within the city of Nîmes. These limestones contain a molluscan association including *Melanoides juliani*, *Brotia albigensis*, *Melanopsis acrolepta*, *Neritina*, *Galba longiscata* which is highly similar to that of the oligohaline, late Priabonian lacustrine limestones from the Issirac basin (Lettéron et al., 2017) and the Butte Iouton. As a consequence, the Puech d'Autel limestones likely represent a relict outcrop of the northwestern shallow carbonate margin of the Vistrenque lake basin.

The proximity of the Priabonian outcrops from the Sommières and Saint-Chaptes basins (10 km) makes a connection with the ASCI saline lake strongly possible. Additionally, in the Issirac basin, Lettéron et al. (2017) argued for a correlation between maximum lacustrine transgressions and periods with the most deficient inflow-evaporation balance. These authors interpreted this apparent paradox as resulting from a connection of the Issirac lake waters with those of the Mormoiron and Vistrenque basins, during a period of relative aridity.

The presence of isolated outcrops of Priabonian lacustrine limestones with brackish fauna, 10 km northeast of the eastern termination of the Saint-Chaptes basin, near Uzès (BRGM, 1968) (**Fig. 3.12**), shows that the ASCI lake basin had a significantly wider extension towards the east and that a connection with the Vistrenque basin is a plausible hypothesis. As a consequence, various potential sills which could have connected the ASCI lake sytem with the Vistrenque-Mormoiron may be identified west of the Nîmes fault. More broadly, the dominant transgressive character of depositional sequences recorded locally in various Priabonian carbonate lake margins from southeast France (Issirac: Lettéron et al., 2017; Saint-Chaptes: Lettéron et al., 2018; Alès: Lettéron et al., 2022; Butte Iouton: this study) associated with a persistence of oligo-mesohaline waters in a context of negative inflow-evaporation balance is indicative of interconnected, subsiding lacustrine area, the total volume of connected waters being much larger than that of individual lake basin (**Fig. 3.12**).

Finally, the oolitic carbonate ramp developing on the margins of the Vistrenque lake margin show significant analogies with various marine oolitic ramps regarding the overall facies model (e.g. Mississipian from Wales: Burchette et al., 1990; Upper Jurassic from Spain: Pomar et al.,

2015; Jurassic from Morocco: Shekhar et al., 2014): 1) oolite shoal developing on the outer ramp, 2) poorly structured oolitic grainstones forming in backshoal setting, 3) mud-supported and/or microbial carbonates developing in the low-energy, innermost area of the ramp and 4) the ramp distally passes into deep water environments.

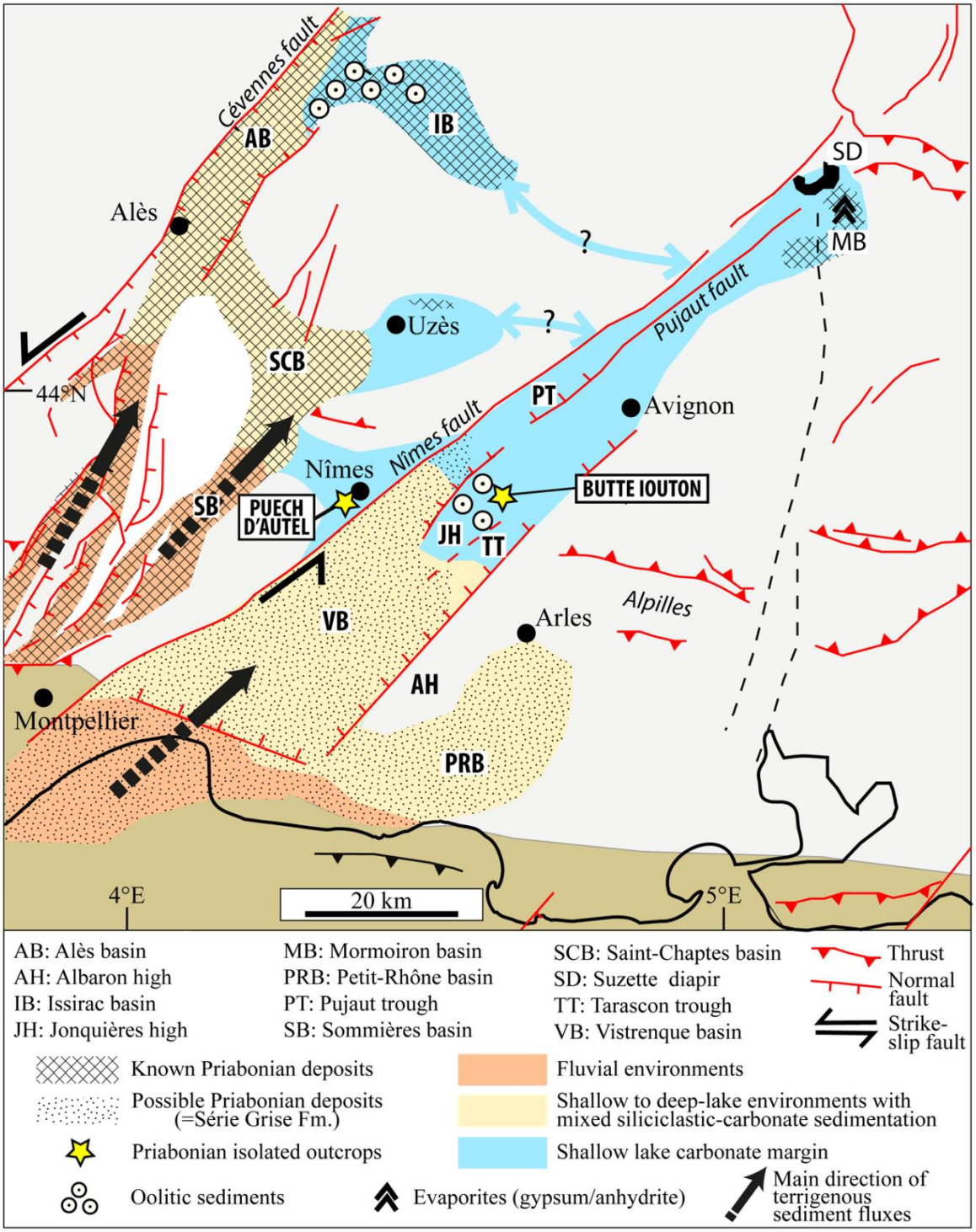

Figure 3.12: Palaeogeographical reconstruction of saline lakes from Languedoc and southern Rhône valley during the late Priabonian. The siliciclastic fluxes are compiled from the previous studies: Lettéron et al. (2022) for the Célas sandstones from Sommières and ASCI systems, and Cavelier et al. (1984) for the plausible late Eocene to early Oligocene siliciclastic infill of the Vistrenque basin.

3.6. Conclusion

The integrative approach (biostratigraphy, paleoecology, carbonate petrography, sedimentology and stable isotope geochemistry) applied to the study of lacustrine carbonates from Butte Iouton outcrops allowed reconstructing a depositional model for an oolitic saline lake margin and providing new insights into the Priabonian paleogeography of southeast France.

1) An oolitic lacustrine ramp model has been evidenced and displays the following facies transition from proximal to distal areas: 1) a shallow marginal saline lake domain with deposition of planar microbial laminites, and molluscan-ostracodal wackestone, 2) a more distal and open lacustrine environments with low to moderate energy characterized by the deposition of peloidal grainstones and 3) a domain of higher energy with accumulation of ooids mixed with peloids. The area of ooid production (not captured by the studied outcrops) likely consisted in oolitic shoals within a high energy outer ramp setting.
2) Carbonate sedimentation dominantly occurred during stages of lake transgression. Subaerial exposure surfaces evidenced at top of depositional cycles are interpreted to result from forced regressions which occurred during periods of negative inflow-evaporation balance.
3) Molluscan associations suggest that oligo- to mesohaline waters dominantly prevailed during the studied time interval.
4) The apparent paradox between a dominant transgressive sedimentation and the persistence of saline conditions suggest that lake transgression is controlled by subsidence and outflows from neighbouring saline waterbodies, and not by an increase in regional lake water volume. The studied carbonate margin belongs to a set of interconnected saline lake waterbodies whose total volume is much greater than that created locally by subsidence.
5) The compilation of existing data regarding regional Priabonian deposits supports the interpretation of interconnected saline lake basins characterized by a siliciclastic-dominated southern margin whose sediment is sourced from the collapsing Pyrenean reliefs and by a carbonate-dominated northern margin with significant oolitic sedimentation in high-energy nearshore area.

3.7. Supplementary data

Table 3.A: Carbon and Oxygen isotope ratio, signal preservation vs alteration and depositional facies.

Height (m)	$\delta^{13}C$ (‰ V-PDB)	$\delta^{18}O$ (‰ V-PDB)	Diagenetic features (macroscopic and/or thin-section observations)	Depositional facies
53,8	-4,01	-3,68	Grain micritization/ microporosity	F1A
53	-4,79	-3,76	Grain micritization/ microporosity	F1A
52,1	-4,55	-3,99	Grain micritization/ microporosity	F1A
43,8	-2,83	-3,56	Grain micritization/ microporosity	F2D
43,6	-2,34	-3,42	Grain micritization/ microporosity	F1A
43,5	-1,74	-1,33	Grain micritization/ microporosity	F1A
42,8	-1,32	-1,91	Grain micritization/ microporosity	F1A
41,8	-1,27	-2,51	Grain micritization/ microporosity	F1A
41,3	-1,61	-2,11	Grain micritization/ microporosity	F1A
40,8	-2,11	-3,07	Grain micritization/ microporosity	F1C
40,65	-2,24	-2,81	Grain micritization/ microporosity	F1C
40,35	-0,53	-3,58	-	F3
38,5	-1,40	-3,35	-	F3
37,7	-1,21	-3,61	-	F3
37,4	-1,32	-3,58	-	F3
37,1	-1,08	-2,86	-	F2B
36,75	-1,20	-3,14	-	F2B
36,7	-0,50	-2,85	Primary	F2B
36,5	-1,16	-3,24	Rare calcite microspar cements	F2A
36,3	-0,90	-2,78	-	F2B
35,9	-1,24	-2,79	Rare calcite microspar cements	F2B
35,5	-1,14	-2,64	-	F2B
35	-0,78	-2,80	Rare calcite microspar cements	F2B
34,7	-1,12	-3,23	-	F2B
34,4	-1,32	-2,80	-	F2B
34	-1,08	-2,79	-	F2B
33,7	-0,88	-2,95	-	F2B
33,2	-1,07	-2,81	-	F2C
32,8	-1,59	-3,38	-	F2C
32,3	-1,15	-3,07	-	F2C
31,9	-0,43	-2,88	-	F2D
31,5	-1,37	-2,70	-	F2C
31,2	-2,09	-3,66	Microspar cements	F2A
31	-1,57	-3,35	Microspar cements	F2A
30,75	-1,17	-2,45	Grain micritization/ microporosity	F1C
30,7	-2,07	-2,95	Microspar cements	F1B
30,55	-2,29	-3,30	Grain micritization/ microporosity	F1B
30,45	-2,22	-3,06	Grain micritization/ microporosity	F1B
30	-0,92	-1,86	Grain micritization/ microporosity	F1A
29,3	-1,04	-1,99	Grain micritization/ microporosity	F1B

29	-1,62	-2,54	Grain micritization/ microporosity	F1B
28,3	-1,24	-2,63	Grain micritization/ microporosity	F1B
27,9	-0,86	-2,39	Grain micritization/ microporosity	F1B
27,5	-0,83	-2,82	Grain micritization/ microporosity	F1A
26,95	-0,76	-3,35	-	F3
26,75	-2,21	-3,02	Grain micritization/ microporosity	F1A
26,6	-1,60	-2,50	-	F2D
26,3	-2,83	-2,08	Pedogenic features/ sparry calcite cements	F4
26,2	-5,21	-2,28	Pedogenic features/ sparry calcite cements	F4
26	-4,57	-3,23	Pedogenic features/ sparry calcite cements	F4
25,75	-2,54	-2,74	Grain micritization/ microporosity	F1A
25,5	-1,58	-2,02	Grain micritization/ microporosity	F1A
24,6	-1,52	-2,28	Grain micritization/ microporosity	F1A
24,35	-1,40	-2,13	Grain micritization/ microporosity	F1A
24,2	-1,84	-2,42	Grain micritization/ microporosity	F1A
23,8	-1,73	-2,52	Grain micritization/ microporosity	F1B
23,5	-2,15	-2,59	Grain micritization/ microporosity	F1B
23,1	-1,70	-2,87	-	F2D

3.8. Références bibliographiques du chapitre 3

Allan JR, Matthews, R. 1982. Isotope signatures associated with early meteoric diagenesis. *Sedimentology* 29 (6): 797-817.

Alonso-Zarza AM. 2003. Palaeoenvironmental significance of palustrine carbonates and calcretes in the geological record. *Earth-Science Reviews* 60: 261–298.

Andrews JE, Riding R, Dennis PF. 1993. Stable isotopic composition of recent freshwater cyanobacterial carbonates from the British Isles: local and regional environmental controls. Sedimentology 40: 303–314.

Andrews JE, Riding R, Dennis PF. 1997. The stable isotopic record of environmental and climatic signals in modern terrestrial microbial carbonates from Europe. Palaeogeogr Palaeoclimatol Palaeoecol 129: 171–189.

Arenas C, Cabrera L, Ramos E. 2007. Sedimentology of tufa facies and continental microbialites from the Paleogene of Mallorca Island (Spain). *Sedimentary Geology* 197: 1-27.

Arthaud F, Ogier M, Séguret M. 1981. Géologie et géophysique du Golfe du Lion et de sa bordure nord. *Bulletin du BRGM* 1(3): 175–193.

Benedicto A, Labaume P, Séguret M, Séranne M. 1996. Low-angle crustal ramp and basin geometry in the Gulf of Lion passive margin: the Oligocene-Aquitanian Vistrenque graben, SE France. *Tectonics* 15(6): 1192–1212.

BRGM. 1968. Notice de la carte géologique de la France au 1/50000: feuille Uzès n°939 : 12 pp.

Bodergat A-M, Briot D, Hugueney M, Poidevin J-L, Picot L, Giraud F, Berger J.P, Levy A, Poignant A. 1999. Incursions marines dans l'environnement lacustre du rift oligocène de Limagne (Massif Central, France) : apport des organismes halophiles et des isotopes du strontium, datation par les mammifères. *Bulletin de la Société Géologique de France* 170: 499–511.

Bouton A, Vennin E, Amiotte-Suchet P, Thomazo C, Sizun, J-P, Virgone A, Gaucher EC, Visscher PT. 2019. Prediction of the calcium carbonate budget in a sedimentary basin: A “source-to-sink” approach applied to Great Salt Lake, Utah, USA. *Basin Research* 32 : 1005-1034.

Briot D, Poidevin JL. 1998. Stratigraphie 87Sr/86Sr de quelques laminites carbonates du Rupélien inférieur du fossé de Limagne : incursions marines dans le rift du Massif central français?. *Compte Rendus de l’Académie des Sciences, Paris* 236: 479–483.

Burchette TP, Wright VP, Faulkner TJ. 1990. Oolitic sandbody depositional models and geometries, Mississippian of southwest Britain: implications for petroleum exploration in carbonate ramp settings. *Sedimentary Geology* 68: 87-115.

Cavelier C, Alabouvette G, Amberger J-P, Cautru J-P, Charollais J, Chateauneuf J-J, Crochet J-Y, Campredon R, Debeglia N, Durand J-P, Feist-Castel M, Freytet P, Gannat E, Gaudant J, Giannerini G, Godinot M, Hartenberger J-L, Hugueney M, Kerckhove C, Lefavrais-Raymond A, Legendre S, Lespinasse P, Magne J, Nury D, Pairis J-L, Plaziat J-C, Rémy J-A, Schlund J-M, Sige, B, Sittler C, Sudre J, Trauth N, Truc G, Valleron M-M, Vianney-Liaud M, Villatte, J. 1984. Paléogène. In : Debrand-Passard ed., *Synthèse géologique du Sud-Est de la France*. *Mémoire du BRGM* 125 : pp. 389-468.

Caziot M. 1896. Sur le Tertiaire inférieur des environs de Nîmes. *Bulletin de la Société Géologique de France* 24: 1–32.

Chen M, Hu X. 2017. Regression-transgression cycles of paleolakes in the Fen River Graben Basin during the mid to late Quaternary and their tectonic implication. *Frontiers in Earth Sciences* 11(4): 703–714.

Cohen AS, Thouin C. 1987. Nearshore carbonate deposits in Lake Tanganyika. *Geology* 15: 414-418.

Coletta P, Pentecost A, Spiro B. 2001. Stable isotopes in charophyte incrustations: relationships with climate and water chemistry. *Palaeogeography, Palaeoclimatology, Palaeoecology* 173: 9-19.

Daley B. 1972. Macroinvertebrate assemblages from the Bembridge marls (Oligocene) of the Isle of Wight, England, and their environmental significance. *Palaeogeography, Palaeoclimatology, Palaeoecology* 11(1): 11–32.

Dalrymple RW. 1992. Tidal depositional systems. In: R. G. Walker and N. P. James, eds. *Facies Models and Sea Level Changes*, *Geological Association of Canada*: 195-218.

Davaud E, Girardclos S. 2001. Recent freshwater ooids and oncoids from western Lake Geneva (Switzerland): indications of a common organically mediated origin. *Journal of Sedimentary Research* 71(3): 423-429.

De Roys M. 1846. Note sur la comparaison des bassins tertiaires du Midi avec celui de Paris. *Bulletin de la Société Géologique de France* (2ème série) (3): 645-652.

Deschamps R, Rohais S, Hamon Y, Gasparrini M. 2020. Dynamic of a lacustrine sedimentary system during late rifting at the Cretaceous–Palaeocene transition: Example of the Yacoraite Formation, Salta Basin, Argentina. *The depositional Record* 6: 490-523.

Dèzes P, Schmid S.M, Ziegler P.A. 2004. Evolution of the European Cenozoic Rift System: interaction of the Alpine and Pyrenean orogens with their foreland lithosphere. *Tectonophysics* 389: 1–33.

Dromart G, Dumas D. 1997. The salt basin of Valence (France). In: Busson G, Schreiber B.C. eds., Sedimentary Deposition in Rift and Foreland Basins in France and Spain. Columbia Univ. Press, New York: pp. 195–239.

Dumas E. 1876. Statistique Géologique, Minéralogique, Métallurgique et Paléontologiques du Département du Gard. Arthus Bertrand ed. : 735 pp.

Dunham RJ. 1962. Classification of Carbonate Rocks According to Depositional Texture. In: Ham, W.E., Ed., Classification of Carbonate Rocks, AAPG, Tulsa, 108-121.

Eardley AJ. 1938. Sediments of Great Salt Lake, Utah. *AAPG Bulletin* 22, 1305–1411.

Embry AF, Klovan JE. 1971. A Late Devonian Reef Tract on Northeasterm Banks Island. *Canadian Petroleum Geology* 19 : 730-781.

Emre T, Truc G. 1978. Mise en évidence d'un contact discordant Oligocène-Trias dans le massif de Suzette. Implciations tectoniques et conséquences sur l'origine des évaporites ludiennes du bassin de Mormoiron (Vaucluse). *Géologie Alpine* 54: 17−23.

Esu D, Girotti O. 2010. The Late Oligocene Molluscan Fauna from Otranto (Apulia, Southern Italy): an example of alternating freshwater, lagoonal and emerged environments. *Palaeontology* 53(1): 137-174.

Fontannes F. 1884. Description sommaire de la faune malacologique des formations saumâtres et d'eau douce du groupe d'Aix (Bartonien – Aquitanien) dans le bas Languedoc, la Provence et le Dauphiné. Georg H, Lyon, and Savy F, Paris: 60 pp.

Fontes J-C, Filly A, Gaudant J, Duringer P. 1991. Origine continentale des évaporites paléogènes de Haute Alsace : arguments paléoécologiques, sédimentologiques et isotopiques. *Bulletin de la Société Géologique de France* 162: 725–737.

Fontes J-C, Gaudant J, Mélières F, Filly A, Schlund J-M. 1996. Origine continentale des évaporites paléogènes du fossé de Valence (Drôme): données minéralogiques, isotopiques et paléoécologiques. *Bulletin de la Société Géologique de France* 167(4): 475–481.

Fretter V, Graham A. (1978). The prosobranch molluscs of Britain and Denmark. Part 3 – Neritacea, Viviparacea, Valvatacea, terrestrial and freshwater Littorinacea and Rissoacea. *Journal of Molluscan Studies*. Suppl. 5: 1-152.

Freytet P, Plaziat J-C. 1982. Continental carbonate sedimentation and pedogenesis – Late Cretaceous and Early Tertiary of Southern France. In: Purser B. H. ed., *Contribution to Sedimentology*, *Schweizerbartsche Verlag*, Stuttgart, 12: 217 pp.

Gallois A, Bosence D, Burgess PM. 2018. Brackish to hypersaline facies in lacustrine carbonates: Purbeck Limestone Group, Upper Jurassic–Lower Cretaceous, Wessex Basin, Dorset, UK. *Facies* 64, 12.

Garcia A. 1994. Charophyta: their use in paleolimnology. *Journal of Paleolimnology* 10(1): 43–52.

Garcia A, Chivas A.R. 2006. Diversity and ecology of extant and Quaternary Australian charophytes (Charales). *Cryptogamie Algologie* 27(4): 323–340.

Garcia-Castellanos D. 2006. Long-term evolution of tectonic lakes: Climatic controls on the development of internally drained basins. *Geological Society of America Special Paper* 398: 283-294.

Gorini C, Le Marrec A, Mauffret A. 1993. Contribution to the structural and sedimentary history of the Gulf of Lions (western Mediterranean), from the ECORS profiles, industrial seismic profiles and well data. *Bulletin de la Société géologique de France* 164(3): 353–363.

Grambast L, Grambast-Fessard N. 1981. Étude sur les Charophytes tertiaires d'Europe occidentale III: le Genre Gyrogona. *Paléobiologie Continentale* 12(2): 1-35.

Hargrave JE, Hicks MK, Scholz CA. 2014. Lacustrine carbonates from Lake Turkana, Kenya: a depositional model of carbonates in an extensional basin. *Journal of Sedimentary Research* 84: 224-237.

Harris M, Faulkner P, Asmussen B. 2015. Macroscopic approaches to the identification of expedient bivalve tools: a case study investigating polymesoda (=Geloina) coaxans (Bivalvia: Corbiculidae) shell valves fromPrincess Charlotte Bay, Queensland, Australia. *Quaternary International* 427: 201–215.

Hasiuk FJ, Kaczmarek SE, Fullmer SM. 2016. Diagenetic origins of the calcite microcrystals that host microposity in limestone reservoirs. Journal of Sedimentary Research, 86, 1163-1178.

Kahle CF. 1974. Ooids from Great Salt Lake, Utah, as analogue for the genesis and diagenesis of ooids in marine limestones. *Journal of Sedimentary Geology* 44(1): 30-39.

Klinger Y, Avouac J-P, Bourlès D, Tisnérat N. 2003. Alluvial deposition and lake-level fluctuations forced by Late Quaternary climate change: the Dead Sea case example. *Sedimentary Geology*: 162 (1-2): 119-139.

Leng MJ, Marshall JD. 2004. Palaeoclimate interpretation of stable isotope data from lake sediment archives. Quaternary Science Reviews 23(7-8): 811-831.

Léonide P, Fournier, F, Reijmer JJG, Vonhof H, Borgomano J, Dijk J, Rosenthal M, van Goethem M, Cochard J, Meulenaars K. 2014. Diagenetic patterns and pore space distribution along a platform to outer-shelf transect (Urgonian limestone, Barremian-Aptian, SE France). *Sedimentary Geology*: 306, 1-28.

Lesueur J-L. 1991. Etude sédimentologique et stratigraphique du Bassin Paléogène d'Apt–Manosque–Forcalquier (Alpes de Haute Provence). Modalités de la transition Burdigalienne. Ph.D. thesis, University M. de Montaigne, Bordeaux III, France : 407 pp.

Lettéron A. 2018. Caractérisation sédimentologique, stratigraphique et paléoenvironnementale du système carbonaté lacustre à salinité variable du bassin d'Alès et des régions limitrophes (Priabonien, SE France) : implications paléoclimatiques et paléogéographiques. PhD thesis, Aix-Marseille University : 344 pp.

Lettéron A, Fournier F, Hamon Y, Villier L, Margerel J-P, Bouche A, Feist M, Joseph P. 2017. Multi-proxy paleoenvironmental reconstruction of saline lake carbonates: Paleoclimatic and paleogeographic implications (Priabonian-Rupelian, Issirac Basin, SE France). *Sedimentary Geology* 358 : 97–120.

Lettéron A, Hamon Y, Fournier F, Séranne M, Pellenard P, Joseph P. 2018. Reconstruction of a saline, lacustrine carbonate system (Priabonian, St-Chaptes Basin, SE France): depositional models, paleogeographic and paleoclimatic implications. *Sedimentary Geology* 367: 20–47.

Lettéron A, Hamoun Y, Fournier F, Demory F, Séranne M, Joseph P. 2022. Stratigraphic architecture of a saline lake system: From lake depocenter (Alès Basin) to margins (Saint-Chaptes and Issirac basins), Eocene-Oligocene transition, south-east France. *Sedimentology, Blackwell Publishing, in press*, ⟨DOI: 10.1111/sed.12920⟩, ⟨hal-03406458⟩.

Li H-C, Ku L. 1997. $\delta^{13}C$ - $\delta^{18}O$ covariance as a paleohydrological indicator for closed-basin lakes. *Palaeogeography, Palaeoclimatology, Palaeoecology* 133: 69 80.

Mauffret A, Gorini C. 1996. Structural style and geodynamic evolution of Camargue and Western Provencal basin, southeastern France. *Tectonophysics* 15(2): 356-375.

Ménillet F. 1973. Carte géologique de la France au 1/50000, feuille Nîmes, BRGM Edition.

Milroy PG, Wright VP. 2002. Fabrics, facies control and diagenesis of lacustrine ooids and associated grains from the Upper Triassic, southwest England. *Geological Journal* 37: 35-53.

Miranda NAF, Perissinotto R, Appleton CC. 2010. Salinity and temperature tolerance of the invasive freshwater gastropod *Tarebia granifera*. *South African Journal of Science* 106(3/4): Art. #156, 7 pages. DOI: 10.4102/sajs.v106i3/4.156.

Morton B, 1983. Mangrove bivalves. In: Russell-Hunter, W.D. ed., *The Mollusca* 6, Academic Press, Orlando: pp. 77–138.

Nutz A, Schuster M, Barboni D, Gassier G, Van Bocxlaer B, Robin C, Ragon T, Ghienne J-F, Rubino J-L. 2020. Plio-Pleistocene sedimentation in West Turkana (Turkana Depression, Kenya, East African Rift System): Paleolake fluctuations, paleolandscapes and controlling factors. *Earth Science Reviews* 111: 103415.

Pellat E, Allard M. 1895. Dépôts lacustres de la Butte Iouton entre Comps et Beaucaire (Gard). *Bulletin de la Société Géologique de France* 23: 434-436.

Plaziat J-C, Younis WR. 2005. The modern environments of Molluscs in southern Mesopotamia, Iraq: A guide to paleogeographical reconstructions of Quaternary fluvial, palustrine and marine deposits. *Carnets de Géologie* 2005/01, (18pp).

Pomar L, Aurell M, Badenas B, Morsilli M, Al-Awwad S.F. 2015. Depositional model for a prograding oolitic wedge, Upper Jurassic, Iberian basin. *Marine and Petroleum Geology* 67: 556-582.

Reichenbacher BA, Uhlig U, Kowalke T, Bassler B, Matzke-Karasz Schenk B. 2004. Biota, paleoenvironments and biostratigraphy of continental Oligocene deposits of the South German Molasse Basin (Penzberg syncline). *Palaeontology* 47(3): 639–677.

Riveline J. 1986. Les charophytes du Paléogène et du Miocène inférieur d'Europe occidentale. Cahiers de Paléontologie, volume 8). Muséum national d'Histoire naturelle, Paris. 304 pp.

Riveline J, Berger J.-P, Feist M, Martin-closas C, Schudack M, Soulié-Märsche I. 1996. European Mesozoic-Cenozoic charophyte biozonation. *Bulletin de la Société Géologique de France* 167(3): 453–468.

Roduit N. 2007. JMicroVision: un logiciel d'analyse d'images pétrographiques polyvalent. PhD thesis, University of Geneva, 128 p.

Roman F. 1903. Contributions à l'étude des Bassins lacustres de l'Éocène et de l'Oligocène du Languedoc. *Bulletin de la Société Géologique de France (4ème série)* 3: 546-616.

Roman F. 1910. Faune saumâtre du sannoisien du Gard. *Bulletin de la Société Géologique de France (4ème série)* 10: 927–955.

Rouchy J-M. 1997. Paleogene continental rift system ofWestern Europe: locations of basins, paleogeographic and structural framework, and the distribution of evaporites. In: Busson, G., Schreiber, B.C. eds., Sedimentary Deposition in Rift and Foreland Basins in France and Spain. Columbia Univ. Press, New York: pp. 45–94.

Rouchy J-M, Blanc-Valleron M-M. 2009. Les évaporites matériaux singuliers, milieux extrêmes. Vuibert, Paris : 184 pp.

Sanchis E, Séranne M. 2000. Structural style and tectonic evolution of a polyphase extensional basin of the Gulf of Lion passive margin: the Tertiary Alès Basin, southern France. *Tectonophysics* 322: 243–264.

Sandberg PA. 1975. New interpretations of Great Salt Lake ooids and of ancient non-skeletal carbonate mineralogy. *Sedimentology* 22: 497-537.

Sandberg PA. 1980. The Pliocene Glenns Ferry oolite: lake-margin carbonate deposition in the southwestern Snake River plain—Discussion and replay. *Journal of Sedimentary Petrology* 50: 997–998.

Séranne M, Benedicto A, Truffert C, Pascal G, Labaume P. 1995. Structural style and evolution of the Gulf of Lion Oligo-Miocene rifting: Role of the Pyrenean orogeny. *Marine and Petroleum Geology* 12: 809–820.

Séranne M, Couëffé R, Husson E, Baral C, Villard J. 2021. The transition from Pyrenean shortening to Gulf of Lion rifting in Languedoc (South France) –A tectonic-sedimentation analysis. *BSGF - Earth Sciences Bulletin* 192, 27.

Shekhar R, Sahni I, Benson G, Agar S, Amour F, Tomas S, Christ N, Always R, Mutti M, Immenhauser A, Karcz Z, Kabiri L. 2014. Modelling and simulation of a Jurassic carbonate ramp outcrop, Amellago, High Atlas Mountains, Morocco. *Petroleum Geoscience* 20, 109–124.

Sissingh W. 2001. Tectonostratigraphy of the West Alpine Foreland: correlation of Tertiary sedimentary sequences, changes in eustatic sea-level and stress regimes. *Tectonophysics*: 333, 361–400.

Schäfer A, Stapf, KRG. 1978. Permian Saar-Nahe Basin and recent Lake Constance (Germany): two environments of lacustrine algal carbonates. In: A. Matter and M.E. Tucker (Eds), Modern and Ancient Lake Sediments. IAS Special Publication, 2, 83-107.

Swirydczuk K, Wilkinson BH. 1979. The Pliocene Glenns Ferry oolite: lake-margin carbonate deposition in the southwestern Snake River plain. *Journal of Sedimentary Petrology* 49: 995–1004.

Swirydczuk K, Wilkinson BH, Smith GR. 1980. The Pliocene Glenns Ferry oolite—II: Sedimentology of oolitic lacustrine terrace deposits. *Journal of Sedimentary Petrology* 50: 1237–1248.

Tabb DC, Moore DR. 1971. Discovery of the Carolina Clam, Polymesoda caroliniana (Bosc), a supposed Florida disjunct species, in Everglades National Park, Florida. *Gulf Research Reports* 3(2): 265–281.

Talbot MR. 1990. A review of the palaeohydrological interpretation of carbon and oxygen isotopic ratios in primary lacustrine carbonates. *Chemical Geology* 80: 261–279.

Tänavsuu-Milkeviciene K, Sarg JF, Bartov Y. 2017. Depositional Cycles and Sequences in an Organic-Rich Lake Basin: Eocene Green River Formation, Lake Uinta, Colorado and Utah, U.S.A. *Journal of Sedimentary Research* 87(3): 210-229.

Triat JM, Truc G. 1974. Evaporites paléogènes du domaine rhodanien. *Revue de Géographie Physique et de Géologie Dynamique* 16: 235–262.

Truc G. 1978. Lacustrine Sedimentation in an Evaporitic Environment: The Ludian (Palaeogene) of the Mormoiron Basin, Southeastern France. *Special Publications of the International Association of Sedimentologists* 2: 189–203.

Valette M. 1991. Etude structural du gisement salifère Oligocène de Vauvert (Gard), *Thèse de doctorat*, Univ. Montpellier II, 229 pp.

Valette M, Benedicto A. 1995. Chevauchements gravitaires halotectoniques dans le basin distensif de Camargue (marge du golfe du Lion, SE de la France). *Bulletin de la Société Géologique de France* 166(2): 137-147.

Veizer J, Ala D, Azmy K, Bruckschen P, Buhl D, Bruhn F, Carden G, Diener A, Ebneth S, Godderis Y, Jasper T, Korte C, Pawellek F, Podlaha O, Strauss H. 1999. $^{87}Sr/^{86}Sr$, $\delta^{13}C$ and $\delta^{18}O$ evolution of Phanerozoic seawater. *Chemical Geology* 161 (1–3): 59–88.

Velasco J, Millán A, Hernández J, Hernández J, Gutiérrez C, Abellán P, Sánchez D, Ruiz M. 2006. Response of biotic communities to salinity changes in a Mediterranean hypersaline stream. *Aquat. Biosyst.* 2, 12. https://doi.org/10.1186/1746-1448-2-12

Van Den Berg MS, Coops H, Simons J, De Keizer A. 1998 – Competition between *Chara aspera* and *Potamogeton pectinatus* as a function of temperature and light. *Aquatic botany* 60: 241-250.

Wanless HR. 1981. Fining-upward sedimentary sequences generated in seagrass beds. *Journal of Sedimentary Petrology* 51: 445-454.

Wattine A, Vennin E, De Wever P, 2003. Evolution d'un environnement carbonaté lacustre à stromatolithes, par l'approche paleo-écologique (Carrière de Montaigu-le-Blin, bassin de Limagne, Allier, France). *Bulletin de la Société Géologique de France* 174 (3): 243-260.

Williamson CR, Picard M.D. 1974. Petrology of carbonate rocks of the Green River Formation (Eocene). *Journal of Sedimentary Petrology* 44(3):738-759.

Ziegler PA. 1992. European Cenozoic srift system. In: Ziegler, P.A. (Ed.), Geodynamics of Rifting, Volume I, Case History Studies on Rifts: Europe and Asia. *Tectonophysics* 208: 91–111.

4. LE DÉPÔT-CENTRE DU BASSIN DE LA VISTRENQUE : CADRE CHRONOSTRATIGRAPHIQUE ET PALÉOGÉOGRAPHIQUE

4. Le dépôt-centre du bassin de la Vistrenque : cadre chronostratigraphique et paléogéographique

Synthèse

Ce chapitre concerne les séries paléogènes de subsurface du dépôt-centre du bassin continental de la Vistrenque connues à travers les nombreux forages des secteurs de Gallician et de Pierrefeu et vise à contraindre le cadre chronostratigraphique de leur formation et à apporter de nouveaux éclairages sur la paléogéographie du Sud-Est de la France au cours de l'Éocène supérieur et de l'Oligocène.

Ce chapitre utilise plusieurs approches pour dater les séries de la Vistrenque, à savoir 1) les datations U-Pb sur la calcite, 2) l'approche de climatostratigraphie basée sur l'analyse de pollen, et 3) la modélisation géochimique des mélanges des compositions isotopiques du Strontium et du soufre sur les sulfates collectés dans les successions paléogènes des bassins de Vistrenque et d'Alès. Cette étude intègre également des données biostratigraphiques et palynologiques des bassins d'Alès, Saint-Chaptes et du Roussillon situés également dans le Sud-Est de la France.

Ce travail a permis de fournir un cadre chronostratigraphique robuste du remplissage paléogène du bassin de la Vistrenque. Les assemblages floristiques sont utilisés pour reconstituer la couverture végétale des systèmes lacustres et de leurs environs (plaines et hautes terres) et pour documenter la détérioration climatique de la transition l'Éocène-Oligocène dans le Sud-est de la France. L'origine des saumures des lacs salins obtenue à partir des analyses isotopiques du Strontium 87 et du Soufre 40 ainsi que la présence de nannofossiles calcaires, de kystes de dinoflagellés et de grains de pollen de mangrove (palétuviers) constituent des preuves de l'intrusion d'eau salée d'origine marine dans le bassin d'Alès au Priabonien et dans le bassin de la Vistrenque au Rupélien et au Chattien.

Les reconstitutions paléogéographiques du Sud-est de la France pendant le Priabonien et le Rupélien supérieur suggèrent fortement des incursions marines depuis la mer alpine via deux voies potentielles : la haute vallée du Rhône via le seuil de Crest et la basse vallée du Rhône via les synclinaux pyrénéens du Haut-Var. D'autre part, les bassins évaporitiques de l'Oligocène supérieur en Camargue sont alimentés en solutés directement depuis la mer Méditerranée occidentale suite à l'effondrement du segment Pyrénéen ayant existé à l'emplacement de l'actuel Golfe du Lion pendant l'extension Oligo-aquitanienne.

Enfin, l'analyse pollinique et la méthode de l'amplitude climatique ont révélé une phase brève mais significative de refroidissement et d'aridification à l'extrême base du Rupélien qui pourrait représenter l'expression régionale et continentale du refroidissement climatique global suivant la transition Éocène-Oligocène.

Ce chapitre est rédigé sous forme d'un article scientifique (**Article 2**) et *a été soumis pour publication à la revue* « ***Palaeogeography, Palaeoclimatology, Palaeoecology*** »

Article 2 - The Paleogene continental basins from SE France: new geographic and climatic insights from an integrated approach

Nazim SEMMANI, François FOURNIER, Jean-Pierre SUC, Séverine FAUQUETTE, Nicolas GODEAU, Abel GUIHOU, Speranta-Maria POPESCU, Mihaela Carmen MELINTE-DOBRINESCU, Christophe THOMAZO, Lionel MARIÉ, Jean BORGOMANO. « **The Paleogene continental basins from SE France: new geographic and climatic insights from an integrated approach** » à soumettre dans la revue : « *Palaeogeography, Palaeoclimatology, Palaeoecology* ».

The Paleogene continental basins from SE France: new geographic and climatic insights from an integrated approach

Nazim Semmani[1,*], François Fournier[1], Jean-Pierre Suc[2], Séverine Fauquette[3], Nicolas Godeau[1,2], Abel Guihou[1], Speranta-Maria Popescu[4], Mihaela Carmen Melinte-Dobrinescu[5], Christophe Thomazo[6], Lionel Marié[1], Jean Borgomano[1]

[1]: Aix Marseille Université, CNRS, IRD, Cerege, Um 34, 3 Place Victor Hugo (Case 67), 13331, Marseille Cedex 03, France

[2]: Sorbonne Université, CNRS-INSU, Institut des Sciences de la Terre Paris, ISTeP, UMR 7193, 75005 Paris, France

[3]: ISEM, Université de Montpellier, CNRS, IRD, EPHE, Montpellier, France

[4]: GeoBioStratData.Consulting, 385 Route du Mas Rillier, 69140 Rillieux-la-Pape

[5]: National Institute of Marine Geology and Geo-Ecology, 23–25 Dimitrie Onciul Street, 70318 Bucharest, Romania

6: Université de Bourgogne Franche-Comté, UMR CNRS/uB6282 Biogéosciences, 6 Bd Gabriel, 21000 Dijon, France

[*]Corresponding author: nazim.semmani@gmail.com

Abstract

The present study concerns the Paleogene successions from the continental Vistrenque (Camargue area) and Alès (Languedoc area) basins and aims to constrain the chronostratigraphic framework of these sedimentary successions. It brings new insights into the palaeogeography of Southeast France during the Late Eocene and Oligocene times.

U-Pb dating on calcite, pollen-based climatostratigraphy and water-mixture geomodelling on Strontium and isotope sulphates conducted on the Paleogene successions from the Vistrenque and Alès basins and integrating data from the Roussillon Basin located in Southeast France allow to provide a strong chronostratigraphic framework for the Paleogene Vistrenque Basin infill. Floral assemblages are used to reconstruct the vegetation cover in the lacustrine systems and their lowlands and highlands surroundings and to document the Eocene-Oligocene climatic deterioration in Southeast France. Saltwater composition inferred from geochemical isotope analyses on Strontium 87 and Sulphur 40 but also the occurrence of calcareous nannofossils, dinoflagellate cysts with pollen grains of mangrove plants provide strong evidence for intrusions of marine influenced saltwater into the Alès Basin during the Priabonian and the Vistrenque Basin during the Rupelian and Chattian.

Palaeogeographic reconstructions of Southeast France during the Priabonian and Late Rupelian strongly suggest marine incursions from the Alpine Sea via two potential pathways:

upper Rhône Valley via the Crest Sill and lower Rhône Valley via the Haut-Var Pyrenean synclines. On the other hand, Upper Oligocene evaporite basins in the Camargue area are fed with dissolved ions directly from the Western Mediterranean Sea following the collapse of the Palaeo-Pyrenean relief at the present location of Gulf of Lion during the Oligocene-Aquitanian extension.

Furthermore, pollen analyses and Climate Amplitude Method calculations reveal a brief but significant stage of cooling and aridification at the very base of the Rupelian which could represent the regional and terrestrial expression of the global climate cooling following the Eocene-Oligocene Transition.

Keywords: Priabonian, Rupelian, U/Pb dating, palynology, marine incursion, palaeoclimate, climatostratigraphy, sulphates, Eocene-Oligocene Transition.

4.1. Introduction

In Southeast France, several continental basins were formed during the Paleogene and are located in Languedoc (e.g. Alès, Saint-Chaptes and Issirac (ASCI) basins, Sanchis and Séranne, 2000; Lettéron et al., 2021; Séranne et al., 2021), Rhone Valley (Mormoiron Basin, Triat and Truc, 1974), Provence (e.g. Apt-Manosque-Forcalquier Basin, Lesueur, 1991; Marseille Basin, Nury, 1990), and Camargue (e.g. Vistrenque Basin, Benedicto et al., 1996). These basins are characterized by thick siliciclastic, carbonate and evaporite sedimentation (e.g. Rouchy, 1997). The formation and the filling of these basins initiated during the Late Eocene (Priabonian) and lasted until the Late Oligocene (Chattian). These basins were interpreted as branches of the European Cenozoic Rift System (ECRIS, **Fig 4.1A**) (Ziegler, 1992) or resulting exclusively from the Oligocene to Aquitanian extension linked to the Liguria-Provence rifting (e.g., Vistrenque Basin, Benedicto et al., 1996), and a few cases as polyphased extensional structures (e.g. Sanchis and Séranne, 2000) (**Fig. 4.1B, 4.1C**). In their recent work, Séranne et al. (2021) reassessed the origin of Priabonian continental basins located in Languedoc, between the Northeast trending Cévennes and Nîmes major regional faults and found that those basins resulted from left-lateral strike-slip movements of these faults which accommodated both the Western European rift system extension (ECRIS) and the still active N-S shortening of the Central and Western Pyrenees.

The origin of evaporites in the saline palaeolakes within the Paleogene basins of Southeast France is poorly understood and is still a matter of controversy that has lasted for decades particularly on the origin of the salt water that may result from marine incursions and/or the recycling of Triassic evaporites (Giraud, 1902; Fontes et al., 1996; Bodergat et al., 1999; Sissingh, 2001, 2006; Dèzes et al., 2004; Ziegler and Dèzes, 2007; Briot, 2008; Lettéron et al., 2017). Questions also remain regarding the patterns of saline water masses connexions and diachronism of the evaporite intervals between the different basins. Also incompletely

understood is the role of changing climate on evaporite deposition and continental depositional system evolution at the key Eocene-Oligocene transition (e.g., Sissingh, 2001; Lettéron et al., 2021) which represents a crucial period for the Cenozoic global climate evolution. Until recently, assumptions have been made about the role of the Camargue area as a saline water corridor into the Languedoc and Rhône Valley continental basins (e.g., Lettéron et al., 2018).

Since the Camargue area is located in a pivotal position within these France south-eastern basins, between the Languedoc basins to the west, the Provence basins to the east, and the Rhone Valley basins to the north (see location in **Figure 4.1B**), the Paleogene Vistrenque Basin occupies a key geographic position for constraining the geodynamic and structural evolution of southeast France and Gulf of Lion areas during the Late Eocene and Oligocene times and provides new insights into these hitherto unresolved palaeogeographic issues.

The Vistrenque Basin is considered as the deepest (~ 5 km) Cenozoic basin in southeast France and in the Gulf of Lion margin (Benedicto et al., 1996). The sedimentary pile is entirely buried beneath the Rhône Delta sediments and the drill cores have yielded very scarce and poorly preserved biota thus preventing the definition of a detailed and well-constrained chronostratigraphic framework (Valette and Benedicto, 1995). The Paleogene sedimentary infill of the Vistrenque Basin is more than 3200 m thick and has been subdivided classically into three main units (**Fig. 4.2F**) (Valette and Benedicto, 1995). The lowermost "Série grise" Unit is more than 2000 m thick and constituted mainly of siliciclastic lacustrine deposits. The intermediate "Série rouge" Unit, around 200 m thick, is dominated by fluvial siliciclastic deposits. The upper "Série Calcaréo-salifère" Unit, a few hundreds of metres thick, mainly consists of carbonates and evaporites (halite and anhydrite). The correlation of the "Calcaréo-salifère" Unit with the Priabonian and Oligocene evaporites from the neighbouring Rhodanian and Languedocian basins is not yet established, thus preventing the reconstruction of a well-constrained palaeogeographic map of these basins during the Paleogene and the elucidation of the question of their potential connection with the marine realm.

A comprehensive and detailed analysis of subsurface data from the Paleogene sedimentary pile of the Vistrenque Basin (cores, cuttings, well logs) as well as from the neighbouring Alès Basin and the integration of data from Canet 1 borehole from the Roussillon Basin (Eastern Pyrenees) (see location in **Figure 4.1B**) has been undertaken to resolve these tectonic and palaeogeographic issues (**Fig. 4.3A, 4.3B, Fig. 4.4**). Based on the integration of different dating methods such as U-Pb absolute dating on carbonates, pollen-based climatostratigraphy, the interpretation of Strontium and Sulphur isotopes measurements, and additional micropalaeontological analyses (dinoflagellate cysts, calcareous nannofossils), the present work aims at: (1) constraining the lithostratigraphic and chronostratigraphic framework of the Paleogene sedimentary succession from the Vistrenque Basin; (2) bringing new insights into the pending issue of the saltwater feeding of the Paleogene saline lakes of Southeast France and the assessment of the hypothesis of marine incursions into these lakes using new geochemical and micropalaeontological data from the Vistrenque and Alès basins, and (3) refining the

palaeogeographic and palaeoclimatic reconstructions of Southeast France during the Late Eocene and Oligocene times.

4.2. Geological setting

4.2.1. The Vistrenque Cenozoic Basin: regional tectonic setting and stratigraphy

Following the Lower Cretaceous platform development, the SE of France region has experienced compressional tectonics from the Upper Cretaceous to Eocene times. During the Late Eocene (Priabonian) and entire Oligocene time intervals, two rifting phases have occurred in the Camargue and Languedoc areas: the Western European rift system (ECRIS, Ziegler, 1992; **Fig. 4.1A**) and the rifting of Gulf of Lion margin (**Fig. 4.1C**; Séranne et al., 1995) respectively. In response to these extensional movements, several continental basins have formed during the Eocene (e.g., ASCI system, Apt-Manosque-Forcalquier and Mormoiron basins) and the Oligocene (e.g., Vistrenque Basin in the Camargue area). Many basins have undergone the two successive extensional movements (Sanchis and Séranne 2000; **Fig. 4.1B**).

The Camargue region occupies an approximately triangular area between Nîmes, Arles, and Marseille towns (**Fig. 4.2A**). The region is constituted of two main Cenozoic basins: the Vistrenque Basin to the West and the Vaccarès Basin (Petit-Rhône Basin) to the East that are separated by the Mesozoic Albaron High (**Fig. 4.2A-B**). The Vistrenque Basin is oriented NE-SW and extends over 50*30 Km². This basin is linked to the northeast with the Pujaut Through along the bounding NNE-SSW trending major Nîmes Fault that separates the basin from the Mesozoic hills of the Garrigues of Nîmes (**Fig. 4.2E**) (Semmani et al., 2022, *see chapter 3 in this PhD manuscript*). The Vistrenque Basin is bounded to the south by the structural highs of Grau-du-Roi and Saintes-Maries-de-la-Mer (**Fig. 4.2B**). The basin is structured by a set of syn-rift faults mostly parallel to the Nîmes Fault (**Fig. 4.2C-D**) that determine tilted blocks within the basin but also by transfer faults that separate different sectors with specific structural styles (e.g., **Fig. 4.2E**; Benedicto et al., 1996 and their figures).

The Nîmes Fault is a major low-angle ramp that played a role during the Gulf of Lion margin rifting and it has been shown that the ramp was newformed in place of the inherited Mesozoic steep normal Nîmes Fault that acted as a triggering weak zone for further movements (**Fig. 4.1C**, **4.2E**). Benedicto et al. (1996) showed that the newly formed Nîmes Fault was active during the Gulf of Lion margin rifting without any reference to possible movements of this fault, likely strike-slipping, during the Late Eocene (Priabonian) to Early Oligocene Western European rift extension recorded in many continental basins of the area as demonstrated recently by Séranne et al. (2021). The latter suggested that the Nîmes Fault is part of an array of sinistrial strike-slip faults of NNE-SSW to NE-SW orientation including the Cévennes Fault along which numerous Languedocian continental basins have been formed (e.g. Alès-Saint-Chaptes-Issirac basins: Lettéron et al., 2021; Hérault, Montpellier and Sommières basins: Séranne et al., 2021). Without any biostratigraphic evidence, Cavelier et al. (1984) suggested

that the continental Cenozoic Vistrenque Basin, located east to the Nîmes Fault, is amongst these numerous basins opened from the Late Eocene to Early Oligocene in the SE of France.

The Oligocene-Aquitanian Gulf of Lion rifting phase accompanied the retreat of slab and is followed by the Burdigalian break-up (**Fig. 4.1C**). Palaeogeographic reconstructions made by Benedicto et al., 1996 suggest a high relief, more than 1 km, at the southern margin while the total normal extension is estimated to 9 to 9.5 km. The break-up event (**Fig. 4.1C**) was dated to the Burdigalian and corresponds to the spreading of the Liguria-Provence Basin which led to the south-eastward drift of the Corsica-Sardinia Block (Gorini et al., 1993; Séranne et al., 1995). During the Burdigalian, a marine transgression followed the break-up and Burdigalian to Tortonian post-rift marine sediments were deposited (**Fig. 4.2E**). By the end of the Miocene, the Messinian Salinity Crisis resulted in valley incision into the Miocene deposits and affected the Oligocene deposits in places. The resulting canyons are overlain by Pliocene and Quaternary sediments (Beaufort, 1954; Benedicto et al., 1996; Leroux et al., 2017).

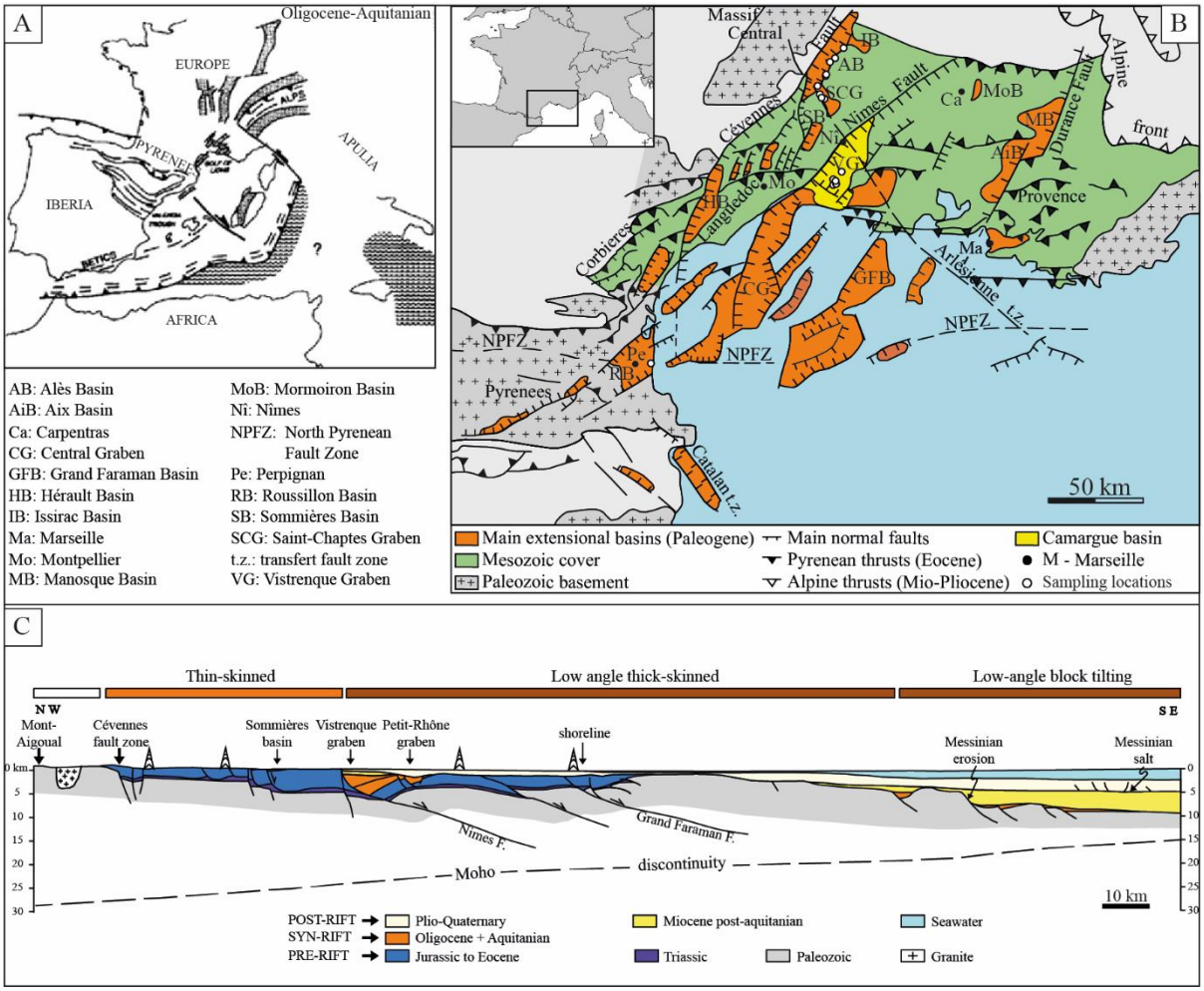

Figure 4.1: A) Palaeotectonic map of Western Europe during the Oligocene-Aquitanian times showing the location of Western European rift basins (ECRIS) and the subduction area to the south and southeast of Corsica-Sardinia, from Bois (1993). B) Structural map of Southeast France and location of the Vistrenque Basin among the various Cenozoic continental basins, modified after Benedicto (1996). Sampling loci for pollen analyses, U/Pb dating, and Sulphur/Strontium isotopes purposes are located in the Alès, Issirac and Saint-Chaptes basins (AB, IB,

SCG), Vistrenque Graben (VG) and Roussillon Basin (RB), locations are given in **§ 4.8. Supplementary data** - **Table S4.1**. C) Geological section across the Gulf of Lion margin (modified after Benedicto, 1996).

4.2.2. The Gallician and Pierrefeu sectors: stratigraphy of the Paleogene sedimentary succession

The maximum thickness of the Cenozoic sedimentary succession of the Vistrenque Basin is known from the Pierrefeu 1 well (4920 m) where it rests on a Lower Cretaceous marine carbonates substratum (**Fig. 4.2E, 4.3C**). The Cenozoic fill of the Vistrenque Basin is subdivided into poorly defined pre-rift series; syn-rift series attributed to the Oligocene-Aquitanian extension; and post-rift series of Burdigalian to Pliocene and Quaternary age (**Fig. 4.2D-E**; Valette and Benedicto, 1995; Benedicto et al., 1996). Below the Aquitanian deposits, the Paleogene strata, up to 3200 metres thick, have been subdivided classically into three main lithological units, comprising from bottom to top: 'Série grise' Formation, 'Série Rouge' Formation, and 'Série Calcaréo-salifère' Formation (**Fig. 4.2F**). These subdivisions have been adopted by Cavelier et al. (1984) in their synthesis on the Paleogene of Southeast France and these authors suggested an Eocene age for the lowermost part of the 'Série Grise' Formation based on the observed similarities in the sedimentary trends with the neighbouring basins.

The compartmentalization of the Vistrenque Basin by transfer faults results in different stratigraphical columns between the northern Parrapon-Pierrefeu sector and the southern Gallician sector (**Fig. 4.3**). In the Gallician sector, the lowermost 'Série Grise' Unit and its upper part, referred to as 'Série Calcaire' Unit (~250 m thick) in this sector, are constituted of carbonate-clastic and siliciclastic sandstones, conglomerates, marlstones and occasional anhydrite and limestones deposited in lacustrine conditions. The overlying 'Série Mixte' Unit, which is not recognized in the Pierrefeu sector, is a few tens of metres thick and is made of an alternation of conglomerates, sandstones, marlstones and bituminous lacustrine to palustrine limestones. The 'Série Mixte' Unit is overlain by the 'Série Rouge' Unit which is approximately 150-200 m thick and consists mainly in variegated marlstones, sandstones, and polymictic conglomerates deposited in fluvial setting. The uppermost 'Série Calcaréo-salifère' Unit is around 300 m-thick in the Gallician sector and is made at its base of lacustrine limestones which are overlain by alternations of sandstones, marlstones and evaporites.

In the Parrapon-Pierrefeu sector, contrasting to the Gallician sector, the same interval is strongly thicker, with 'Série Grise' Unit reaching ~2000 m, 'Série Rouge' Unit of comparable thickness to the Gallician sector, and a thicker 'Série Calcaréo-salifère' Unit. The considerable thickness of the evaporite-rich 'Série Calcaréo-salifère' Unit (~900 m) from the Pierrefeu sector results from the abnormal superposition of evaporite intervals caused gravity halotectonic thrusts linked to the Oligocene-Aquitanian extension (Valette and Benedicto, 1995).

The Paleogene continental infill of the Vistrenque Basin is overlain by Aquitanian and Burdigalian marine deposits (**Fig. 4.2E**). The Burdigalian post-rift deposits are overlain by Middle to Late Miocene deposits (interrupted and partially eroded during the Messinian Event

as evidenced by the incision of valleys; **Fig. 4.1C**). These valleys are infilled with siliciclastics during the Pliocene while new fluvial erosion characterizes the Quaternary. During the Holocene, the thick sediments of the Rhône Delta have buried the Tertiary pile.

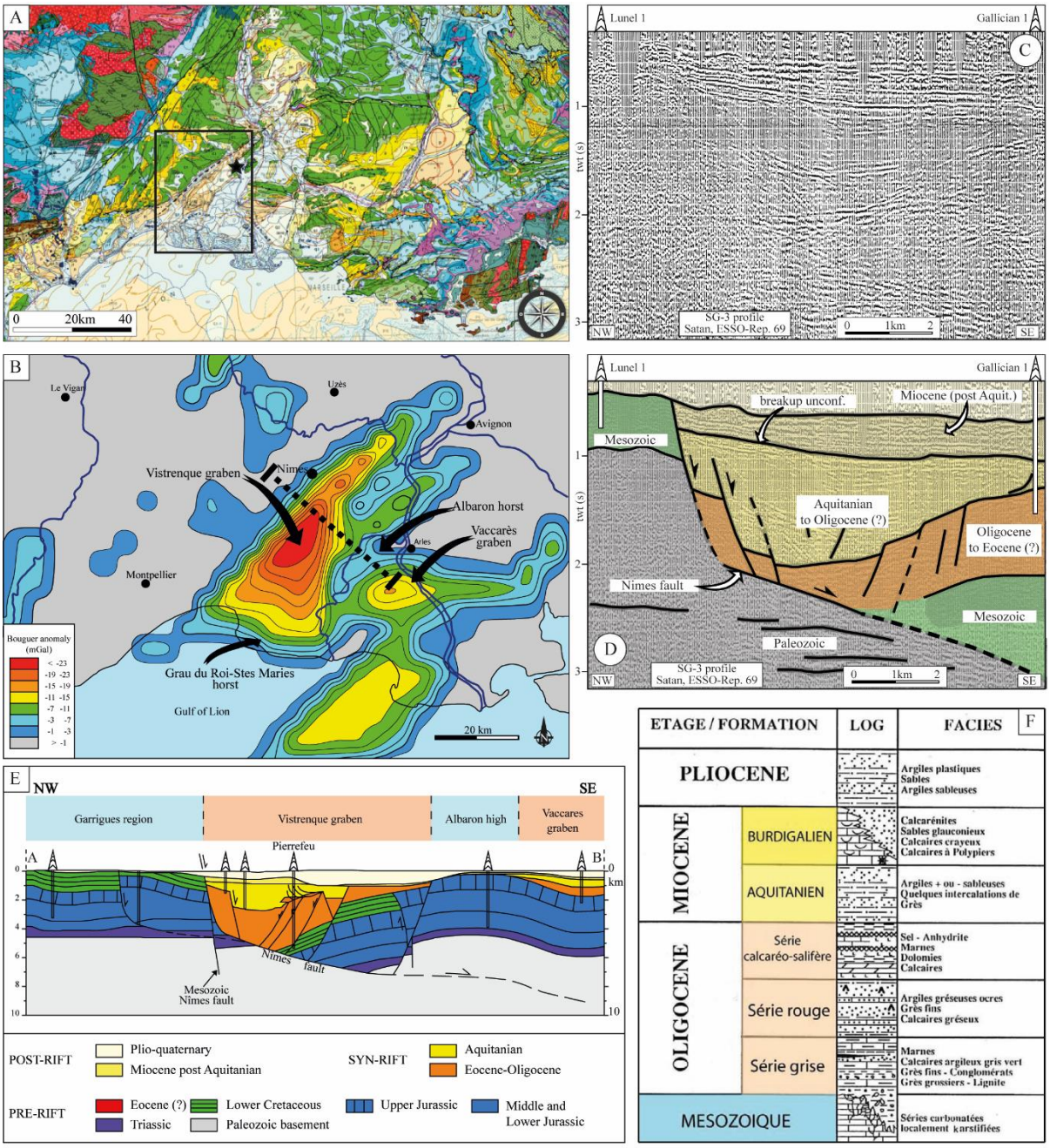

Figure 4.2: A) Geological map of Southeast France showing the Vistrenque Basin indicated by the rectangular box. The NE-SW trending Nîmes Fault separates the Mesozoic substratum of the 'Garrigues nîmoises' from the Cenozoic basins currently almost buried beneath the Rhône Delta sediments (modified after BRGM geological map: 1-1.000.000). The black star indicates the position of the Priabonian northern carbonate succession at Butte Iouton (e.g., Pellat and Allard, 1895; Semmani et al., 2022, *see chapter 3 in this PhD manuscript*). B) Map of the Bouguer gravity anomaly, modified after Chauvin and Follin-Arbelet (1985). C) Non-migrated and D) interpreted seismic profile SG3 in the Northern Vauvert compartment, after Benedicto (1996), (see location in Figure 4.3 hereinafter). E) NW-SE geological cross-section through the Vistrenque Basin on the northern Vauvert

compartment (modified after Benedicto et al., 1996). F) Stratigraphic synthesis of the Vistrenque Basin compiled from borehole data by Gorini (1993), modified after Bache (2008).

4.3. Material and methods

4.3.1. Database and lithostratigraphic framework

This work is based on the analysis of cores, drilling cuttings and well logs from boreholes drilled in the Gallician and Parrapon-Pierrefeu sectors of the **Vistrenque Basin** (South of Nîmes), boreholes and exposed sections from the **ASCI system** (north of Nîmes), and the Canet 1 borehole from the **Roussillon Basin** (near Perpignan). Sampling locations are shown in **Fig. 4.1B**, **Fig. 4.3A-B** and **Fig. 4.4** and listed in **§ 4.8. Supplementary data - Table S4.1**.

In the Gallician sector located in the southern part of the Vistrenque Basin, the density of subsurface data (average distance between the wells < 1km) allowed to build a detailed lithostratigraphic framework. Lithostratigraphic correlations between the wells are based on the Gamma Ray (GR) curves and major vertical lithological changes (**Fig. 4.5**). The ASCI basins have been recently studied and documented in the publications of Lettéron et al. (2017, 2018, 2021). The Canet 1 well was drilled in the Roussillon Basin and intersects a 1785 m thick sedimentary succession overlying the ante-Hercynian substratum and running from Permian-Triassic to Quaternary in which ca. 700 m of sandy-clayey-lignitic deposits might represent the time interval from the Late Oligocene to the Early Miocene (Gottis, 1958).

4.3.2. Chronostratigraphic framework construction

Since the subsurface Paleogene sedimentary succession from the Vistrenque Basin lacks identifiable macrofauna, the chronostratigraphic framework was established using, besides the lithostratigraphic framework based on well correlations, alternative dating approaches, such as U-Pb dating on carbonates, pollen-based climatostratigraphy and geochemical modelling on Strontium and Sulphur in sulphates.

U-Pb analyses were performed at the DatCarb A*midex platform (CEREGE, Aix-Marseille University). The obtained absolute ages have been calibrated on the Geological Time Scale of Gradstein et al. (2012). Pollen grains have been extracted at the GeoBioStratData.Consulting laboratory (Rillieux-la-Pape, France) and the results have been integrated within a regional climatostratigraphic chart. Geochemical modelling was performed on the Strontium and Sulphur isotopes measurements on evaporites from the ‘Série Calcaréo-salifère’ Unit using the two-component mixture of Denison et al. (1998). Further details on each method are given in the following sections.

4.3.3. U-Pb geochronology

a. Sampling:

The ‘Série Grise’ Formation is almost entirely detrital in such a way that the U-Pb method is not suitable except for calcite veins. In contrast, the ‘Série Rouge’ and Série Calcaréo-

salifère' formations are carbonate-rich and present various carbonate mineral phases (cements, pedogenic carbonates, root calcifications, molluscan shells -*neomorphs*) allowing their dating.

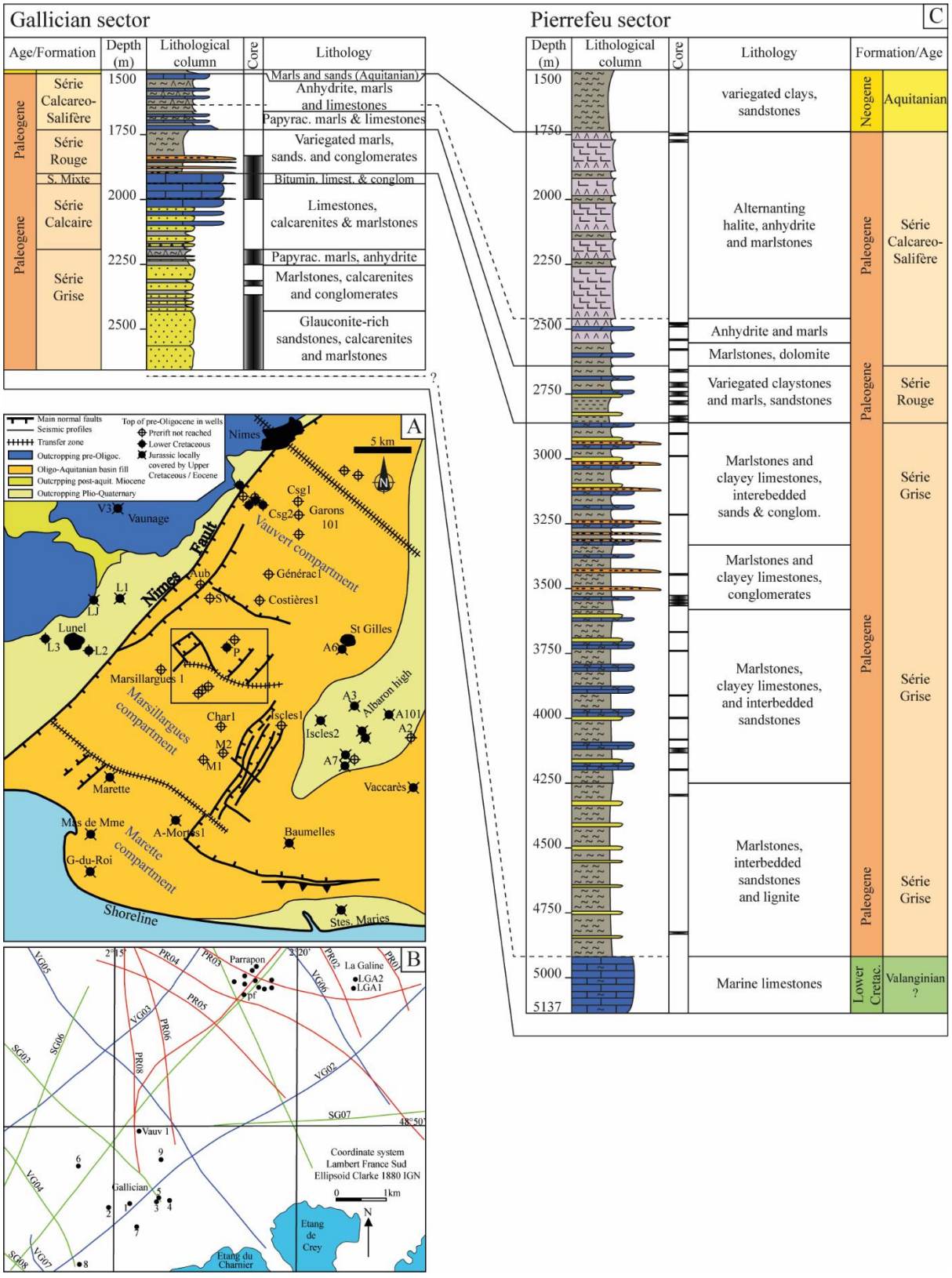

Figure 4.3: A) Structural map of the Vistrenque Basin showing location of deep boreholes, modified after Benedicto et al. (1996). V3: Vaunage 3 - LJ: La Jasette - L1: Lunel 1 - L2: Lunel 2 - L3: Lunel 3 - Csg: Caissargues Aub: Aubord 1 - SV: Saint-Véran 1 - P: Pierrefeu 1 - A6: Albaron 6 - A3: Albaron 3 - A7: Albaron 7 - A101:

Albaron 101 - A2: Albaron 2 - Char 1: Charnier 1 – M1: Montcalm 1 – M2: Montcalm 2 – P: Pierrefeu 1 – Stes. Maries: Saintes-Maries-de-la-Mer 101. t.z.: transfer zone. B) Geographical map of the rectangle in (A) showing the location of subsurface database (wells and seismic lines) pf=Pierrefeu 1 well, LGA=LaGaline, Vauv=Vauvert 1, numbers refer to the Gallician wells. PR, VG, SG: Parrapon (1986), Vauvert-Gallician (1986) and Saint-Gilles (1969) seismic surveys respectively, modified after Valette (1991). C) lithological columns and correlations of Gallician 9 and Pierrefeu 1 wells located in the Gallician and Pierrefeu sectors respectively.

The dating of calcite phases, and therefore the corresponding geological events (e.g., subaerial exposure) helps to approximate the depositional age of the sedimentary formations by the determination of the ages of post-depositional (younger) and earlier (older) events. The stratigraphy uses crosscuttings and superposition laws and, with the help of the absolute dating clues, allows to build a relevant chronostratigraphic framework of the Paleogene sedimentary infill of the Vistrenque Basin.

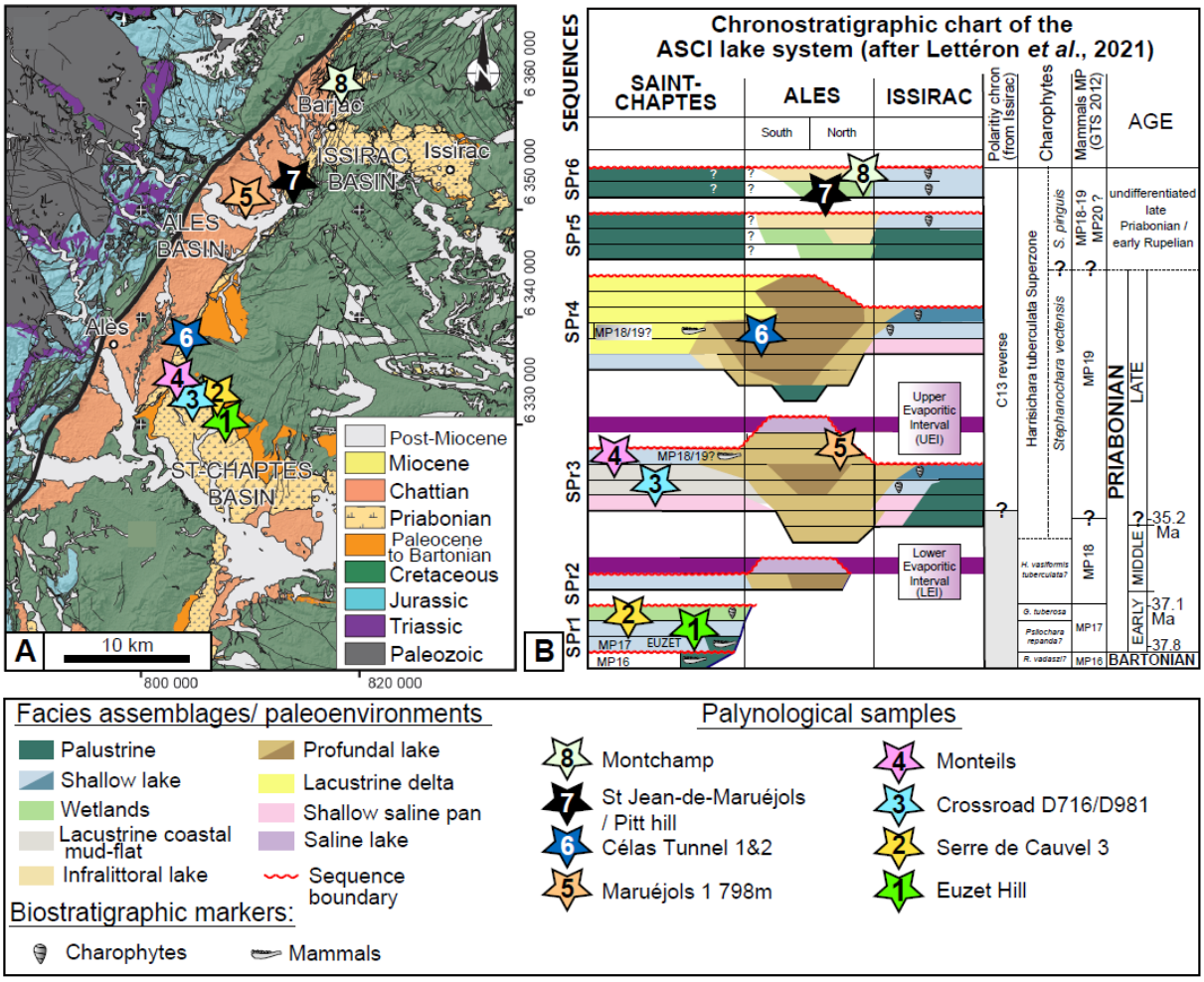

Figure 4.4: A) Geological map of the Alès-Saint-Chaptes-Issirac (ASCI) basins and location of the pollen sampling. B) Chronostratigraphic chart of the ASCI lake system (after Lettéron et al., 2021) and location of the pollen samples.

To perform U-Pb absolute dating on the Paleogene succession from the Vistrenque Basin, samples which contain enough calcite were collected from drill cores. Microscopic petrographic

analyses and diagenetic studies allowed to choose eleven samples to analyse with LA-ICP-MS (*in situ* Laser Ablation Inductively-Coupled-Plasma Mass Spectroscopy).

b. Analytical procedure

In order to carry out U-Pb dating on calcite, the samples containing a calcite mineral phase were selected for the confection of a set of two geological slides: a thin section (30 µm) for petrographic observations and a thick section (100 µm) for the sampling of material by laser ablation for spectrometric analyses. These geological sections were polished up to 1 µm.

Prior to the analyses, sedimentological and diagenetic observations were carried thoroughly in order to identify the relevant mineral phases that should be dated and to avoid sampling from two different mineral phases; sampling from different calcite generations would result in misinterpretations of ages. Diagenetic studies were performed either by cathodoluminescence or fluorescence microscopy to define the areas of interest for the dating. Cement sequence stratigraphy is established using superposition and crosscutting principles. In a few cases, confocal fluorescence observations allowed more details to be captured than would be possible with cathodoluminescence, especially with non-luminescent cement phases. Confocal observations have been performed at the PRATIM (Aix-Marseille University) using an Axio-observer Z1 inverted confocal microscope with single or two-photon laser scanning comprising 04 visible lasers (Argon multi-ray laser: 458, 488 and 514 nm, DPSS 561 nm, He-Ne 594 nm, and He-Ne 633 nm) and a Chaméléon Vision II IR laser with pre-compensation system coupled with a ZEN 2010 software. Cathodoluminescence observations have been made at the CEREGE (Marseille, France) using a Cathodyne cold-cathodoluminescence from NewTec ® operating at 16 to 18 Kv and 160 to 200 µA coupled to an Olympus BH-2 microscope and Olympus-UPMTVC camera.

Once the petrography and diagenetic sequence are understood and the mineral phase(s) corresponding to the geological event to be dated have been identified under microscopy, the next step consists of the screening on this area of interest for U and Pb content on thick section in order to have an indication concerning the variability of U/Pb ratios. For this purpose, elemental mapping of the U, Pb, Fe and Sr were performed on the area of interest of the thick section (e.g., **Fig. 4.6B**). U-Pb dating on calcite is based on the LA-ICP-MS (*in situ* Laser Ablation Inductively Coupled Plasma Mass Spectrometry) method which requires dispersed U/Pb ratios in order to make robust statistical calculations thus allowing a strong age with the least uncertainty to be obtained.

Where the screening shows the U and Pb concentrations variability, about 30 circular spots of 100 µm diameter are picked along the mineral phase to perform the Laser Ablation. Calcite ablation on thick sections was performed using an ESI (Electro Scientific Industries) laser (193nm ArF Excimer laser) the resolution of which is 100 µm. Reference standards were used to correct the inter-elemental fractionation. The raw data were processed with the Lolite ® software designed for laser ablation analyses. An Excel macro, inhouse to the CEREGE, is used

to handle the U-Pb data. Finally, the U-Pb age is calculated by using the Tera-Wasserburg diagram with add-on isoplot 4.15 (Excel) (**Fig. 4.6-4.7**). Further details on the methodology and the analytic parameters can be found in (Godeau et al., 2018) and their online supporting data section.

4.3.4. Pollen-based climatostratigraphy

52 samples of about 20-30 grams weight have been processed in order to obtain pollen floras using the classical method (acid digestions with hydrochloric acid (HCl) and hydrofluoric acid (HF), concentration in $ZnCl_2$ at density 2, and sieving at 10 µm). Only 18 samples yielded pollen grains in sufficient quantities (their geographic distribution is shown in **Figure 4.1.B** and specified in **§ 4.8. Supplementary data - Table S4.1**. The palynological residues are mounted within glycerol between the slide and coverslip that allows to slightly move each pollen grain for observation purposes under various sides. Some pollen records, from the wells (Gallician 1, 4 and 9, Maruéjols 1) and the exposed Monteils section (Saint-Chaptes Basin, ASCI system), display a number of taxa that is lower than 25 (= systematic entities equivalent to families or genera). This value is the diversity threshold required to reliably assess the representativeness of a pollen flora sample. These non-representative samples should be interpreted with caution.

The main advantage of this new pollen analysis approach based on a detailed taxonomic investigation is that it aims to reconstruct the botanical flora and is therefore a peculiar approach for the Paleogene times. The accurate examination of the morphological characters of fossil pollen grains and their comparison with modern pollen grains of rich and varied collections (ISEM mainly, GeoBioStratData.Consulting) and iconographic databases allow to confidently identify fossil pollen grains at least at the family level and very often at the genus level. A powerful ecological interpretation of pollen floras results from such botanical identifications. These botanical identifications are robust as it has been demonstrated that almost all the modern genera of plants already existed since the Early Paleogene and were altitudinally-latitudinally distributed similarly to the present time (Suan et al., 2017; Salpin et al., 2019; Suc et al., 2020). The significance of our pollen records in terms of ecological-climatological changes are also enhanced thanks to pollen countings. To date, pollen counting approach has been a routine investigation for the Pliocene and Quaternary and less used for ancient series.

High-quality pollen identification and countings have allowed to successfully apply on these pollen floras the ‘Climatic Amplitude Method’ (Fauquette et al., 1998) in order to quantify the Paleogene palaeoclimatic conditions (Suan et al., 2017; Salpin et al., 2019; Suc et al., 2020). The analyses have been performed on a AX10 Zeiss light microscope at X250 magnification, each pollen grain being observed at X1000 magnification for its identification.

A minimum of 150 pollen grains were counted per sample extra those of *Pinus* (a cosmopolitan genus), those of meso-microthermal trees, inhabiting mid-altitudes (*Cathaya*, *Podocarpus*, *Fagus*, *Cedrus*, *Tsuga*), and those of microthermal trees, inhabiting higher altitudes (*Abies* and *Picea*). The detailed pollen analyses are provided in **§ 4.8. Supplementary**

data -Table S4.2. Taxa are grouped according to the climatic and/or ecological significance of their modern representatives (**Table S4.2**), resulting in two types of synthetic pollen diagrams (**Fig. 4.8**). The first type includes all the pollen grains excepted those of *Pinus* and provides a local and regional image of the vegetation (including that growing on reliefs); the second type excludes the mid- and high-altitude plants and provides a perception of the local vegetation (i.e., that of low altitudes). In such diagrams, plants are grouped mainly according to the classification of Nix (1982) based on the mean annual temperature (MAT), the concerned taxa usually requiring relatively elevated to high precipitation: megatherms (MAT > 24 °C), mega-mesotherms (20 °C < MAT < 24 °C), mesotherms (14 °C < MAT < 20 °C), meso-microtherms (12 °C < MAT <14 °C), and microtherms (MAT < 12 °C). The other groups have various significations: environmental for the herbaceous plants (more often not-identifiable at the infra-family level), ecological for the water plants, indicative of some dryness (Mediterranean sclerophyllous plants, steppe plants and subdesertic plants), insignificant (for example, the Cupressaceae with a *Cupressus-Juniperus* like pollen unidentifiable at the genus level). Details about taxa composing the groups are provided in **Table S4.2**.

In **Figure 4.8**, the vertical arrangement of samples first follows the stratigraphic knowledge of the studied basins (Gottis, 1958; Clauzon, 1990; Biteau et al., 1993 (*unpublished*); Séranne, 1999; Lettéron et al., 2017, 2018, 2021) and chronology is specified thanks to informations provided by mammal faunas (Depéret, 1917; Rémy, 1985; Rémy, 1994; Rémy and Fournier, 2003; Rémy and Lesage, 2005). Calcareous nannofossils have been searched in the samples containing frequent to abundant marine dinoflagellate cysts (**Table S4.2**): they are specified in **§ 4.8. Supplementary data - Table S4.3**.

The varying content of successive pollen locations is mostly considered as markedly driven by global climate changes which was affected by major and secondary fluctuations during the time interval 38–23 Ma as illustrated by the global oxygen reference isotope curve (**Fig. 4.8**; Westerhold et al., 2020). Accordingly, pollen floras are hypothesized to correlate with the global climatic evolution, that constitutes the principle of climatostratigraphy (**Fig. 4.8**; Suc, 1984; Suc et al., 1995, 2018, 2020; Popescu et al., 2010). This approach contrasts with the traditional palynostratigraphy approach based on the direct attribution of a chronological value to a described pollen grain (Sittler and Schuler, 1975; Châteauneuf, 1980; Châteauneuf et al., 2019) that may lead to misinterpretations (Further discussion on the two approaches in **§ 4.8. Supplementary data - Appendix A**.

4.3.5. Climatic Amplitude Method

The investment in pollen identification and counting implies the possibility to use the Climatic Amplitude Method to reconstruct climate conditions during the deposition of the sediments. This method, after comparison with more than 6,000 present-day pollen records distributed worldwide, relies on the relationship between the relative abundance of each individual taxon and the climate because the method accounts not only for the presence/absence criterion but also percentages (Fauquette et al., 1998). The estimated mean annual temperatures

(MAT), mean temperatures of the coldest (MTC) and warmest (MTW) months and mean annual precipitation (MAP) concern low-elevation vegetation because meso-microthermal and microthermal taxa (*Cedrus*, *Fagus*, *Tsuga*, *Cathaya*, *Podocarpus Abies* and *Picea* which live today at higher elevations in tropical-subtropical regions) were excluded from the process (but not from the percentages) to avoid a cold bias linked to transport from higher elevations. *Pinus*, which may inhabit different vegetation belts, is also excluded from the calculation. The excluded taxa were defined based on the distribution of vegetation today. Indeed, the types of vegetation deduced from our pollen data are found in South-eastern China today at around 25°N and 110 to 120°E (Hou, 1983). In this region, the vertical distribution of the vegetation is characterized, from the base to the top of the massifs by evergreen broad-leaved forest, mixed evergreen and deciduous (*Betula*, *Acer*) broad-leaved forest, *Cathaya*/*Tsuga* forest, *Picea*/*Abies* forest and high mountain meadows (Hou, 1983). In the Climatic Amplitude Method, the estimates for each climatic parameter are given as an interval (minimum and maximum values of the parameter) and a most likely value (MLV) corresponding to a weighted mean. The MLV has been statistically tested on modern pollen data and has provided reliable results (Fauquette et al., 1998).

4.3.6. Geochemical modelling of Strontium and Sulphur isotopes on sulphates

The geochemical modelling of $\delta^{34}S$ and $^{87}Sr/^{86}Sr$ on sulphates is carried out to assess the relevance of different scenarios of mixed saltwater compositions. The compositions of mixed saltwaters allow to identify the context (continental vs marine) and timing (age) of the salinisation of the lacustrine sedimentary basins.

a. Sampling and measurements

Five anhydrite samples from Pierrefeu-1 well (Vistrenque Basin, see positions in **Fig. 4.5**) and three anhydrite samples from Les Fumades wells (SC-1 and SC-2, Alès Basin, see position in **Fig. 4.4**) have been selected for $\delta^{34}S$ and $^{87}Sr/^{86}Sr$ laboratory measurements.

Strontium isotope measurements were carried by the SARM-CRPG laboratory (Vandoeuvre-lès-Nancy, France). Samples have been powdered (<50 µm), weighed and mixed with HNO_3 and HF and after evaporation, mixed with concentrated HCl. After complete digestion of the sample and Sr separation, $^{87}Sr/^{86}Sr$ was measured using a TIMS Triton Plus (Thermo electron) in static mode. The standard NBS987 has been used as a reference. All measurements have 2σ error lower than 0.000012.

Anhydrite samples were measured in duplicate for their S and O isotopic composition on an Elementar vario PYRO cube elemental analyzer (Elementar GmbH) in-line with an Isoprime 100 mass spectrometer (Manchester, UK) in continuous flow mode at the University of Burgundy in Dijon, France.

For Oxygen isotopes, samples were measured through pyrolysis. The data are expressed in delta notation, $\delta = (R_{Sample}/R_{Standard}) - 1$, where R is the mole ratio of $^{18}O/^{16}O$ and reported in

units per mille (‰, i.e., × 1000). The $\delta^{18}O$ data are reported with respect to the international standard Vienna Standard Mean Ocean Water (VSMOW). Analytical errors are ± 0.4 ‰ (2σ) based on long term replicate analyses of the international barite standard NBS-127, which was used for data correction via standard-sample-standard bracketing.

For sulphur isotopes, samples were measured through combustion. Sulphur isotope data are expressed in delta notation and reported in units per mil (‰). The $\delta^{34}S$ data are reported with respect to the international standard Vienna Cañon Diablo Troilite (VCDT). Analytical errors are ± 0.3 ‰ (2σ) based on replicate analyses of the international barite standard NBS-127, which was used for data correction assuming a $\delta^{34}S$ value of + 20.3 ‰ on the VCDT scale.

b. Modelling of Strontium and Sulphur isotope composition of mixed waters

Strontium and sulphur isotope compositions of gypsum and anhydrite have been proved to be reliable markers of the origin of the waters from which they precipitated and make it possible to quantify the proportions of different waters in the case of a mixture (Denison et al., 1998).

The Sr isotope composition of two-component mixtures/endmembers has been described in detail by Faure (1986) and applied to Sr and Sulphur isotopes (Andersson et al., 1992; Denison et al., 1998). The isotopic ratio ($^{87}Sr/^{86}Sr$ and $^{34}S/^{32}S$) Im is computed as follows:

$$\mathbf{Im=[f1.C_1.I_1+(1-f_1).C_2.I_2] / [f_1.C_1 + (1-f_1).C_2] \ (1)}$$

Where I_1 and I_2 represent the isotopic ratios of the first and second end member, respectively. C_1 and C_2 are the Sr or SO_4^{2-} concentration in the first and second end members, respectively and f1 is the volume fraction of the first end member water in the mixture.

Various endmembers have been selected for the modelling: 1) seawater, 2) continental water whose Sr and S content is controlled by the leaching of Triassic evaporites, 3) continental water whose composition is derived from the leaching of metamorphic rocks.

The Sr concentration of Paleogene seawater (15 ppm) is derived from the estimations by Vollstaedt et al. (2014); such a value is slightly higher to modern concentrations (~8 ppm). Sulphur concentration was assumed to be similar to that of modern seawater (2800 ppm). The $^{87}Sr/^{86}Sr$ values for Priabonian to Chattian seawater range from 0.7077 to 0.7083 (Mc Arthur et al., 2012) while $\delta^{34}S$ is assumed to be close to modern values (+20‰).

Riverine waters influenced by the leaching of Triassic evaporites have been considered to have retained the $^{87}Sr/^{86}Sr$ and $\delta^{34}S$ of the original gypsum or anhydrite. $^{87}Sr/^{86}Sr$ values ranging from 0.7076 to 0.7080 have been reported for Triassic (Keuper) evaporites from the French Pyrenees (Albarède and Michard, 1987), Italy (Dinelli et al., 1999), Spain (Alonso-Azcarate et al. 2006; Ortí et al., 2014), while $\delta^{34}S$ values range from +10 ‰ to +17 ‰ (Utrilla et al., 1992; Dinelli et al., 1999; Boschetti et al., 2011).

Riverine waters flowing across metamorphic or igneous rocks should have higher $^{87}Sr/^{86}Sr$ ratios as shown in present time in the Cevennes Massif, with values ranging from 0.712 to 0.714

for waters draining granites and from 0.714 to 0.717 for waters draining schists (Petelet-Giraud et al., 2006). Regarding sulphur isotope composition, magmatic and metamorphic rocks are known to be characterized by $\delta^{34}S$ ranging from -12 ‰ to +12‰ (Chaussidon et al., 1989; Giacometti et al., 2014).

4.4. Results and interpretations

4.4.1. Lithological framework of the Vistrenque Basin

The lithological correlations within the Paleogene succession between the studied wells from the Gallician sector (Gallician 1, Gallician 4, Gallician 9, Vauvert 1) and Pierrefeu sector (Pierrefeu 1) are based on GR signal and major lithological changes. These correlations are given in **Figure 4.5**.

The reference section of the Gallician 9 well from the Gallician sector provides the most complete lithological column of the Vistrenque Basin. In this borehole, the lowermost 'Série Grise' Formation is several hundred metres thick (the base of the Paleogene is not reached in this sector) and is constituted of a monotonous succession of sandstones (calcarenites), conglomerates, marlstones and less common evaporites deposited in lacustrine settings. The overlying 'Série Calcaire' Formation is 251 m thick and is made essentially of sandstones (calcarenites) and calcisiltites (siltstones), and a few monomictic conglomerates at the base. These lithologies become scarce upward while variegated calcareous claystones and vacuolar limestones become more frequent, and the unit is capped by a major subaerial exposure surface.

The 'Série Mixte' Formation is 42 m thick and characterized by alternation of dominantly polymictic conglomerates, siliciclastic sandstones, variegated calcareous claystones and limestones. The Série Rouge Formation is made of alternations of siliciclastic sandstones and marlstones, and conglomerates at the base. This unit is capped by a major unconformity that separates it from the overlying 'Série Calcaréo-Salifère' Unit.

The 'Série Calcaréo-salifère' Formation is around 300 m thick in the Gallician sector and constituted mainly of limestones and papyraceous marlstones at the base. The upper part of the unit is made of two sequences made of alternation of sandstones, marlstones, limestones, anhydrite, and halite.

In Vauvert 1 well, the Paleogene succession is encountered with increased thickness (>1700 m) and the base of the Paleogene is not reached. The 'Série Grise' is thick (1200 m) and display similar lithologies with the Gallician 9 well counterpart. The 'Série Mixte' is around 400 m thick and the 'Série Rouge' is more than 100 m thick.

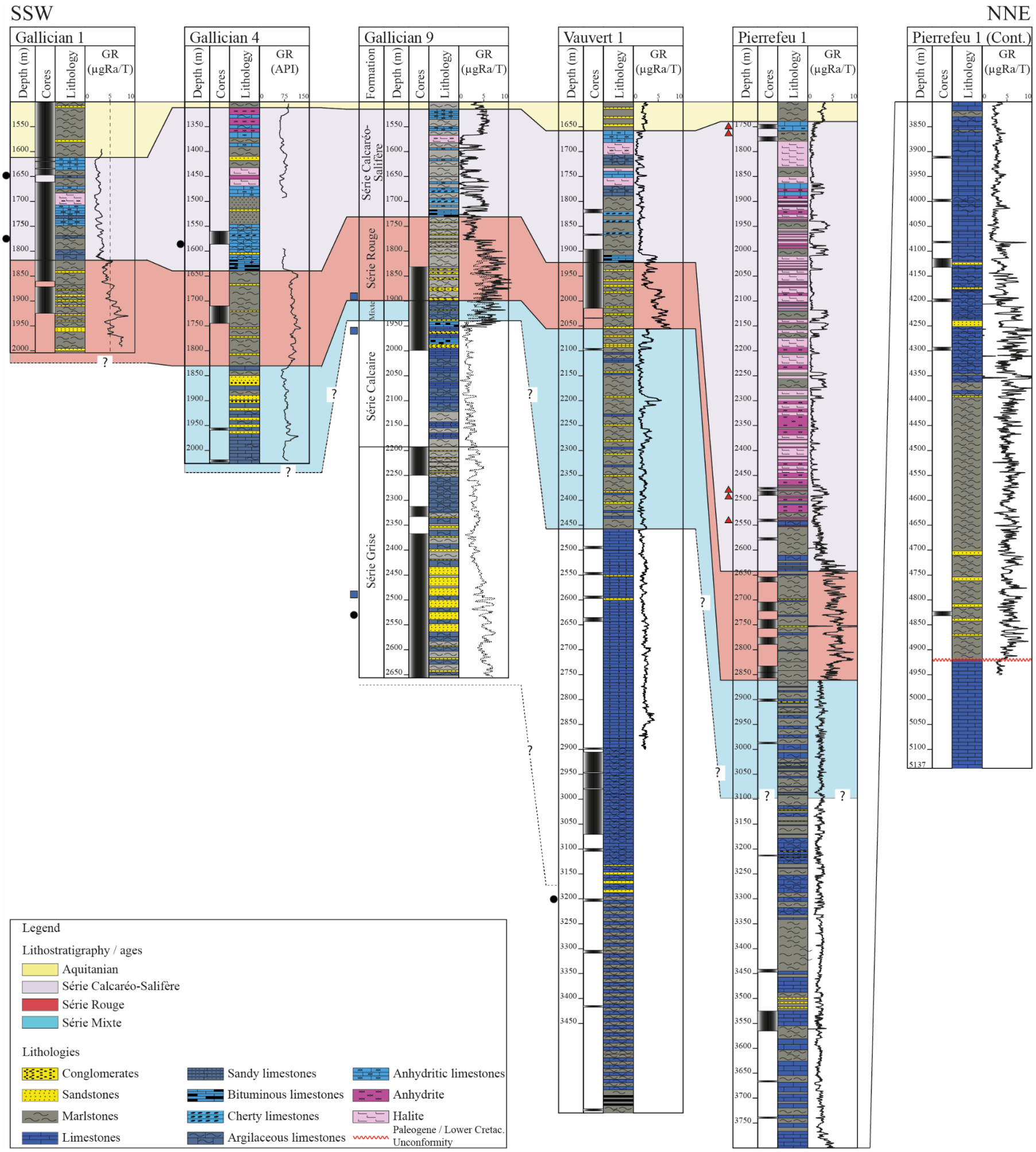

Figure 4.5: Correlation panel of wells Gallician 1, Gallician 4, Gallician 9, Vauvert 1 and Pierrefeu 1 from the Vistrenque Basin showing the sedimentary units, lithologies and lithostratigraphic correlations. Lithostratigraphic correlations are carried out using lithological similarities and gamma ray (GR) signal. Drill core locations and the positions of samples used for U/Pb dating (squares) and pollen analyses (circles), and $^{87}Sr/^{86}Sr$ & $\delta^{34}S$ measurements (triangles) are also plotted.

In Pierrefeu 1 well, the Paleogene interval is still thicker (~3200 m) and the nomenclature is slightly different. The 'Série Calcaire' and 'Série Mixte' formations have not been recognized probably because of lateral variations of facies. The top of the Série Grise from the Pierrefeu 1 well likely corresponds to the 'Série Calcaire' defined in the Gallician sector. The 'Série Mixte' Unit from Gallician 9 well probably corresponds to the base of the 'Série Rouge' Unit in the Pierrefeu sector.

Sedimentological and stratigraphic analyses of 'Série Rouge' and underlying units have been carried out in a further detailed work (Semmani et al., in prep, *see chapter 5 in this PhD manuscript*). Main lithofacies defined in these units and their palaeoenvironmental interpretations are given in **Table 4.1**.

Table 4.1: Depositional lithofacies, their facies associations and palaeoenvironmental interpretations defined in the Paleogene 'Série Rouge' and underlying units from the Vistrenque Basin (Camargue, SE France), see further details in (Semmani et al., *in prep*, see chapter 5 in this PhD manuscript).

Facies association	Code	Facies	Palaeoenvironmental interpretation	Occurrence
FA1 Evaporite-rich perennial lake	F1	Anhydritic marlstones and anhydrite	Evaporative perennial lake	Uncommon, reported only from one thick interval from Série Grise formation (Fm).
FA2 Profundal lake	F2	Finely laminated argillaceous limestones and papyraceous marlstones	Profundal perennial lake with poorly oxygenated conditions	Frequent in the Série Calcaire & occasional in the Série Grise
	F3	Dark grey marlstones with scarce fauna		Common in the Série Grise and in the Série Calcaire formations
FA3 Lake slope and offshore lake	F4	Glauconite-rich sandstones and fine-grained calcarenites	Gravity-driven currents in the lake slope and offshore lake	Common in the Série Grise Fm
	F5	Coarse calcarenites and microconglomerates		Frequent in the upper part of the Série Grise formation
	F6	Matrix-supported conglomerates		Occasional to frequent in the Série Grise formation
FA4 Deltaic and littoral lake	F7	Bedded quartzose calcarenites	Vicinity of a riverine mouth (lacustrine delta) and lake littoral	Frequent in the upper part of the Série Calcaire Fm but also at the base of the S. mixte Fm
	F8	Oncolitic limestones		Occasional in the Serie Mixte formation
	F9	Microbial limestones (tufa?)		Frequent in the Série Mixte & Série calcaire formations
FA5 Fluvial association	F10	Polymictic conglomerates and microconglomerates	Channelized and overbank deposits	Frequent in the Série Rouge and less the Série Mixte Fm
	F11	Fine to medium sandstones (Quartzose sandstones)		Common in the Série Rouge and occasional in the Série Mixte Fms.
FA6 Floodplain association	F12	Variegated and mottled calcareous claystones	Floodplain and very shallow pond/ephemeral water pans	Common in the Série Rouge and Série Mixte formations Occasional in the Série Calcaire formation.
	F13	Pedogenically modified carbonates (Brecciated limestones)		Frequent in the Serie Mixte and occasional in Série Rouge (lowermost parts) and Série Calcaire formation.

4.4.2. U-Pb dating

The new results from 1) U/Pb dating on calcite, 2) Pollen-based climatostratigraphy, and 3) geochemical modelling on sulphates are summarized in **Table 4.2**. These results are presented and interpreted in the following sections.

Among the eleven samples that were selected for U-Pb dating, three of them have been tested without success while five samples display large uncertainties and have therefore been excluded from the stratigraphic interpretations. Because the requirements for a robust U-Pb dating are not satisfied in those samples (i.e., U and Pb concentrations, and U/Pb ration variability), only the three successful analyses from Gallician 9 well are described in the following sections: (a) G9 13D, (b) G9 7, and (c) G9 K35. Details are provided on the microscopic analyses that allowed to determine the calcite phase to perform the LA-ICP-MS method on the samples and the resulting U-Pb ages are interpreted.

Table 4.2: Dating results obtained in the Vistrenque Basin using U-Pb dating on calcite, Pollen-based climatostratigraphy and geochemical modelling on sulphates. Samples presented come from the Paleogene succession of the Gallician and Pierrefeu sectors. Samples from the Alès and Roussillon basins are given in § 4.8. supplementary data (**Table S4.1**; **S4.2**). Sample G9 K35 (2487m) does not give concluding age to approximate depositional age and is therefore excluded from chronological framework interpretations (see text for details).

Lithostratigraphic units	Age	Dating approach	Analysed samples	Well – depth (m)
Série Calcaréo-salifère	Late Chattian to earliest Aquitanian?	Geochemical modelling on sulphates	Anhydrite	Pierrefeu 1 – 1750 Pierrefeu 1 – 1775 Pierrefeu 1 – 2485 Pierrefeu 1 – 2545
	Early to middle Chattian	Pollen climatostratigrpahy	Pollen assemblage	Gallician 1 – 1648 Gallician 1 – 1775 Gallician 4 – 1580
Série Rouge	Early Chattian [a]	U/Pb dating * Absolute age: 27.88 +/1.71 Ma [b]	Vadose cement	Gallician 9 – 1894
Série Mixte	Middle Rupelian to early Chattian	Bounding	/	/
Série Calcaire	Early to middle Rupelian [a]	U/Pb dating * Absolute age: 31.27 +/1.90 Ma [b]	Vadose cement	Gallician 9 – 1960
Série Grise	Priabonian (?) to early Rupelian	Pollen climatostratigraphy	Pollen assemblage	Gallician 9 – 2530 Vauvert 1 – 3200

[b] Ages are calibrated with the Geological time Scale after Gradstein et al. (2012).

[a] Errors include measurements errors and errors associated with statistic calculations, considering 95% confidence interval

a. G9 13D Sample: *subaerial exposure on top of the 'Série Calcaire' Unit*

In this sample, microstalactitic calcite (A1) lines the cavity and is post-dated by an anisopachous calcite cement (A2) which is in turn post-dated by an isopachous equant sparry calcite cement (I1) (**Fig. 4.6A**). Only cement A1 displays dull luminescence while the following cements are non-luminescent and thus cannot be distinguished under cathodoluminescence. However, observations under confocal microscope made it possible to distinguish the cement generations (**Fig. 4.6C**). Uranium concentrations are very low in the A2 and I1 cements thus precluded dating analyses (**Fig. 4.6B**). However, the cement stage A1 displays enough U and

Pb thus allowing the dating method to be applied (**Fig. 4.6D**). The calculated age of the early diagenetic microstalactitic cement A1 is **31.27 +/- 1.90 Ma** which gives a lower to middle Rupelian age after GTS2012 (Gradstein et al., 2012).

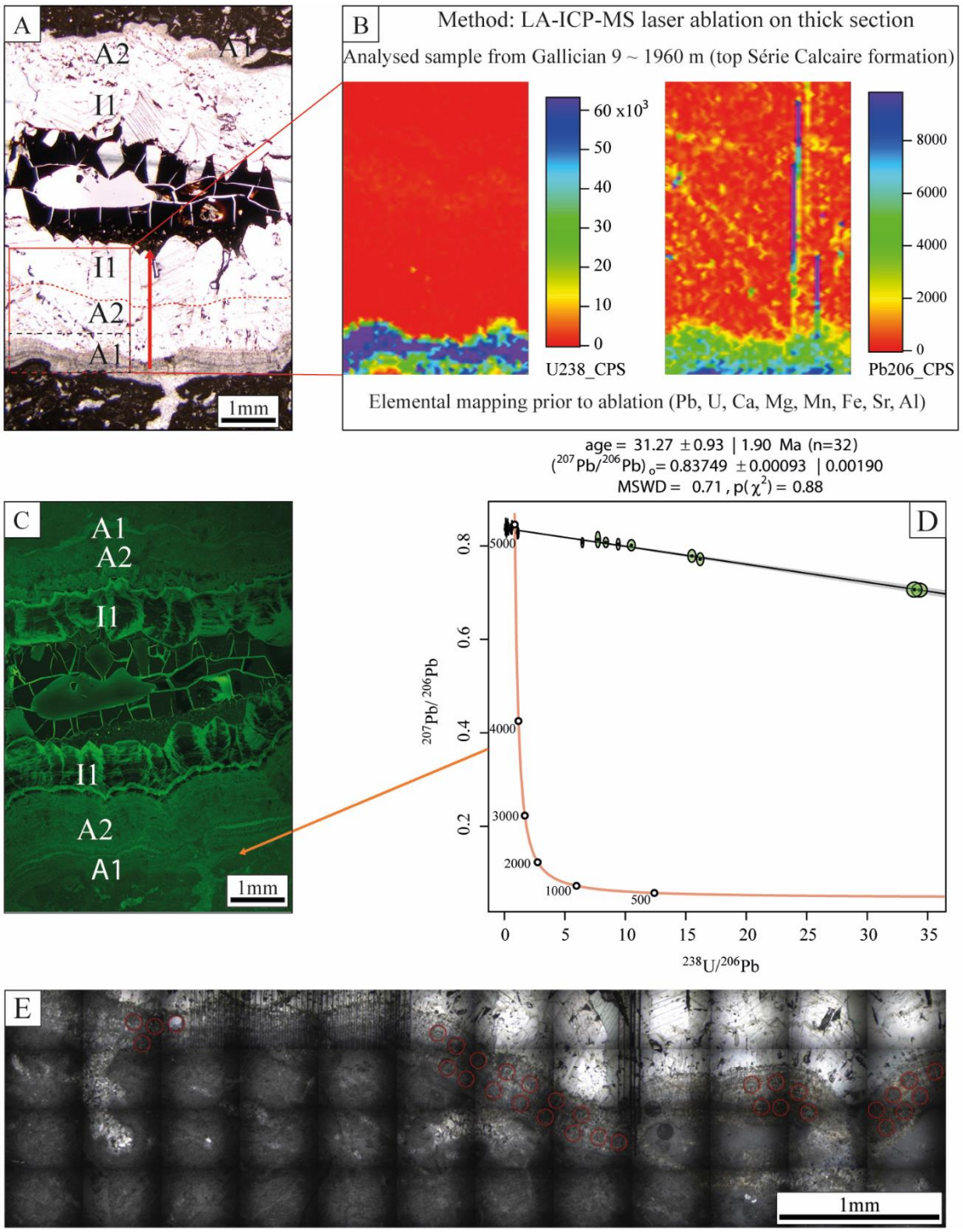

Figure 4.6: A) Microphotograph of the cavity in thin section of the sample G9 13D from Gallician 9 well (depth ~ 1960 m) displaying the growth of successive cement stages: microstalactitic cements A1 & A2, and coarse bladed calcite I1 with further bitumen infill. B) elemental mapping of the red box in A) showing the concentrations of ^{238}U and ^{206}P. C) Confocal microscopy photograph of the cavity in (A) where the fluorescence allows to observe the different generations of cement. The cementation stages A2 and I1 are non-luminescent and therefore indistinguishable under cathodoluminescence. D) Tera-Wasserburg plots displaying $^{238}U/^{206}Pb$ versus $^{207}Pb/^{206}Pb$

from the A1 cement (early diagenetic anisopachous cement). E) panorama image of the dashed line contour box in A) showing the Laser Ablation (red circles) craters within the A1 cement, (number of spots = 32).

b. G9 7 sample: *vadose cement within the lowermost interval of the 'Série Rouge' Unit*

This sample displays anisopachous pendant microsparite cements, up to 600 µm thick around clasts in a polymictic conglomerate (**Fig. 4.7A**). In this sample, carbone and oxygen isotope analyses on the calcite yielded very negative values ($\delta^{18}O$ = -5.11 ‰ V-PDB & $\delta^{13}C$ = -5.59 ‰ V-PDB) thus indicating meteoric origin of the precipitation water. In addition, the anisopachous nature of the cement suggests precipitation under vadose meteoric conditions. Such cements represent the earliest phase of cementation and formed prior to burial and mechanical compaction. The cement therefore likely formed shortly after deposition and infill of the fluvial channel, in a vadose environment within an alluvial plain. U and Pb concentrations are favourable thus making it possible to perform the dating method. 74 spots have been used and the concentrations show sufficient dispersal of the U/Pb ratio thus enhancing the accuracy of the method (**Fig. 4.7B**). The U-Pb age found for this carbonate phase using the Tera-Wasserburg diagram is **27.88 +/- 1.71 Ma** which indicates an upper Rupelian to lower Chattian age according to the GTS (Gradstein et al., 2012). The initial composition ratio of $^{207}Pb/^{206}Pb$ is 0.8321 +/- 0.034.

c. G9 K35 sample: *calcite veins within the lower 'Série Grise' Unit*

The K35 sample is from the terrigenous-rich 'Série Grise' Unit. In this sample, the calcite analysed for U-Pb dating consists of the filling of fractures (veins) within the silty marlstones host rock (**Fig. 4.7C**). The vein is around 1 mm large and is filled with equant to fibrous calcite, the crystals sizes average 200 µm.

Under cathodoluminescence, the calcite vein is non-luminescent and seems to be formed in one cementation stage as indicated by the absence of features indicating vein growth (**Fig. 4.7D**). In the calcite vein, U and Pb concentrations are favourable to the dating method (**Fig. 4.7E**). The calculated Tera-Wasserburg U-Pb age for the calcite vein infill is 21.46 +/- 2.19 Ma corresponding to a mid-Aquitanian age according to GTS2012 (Gradstein et al., 2012).

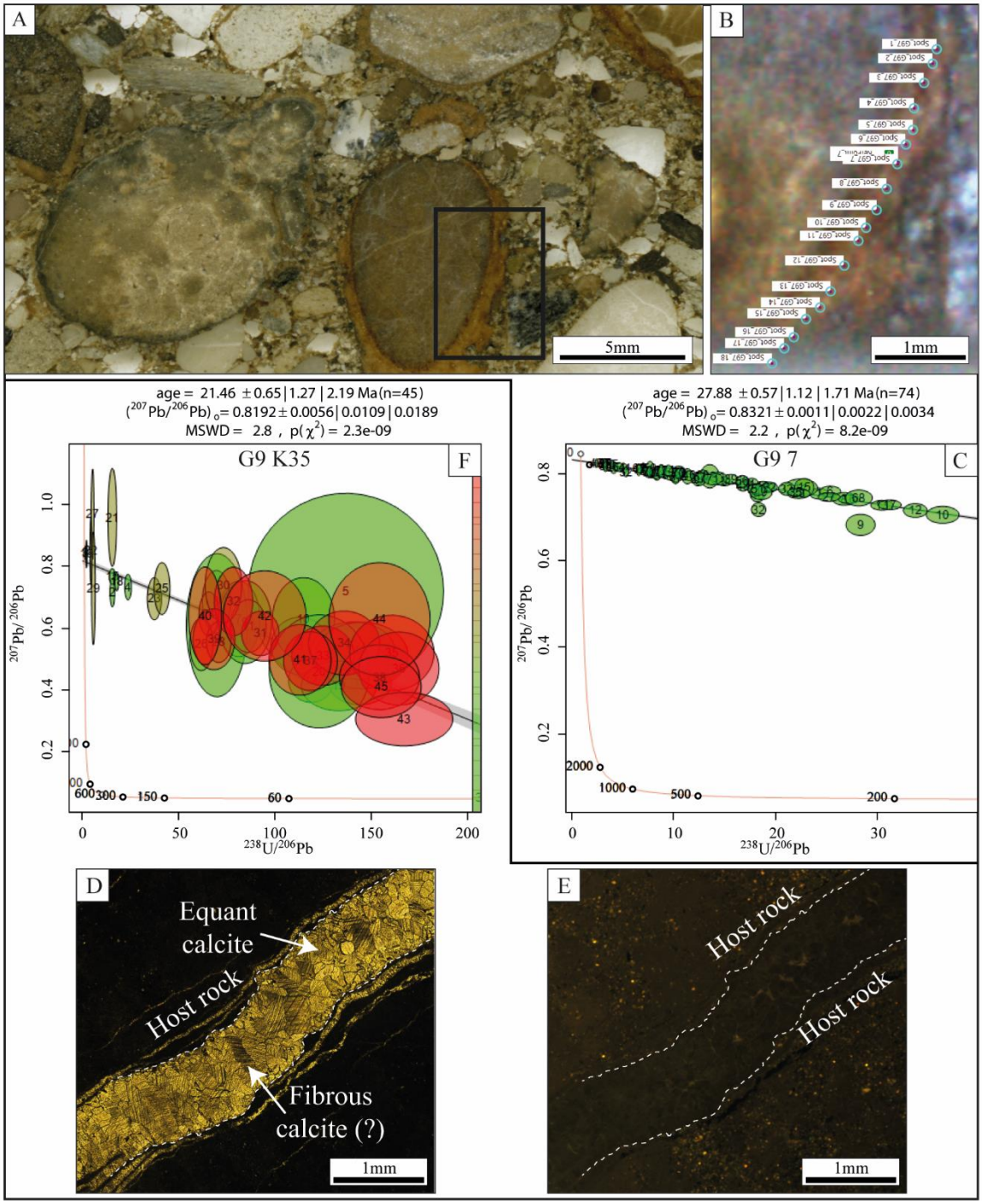

Figure 4.7: A) Thick geological section scan (sample G9 7; Gallician 9 well, depth ~ 1894 m) showing the yellowish beige pendant anisopachous cement around clasts in a fluvial conglomerate. B) close-up view of the rectangular box in A) displaying the position of the laser ablation spots alongside the cement. C) Tera-Wasserburg plots displaying $^{238}U/^{206}Pb$ versus $^{207}Pb/^{206}Pb$ from the anisopachous cement of the G9 7 sample (number of spots = 74). D) and E) Microphotographs of the vein calcite infill within the G9 K35 sample (Gallician 9, depth ~ 2487 m) under plane polarized light and cathodoluminescence respectively. Note the dull luminescence of the calcite fill (right hand picture). F) Tera-Wasserburg plots displaying $^{238}U/^{206}Pb$ versus $^{207}Pb/^{206}Pb$ from the calcite vein infill of the G9 K35 sample (number of spots = 45).

4.4.3. Pollen-based reconstructed palaeoclimates and climatrostratigraphy

a. Results

A total of 122 taxa have been identified in the 18 pollen records (**Table S4.3**). These pollen floras show prevalent mega-mesothermal plants and, secondarily, mesothermal plants and the conifers *Cathaya* and *Podocarpus*. Megathermal elements are mostly present in the Priabonian samples where they show relevant variations. Steppe elements mainly occur in the Rupelian samples. The other plant groups are intermittently represented (see morphological description of some pollen grains in **§ 4.8. Supplementary data** - **Appendix A**).

Pollen record of five samples from wells in the Vistrenque Basin (Gallician 1 1648m, Gallician 1 1775m, Gallician 4 1580m, Gallician 9 2530m, and Vauvert 1 3200m; **Fig. 4.8**, see location in **Figure 4.5**) was relatively poorly diversified and poorly preserved. Indeed, these pollen grains have been partially vitrified and therefore some of their morphological characters (ornamentation, structure) are severely altered. A certain amount of pollen can still be identified even though a great percentage of undeterminable pollen grains may lead to lessen the significance of some of these microflora (percentage of unidentifiable pollen grains: Gallician 1 1648 m: 8.19%; Gallician 4 1580 m: 37.36%; Vauvert 1 3200 m: 10.81%).

In addition, some of these pollen floras are characterized by a low number of taxa (Gallician 1: 24 taxa at 1648 m, 19 taxa at 1775 m; Gallician 4 1580 m: 13 taxa; Gallician 9 2530 m: 20 taxa). Among the possible hypotheses to explain such biases in preservation and plant diversity (oxidation, transport, diagenesis), the usual occurrence of oil traces during the sample processing points to a thermal diagenesis in relation with sediment maturation within the oil window. In the Gallician samples, the dominant pollen grains are those of Gymnosperms which remain often identifiable despite their poor preservation, especially of meso-microthermal (*Cathaya*, *Podocarpus*, and some *Tsuga*) and microthermal (*Abies*) trees which may reflect the relief of the Pyrenees and subsidiarily of the Alps.

The pollen record of the Gallician 9 2530m sample shows the dominance of mega-mesothermal (Cupressaceae papillate pollen representative of the former ‘Taxodiaceae’ family) and both *Cathaya* and *Podocarpus* but a significant feature of this sample is the occurrence of some mesothermal plants, Cupressaceae *(Cupressaceae-Juniperus*-type*)* and *Ephedra* (steppe plants).

The climate has been quantified for all the pollen spectra except for Gallician 1 1775 m, Gallician 4 1580 m and Saint-Jean de Maruéjols – Pit hill samples because of the low taxa diversity. The results are given, for each climatic parameter, as a min-max interval and a Most Likely Value (in bold) for each site (**Table 4.3**).

Table 4.3: Climatic reconstruction based on pollen data. Mean annual temperatures (MAT), mean temperature of the coldest (MTC) and of the warmest (MTW) months and mean annual precipitation (MAP) are reconstructed using the Climatic Amplitude Method (Fauquette et al., 1998). The results are given as a min-max interval and a Most Likely Value (in bold) for each site where the diversity threshold is reached (n=15); climatic parameters are not quantifiable for Gallician 1 1775 m, Gallician 4 1580 m and Saint-Jean de Maruéjols – Pit hill samples. Samples sorting follows chronostratigraphic attributions (see **Figure 4.8** for biostratigraphic and climatostratigraphic age attributions).

Site	MAT (°C)	MTC (°C)	MTW (°C)	MAP (mm)
Gallician 1 - 1648 m	16-**18.9**-25	5-**9**-14	25-**26.2**-29	1100-**1560**-1960
Canet 1 - 1100 m	16-**19**-25	10-**11.6**-14	25-**26.2**-29	1100-**1640**-2200
Canet 1 - 1186 m	15-**18.4**-25	2.5-**10.4**-14	25-**26.2**-29	1000-**1260**-1400
Canet 1 - 1470 m	16-**19**.1-24	10-**11.7**-14	25-**26.1**-28	1100-**1230**-1300
Canet 1 - 1701 m	19-**20.7**-25	10-**12.7**-16.5	26-**26.7**-28	1200-**1530**-1960
Gallician 9 - 2530 m	12-**15.8**-20	2.5-**7.3**-14	20-**23.3**-27	800-**870**-2200
Vauvert 1 - 3200 m	17-**19.7**-25	12-**13.2**-15	25-**26.2**-28	1200-**1325**-1400
Montchamp	20-**21.4**-25	12-**14.4**-15	26-**26.4**-28	1100-**1530**-1800
Celas Tunnel 2	19-**20.9**-25	12-**14.5**-17	25-**26.7**-29	1500-**1670**-1800
Celas Tunnel 1	19-**20.9**-25	10-**12.5**-15	26-**26.9**-28	1500-**1760**-2000
Maruéjols 1 - 798 m	19-**20.9**-25	12-14-17	26-**27.1**-29	1100-**1630**-2000
Monteils	15-**18.7**-25	10-**11.7**-14	25-**26.1**-28	1500-**1650**-1800
Crossroads D716/D981	19-**21.1**-25	12-**13**-14	26-**27**-29	1000-**1400**-1560
Serre de Cauvel 3	18-**20.2**-25	12-**12.8**-14	25-**26.2**-28	1100-**1540**-1800
Euzet Hill	17-**20.1**-24	12-**13.9**-16	25-**26.3**-28	1200-**1530**-1600

b. Interpretations:

The analysed pollen records allow to reconstruct the local and regional vegetation, from low altitude to elevated reliefs (**Fig. 4.8**). Lower places were sporadically occupied by *Avicennia* mangrove with probably Rhizophoraceae, suggesting nearby marine environments, which are also supported by the occurence of marine dinoflagellate cysts. Occurrence of lakes is revealed by frequent freshwater plants (*Aglaoreidia*, *Myriophyllum*, Oenotheraceae, Restionaceae, etc.) and the *Botryococcus* microalga. The coastal environments and lake banks were also inhabited by riparian swamps with *Taxodium-Glyptostrobus* (i.e., illustrated by the *Taxodium*-type pollen grains). Lowlands were occupied by an evergreen subtropical forest rich in mega-mesothermal plants (*Alangium*, *Engelhardia*, *Embolanthera*, *Distylium*, *Nyssa*, *Mussaenda*-type, *Rhoiptelea*, Sapotaceae, *Symplocos*, *Uncaria*-type, Cupressaceae former 'Taxodiaceae', etc.) including some megathermal plants (*Amanoa*, *Bombax*-type, *Afzelia-Peltophorum*-type, *Canthium*-type, *Croton-Jatropha*, *Peltophorum*-type, *Mappianthus*, *Phyllanthus*, *Peltogyne*-type, *Sapindaceae*, *Thumbergia*, etc.). Vicinity of higher lands is attested by abundant mesothermal plants (*Acer*, Araliaceae, *Carpinus*, *Carya*, *Eucommia*, *Liquidambar*, *Parrotia*, *Pterocarya*, *Quercus*, *Ulmus*, *Zelkova*, etc.), which constituted a mesophilous deciduous forest. The development of altitudinal forest vegetation (*Cathaya*, *Podocarpus*, *Cedrus*, *Tsuga*, *Abies*, *Picea*) suggests the

occurrence of reliefs, especially of high reliefs to the south as evidenced by Canet 1 well and Gallician wells pollen floras.

Cupressaceae trees (*Cupressus-Juniperus*-type) may contribute to the lowland and higher vegetation as they can be represented by diverse taxa growing today in subtropical to high altitude forests, because of our inability to distinguish their pollen. Sclerophyllous Mediterranean elements (*Olea* mainly, *Phillyrea*, *Quercus ilex*-type) episodically developed, simultaneously with decrease in taxa requiring great humidity and increase in herbaceous taxa. It is possible to conceive that these plants already grew on drier soils and tolerated less humid periods. Drier conditions are revealed by development of steppe assemblages (mainly constituted of *Ephedra*), in parallel with reducing of taxa requiring humid climate.

Variability observed in the Priabonian pollen assemblages appears to be related to climate fluctuations during a warmer phase. All these pollen records come from exposed sections and are not concerned by biases in preservation which often affect deep sediments from boreholes. They mainly consist in opposed amounts of thermophilous forest elements (megatherms and mega-mesotherms) and herbaceous and steppe elements (*Ephedra*) pointing to more open and drier environments. Variability observed in the Oligocene pollen assemblages could refer to climate fluctuations during a cooler phase resulting in alternations of drier and more humid episodes.

All the Oligocene pollen records come from drilled sediments in which pollen preservation may be poor, making their palaeoenvironmental interpretation uncertain. However, these major (Priabonian–Rupelian transition) and minor (intra-Priabonian and intra-Rupelian–Chattian) changes displayed by pollen assemblages are consistent with the reference oxygen isotope curve (**Fig. 4.8**; Westerhold et al., 2020).

Palaeogeographic reconstructions indicate the existence of elevated topography south of the Camargue and Languedoc areas (Benedicto et al., 1996). These reliefs supplied detrital sediments and pollen grains of high-altitude plants that have undergone low to moderate transport to the depositional areas of the Vistrenque and of the Alès basins. The abundance of *Podocarpus* in the Gallician samples, a marker of the Pyrenean flora during the Paleogene (Fauquette et al., in progress), indicates that the pollen material of these samples is sourced from these highlands.

In the Alès Basin, the climatic deterioration at the Eocene-Oligocene transition is expected to follow the Montchamp pollen flora, indicating persistent warm conditions. The reconstructed MAT and MTC are very high for this pollen spectra (**Table 4.3**). Because of their low percentage in megathermal plants in contrast to the occurrence of *Ephedra*, the pollen records of Monteils and of the Pit hill of Saint-Jean de Maruéjols attest less warm and weakly drier conditions than the Crossroads D716/D981, Célas, and Montchamp microfloras. The estimated MAT at Monteils is the lowest for this time period (Most Likely value around 18.7°C instead of 20 to 21°C, **Table 4.3**). Some cooling is also evidenced by the Serre de Cauvel pollen

assemblage with respect to decreased megathermal plants and increased Mediterranean sclerophyllous elements. However, this cooling should be less important as it is not observed in the estimated climate. The Monchamp microflora contains *Avicennia* and Rhizophoraceae pollen grains. The latter are also recorded at Serre de Cauvel while *Avicennia* is also recorded at Saint-Jean de Maruéjols Pit hill, Célas Tunnel and Crossroads D716/D981. Mean temperature of the warmest month (MTW) is stable all along the period (**Table 4.3**).

In the Vauvert 1 3200 m sample, the presence of relatively frequent pollen of Mediterranean sclerophyllous plants may point to the climatic cooling at earliest Oligocene, supported by few megathermal plants, reduced mega-mesothermal plants and increasing herbaceous open environments in a context of shortening freshwater bodies. This cooling and lower humidity are also well marked in the estimated mean annual temperature (MAT), mean temperature of the coldest month (MTC) and mean annual precipitation (MAP) (**Table 4.3**). The estimated MAT at Vauvert is in agreement with the value obtained at Saint-Lions, to the South of Digne, for the same period (Fauquette et al., 2015). In the Gallician 9 2530 m sample, some aridification of the climate is suggested by the local expansion of *Ephedra* that leads to a low estimate of mean annual precipitation (**Table 4.3**). Pollen assemblages of Gallician 4 1580 m and Gallician 1 1648 m are consistent with a Late Oligocene age.

Our ascription of the studied interval of Canet 1 well (1701–1100 m) to Oligocene is based on the presence-abundance of *Podocarpus* pollen, never recorded in Southern France since the earliest Aquitanian (Bessedik, 1984). The Canet 1 samples at 1701 and 1470 m depths are considered to belong to the Rupelian by analogy with the Galician 9 2530 m sample because of frequent elements living in dry environments. Climate reconstruction of Canet 1 well show that MAT are 1 to 2°C and MTC are 1 to 5°C lower than during the Priabonian. MAP are also slightly lower than during the Priabonian (**Table 4.3**).

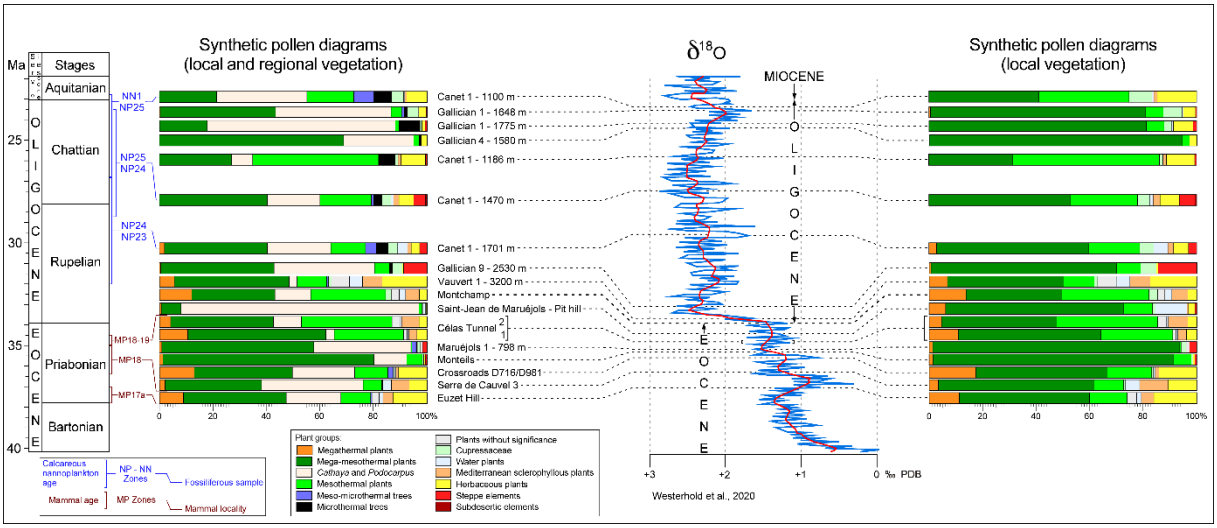

Figure 4.8: Synthetic pollen diagrams (*Pinus* excluded) illustrating (1) to the left the local to regional palaeovegetation (including altitudinal trees) and (2) to the right the local palaeovegetation (the latter trees excluded) – their proposed climatostratigraphic correlations with the reference oxygen isotope curve (smoothed

curve over 20 ka in blue, smoothed curve over 1 Ma in red; Westerhold et al., 2020). Pollen diagrams are vertically arranged according to the basin stratigraphy and available chronostratigraphic information. Pollen group composition is specified in the text and more in **§ 4.8. Supplementary data - Table S4.3**.

Euzet Hill, Serre de Cauvel, Crossroads D716/D981, Maruéjols 1 798 m, and Saint-Jean de Maruéjols Pit hill samples contain high proportions of conifers (*Podocarpus*, *Cathaya*) that do not result from preservation bias because of their high floristic diversity (>30 taxa) but from high pollen supply from mid-altitude.

4.4.4. Calcareous nannofossils

Calcareous nannofossils are recorded in four samples (**Table S4.2**), supporting some marine water incursions into the Alès Basin during the Priabonian, in agreement with the occurrence of dinoflagellate cysts and mangrove pollen grains. Some other marine water incursions are indicated in the Gallician 1 borehole at depths 1810 m (from the lowermost 'Série Calcaréo-salifère' Unit ascribed to late Chattian) and 1594 m (ascribed to earliest Aquitanian), consistently with the occurrence of marine dinoflagellate cysts in the studied samples from the Canet 1 borehole. The four recorded calcareous nannofloras are poor in species with a short biostratigraphic range: only *Reticulofenestra bisecta* and *R. lockeri* point out a chronological interval from ca. 38 Ma to ca. 23 Ma (Anthonissen and Ogg, 2012 in Gradstein et al., 2012) i.e., covering the time interval investigated in this study including the Priabonian and the entire Oligocene.

4.4.5. Geochemical modelling of the Strontium and Sulphur isotopes of sulphates

a. Pierrefeu-1 well (Vistrenque Basin)

Anhydrite samples from Pierrefeu 1 well display $^{87}Sr/^{86}Sr$ values ranging from 0.70777 to 0.708201 and $\delta^{34}S$ values comprised between +10.92 ‰ and +17.10 ‰ **(Table 4.4)**. Anhydrites from core K2 fall within the domain of Triassic evaporites while samples from cores K5 and K6 display significantly higher $^{87}Sr/^{86}Sr$ values (**Figure 4.9A**).

Mixing fluid models revealed that Sr and S isotope composition of anhydrites from Pierrefeu-1 is consistent with a formation from a mixed water composed of a riverine end-member whose Sr and S content is controlled by the leaching of Triassic evaporites and a marine end-member. The Sr and S concentrations and isotope composition of the volume fraction of each end-member for the best-case scenario, are given in **Table 4.5**. Matching between mixed-water models and isotope measurements on anhydrites integrates the effect of fractional precipitation which may lead to a difference of up to +2 ‰ in $\delta^{34}S$ between sulphates and precipitating water (Raab and Spiro, 1991).

Table 4.4: $^{87}Sr/^{86}Sr$ and $\delta^{34}S$ measurements on anhydrite/gypsum samples and native sulphur from Pierrefeu 1 well (Vistrenque Basin), SC-1 and SC-2 wells (Alès Basin, Les Fumades). The stratigraphic sequences of the Alès basin are defined in Lettéron et al. (2021).

Well	Core	Sample ID	Depth (m)	Lithology	Age	$^{87}Sr/^{86}Sr$	$\delta^{34}S$ ‰VCDT
Pierrefeu 1 (Vistrenque Basin)	core K2	PF1-K2-3-8	1749	anhydrite	Oligocene	0,707777	+10,92
	core K2	PF1-K2-5-8	1751	anhydrite	Oligocene	0,707772	+11,75
	core K5	PF1-K5-1-10	2481	anhydrite	Oligocene	0,708061	+13,87
	core K5	PF1-K5-4-10	2484	anhydrite	Oligocene	0,708031	+15,02
	core K6	PF1-K6-5-5	2546	anhydrite	Oligocene	0,708201	+17,11
SC-1 well (Alès Basin) SC-2 well (Alès Basin)	Sequence SPr2	SC1-108-2	108.20	anhydrite/gypsum	Priabonian	0,707685	+12,11
	Sequence SPr3	SC2-103	103	anhydrite/gypsum	Priabonian	0,707903	+26,98
	Sequence SPr3	SC2-89	89	anhydrite/gypsum	Priabonian	0,707870	+25,59
	Sequence SPr3	SC2-89	89	native sulphur	Priabonian		-6.42
	Sequence SPr3	SC2-89	89	native sulphur	Priabonian		-5.99

b. SC-1 and SC-2 wells (Alès Basin, Les Fumades)

Anhydrite from the Alès Basin (SC-1 and SC-2 wells, Les Fumades location) display a narrow range of $^{87}Sr/^{86}Sr$ values (0.70768-0.70790) while $\delta^{34}S$ is comprised between +12.11 ‰ and +26.98 ‰ **(Table 4.4)**. The sample from SC-1 well falls within the domain of Triassic evaporites while samples from SC-2 exhibit $\delta^{34}S$ values which are significantly higher than those of Priabonian sea-water (**Figure 4.9B**).

Table 4.5: Sulphur and Strontium isotope composition and concentrations for the late Oligocene seawater and riverine end-members (best-case scenario).

	Late Oligocene seawater end-member	Riverine end-member
$^{87}Sr/^{86}Sr$	0.70825	0.7077
$\delta^{34}S$ VCDT	20	11
[Sr]	15	0.1
$[SO_4^{2-}]$	2800	70

The high $\delta^{34}S$ values of gypsum minerals from SC-2 most likely arise from isotope fractionation during microbially mediated reduction of sulphates. If sulphate reduction takes place in a closed basin, the $\delta^{34}S$ of residual dissolved sulphates will be higher compared to the original fluid (Utrilla et al., 1992; Palmer et al., 2004). Additionally, measurements on native sulphur formed within anhydrite-bearing horizons in SC-2 well yielded negative $\delta^{34}S$ values ranging from -5.99 ‰ to -6.43 ‰. These negative $\delta^{34}S$ values strongly suggest that the elemental sulphur from SPr3 evaporitic interval is a byproduct of sulphate-reducing bacterial activity (Lindke et al., 2011).

As a consequence, although the SC-1 sample unequivocally indicates precipitation from a water influenced by the dissolution of Triassic sulphates, the bacterial sulphate-reduction

processes affecting the anhydrites from SC-2 prevent to draw any conclusion regarding a possible mixing with marine water.

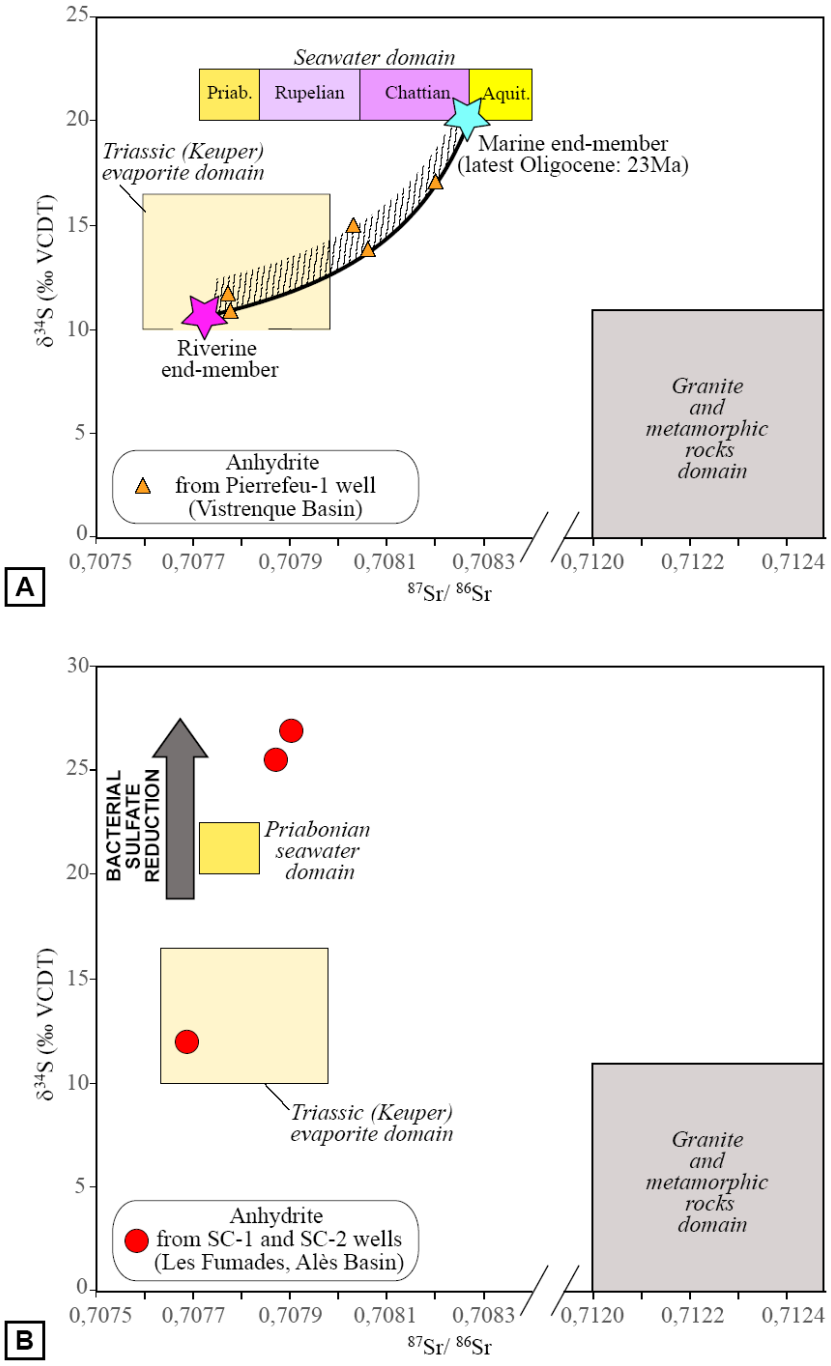

Figure 4.9: $\delta^{34}S$ vs $^{87}Sr/^{86}Sr$ crossplot for Paleogene anhydrites from SE France: A) Vistrenque Basin (Pierrefeu 1 well); the solid line represents the water-mixing model for a mixture of a Late Oligocene seawater with a riverine water whose composition is influenced by recycling of Triassic evaporites (see **Table 4.4** for Sr and S isotope compositions and concentrations of each end-member); the dashed area represents possible isotope compositions of sulphates having precipitated from the modelled water mixture by considering the fractional crystallization effect; B) Alès Basin (Les Fumades: SC-1 and SC-2 wells). The arrow indicates how bacterial sulphate reduction is likely to result into higher $\delta^{34}S$.

4.5. Discussion

4.5.1. Chronostratigraphic framework of the Paleogene of the Vistrenque Basin

The U/Pb age obtained on the first stage of calcite cementation (**Fig. 4.6-4.7**) infilling a dissolution cavity located 20 metres below the top of the 'Série Calcaire' Unit indicates that the underlying "Série Grise" and "Série Calcaire" units are older than early to middle Rupelian (**31.27 +/- 1.90 Ma**). Sedimentological and diagenetic studies, and petrographical observations on core from the Paleogene succession in the Gallician 9 well (Semmani et al., *in prep, see chapter 5 in this PhD manuscript*) revealed that the top of the "Série Calcaire" and the whole overlying "Série Mixte" are affected by repeated subaerial exposition as suggested by the occurrence of pedogenic limestones and karst features (**Fig. 4.3C**). The development of dissolution vugs and the subsequent formation of anisopachous calcite cements (meteoric vadose environment) in the sample G9 13D (Gallician 9: 1960 m depth) are linked to these repeated stages of subaerial exposition affecting the top of the 'Série Calcaire' Unit and the whole overlying 'Série Mixte' Unit. The obtained age for the subaerial exposure of the 'Série Calcaire' Unit therefore predates the deposition of the 'younger' overlying 'Série Mixte' Unit.

The U/Pb age obtained in Gallician 9 well at 1894 m depth in an early vadose cement from a fluvial conglomerate (**27.88 +/- 1.71 Ma**: G9 7 sample) suggests a late Rupelian to early Chattian age for the lower part of the 'Série Rouge' Unit. The difference between the two absolute ages (~ 3.4 Ma) corresponds therefore to the deposition duration of the 'Série Mixte' unit and the lower part of the 'Série Rouge' unit. Such a long duration, compared to the preserved thickness (~ 45 m) is consistent with low sedimentary rates and the occurrence of the numerous hiatuses that punctuate the sedimentation.

In addition, pollen-based climatostratigraphic approach suggests that the sediments from Vauvert 1 well at 3200 m depth were deposited very close to the Priabonian to Rupelian transition, thus likely indicating a late Eocene (Priabonian) age for the lowermost part of the 'Série Grise' Unit. This is consistent with the early Rupelian assemblage evidenced at 2530m in Gallician 9, located in an upper stratigraphic level within the "Série Grise" Unit. Pollen records from Gallician 4 1580m and Gallician 1 1648m suggest a Late Oligocene (early Chattian) age for the lowermost part of the 'Série Calcaréo-salifère' Unit. These findings agree with Chattian to Aquitanian age derived from the Sr and S isotope modelling on sulphates from this unit in the Pierrefeu 1 well. Based on this upper age bounding, the Série Rouge Unit is upper Rupelian to early Chattian in age.

Furthermore, the Aquitanian absolute U-Pb age (21.46 +/- 2.19 Ma) of the calcite vein affecting the "Série Grise" Unit in sample G9-K35 from Gallician 9 well is consistent with the infill of a fracture formed during the Oligocene-Aquitanian rifting of the Gulf of Lion margin (Séranne et al., 1995).

Based on the integration of these new dating results, namely the U-Pb absolutes ages, pollen-based climatostratigraphy, and geochemical modelling on sulphates, together with the lithostratigraphic framework, a robust chronostratigraphic framework of the Paleogene of the Vistrenque Basin can be provided (**Fig. 4.10**).

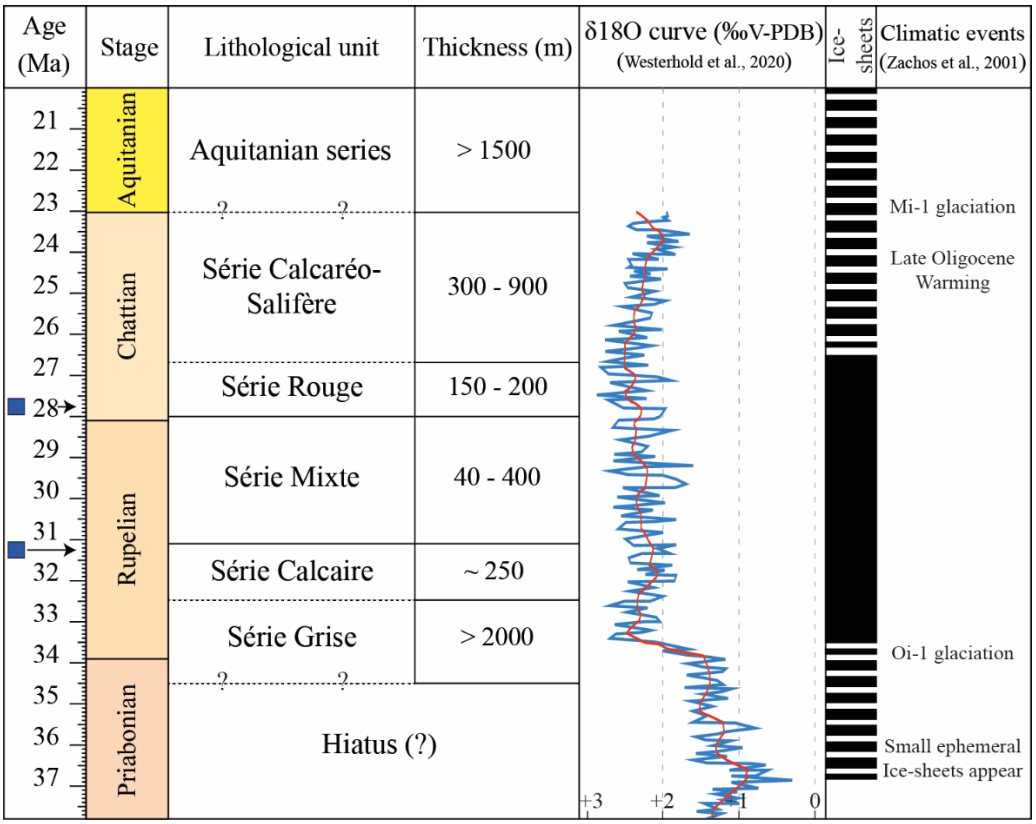

Figure 4.10: Chronostratigraphic framework of the Paleogene succession of the Vistrenque Basin. Stratigraphic attributions for the main lithological units are obtained using U/Pb absolute dating (blue squares), pollen analyses and geochemical modelling on sulphates, see text for details about the dating results. Reference oxygen isotope curve (smoothed curve over 20 ka in blue, smoothed curve over 1 Ma in red; Westerhold et al., 2020). Climatic events and Antarctic ice-sheets coverage history are derived from Zachos et al. (2001).

4.5.2. Evidence of marine incursions into Priabonian to Chattian continental basins from Southeast France

Saline lake sedimentation associated with the deposition of sulphates (gypsum and anhydrite) occurred during the Priabonian and/or Rupelian in various basins from SE France: Alès, Saint-Chaptes and Issirac basins (Busson et al., 1992; Lettéron et al., 2017, 2018, 2021) as well as in the Mormoiron–Carpentras and Apt–Manosque–Forcalquier basins (e.g. Triat and Truc, 1974; Cavelier et al., 1984). The present work documents saline lake conditions and deposition of evaporites in the Vistrenque Basin as early as the early Rupelian (within the 'Série Grise' Formation) and during the Chattian ('Calcaréo-salifère' Formation).

The origin of dissolved ions (Briot, 2008) in the Paleogene saline lake waters, and the possibilities and pathways of salinization of these lacustrine systems of Southeast France and Western-European rift system are still discussed (e.g., Lettéron et al., 2017, 2018, 2021;

Semmani et al., 2022, *see chapter 3 in this PhD manuscript*). Lettéron et al. (2017) examined the relevance of the occurrence of benthic foraminifera and halophile molluscs in the lacustrine deposits from the Issirac Basin to demonstrate marine connections and discarded evidence of marine connections based on these faunal contents. Moreover, these organisms have been shown to be tolerant to salinity variations and to be able to thrive in athalassic lakes (Plaziat and Younis, 2005). Nevertheless, strong evidence of incursions of marine-influenced waters into the ASCI lake system during the Priabonian and into the Vistrenque Basin during the Late Eocene to Late Oligocene period can be provided by the occurrence of microfossils such as calcareous nannofossils, dinoflagellate cysts and halophilous plant pollen. These micropalaeontological evidence are also supported by the results of geochemical modelling performed in this study.

In the ASCI system, the occurrence of marine dinoflagellate cysts in Serre-de-Cauvel and at crossroad D716/D981 (Saint-Chaptes Basin) is indicative of marine connections as early as the early-to-middle Priabonian. Additionally, the presence of *Avicennia* pollen grains in the Saint-Chaptes (Crossroads D716/D981) and Alès basins (Célas Tunnel, Saint-Jean de Maruéjols Pit hill and Montchamp) suggests the persistent influence of marine water from the middle to the latest Priabonian. The occurrence of Rhizophoraceae pollen grains from Serre de Cauvel and Montchamp is consistent with such an interpretation. Finally, the Sr and S isotope signatures of evaporites from the Ales Basin, although altered by sulphate-reduction processes likely derive from a mixture between a continental water influenced by Triassic evaporites and seawater.

In the Vistrenque Basin, the presence of the dinoflagellate *Deflandrea phosphoritica* (chronological range: 54.6-21.2 Ma; Powell et al., 1996) in Gallician 9 well at 2530 m depth (‘Série Grise’ Formation) provides evidence of marine incursion into the Vistrenque Basin during the early Rupelian times. The presence of pollen grains of *Ephedra* in this pollen record may also be a sign of marine incursion, although it can also be an indicator of both cooling and aridification phase. To support the climatic interpretation, it is important to indicate that *Ephedra* pollen is very scarce in present-day pollen assemblages from the Camargue and Roussillon coastal areas (Cambon et al., 1997; Beaudouin et al., 2005a; Suc and Fauquette, 2012; Suc, unpublished) and from the pollen records of warm phases (Holocene and older interglacials) although it is frequent to abundant during the drier episodes corresponding to cold phases (Beaudouin et al., 2005b; Tesson et al., 2011; Arnaud-Fassetta and Suc, 2015; Suc et al., in progress). In addition, the Sr and S isotope signatures of sulphate evaporites from the ‘Série Calcaréo-salifère’ Formation and mixing-water modelling strongly suggest an intrusion of marine water into the Vistrenque Basin during the late Chattian.

4.5.3. Palaeogeographic reconstructions of Southeast France during the Late Eocene and Oligocene

The possibilities of marine incursions into the ASCI system and Camargue area evidenced in the previous section allow to draw palaeogeographic maps that show the pathways of saltwater intrusion into these Paleogene lacustrine systems. These palaeogeographic

reconstructions are constrained by the regional structural framework and by the sedimentary record, the potential pathways for marine incursions are given in (**Fig. 4.11**) for the Priabonian, (**Fig. 4.12**) for the Rupelian, and (**Fig. 4.13**) for the Chattian.

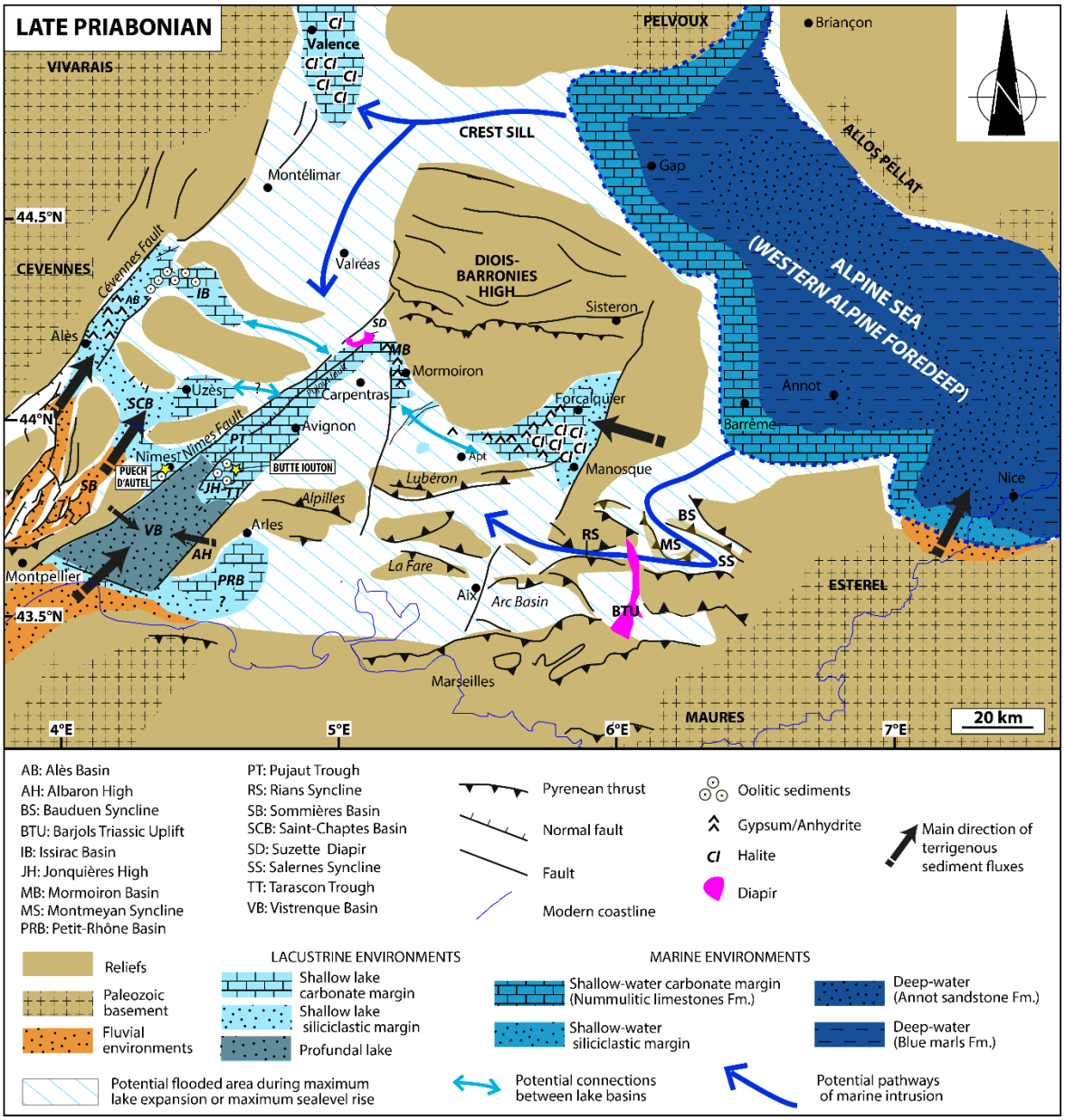

Figure 4.11: Palaeogeographic map of Southeast France during the late Priabonian. Locations of continental basins are compiled from Lettéron et al. (2017, 2021) and Semmani et al. (2022, *see chapter 3 in this PhD manuscript*). Palaeogeography of marine domain is modified after Joseph and Lomas (2004). The structural framework is compiled from Séranne et al. (2021) and Semmani et al. (2022, *see chapter 3 in this PhD manuscript*) west of the Diois-Barronies High and from Balansa et al. (2022) for Northern and Eastern Provence.

During the Priabonian and Rupelian, the Southeast France lake basins as well as the West Alpine Sea were bounded to the south by the EW-trending Pyrenean-Corsica-Sardinia Massif (Joseph and Lomas, 2004; Séranne et al., 2021). This relief likely yielded most of the terrigenous supply of the ASCI and Vistrenque lake basins (Lettéron et al., 2021; Semmani et al., 2022, *see chapter 3 in this PhD manuscript*) and of the deep-marine West Alpine foreland

Basin (Joseph and Lomas, 2004). The relief was likely sufficiently continuous and elevated to prevent from connections with the Western Neotethys to the south. In addition, in the Aquitaine Basin, the oceanic shoreline was located at more than 300 km west of the Alès Basin during the Priabonian and Rupelian times (Gely and Sztrákos, 2000; Sztrákos and Steurbaut, 2017), thus making unlikely any marine intrusion from the Atlantic Ocean into Languedoc, Rhône Valley and Camargue areas. In contrast, the proximity of the West Alpine foredeep (<30 km from the Manosque-Forcalquier Basin, and <50 km from the Valence Basin), and the probable interconnection between the different SE France saline lake basins, as suggested by previous studies (Lettéron et al., 2021; Semmani et al., 2022, *see chapter 3 in this PhD manuscript*) makes marine intrusions more plausible from the West Alpine Sea during the Priabonian and Rupelian (**Fig. 4.11** and **Fig. 4.12**).

The reconstruction of Pyrenean structures and their differentiation from later Alpine deformation (Balansa et al., 2022) provides a structural framework allowing a realistic reconstruction of continental palaeo-reliefs during the Priabonian and Rupelian and the identification of two potential marine incursion pathways, from the West Alpine Sea to the Southeast France lake basins (**Fig. 4.11** and **Fig. 4.12**). A northern potential pathway would connect the West Alpine Sea with the Valence Graben, north of the Diois-Barronies High. This corresponds to the "Crest Sill" identified by Sissingh (2001) as a possible marine corridor supplying seawater into the Western European rift basins. A connection of the Valence lake Basin with the Mormoiron and Vistrenque to the south and finally with the ASCI system during periods of maximum lake expansion would therefore explain the occurrence of calcareous nannofossils, dinoflagellate cysts and mangrove pollen grains within the Alès Basin during the Priabonian and in the Vistrenque Basin during the Rupelian.

A southern potential pathway of marine incursion would connect the West Alpine Sea with the Manosque-Forcalquier, Mormoiron and Vistrenque-ASCI basins through a set of Pyrenean synclines in the Haut-Var region (Bauduen, Montmeyan, Salernes and Rians basins). The hypothesis of such a marine corridor is corroborated by the presence of Paleogene marine markers such as calcareous nannofossils and dinoflagellate cysts in the "Sables Bleutés du Var" Formation in the Montmeyan Basin (Châteauneuf et al., 2019) even though the age of these deposits remains very much debated (e.g., Philip et al., 2017). Such a southern sea-water pathway may also explain the occurrence of dinoflagellate cysts in the Rupelian from the Marseilles Basin (Châteuneuf and Nury, 1995).

The Chattian palaeography of SE France (**Fig. 4.13**) differs significantly from that of Priabonian-Rupelian times, since the West Alpine Sea closed as a result of sedimentary infill and westward accretion of the Alpine orogenic wedge (Joseph and Lomas, 2004) during the late Rupelian. In addition, the Chattian is regionally characterized by an active and widespread stage of rifting leading to the collapse of the Pyrenean-Corsica-Sardinia Massif and the formation of NE-SW-oriented rift basins onshore and offshore in the Gulf of Lion. This resulted in marine intrusions from the southern Western Neotethys, into Provence as evidenced by the

occurrence of late Chattian, strictly marine, shallow-water carbonate sediments west of Marseilles ('Côte Bleue' shoreline: Oudet et al., 2010) and marine biological markers including dinoflagellate cysts, coelenterates and marine fishes in brackish-water lacustrine/lagoonal deposits from the Aix-en-Provence Basin (Nury and Thomassin, 1994).

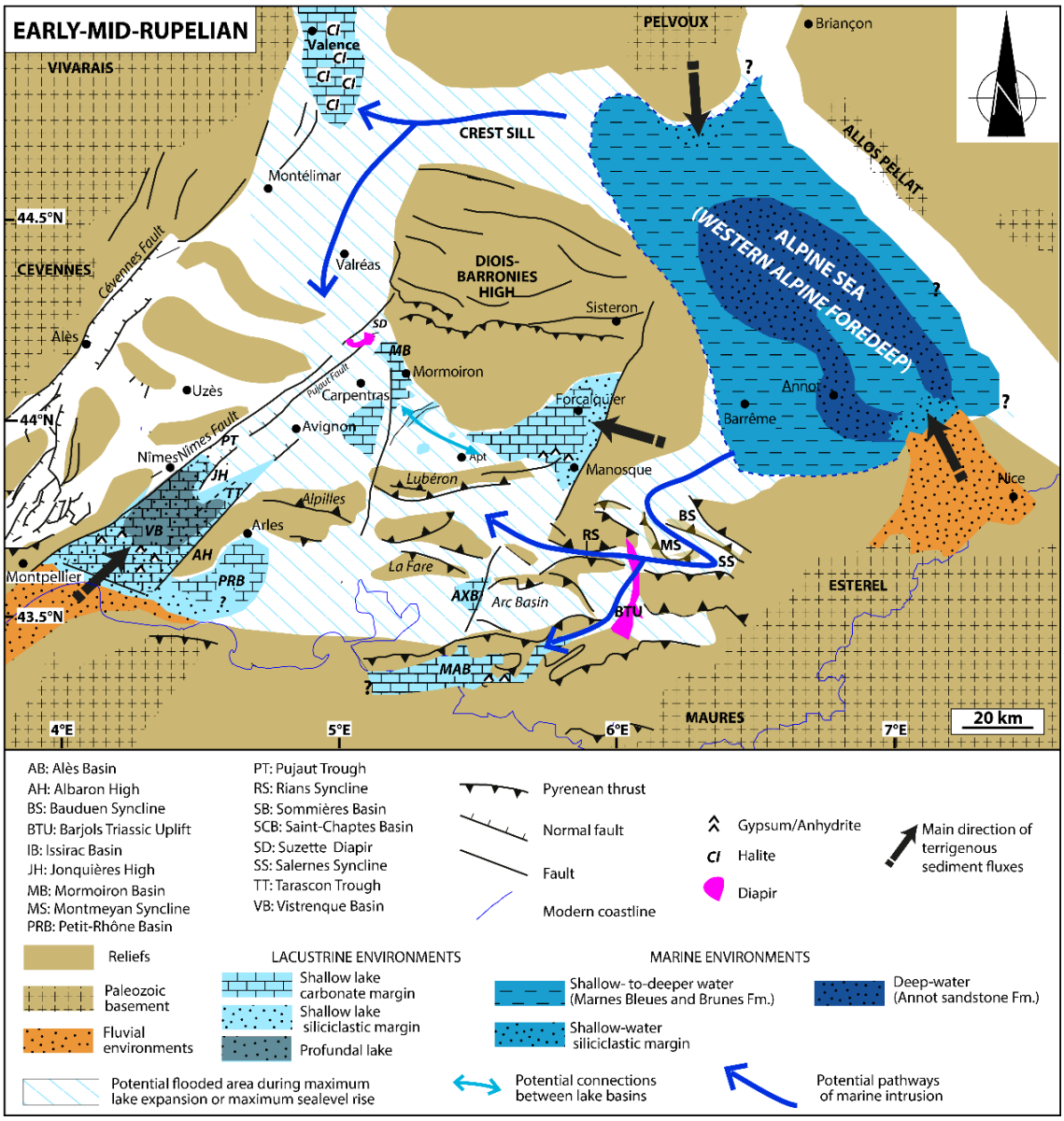

Figure 4.12: Palaeogeographic map of Southeast France during the early-middle Rupelian. Locations of continental basins are compiled from Nury (1990), Lettéron et al. (2017, 2021), Semmani et al. (2022, *see chapter 3 in this PhD manuscript*). Palaeogeography of marine domain is modified after Joseph and Lomas (2004). The structural framework is compiled from Séranne et al. (2021) and Semmani et al. (2022, *see chapter 3 in this PhD manuscript*) west of the Diois-Barronies High and from Balansa et al. (2022) for Northern and Eastern Provence.

The marine influence revealed by Strontium and Sulfur isotope signatures of Chattian evaporites from the Vistrenque Basin could therefore result from a marine connection to the south through the offshore Vistrenque rift Basin (**Fig. 4.13**). The Chattian carbonate and evaporite sediments from the Vistrenque Basin 'Calcaréo-salifère' Formation could therefore

have deposited in a saline lake with transient connections with seawater during sea-level or lake-level highstands, or within a coastal sabkha with periodic marine intrusions.

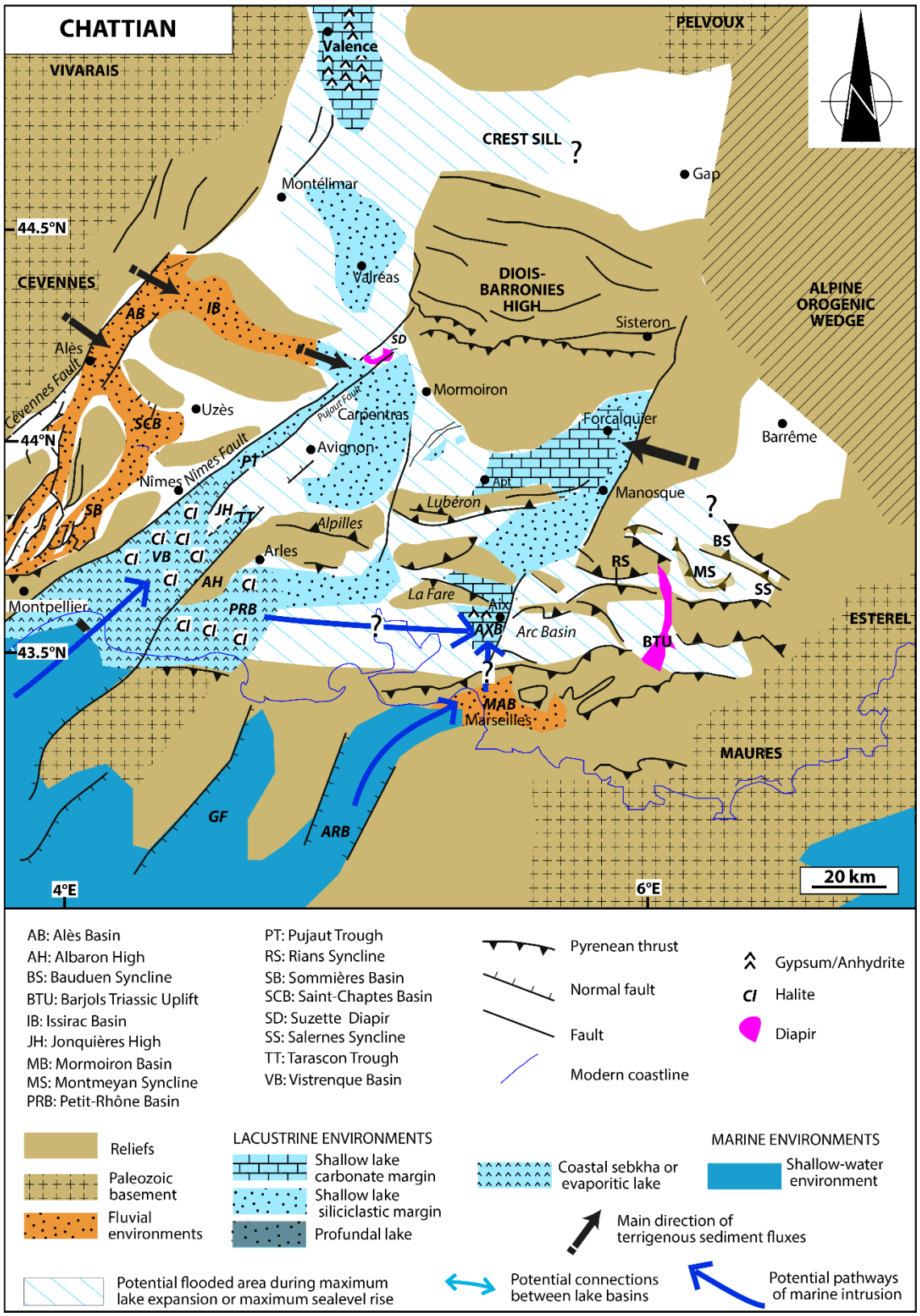

Figure 4.13: Palaeogeographic map of South-East France during the Chattian. Locations of continental basins are compiled from Cavelier et al. (1984), Nury (1990), Séranne et al. (2021). Palaeogeography of marine domain

is modified after Oudet (2008). The structural framework is compiled from Séranne et al. (2021) and Semmani et al. (2022, *see chapter 3 in this PhD manuscript*) west of the Diois-Barronies High and from Balansa et al. (2022) and Ford and Lickorish (2004) for Northern and Eastern Provence.

4.5.4. Palaeoclimatic implications

This study is the first on Late Eocene and Oligocene deposits to be both based on full botanical identification of pollen grains and their counting, allowing an outstanding and robust interpretation of climate evolution between 38 and 23 Ma. Four pollen data from the Canet 1 borehole have been added to complete those from the Alès and Vistrenque basins for documenting the climate knowledge during the late Rupelian and early Chattian.

Looking at pollen data, the Eocene–Oligocene transition is marked by the suddenness and the great amplitude of the climate deterioration with lowering temperature and increasing dryness at low elevations while high humidity continued in higher altitude. The climate estimated from pollen data does not show a so great climatic deterioration as the reconstructed intervals are relatively large. Indeed, some plants may live under large temperature and/or precipitation amplitudes. However, the cooling between the Priabonian and the Rupelian is indicated by a decrease in mean annual temperature, mean temperature of the coldest month and in mean annual precipitation at Vauvert but more particularly at Gallician 9 2530 m. After that event, temperatures and precipitations increase but stay a little lower than during the Priabonian. Vegetation and climate changes seem to indicate that the cooling in Southeast France was brief and took place at the very early Rupelian. From a vegetation and climatic point of view, the Mediterranean region is considered as a very particular region since the Paleogene as it was certainly sheltered from cold air masses (Pospescu et al., 2021; Fauquette et al., in progress). The cooling phases were thus certainly less pronounced than elsewhere in Europe.

Finally, the upper Chattian shows a progression of climate towards the Aquitanian conditions with very scarce megathermal plants as described by Bessedik (1984), Zheng (1990) and Suc et al. (2018), despite persistence of *Podocarpus* in the mountains up to the latest Chattian.

4.6. Conclusion

This study addressed the question of the origin of saltwater in the Paleogene saline lakes of Languedoc and Camargue areas in Southeast France and assessed the assumptions on evaporites recycling from the Triassic diapirs of the Rhône Valley and on incursion of marine influenced waters into these basins and their potential pathway using new data from the Vistrenque Basin (Camargue area) and Alès Basin. It also investigated the record of the Eocene-Oligocene transition in Southeast France.

This work is the first to provide a strong chronological framework for the Paleogene succession of the Vistrenque Basin using a multiproxy approach integrating lithostratigraphic correlations, and newly acquired age data using U-Pb dating on calcite, pollen-based

climatostratigraphy and water-mixture geochemical modelling on Strontium and Sulphur isotopes on sulphates. Our age data have shown that the lower infill of the Paleogene Vistrenque Basin ('Série Grise' Formation) is late Priabonian to early Rupelian in age, while the 'Série Mixte' is middle Rupelian to early Chattian in age. The 'Série Rouge' Formation is upper Rupelian to early Chattian in age and the 'Calcaréo-Salifère' Formation is early Chattian to Aquitanian in age.

In addition to the chronological information, pollen analyses made it possible to reconstruct a mangrove and freshwater lake vegetation in the Alès Basin, and a dominant evergreen subtropical forest in the surroundings of the lake which also record fluctuations with a high-altitude vegetation in the southern palaeo-Pyrenean relief during the Priabonian. Vegetation cover has been shown to be rather dominated by mesothermal and herbaceous plants with a significant highly influencing altitude vegetation cover in the southern palaeo-Pyrenean relief during the early Rupelian and Chattian times reflecting cooler and drier climate in the surroundings of the Camargue area. In addition, the new U/Pb ages obtained from the Vistrenque basin and the use of the Climate Amplitude Method allowed evidencing a short but significant stage of climate cooling and aridification in the early Rupelian which could result from the global climate cooling following the Eocene-Oligocene Transition.

Composition and provenance of dissolved ions in the Vistrenque Basin during the Chattian to Aquitanian deposition of the evaporites of the 'Série Calcaréo-salifère' Formation strongly suggest influence of marine influenced waters incursions into the Vistrenque lacustrine system. Potential influence of marine water is also suggested by the geochemical modelling of the Priabonian evaporites from the Alès Basin. In addition to the geochemical evidence, strong evidence for intrusions of marine-influenced saltwater into the Languedoc and Camargue areas during the Priabonian, lower Rupelian and Chattian times are provided by the occurrence of calcareous nannofossils, dinoflagellate cysts and the halophilous *Avicennia* and Rhizophoracea plants documented by their pollen.

Our palaeogeographic reconstructions of the Southeast France integrating this new evidence of marine water influence and the latest advances in tectonic framework of the studied areas rule out any marine corridor to the south via Camargue during the Priabonian and earliest Rupelian. The presence of an elevated relief at the present Gulf of Lion location prevented marine incursion from the south and the pathways of these marine incursions are to be found from the Western Alpine Sea through the Crest Sill north to the Diois-Barronies High and/or the Pyrenean synclines in the Haut-Var area south of the Diois-Barronies High. Dramatic palaeogeographic changes occurred during the Chattian with the closure of the Alpine Sea and the collapsing of the Pyrenean relief at the presence Gulf of Lion location followed by the opening of the Western Mediterranean Sea that constituted a pathway of marine intrusion into the Gulf of Lion and Camargue areas which then allowed the deposition of the thick Upper Oligocene evaporite interval in the Vistrenque Basin in marginal-littoral setting.

The floral assemblages from the Priabonian and Rupelian of the neighbouring Languedoc and Camargue areas constitute a powerful tool to document the climatic deterioration at the Eocene-Oligocene transition. Evidence of marine connection during the late Priabonian and early Rupelian to the Southeast France areas and their pathways is provided by micropalaeontological data comprising occurrence of mangrove pollen, calcareous nannofossils, and dinoflagellate cysts, and the contribution of water-mixture geochemical modelling on Strontium and sulphur on sulphates in the Upper and Lower Rhône Valley segments.

4.7. Acknowledgements

This work was funded by the France's Ministry of Higher Education and Research and is part of the PhD of the first author (NS). This work also benefited from the financial supports of CEREGE (APIC 2018 RRH) and Carb3E TotalEnergies-AMIDEX Chair and we thank them profoundly for their support. Sampling and analyses on the Canet 1 borehole were carried out thanks to the financial support of the ANR 'PYRAMID', to which this paper is a contribution. This work benefited from internal documents provided by TotalEnergies (Contract of cooperation and data exchange TotalEnergies - Aix-Marseille University FR00040451). The authors are also grateful to Gilles Graffin (STC core library, Boussens) for giving access to samples on the Camargue wells cores. Alain Tonetto (head of PRATIM, Aix-Marseille University) is also thanked for their help to carry out confocal microscope analyses. The authors would also like to thank Christophe Nussbaumer (TotalEnergies) for his comments and suggestions to improve this manuscript.

4.8. Supplementary data

Table S4.1: Latitude, longitude, and elevation of the pollen sampling locations. For boreholes, elevation refers to depth of samples with respect to elevation of the hole top.

N°	Location	Basin	Type	North Latitude	East Longitude	Elevation (m)
1	Canet 1	Roussillon	Borehole	42°41’23.41”	3°04’66.00”	-1099
2	Canet 1	Roussillon	Borehole	42°41’23.41”	3°04’66.00”	-1186
3	Canet 1	Roussillon	Borehole	42°41’23.41”	3°04’66.00”	-1470
4	Canet 1	Roussillon	Borehole	42°41’23.41”	3°04’66.00”	-1700
5	Gallician 9	Vistrenque	Borehole	43°38’35.64”	4°16’58.49”	-2530
6	Gallician 4	Vistrenque	Borehole	43°38’13.86”	4°17’06.36”	-1581
7	Gallician 1	Vistrenque	Borehole	43°38’14.98”	4°16’58.22”	-1647
8	Gallician 1	Vistrenque	Borehole	43°38’14.98”	4°16’58.22”	-1775
9	Vauvert 1	Vistrenque	Borehole	43°38’58.04”	4°16’39.43”	-3200
10	Euzet hill	Saint-Chaptes	Exposed	44°04’35.71”	4°12’41.02”	127
11	Serre de Cauvel	Saint-Chaptes	Exposed	44°04’36.90”	4°12’28.10”	120
12	Crossroad D716/D981	Saint-Chaptes	Exposed	44°04’50.50”	4°11’57.50”	132
13	Monteils	Saint-Chaptes	Exposed	44°05’08.00”	4°11’39.00”	168
14	Célas Tunnel 1	Alès	Exposed	44°07’37.70”	4°10’34.80”	201
15	Célas Tunnel 2	Alès	Exposed	44°07’37.70”	4°10’34.80”	201
16	Saint-Jean-de-Maruéjols Pit hill	Alès	Exposed	44°15’59.05”	4°17’48.36”	128
17	Maruéjols 1	Alès	Borehole	44°15’35.76”	4°15’20.78”	-633
18	Montchamp	Alès	Exposed	44°19’56.20”	4°21’29.30”	220

Table S4.2: Occurrences of calcareous nannofossils.

Sample	**Calcareous nannofossils**
Gallician 1 – 1594 m	*Coccolithus pelagicus, Cyclicargolithus floridanus, Pontosphaera multipora, Reticulofenestra bisecta, R. lockeri, Sphenolithus moriformis, Zygrablithus bijugatus*
Gallician 1 – 1810 m	*Coccolithus pelagicus, Sphenolithus moriformis, Zygrablithus bijugatus, Reticulofenestra cf. lockeri*
Canet 1 – 1100 m	*Calcidiscus pataecus, Coccolithus pelagicus, Cyclicargolithus abisectus, C. floridanus, Discoaster deflandrei, Helicosphaera carteri, Pontosphaera discopora, P. multipora, Reticulofenestra bisecta, small reticulofenestrids, Sphenolithus cf. delphix, S. moriformis, Zygrhablithus bijugatus*
Canet 1 – 1470 m	*Calcidiscus pataecus, Chiasmolithus altus, Coccolithus pelagicus, Cyclicargolithus abisectus, C. floridanus, Discoaster deflandrei, Helicosphaera mediterranea, Pontosphaera enormis, P. multipora, Reticulofenestra bisecta, small reticulofenestrids, Sphenolithus moriformis, Zygrhablithus bijugatus*
Canet 1 – 1701 m	*Chiasmolithus altus, Coccolithus pelagicus, Cyclicargolithus abisectus, C. floridanus, Helicosphaera ethologa, Pontosphaera enormis, P. multipora, Zygrhablithus bijugatus, Reticulofenestra bisecta, Sphenolithus moriformis*
Maruéjols 1 – 433 m	*Coccolithus pelagicus, Cyclicargolithus floridanus, Pontosphaera multipora, Reticulofenestra bisecta, R. lockeri, Sphenolithus moriformis, Zygrablithus bijugatus*
Crossroad D716/D981	*Coccolithus pelagicus, Sphenolithus moriformis, Helicosphaera sp.*

Table S4.3: Detailed content in pollen grains and other palynomorphs (spore, dinoflagellate cysts, etc.) of the analysed samples.

Site	Canet 1				Gallician 1		Gallician 4		Gallician 9	Vauvert 1	Montchamp	Saint-Jean de Maruéjols	Célas Tunnel		Maruéjols 1	Monteils	Crossroads D716/D981	Serre de Cauvel	Euzet Hill
Taxa Depth (m) or sample name or sample number	1100 m	1186 m	1470 m	1701 m	1648 m	1775 m	1580 m		2530 m	3200 m		Pit hill	1	2	798 m			3	
MEGATHERMS (MAT>24°C)*																			
Amanoa (Euphorbiaceae)										1				1			3	2	
Bambusa (Poaceae)																	1		
Avicennia (Acanthaceae)				1	1						1	3	1	1	1		3		
Bombax-type (Malvaceae)																	1		1
Buxus bahamensis-type (Buxaceae)												1		1					
Afzelia-Peltophorum-type (Leguminosae)				1					1								5		2
Canthium-type (Rubiaceae)											9	2	11				1		
Peltogyne-type (Leguminosae)																			1
Croton-Jatropha (Euphorbiaceae)				1							4	2	1				6		1
Euphorbiaceae											1		4						
Leguminosae Caesalpinioideae											1						1		
Malpighiaceae																			1
Mappianthus (Icacinaceae)				1															3
Mussaenda-type (Rubiaceae)										1				2	1		2	3	2
Phyllanthus (Phyllanthaceae)																			2
Rhizophoraceae											3							2	
Rubiaceae																		1	
Sapindaceae										1	2			1		2			1
Theaceae																	2		1
Thunbergia (Acanthaceae)																			1
Uncaria-type (Rubiaceae)										6		1		1			1		3
MEGA-MESOTHERMS (20 °C<MAT<24 °C)*																			
cf. *Alfaroa* (Juglandaceae)										2				1				2	
Alangium (Cornaceae)										1		1	4	1		1			
Arecaceae				4					1	1		1		2					1
Castanopsis-Lithocarpus (Fagaceae)			3										2	5	1	1			1
Cissus (Vitaceae)																	1		
Cyrillaceae-Clethraceae															1				
Distylium (Hamamelidaceae)			1	1		1	1		1	2	9	13	2	2	1	6	6	3	10
Dodonaea (Sapindaceae)														1			1		
Embolanthera (Hamamelidaceae)										4	4	1	2		2	2			1
Engelhardtia (Juglandaceae)	3	19	22	18	2	3	1		7	48	9	14	24	13	2	33	8	49	54
Fothergilla (Hamamelidaceae)																			2
Hamamelis (Hamamelidaceae)																			1
Ilex floribunda-type (Aquifoliaceae)													1				1		1
Leea (Vitaceae)												3						1	
Menispermaceae			1								25	2	35	23		11	6	1	6
Microtropis (Celastraceae)										1									
Myrica (Myricaceae)		2	2			1					1			3		1			
Nyssa aquatica-type (Cornaceae)																			1
Nyssa cf. *sinensis* (Cornaceae)	2													1					
cf. *Phyllostylon* (Ulmaceae)														1			1		
Platycarya (Juglandaceae)			1	2						1	1	2	1					1	
Rhodoleia (Hamamelidaceae)										5		16				1			1
Rhoiptelea (Juglandaceae)			1																
Ricinus-type (Euphorbiaceae)														1					
Sapotaceae	1	4	5		2	1				2	1	6	4	7	2	3	11		1
Sciadopitys (Sciadopityaceae)	9		1	1															
Symplocos (Symplocaceae)										2	2		5	4			5		2
Taxodium-type (Cupressaceae)	3		2	11	7				1	2	1				46			16	
Cupressaceae papillate pollen grains (former 'Taxodiaceae')	44	23	43	49	185	116	140		97		2	51	4	1	88	78	39	13	
Cathaya (Pinaceae)	74	11	10	24	55	352	26		22		6	1127		1	27	3	3	4	5
Podocarpus (Podocarpaceae)	24	3	30	29	101	134	28		73	5	17	214	5	17	64	18	46	89	39
MESOTHERMS (14 °C<MAT<20 °C)*																			
Acer (Sapindaceae)												16					1	1	1
Alnus (Betulaceae)	4	3	1	2															
Anacardiaceae	1																		
Araliaceae	1				1	1				1	27		33	37			5	1	
Betula (Betulaceae)	1																		
Buxus sempervirens-type (Buxaceae)		1									3	1	2	5					
Carpinus (Betulaceae)	3	1							3	1									
Carya Juglandaceae)	10	38	12	6	4	2			6				1				2	2	3
Celtis (Cannabaceae)														2					
Ericaceae	7	1	1	1	1	1						2		1					
Eucommia (Eucommiaceae)																		1	
Hedera (Araliaceae)												1							2
Ilex (Aquifoliaceae)																			
Juglans (Juglandaceae)				1															
Liquidambar (Hamamelidaceae)			1	3			1		1		3	1	1	3				1	
Lonicera (Caprifoliaceae)																	2	1	
Parrotia (Hamamelidaceae)					1					4		6							8
Populus (Salicaceae)			1	1	1						1			1			1	1	
Pterocarya (Juglandaceae)	1	4	1	1	2						1	1							3
Quercus (Fagaceae)	23	11	22	13	3	2	3		1	6	4	4	3	2	1	2	18	6	1
Salix (Salicaceae)																	1		
Sambucus (Adoxaceae)																			1
Taxaceae																			3
Ulmus (Ulmaceae)		6		1	2	1			2	4	11	1	2	4		8	1	6	2
Zelkova (Ulmaceae)		19			1	3			1	2		1		1				1	
MESO-MICROTHERMS (12 °C<MAT<14 °C)*																			
Cedrus (Pinaceae)	12		1							1					1		4		
Fagus (Fagaceae)	4		1	2															1
Tsuga (Pinaceae)	6			7	4										3				
MICROTHERMS (MAT<12 °C)*																			
Abies (Pinaceae)	7	4	5	4	2	19	1		1						1				
Picea (Pinaceae)	12	7	1	6	2	34	1		2										
TAXA WITHOUT ECOLOGICAL SIGNIFICANCE															4				
Pinus diplostellate-type (Pinaceae)	172	9	2	19	11		39		18	3	5	161	1	2	111	2	79		11
Indeterminable pollen grains of Pinaceae	259	109	81	135	187	9427	264		310	3	4	3864	5	3		37	166	93	15
***Cupressus-Juniperus*-type (**Cupressaceae)	13	2	7	8	17	4			9	2	5	2			3	1	1	1	
Aristolochia (Aristolochiaceae)														1					
cf. Cucurbitaceae																			
Ranunculaceae										4				1					4
Rosaceae										2				1					
WATER PLANTS																			
Aglaoreidia (fossil taxon)												13						3	
Lemna (Lemnaceae)										4									
Lythraceae											1								
Myriophyllum (Haloragaceae)				1						1	1								
Nympheaceae				*4*									*1*						
Oenotheraceae				2										1					
Potamogeton (Potamogetonaceae)	1										1								
Restio (Restionaceae)				1														2	
Restionaceae			2		1					3	1						1	3	3
SCLEROPHYLLOUS MEDITERRANEAN PLANTS																			
Jasminum (Oleaceae)														1					
Olea (Oleaceae)	1	1								10	5	1	5	9			2	16	6
Phillyrea (Oleaceae)	1									2	4			1				2	2
Quercus ilex-type (Fagaceae)		1	4	3															
HERBACEOUS PLANTS																			
Amaranthaceae	4		1	3						1	1	1	1				1	1	
Brassicaceae																		1	1
Campanulaceae										3							1		7
Caryophyllaceae	1																		
Compositae Asteroideae	1		4										1			1	1		4
Compositae Cichorioideae	1		2														1		
Convolvulus (Convolvulaceae)	1												1				13	1	1
Cyperaceae	2		3	1						2	1	1						12	4
Lamiaceae																			1
Leguminosae Papilionideae											3								
Liliaceae							1												
Plantago (Plantaginaceae)	3									2			1				1		3
Plumbaginaceae	2	1				2			1										
Poaceae	7	15	1	3	11	9	2			19		2	1				2		2
Resedaceae																			1
Rumex (Polygonaceae)													1					1	2
Sanguisorba-type (Rosaceae)																			1
Thymeleaceae																	1		
STEPPE PLANTS																			
Artemisia (Compositae)			1																
Ephedra		1	8	6	1	2			22			1			4	1			
SUBDESERTIC PLANTS																			
Calligonum (Polygonaceae)			1																
Number of identified pollen grains	**721**	**296**	**286**	**377**	**605**	**10115**	**508**		**580**	**165**	**181**	**5541**	**166**	**167**	**364**	**212**	**459**	**344**	**238**
Unidentified pollen grains											4	1	2	2					
Indeterminable pollen grains	10	39	116	37	54	229	303		8	20	36	14	43	40	2	15	60	17	19
PTERIDOPHYTES														334					
Osmunda (Osmundaceae)															3			5	
Polypodiaceae	1																		
Pteris (Pteridaceae)																			1
Unidentified monolete spores	21	4	4	5					1	3	4	2	1	1	5	2	3	128	5
Unidentified trilete spores	12	4	1	5			3		7		9		12	2	8		21	199	4
Unidentified spores	4		4	1	5		3		3	1	8	1	2	2	6	3		2	12
ALGAE																			
Botryococcus											Present	Present	Present	Present		Abundant	Present		Present
OTHER PALYNOMORPHS																			
Fungi	2	1			1				2	1	1		1		2			2	1
Marine dinoflagellate and acritarch cysts	92	2	15	24	2	3	1		48						4		16	1	1
Freshwater dinoflagellate cysts	3																		
REWORKED PALYNOMORPHS																			
Pollen grains	35	4	16	102	65	1			205		2	1	18	2	21	1	7	24	
Fern spores	16	2	5	3					3	1					1				
Dinoflagellate cysts	3	1		1	1				5	2									

* MAT (mean annual temperature) with respect to the Nix (1982)'s temperature gradient

Appendix A- Details and discussions about the Climatostratigraphy approach and description of the observed specimens.

a- Advances with respect to previous palynological records.

Several palynological records were previously performed in the studied region. Most of them are characterized by a listing of the most usually identified plants with a limited or missing counting of pollen grains (Provence: Sittler, 1965; Schuler and Sittler, 1976; Marseilles Basin: Châteauneuf, 1977; Alès Basin: Michoux, 1983). Such studies are particularly damaged by the non-recognition of most of the triporate, tricolpate and tricolporate pollen grains, which often belong to subtropical and tropical plants, i.e., meaningful elements for palaeoenvironmental reconstructions. The use of these poor pollen records is thus very limited for understanding palaeovegetation and palaeoclimate. Even lesser elaborated palynological analyses have been performed on few Camargue wells and do not provide significant information (Jan du Chêne, 1989; Buisson, 1993).

Because of improvements in botanical identification of pollen grains achieved in the seventies on the Neogene pollen floras thanks to the use of the rich ISEM pollen collection in Montpellier (Suc, 1976; Bessedik, 1980, 1981; Suc and Bessedik, 1981), supported by pollen photographs, some progress was introduced in Paleogene microfloras (Célas: Gruas-Cavagnetto, 1973; Provence: Châteauneuf and Nury, 1995), unfortunately still devoid of countings. Accordingly, these pollen records have a limited interest.

Our pollen study confirms the same differences and similarities between the Célas macroflora and microflora than previously indicated by Gruas-Cavagnetto (1973) but emphasizes the important role in the local vegetation made by Hamamelidaceae (*Distylium*, *Embolanthera*, *Rhodoleia*), Sapotaceae, Euphorbiaceae (*Croton*, *Amanoa*, *Canthium*-type) in addition to Araliaceae and Menispermaceae listed in the macroflora. One matter persists due to abundant cones of the fossil genus *Doliostrobus* Marion in the macroflora that Kvacek (2002) ascribed to an extinct family, Doliostrobaceae, expected close of both Araucariaceae and Cupressaceae. Cupressaceae pollen grains (including those of the former Taxodiaceae) are very scarce in the Célas microflora while those of Araucariaceae have not been observed.

b- Dinoflagellate cysts

Dinoflagellate cysts have been recorded in some samples (**Plate 4**): Canet 1 (1100 m, 1470 m, 1701 m), Gallician 4 (1580 m), Gallician 9 (2530 m), Crossroads D716/D981, and Serre de Cauvel (samples 1 and particularly 2, the sample in which dinoflagellate cysts are the most abundant). On the whole, dinoflagellate cysts are not well preserved, often broken and thus identifiable with great difficulty. Many reworked dinoflagellate cysts occur. All the individuals have been observed both in transmitted light microscopy (TLM) and under fluorescent UV light microscopy (FLM) in order to detect the reworking (Doláková and Burešová, 2007; Hoyle et al., 2018) : the reworked dinoflagellate cysts show a dull brown colour at the difference of the non-reworked specimens which show a bright yellow colour as illustrated in **Plate 4**.

c- Morphological description of some pollen grains.

These descriptions are based on observations at transmitted light microscope (TLM) according to LO-analysis (*Lux* = light vs. *Obscuritas* = darkness) technique and/or scanning electronic microscope (SEM).

Afzelia-Peltophorum-type (Leguminosae) (**Plate 1**, **Figs. 2a-e**, **3a-d**, **4**).

Oblate to equiaxal tricolporate and reticulate pollen grains show large and short non-linear ectoapertures (colpi), endoapertures (pori) being often indistinct. The supratectal reticulum is made of large lumina. Muri are densely micro-echinate. Columellae with large head structurate the tectum, also supported by smaller other ones. This pollen has been recorded in several locations (Canet 1, Gallician 9, Crossroads D716/D981, Euzet Hill; **Table S4.3**).

Similar pollen types are found in the tribes Detarioideae (*Afzelia*, *Intsia*) and Caesalpinioideae (*Peltophorum*, *Delonix*) (**Plate 1**, **Figs. 1a-e**; Banks and Lewis, 2018) but none of the observed species from the ISEM Collection shows small spines.

Peltogyne-type (Leguminosae; **Plate 3**, **Figs.6a-d, 7**).

Oblate tricolporate and clavate pollen with thick costae along the ectoapertures (colpi) and a distinct thin annulus bordering the endoapertures (pori). Large and smaller clavae constitute the ornamentation of the pollen. This pollen has been recorded in the Euzet Hill location.

This pollen morphology is similar to that of the modern species Peltogyne confertiflora (Hayne) Benth. (Detarioideae) (Graham and Barker, 1981: plate 12, fig. E).

Croton-Jatropha (Euphorbiaceae; **Plate 2**, **Figs. 3, 5a-b**).

Inaperturate spheroidal pollen grain with a coarsely reticulate ornamentation constituted by more or less dense clavae, which have an almost triangular shape that provides the so-called *Croton*-pattern. This pollen has been recorded in several locations (Canet 1, Montchamp, Saint-Jean de Maruéjols Pit hill, Célas Tunnel, Crossroads D716/D981, Euzet Hill; **Table S4.3**). Such very peculiar pollen types are characteristic of Croton (**Plate 2**, **Figs. 4a-c**) and *Jatropha* genera (Carreira et al., 1996; Ribes de Lima, 2007; Ribeiro de Souza et al., 2020).

Amanoa (Phyllanthaceae; **Plate 1**, **Figs. 6a-c**).

Tricolporate oblate pollen showing a large semi-tectate curvilinear reticulum (a thin membrane covers the lumina), with long colpi (ectoapertures) resulting in a small apocolpium, bordered by costae. Endoapertures are rectangular. This pollen has been recorded in several locations (Vauvert 1, Célas Tunnel, Crossroads D716/D981, Serre de Cauvel; **Table S4.3**).

This pollen morphology is characteristic of the genus *Amanoa* (**Plate 1**, **Figs. 5a-b**; Punt, 1962; Köhler, 1965).

Dodonaea (Sapindaceae; **Plate 2**; **Figs. 6a-b**).

Equiaxal tricolporate pollen, subtriangular in polar view, with prominent apertural areas characterized by thickening endexine, especially around the rectangular endoapertures. The ornamentation can be psilate, rugulate or slightly reticulate. This pollen has been recorded at Célas Tunnel and Crossroads D716/D981 locations (**Table S4.3**).

Because of its distinctive shape, this pollen corresponds in part to the fossil 'genus' *Pentapollenites* conceived by Krutzsch (1962), manifestly illustrated at the scanning electronic microscope by Châteauneuf (1980: plate 17, fig. 7), which now receives a robust botanical ascription as *Dodonaea* (**Plate 2, Figs. 7a-c**; Merville, 1965), a primitive genus within the Sapindaceae (Muller and Leenhouts, 1976). Henceforth, the name *Pentapollenites* must be rejected as it probably also includes other botanical genera.

Alangium (Cornaceae; **Plate 1**, **Figs. 7, 8**).

Prolate tricolporate and reticulate pollen, elliptic in equatorial view, with long ectoapertures (colpi) edged by thick costae. Lalongate endoapertures (pori) are surrounded by a thin annulus. The supratectate reticulum is somewhat lengthened along the pole axis. The tectum is thick and clearly separated from the endexine. This pollen has been recorded at Vauvert 1, Célas Tunnel, Saint-Jean de Maruéjols Pit hill and Monteils locations (**Table S4.3**).

Such a pollen is characteristic of several species of the *Alangium* genus (**Plate 1**, **Fig. 9**; Reitsma, 1970).

Plate 1. Photographs at TLM and SEM of some fossil and modern pollen grains (shots by J.-P. Suc). Modern pollen grains originate from the ISEM - Montpellier Collection. Scale bar = 10 µm.

Figs 1a-e. *Afzelia cochinchinensis* (Pierre)J.Léonard = *A. xylocarpa* (Kurz)Craib (Leguminosae) – ISEM Collection number: 9427 (plant specimen collected in Vietnam); equatorial view aperture facing at TLM.
LO-analysis: **a**, reticulate ornamentation; **b**, focus on the head of columellae; **c**, focus on the foot of columellae; **d**, optical section.

Figs. 2a-e. *Afzelia-Peltophorum*-type (Leguminosae) – Euzet Hill; equatorial view (intercolpium) at TLM.
LO-analysis: **a**, reticulate ornamentation; **b**, focus on the head of columellae; **c**, focus on the foot of columellae; **d**, aperture; **e**, optical section.

Figs. 3a-d. *Afzelia-Peltophorum*-type (Leguminosae) – Crossroad D716/D981; equatorial view (intercolpium) at TLM.
LO-analysis: **a**, reticulate ornamentation; **b**, focus on the head of columellae; **c**, focus on the foot of columellae; **d**, optical section.

Fig. 4. *Afzelia-Peltophorum*-type (Leguminosae) – Euzet Hill; equatorial view aperture facing at SEM.

Figs. 5a-b. *Amanoa caribaea* Krug & Urb. (Phyllanthaceae) – ISEM Collection number: 41784 (plant specimen collected in Cameroon); equatorial views aperture facing (**a**) and polar view (**b**) at TLM.
LO-analysis: **a**, reticulate ornamentation and apertures; **b**, optical section.

Figs. 6a-c. *Amanoa* (Phyllanthaceae) – Crossroad D716/D981; equatorial view aperture facing (**a-b**) and polar view (**c**) at TLM.
LO-analysis: **a**, reticulate ornamentation and aperture; **b**, optical section.

Fig. 7. Alangium (Cornaceae) – Célas Tunnel 1; equatorial view (intercolpium) at TLM.

Fig. 8. Alangium (Cornaceae) – Saint-Jean de Maruéjols Pit hill; equatorial view aperture facing at TLM.

Fig. 9. *Alangium barbatum* (R.Br. ex C.B.Clarke) Baill. ex Kuntze (Cornaceae) – ISEM Collection number: 17360 (plant specimen collected in Burma); equatorial views aperture facing and optical section at TLM.

Figs. 10a-b. *Bombax*-type (Malvaceae) – Crossroad D716/D981; polar view at TLM.
LO-analysis: **a**, reticulate ornamentation; **b**, optical section.

Figs. 11a-b. *Avicennia* (Acanthaceae) – Montchamp; equatorial view aperture facing at TLM.

LO-analysis: **a**, reticulate ornamentation; **b**, optical section.

Figs. 12a-c. *Avicennia* (Acanthaceae) – Saint-Jean de Maruéjols Pit hill; equatorial view (intercolpium) at TLM.
LO-analysis: **a**, reticulate ornamentation; **b**, focus at base of columellar, colpi; **c**, optical section.

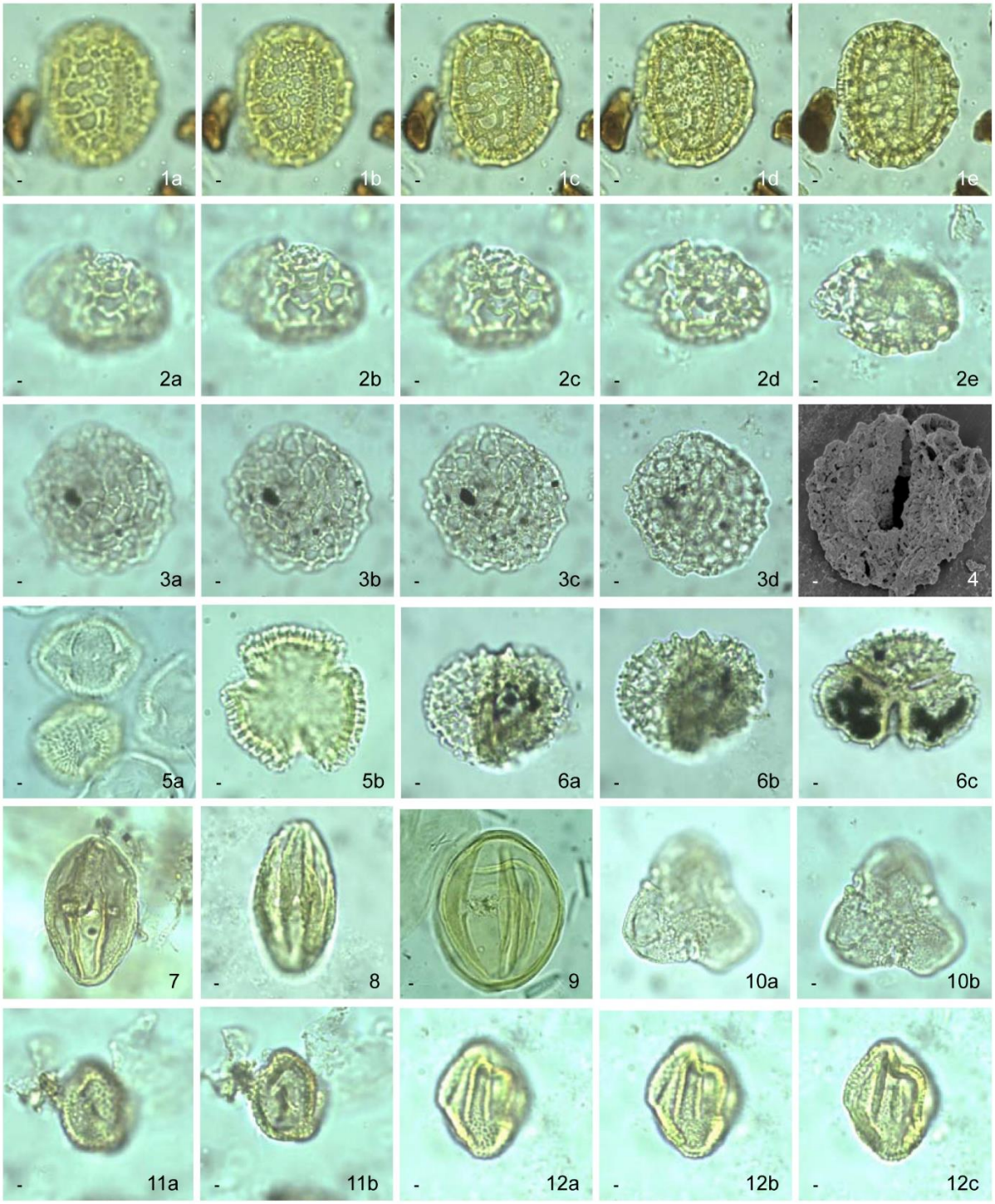
- 1a
- 1b
- 1c
- 1d
- 1e
- 2a
2b
- 2c
- 2d
- 2e
- 3a
- 3b
- 3c
- 3d
- 4
- 5a
- 5b
- 6a
- 6b
- 6c
7
- 8
- 9
10a
- 10b
- 11a
- 11b
- 12a
- 12b
- 12c

Plate 2. Photographs at TLM and SEM of some fossil and modern pollen grains (shots by J.-P. Suc). Modern pollen grains originate from the ISEM - Montpellier Collection or from the GeoBioStratData – Rillieux la Pape Collection. Scale bar = 10 µm.

Figs 1a-b. Araliaceae – Célas Tunnel 2.; equatorial view (intercolpium) at TLM.

LO-analysis: **a**, reticulate ornamentation and apertures; **b**, optical section.

Figs. 2a-b. Araliaceae – Montchamp; equatorial view aperture facing at TLM.
LO-analysis: **a**, reticulate ornamentation and apertures; **b**, apertures and optical section.

Fig. 3. *Croton* (Euphorbiaceae) – Euzet Hill; view at SEM.

Figs. 4a-c. *Croton scabiosus* Bedd. (Euphorbiaceae) – ISEM Collection number: 15339 (plant specimen collected in India); view at TLM.
LO-analysis: **a**, reticulate ornamentation; **b**, focus on the foot of columellae; c, optical section.

Figs. 5a-b. *Croton* (Euphorbiaceae) – Saint-Jean de Maruéjols Pit hill; view at TLM.
LO-analysis: **a**, reticulate ornamentation; **b**, focus on the foot of columellae and optical section.

Figs. 6a-b. *Dodonaea* (Sapindaceae) – Crossroad D716/D981; equatorial view aperture facing at TLM.
LO-analysis: **a**, aperture; **b**, aperture and optical section.

Figs. 7a-c. *Dodonaea triquetra* J.C.We,dl. (Sapindaceae) – ISEM Collection number: 36963 (plant specimen collected in Australia); equatorial view aperture facing at TLM.

LO-analysis: **a**, psilate ornamentation and apertures; **b**, aperture; **c**, aperture and optical section.

Figs. 8-c. *Embolanthera glabrescens* H.L.Li (Hamamelidaceae) – ISEM Collection number: 14245 (plant specimen collected in Vietnam); polar view at TLM.
LO-analysis: **a**, reticulate ornamentation; **b**, focus on the foot of columellae; **c**, optical section.

Figs. 9a-c. *Embolanthera* (Hamamelidaceae) – Vauvert 1 3200 m; polar view at TLM.
LO-analysis: **a**, reticulate ornamentation; **b**, focus on the foot of columellae; **c**, optical section.

Figs. 10a-c. *Fothergilla gardenii* L. (Hamamelidaceae) – GeoBioStratData Collection number: 839 (plant specimen collected in North America); polar view at TLM.
LO-analysis: **a**, reticulate ornamentation; **b**, focus on the foot of columellae; **c**, optical section.

Figs. 11a-c. *Fothergilla* (Hamamelidaceae) – Euzet Hill; polar view at TLM.

LO-analysis: **a**, reticulate ornamentation; **b**, focus on the foot of columellae; **c**, optical section.

Figs. 12a-b. Mappianthus (Icacinaceae) – Euzet Hill; equatorial view at TLM.
LO-analysis: **a**, echinulate ornamentation and aperture; **b**, optical section.

Fig. 13. *Leea* (Vitaceae) – Saint-Jean de Maruéjols Pit hill; equatorial view at TLM.
LO-analysis: reticulate ornamentation and aperture.

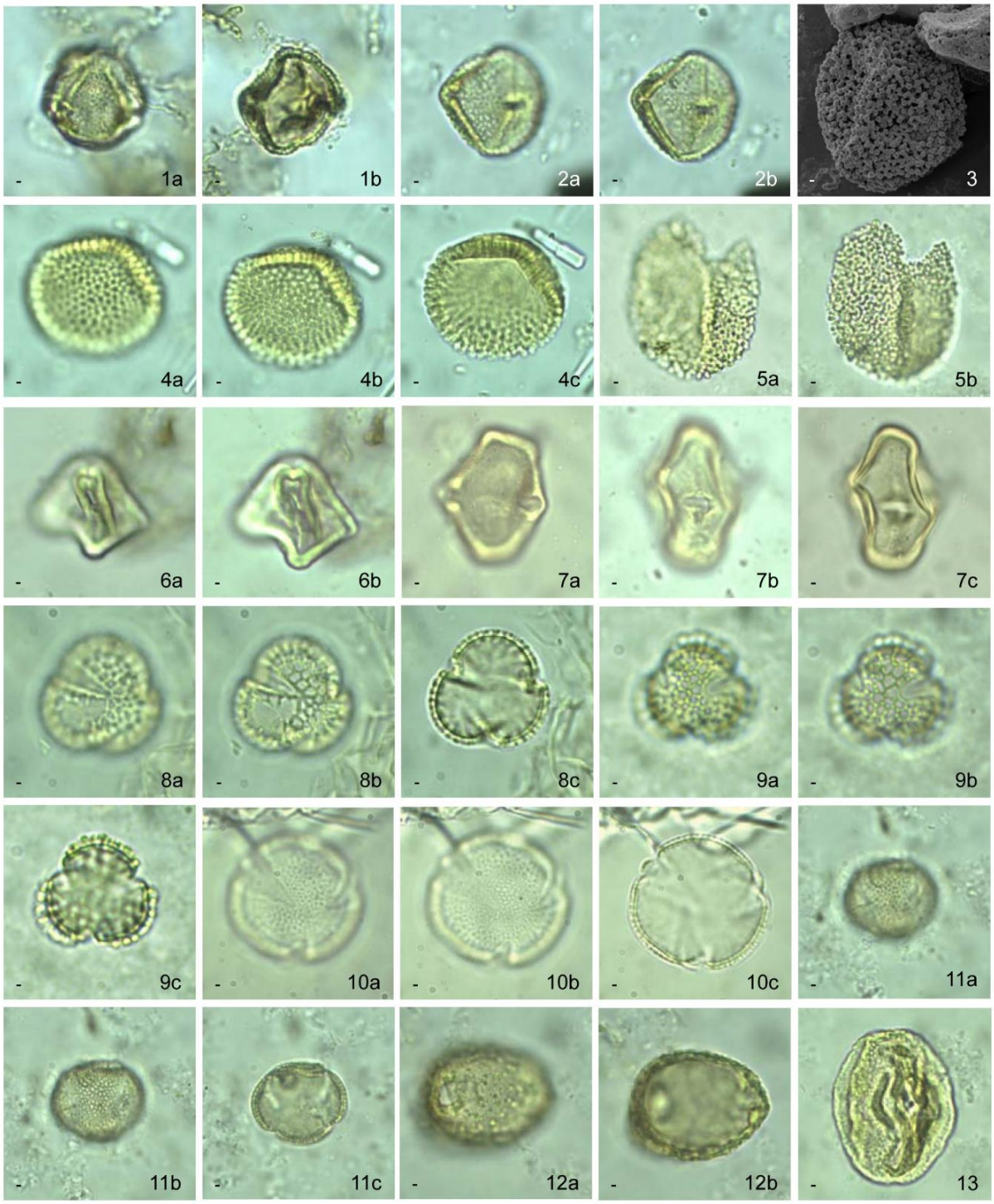
- 1a
- 1b
- 2a
- 2b
- 3
- 4a
- 4b
- 4c
- 5a
- 5b
- 6a
- 6b
- 7a
- 7b
- 7c
- 8a
- 8b
- 8c
- 9a
- 9b
- 9c
- 10a
- 10b
- 10c
- 11a
- 11b
- 11c
- 12a
- 12b
- 13

Plate 3. Photographs at TLM and SEM of some fossil and modern pollen grains (shots by J.-P. Suc). Modern pollen grains originate from the ISEM - Montpellier Collection. Scale bar = 10 µm.

Figs 1a-e. *Distylium* (Hamamelidaceae) – Euzet Hill; polar view at TLM.
LO-analysis: **a**, reticulate ornamentation; **b**, apertures and optical section.

Figs. 2a-c. Menispermaceae – Euzet Hill; equatorial view aperture facing at TLM.
LO-analysis: **a**, reticulate ornamentation and aperture; **b**, focus on the base of columellae; **c**, optical section.

Figs; 3a-c. *Olea* (Oleaceae) – Euzet Hill; equatorial view (intercolpium) at TLM.
LO-analysis: **a**, reticulate ornamentation; **b**, focus on the base of columellae; **c**, optical section.

Fig. 4. *Mussaenda laxa* (Hook.f.)Hutch. ex Gamble (Rubiaceae) – ISEM Collection number: 9954 (plant specimen collected in India); polar view, optical section at TLM.

Fig. 5. *Mussaenda*-type (Rubiaceae) – Serre de cauvel 3; polar view, optical section at TLM.

Figs. 6a-d. *Peltogyne*-type (Leguminosae) – Euzet Hill; polar view at TLM.
LO-analysis: **a**, clavate ornamentation; **b**, focus on the base of clavae; **c**, apertures; **d**, optical section.

Fig. 7. Peltogyne-type (Leguminosae) – Euzet Hill; view with aperture at SEM.

Figs. 8a-c. *Phyllanthus simplex* Retz. = *P. virgatus* G.Forst. (Phyllanthaceae) – ISEM Collection number: 10100 (plant specimen collected in India); polar view at TLM.
LO-analysis: **a**, reticulate ornamentation and apertures; **b**, focus on the base of columellae and apertures; **c**, optical section.

Figs. 9a-c. *Phyllanthus* (Phyllanthaceae) – Euzet Hill; polar view at TLM.
LO-analysis: **a**, reticulate ornamentation and apertures; **b**, focus on the base of columellae and apertures; **c**, optical section.

Fig. 10. *Phyllanthus* (Phyllanthaceae) – Euzet Hill; view at SEM showing the reticulum and apertures.

Fig. 11. *Rhizophoraceae* – Montchamp; equatorial view at TLM showing the apertures.

Fig. 12. *Rhoiptelea* (Juglandaceae) – Canet 1 1470 m; polar view, optical section at TLM.

Fig. 13. *Symplocos* (Symplocaceae) – Euzet Hill; polae view showing apertures at TLM.

Fig. 14. *Cedrus* (Pinaceae) – Crossroad D716/D981; profile view at TLM.

Fig. 15. *Podocarpus* (Podocarpaceae) – Célas Tunnel 2; proximal view at TLM.

Fig. 16. *Podocarpus* (Podocarpaceae) - Crossroad D716/D981; distal view at TLM.

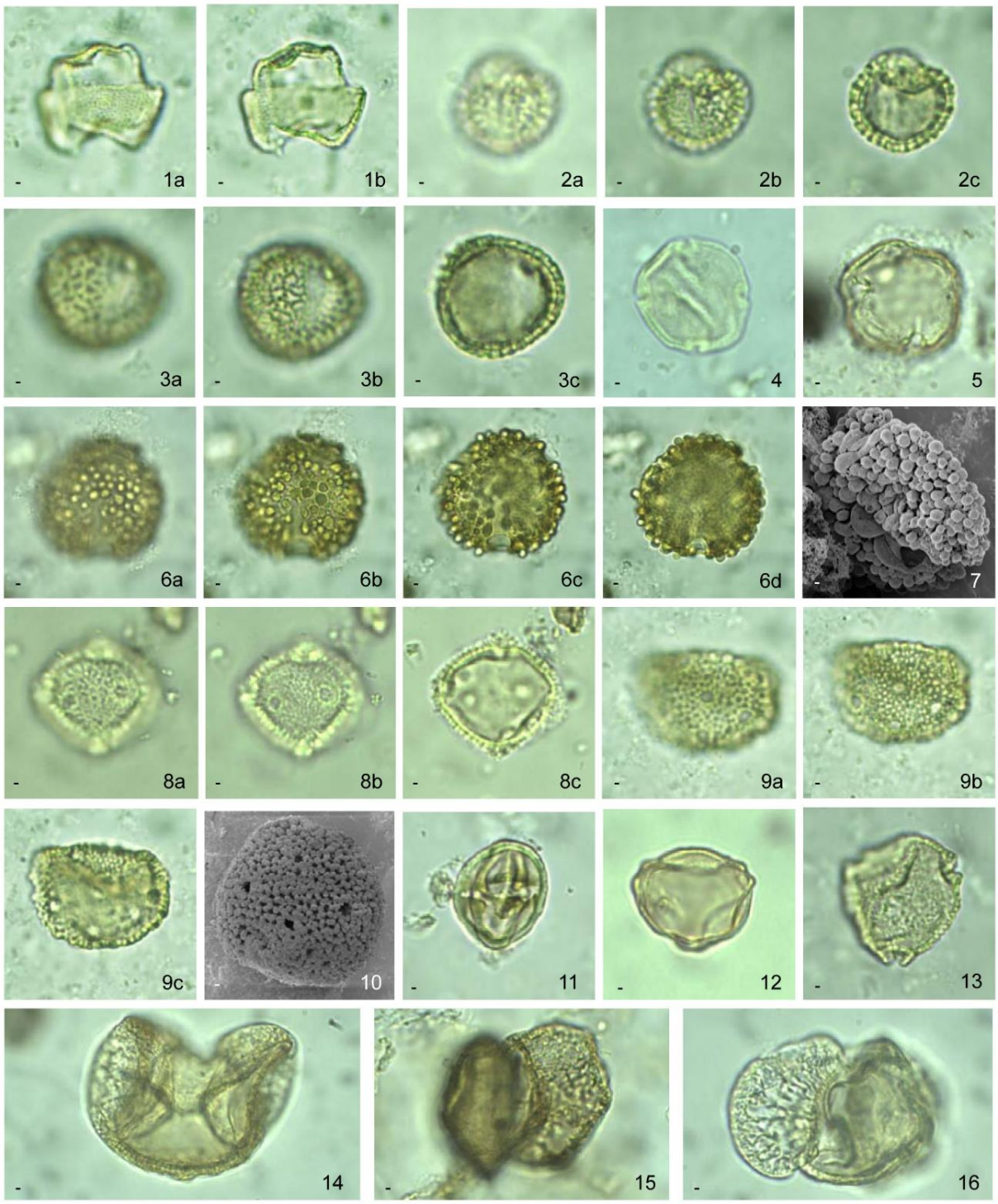
1a
1b
2a
2b
2c
3a
3b
3c
4
5
6a
6b
6c
6d
7
8a
8b
8c
9a
9b
9c
10
11
12
13
14
15
16

Plate 4. Photographs at TLM and FLM of some fossil dinoflagellate cysts (shots by S. -M. Popescu). Scale bar = 10 µm.

Figs. 1a-c. Deflandrea phosphoritica – Gallician 9 (2530 m): a-b, TLM; c, FLM.

Figs. 2a-c. Spiniferites sp. – Gallician 9 (2530 m): a-b, TLM; c, FLM.

Figs. 3a-c. Nematosphaeropsis sp. – Crossroad D716/D981: a-b, TLM; c, FLM.

Figs. 4a-c. Cleitosphaeridium sp. – Serre de Cauvel (sample 2): a-b, TLM; c, FLM.

Figs. 5a-c. Impagidinium sp. – Serre de Cauvel (sample 2): a-b, TLM; c, FLM.

Figs. 6a-c. Lingulopdinium machaerophorum – Serre de Cauvel (sample 2): a-b, TLM; c, FLM.

Figs. 7a-c. Glaphyrocysta sp. – Canet 1 (1100 m): a-b, TLM; c, FLM.

Figs. 8a-c. Impagidinium patulum – Canet 1 (1100 m): a-b, TLM; c, FLM.

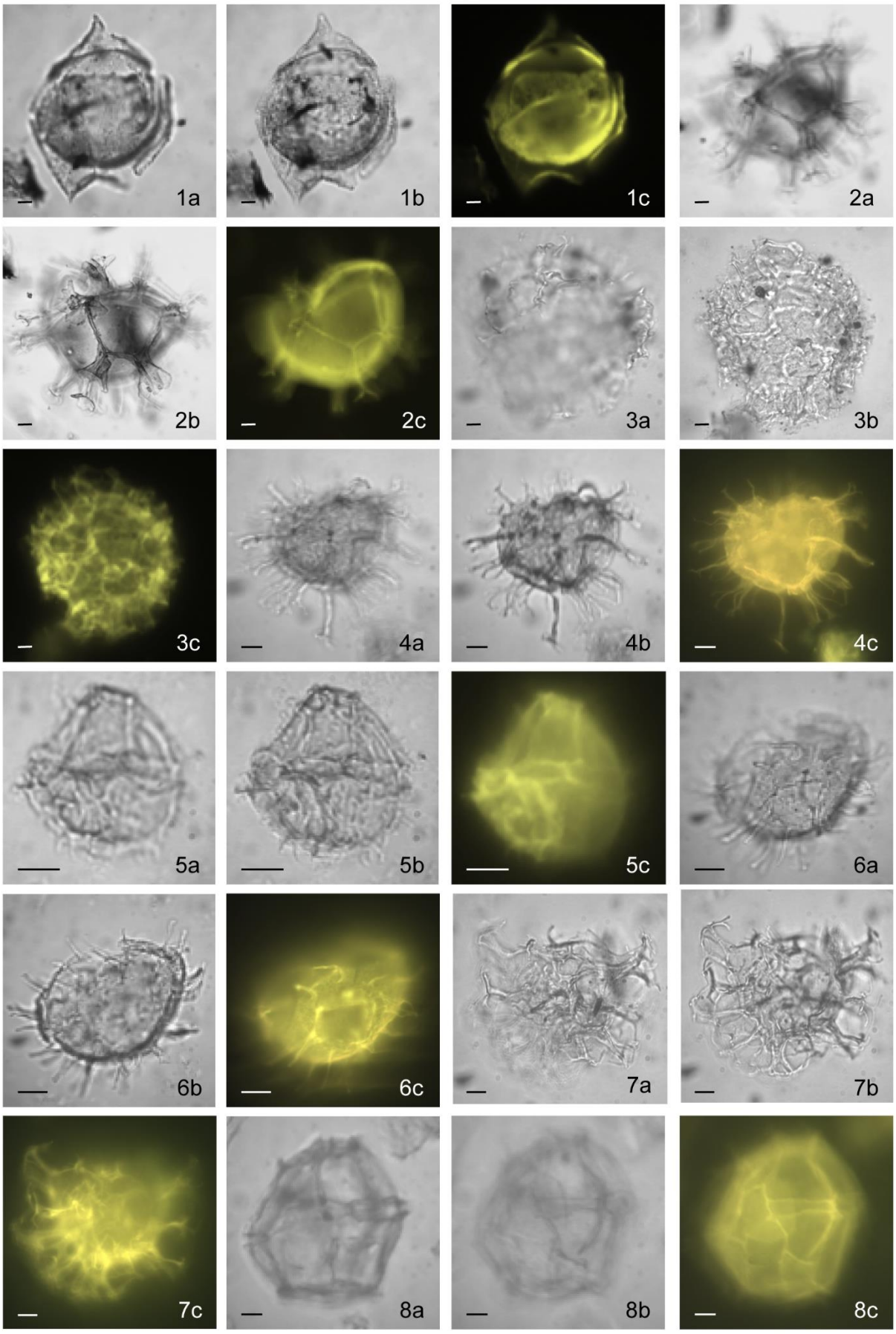
1a
1b
1c
2a
2b
2c
3a
3b
3c
4a
4b
4c
5a
5b
5c
6a
6b
6c
7a
7b
7c
8a
8b
8c

d- Climatostratigraphy vs. palynostratigraphy.

Two obvious items imply to use pollen data as a climatostratigraphic tool (numerical variability) in contrary to a classical biostratigraphic tool (first occurrence and last occurrence datums):

- plants evolve along geological times but evolution only affects the species level during the Cenozoic period, usually unattainable through the pollen morphology;
- plants shift in latitude and altitude along geological times with respect to changes in temperature and precipitation.

As a consequence, palynostratigraphy based on occurrences of supposed species is to be considered as an old-fashioned approach and must be definitely abandoned. One of the most critical examples of such an obsolete use is provided by the use of the pseudo-species *Boelhensipollis hohli*, which has been proposed as a marker of the Oligocene series (Sittler and Schuler, 1976) and hence abundantly indeed excessively exploited (e.g., Châteauneuf, 1980; Olivier-Pierre, 1980; Schuler, 1988; Châteauneuf and Nury, 1995; Cavagnetto, 2002; Châteauneuf et al., 2019).

The problem resulting from this deficient concept shows multiple aspects:

- quality of the published photographs is often insufficient to convince that an unique taxon corresponds to the so-called *Boelhensipollis hohli* pollen;
- Sittler and Schuler (1976) suppose that two pollen-types are included within their *Boelhensipollis hohli* that makes more inappropriate the use of a species designation;
- these authors describe the *Boelhensipollis hohli* pollen-type as heteropolar, i.e., non-joined colpi (strictly tricolporate pattern) on one side of the polar view and joined colpi (syncolporate pattern) on the other side, and they propose two possible botanical ascriptions: *Elaeagnus* (Elaeagnaceae) and *Serjania* (Sapindaceae); *Elaeagnus* modern species do not show heteropolar pollen while some *Serjania* modern species show heteropolar pollen (Muller and Leenhouts, 1976);
- in addition, it is difficult to conceive the sudden appearance of the temperate genus *Elaeagnus* at the earliest Oligocene, while it has been already recorded in Northern Canada during the Early Eocene Climatic Optimum (Salpin et al., 2019);
- it is also unbelievable that *Serjania*, a tropical genus, appeared simultaneously with a significant climate cooling, while several pollen grains belonging to Sapindaceae have been recorded in the Priabonian samples (**Table S4.3**) and are present in Eocene sediments from Southwestern France (Fauquette et al., in progress).

4.9. Références bibliographiques du chapitre 4

Albarède, F. Michard, A. 1987. Evidence for Slowly Changing Sr-87/Sr-86 in Runoff from Fresh-Water Limestones of Southern France. *Chemical Geology* 64: 55-65.

Alonso-Azcárate, J. Bottrell, S.H. and Mas, J.R., 2006. Synsedimentary versus metamorphic control of S, O and Sr isotopic compositions in gypsum evaporites from the Cameros Basin, Spain. *Chemical Geology* 234: 46-57.

Andersson, P.S., Wasserburg, G.J., Ingri, J. 1992. The sources and transport of Sr and Nd isotopes in the Baltic Sea. *Earth and Planetary Science Letters* 113: 459-472.

Anthonissen D.E., Ogg J.G, 2012. Cenozoic and Cretaceous biochronology of planktonic foraminifera and calcareous nannofossils. In "The geologic time scale 2012", Gradstein, F.M., Ogg, J.G., Schmitz, M.D., Ogg, G.M. (eds.), Elsevier, Amsterdam, Appendix 3, 1083–1127.

Arnaud-Fassetta, G., Suc, J.-P., 2015. Dynamique hydrogéomorphologique et diversité végétale dans le delta du Rhône (France) de -10.000 ans à demain. *In* " Le Rhône, entre nature et société ", Reynard, E., Evéquoz-Dayen, M., Borel, G. (eds.), *Cahiers de Vallesia*, 29, 63–98.

Arthaud F, Ogier M, Séguret M. 1981. Géologie et géophysique du Golfe du Lion et de sa bordure nord. *Bulletin du BRGM* 1(3): 175–193.

Balansa J, Espurt N, Hippolyte J-C, Philip J, Séverine Caritg. 2022. Structural evolution of the superimposed Provençal and Subalpine fold-thrust belts (SE France). *Earth-Science Reviews* 227, April 2022, 103972. Doi : https://doi.org/10.1016/j.earscirev.2022.103972

Banks H, Lewis G. 2018. Phylogenetically informative pollen structures of 'caesalpinioid' pollen (Caesalpinioideae, Cercidoideae, Detarioideae, Dialioideae and Duparquetioideae: Fabaceae). *Botanical Journal of the Linnean Society* 187: 59–86.

Beaudouin, C., Suc, J.-P., Cambon, G., Touzani, A., Giresse, P., Pont, D., Aloïsi, J.-C., Marsset, T., Cochonat, P., Duzer, D., Ferrier, J., 2005a. Present-day rhythmic deposition in the Grand Rhône prodelta (NW Mediterranean) according to high-resolution pollen analyses. *Journal of Coastal Research*, 21, 2, 292–306.

Beaudouin, C., Suc, J.-P., Acherki, N., Courtois, L., Rabineau, M., Aloïsi, J.-C., Sierro, F.J., Oberlain, C., 2005b. Palynology of the northwestern Mediterranean shelf (Gulf of Lions): First vegetational record for the last climatic cycle. *Marine and Petroleum Geology*, 22, 6–7, 845–863.

Beaufort L, Bruneau J, Crepin A, Julian Y. 1954. Ampleur de l'érosion pontienne et du comblement Pliocène en Camargue. Bulletin de la Société Géologique de France 6(4) : 157-184.

Benedicto A, Labaume P, Séguret M, Séranne M. 1996. Low-angle crustal ramp and basin geometry in the Gulf of Lion passive margin: the Oligocene-Aquitanian Vistrenque graben, SE France. *Tectonics* 15(6): 1192–1212.

Bessedik M. 1980. La flore pollinique d'un niveau gypseux de la série de Portel (Aude-France): Oligocène terminal. Mémoires *du Muséum national d'histoire naturelle*, ser. 8, Botanique, 27: 196–203.

Bessedik M. 1981. Recherches palynologiques sur quelques sites du Burdigalien du midi de la France. PhD thesis, Univ. Montpellier 2, 43 pp.

Bessedik M. 1984. The early Aquitanian and upper Langhian-lower Serravallian environments in the Northwestern Mediterranean region. *Paléobiologie continentale*, 14, 2, 153–179.

Biteau, Morash, Mervoyer, Canard, Buisson. 1993. Permis Vauvert-Gallician – « Farm out » Coparex. Compte rendu de visite chez Coparex. Synthèse sur le secteur de Gallician. *Elf Aquitaine Production, Document interne*. 27 pp.

Bois C. 1993. Initiation and evolution of the Oligo-Miocene rift basins of southwestern Europe: contribution of deep seismic profiling. *Tectonophysics* 226 : 227-252.

Boschetti, T., Cortecci, G., Toscani, L., Iacumin, P. 2011. Sulfur and oxygen isotope compositions of Upper Triassic sulfates from northern Apennines (Italy): paleogeographic and hydrogeochemical implications. *Geologica Acta* 9(2): 129-147.

Bodergat A-M, Briot D, Hugueney M, Poidevin J-L, Picot L, Giraud F, Berger J.P, Levy A, Poignant A. 1999. Incursions marines dans l'environnement lacustre du rift oligocène de Limagne (Massif Central, France) : apport des organisms halophiles et des isotopes du strontium, datation par les mammifères. *Bulletin de la Société Géologique de France* 170: 499–511.

Briot D, 2008. Sr isotopes of the shells of the euryhaline gastropod *Potamides lamarcki* from the Oligocene of the French Massif Central and Paris Basin – A cule to its habitats. Palaeogeography, Palaeoclimatology, Palaeoecology 268 : 116-122.

Buisson J.-J. 1993. Permis Vauvert-Gallician – 'Farm out' Coparex. Synthèse sur le secteur de Gallician. Document interne n° 93-0345 Elf-Aquitaine Production, 27 pp.

Cambon, G., Suc, J.-P., Aloïsi, J.-C., Giresse, P., Monaco, A., Touzani, A., Duzer, D., Ferrier, J., 1997. Modern pollen deposition in the Rhône delta area (lagoonal and marine sediments), France. *Grana*, 36, 105–113.

Carreira L.M.M, de Souza Secco R, Barth O.M. 1996. Pollen morphology of the lianescent species of the genus *Croton* (Euphorbiaceae). *Grana* 35: 74–78.

Cavagnetto C. 2002. La palynoflore du basin d'As Pontes en Galice dans le nord-ouest de l'Espagne à la limite Rupélien–Chattien (Oligocène). *Palaeontographica* B 263: 161– 204.

Cavelier C, Alabouvette G, Amberger J.P, Cautru J.-P, Charollais J, Châteauneuf J.-J, et al. 1984. Paléogène. In : Debrand-Passard ed., *Synthèse géologique du Sud-Est de la France*. *Mémoire du BRGM* 125 : pp. 389-468.

Châteauneuf J.-J. 1977. Etude palynologique de l'Oligocène du bassin de Marseille. *Géologie méditerranéenne* 4 (1): 37–46.

Châteauneuf, J.-J. 1980. Paléostratigraphie et paléoclimatologie de l'Éocène supérieur et de l'Oligocène du bassin de Paris. *Mémoires du Bureau de Recherches géologiques et Minières* 116: 357 pp.

Châteauneuf, J.-J., Nury, D., 1995. La flore de l'Oligocène de Provence méridionale : implications stratigraphiques environnementales et climatiques. *Géologie de la France* 2 : 43-55.

Châteauneuf, J.-J., Villeneuve, M., Nury, D. 2019. La transgression rupélienne (stampienne) dans les « Sables bleutés » du Haut-Var, démontrée par l'étude palynologique à Saint-Maime (Fossé de Montmeyan, Sud-Est France). *Géologie de la France* 1: 1–17.

Chaussidon, M., Albarède, F., Sheppard, S.M.F. 1989. Sulphur isotope variations in the mantle from ion microprobe analyses of micro-sulphide inclusions. *Earth and Planetary Science Letters* 92: 144-156.

Clauzon, G. 1990. Restitution de l'évolution géodynamique néogène du bassin du Roussillon et de l'unité adjacente des Corbières d'après les données écostratigraphiques et paléogéographiques. *Paléobiologie continentale* 17: 125–155.

Denison, R.E., Kirkland, D.W., Evans, R., 1998. Using Strontium Isotopes to Determine the Age and Origin of Gypsum and Anhydrite Beds. *Journal of Geology*, 106, 1-17.

Depéret C. 1917. Monographie de la faune de mammifères fossiles du Ludien inférieur d'Euzet-les-Bains (Gard). *Annales de l'Université de Lyon, Sciences, Médecine*, Lyon (N° 40-288pp).

Dèzes P, Schmid S.M, Ziegler P.A. 2004. Evolution of the European Cenozoic Rift System: interaction of the Alpine and Pyrenean orogens with their foreland lithosphere. *Tectonophysics* 389: 1–33.

Dinelli E, Testa G, Cortecci G, Barbieri M. 1999. Stratigraphic and petrographic constraints to trace element and isotope geochemistry of Messinian sulfates of Tuscany. *Memoria della Società Geologica Italiana* 54: 61-74.

Doláková N, Burešová A. 2007. Use of fluorescent microscopy in the study of redeposited palynomorphs in the cave and marine sediments of Moravia (Czech Republic). *Acta Palaeobotanica* 47(1): 275–279.

Fauquette, S., Guiot, J., Suc, J.-P. 1998. A method for climatic reconstruction of the Mediterranean Pliocene using pollen data. *Palaeogeography, Palaeoclimatology, Palaeoecology* 144: 183–201.

Fauquette S, Bernet M, Suc J.-P, Grosjean A.-S, Guillot S, van der Beek P, Jourdan S, Popescu S.M, Jiménez-Moreno G, Bertini A, Pittet B, Tricart P, Dumont T, Schwartz S, Zheng Z, Roche E, Pavia G, Gardien V. 2015. Quantifying the Eocene to Pleistocene topographic evolution of the southwestern Alps, France and Italy. *Earth and Planetary Science Letters* 412: 220-234.

Faure, G., 1986. Principles of Isotope Geology, 2nd edition, New York, Chichester, Brisbane, 589 pp.

Fontannes, F. 1885. Etudes stratigraphiques et paléontologiques pour servir à l'histoire de la période Tertiaire dans le bassin du Rhône, *Société Géologique de France*, Paris (195pp).

Fontes J.-C, Gaudant J, Mélières F, Filly A, Schlund J.-M. 1996. Origine continentale des évaporites paléogènes du fossé de Valence (Drôme): données minéralogiques, isotopiques et paléoécologiques. *Bulletin de la Société Géologique de France* 167(4): 475–481.

Ford M, Lickorish H. 2004. Foreland basin evolution around the western Alpine Arc. *Geological Society, London, Special Publications* 221 :39-63.

Giraud J. 1902. Études géologiques sur la Limagne. *Bulletin du Service de la Carte Géologique de France* 13(87): 410 p.

Gely, J.-P., Sztrákos, K., 2000. L'évolution paléogéographique et géodynamique du Bassin aquitain au Paléogène : enregistrement et datation de la tectonique pyrénéenne. *Géologie de la France* 2 : 31-57.

Giacometti, F., Evans, K. A., Rebay, G., Cliff, J., Tomkins, A. G., Rossetti, P., Vaggelli, G. and Adams, D. T., 2014. Sulfur isotope evolution in sulfide ores from Western Alps: Assessing the influence of subduction-related metamorphism, Geochemistry, Geophysics, Geosystems, 15, 3808–3829.

Gorini C, Le Marrec A, Mauffret A. 1993. Contribution to the structural and sedimentary history of the Gulf of Lions (western Mediterranean), from the ECORS profiles, industrial seismic profiles and well data. *Bulletin de la Société géologique de France* 164(3): 353–363.

Gottis, M. 1958. L'apport des travaux de la Compagnie d'exploration pétrolière (C.E.P.) dans la connaissance du basin tertiaire du Roussilon. *Bulletin de la Société géologique de France* ser. 6, 8, 8, 881–883.

Gradstein, F.M., Ogg, J.G., Schmitz, M.D., Ogg, G.M. (eds.), 2012. The geologic time scale 2012, Elsevier, Amsterdam, 1144 pp.

Graham A, Barker G. 1981. Palynology and tribal classification in the Caesalpinioideae. *In* 'Advances in Legume Systematics', Polhill R.M and Raven P.H. eds., *Royal Botanic Garden*, Kew, 801–834.

Gruas-Cavagnetto C. 1973. Première contribution à l'étude de la palynoflore de la Formation de Célas (Bassin d'Alès, Gard). *Paléobiologie continentale* 4 (2) 1–13.

Hou H.-Y. 1983. Vegetation of China with reference to its geographical distribution. *Annals of Missouri Botanical Garden* 70: 509-548.

Hoyle T.M, Leroy S.A.G, López-Merino L, Richards K. 2018. Using fluorescence microscopy to discern in situ from reworked palynomorphs in dynamic depositional environments – An example from sediments of the late Miocene to early Pleistocene Caspian Sea. *Review of Palaeobotany and Palynology* 256: 32–49.

Jan du Chêne R. 1989. Etude palynologique du sondage EURAFREP (Camargue) : BAM 1. Aanalyse des échantillons 980 m à 1160 m et 1475 à 1950 m. In 'Rapport de fin de sondage Baumelles 1 (BAM 1). Permis Vauvert-Gallician', *Document interne EURAFREP* pp. 29–36.

Joseph P, Lomas S. 2004. Deep-water sedimentation in the Alpine Foreland Basin of SE France: new perspectives on the grès d'Annot and related systems - An introduction. Dans P. Joseph, & S. Lomas (Éds.), Deep-water sedimentation in the Alpine Foreland Basin of SE France: new perspectives on the grès d'Annot and related systems (Vol. 1, pp. 1-16). *The Geological Society of London, Special Publications*.

Köhler E. 1965. Die pollenmorphologie der biovulaten Euphorbiaceae und ihre bedeutung für die taxonomie. *Grana Palynologica* 6 (1) 26–120.

Krutzsch W. 1962. Mikropaläontologische (sporenpaläontologische) untersuchungen in der braunkohle des Geiseltales. II. Die formspezies des pollengattung Pentapollenites Krutzsch (1958). *Paläontologie*, 1, H. 2, 73–103.

Kvacek Z. 2002. Novelties on Doliostrobus (Doliostrobaceae), an extinct conifer genus of the European Palaeogene. *Časopis Národního muzea, Řada přírodovědná*171 (1–4): 131– 175.

Leroux, E., Rabineau, M., Aslanian, D., Gorini, C., Molliex, S., Bache, F., Robin, C., Droz, L., Moulin, M., Poort, J., Rubino, J.-L., Suc, J.-P. 2017. High-resolution evolution of terrigenous sediment yields in the Provence Basin during the last 6 Ma: relation with climate and tectonics. *Basin Research*, 29 (3): 305–339.

Lesueur J.-L. 1991. Etude sédimentologique et stratigraphique du Bassin Paléogène d'Apt–Manosque–Forcalquier (Alpes de Haute Provence). Modalités de la transition Burdigalienne. Ph.D. thesis, University M. de Montaigne, Bordeaux III, France : 407 pp.

Lettéron, A., Fournier, F., Hamon, Y., Villier, L., Margerel, J.-P., Bouche, A., Feist, M., Joseph, P. 2017. Multi-proxy paleoenvironmental reconstruction of saline lake carbonates:

paleoclimatic and paleogeographic implications (Priabonian-Rupelian, Issirac Basin, SE France). *Sedimentary Geology* 358: 97–120.`

Lettéron, A. 2018. Caractérisation sédimentologique, stratigraphique et paléoenvironnementale du système carbonaté lacustre à salinité variable du bassin d'Alès et des régions limitrophes (Priabonien, SE France) : implications paléoclimatiques et paléogéographiques. PhD thesis, Aix-Marseille University : 344 pp.

Lettéron A, Hamoun Y, Fournier F, Demory F, Séranne M, Joseph P. 2021. Stratigraphic architecture of a saline lake system: From lake depocenter (Alès Basin) to margins (Saint-Chaptes and Issirac basins), Eocene-Oligocene transition, south-east France. *Sedimentology, Blackwell Publishing, in press*, ⟨DOI: 10.1111/sed.12920⟩, ⟨hal-03406458⟩.

Lindtke, J., S.B. Ziegenbald, B. Brunner, J.M. Rouchy, C. Pierre, and J. Peckmann. 2011. Authigenesis of native Sulphur and dolomite in a lacustrine evaporitic setting (Hellín basin, Late Miocene, SE Spain). *Geological Magazine*: 148 (4) 655-669.

Mauffret A, Gorini C. 1996. Structural style and geodynamic evolution of Camargue and Western Provencal basin, southeastern France. *Tectonophysics* 15(2): 356-375.

Merville M. 1965. Le pollen des Sapindacées d'Afrique occidentale. *Pollen et Spores* 7(3) 465–489.

Michoux D. 1983. Etude palynologique des sédiments ludiens du fossé d'Alès (Gard). In "Inventaire des ressources nationales de charbon. Lignites du fosse d'Alès-Barjac", Alabouvette B, Chedhomme J, Fredet J.M, Lartaud V. *Rapport du B.R.G.M* 83 SGN 519 GEO/LRO, Annexe 4, 9 pp.

Muller J, Leenhouts P.W. 1976. A general survey of pollen types of Sapindaceae in relation to taxonomy. *In* "The evolutionary significance of the exine", Ferguson I.K, Muller J. eds., *Linnean Society Symposium Series* 1 : 407–445.

Nury D. 1990. L'Oligocène de Provence méridionale: stratigraphie, dynamique sédimentaire, reconstitutions paléogéographiques. Document du BRGM n°163. Editions du BRGM, 412pp.

Nury D, Thomassin B.A, 1994. Paléoenvironnements tropicaux, marins et lagunaires d'un littoral abrité (fonds meubles à bancs coralliens, lagune évaporitique) à l'Oligocène terminal, en Basse-Provence (région d'Aix-en-Provence, Marseille, France). *Géologie Méditerranéenne* 21(1-2): 95-108.

Ollivier-Pierre M.-F. 1980. Etude palynologique (spores et pollens) de gisements paléogènes du Massif Armoricain. Stratigraphie et paléogéographie. *Mémoires de la Société géologique et minéralogique de Bretagne* 25 : 1–239.

Ortí, F., Pérez-López, A., García-Veigas, J., Rosell, L., Cendón, D.I., Pérez-Valera, F. 2014. Sulfate isotope compositions (δ34S, δ18O) and strontium isotopic ratios (87Sr/86Sr) of Triassic

evaporites in the Betic Cordillera (SE Spain). *Revista de la Sociedad Geológica de España* 27: 79-89.

Oudet, J. 2008. Etude terre-mer de la transition syn-rift/post-rift sur les marges de l'océan Liguro-Provençal: apports de la modélisation géologique 3D et de la chronostratigraphie intégrée (Ph.D thesis). Marseille, France: Université de Provence.

Oudet J, Münch Ph, Borgomano J, Quillévéré F, Melinte M, Demory F, Viseur S, Cornée J.-J. 2010. Land and sea study of the northeastern golfe du Lion rifted margin. In: X. Le Pichon and C. Rangin, Eds, Geodynamics of the France Southeast Basin. *Bulletin de la Société géologique de France* 181 (6) 591-607.

Palmer, M.R., C. Helvaci, and A.E. Fallick. 2004. Sulphur, sulphate oxygen and strontium isotope composition of Cenozoic Turkish evaporites. *Chemical Geology* (209) 341-356.

Pellat E, Allard M. 1895. Dépôts lacustres de la Butte Iouton entre Comps et Beaucaire (Gard). *Bulletin de la Société Géologique de France* 23: 434-436.

Petelet-Giraud, E., Desprats, J.F., Izac, J.L., Foucher, J.C., 2006. Caractérisation géochimique du bassin versant du Gardon d'Anduze. Approche des isotopes du strontium du phénomène de « crue éclair ». Final Report. BRGM/RP-54662-FR public report, 50 pp.

Philip J, Vianey-Liaud M, Martin-Clausas C, Tabuce R, Leonide P, Margerel J.-P, Noël J. 2017 - Stratigraphy of the Haut Var Paleogene continental series (Northeastern Provence, France) : New insight on the age of the « Sables bleutés du Haut Var » Formation. *Géobios* 50 : 319-339.

Plaziat J.-C, Younis W.R. 2005. The modern environments of Molluscs in southern Mesopotamia, Iraq: A guide to paleogeographical reconstructions of Quaternary fluvial, palustrine and marine deposits. *Carnets de Géologie* 2005/01, (18pp).

Popescu S.-M, Biltekin, D, Winter H, Suc J.-P, Melinte-Dobrinescu M.C, Klotz S, Combourieu-Nebout N, Rabineau, M, Clauzon, G, Deaconu F. 2010. Pliocene and Lower Pleistocene vegetation and climate changes at the European scale: Long pollen records and climatostratigraphy. *Quaternary International* 219: 152–167.

Popescu S.-M, Suc J.-P, Fauquette S, Bessedik M, Jiménez-Moreno G, Robin C, Labrousse L. 2021. Mangrove distribution and diversity during three Cenozoic thermal maxima in the Northern Hemisphere (pollen records from the Arctic – North Atlantic – Mediterranean regions). *Journal of Biogeography* 48: 2771-2784.

Powell A.J, Brinkhuis H, Bujak J.P. 1996. Upper Paleocene-Lower Eocene dinoflagellate cyst sequence biostratigraphy of southeast England. In: Knox R.W.O'B, Corfield R.M, Dunnay R.E. (eds), 1996, Correlation of the Early Paleogene in Northwest Europe, *Geological Society Special Publication*, n° 101.

Punt W. 1962. Pollen morphology of the Euphorbiaceae with special reference to taxonomy.

Wentia 7: 1–116.

Raab M, Spiro B. 1991. Sulfur isotopic variations during seawater evaporation with fractional crystallization. *Chemical Geology* 86: 323-333.

Reitsma Tj. 1970. Pollen morphology of the Alangiaceae. *Review of Palaeobotany and Palynology* 10: 249–332.

Rémy J.A. 1985. Nouveaux gisements de mammifères et reptiles dans les grès de Célas (Éocène sup. du Gard). Etude des paléothériidés (Perissodactyla, Mammalia). *Palaeontographica, Abteilung A*, 189, 171-225.

Rémy J.A. 1994. Une faunule de vertébrés sous la base des Grès de Célas (Éocène supérieur) à St-Dézery (Gard). *Palaeovertebrata* 23(1-4) : 211-216.

Rémy J.A., Fournier F. 2003. Mammifères fossiles de Grès de Célas (Éocène supérieur du Gard) : Découvertes récentes. *Bulletin de la Société des Sciences Naturelles de Nîmes et du Gard*, Nîmes, 64 :18-30.

Rémy J.A., Lesage J.-L. 2005. Un nouveau gisement de vertébrés d'âge Priabonien et son contexte géologique (Tranchée de Nozières, Gard). *Bulletin de la Société Géologique d'étude des Sciences Naturelles de Nîmes et du Gard* 65 : 7-14.

Ribes de Lima L, Vitorino da Cruz-Barros A, Pirani J.R, da Silva Corrêa A.M. 2007. Pollen morphology of *Croton* sect. *Lamprocroton* (Müll. Arg.) Pax (Euphorbiaceae) and its taxonomic implications. *Nordic Journal of Botany* 25 : 206–216.

Ribeiro de Souza L, Marques da Silva O.L, de Assis Ribeiro dos Santos F, Carneiro- Torres, D.S. 2020. Pollen morphology of Croton of the New World and pollen evolution of tribe Crotoneae (Euphorbiaceae). *Review of Palaeobotany and Palynology* 281 : 104279.

Rouchy J.-M. 1997. Paleogene continental rift system ofWestern Europe: locations of basins, paleogeographic and structural framework, and the distribution of evaporites. In: Busson, G., Schreiber, B.C. eds., Sedimentary Deposition in Rift and Foreland Basins in France and Spain. Columbia Univ. Press, New York: pp. 45–94.

Rouchy J.-M, Blanc-Valleron M.-M. 2009. Les évaporites matériaux singuliers, milieux extrêmes. Vuibert, Paris : 184 pp.

Salpin M, Schnyder, J., Baudin, F., Suan, G., Suc, J.-P., Popescu, M.-S., Fauquette, S., Reinhardt, L., Schmitz, M., Labrousse, L. 2019. Evidence for subtropical warmth in Canadian Arctic (Beaufort-Mackenzie, Northwest Territories, Canada) during the early Eocene. In 'Circum-Arctic Structural Events: Tectonic Evolution of the Arctic Margins and Trans-Arctic Links with Adjacent Orogens', *Geological Society of America Special Paper* 541 (27) : 637–664.

Sanchis E, Séranne M. 2000. Structural style and tectonic evolution of a polyphase extensional basin of the Gulf of Lion passive margin: the Tertiary Alès Basin, southern France. *Tectonophysics* 322: 243–264.

Schuler M. 1980. Environnements et paléoclimats paléogènes. Palynologie et biostratigraphie de l'Eocène et de l'Oligocène inférieur dans les fosses rhénan, thodanien et de Hesse. PhD thesis, University L. Pasteur Strasbourg, 383 pp.

Schuler M, Sittler C. 1976. Données paléoclimatiques à l'aube des temps néogènes en Haute Provence (France). *Géologie méditerranéenne* 3(3): 155–160.

Semmani N, Fournier F, Léonide P, Feist M, Boularand S, Borgomano J. 2022 Transgressive-regressive cycles in saline lake margin oolites: paleogeographic implications (Priabonian, Vistrenque Basin, SE France). *BSGF Earth Science Bulletin*: 193, 8.

Semmani N, Fournier F, Léonide P, Suc J-P, Marié L, Borgomano J. The continental depositional record of climate and tectonics around the Eocene-Oligocene transition in the Vistrenque Basin (Camargue, Southeast France), *in prep*.

Séranne M, Benedicto A, Truffert C, Pascal G, Labaume P. 1995. Structural style and evolution of the Gulf of Lion Oligo-Miocene rifting: Role of the Pyrenean orogeny. *Marine and Petroleum Geology* 12: 809–820.

Séranne, M. 1999. The Gulf of Lion continental margin (NW Mediterranean) revisited by IBS: an overview. In: Durand, B, Jolivet, L, Horváth, F, Séranne, M, eds. The Mediterranean basins: Tertiary extension within the Alpine Orogen. Volume Special Publication, 156. London: *The Geological Society* 15–36.

Séranne M, Couëffé R, Husson E, Baral C, Villard J. 2021. The transition from Pyrenean shortening to Gulf of Lion rifting in Languedoc (South France) –A tectonic-sedimentation analysis. *BSGF - Earth Sciences Bulletin* 192, 27.

Sissingh W. 2001. Tectonostratigraphy of the West Alpine Foreland: correlation of Tertiary sedimentary sequences, changes in eustatic sea-level and stress regimes. *Tectonophysics*: 333, 361–400.

Sissingh W. 2006. Synkinematic paleogeographic evolution of the West European Platform: correlation with Alpine plate collision and foreland deformation. *Géologie en Mijnbouw, Nehterlands Journal of Geosciences* 85(2):131-180.

Sittler C. 1965. Le Paléogène des fosses rhénan et rhodanien. Etudes sédimentologiques et paléoclimatiques. *Mémoires du Service de la carte géologique d'Alsace et de Lorraine* 24: 392 pp.

Sittler C, Schuler M. 1975. Extension stratigraphique, répartition géographique et écologie de deux genres polliniques paléogènes observes en Europe occidentale: *Aglaoreidia* et *Boehlensipollis*. *Société botanique de France, Colloque Palynologie*, 231–245.

Suan, G., Popescu, S.-M., Suc, J.-P., Schnyder, J., Fauquette, S., Baudin, F., Yoon, D., Piepjohn, K., Sobolev, N., Labrousse, L. 2017. Subtropical climate conditions and mangrove growth in Arctic Siberia during the early Eocene. Geology 45: 539–542.

Suc J.-P. 1976. Quelques taxons-guides dans l'étude paléoclimatique du Pliocène et du Pléistocène inférieur du Languedoc (France). Revue de Micropaléontologie, 18 (4) 246– 255.

Suc J.-P, Bessedik M. 1981. A methodology for Neogene palynostratigraphy. International Symposium on Concept and Method in Paleontology, Barcelona, pp. 205–208.

Suc J.-P. 1984. Origin and evolution of the Mediterranean vegetation and climate in Europe. Nature 307: 429–432.

Suc, J.-P., Diniz, F., Leroy, S., Poumot, C., Bertini, A., Dupont, L., Clet, M., Bessais, E., Zheng, Z., Fauquette, S., Ferrier, J. 1995. Zanclean (~ Brunssumian) to early Piacenzian (~ early-middle Reuverian) climate from 4° to 54° north latitude (West Africa, West Europe and West Mediterranean areas). *Mededelingen Rijks Geologische Dienst* 52: 43–56.

Suc, J.-P., Fauquette, S., 2012. The use of pollen floras as a tool to estimate palaeoaltitude of mountains: the eastern Pyrenees in the Late Neogene, a case study. *Palaeogeography, Palaeoclimatology, Palaeoecology*, 321–322, 41–54.

Suc, J.-P., Fauquette, S., Popescu, S.-M., Robin, C. 2020. Subtropical mangrove and evergreen forest reveal Paleogene terrestrial climate and physiography at the North Pole. *Palaeogeography, Palaeoclimatology, Palaeoecology* 551, 109755.

Suc, J.-P., Popescu, S.-M., Fauquette, S., Bessedik, M., Jiménez-Moreno, G., Bachiri Taoufiq, N., Zheng, Z., Médail, F. 2018. Reconstruction of Mediterranean flora, vegetation and climate for the last 23 million years based on an extensive pollen dataset. *Ecologia mediterranea* 44 (2): 53–85.

Sztrákos K. & Steurbaut E. 2017. — Révision lithostratigraphique et biostratigraphique de l'Oligocène d'Aquitaine occidentale (France). *Geodiversitas* 39(4) : 741-781.

Tesson, M., Labaune, C., Gensous, B., Suc, J.-P., Melinte-Dobrinescu, M.C., Parize, O., Imbert, P., Delhaye-Prat, V., 2011. Quaternary "compound" incised valley in a microtidal environment, Roussillon continental shelf, Western Gulf of Lions, France. *Journal of Sedimentary Research*, 81, 708–729.

Triat J.M, Truc G. 1974. Evaporites paléogènes du domaine rhodanien. *Revue de Géographie Physique et de Géologie Dynamique* 16: 235–262.

Utrilla, R., Pierre, C., Orti, F., Pueyo, J.J., 1992. Oxygen and sulphur isotope composition as indicators of the origin of Mesozoic and Cenozoic evaporites from Spain. *Chem. Geol.* 102: 229– 244.

Vollstaedt, H., Eisenhauer, A., Wallmann, K., Böhm, F., Fietzke, J., Liebetrau, V., Krabbenhöft, A., Farkaš, J., Tomašových, A., Raddatz, J., Veizer, J., 2014. The Phanerozoic

δ88/86Sr record of seawater: New constraints on past changes in oceanic carbonate fluxes. *Geochimica and Cosmochimica Acta,* 128, 249–265.

Westerhold, T., Marwan, N., Drury, A.J., Liebrand, D., Agnini, C., Anagnostou, E., Barnet, J.S.K., Bohaty, S.M., De Vleeschouwer, D., Florin, D., Lauretano, V., Littler, K., Lourens, L.J., Lyle, M., Pälike, H., Röhl, U., Tian, J., Wilkens, R.H., Wilson, P.A., Zachos, J.C. 2020. An astronomically dated record of Earth's climate and its predictability over the last 66 million years. *Science* 369: 1383–1387.

Zachos J, Pagani M, Sloan L, Thomas E, Billups K, 2001. Trends, rythms and aberrations in global climate 65 Ma to present. *Science* 292, 686-693.

Zheng Z. 1990. Végétation et climats néogènes des Alpes maritimes franco-italiennes d'après les données des analyses palynologiques. *Paléobiol. cont.* 17: 217-244.

Ziegler, P.A. 1992. European Cenozoic srift system. In: Ziegler, P.A. (Ed.), Geodynamics of Rifting, Volume I, Case History Studies on Rifts: Europe and Asia. *Tectonophysics* 208: 91–

Ziegler P.A, Dèzes P. 2007. Cenozoic Uplift of Variscan Massifs in the Alpine Foreland: Timing and Controlling Mechanisms. *Global Planetary Change* 58: 237-269.

5. LE DÉPÔT-CENTRE DU BASSIN DE LA VISTRENQUE : ANALYSE SÉDIMENTOLOGIQUE ET STRATIGRAPHIQUE

5. Le dépôt-centre du bassin de la Vistrenque : analyse sédimentologique et stratigraphique

'*If, like me, you have a more nihilistic view of life, the universe and everything, then you have to admit an infinite number of environments, facies and models*'

(Anderton, 1985, p.33 ; *in* Walker, 1992).

Synthèse

Ce chapitre concerne l'analyse sédimentologique, stratigraphique et géochimique du remplissage paléogène dans les secteurs de Gallician et de Pierrefeu situés dans le centre du bassin de la Vistrenque. Ce chapitre intègre les résultats obtenus dans le **chapitre 4** notamment le nouveau cadre chronostratigraphique du remplissage du bassin de la Vistrenque (SE France).

L'étude sédimentologique détaillée des carottes et les mesures de la composition isotopique du carbone et de l'oxygène des carbonates lacustres ont permis de reconstituer les paléoenvironnements de dépôts et l'évolution de l'architecture sédimentaire du bassin continental paléogène de la Vistrenque.

L'analyse de 6 forages a permis de définir 12 faciès de dépôt regroupés en 6 associations de faciès reflétant des aires de dépôt de lac profond, de pente de lac soumis à des apports terrigènes importants, de lac peu profond à sédimentation littorale et deltaïque et d'environnements fluviatiles et palustres. Trois modèles de dépôt ont été proposés pour rendre compte du remplissage paléogène « anté-salifère » du bassin de la Vistrenque entre le Priabonien-Rupélien basal et le Chattien inférieur : 1) un modèle de lac profond d'eau douce à oligohalin ; 2) un modèle de lac évaporitique ; 3) un modèle de lac peu profond avec un développement d'une plaine d'inondation.

L'évolution verticale des faciès dans les forages étudiés a révélé trois étapes principales de l'évolution du remplissage du bassin : 1) un bassin lacustre profond transgressif (Priabonien (?) - Rupélien basal) dans lequel la sédimentation était dominée par des dépôts terrigènes gravitaires sous climat humide dominant pendant une période marquée par des taux de subsidence élevés et une importante activité des failles ; 2) un bassin lacustre profond évaporitique et à régression forcée (Rupélien inférieur) caractérisé par une réduction drastique des apports terrigènes et par le dépôt d'évaporites dans des sous-bassins déconnectés de la masse d'eau lacustre ; 3) un stade de régression normale à long-terme (Rupélien moyen à supérieur / Chattien inférieur) et de remplissage du lac caractérisé par une augmentation des apports

terrigènes et une transition verticale ascendante des dépôts gravitaires de lac profond vers une sédimentation en milieu lacustre marginal dans des plaines alluviales, interprétée comme résultant à la fois d'une humidification du climat et d'une diminution du taux de subsidence et de l'activité des failles. Le début de la réduction du volume du lac et de la régression forcée pendant le Rupélien inférieur est enregistré par 1) le remaniement des carbonates intra-formationnels de la marge lacustre dans le dépôt-centre du lac, 2) le dépôt de sédiments riches en matières organiques (TOC>10%) associés à des processus de sulfato-réduction dans les zones les plus profondes du lac, 3) une forte diminution des apports terrigènes couplée à une forte augmentation du $\delta^{18}O$ des carbonates.

La régression forcée du début du Rupélien du bassin du lac Vistrenque est interprétée comme le résultat de l'aridification terrestre en réponse au refroidissement global à la transition Éocène-Oligocène (EOT). A la suite de cet épisode d'aridification et de refroidissement du climat au Rupélien inférieur, le remplissage final du lac et la transition vers des dépôts de plaine d'inondation se sont produits dans un environnement plus humide, pendant une phase de diminution de l'activité de la faille de Nîmes, avant sa réactivation pendant le rifting du Golfe du Lion.

*Ce chapitre est rédigé en anglais sous format d'un article scientifique (***Article 3***) qui sera soumis prochainement pour publication à une revue scientifique.*

Article 3 - The continental depositional record of climate and tectonics around the Eocene-Oligocene transition in the Vistrenque Basin (Camargue, Southeast France)

Nazim SEMMANI, François FOURNIER, Philippe LÉONIDE, Jean-Pierre SUC, Lionel MARIÉ, Jean BORGOMANO. «The continental depositional record of climate and tectonics around the Eocene-Oligocene transition in the Vistrenque Basin (Camargue, Southeast France)». *In prep.*

The continental depositional record of climate and tectonics around the Eocene-Oligocene transition in the Vistrenque Basin (Camargue, Southeast France)

Nazim Semmani[1,*], François Fournier[1], Philippe Léonide[1], Jean-Pierre Suc[2], Lionel Marié[1], Jean Borgomano[1]

[1]: Aix Marseille Université, CNRS, IRD, Cerege, Um 34, 3 Place Victor Hugo (Case 67), 13331, Marseille Cedex 03, France.

[2]: Sorbonne Université, CNRS-INSU, Institut des Sciences de la Terre Paris, ISTeP, UMR 7193, 75005 Paris, France

[*]Corresponding author: nazim.semmani@gmail.com

Abstract

Based on detailed sedimentological analysis of core data and measurements of carbon and oxygen isotope composition of lacustrine carbonates, the palaeoenvironmental evolution and the sedimentary architecture of the Paleogene continental Vistrenque Basin (SE France) have been reconstructed.

The analysis of sedimentary archives revealed three main stages of basin infill evolution: 1) a transgressive deep-lake basin (Priabonian-earliest Rupelian) whose sedimentation was dominated by terrigenous gravity-driven deposits during a period of high subsidence rate and fault activity and under a prevailing humid climate; 2) a forced-regressive, evaporative deep lake (early Rupelian) characterized by a drastic reduction in terrigenous supplies and deposition of evaporites in disconnected compartmentalized sub-basins; 3) an overall long-term normal regressive stage (middle Rupelian to earliest Chattian) of lake infill characterized by an increase in terrigenous supplies and a vertical upward transition from deep-lake gravity-driven deposits to marginal lake and floodplain sedimentation, interpreted as resulting from both a climate humidification and a decrease in subsidence rates and fault activity. The onset of lake volume reduction and forced regression during the early Rupelian is recorded by 1) the reworking of marginal lake carbonates into the deep lake areas, 2) the deposition of organic-rich sediments (TOC>10%) associated with sulphate-reduction processes in the deepest areas of the lake, 3) an important decrease in terrigenous supplies coupled with a long-term increase in $\delta^{18}O$ of matrix-supported carbonates.

This early Rupelian forced regression of the Vistrenque lacustrine system is interpreted to result from terrestrial aridification in response to global cooling during the Eocene-Oligocene Transition (EOT). Following this Early Rupelian stage of aridification and climate cooling, the final infill of the Vistrenque lake system and the installation of a floodplain occurred in more humid conditions during a stage of decreased activity of the Nîmes fault, prior to the further extensional phase related to the Chattian to Aquitanian Gulf of Lion rifting.

Keywords: Paleogene, continental basin, gravity-driven sedimentation, carbonate, lacustrine evaporites, floodplain, Eocene-Oligocene transition, palaeoclimate

5.1. Introduction

Continental sediments revealed to be very sensitive to climate changes because they result from physical or biological processes occurring in nearby areas or in direct contact with atmosphere (e.g., Fabre and Mainguet, 1991; Nutz et al., 2019). Among continental depositional systems, lakes have been shown to constitute comprehensive and reliable archives of the evolution of environmental parameters at various time scales due to fluctuations in their level which respond to climate and hydrologic changes and to the ability of biologically or chemically-produced carbonates to record palaeotemperature, pCO2, salinity and hydrologic balances (e.g., Talbot, 1990; Tanner, 2010; Lettéron et al., 2017). Additionally, continental sedimentation is also extremely sensitive to tectonic setting (e.g., Ashley and Renaut, 2002) since the latter controls the formation and location of reliefs and terrigenous sediment sources as well as those of subsident areas where sediments are deposited and preserved.

The time interval ranging from the Priabonian (Late Eocene) to the Rupelian (Early Oligocene) is marked at a global scale by the most important climate change of the Cenozoic resulting in the establishment of Antarctic ice sheets (Liu et al. 2009) and records the transition from greenhouse to icehouse conditions (Wade et al. 2012). In terrestrial mid-to-high latitude environments, long-term cooling during the Eocene-Oligocene transition (EOT) resulted in major changes in floristic and faunistic associations, and regional hydrological cycles (Hutchison et al. 2021), and promoted climate aridity (Yancey et al. 2003; Page et al., 2019) and seasonality (Eldrett et al. 2009). Moreover, this period is characterized in Western Europe by a major transition in tectonic regime from compressional (Pyrenean compression) to extensional (West-European and Liguro-Provençal extension) (Séranne et al., 2021) which occurred coevally with the development of the marine Western Alpes foreland basin to the east (Joseph and Lomas, 2004).

Late Eocene and Oligocene continental sedimentary basins have been extensively documented in the literature in Western Europe, onshore (e.g., Upper Rhine Graben: Blanc-Valleron and Schuler, 1997; Bresse Graben: Curial and Moretto, 1997; Valence Basin: Dromart and Dumas, 1997; Apt-Manosque-Forcalquier Basin: Lesueur, 1991; Alès-Saint-Chaptes-Issirac basins (ASCI system): Lettéron et al., 2017, 2018, 2021; Camargue Basin: Benedicto et al., 1996) and offshore in the Gulf of Lion (Central Graben, Grand Faraman Basin: Séranne et al., 1995) (see location in **Fig. 5.1**). These basins are characterized by thick siliciclastic, carbonate and evaporite sedimentation (e.g., Benedicto,1996; Rouchy, 1997).

The Vistrenque Basin is located in the western part of the Camargue area. It is the deepest Cenozoic continental basin in Southeast France with more than 3200 m thick Paleogene succession. This basin is bounded to the west by the Nîmes fault which acted as a sinistral strike-slip fault as early as the Priabonian in Languedoc (Séranne et al., 2021). This major fault may also have triggered the formation of the Vistrenque Basin during the Priabonian and Early Oligocene, a few million years before the Gulf of Lion extension. The Paleogene sedimentary

infill of the Vistrenque Basin has been subdivided into three main units: the lowermost terrigenous-rich lacustrine 'Série Grise' unit is more than 2000 m thick; an intermediate siliciclastic-rich fluvial 'Série Rouge' unit, around 200 m thick; and an evaporite-rich 'Série Calcaréo-salifère' unit, of few hundreds of metres thick, at the top (**Fig. 5.3C**). Since the Série Calcaréo-Salifère unit has been shown to be linked to the Upper Oligocene to Aquitanian rifting (Benedicto et al., 1996; Semmani et al., *under review, see Chapter 4 in this PhD manuscript*), this study focuses only on the ante-saliferous units, namely the Série Rouge and underlying units.

The density of subsurface data (cores, cuttings, well logs) from the Gallician and Pierrefeu-Parrapon sectors (see location in **Fig. 5.2A** and **5.3A**) makes it possible to investigate the sedimentary record of tectonic evolution from the Pyrenean compression and Western European extension to the Gulf of Lion margin rifting, and dramatic global climate change at the Eocene-Oligocene transition in the continental Vistrenque Basin. The present study aims to: 1) define the depositional facies and reconstruct the depositional palaeoenvironments, 2) reconstruct the evolution of depositional systems and patterns of the Paleogene sedimentary infill of the Vistrenque Basin, 3) link the evolution of these depositional systems to changes in climate and tectonic regimes in Southeast France during the Priabonian-Rupelian times, and 4) discuss the relevance of continental sedimentary record as an archive of past climate changes in Southwestern Europe during around the Eocene-Oligocene transition.

5.2. Geological setting

5.2.1. Regional tectonic setting

The Camargue area is located in Southeast France near the Rhône delta between the limestone plateaus of the 'Garrigues Nîmoises' and the Mediterranean (**Fig. 5.1A**). This area has an approximately triangular form and is constituted of two Cenozoic sedimentary basins entirely buried beneath the Rhône delta sediments: the Vistrenque Basin to the west and the Vaccarès Basin to the east. The Paleogene Vistrenque Basin (50*30 km²) is controlled by the major Nîmes fault and belongs to the numerous continental basins opened during the late Eocene and Oligocene in Southeast of France (Cavalier et al. 1984, Semmani et al., *under review, see Chapter 4 in this PhD manuscript*). These basins result from the Priabonian-Rupelian Western European Rift extension (ECRIS, Ziegler, 1992) and Oligo-Aquitanian Gulf of Lion margin rifting (Benedicto et al., 1996) in Languedoc, Provence, Rhône Valley and Gulf of Lion areas (**Fig. 5.1B**). In Languedoc, the Nîmes fault has been shown to accommodate sinistral strike-slip movements as early as the Priabonian in response to both the Pyrenean shortening and Western European Rift extension (Séranne et al., 2021). As a result of the convergence and collision of the Iberia-Corsica-Sardinia block with the European plate, the Mesozoic to Eocene cover has been folded and thrusted during the Pyrenean shortening in

Languedoc and Provence (e.g., Mascle et al., 1994; Arthaud and Laurent, 1995; Séranne et al., 1995; Bestani et al., 2015).

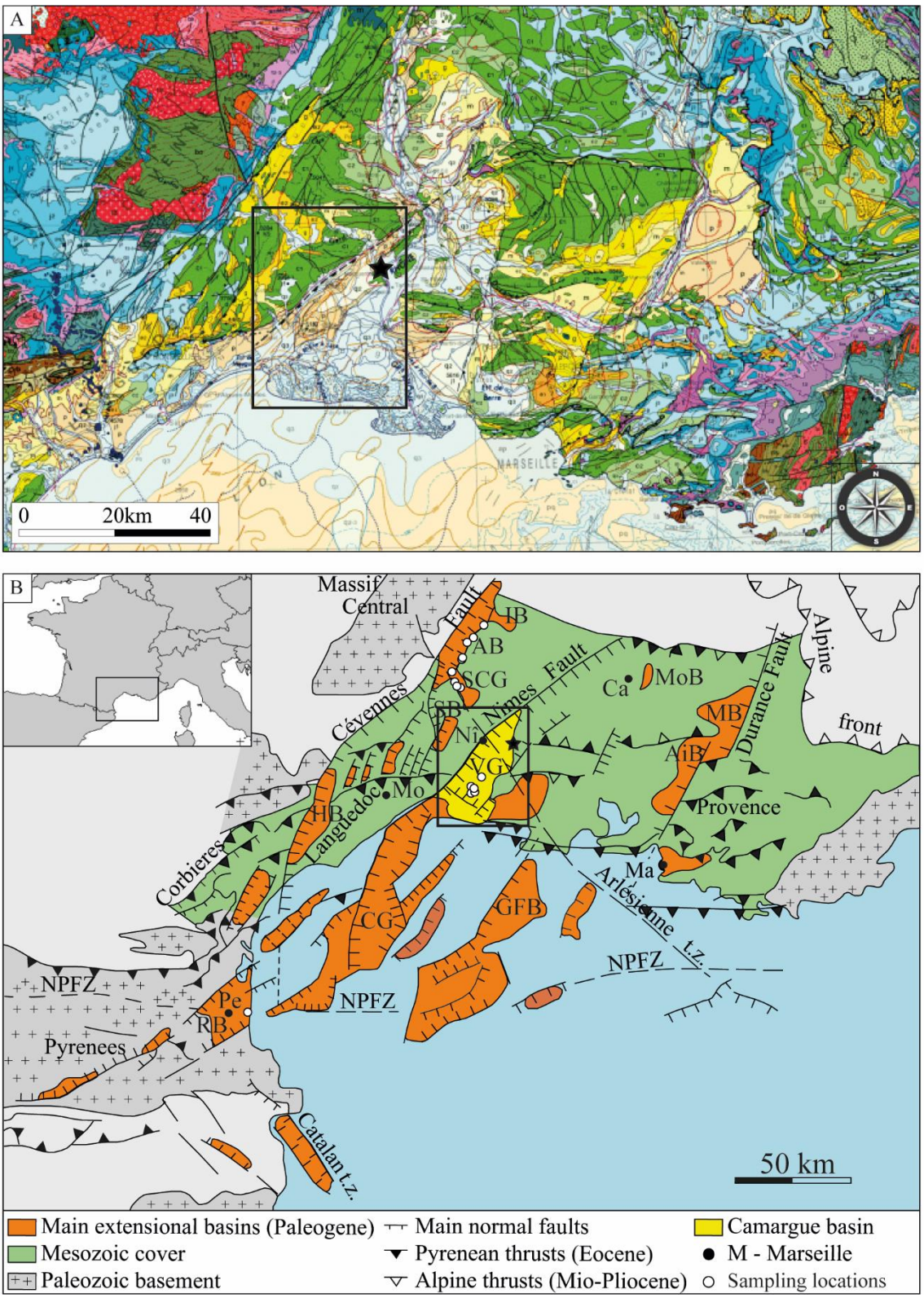

Figure 5.1: A) Geological map of the Southeast France showing the Vistrenque Basin indicated by the rectangular box. The NE-SW trending Nîmes Fault separates the Mesozoic substratum of the 'Garrigues nîmoises' from the Cenozoic basins currently almost buried beneath the Rhône Delta sediments (modified after BRGM

geological map: 1-1.000.000). The black star indicates the position of the Priabonian northern carbonate succession at Butte Iouton (e.g., Pellat and Allard, 1895; Semmani et al., 2022, *see chapter 3 in this PhD manuscript*); B) Structural map of the Southeast France and location of the Vistrenque Basin among the various Cenozoic continental basins, modified after Benedicto (1996). AB: Alès Basin, AiB: Aix Basin, Ca: Carpentras, CG: Central Graben, GFB: Grand Faraman Basin, HB: Hérault Basin, IB: Issirac Basin, Ma: Marseille, Mo: Montpellier, MB: Manosque Basin, MoB: Mormoiron Basin, Nî: Nîmes, NPFZ: North Pyrenean Fault Zone, Pe: Perpignan, RB: Roussillon Basin, SB: Sommières Basin, SCG: Saint-Chaptes Graben, t.z.: transfer fault zone, VG: Vistrenque Graben.

The Mesozoic basement is constituted mainly of Jurassic and Cretaceous marine carbonates and is exposed in the 'Garrigues Nîmoises'. These carbonates also constitute the buried structural highs that bound the Paleogene Vistrenque Basin to the east (Albaron high; Jurassic), to the north (Jonquières high; Lower Cretaceous), and to the south (Grau-du-Roi and Saintes-Maries highs; Jurassic) (**Fig. 5.2C**). The Palaeozoic basement is known from the Massif Central, and Provençal Maure and Esterel massifs. Offshore in the present Gulf of Lion, the Palaeozoic basement was intersected by Paleogene extensional basins (e.g., Grand Faraman Basin, Central Graben) formed during the Oligo-Aquitanian extension (Séranne et al., 1995). Séranne et al. (2021) have reconstructed a Pyrenean relief, south of Camargue and Languedoc that links the French-Spanish Pyrenees to the Provence segment of the Pyrenean orogen and dated the onset of its dismantling to the Priabonian (late Eocene).

5.2.2. Stratigraphic framework of the Vistrenque Basin

Except for the Priabonian carbonate succession exposed at the Butte Iouton hill in its Northern margin (Pellat and Allard, 1895, Semmani et al., 2022, *see chapter 3 in this PhD manuscript*), the Paleogene sedimentary succession of the Vistrenque Basin is almost entirely buried beneath the Miocene marine deposits and Plio-Quaternary sediments of the Rhône delta. Within the Vistrenque Basin, the Paleogene stratigraphic column changes laterally in both lithologies and thickness between the Gallician and Pierrefeu sectors since the basin is affected by transfer faults resulting in the compartmentalization of the basin (**Fig. 5.2A**). In the Pierrefeu sector, the Paleogene succession (~3200 m thick) has been subdivided into three main lithological units, from bottom to top: 'Série Grise', 'Série Rouge', and 'Série Calcaréo-salifère' formations (Valette and Benedicto, 1995) (**Fig. 5.3B-C**).

Very recently, Semmani et al. (*under review, see Chapter 4 in this PhD manuscript*) proposed a revised chronological framework of the Paleogene of the Vistrenque Basin. In the Gallician sector (**Fig. 5.3D**), the lowermost lacustrine-dominated 'Série Grise' and 'Série Calcaire' formations are Priabonian (?) to Middle Rupelian in age. The overlying fluvio-lacustrine 'Série Mixte' and 'Série Rouge' formations are middle Rupelian to earliest Chattian in age. A return to lacustrine conditions occurred with the deposition of a thick carbonate and evaporite succession ('Série Calcaréo-Salifère' formation) (e.g., Valette and Benedicto, 1995) and attributed to ages from upper Oligocene to Aquitanian by Semmani et al. (*under review, see Chapter 4 in this PhD manuscript*).

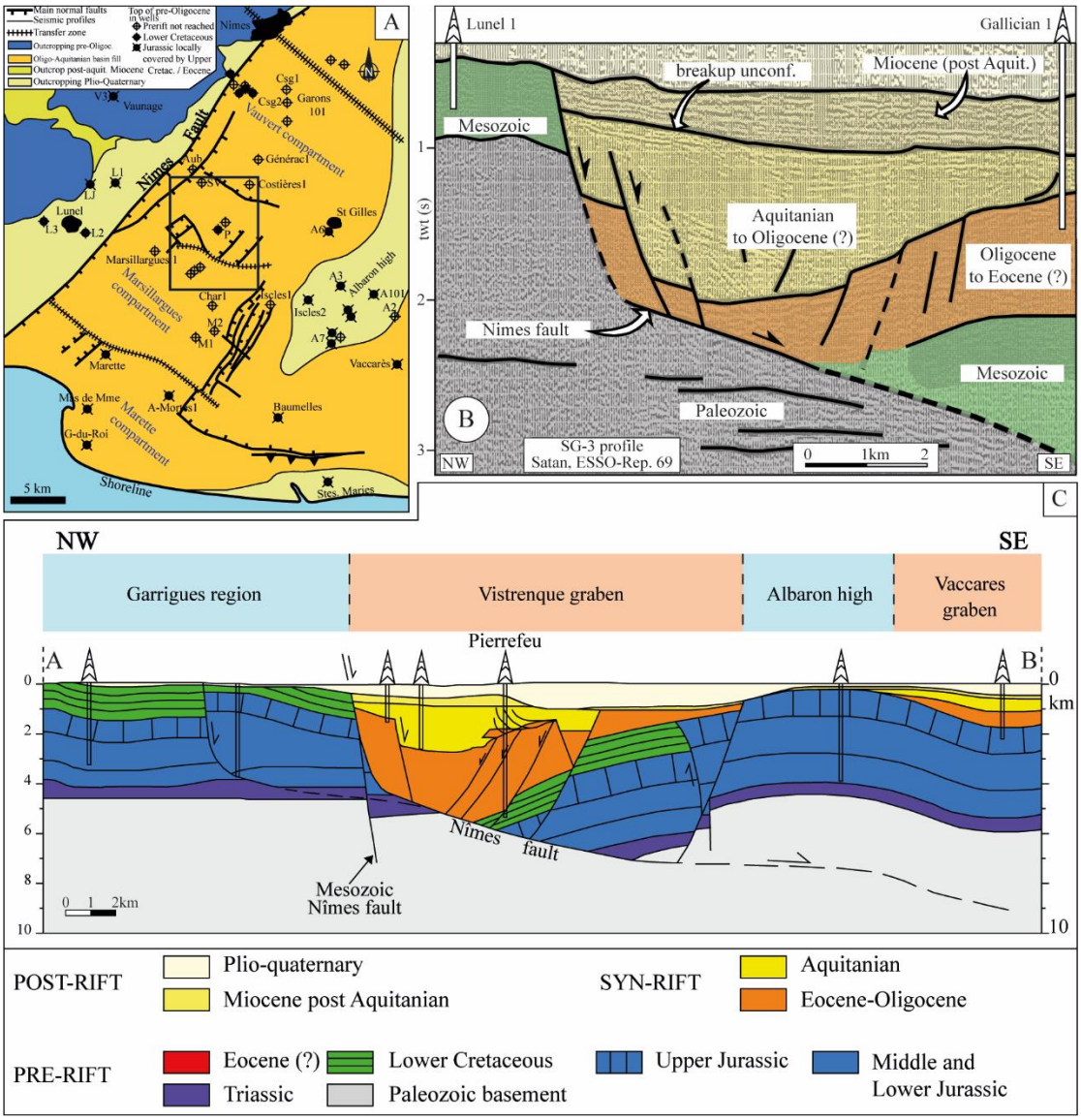

Figure 5.2: A) Structural map of the Vistrenque Basin showing location of deep boreholes, modified after Benedicto et al. (1996). V3: Vaunage 3 - LJ: La Jasette - L1: Lunel 1 - L2: Lunel 2 - L3: Lunel 3 - Csg: Caissargues Aub: Aubord 1 - SV: Saint-Véran 1 - P: Pierrefeu 1 - A6: Albaron 6 - A3: Albaron 3 - A7: Albaron 7 - A101: Albaron 101 - A2: Albaron 2 - Char 1: Charnier 1 – M1: Montcalm 1 – M2: Montcalm 2 – P: Pierrefeu – Stes Maries: Saintes-Maries-de-la-Mer 101. t.z.: transfer zone. The rectangle shows the studied area (Pierrefeu-Parrapon and Gallician sectors) shown in the geographical map of Fig. 5.3A. B) Non-migrated seismic profile SG3 interpreted, after Benedicto (1996), see location in map in Figure 5.3A; (C) NW-SE Cross-section through the Vistrenque Basin on the northern Vauvert compartment (modified after Benedicto et al., 1996).

Seismic data interpreted by Valette (1991) suggest that the Série Calcaréo-Salifère formation unconformably overlies the Série rouge and underlying units. Chronostratigraphic data (Semmani et al., *under review, see Chapter 4 in this PhD manuscript*) revealed that such unconformity can be dated to the early Chattian. Syn-rift sedimentation lasted until the late Aquitanian and the break-up event that separates syn-rift from post-rift deposits was dated to the Burdigalian and corresponds to the spreading of the Liguria-Provençal Basin (Gorini et al., 1993). The post-Aquitanian Miocene and Plio-Quaternary correspond to the post-rift stage of the Gulf of Lion margin (**Fig. 5.2B-C**; Séranne et al., 1995).

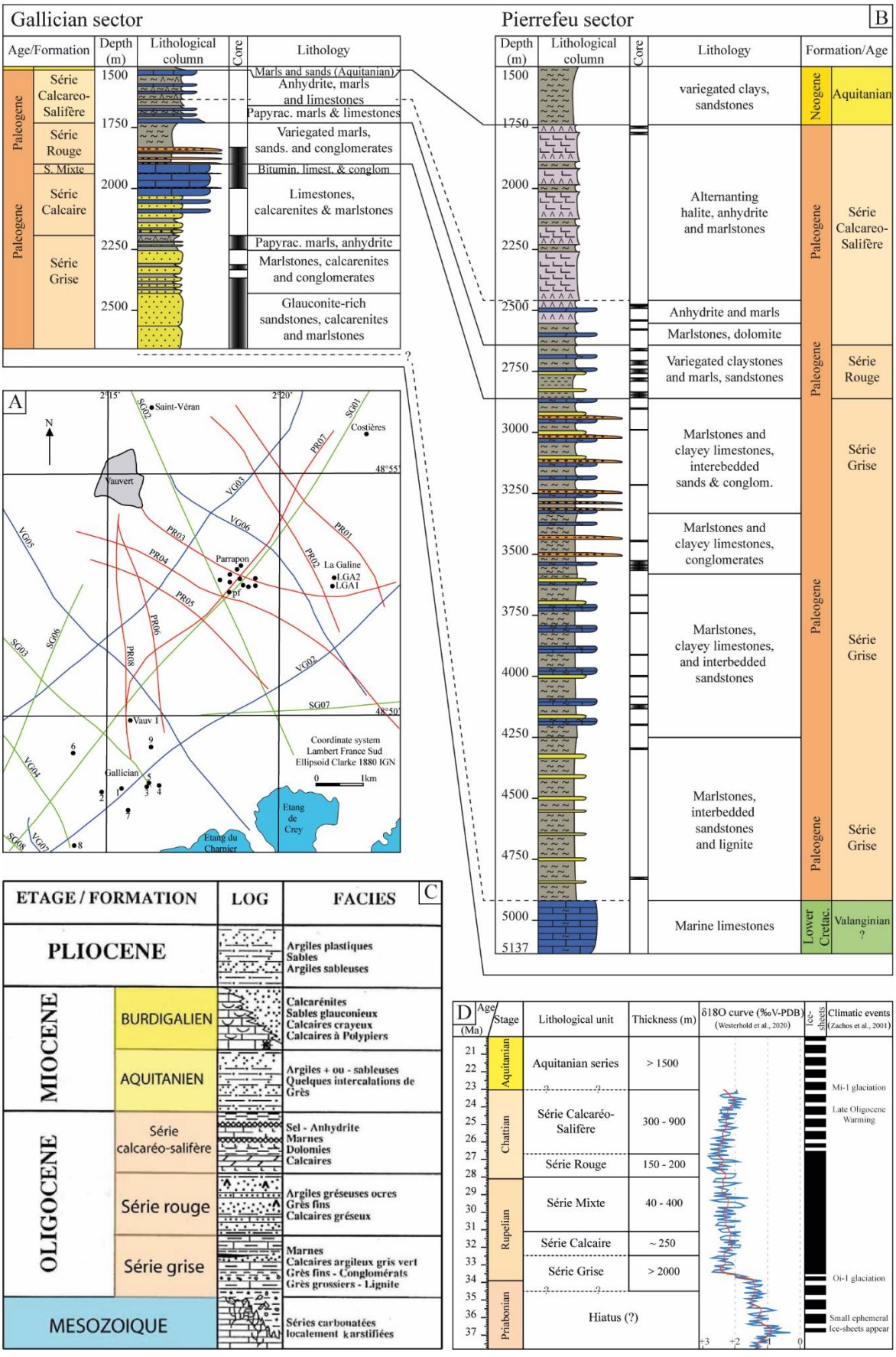

Figure 5.3: (A) Geographical map of the Gallician and Pierrefeu areas (enlargement of the quadrangle shown in Fig. 5.2A) showing the location of subsurface database (wells and seismic lines) pf=Pierrefeu 1 well,

LGA=LaGaline, numbers refer to the Gallician wells, modified after Valette (1991). B) lithological columns and correlations of Gallician 9 and Pierrefeu 1 wells located in the Gallician and Pierrefeu sectors respectively. C) Stratigraphic synthesis of the Vistrenque Basin compiled from borehole data by Gorini (1993), modified after Bache (2008). D) Chronostratigraphic framework of the Paleogene succession of the Vistrenque Basin. Reference oxygen isotope curve (smoothed curve over 20 ka in blue, smoothed curve over 1 Ma in red; Westerhold et al., 2020). Climatic events and Antarctic ice-sheets coverage history are derived from Zachos et al. (2001), from Semmani et al. (*under review*, *see Chapter 4 in this PhD manuscript*).

5.3. Database and methods

5.3.1. Database

Borehole data were acquired by oil companies (SNPLM, CEP: current TotalEnergies) as part of the petroleum exploration in the Gallician sector in the 1950's and later during a development drilling survey with the Pierrefeu 1 well drilled in 1963. Since the 1970's, salt mining using halite leaching led to the drilling of more than 20 well doublets in the Pierrefeu-Parrapon sector in order to extract brine from the thick evaporite accumulation of the Série Calcaréo-Salifère formation. However, these wells are not considered in this work since the studied intervals (Série Rouge formation and underlying units) have not been reached.

This study is based on data from 6 wells (cores and drilling cuttings, well logs, geological reports) from the Gallician and Pierrefeu-Parrapon sectors: Gallician 1, Gallician 3, Gallician 7, Gallician 9, Vauvert 1, and Pierrefeu 1 (see location in **Figure 5.3A**). All these wells have reached the Série Rouge formation and investigated variably the underlying units. The maximum depth, the deepest explored stratigraphic levels, and the available well log data and geological reports are summarized in **Table 5.1**.

Table 5.1: List of the wells studied in this work and the dataset used. Core intervals are indicated for the Paleogene series, Fm: formation (see location in Fig. 5.3A).

Well	Location	Year of completion	Depth (reached formation)	Dataset (well logs, documents)	Cores and cuttings data
Gallician 1	Vauvert (Gard)	1951	2004 m (Série Rouge Fm)	Electrical logs, Gamma Ray (GR), geological reports, master-log	Cores: 1612 - 1929 m
Gallician 3	Vauvert (Gard)	1951	1871 m (Série Mixte Fm)	Electrical logs, Gamma Ray (GR), geological reports, master-log	Cores: 1720 - 1871 m
Gallician 7	Vauvert (Gard)	1952	2087 m (Série Mixte Fm)	Electrical logs, Gamma Ray (GR), geological reports, master-log	Cores: 2007 - 2087 m
Vauvert 1	Vauvert (Gard)	1952	3626 m (Série Grise Fm)	Electrical logs, Gamma Ray (GR), geological reports, master-log	Cores, essentially: 1897 - 2014 and 2902-3067 m
Gallician 9	Vauvert (Gard)	1956	2653 m (Série Grise Fm)	Electrical logs, Gamma Ray (GR), geological reports, master-log	Cores: 1830 - 1997 / 2190 - 2247 / 2365- 2653 Cuttings: 2000-2190 m
Pierrefeu 1	Vauvert (Gard)	1963	5137 m (Lower Cretaceous) Base of Paleogene: 4920m	Electrical logs, Gamma Ray (GR), geological reports, master-log	Discontinuous cores between 1740 and 4830 m

Many wells are not analysed in this study (e.g., Gallician 2, 4, 5, 6, and 8) due to a lack of core data. However, the studied wells, listed in **Table 5.1** are a representative selection of the sedimentary record of the Paleogene of the Vistrenque Basin. **Figure 5.4** provides a correlation panel of the Paleogene sections from these wells.

5.3.2. Depositional facies and palaeoenvironmental interpretations

The definition of the depositional facies is based on the description of the sedimentological features observed both macroscopically on cores and microscopically on thin sections (>3000 thin sections were examined). The thin sections were made by the geological departments of the oil companies during the 1950's and 1960's. The thin sections dataset was prepared with a close vertical spacing (ranging from 5 cm to 1 m).

Microscopic analyses on thin sections were carried out essentially qualitatively to identify the depositional facies (**Table 5.2**). Qualitative description includes measurement of average grain size, estimation of grain sorting and morphoscopic features, and proportion of fines (carbonate mud and silt matrices). Other features examined to define the depositional facies are biological content, sedimentary structures, stratal patterns, and vertical stacking patterns. Depositional palaeoenvironments are inferred from the depositional facies grouped within facies associations (FA, **Table 5.3**) and from the vertical evolution of facies.

5.3.3. Stable carbon and oxygen isotope analyses of carbonates

Carbon and oxygen stable isotopic compositions of bulk-rock carbonates have been measured on 117 samples from Gallician 9 well, 89 samples from Pierrefeu 1 well and 35 samples from Vauvert 1 well in order to provide insights into lake palaeohydrology. Measurements have been performed on matrix-supported fabrics (calcareous claystones, marlstones, argillaceous limestones and limestones of mudstone-wackestone textures) from the "Série Grise", "Série Calcaire" and "Série Mixte" formations. Carbon and oxygen isotopes signatures of carbonates from the Série Mixte and Série Rouge units are altered by the intense pedogenic modifications that these limestones underwent and are therefore not considered. The isotope analyses were performed at the Laboratory of Analytic Geochemistry of the Faculty of Earth Sciences at Friedrich-Alexander-University of Erlangen-Nürnberg, Germany. Carbonate powders were reacted with 100% phosphoric acid at 70°C using a Gasbench II connected to a ThermoFisher DELTA V Plus mass spectrometer. All values are reported in per mil relative to V-PDB. Reproducibility for $\delta^{13}C$ and $\delta^{18}O$ was ±0.07‰ and ±0.05‰ (1 standard deviation), respectively. Carbon and oxygen stable isotope measurements have been reported in **§ 5.8. Supplementary data** – **Table S5.1**.

5.3.4. Organic matter and $CaCO_3$ concentrations

The present work integrates unpublished measurements of total organic matter content (TOC) and calcimetric analyses from oil companies inhouse reports. The TOC measurements have been performed in 1992 at the IFP (French Institute of Petroleum) by using a Rock Eval apparatus and following the methodology established by Espitalié et al. (1985). The data are displayed in **§ 5.8. Supplementary data** – **Table S5.2**.

SSW-NNE Correlation panel of the studied wells from the Gallician and Pierrefeu sectors

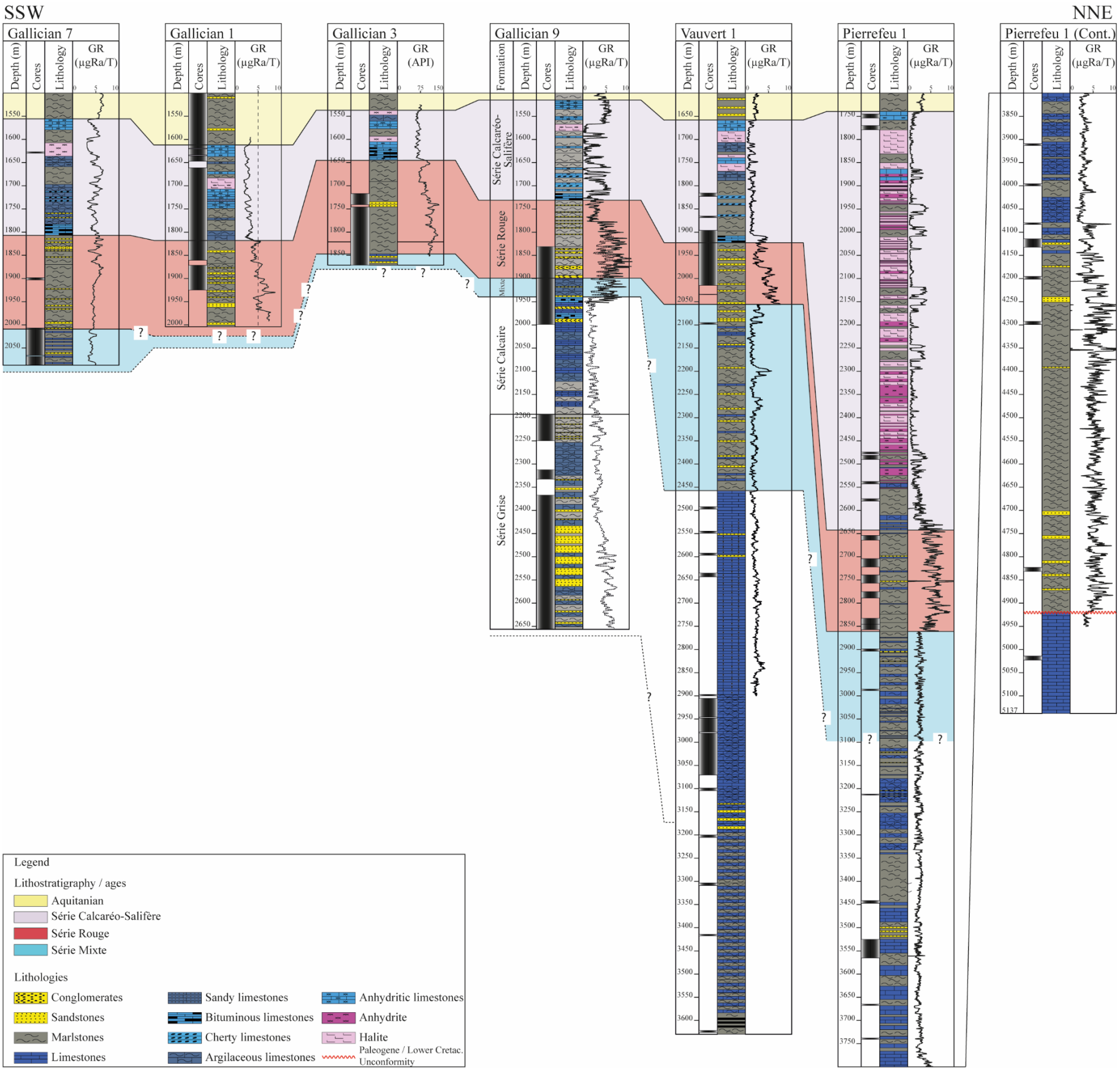

Figure 5.4: Correlation panel of wells Gallician 7, Gallician 1, Gallician 3, Gallician 9, Vauvert 1 and Pierrefeu 1 from the Gallician and Pierrefeu-Parrapon sectors showing the sedimentary units, litholologies and lithostratigraphic correlations. Lithostratigraphic correlations are carried out using lithological similarities and gamma ray (GR) signal. µgRa/T: microgram of Radium / Time (radioactivity measurement).

5.3.5. Sequence stratigraphy analysis and well correlations

Sequential analysis was carried out at the metric to decametric scale in the cored intervals. High-resolution depositional cycles are defined using vertical evolution of facies associations. Since the studied formations are very thick and fine-scale correlations between the wells are difficult to make, only the major sedimentary cycles recorded during the Paleogene in the Vistrenque Basin will be described.

Well correlations are based on lithological criteria and well log data (Gamma Ray), the recognition of transgressive-regressive cycles and the identification of the major uncoformities from the vertical stacking pattern, and the vertical evolution of carbon and oxygen isotope composition of lacustrine carbonates and the corresponding long-term trends of inflow-evaporation balance. Sequence boundaries have been defined as major, correlatable subaerial exposure surfaces or may correspond to conformable surface of maximum regression of the lake (basinal correlative conformity).

5.4. Results and interpretations

5.4.1. Depositional facies and palaeoenvironmental interpretations

In the studied wells, the investigated Paleogene intervals display a great diversity of depositional facies including strictly terrigenous, carbonate and evaporite-rich deposits as well as mixed terrigenous-carbonate deposits. The carbonates have been described using the Dunham classification system (Dunham, 1962) modified by Embry and Klovan (1971) and the terrigenous deposits have been classified using the granulometric classification of Wentworth (1922). Thirteen depositional facies (F1 to F13) have been described, their main characteristic features and palaeoenvironmental interpretations are summarized in **Table 5.2**. Due to the difficulty to capture large-scale sedimentary geometries in drill cores, interpretations of detrital carbonates and siliciclastics in terms of depositional environments are based on the vertical and distribution of facies (F1 to F13) and on their facies associations (FA1 to FA6, **Table 5.3**). Fluvial systems are often divided from upstream to downstream into braided, meandering, and anastomosed parts to which are added the distal areas (e.g., deltas) at the riverine mouth in the ocean or lake margin. Miall (1985) stated that the recognition of the fluvial configurations is often not straightforward, and the identification of fluvial depositional systems requires the use of *architectural elements analyses* observable in general at large-scale outcrops.

Hemipelagic lacustrine marls and evaporite facies: F1, F2 and F3

F1. Anhydritic marlstones and anhydrite:

Anhydritic marlstones and banded anhydrite are uncommon facies within the studied intervals since these are reported only from the upper part of the Série grise formation. Anhydritic marlstones consist of dark-grey marls encasing sparse nodules of anhydrite (up to 2 cm in size, **Fig. 5.5A**) while banded anhydrite consists of centimetre-thick layers of nodular

anhydrite, alternating with thin, millimetre-thick, micrite laminae (**Fig. 5.5B**). Anhydrite has also been observed infilling fractures. The anhydritic marlstones are organized in two pluri-metre thick intervals of finely laminated platelet marls intercalated with fine silty sandstones and organic-rich layers. The banded anhydrite interval (~ 1 m thick) is bracketed between those two anhydritic marlstones intervals. In thin section, anhydrite nodules display a microcrystalline structure made of little needle crystals (**Fig. 5.5C**). A few relicts of small prismatic to lenticular crystals have been evidenced within anhydrite nodules (**Fig. 5.5D**) thus suggesting a gypsum precursor.

Interpretation: The nodular habit of the anhydrite is a common diagenetic fabric which does not necessarily indicate subaerial sabkha environments (Dean et al., 1975). The occurrence of relicts of pseudomorphs after gypsum crystals suggests that laminated anhydrite derives from the diagenetic transformations (under burial conditions?) of laminated gypsum deposits. The original alternation of gypsum and organic-rich carbonate layers reflects fluctuations between more and less arid conditions leading to precipitation of these minerals on a shallow perennial lake floor while the nodular texture results from subsequent diagenetic transformation of gypsum into anhydrite (Orti and Salvany, 2004). Large and scattered prismatic anhydrite crystals embedded in a marlstone background are likely to form and grow within the mud matrix during early diagenesis.

F2. Finely laminated argillaceous limestones and papyraceous marlstones (laminites):

This facies consists of alternations of light beige and dark grey, greenish grey and brown finely laminated argillaceous limestones to papyraceous marlstones. Laminae are often millimetric to submillimetric in thickness, plane-parallel to wavy and may also be crumpled (**Fig. 5.5E-G**). The dark layers are enriched in organic matter and in detrital particles of mud to silt size. In contrast, light laminae are dominated by micrite, with low detrital and organic matter content. Preserved fossils are lacking in these facies although the papyraceous marlstones may contain high amounts of terrestrial plant debris intercalated between the laminae. These laminites are organized into thick intervals with a thickness ranging from several decimetres to few metres. This facies is particularly frequent in the upper part of the *Série Calcaire* and less frequent in the top of the *Série Grise* formation while the lowermost intervals of the *Série Grise* do not contain this facies.

Interpretation: The fine grain-size in the laminates indicates deposition in areas located far from the clastic sources. The lack of fauna suggests anoxic conditions, and the preservation of the original laminae indicates that they have not been affected by bioturbation. The preservation of organic matter also suggests stratified water preventing oxygenation of the lake bottom. Finally, the absence of subaerial exposure features (e.g., root traces) in these marlstones indicates deposition in deep and perennial lake conditions.

Table 5.2: Depositional facies classification of the Paleogene sedimentary succession of the Série Rouge and underlying units in the Vistrenque Basin: biological contents, sedimentary and diagenetic features, and their palaeoenvironmental interpretations (Fm: Formation)

Code	Facies	Biological content	Sedimentary structures	Stratal pattern	Diagenetic features	Occurrence	Palaeoenvironmental interpretation
F1	Anhydritic marlstones and anhydrite	---	Nodular and banded structure	Metre anhydrite banded interval enclosed between anhydrite marlstones	Replacement of gypsum by anhydrite	Uncommon, reported only from one thick interval from Série Grise formation (Fm)	Evaporitic perennial lake
F2	Finely laminated limestones and papyraceous marlstones	Terrestrial plant remains	Millimetre laminations Wavy to plane-parallel	Several decimetres to metre thick intervals	---	Frequent in the Série Calcaire & occasional in the Série Grise	Profundal perennial lake with anoxic condition
F3	Dark grey marlstones with scarce fauna	Terrestrial plant remains, few ostracod shells	Structureless	Massive and structureless interval. Frequent alternations with the F4 sandstones	Occasional pyrite precipitation	Common in the Série Grise and in the Série Calcaire formations	Profundal perennial lake with poorly oxygenated conditions
F4	Glauconite-rich sandstones and fine calcarenites	Azoic. Terrestrial plant remains	Plane parallel laminations and current ripples. Load casts and flame structures	Centimetre to few cm layers in alternation with marlstones/siltstones	---	Common in the Série Grise Fm	Gravity-driven currents in the offshore lake
F5	Coarse calcarenites and microconglomerates	Azoic. Terrestrial plant remains	Vertical normal grading, parallel laminations	Centimetre to decimetre beds overlying F3 marlstones and overlain by F4 sandstones	---	Frequent in the upper part of the Série Grise formation	Gravity-driven currents in the offshore lake
F6	Matrix-supported conglomerates	Mostly azoic. Occasional characean grains in the matrix	---	Decimetre beds intercalated with F3, F4 and F5 facies	---	Occasional to frequent in the Série Grise formation	Gravity-driven currents in the offshore lake
F7	Bedded quartzose calcarenites	Azoic. Few terrestrial plant remains	---	Decimetre tabular beds to metre beds. May alternate with F2 marlstones and display subaerial exposure features	Pedogenic modifications at the top of the beds including dessication cracks	Frequent in the upper part of the Série Calcaire Fm but also at the base of the S. mixte Fm	Vicinity of a riverine mouth (lacustrine delta) with local detrital fluxes
F8	Oncolitic limestones	---	---	Decimetre to metre beds with subaerially exposed tops	Pedogenic modifications at the top of the beds including dessication cracks	Occasional in the Serie Mixte formation	Shallow lake littoral and riverine mouth in the lake

Table 5.2 (continued): Depositional facies classification of the Paleogene sedimentary succession of the Série Rouge and underlying units in the Vistrenque Basin: biological contents, sedimentary and diagenetic features, and their palaeoenvironmental interpretations (Fm: Formation)

Code	Facies	Biological content	Sedimentary structures	Stratal pattern	Diagenetic features	Occurrence	Palaeoenvironmental interpretation
F9	Microbial limestones	microbial crusts (?)	---	Metre thick beds in alternation with palustrine carbonates (F13)	Occasional incipient pedogenic modifications (cracking)	Frequent in the Série Mixte & Série Calcaire formations	Littoral lake in the vicinity of streams and springs
F10	Polymictic Conglomerates and microconglomerates	Azoic	Erosive base (?), grading into F11 and F12 facies. Preferential clast imbrication	Inframetric to metre beds alternating with sandstones and marlstones (F11/F12)	Occasional pendular cements and micrite coating around clasts	Frequent in the Série Rouge and less frequent the Série Mixte formation	Bed load fill of channels
F11	Fine to medium sandstones (Quartzose sandstones)	Azoic.	Vertical normal grading, Current ripples (?)	Decimetre to metre beds in alternation with F10 and F11 facies	---	Common in the Série Rouge and occasional in the Série Mixte formations	Slowdown of fluvial stream deposits, overbank deposits
F12	Variegated and mottled calcareous claystones	Azoic	---	Metre to several metres intervals alternating with F10, F11 and F13 facies	Mainly pedogenesis: root traces, marmorization vermicular mottling & vivid red coloration, peds	Common in the Série Rouge and Série Mixte formations Occasional in the Série Calcaire formation	Floodplain deposits
F13	Brecciated limestones (pedogenically modified carbonates)	Undetermined numerous molluscs, ostracods	---	Decimetre to few decimetres beds. Often, pedogenesis modify the top of F7/F8/F9 and F12 facies beds	Pedogenesis: perigranular cracks, root traces, pseudo-microkarst, vadose pisoids may also be found. Geopetal silt and blocky calcite in cavities	Frequent in the Serie Mixte and occasional in the Série Rouge (lowermost parts) and Série Calcaire formation	Very shallow pond/lake or abandoned channel subjected to exposure and vegetation development

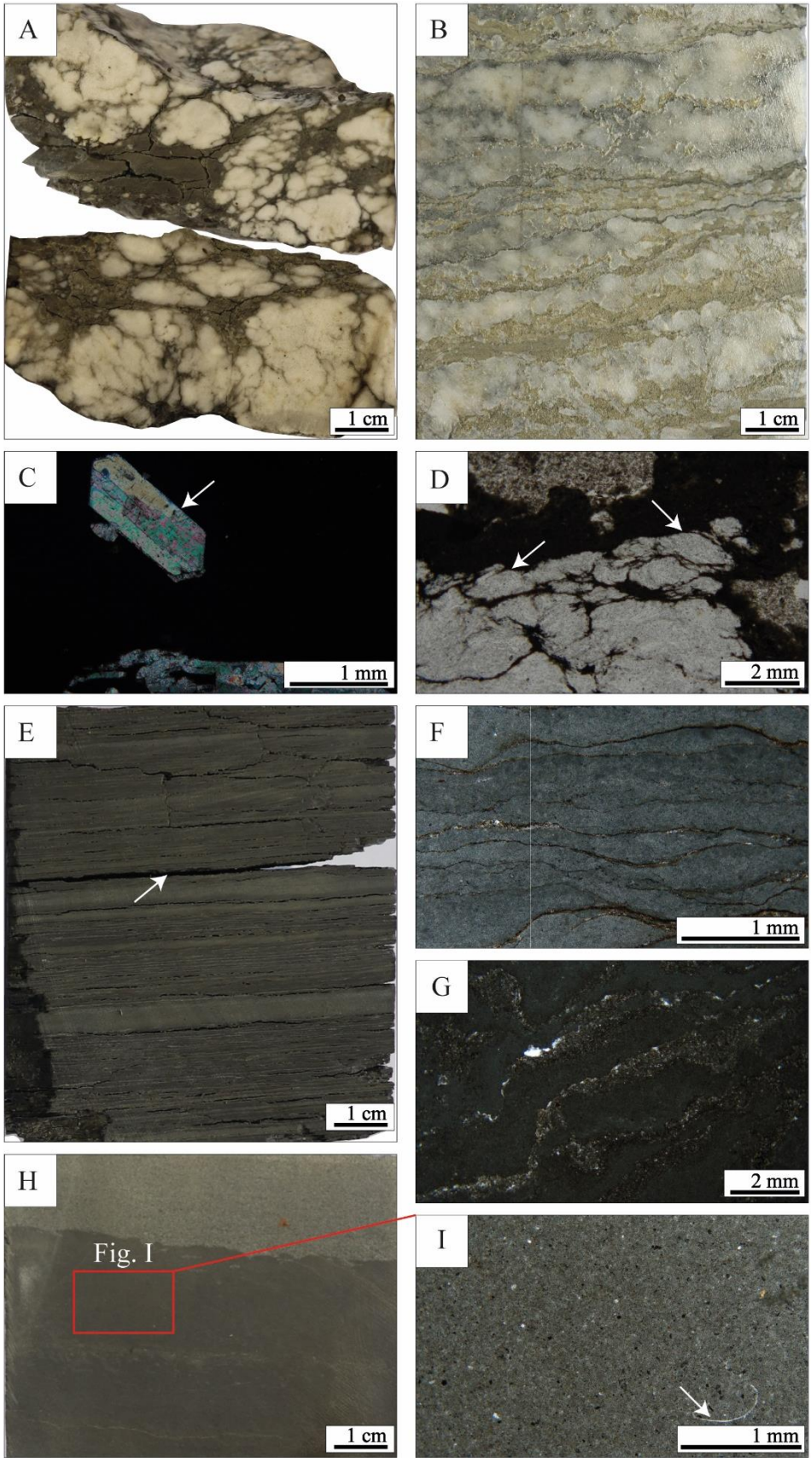

Figure 5.5: Anhydritic marls and anhydrite (F1), finely laminated limestones and papyraceous marlstones (F2), dark grey marlstones with scarce fauna (F3) facies. A) and B) Hand sample images showing the white anhydrite sparce nodules set in the marlstone matrix (A) and the banded anhydrite resulting from the coalescence of the

anhydrite nodules (B). C) Thin section of the facies F1 showing the needle microcrystalline structure of the anhydrite nodules embedded in a marlstone background (white arrow, XPL). D) Thin section of the banded anhydrite (F1 facies) displays the relicts of prismatic to lenticular crystals (white arrows) within the anhydrite nodules (PPL). E) core photograph showing the alternation of white and dark millimetre-thick laminae within the papyraceous marlstones (F2 facies), the white arrow indicates horizontally settled plant leaves. F) Thin section of the laminated limestones (F2 facies) exhibiting the alternation of wavy to crumpled submillimetre to millimetre laminae (PPL). G) Thin section (under PPL) exhibiting the alternation of carbonate-rich laminae (dark) and silt-rich laminae (clear), the laminae are wavy, and this may result from seismic destabilization. H) Hand sample shows a dark grey marlstone interval that lies below a grey sandstone interval (further detailed images on sandstones in Figure 5.6) I) close-up view of the box in H) showing the microscopic characteristics of the dark grey marlstones (facies F3), the arrow indicates an ostracod shell.

F3. Dark grey marlstones with scarce fauna:

Marlstones are very common in the *Série Grise* formation and are found occasionally in the *Série Calcaire* and *Série Mixte* formations. F3 facies occur in massive and structureless intervals in alternation with calcarenites and conglomerates (F4 to F7 facies, see description hereinafter) (**Fig. 5.5H**). These marls may contain significant amounts of silt-sized quartz and mica particles (=silty marlstones), and minor proportions of scattered coarse grains. Laminations are lacking and the marls are organic-rich thus resulting into the grey to dark grey colour; terrestrial plant remains are sometimes frequent. The preserved carbonate biotic remains are very scarce and consist mainly of ostracod shells (**Fig. 5.5I**). Pyrite mineral is also reported from these marlstones.

Interpretation: The detrital fraction is made of fine-sized particles (silt, clay) indicating sedimentation in quiet areas located far from the sources hence in distal and central parts of a perennial lake. Preservation of organic matter as well as the extreme scarcity of carbonate skeletal grains suggests low oxygen conditions on the lake bottom as observed in ancient and modern perennial lakes with water stratification (Basilici, 1997). The occurrence of pyrite is also consistent with anoxic conditions in a lake bottom affected by sulphate reduction processes (Peckmann et al., 1999). Dark grey marlstones are therefore interpreted to form in the distal, deeper, and poorly oxygenated areas of a lake which is subjected to detrital fluxes carrying the fine grains and the plant remains.

Gravity-driven lacustrine facies: F4, F5 and F6

F4. Glauconite-rich sandstones and fine-grained calcarenites:

F4 facies occurs within the *Série Grise* formation and consists of moderately to well-sorted, fine mixture dominated by angular quartz, oxides minerals, glauconite and mica grains with reworked miscellaneous siliceous and carbonate elements. The latter include small-sized peloids and broken bioclasts (e.g., benthic foraminifera, bryozoans, and echinoderms) derived from the reworking of Mesozoic marine limestones cropping out in the catchment area, as well as *microcodium* debris likely reworked from the neighbouring Paleogene continental limestones (**Fig. 5.6A, D-G**). Terrestrial plant remains are common whereas coeval lacustrine carbonate grains are scarce and could be represented by only a few ooids or peloids and characean remains. Sedimentary structures are represented by plane parallel laminations and

current ripples (**Fig. 5.6A**). These sandstones may also grade downwards into medium-sized sandstones and upwards into siltstones and marlstones (F3 facies, **Fig. 5.6A-C**). These sandstones may occur in several centimetres thick intervals (**Fig. 5.6B**) but also frequently alternating with marlstones in the form of millimetre to few centimetres thick layers thus forming banded intervals (**Fig. 5.6C**; "banded sandstones" *sensu* Lowe and Guy, 2000). In such banded sandstones, the bounding surfaces of the layers may be erosive with rip-up clasts (**Fig. 5.6B**) and may exhibit soft sediment deformation and load structures such as flame structures and pendulous load cast. (**Fig. 5.6B-C**).

F5. Coarse calcarenites and microconglomerates:

Coarse-grained quartzose calcarenites and microconglomerates are reported mostly from the upper part of the *Série Grise* formation. Clasts are made of various lithologies including limestones, sandstones, and more rarely siliceous elements (**Fig. 5.7A)**. Ripped up elements are also found among these grains (**Fig. 5.7A**). In F5 facies, carbonate grains are essentially lithoclasts or fragments of marine bioclasts (e.g., foraminifers, echinoderms, bryozoans) which can be found both within the lithoclasts or as separate grains within the sandy matrix thus suggesting that they are reworked. These microconglomerates generally display a grain-size break with the subjacent marlstones (F3 facies) and may show parallel laminations and grade upward into medium and fine sandstones. This facies occurs generally in several centimetres to few decimetres thick intervals intercalated between the sandstones (F4 facies) and the silty marlstones (F3 facies).

F6. Matrix-supported conglomerates:

This facies consists of sub-rounded to angular poorly sorted clasts, ranging in size from several millimetres to 1 cm and that reach up to 3 cm for the coarsest elements, embedded within a marlstone or silty sandstone matrix (**Fig. 5.7B-C, Fig. 5.7F**). F6 intervals show neither grading nor internal bedding. In the lower and middle parts of the *Série Grise* formation, conglomerates are oligomictic and clasts generally consist in light grey marly limestones of Mesozoic age bearing a clearly defined Mesozoic fauna with associated with some quartz grains and reworked calcite phenocrysts (**Fig. 5.7C, 5.7E, 5.7F**). In the upper levels of the formation, the conglomerates are also oligomictic and the matrix may contain lacustrine carbonate grains (**Fig. 5.7D**). The conglomerates and breccias are found in alternation with the F2, F3 and F4 facies described in the previous sections.

Interpretation of F4, F5 and F6 facies:

In the Série Grise formation, F4 sandstones are characterized by good sorting and grading, and they display sedimentary structures such as parallel laminations and current ripples (**Fig. 5.6A**). These sedimentary structures are described together in the turbidite sequence of Bouma: the parallel laminations are reported from the sandy level Tb, and the current ripples are indicative of the Tc interval (Bouma, 1962). Such sedimentary structures and vertical stacking of facies have been associated with turbidity currents (Bouma, 1962, Tinterri et al., 2020).

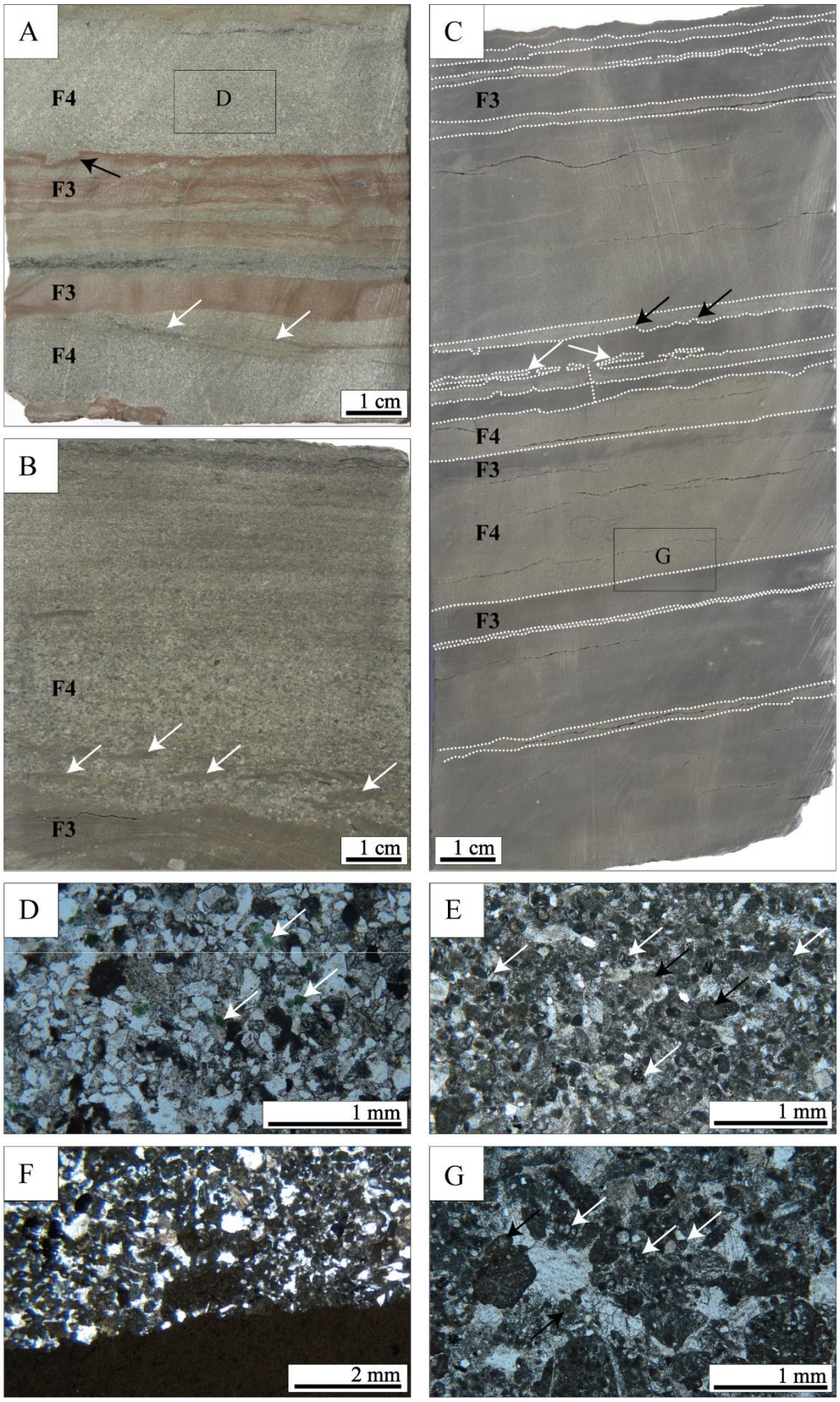

Figure 5.6: Glauconite-rich sandstones and fine calcarenites. A) Core photograph of glauconite-rich sandstone (F4 facies) alternating with marlstone/siltstone like that described previously (F3) in the form of planar parallel laminations similar to the upper parallel laminations of the Td member of the Bouma sequence (Bouma, 1962).

The white arrows indicate current ripples within the sandstones recalling those from the Tc layer of the Bouma sequence, and the black arrow indicate a flute cast. As an indication, the direction of the current would be from the left to the right of the picture. Darker areas in the core sample indicate the accumulation of leaves. B) Hand sample of fine to medium sandstone (F4 facies) displaying parallel lamination (lower parallel laminations of the Tb of a Bouma sequence) with an erosive base and grain size cut-off with the underlying marlstone layer (F3 facies). The white arrows in F4 facies indicate rip-up clasts ripped from the F3 facies marls. C) Core photograph displays alternation of the glauconite-rich sandstones (F4) and marls/siltstones (F3). Load structures are indicated by the arrows: white arrows indicate pendulous load cast while black arrows indicate flame structures. D) Close-up view of the F4 sandstones from A) showing the dominance of well sorted fine quartz and the abundance of glauconite mineral indicated by the white arrows (PPL microphotograph). E) Thin section of the fine calcarenites (F4 facies) displaying the mixture of miscellaneous grains with the noticeable abundance of reworked Mesozoic foraminifera (white arrows) and the presence of lacustrine ooids/peloids (black arrows). F) Thin section under PPL exhibiting a grain size cut-off between the calcarenite (F4 facies) and the underlying marlstone (F3 facies). G) Thin section under PPL of a medium-sized calcarenite (F4 facies) displaying dominant carbonate extraclasts, some of which containing foraminifera within them (white arrows), the black arrow indicates a lacustrine ooid/peloid.

The presence of preserved plant fossils and the interbedding of these sandstones with the F3 marlstones together with the lack of subaerial features suggests deposition in perennial lake conditions. The abundance of marine carbonate clasts, including bryozoans and reworked Mesozoic foraminifers (e.g., *Cuneolina*) together with siliceous elements (sponge spicules) and glauconite mineral grains, suggests feeding from the erosion of the Mesozoic sedimentary cover that forms the neighbouring catchment area. Part of the siliciclastic material supply, especially the quartz grains, may also be sourced from the dismantling of metamorphic and igneous rocks from distal areas (Pyrenean relief to the south and/or Cévennes Massif to the northwest).

The occurrence of sandstones in alternation with dark grey marlstones (F3 facies) which together form the ‘banded sandstones’ intervals displaying rip-up clasts, flame structures and pendulous load casts suggests that F4 facies results from transitional gravity-driven flows in the deep parts of the lake (Haughton et al., 2009, Tinterri et al., 2020). Those soft sediment deformations have been described in marine-gravity driven sediments and have been interpreted to result from a transitional flow, the characteristics of which are intermediate between a cohesive flow and low-density current (Tinterri et al. 2016, Tinterri et al. 2020).

In the microconglomerates (F5 facies) and conglomerates (F6 facies), the limestone detrital grains can either be made of irregularly shaped and dominantly subangular to subrounded mudstone clasts (rip-up) and reworked marine limestones.

The grain-size break with the subjacent marlstones and the presence of parallel laminations within the coarse sandstones and microconglomerates (F5 facies) are characteristic of a density flow current (Ta layer in Bouma (1962), S3 layer in Lowe (1982)).

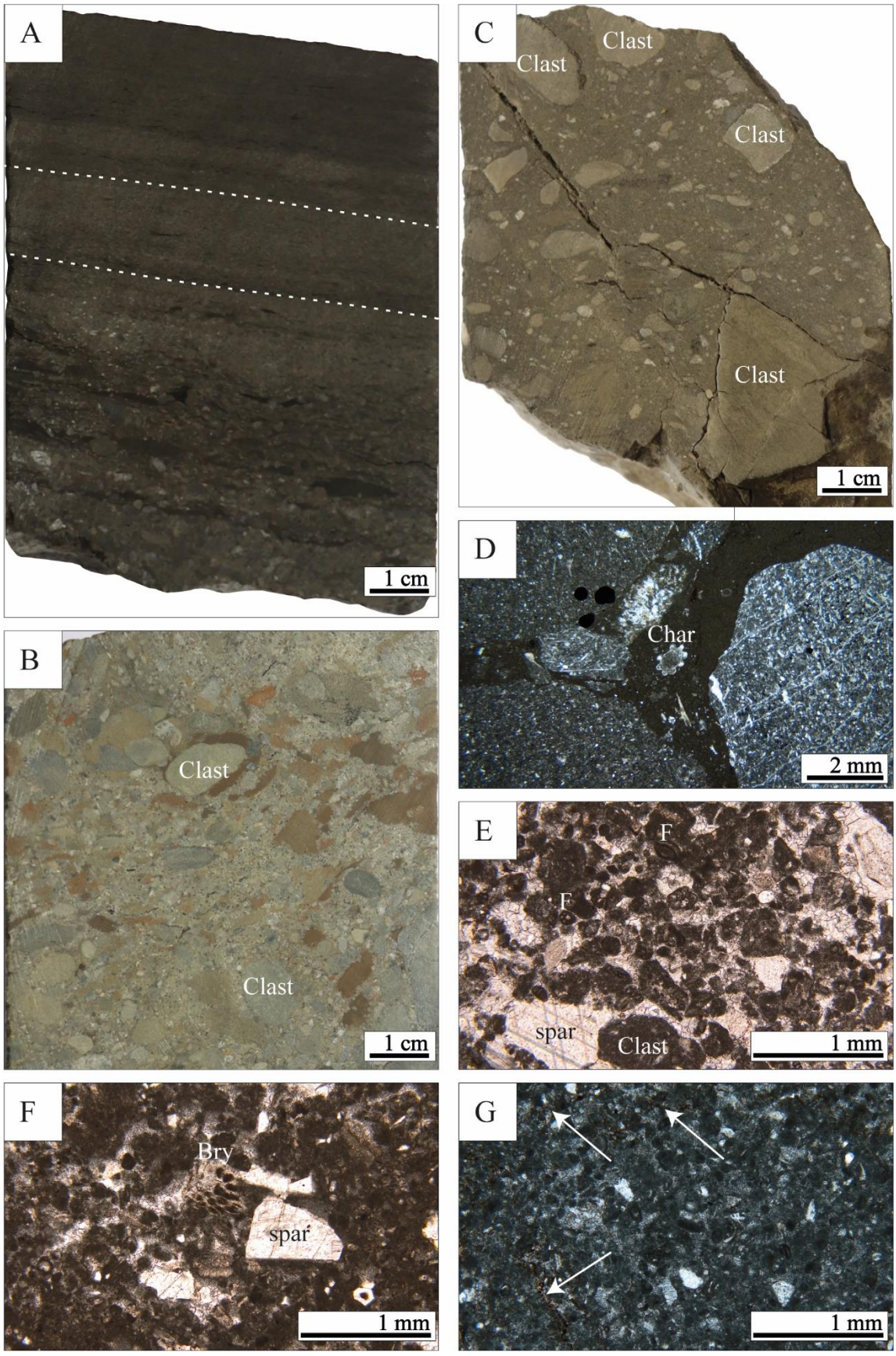

Figure 5.7: A) Core photograph showing the coarse calcarenite (F5 facies). Note that base of the sample contains coarse grains while the grain size becomes finer at the top, the dashed lines indicate parallel lamination.

B) Core photograph of a matrix-supported conglomerate (F6 facies) where the clasts are floating in the sandy matrix. C) Core photograph showing a matrix-supported conglomerate with particularly a monomictic composition of the angular clasts (Clast). D) Thin section under plane polarized light showing the nature of the clasts and the matrix. For instance, the clast on the right-hand side of the picture contains a marine limestone made of abundant sponge spicules. The marlstone matrix may contain in situ lacustrine elements like characean remains (Char). E) Thin section of a sandy matrix showing the wide variety of reworked elements: calcite phenocrysts (spar), foraminifera (F) and clasts (Clast) (PPL). F) Thin section (under PPL) showing a sandy matrix with miscellaneous reworked grains (Bry: bryozoans, calcite phenocrysts (spar). G) Microphotograph under plane polarized light of a bedded quartzose calcarenite (F7 facies) from the upper interval of the *Série Calcaire* formation. The detrital elements are similar to those from the previously defined calcarenites and microconglomerates. These calcarenites (F7 facies) are characterized by the presence of pedogenic modifications like perigranular cracks (white arrows).

In the F6 conglomerate facies, size and shape of carbonate clasts indicate low to moderate transport and the proximity of the source. Within these conglomerates, the occurrence of reworked lacustrine carbonate grains (e.g., characean remains, ooids) suggests that the lake margins are also subjected to mechanical erosion during the deposition of these conglomerates. The poor sorting of the grains and the matrix-supported texture suggest *en masse* deposition as described by Tinterri et al. (2020). F6 facies are interpreted as resulting from the freezing of a cohesive debris flows (Talling et al., 2012, Tinterri et al., 2020).

The F4, F5 and F6 facies form, together with the F3 marlstones, hectometre-scale intervals in the Gallician sector which is located in the central part of the Vistrenque Basin. These facies that stack vertically indicate close sedimentation areas. Haughton et al. (2009) related the different stratal morphologies and their sedimentary features (current and load structures, bedding geometry) to the basinward evolution of density current. F4, F5 and F6 are therefore interpreted to result from gravity-currents (hyperpycnal flow) that initiated on the slopes of the lacustrine basin and reached the profundal and central areas of the lake. Similar stratal pattern within lacustrine gravity-driven deposits have been described in the lacustrine delta front of the Ediacaran Camaquã Basin (Western Santa Bárbara Rift, Southernmost Brazil) and attributed to fluvial floods entering the lake system in the form of hyperpycnal flow (Lehn et al., 2018).

Terrigenous lake margin facies: F7

F7. Bedded quartzose calcarenites:

The bedded quartzose calcarenites occur mostly in the upper levels of the *Série Calcaire* formation and at the base of the *Série Mixte* formation. This facies forms massive decimetre to metre beds topped by calcarenites displaying pedogenic modifications (F13 facies) (**Fig. 5.7G**).

In addition to this characteristic feature, the F7 facies do not display the sedimentary features of the F5 facies (e.g., alternations with siltstones/marlstones in the form of centimetre layers). In thin section, however, the F7 facies exhibits similar grain contents such as quartz and miscellaneous reworked grains from the Mesozoic limestones.

Interpretation: The high content of carbonate clasts and quartz grains suggests high terrigenous flux in the depositional area. The carbonate grains are dominated by extraclasts

sourced by the erosion of the Mesozoic cover from the neighbouring drainage area of the lake. The low matrix content (mud and silt) suggests winnowing of the sediment. However, the presence of pedogenic features (e.g., cracking) at the top of the calcarenite beds indicate subaerial exposure. In addition, the occurrence of this facies in alternation with grey marlstones (F3 facies) and palustrine limestones (F13 facies, see description hereinafter) indicates the vicinity of the stream mouth and thus may be interpreted to be the delta or lacustrine shoreface deposits in the lake margin subjected to lake level fluctuations.

Carbonate lake margin facies: F8 and F9

F8. Oncolitic limestones:

Oncolitic limestones are found occasionally in the upper part of the *Série Calcaire* formation. F8 facies is dominated by spherical to elongate oncoids and may be classified as a floatstone of oncoids according to the classification of Dunham (Dunham, 1962) modified by Embry and Klovan (1971). In thin section, these oncoidal-rich carbonates display highly porous zones and the oncoids display fine micrite coatings (**Fig. 5.8A-B**). This facies occurs in the form of brown vacuolar limestones of inframetric beds, and the top of the beds display pedogenic features such as circumgranular cracks and root traces. F8 limestones are found intercalated between red calcareous marlstones (F12 facies, see description hereinafter) and palustrine limestones (F13).

Interpretation: The occurrence of these limestones interbedded with red marlstones and palustrine limestones may suggest deposition in alluvial to nearshore settings, probably in the form of bedload fill of channel or overbank deposits in the fluvial system or as littoral deposits at the vicinity of a riverine mouth in a lake. The lack of matrix suggests strong hydrodynamic setting. The presence of pedogenic features on top of F8 beds indicates subaerial exposure and therefore confirms the shallow water setting which may be consistent with deposition in an ephemeral shallow lake. Oncolitic grainstones are reported from the margin of a saline lake setting in the neighbouring Priabonian Saint-Chaptes basin (Lettéron et al., 2018) while Arenas et al. (2007) described overbank oncoid-rich deposits in a floodplain from the Paleogene of Mallorca Island (Spain).

F9. Microbial limestones (tufa?):

Microbial limestones occur in the form of metre-thick beds of brown vacuolar limestones made up of accumulation of millimetre to centimetre-scale microbial crusts (tufa fragments?) with minor proportions of fine angular quartz (**Fig. 5.8C-D**). In thin section, these microbial limestones consist of irregularly arranged micrite and sparite millimetre laminae alternating with highly porous areas. The laminae are slightly broken (**Fig. 5.8F**) and show little displacement. Other features may include micrite encrustations around unpreserved elements (leaves?). These limestones may display pedogenic modifications at the top of the beds including circumgranular cracking (**Fig. 5.8G**).

These limestones are frequent in the upper intervals of the *Série Calcaire* formation and in the *Série Mixte* formation. Microbial limestones are found in alternation with brecciated limestones (F13 facies defined hereinafter).

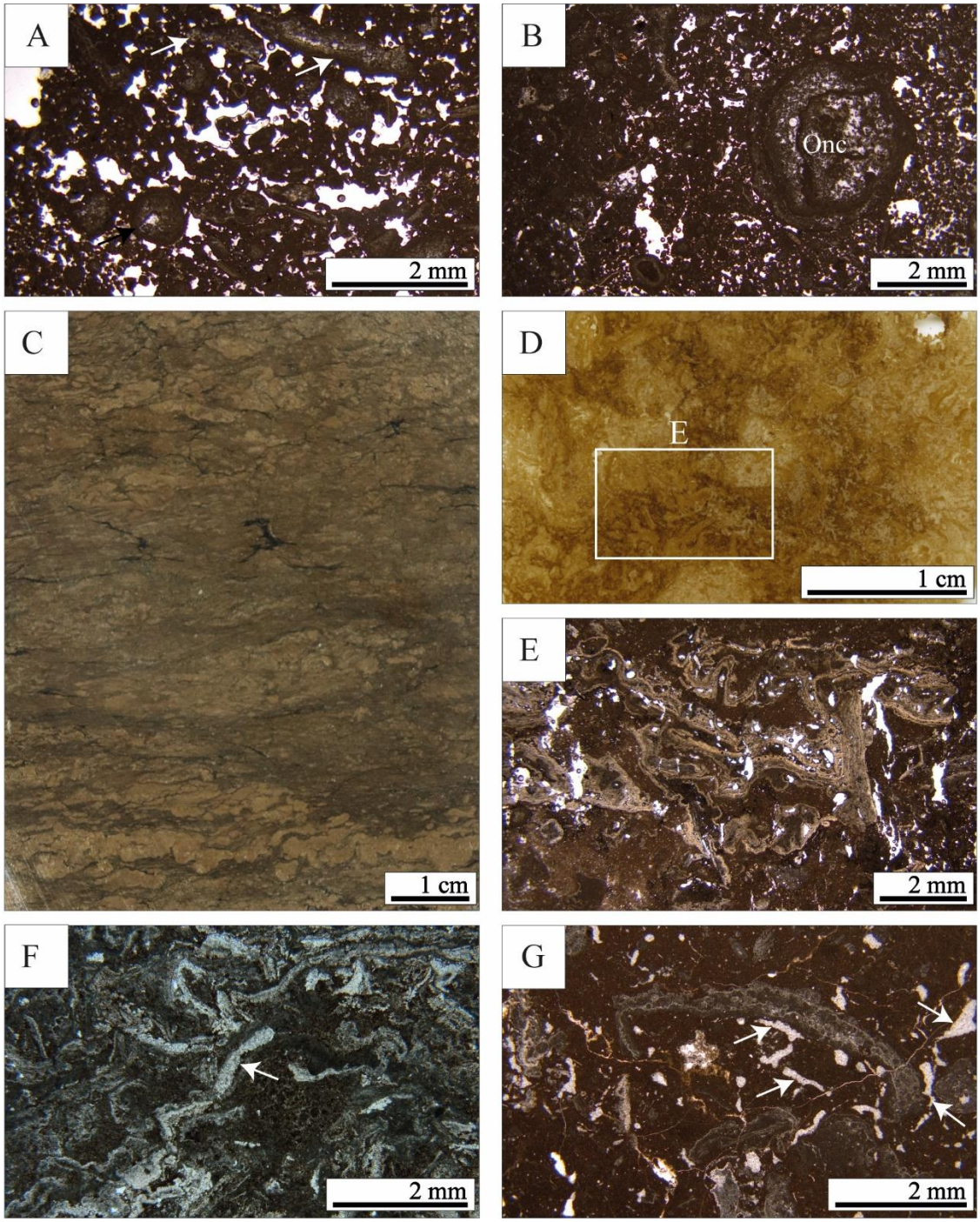

Figure 5.8: Fluvial continental carbonate facies (F8 and F9). A) Thin section of an oncolitic limestone (F8 facies) displaying various oncoid shapes, spherical (black arrow) and elongate (white arrows) within a interparticle porous zone. The texture of the limestone after the Dunham classification (Dunham, 1962) is floatstone to rudstone. B) Detail of an oncolitic limestone showing the coatings of a spherical oncoid (Onc). C) Core photograph showing beige microbial crusts (tufa fragments?) within a microbial limestone (F9 facies) D) Scan of a thick (100 µm) geological section showing the microbial crusts of the facies F9. E) Thin section under plane polarized light of the box in (D) showing the alternation of micrite (dark) and sparite (light) laminae in the form of irregular laminations

(PPL). F) Microphotograph under plane polarized light showing microbial crusts (probable tufa fragments) that are non-organized and some of which look like broken crusts (white arrow). G) Floatstone of microbial limestones showing micrite coating on thin grains (encrustations around leaves?). The white arrow indicates incipient pedogenic imprints expressed by the development of cracks filled with calcite.

Interpretation: The presence of microbial crusts (tufa fragments) and encrustations indicate deposition in lacustrine, fluvial and water spring settings (Arenas et al., 2010). Limestone bedrock availability is required to provide carbonate solutes to the fluvial system (Pentecost, 2005). The substratum of the Vistrenque Basin and the surroundings are dominated by Mesozoic marine carbonates thus making it possible for fluvial waters to be enriched in carbonate solutes. Tufa limestones can form within a broad range of climates (Arenas et al., 2010) even though alternation of clear and dark laminae points to temperate to semi-arid climate (Viles et al., 2007). However, tufa facies have been described from the fluvial and lacustrine settings from the middle Eocene and Oligocene of Mallorca Island (Spain) (Arenas et al., 2007 in Arenas et al., 2010) under tropical and subtropical climate.

The limited displacement of microbial crusts indicates the proximity of the location where these are formed to the lake littoral. The presence of mud matrix in these facies indicates rather a lacustrine depositional environment. Moreover, the presence of incipient pedogenic modifications suggest short-term subaerial exposure. The F9 facies is therefore interpreted to form within a lake littoral by reworking of carbonate crusts formed within nearby fluvial stream and spring waters in a carbonate-rich bedrock.

Fluvial facies: F10 and F11

F10. Polymictic conglomerates & microconglomerates

These conglomerates and microconglomerates are poorly sorted heterometric deposits and consist of a mixture of coarse sand through to granule and pebble size gravels (**Fig. 5.9A-C**). The mean size of the clasts is 1 cm and the largest may reach up to 4 cm in size. The clasts are subangular to subrounded and are of diverse lithologies, these are dominantly made of quartz, feldspar, and mica, but also brown and beige limestone clasts of Mesozoic and Tertiary ages with accessory glauconite (**Fig. 5.9B-C**). Some grains display anisopachous pendent cement and micrite coating around them (**Fig. 5.9A**). These polymictic conglomerates are clast-supported and have a sandy matrix made of fine to medium sandstones that fills the voids between the clasts, the sandstones are medium-sized (average size ~ 1 mm). The conglomerates have no obvious internal grading or sedimentary features. Moreover, preferential imbrication is very crude or even roughly displayed.

F10 facies are frequent in the lower part of the *Série Rouge* formation and are less frequent in the underlying *Série mixte* formation. Conglomerates are also present in the *Série calcaire* but are mainly made of limestone clasts and contains less terrigenous siliciclastic grains; these "monomictic" conglomerates have been described above (see F6 facies).

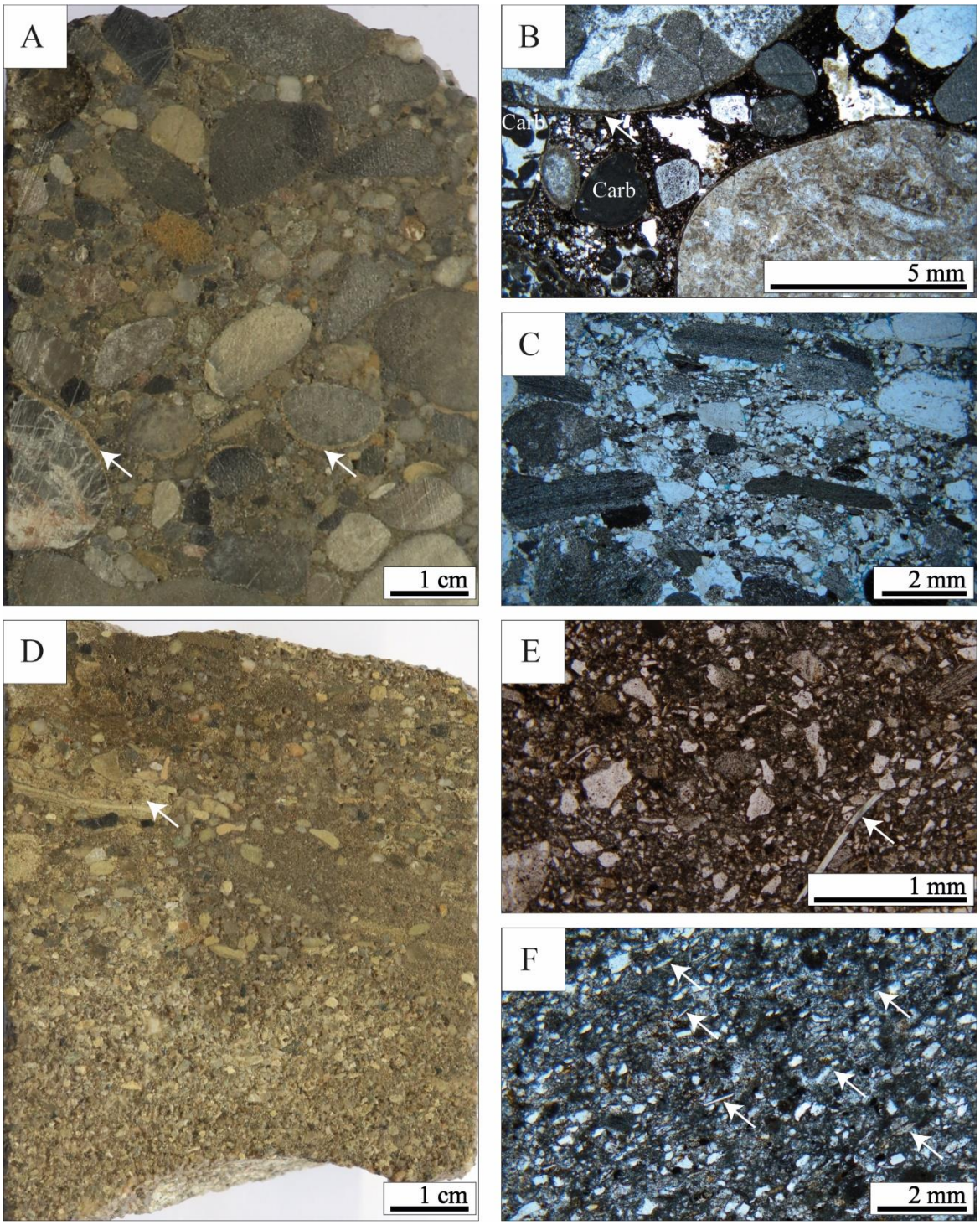

Figure 5.9: Conglomerates (F10 facies) and sandstones (F11 facies). A) Core photograph showing a polymictic clast supported conglomerate. The white arrows indicate pendular cements and/or micrite coating around the clasts. B) Thin section showing the poor sorting of the clasts and the sandy matrix within the conglomerates (Carb = carbonate lithoclasts). Notice the thin micritic coating around the grains C) Thin section exhibiting the preferential imbrication of the grains in the microconglomerate/coarse sandstone (F10/F11 facies) suggesting deposition under traction current. Small green grains are glauconite minerals. D) Core photograph of a siliciclastic-rich sandstone (F11 facies). The lithic fragment indicated by the white arrow consists of a tufa clast (further details in figure 5.8). E) Thin section under plane polarized light showing the abundance of fine angular quartz grains and the silty

matrix of the sandstone. The white arrow indicates a mica grain. F) Thin section photograph exhibiting the arrangement of sheet minerals (e.g., mica) as outlined by the arrows and suggesting current ripples (PPL).

The terrigenous polymictic conglomerates are organized into inframetric to metric beds and are found in alternation with sandstones and marlstones (F11 and F12, see descriptions hereinafter). The preservation of the cores does not allow to observe the stacking of the conglomerate beds, but the geological reports indicate that these conglomerates may grade upwards into medium and fine sandstones and then marlstones. These conglomerates may be found to overly sandstones, marlstones but also conglomerate beds from which these are separated by a sharp contact.

F11. Fine to medium sandstones (quartzose sandstones):

These sandstones are mainly made of very fine to medium-sized quartz grains with associated micas, feldspars, and glauconite/chlorite; less common centimetre-scale lithic mudstone fragments are also present (**Fig. 5.9D-F**). These quartzose sandstones are well to moderately sorted and carbonate mud fraction is very low or even lacking; grain size ranges from 80 to 250 µm (average ~ 170 µm) while the matrix may be constituted of silts and clays. Sandstones are azoic except the occurrence of scarce plant debris. In thin section, current ripples are highlighted by the arrangement of sheet minerals (e.g., mica, **Fig. 5.9F**).

F11 quartzose sandstones are common in the *Série Rouge* formation and occur in decimetre to metre-thick beds in alternation with conglomerates and marlstones. This terrigenous facies becomes less frequent in the subjacent *Série Mixte* formation and scarce or even absent in the lowermost *Série Calcaire* formation. The sandstone beds of metric thickness may lie over conglomerate intervals and exhibit vertical normal (fining-up) grading to marlstones and thus form plurimetric stacks of conglomerates, sandstones and marlstones. However, in some cases, structureless fine sandstones may also occur as discrete and isolated decimetric beds interbedded with calcareous siltstones and claystones (F12 facies, see description hereinafter).

Interpretation (of F10 and F11 facies): The clast-supported fabric of the conglomerates (F10 facies) suggests bed load transport within a channel. The wide range of the lithological nature of the clasts suggest feeding from both nearby and far source catchment areas. An example of nearby source includes tufa elements resulting from the erosion of contemporaneous upstream fluvial carbonates (**Fig. 5.9D**). The upwards grading of the conglomerates into sandstones (F11 facies) and calcareous claystones (F12 facies described hereinafter) reflects slowdown of fluvial currents, the energy of which gradually decreases allowing further deposition of fine sand grains and then fine particles (silts and clays), and therefore channel infill. F10 facies therefore represents deposition as bedload infill of braided and/or meandering streams in the proximal to medial parts of the alluvial plain; the presence of outsize clasts would indicate more proximal (braided?) areas of the alluvial plain.

The dominance of quartz, silicate and metamorphic minerals in these polygenic conglomerates and siliciclastic sandstones indicates feeding from the weathering of crystalline

rocks. Since the nearby catchment area of the basin is made essentially of Mesozoic limestones and glauconite sandstones, the origin of the minerals, especially metamorphic ones, is to be found in the mountain ranges that where being dismantled at those times, probably the Pyrénées that bordered the basin to the South (Séranne et al., 2021) or in the Massif Central further to the north. Moreover, the frequency of polycrystalline quartz suggests a metamorphic origin for this mineral. The contribution of the Albian glauconite-rich sandstones to the feeding of the fluvial streams is very low or next to nil since glauconite mineral is rarely observed in the F10 and F11 facies in contrast to the glauconite-rich sandstone interval from the Série Grise where the high proportion of this mineral suggests direct and significant feeding from the erosion from the Albian sandstones bedrock. Apart from the upwards grading into fine deposits, other evidence for fluvial deposition setting includes the presence of pedogenic features characteristic of alluvial plain in these claystones thus supporting the fluvial depositional setting for these conglomerates. In addition, sedimentary structures (current ripples) highlighted by the arrangement of sheet minerals (e.g., mica, cf. **Fig. 5.9**) in the sandstones suggest deposition under water stream. However, when the sandstones are found in the form of thin beds intercalated within the variegated claystones (F12 facies below), these rather represent overbank deposits/sheet flood in the floodplain.

Floodplain and palustrine carbonate facies: F12 and F13

F12. Variegated and mottled calcareous claystones:

Lithofacies F12 consists of predominantly vivid red sandy calcareous claystones, variegated with brown, yellow, green, and occasionally orange colours (**Fig. 5.10A-C**). In thin section, these marlstones are made up of very fine sand size (or silt size) siliciclastics including abundant quartz, feldspar, and mica (muscovite and biotite), with clays and oxides and very scarce glauconite. Silt is abundant (<30µm in size) while quartz grain size averages 50 µm and coarser quartz grains (>100µm) are found to be dispersed within the silty matrix (**Fig. 5.10D**). F12 facies is in general azoic and displays marmorisation patches (mottling). Other pedogenic features are found in these marlstones and include root traces (**Fig. 5.10C-E**).

These variegated and mottled claystones are widespread across the Vistrenque Basin especially in the *Série Rouge* formation where these form the essential part of this stratigraphic interval but are also frequent in the underlying upper and middle parts of the *Série Mixte* and are also reported in two levels within the *Série Calcaire* formation (geological reports). In cores, the calcareous claystones are organized into thick intervals the thickness of which may reach up to 2.20 m. These calcareous claystones occur alternating with sandstones (F11), conglomerates (F12) and brecciated limestones (F13 facies, see description hereinafter).

Interpretation: The high content of clays and silts in these calcareous claystones indicates settle-out of fine siliciclastic in calm areas (Arenas et al., 2010). The depositional setting may be ephemeral lake and/or floodplain. However, the association of these claystones with the fluvial deposits (F10 and F11) rather suggests floodplain area. The dominant reddish mottling

in these calcareous claystones results from the concentration of iron and manganese and indicates redox concentration conditions during the pedogenesis and later dehydration and oxidation of hydrate minerals which are transformed to crystalline hematite (Tabor et al., 2017).

The presence of root traces within these claystones indicates development of vegetation over the floodplain. Moreover, the alternation of thin sandstone beds with the marlstones suggests overbank deposition over the floodplain. Furthermore, these marlstones are stacked in the form of plurimetre thick intervals; the widespread record of the variegated marlstones across the Vistrenque Basin suggests aggrading floodplain.

F13. Brecciated limestones (Pedogenically modified carbonates)

F13 consists of white-beige brecciated limestones with occasional amounts of siliciclastics and detrital carbonates (**Fig. 5.11A-C**). The lacustrine host rocks may consist of gastropod mudstones to wackestones with ostracod shells and characean remains that display incipient and evolved pedogenic features *sensu* Freytet and Plaziat (1982) resulting in a nodular and brecciated texture. In many cases, the host rock consists of the calcarenites (F7 facies) and intraclastic limestones (F8 and F9 facies) defined previously that display those pedogenic modifications (**Fig. 5.11D-F**).

Incipient pedogenesis is expressed by perigranular cracks, weakly differentiated glaebules and sparse root traces. Root cavities are wider at the top of the bed and taper off downwards (**Fig. 5.11G**). The limestones that are most extensively affected by pedogenesis display abundant and/or enlarged root traces, well developed perigranular cracks but also well differentiated glaebules and pseudomicrokarst features (**Fig. 5.11F, 5.11H**). The cavities may reach few centimetres in size and may be filled with bitumen and/or different materials (e.g., ostracodal mudstone in **Fig. 5.11F**).

In thin section, theses limestones display dense dark micrite with sparse detrital grains. The perigranular cracks are filled with calcite while the dissolution cavities are filled with geopetal vadose silt and further cemented with blocky calcite spar (**Fig. 5.11F**). Beta calcrete fabrics *sensu* Alonso-Zarza and Wright (2010) (e.g., *Microcodium* features) are also reported from a few levels (**Fig. 5.11I**).

F13 facies occurs mainly in the uppermost part of the Série *Calcaire formation* and within the *Série Mixte* formation, and less frequently in the *Série Rouge* formation. The F13 limestones beds are decimetre-thick and typically cap the plurimetre-thick transition from the conglomerates (F10 facies) to quartzose sandstones (F11 facies) and calcareous claystones (F12 facies) in the *Série Mixte* and *Série Rouge* formations. In the *Série Calcaire* formation, however, pedogenically modified limestones (F13 facies) cap the calcarenite beds (F7 facies) and the intraclastic limestones (F8 and F9 facies).

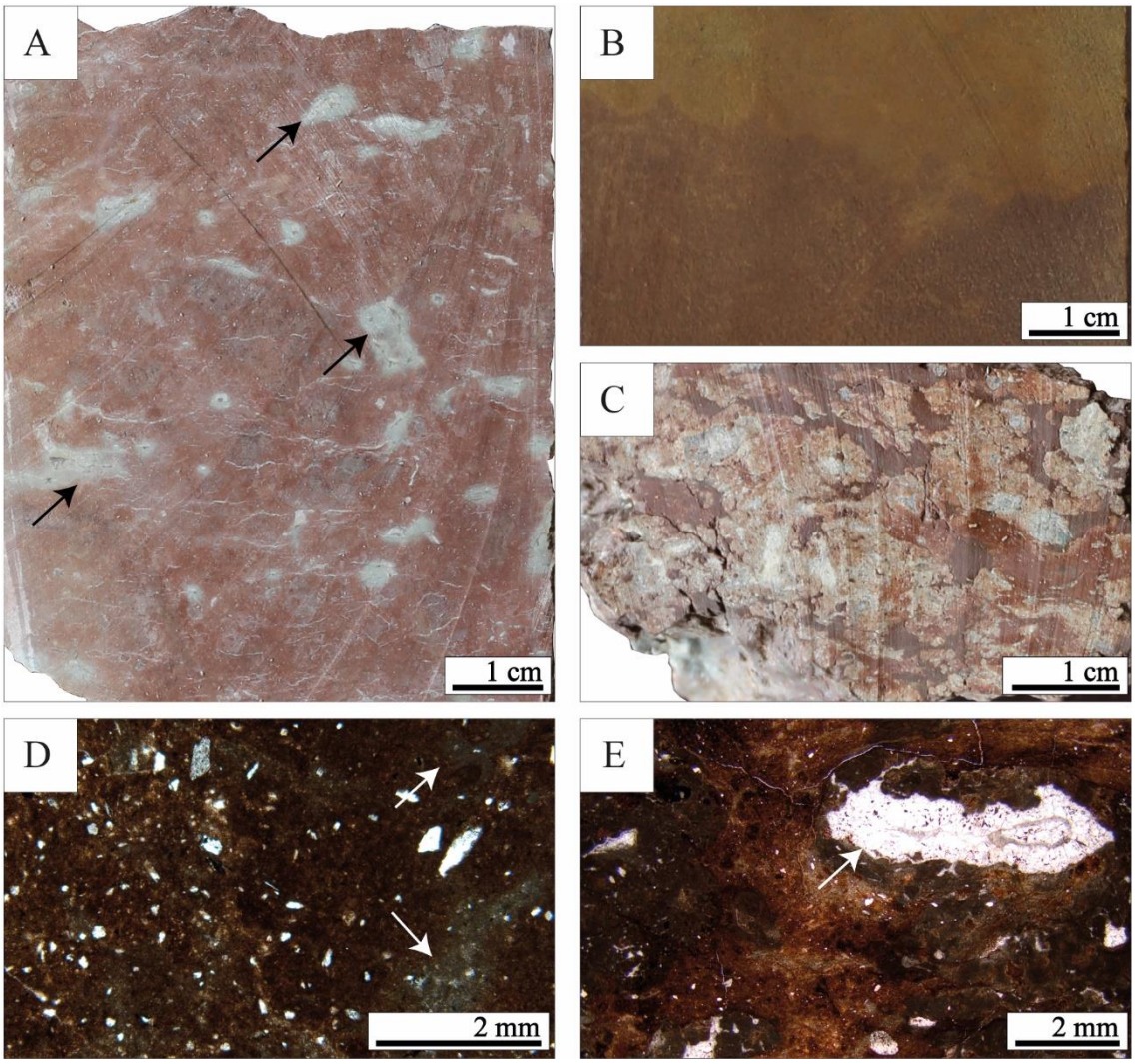

Figure 5.10: Variegated and mottled calcareous claystones (F12 facies). A) Core photograph from the Série Rouge formation showing a dominantly red calcareous claystone displaying green mottles (black arrows). B) Core photograph showing different hues of red and orange colours within a sandy claystones (F12 facies). C) Core photograph showing different ped structures with a broad palette of colours in the variegated marlstones. D) Thin section photograph showing green mottles (white arrows) within a dominantly brown sandy claystone (PPL). E) Thin section photograph showing cross-cut root filled with blocky sparite (white arrow) within a variegated calcareous claystone (PPL).

Interpretation: The features observed in F13 facies (perigranular cracks, glaebules, root traces) characterize very shallow lake margin environments subjected to repeated short-term exposure (Freytet, 1973; Platt and Wright, 1992). However, pseudomicrokart features suggest longer duration of subaerial exposure leading to the dissolution of limestones around the root traces resulting in the formation of cavities and their further filling with geopetal silt (vadose silt). Blocky and mosaic cements point to phreatic meteoric environments subsequently to reflooding and burial beneath the overlying sediments.

The occurrence of pedogenically modified carbonates (F13 facies) on top of F7 facies suggests the regression of the lake shoreline and/or progradation of the deltaic system of the

lake, and formation of very shallow and ephemeral water bodies. In the same way, pedogenesis modifying the oncolitic and microbial limestones confirms the subaerial exposure of their depositional settings (littoral shoreline). Moreover, the occurrence of F13 palustrine limestones beds in alternation with fluvial conglomerates and sandstones (F10 and F11 facies) and variegated calcareous claystones (F12 facies) is indicative of ephemeral carbonate pond environments developed within the floodplain.

Palustrine limestones are known from semi-arid to sub-humid climate settings (Platt and Wright, 1992). However, the lack of evaporites and the absence of coal intervals interbedded with these limestones excludes semi-arid and sub-humid conditions. Moreover, these authors suggest that microkarst cavities, vadose cements and rhizocretions are characteristic of intermediate climate conditions. Those features, including also *Microcodium*, have been described by Freytet and Plaziat (1982) in the Upper Cretaceous and Lower Tertiary of Languedoc (Southestern France). Palustrine limestones are also documented in the Priabonian lacustrine deposits from the Issirac Basin (ASCI system, Lettéron et al., 2017).

5.4.2. Vertical facies stacking pattern within the lithostratigraphic units

Only Pierrefeu-1 well intersected completely the whole Paleogene succession in the depocenter of the Vistrenque Basin and reached the lower Cretaceous substratum. In the Gallician sector, the Paleogene interval has not been completely drilled to the Mesozoic substratum. In these sectors, the subsurface data allow to investigate the vertical evolution of depositional facies and palaeoenvironments (**Fig. 5.12**). Detailed logs at core scale are given in **§ 5.8. Supplementary data** - **Appendix A**.

5.4.2.1. Lithological units and facies stacking pattern from Gallician 9 well:

5.4.2.1.1. Série Grise formation

Both Série Grise and Série Calcaire formations are characterized by the abundance of clastic deposits: marlstones (F2-F3), sandstones and calcarenites (F4), conglomerates and breccias (F5-F6). The Série Calcaire formation, however, is characterized by a carbonate enrichment trend towards the top recorded by bedded calcarenites (F7) the occurrence of intraclastic limestones (F8-F9) together with brecciated limestones (F13). The Série grise (2189 m - 2653 m) is subdivided into four intervals, from bottom to top: Glauconite complex, conglomerates, calcarenites, and evaporites intervals. It is cored continuously between the depths 2364 m and 2653 m (i.e., 289 m long core) and between 2309.50 m and 2329.70 m (i.e., 20 m long core). The base of the Paleogene is not reached in the Gallician 9 well (**Fig. 5.12A**).

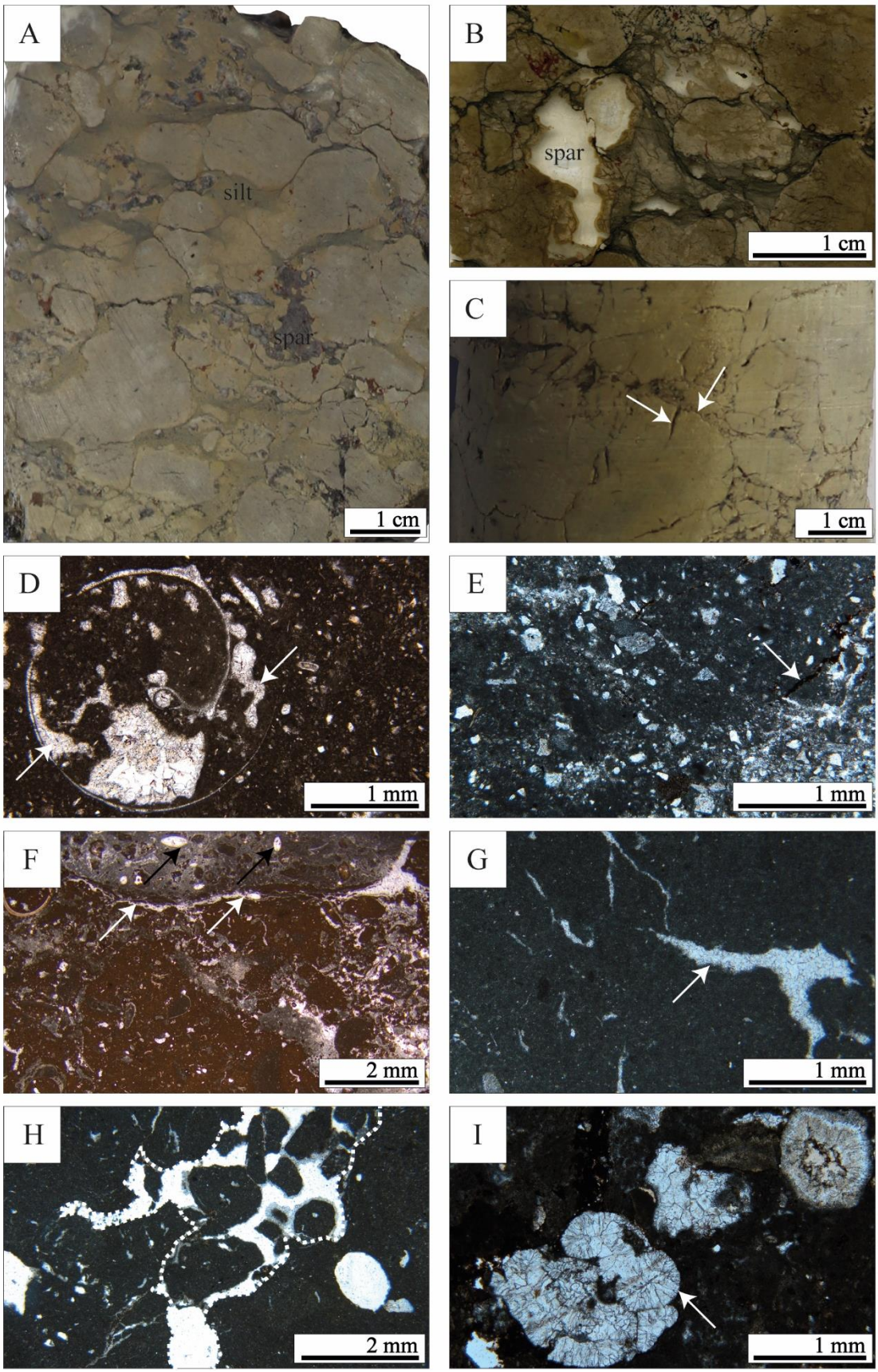

Figure 5.11: Brecciated and palustrine limestones (F13 facies). A) Core photograph of a nodular limestone (F13 facies). The nodules (glaebules) are well differentiated indicating long-time pedogenic processes, the voids

between the nodules are filled with silt and blocky calcite (spar). B) Scan of thick geological section (100 µm) showing a nodular carbonate similar to that from (A). C) Hand sample showing white brecciated limestone with fractures and individualized angular blocks. D) microphotograph of a lacustrine limestone with a cross section of a thin-shelled gastropod. The white arrows indicate cracks initiated in the gastropod limestone. E) Thin section of a pedogenically modified calcarenite (F7 facies) displaying cracks lined with the clay material (white arrow). This facies is frequent at the top of the F7 calcarenite beds. F) Thin section of an intraclastic limestone with microbial crusts (F9 facies) displaying subaerial exposure features (silt fill, cavity (white arrows) filled with different material which is in this case an ostracodal mudstone (black arrows indicate those ostracods). G) Thin section showing a palustrine limestone made of dense dark micrite and displaying cracks filled with calcite as indicated by the white arrow. The white fine lines on the upper part of the picture are likely root since they display downward ramifying (PPL). H) Microphotograph showing a cavity (outlined by the dashed line) within a dense dark micrite filled with clasts of the same micrite, resulting probably from the enlargement of a root cavity (PPL). I) Thin section of a palustrine carbonate made of dense dark micrite and showing well developed cluster of calcified roots (white arrow) displaying prismatic structures resembling to those of the *Microcodium*.

Glauconite complex (2430-2653 m):

The lowermost interval consists of a glauconite-rich sandstone interval (2430 – 2653 = 223 m) made essentially of alternations of glauconite-rich sandstones and calcarenites (F4), marlstones (F3) thus indicating deposition in profundal lake setting with important gravity-driven clastic supply. The supply of carbonate clasts (foraminiferal-rich limestones, bryozoan-echinodermal limestones, sponge spicules), quartz grains and glauconite mineral is potentially sourced from the erosion of the Albian marine glauconite-rich sandstones and lower Cretaceous marine carbonates that are widespread in the catchment area (Mesozoic substratum).

In the glauconite complex interval, laminites (F2), and matrix-supported conglomerates and microconglomerates (F6) are scarce in the lower part but increase in abundance upwards.

Conglomerates interval (2307-2430 m):

This interval (123 m thick) overlies the glauconite complex and is cored between 2365 m and 2430 m (i.e., 65 m core) and between 2309.50 m and 2329.70 m (i.e., 20 m core); the two cores are separated by a gap of 35 m. This interval is made essentially of matrix-supported conglomerates (F6) and calcarenites (F4 and F5) interbedded with papyraceous marls and laminites (F2). Glauconite-rich sandstones are absent in this interval and the calcarenites contain significant proportions of lacustrine clasts and grains, probably penecontemporaneous, such as ostracods, ooids and charophytes remains. The depositional facies (F2, F4, F5 and F6) display arrangements in the form of several metres-thick cycles showing an upward grading from conglomerates to sandstones through marlstones and laminites on top of cycle thus suggesting deposition in profundal lake and slope settings subjected to gravity-driven fluxes.

Calcarenites interval (2253-2307 m):

Core and cutting data are lacking in this interval. However, daily geological reports indicate that it is dominated by sandstones and calcarenites (F4? F5?), grey marlstones (F3), and anhydrite (F1). Anhydrite is particularly abundant at the top of this interval between the depths 2247.50 and 2285 m.

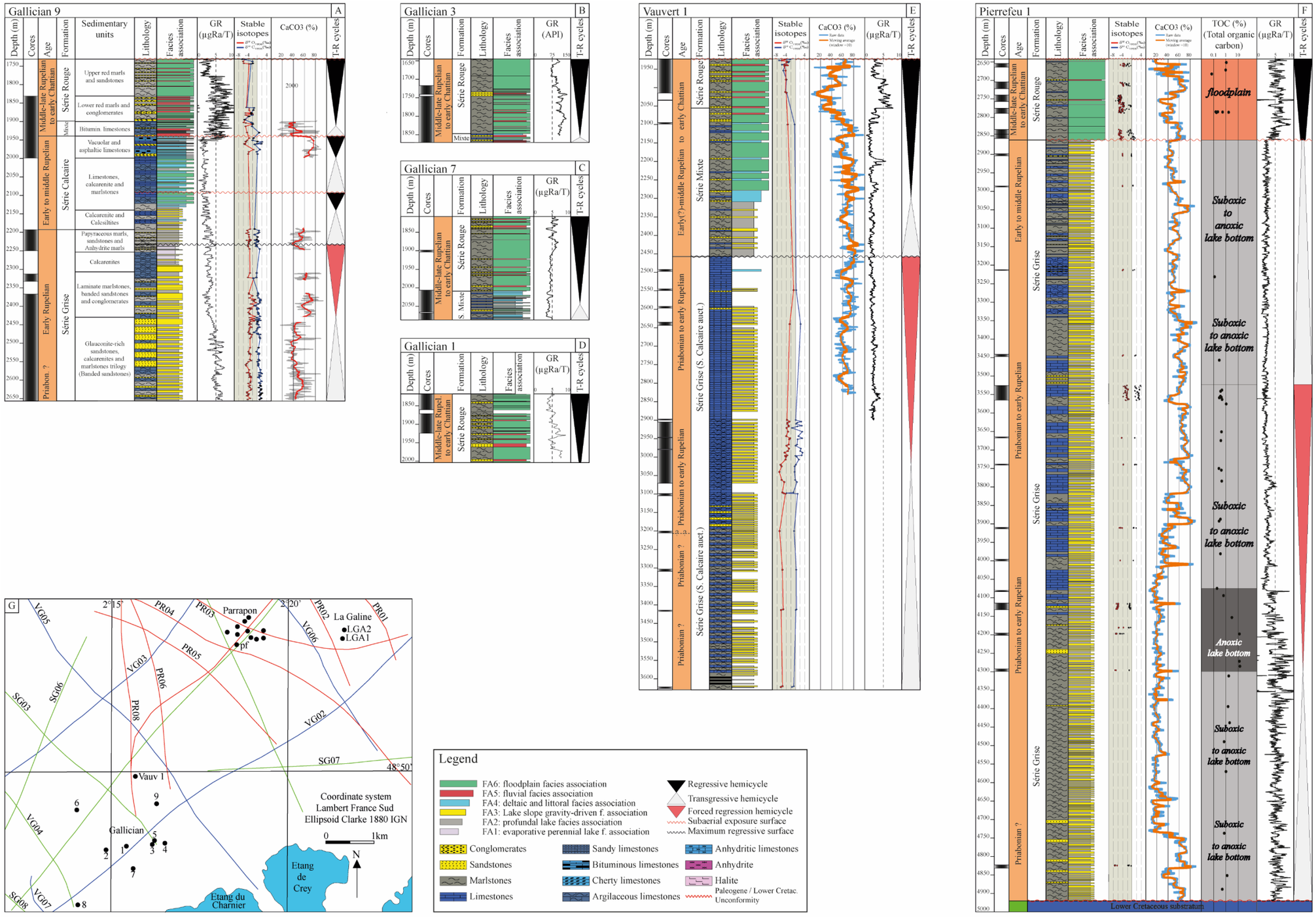

Figure 5.12: Sedimentary units, lithology and depositional lithofacies associations and transgressive-regressive cycles of Priabonian (?) to Early Chattian deposits from the Vistrenque basin wells: A) Gallician 9; B) Gallician 3; C) Gallician 7; D) Gallician 1; E) Vauvert 1; F) Pierrefeu 1. See text for details on facies associations definition.

Evaporite interval (2189-2253 m):

This 64 m-thick interval is entirely cored and dominated by anhydrite and anhydrite marlstones (F1) and papyraceous marlstones and laminites (F2) with less frequent calcarenites (F4-F5), and matrix-supported conglomerates (F6). Grouped with those from the underlying *Calcarenite* interval, the total thickness of the evaporites reaches up to 52 metres (between the depths 2233 m and 2285 m) indicating evaporitic conditions with a saline lake. Above this evaporite interval, the uppermost part of the Série Grise formation is characterized by frequent intercalations of calcarenites and conglomerates (F4-6) with marlstones (F2-F3) similar to those recorded below the evaporite interval.

5.4.2.1.2. Série Calcaire formation

The Série Calcaire unit (1939m-2189m) is in turn subdivided into three intervals, each characterized by dominant lithofacies, and is bounded at the top by a long-term subaerial exposure surface. This unit is cored only at the top between 1939 m and 1997 m (58 m long continuous core) while the two lowermost intervals (2000 – 2140 m and 2140 – 2189 m respectively) are not cored. However, the abundance of thin sections made on drilling cuttings together with the interpretation of the daily geological reports allow to determine the depositional facies and their vertical evolution.

Calcarenites et calcisiltites interval (2140-2189 m, not cored):

The lower interval (2140 m – 2189 m, i.e., 49 m thick) is made essentially of clastic carbonates, such as calcarenites and calcisiltites (F4-F5), matrix-supported microconglomerates (F6) reworking Mesozoic limestones (foraminifers, peloids, sponge spicules), and grey marlstones (F3). This interval displays similar vertical evolution of facies with the topmost interval of the underlying Série Grise formation and suggests deposition in profundal lakes subjected to gravity-driven sedimentary fluxes.

Limestones, calcarenites and marlstones interval (2000-2140m, not cored):

This intermediate interval (2000 m – 2140 m, 140 m thick) consists of alternations of dark grey marlstones (F3), calcarenites (F4), calcarenites and sandy limestones displaying pedogenic features (F7), red variegated calcareous claystones (F12) and less common microconglomerates (F6). The pedogenic imprints on calcarenites and limestones are frequent in this interval indicating subaerial exposures. The conglomerates are enriched in lacustrine elements and reworked *Microcodium* provided from the erosion of Upper Cretaceous to Paleogene continental carbonates from the surroundings. The variegated calcareous claystones (F12) occur particularly between the depths 2090-2123 m and 2040-2050 m.

Vacuolar and asphaltic limestones interval (1939-2000m, cored):

This interval is cored continuously between 1939 m and 1997 m (i.e., 58 m long core) and consists essentially of alternating marlstones (F3), calcarenites with pedogenic modifications (F7), and matrix-supported microconglomerates (F6) together with intraclastic limestones (F8-9) and palustrine limestones (F13). F3, F6 and F7 facies are dominant in the lowermost parts while the palustrine and intraclastic limestones (F8-9-13) are more frequent in the upper part of the interval. In the upper part of this interval, these facies occur in the form of plurimetre-thick units bounded at their top by subaerial exposure surfaces.

5.4.2.1.3. Série Mixte formation:

The Série Mixte formation is 42 m thick (1897-1939m) and is entirely cored. The dominant facies are: polymictic conglomerates (F10), quartzose sandstones (F11), oncolithic and microbial limestones (F8-F9), marlstones (F3? - F12) and pedogenically modified limestones (F13). Depositional facies are vertically organized into metre-scale units ideally displaying from bottom to top: grey and red marlstones (F3-F12), conglomerates (F10), sandstones (F11) and/or intraclastic limestones (F8-F9), variegated calcareous claystones (F12) and palustrine limestones (F13). Conglomerates from the Série Calcaire formation (F6 and F7(?)) differ from those occurring within the Série Mixte formation (F10) in their clast contents: those from the Série Calcaire contain essentially carbonate clasts whereas those from the Série Mixte are polymictic with a significant proportion of metamorphic and igneous elements. The change in clastic provenance is consistent with the unconformity recorded at top of the Série Calcaire formation. However, the facies transition to the overlying Série Rouge is gradational and is indicated by the decrease of the proportion of the limestone beds (F8-F9 and F13; intraclastic and palustrine limestones).

5.4.2.1.4. Série Rouge formation:

The Série Rouge formation is encountered in many wells across the Vistrenque Basin and displays low lateral variations in thickness (average thickness ~ 200 m). In the Gallician 9 well, the Série Rouge formation (1730-1897m) is subdivided into two intervals: a lower interval (1830-1897m) made of interbedded polymictic conglomerates (F10), sandstones (F11) and red variegated claystones (F12), and an upper interval (1730-1830 m) made essentially of red calcareous claystones (F12) and sandstones (F11).

Lower Série Rouge interval (1830-1897, cored):

The lower interval is entirely cored (67 m core). As in the subjacent Série Mixte formation, the plurimetre-thick units of alternating polymictic conglomerates (F10), quartzose sandstones (F11), variegated calcareous claystones (F12), and in a lesser extent palustrine carbonates (F13) are also found in the Série Rouge thus indicating depositional in fluvial and floodplain setting.

-Upper Série Rouge interval (1730-1830, not cored):

The upper interval (1730- 1830 m) of the Série Rouge unit is 100 m thick and is not cored. Daily geological reports indicate that this interval is dominated by red and variegated calcareous claystones (F12) with less frequent sandstones (F11) thus indicating floodplain and fluvial sedimentation environment.

5.4.2.2. Lithological units and facies stacking pattern from Gallician 3 well:

5.4.2.2.1. Série Mixte formation:

In Gallician 3 well, the Série Mixte formation has been drilled only in the uppermost 24 metres (**Fig. 5.12B**). This interval (1847-1870.80m) is cored continuously and displays alternations of polymictic conglomerates (F10) with occasional oncolithic and microbial limestones (F8-F9), siliciclastic-rich sandstones (F11), marlstones and claystones (F12), and palustrine limestones (F13). Depositional facies are organised into several metres thick normally graded units similar to those described in the Gallician 9 well and suggest sedimentation within fluvial (F10, F11), lacustrine margin (F8, F9) and floodplain (F12, F13).

5.4.2.2.2. Série Rouge formation:

This formation (202 m thick) overlying the Série Mixte formation is subdivided into two intervals. The ***lower red*** interval (1691-1847m) is almost entirely cored and is dominated by variegated calcareous claystones (F12) with interbedded sandstones (F11) reflecting deposition within fluvial and floodplain setting. The ***upper red*** interval (1645-1691m) is not cored but daily geological reports indicate lithologies similar to those from the ***lower red*** interval.

5.4.2.3. Lithological units and facies stacking pattern from the Gallician 7 well:

5.4.2.3.1. Série Mixte formation:

The Gallician 7 well reached the upper part of the Série Mixte formation and has been cored between 2009 m and 2087 m (i.e., 78 m long core, **Fig. 5.12C**). This interval is characterized by an alternation of dark grey marlstones (F3 ? or reduced F13 alluvial marlstones), sandstones and conglomerates (F10-F11), intraclastic limestones (F8-F9), and palustrine limestones (F13). The depositional facies indicate organization in the form of plurimetre-thick units topped by subaerial exposure surfaces as indicated by the frequence of pedogenic features. The lowermost parts are dominated by carbonate beds (intraclastic and palustrine) whereas the siliciclastic facies become more frequent to the top.

5.4.2.3.2. Série Rouge formation:

The Série Rouge formation has not been cored in this well although daily geological reports indicate similar lithologies with the neighbouring wells.

5.4.2.4. Lithological units and facies stacking pattern from the Gallician 1 well:

5.4.2.4.1. Série Rouge formation:

In Gallician 1 well, the Série Mixte formation has not been reached. The Série Rouge formation has a thickness of at least 186 m and is subdivided into two intervals: 1818-1867m and 1867-2004 m respectively. This formation is cored continuously between 1818 and 1925 (~ 100 m long core) and displays alternation of variegated calcareous claystones (F13), and sandstones (F12) thus suggesting deposition in fluvial and floodplain settings (**Fig. 5.12D**).

5.4.2.5. Lithological units and facies stacking pattern from the Vauvert 1 well:

5.4.2.5.1. Série Grise (Série Calcaire auct.) formation:

Although Vauvert 1 is the deepest well in the Gallician sector, the base of the Paleogene has not been reached (**Fig. 5.12E**). The lowermost Série Grise unit (2457-3630m), referred to as *Série Calcaire* in the geological reports is 1173 m thick. Some intervals have been cored and the unit is dominated by dark grey marlstones (F3) sandstones and calcarenites (F4-F5), matrix-supported conglomerates (F6), with less frequent papyraceous marlstones (F2) indicating deposition in profundal lake subjected to gravity-driven fluxes.

5.4.2.5.2. Série Mixte formation:

Core and cuttings are lacking from this interval (2055-2457m). However, daily geological reports indicate that this interval is made of an alternation of limestones, marlstones and sandstones. The lithological change from the underlying *Série Grise* formation is ambiguous and the thickness of the Série Mixte formation (>400 m) is very large compared to the neighbouring wells. This interval needs stratigraphic revisions to enable depositional palaeoenvironments interpretations.

5.4.2.5.3. Série Rouge formation:

The Série Rouge formation from Vauvert 1 well is ~130 m thick (1923-2055m) and is almost entirely cored (90m long core). This unit is dominated by variegated calcareous claystones (F12) with a siliciclastic-rich sandstones (F11) indicating deposition in fluvial setting.

5.4.2.6. Lithological units and facies stacking pattern from Pierrefeu 1 well:

5.4.2.6.1. Série Grise formation

The Pierrefeu 1 well is the deepest well in the Vistrenque Basin and has reached at the depth of 4920 m a lower Cretaceous substratum constituted of Lower Cretaceous marine carbonates (**Fig. 5.12F**). The lowermost lithostratigraphic unit (Série Grise formation, 2861-4920m) from Pierrefeu 1 well is approximately 2000m thick and was cored on non-continuous intervals. This formation consists of a relatively monotonous succession of grey marlstones (F3) and fine

turbidite sandstones (F4) with few conglomerates (F5-F6) indicative of profundal lake and slope depositional settings.

5.4.2.6.2. Série Rouge formation

The Série Grise formation is overlain by the Série Rouge formation. The Série Calcaire and Série Mixte formations described in the Gallician wells were not encountered in Pierrefeu 1 well, thus probably passing laterally into the uppermost part of the Série Grise formation and the lowermost part of the Série Rouge respectively. The Série Rouge formation from Pierrefeu 1 well is 173 m thick (2642-2861m) and is cored non-continuously. It is constituted mainly of variegated claystones (F12) with sandstones (F11) thus suggesting deposition in fluvial and floodplain settings.

5.4.3. Facies associations and palaeoenvironmental interpretations

The vertical distribution of the thirteen depositional facies defined previously in the studied wells allowed to identify six facies associations that enable to infer the depositional environments. The facies associations are: **evaporite-rich perennial lake** facies association (FA1), **profundal lake** facies association (FA2), **gravity-driven lake slope and offshore lake** facies association (FA3), **Deltaic and littoral lake** facies association (FA4), ***fluvial stream*** facies association (FA5), **palustrine and floodplain** facies association (FA6). These facies associations are described hereinafter and summarized in **Table 5.3**. The vertical distribution of these facies associations are displayed in **Figure 5.12** for the six studied wells.

Evaporite-rich perennial lake facies association (FA1) consists of the anhydritic marls and anhydrite grouped under the facies F1. Based on the petrographic characters, the lack of subaerial exposure evidence, and the alternation with deep lake dark grey marlstones (F3), facies F1 has been shown to form in evaporative perennial saline lake subjected to negative inflow-evaporation balance.

Profundal lake facies association (FA2) includes the finely laminated argillaceous limestones and papyraceous marlstones (F2 facies) and the dark grey marlstones with scarce fauna (F3 facies) that indicate deposition in the deep part of a perennial lake with poorly oxygenated waters.

Lake slope and offshore lake density currents facies association (FA3) encompasses lacustrine terrigenous-dominated facies (glauconite-rich sandstones and fine calcarenites F4, coarse calcarenites and microconglomerates F5, and conglomerates/breccias F6). The presence of sedimentary structures (e.g., current ripples, parallel laminations, load structures) and the vertical evolution of facies allowed to interpret these facies to be formed in slope and offshore lake conditions (delta front) by gravity-driven currents that evolve downwards from a cohesive flow to a low-density flow. Perennial lake conditions are evidenced from the lack of subaerial

exposure features. The terrigenous flux is high during the deposition of these facies and enters the lake in the form of hyperpycnal flow during fluvial floods in the upstream.

Deltaic and littoral lake facies association (FA4) consists of bedded calcarenites (F7) that are sometimes grading into coarse-grained deposits (calcirudites) downwards and fine-grained deposits (calcisiltites) upwards, and intraclastic limestones (F8-F9). These three facies have been shown to be topped by pedogenically modified limestones (F13 facies). On one hand, the F7 calcarenite beds deposited in the riverine mouth may be affected by pedogenic modifications. The presence of subaerial exposure features and the lack of sedimentary structures related to gravity-driven currents (e.g., parallel laminations, erosive base, load structures) strongly suggest deposition in littoral and deltaic setting, upstream to the FA3 depositional setting. On the other hand, carbonate-rich margin littoral depositional setting is indicated by deposition of oncoliths and reworked intraclasts (tufa fragments) formed in a nearby water spring. FA4 reflects therefore deposition in the vicinity of a riverine mouth where the progradational lake shoreline regression may lead to subaerial exposure of the littoral areas and installation of shallow waterbodies instead (palustrine margin).

Fluvial facies association (FA5) comprises the F10 (polymictic conglomerates) and F11 (quartzose sandstones) corresponding to the filling of a channel with both siliciclastic and carbonate clasts. This facies association characterizes fluvial depositional environments probably under high to moderate energy streams (braided to meandering rivers).

Floodplain facies association (FA6) consists of variegated and mottled calcareous claystones (F12) and brecciated limestones (F13) with less frequent thinly bedded siliciclastic sandstones (F11). The calcareous claystones may reflect either floodplain deposition or oxidation and decarbonation of lacustrine marls after subaerial exposure. The lack of fauna within these claystones and the occurrence of interbedded overbank sandstones (F11) point to fine particles settlement over the floodplain. The floodplain may be intersected by channels which in turn may be abandoned in the form of ponds and oxbow lakes. The latter ephemeral water pans undergo short-term drying and wetting cycles leading to the development of the F13 palustrine limestones.

Table 5.3: Depositional facies associations of the Paleogene 'Série Rouge' and underlying units ('Série Mixte', 'Série Calcaire', 'Série Grise') from the Vistrenque Basin (Camargue, SE France) defined in the Gallician and Pierrefeu sectors and their palaeoenvironmental interpretations.

Facies association	Facies Code	Depositional facies	Occurrence	Palaeoenvironmental interpretation
FA1 Evaporite-rich perennial lake	F1	Anhydritic marlstones and anhydrite	Uncommon, reported only from one thick interval from Série Grise Formation.	Evaporative perennial lake
FA2 Profundal lake	F2	Finely laminated argillaceous limestones and papyraceous marlstones	Frequent in the Série Calcaire Formation & occasional in the Série Grise Formation	Profundal perennial lake with poorly oxygenated conditions
	F3	Dark grey marlstones with scarce fauna	Common in the Série Grise and in the Série Calcaire formations	
FA3 Lake slope and offshore lake	F4	Glauconite-rich sandstones and fine-grained calcarenites	Common in the Série Grise Formation	Gravity-driven currents in the lake slope and offshore lake
	F5	Coarse calcarenites and microconglomerates	Frequent in the upper part of the Série Grise Formation	
	F6	Matrix-supported conglomerates	Occasional to frequent in the Série Grise Formation	
FA4 Deltaic and littoral lake	F7	Bedded quartzose calcarenites	Frequent in the upper part of the Série Calcaire Formation but also at the base of the Série mixte Formation	Vicinity of a riverine mouth (lacustrine delta) and lake littoral
	F8	Oncolitic limestones	Occasional in the Série Mixte formation	
	F9	Microbial limestones (tufa?)	Frequent in the Série Mixte & Série calcaire formations	
FA5 Fluvial association	F10	Polymictic conglomerates and microconglomerates	Frequent in the Série Rouge and less the Série Mixte Formation	Channelized and overbank deposits
	F11	Fine to medium sandstones (Quartzose sandstones)	Common in the Série Rouge and occasional in the Série Mixte Formation.	
FA6 Floodplain association	F12	Variegated and mottled calcareous claystones	Common in the Série Rouge and Série Mixte formations and occasional in the Série Calcaire Formation.	Floodplain and very shallow pond/ephemeral water pans
	F13	Brecciated limestones (Pedogenically modified carbonates)	Frequent in the Serie Mixte and occasional in Série Rouge (lowermost parts) and Série Calcaire formation.	

5.4.4. Carbon and oxygen stable isotope signatures of lacustrine carbonates

The dataset used in this chapter is listed extenso in **§ 5.8. Supplementary data** – **Table S5.1**. The C&O isotope signatures are graphically illustrated on the multi-well correlation of **Fig. 5.12**, on the crossplots in **Fig. 5.13** and on the panels of **Fig. 5.14**.

5.4.4.1. Gallician 9 well

In the Série Grise formation between 2189 m and 2652m depths, $\delta^{13}C$ of bulk rock carbonates values have a wide range and vary from -1.80 ‰ PDB to 2.05 ‰ PDB. $\delta^{18}O$ values

are also widely distributed since these range between -5.02 ‰ PDB and -0.54 ‰ PDB (**Fig. 5.13A**). Within the Série Calcaire formation, measurements exhibit similar ranges of values of oxygen and carbon isotopes ratios as those from the underlying Série Grise unit. $\delta^{13}C$ values range from -2.03 ‰ PDB to 2.03 ‰ PDB while $\delta^{18}O$ vary between -5.67 ‰ PDB and -1.64 ‰ PDB. Geochemical signal from the Gallician 9 well carbonates is probably polluted due to the abundance of carbonate detrital fraction within the sedimentary succession of this section.

5.4.4.2. Pierrefeu 1 well

In Pierrefeu 1 well, carbonates from matrix-supported samples (calcareous claystones, marlstones, argillaceous limestone and micritic limestones) from the Série Grise formation exhibit a wide range of $\delta^{13}C$ (from -5.36 to +3.83‰ V-PDB) and $\delta^{18}O$ values (from –7.59‰ to –1.32‰ V-PDB) (**Fig. 5.13A**). Within the lower interval (4830 m – 4080 m) covered by cores K30 to K26, a positive covariant trend is evidenced at hectometre scale and the lowermost cores (K29 and K30) exhibit moderately negative $\delta^{13}C$ values (-1.76 to -0.39‰) while $\delta^{18}O$ values (-7.59 to -6.40‰) are the more negative within the Série Grise formation. Toward the top of this interval, however, $\delta^{18}O$ and $\delta^{13}O$ display less negative values (~ - 6‰ V-PDB) while ^{13}C is less important (~ -1‰ V-PDB). In addition, a positive covariant trend is observed at metre to decametre scale between the $\delta^{13}C$ and $\delta^{18}O$ signals except for the core K28 made of organic-rich marlstones where $\delta^{13}C$ values are very negative (-5.36‰ V-PDB à -3.56‰ V-PDB) although $\delta^{18}O$ values remain similar to the values observed at hectometre scale (~ -7‰ V-PDB).

From 4000 m (core K25) to 3525m (core K19), both $\delta^{13}C$ and $\delta^{18}O$ exhibit an increasing upward trend, the maximum values on top of this interval being respectively +3.83‰ and -1.32‰ (**Fig. 5.13B**). Conversely to the underlying interval (4830m – 4080m), $\delta^{13}C$ values are positive within this interval. Like the 4830-4080m interval, positive covariant trends are also evidenced between $\delta^{13}C$ and $\delta^{18}O$ at core (metre to decametre) scale. However, in the upper interval of the Série Grise formation (3447 m – 2900 m: cores K18 to K15), the available dataset suggests an overall slightly decreasing upward trend in both $\delta^{13}C$ and $\delta^{18}O$.

5.4.4.3. Vauvert 1 well

In Vauvert 1 well, carbonates from samples with matrix-supported fabrics exhibit a wide range of $\delta^{13}C$ (from -3.83 to +3.05‰ V-PDB) and $\delta^{18}O$ values (from –6.96‰ to –0.79‰ V-PDB) (**Fig. 5.13C**). In the lower part of the studied section (3622-3020m, cores K62 to K53), available carbon and oxygen isotope measurements display apparent low vertical variations with $\delta^{13}C$ values ranging from -1.51 to +0.92‰ and $\delta^{18}O$ values from -6.87 to -4.36‰ in spite of the relative scarcity of measurements (14 values) within this interval. From 3020m to 2548 m (cores K52 to K34), $\delta^{13}C$ and $\delta^{18}O$ values are widely distributed although an overall increasing upward trend in $\delta^{18}O$ (up to -0.79‰), a shift toward more positive values (maximum $\delta^{13}C$: +3.05‰) and a roughly positive covariant trend may be observed.

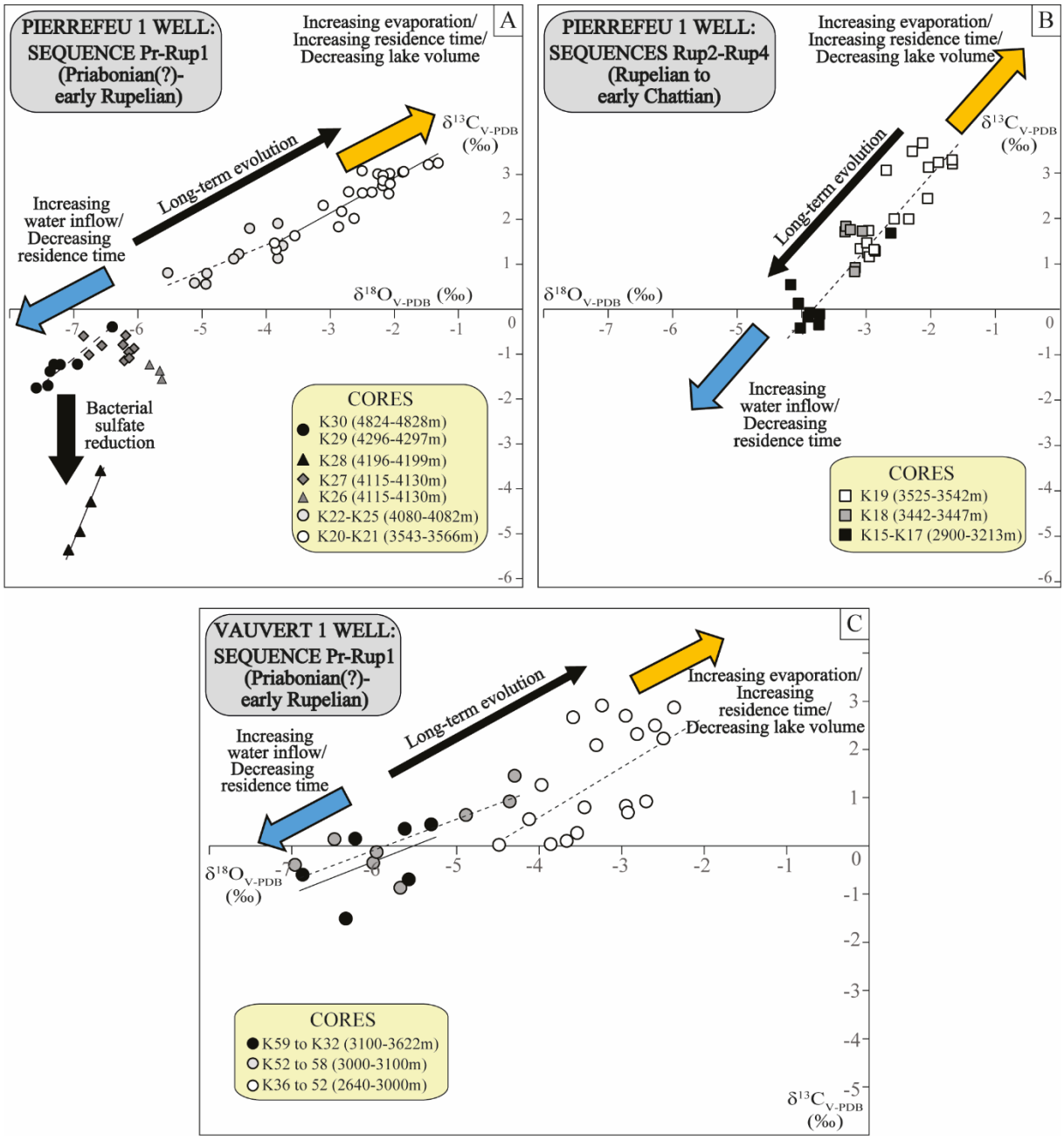

Figure 5.13 : $\delta^{13}C$ and $\delta^{18}O$ cross-plots of carbonates from Pierrefeu 1 well (A, B) and Vauvert 1 well (C) within the Série Grise formation.

Palaeohydrological interpretation of stable isotope signatures

Covariance of $\delta^{13}C$ and $\delta^{18}O$ usually occurs in carbonate lake sediments under the condition of long-term hydrological closure, typically for time periods greater than 5,000 yr (Li and Ku, 1997). Covariant trends have been identified in Pierrefeu-1 at metre-to-decametre scale and likely reflect variations through times of lake hydrological balance and vapor exchange (Li and Ku, 1997; Leng and Marshall, 2004) in a closed lake. The highest isotopic values reflect high degree of equilibration of the TDIC with atmospheric CO_2 related to increased water residence time, and preferential evaporative loss of the ^{16}O (Talbot, 1990; Leng and Marshall, 2004) while

the lowest values reflect lower time residence, less evaporated water and therefore isotopic compositions that are closer to those of inflows.

In Vauvert 1 well, a covariant trend is also evidenced but is weak and values are more scattered possibly because of higher and variable concentrations in carbonate detrital particles within the matrix, as also observed in Gallician 9 well, compared to Pierrefeu 1 counterpart: the Vauvert 1 and Gallician 9 wells are located around 3.5 km to the south of Pierrefeu 1 well.

The highly negative $\delta^{18}O$ values (down to –7.59‰) evidenced in the lower 'Série Grise' formation in both Pierrefeu-1 and Vauvert-1 wells are consistent with values measured in Priabonian meteoric cements (-7 to -8‰) in the Saint-Chaptes basin (Lettéron et al., 2018). The very negative $\delta^{18}O$ values that have been measured in the lower part of the Série Grise formation in Pierrefeu 1 (4830 m – 4080 m) and Vauvert 1 (3622 m - 3020 m) wells suggest relatively short residence time of waters and constant or increasing average lake volume through the considered time interval. In addition, the negative $\delta^{13}C$ values in these intervals suggests that the dissolved inorganic carbon from the freshwater inflows was significantly depleted in ^{13}C which is indicative of a densely vegetated catchment area in a relatively humid climatic setting (Talbot, 1990).

A major break in the vertical evolution of carbon and oxygen isotope compositions of carbonate sediments occurs in Pierrefeu 1 around 4070 m and in Vauvert 1 around 3020 m and which display a significant increase upward and covariant trend of $\delta^{13}C$ and $\delta^{18}O$. Within the intervals overlying these depths (i.e., 4000 - 3525 m in Pierrefeu 1 and 3020 - 2548 m in Vauvert 1), $\delta^{13}C$ values are positive. In these intervals, covariant trends evidenced at metre-to-decametre scale likely reflect high-frequency secular changes of volume of a closed lake while the overall (few hundred metre scale) increasing upward trend in $\delta^{18}O$ is indicative of long-term reduction of lake volume.

In Pierrefeu 1 well, the very negative $\delta^{13}C$ excursion that occurs in the organic-enriched intervals from the Série Grise formation (K28 core) likely results from CO_2 released from the organic matter consumption on the lake bottom by sulphate-reducing bacteria as evidenced in other organic-rich lake basins (Carothers and Kharaka, 1980; Kelts and Talbot, 1990). Such sulphate-reduction processes may have been triggered by the development of anoxic conditions on lake bottom as a result of significant organic-matter supply coupled with strengthened water stratification. Water stratification may have been favoured by an increase in lake salinity and associated enhancement of the density difference between the epilimnion and the hypolimnion and thus limiting water mixing and favouring anoxia on lake bottom (e.g., Sonnenfeld, 1985). This interpretation is consistent with the saline nature of the lake during the entire Priabonian and at least episodically during the Rupelian as established by previous studies (Semmani et al., 2022; *under review*; *see chapters 3 and 4 in this PhD manuscript*) and by the coeval onset of $\delta^{18}O$ increase which reflects deficient inflow-evaporation balance, lake volume reduction and therefore increased salinity.

Above the organic-rich interval from Pierrefeu 1 well (between 4300 m and 4100 m, TOC >5% and up to 10%) and above the depth of 3020 m in Vauvert 1 well, the overall increasing upward trend in $\delta^{13}C$ is likely indicative of both higher water residence time and weakly-vegetated catchment area thus strongly suggest dryer climate during the deposition of these intervals. Changes in nature of the substrate of the drainage area through times may also have modified the long-term variation of $\delta^{13}C$ of the DIC (Dissolved Inorganic Carbon) and subsequently of the lacustrine carbonates. Finally, the upward decreasing trend in $\delta^{13}C$ and $\delta^{18}O$ recorded in the upper part of the 'Série Grise' from Pierrefeu 1 well (K18-K15: 3447 – 2900 m) is interpreted to result from a long-term increase in connected volume of lake water.

The analysis of carbon and oxygen isotope compositions of lacustrine carbonates that are common in the Série Grise and Série Calcaire formations (Priabonian (?) to Middle Rupelian) from both Pierrefeu 1 and Vauvert 1 wells show that these signals record an overall similar evolution between the two wells. The early stage of lake basin infill (Priabonian (?) to early Rupelian: 4920 - 4080m in Pierrefeu 1, 3622 – 3020 m in Vauvert 1) occurred within a constant or increasing lake volume and is followed by a stage of lake contraction (Early Rupelian: 4080 – 3525 m in Pierrefeu 1, 3020 - 2458m in Vauvert 1). This cycle of long-term lake waxing and waning is followed by a later stage of increasing volume of connected lake water during the Early to Middle Rupelian times (3525 – 2860 m in Pierrefeu, 2458 - 2300m in Vauvert 1).

5.4.5. Sedimentary cycles and well correlations

The vertical stacking pattern of facies associations and corresponding depositional environments allow to identify depositional sequences defined as transgressive-regressive (T-R) cycles. The interpretation of T-R cycles has been complemented by the identification of vertical trends of carbon and oxygen isotope ratios of lacustrine micrites from the Série Grise and Série Calcaire formations. The chronostratigraphic framework used in this section was constructed by Semmani et al. (*under review, see Chapter 4 in this PhD manuscript*) using U/Pb absolute ages and pollen-based climatostratigraphy approaches.

Four medium-scale (few hundreds of metres thick) depositional sequences (Pr-Rup1 to Rup4) can be defined within the studied units ('Série Rouge' and underlying formations) of the reference section of Gallician 9 well. The depositional sequences described below are shown on the reference section of Gallician 9 and on the sections of the other studied wells (**Fig. 5.12**).

5.4.5.1. Gallician 9 well

Sequence Pr-Rup1: Priabonian (?) to early Rupelian

In the Gallician sector, the studied wells have not reached the base of the Paleogene. The base of sequence Pr-Rup1 is placed at the base of the glauconite-rich interval. The age of the glauconite-rich interval is not fully known although pollen data suggest an earliest Rupelian

age at the depth of 2530 m. In this sector, the lowermost intervals of the Série Grise formation that are not drilled, hundreds of metres thick according to seismic data (**Fig. 5.2B**), may have been deposited as early as the Priabonian (Semmani et al., *under review, see chapter 4 in this PhD manuscript*). The sequence boundary SB1 that separates the Priabonian – Rupelian deposits from the Cretaceous substratum is only known from the Pierrefeu 1 well in the Pierrefeu-Parrapon sector. The glauconite-rich interval is made of a succession of gravity-driven elemental sequences dominated by fine sandstones (low-density turbidites, FA3 association) intercalated with marlstones (FA2) in the lower interval while coarser material (matrix-supported conglomerates, F6 facies) becomes more frequent upwards and dominant in the overlying conglomerates interval. The lower fine-grained turbidites constituting the glauconite-rich interval are interpreted to be a transgressive and/or stillstand hemicycle of the sequence Pr-Rup1 recorded in a deep-lake setting dominated by gravity-driven sedimentation. The top of the glauconite-sandstone interval is characterized by chaotically organized conglomerates with lacustrine/palustrine carbonate elements which are likely to be reworked from the lake margins (=intraformational), but also by the change of the provenance of the clastic material in the overlying interval. The occurrence of significant amounts of marginal lacustrine clasts reworked within profundal deposits suggests a long-duration subaerial exposition of the lake margins and their subsequent erosion and is therefore consistent with a significant lake regression associated with a major fall in lake level.

Although sedimentary processes are similar, the abundance of reworked marginal lacustrine carbonates (intraclasts) in this regressive cycle contrasts with the dominantly extraclastic flux (e.g., glauconite-rich sands) of the transgressive hemicycle of sequence Pr-Rup1. In the Gallician 9 well, the maximum transgression surface may be placed at the top of the glauconite sandstones interval (i.e., 2430 m depth) and records the maximum spread of extraclastic fine-grained gravity fluxes into the lake. In these gravity driven deposits, elemental ‘short-term’ to ‘very-short term’ sequences ranging from decimetres to metres in thickness can be identified and correspond to autocyclic processes.

Evaporites (FA1 facies association) are abundant in the overlying interval which constitutes the uppermost part of the Pr-Rup1 sequence and indicate the maximum of forced regression of the lake resulting from long-term negative inflow-evaporation balance. The top of the evaporites interval does not display evidence of subaerial exposure and the FA1 facies association has been shown to form in a perennial evaporative lake. The sequence boundary SB2 which corresponds to the top of the evaporites interval is therefore a maximum regression surface corresponding to the lowermost lake level prior to the water replenishment of the basin at the onset of the deposition of the overlying Rup 2 sequence.

Sequence Rup2: early Rupelian

Sequence Rup2 overlies the evaporites of the sequence Pr-Rup1 and the transgressive hemicycle is constituted of alternation of marlstones (FA2) and gravity-driven sandstones (FA3). In the Gallician 9 well, this hemicycle corresponds to the upper part of the papyraceous

marls interval and the entire calcarenites and calcisiltites interval (2233.4-2140m). FA2 becomes less frequent in the regressive hemicycle which is characterized by upward increase of frequency of the FA4 (F7), and FA6 (F12/F13) facies associations which constitute a thick interval that caps the sequence at the top. The regressive hemicycle therefore records the transition from deep lake conditions (FA2) to deltaic and littoral conditions (FA4) which are accompanied by the development of shallow ephemeral lake and floodplain conditions (FA6). The top of sequence Rup2 is therefore a sequence boundary (SB3) that records the filling of the lake system and subaerial exposure of the lake.

Sequence Rup3: early to middle Rupelian

Sequence Rup3 is defined between SB3 and the top of the Série Calcaire formation. In the Gallician 9 well, the lower part is made of alternation of FA4 and FA6 facies associations which may correspond to the transgressive hemicycle of the lake. This hemicycle is constituted of smale-scale sequences of filling of a shallow lake by reworked Mesozoic to Eocene carbonates supplied from the nearby catchment area. Toward the top of this hemicycle, offshore lake conditions are recorded by the frequent marlstones deposits (FA2) that corresponds to the maximum transgression surface. Regressive hemicycle corresponds to the vacuolar and asphaltic limestones formation made of alternation of deep lake (FA2) to deltaic and littoral conditions (F7, F8 and F9 facies) that evolve upwards to palustrine settings at the topmost part. Short-term sequences have been identified within this regressive hemicycle and consist mostly of metre to plurimetre thick lacustrine deltaic and littoral deposits capped by repeated subaerial exposure surfaces. An example of these subaerial exposure surfaces it that dated with U/Pb dating method on calcite which provided an absolute age of **31.27 +/- 1.90** Ma for the earliest filling of the microkarst cavities resulting from meteoric diagenesis (Semmani et al., *under review, see Chapter 4 in this PhD manuscript*).

The regressive hemicycle of sequence Rup3 is bounded at top by a long-term subaerial exposure surface (SB4) which is marked by dramatic changes in sedimentation patterns within the overlying Série Mixte and Série Rouge formations. The most significant change concerns the nature of the clastic supply origin where crystalline (metamorphic and igneous) sources are involved in the place of local Mesozoic to Eocene carbonate clastic supply.

Sequence Rup4: middle-late Rupelian to Early (?) Chattian

In the Gallician sector, this sequence corresponds to the Série Mixte and Série Rouge formations. At the base of the sequence, the Série Mixte formation is bounded by the major subaerial exposure surface SB4 which separates it from the underlying Série Calcaire formation. At top of the sequence, the overlying Série Rouge formation is bounded by the sequence boundary SB5 which separates it from the overlying Série Calcaréo-Salifère formation (**Fig. 5.12A-F**).

The base of sequence Rup4 (Série Mixte formation) is characterized by the repetitive occurrence of plurimetre-thick parasequences made of fluvial (FA5), floodplain (FA6) facies

associations and in less extent profundal lake facies association (FA2). The lower part of the Série Rouge formation is made of plurimetre-thick channel fill sequences (FA5 and FA6) while the upper part records mostly floodplain deposits (FA6). The Série Mixte formation records repetitive filling of a shallow lake while the Série Rouge indicates rather fluvial and floodplain settings, and the lack of palustrine carbonates is the unique distinguishing feature. In both formations, clastic deposits indicate feeding from the erosion of crystalline rocks. Laterally, the Série Mixte formation was not encountered in the Pierrefeu 1 well and this likely results from lateral variation of facies. However, the thick Série Rouge formation has been encountered in many wells accross the Vistrenque Basin and constitutes a correlatable unit. These considerations suggest that the two units should be grouped in the same depositional sequence.

The Série Mixte formation is interpreted to form the transgressive hemicycle of sequence Rup4, and the maximum transgression can be placed within the lacustrine interval (FA2) close to the formation top. The uppermost part of the Série Mixte formation together with the Série Rouge formation record the regressive hemicycle of sequence Rup4 with a return to dominant fluvial sedimentation. The fluvial 'short-term' sequences recorded in sequence Rup4 are autocyclic and lateral variations between wells are difficult to capture. The upper aggrading variegated marlstones interval (FA6) of sequence Rup4 record a regressive trend that is expressed by the development of a thick palaeosol.

U/Pb dating on calcite at the base of the Série Rouge formation provided an absolute age of **27.88+/-1.71** Ma (Semmani et al., *under review, see chapter 4 in this PhD manuscript*). SB5 is a major subaerial exposure surface that separates the floodplain deposits from the overlying lacustrine carbonates and evaporites of the Chattian to Aquitanian Série Calcaréo-Salifère formation. SB5 is a major stratigraphic surface in the Vistrenque Basin since it separates the floodplain deposits dominated 'Série Rouge' formation from the overlying thick lacustrine carbonates and evaporites of the 'Série Calcaréo-salifère' formation and correspond to the onset of the gulf of Lion rifting (Benedicto et al., 1996).

5.4.5.2. Vauvert 1 well

In a similar way to Gallician 9 well located 735 m to the southeast, the Série Grise (Série Calcaire *auct.*) formation is dominated in Vauvert 1 well by gravity-driven deep lacustrine carbonate-dominated terrigenous sedimentation. The stable isotope measurements revealed a major break in $\delta^{13}C$ and $\delta^{18}O$ signatures around the depth of 3020 m suggesting the onset of long-term negative inflow-evaporation balance and associated reduction of lake volume. This event coincides with the occurrence of conglomerate intervals of similar petrographic nature to those observed in Gallician 9 in the lower part of the Pr-Rup1 forced regressive hemicycle. Above this level and up to 2458m, the significant decrease of terrigenous content, coupled with the increasing upward trend in $\delta^{13}C$ and $\delta^{18}O$ (**Fig. 5.14A**) suggest an important reduction in water inflow and lake volume and therefore point to a correlation of the 2458 – 3020 m interval

from Vauvert 1 well with the Pr-Rup1 forced regressive hemicycle evidenced in the Gallician 9 well.

The interval 2458 – 2300 m made essentially of gravity driven and profundal lake deposits (FA2 and FA3 facies associations) reflects a transgression of the lake after the forced regression hemicycle. Sedimentation is dominated by deltaic and littoral lake and floodplain deposits (FA4 and FA6 facies associations) within the upper part of Série Mixte formation (2458 - 2056 m) and by fluvial and floodplain deposits (FA5 and FA6) within the Série Rouge formation (2056-1922 m). This upward transition toward the installation of a floodplain is indicative of an overall normal lake regression as evidenced in the Rup 2 to Rup 4 sequences previously described in Gallician 9 well. The scarcity of core data in the Série Mixte formation (2056 - 2458 m) in Vauvert 1 well prevents from the identification of the boundaries of sequences Rup 2, Rup 3 within this package: these sequences are here merged into a single lower-order transgressive-regressive sequence (**Fig. 5.12E, 5.14A**).

5.4.5.3. Pierrefeu 1 well

As in Gallician 9 and Vauvert 1 wells, the lower part of the Série Grise shows frequent gravity-driven deep lacustrine terrigenous sedimentation. Stable isotope signatures allowed to identify a major turnover in lake palaeohydrology between 4300 and 4070 m depths and the onset of long-term negative inflow-evaporation balance conditions which are persistent up to around 3525m. The significant reduction in terrigenous supplies within the 4300 m – 3525 m interval as evidenced by core observations and by a decrease in gamma-ray (**Fig. 5.14B**) and an increase in $CaCO_3$ content is consistent with a drastic decrease in water inflow and therefore with a long-term negative inflow-evaporation balance. This interval may therefore be considered to correlate with the forced regressive hemicycle of sequence Pr-Rup 1 described in the Gallician-9 section. The lower interval (4920-4300m) therefore corresponds to the transgressive hemicycle of sequence Pr-Rup 1.

Above this level, the interval 3525 – 2860 m (upper part of the Série Grise) is constituted of a monotonous succession of alternating gravity-driven deposits and profundal marls (FA2 and FA3 facies associations) and the overall decrease in $\delta^{13}C$ and $\delta^{18}O$ signals attributed to the long-term increase of connected volume of lake water indicate a transgressive trend (**Fig. 5.14B**). The sharp lithological change supported by Gamma Ray signal shift at the contact between the top of the Série Grise and the overlying Série Rouge formation and the lack of lateral equivalent of the Série Calcaire and Série Mixte formation described in Gallician 9 well strongly suggest a lack of these stratigraphic interval within the Pierrefeu 1. The Pierrefeu 1 may have intersected a fault thus the latter intervals are not encountered. Sequence Rup 2 may therefore have been truncated (**Fig. 5.14B**). Nevertheless, the long-term evolution of the sedimentation in the Pierrefeu sector is similar to that in the Gallician sector and the upward transition to the floodplain deposits of the Série Rouge formation suggest an overall normal regression of the

lake. As in Vauvert 1, sequences Rup2 to Rup4 have been merged into a single transgressive-regressive cycle (**Fig. 5.12F**, **5.14B**).

5.5. Discussion

5.5.1. Depositional models for the Paleogene lacustrine succession

The analysis of the vertical stacking pattern of the studied sedimentary succession (Série Rouge and underlying units) and the lateral relationships of the defined depositional facies associations within the correlatable sedimentary units enable to construct three depositional models that characterize the infill of the Vistrenque Basin during the Priabonian to early Chattian times (**Fig. 5.15**).

The Vistrenque Basin has recorded three depositional systems during the Priabonian to early Chattian times depending on tectonic, climatic, and hydrological setting: 1) profundal freshwater to oligohaline lake, 2) Perennial evaporative lake, and 3) shallow lake with extensive floodplain.

- ***Profundal freshwater to oligohaline lake: Fig. 5.15A***

FA2 and FA3 facies associations indicate profundal lake setting subjected to high clastic supply. Their dominance in transgressive/stillstand hemicycle and lowermost part of regressive hemicycle of sequence Pr-Rup1 and transgressive hemicycle of sequence Rup2 allows to reconstruct for these intervals a profundal lake depositional model and assess the clastic and water supplies, water salinity, topography, bedrock composition and tectonic setting.

The abundance of FA3 in these sequences indicates high clastic fluxes entering the lake system. Clastic fluxes are transported into the lake system by fluvial streams and therefore a significant riverine freshwater input enters the lake during the deposition of these gravity-driven deposits in the profundal areas. The deposition of cohesives debrites and turbidites in the lake slope and bottom accompanies hyperpycnal flows and the water input therefore results in lake transgression. Riverine inputs that feed the lake mostly drain igneous and metamorphic rocks from the southern Pyrenean reliefs and Mesozoic marine carbonates from the neighbouring of the lake. Such meteoric-derived river streams most likely consist of freshwater. However, oligo-mesohaline conditions in the northern margin of the Priabonian lake at Butte Iouton evidenced by Semmani et al. (2022, *see chapter 3 in this PhD manuscript*) strongly suggest contribution by saline water, albeit very diluted by riverine freshwater inputs, in the central and southern parts of the lake, particularly in Pierrefeu-Parrapon and Gallician sectors.

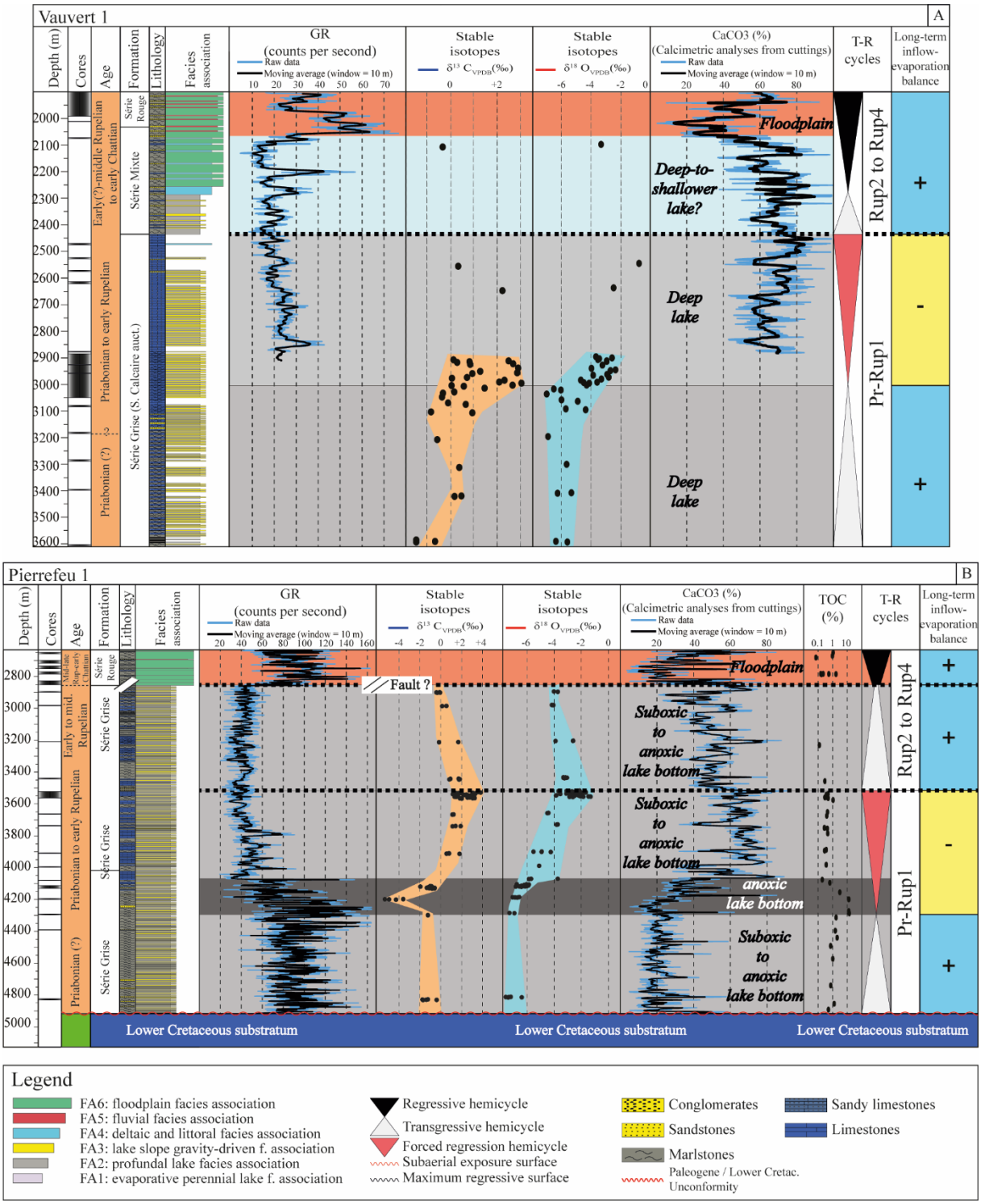

Figure 5.14 : Synthetic panel of vertical variations in $\delta^{18}O$, $\delta^{13}C$, $CaCO_3$ content, Gamma Ray signal, TOC (total organic carbon), and the interpreted lacustrine transgressive and regressive trends and long-term inflow-evaporation balance: A: Vauvert 1 well; B: Pierrefeu 1 well.

The high clastic fluxes entering the lake indicate important weathering, upstream, in the catchment area. In the lower units (Série grise) from the Gallician area, clasts nature (e.g., marine carbonates, glauconite mineral) suggests detrital feeding from the erosion of the Mesozoic cover that forms the bedrock of the catchment area. The monomictic nature of the

matrix-supported conglomerates suggests dominant clastic supply from the surroundings and indicates that far crystalline basement constitute a less dominant source for the feeding of clastic material. The Série Grise formation overlies unconformably the Mesozoic cover constituted at top by the Albian glauconite sandstones, and the Neocomian (Lower Cretaceous) and Jurassic marine carbonates which provide the mixed detrital material to the lake. Compared to the Gallician counterpart, sedimentation is dominated by fine grained deposits in the Pierrefeu sector which constitutes the distal area of the basin.

Moreover, the abundance of plant debris (leaves, stems) within the FA3 facies association suggests dense vegetation cover in the surroundings of the lake. Dense vegetation cover and high riverine inflows are consistent with relatively humid conditions. The lack of subaerial exposure features (e.g., perigranular cracks, root traces, dissolution cavities) within these units strongly suggests persistence of perennial lake conditions. In addition, the persistently very negative $\delta^{18}O$ values of carbonate matrix in the lower Série Grise formation (**Fig. 5.14**), close to those of calcite precipitated from meteoric waters within the neighbouring Priabonian Saint-Chaptes basin (Lettéron et al., 2018) support also significant freshwater supplies (riverine, groundwater and/or precipitation). The covariant trends between $\delta^{18}O$ and $\delta^{13}C$ are consistent with increased water residence times (**Fig. 5.13**).

On the other hand, FA2 facies association, especially the laminated argillaceous limestones and papyraceous marlstones (F2 facies) suggest lake stratification and deposition in deep poorly oxygenated lake bottom (Platt and Wright, 1991). Water stratification may result from a thermal or a density process. Stratification may be enhanced by the saline nature of the water and by seasonal evaporation of the surface waters (epilimnion). Deposition of marlstones and argillaceous limestones during low clastic supply periods suggests a tendency for hydrological lake closure. Organic matter preservation in the lake bottom is consistent with the water stratification, poor oxygenation of lake bottom, and perennial lake conditions.

The thicknesses of the transgressive and stillstand hemicycle (223m) and lower part of regressive hemicycle (145m) of sequence Pr-Rup1 and of the transgressive hemicycle (93 m) of sequence Rup2 in the reference section of Gallician 9 well are important and these thicknesses are found to be much more important in the Pierrefeu 1 well. Theses intervals are characterized by monotonous accumulation of interbedded gravity driven deposits with profundal marls without any evidence of subaerial exposure. This stacking pattern reflects persistence of deep lake conditions in the studied areas (Gallician and Pierrefeu sector). The persistence of deep lake conditions and steep lacustrine slope allowing deposition of hectometre scale turbidite stacks may result from the absence of a topographic sill in the lake system that would result in water outflow and/or from a high subsidence rate leading to continuous creation of accommodation space and keeping the studied area in profundal lake conditions during these time intervals.

Finally, these intervals from Sequences Pr-Rup 1 (transgressive/stillstand and lower regressive hemicycle) and Rup 2 (transgressive hemicycle) were formed within a freshwater to

oligohaline highly subsiding lake system comprising a slope break into the bottom and fed by high siliciclastic and carbonate detrital inputs from the southern Pyrenean reliefs and from the neighbouring highs of the catchment area within humid to semi-humid conditions (**Fig. 5.15A**).

- ***Perennial evaporative lake: Fig. 5.15A***

In Gallician 9 well, FA1 facies association is the dominant facies association within the upper part of the regressive hemicycle of Sequence Pr-Rup1 with FA2 and FA3 found in lesser extent. The alternation of anhydrite with organic-rich grey marlstones in the evaporative interval and the lack of subaerial exposure evidence allowed to interpret their formation within perennial evaporative lake conditions. Hypersaline conditions and arid climate are required to precipitate these evaporites (gypsum and anhydrite). Concentration of solutes into brine results in water stratification. Stratified waters are associated with poorly oxygenated bottom, and this is consistent with the preservation of organic matter in the anhydritic marls (F1 facies).

The lack of evaporites in the correlative levels from Vauvert 1 and Pierrefeu 1 suggests transient disconnection between lake waters from Gallician 9 area and those from deeper areas in the lake basin. This is consistent with a tectonic compartmentalization of the basin controlling the lake bottom topography and with the formation of a localized evaporative ponded areas developing on the hanging-wall of a tilted block. For instance, the compartmentalization between the Gallician and Pierrefeu sectors may likely be caused by the Gallician transfer zone that separates the Marsillargues and Vauvert compartments (**Fig. 5.2A**). The forced regression of the lake and the significant reduction of the clastic fluxes into the lake bottom strongly suggest a very negative inflow-evaporation balance. No direct information is available about the expression of the forced regression surface in the lake margins, but the occurrence of reworked ooids, of similar size, shape, and structures with those from the Priabonian northern lake margin (Butte Iouton, Semmani et al., 2022, *see chapter 3 in this PhD manuscript*) in the upper regressive hemicycle of sequence Pr-Rup1 reflects exposure and incision of the Priabonian to Rupelian lake margins during the early Rupelian forced regression.

The evaporative lake system in which the regressive hemicycle of sequence Pr-Rup1 formed is therefore a perennial, saline to hypersaline, profundal lake in arid to semi-arid climate conditions and subjected to reduced clastic gravity-driven flux and the depositional area of evaporites is plausibly disconnected from the main waterbody by strong topographic control (**Fig. 5.16**).

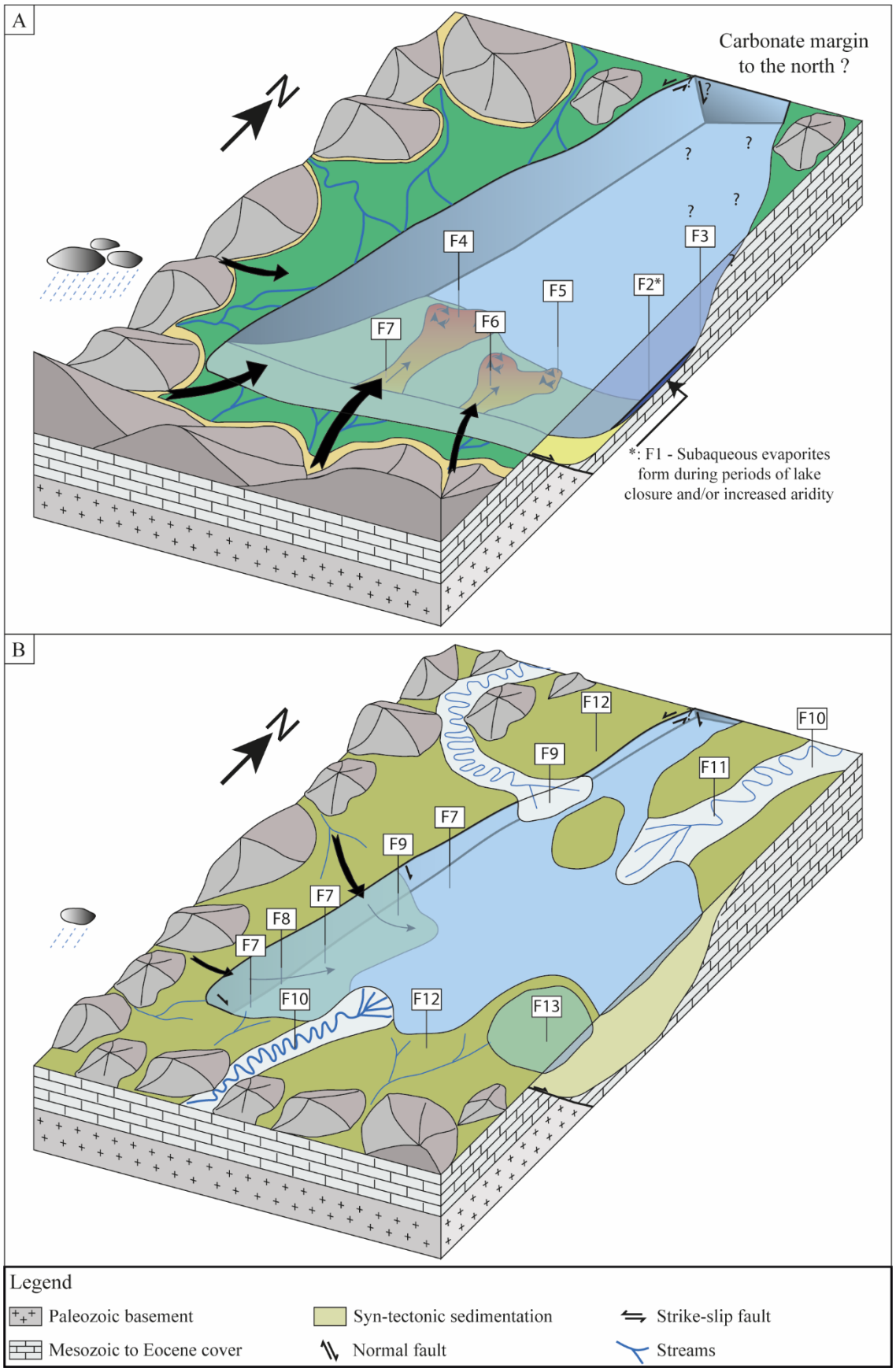

Figure 5.15: Simplified block diagrams showing the depositional models for A) Profundal perennial lake, and B) Shallow lake with extensive floodplain. Evaporites (F1 facies) formed within perennial lake conditions

precipitate in compartmentalized areas with maximum reduction of connection to the main saline waterbody (see Figure 5.16 for further details).

- ***Shallow lake with extensive floodplain: Fig. 5.15B***

In the regressive hemicycles of sequence Rup2, and the entire sequences Rup3 and Rup4, facies associations FA4, FA5 and FA6 are dominant and indicate lacustrine littoral delta, fluvial and floodplain settings (**Fig. 5.15B**). Profundal lake deposits such as organic-rich marls are rare and correspond to the maximal expansion of the lake. In contrast to the profundal lake system described previously, this lacustrine system is rapidly and repeatedly filled and exposed. These rapid fluctuations of the shoreline are evidenced by the frequent subaerial exposure surfaces and pedogenesis occurring at top of plurimetre-thick shallow lake sequences. The almost lack of gravity driven deposits (FA3) and dominance of marginal lacustrine facies (FA4) suggest a gentler basin topography. Moreover, the lack of laminated marlstones and the poor preservation of organic matter suggests a non-stratified water body, which is consistent with the shallow water conditions.

Pedogenic carbonates occur in semi-arid to semi-humid conditions. The presence of pseudomicrokarst features in the Série Calcaire and Série Mixte formations is indicative of intermediate climate conditions (Platt and Wright, 1992). The abundance of lacustrine detrital calcarenites in the top of Série Calcaire formation and the upward transition to floodplain deposits suggests progradation of a deltaic system into the lake. Deltaic progradation and infill of the lake system may have been promoted by slowing of subsidence.

In sequences Rup3 and Rup4, the dominant siliciclastic fluxes strongly suggest uplift and erosion of crystalline rocks. Crystalline basement that constitutes the continuation of the French-Spanish Pyrénées to the east covers large areas to the south of the Vistrenque Basin, in place of the present Gulf of Lion and therefore may have acted as a source of igneous and metamorphic clasts into the lake. Northern direction of clastic fluxes has also been documented in the Grès de Célas formation in the Alès and Saint-Chaptes basin (Lettéron et al., 2018; 2021). The increasingly important involvement of far crystalline sources compared to the nearby Mesozoic marine carbonates suggests low relief creation in the margins of the lake and therefore slowdown of the erosion of these rocks. Low topography creation, i.e., slow subsidence across the Vistrenque Basin allowed the progradation of far detrital fluxes into the lacustrine system. This is also consistent with the slowdown of accommodation space creation during the deposition of sequence Rup4 as evidenced by the widespread development of a floodplain across the Vistrenque Basin.

In conclusion, the sedimentary system of the deposition of the marginal lacustrine and fluvial to floodplain deposits of the regressive hemicycle of sequence Rup2 and sequences Rup3 and Rup4 consists of a shallow lake subjected to both carbonate and crystalline terrigenous fluxes under semi-arid to semi-humid conditions and undergoing frequent subaerial exposure (**Fig. 5.15B**). An analogue of a such mixed fluvio-lacustrine systems is known in the basal Cretaceous

from the Central northern Spain Rupelo formation of the Western Cameros Basin (Platt, 1989 in Platt and Wright, 1992) where abundant marlstones (calcareous claystones) of red and green colours are abundant in the alluvial setting and floodplain near a low energy gentle slope margin.

5.5.2. Tectonic and climatic controls on the Paleogene Vistrenque Basin infill

In the Vistrenque Basin, the present study shows a significant development of clastic gravity-driven sedimentation, especially in the southern part of the basin (Gallician sector). In the Pierrefeu sector, these deposits are more fine-grained, and this polarity trend suggests a dominant South-to-north direction of sedimentary fluxes. Detrital fluxes sourced from the south are documented in the neighbouring Sommières, Saint-Chaptes and Alès basins during the Priabonian (Rémy, 1985; Rémy and Fournier, 2003; Lettéron et al., 2018, 2021).

In contrast to these Languedoc siliciclastic fluxes, the almost monogenic character of the carbonate extraclasts in the lower part of the Vistrenque Paleogene infill suggests significant involvement of the Mesozoic cover from the surroundings of the basin in the supply of sedimentary fluxes to the depositional system. The nature of the sedimentary fluxes is consistent with the nature of the basin substratum revealed in the wells. The substratum is Lower Cretaceous in age to the North and the West, while the Lower Cretaceous cover is absent to the South and to the East in the Grau-du-Roi-Saintes-Maries-de-la-Mer and Albaron highs (**Fig. 5.2A**, **5.2C**). The lack of the Cretaceous cover suggests its erosion and reworking in these high areas immediately adjacent to the Gallician sector in the Vistrenque Basin.

The thick accumulation of gravity-driven deposits (hectometre scale units) during the Priabonian (?) and Lower Rupelian required both a strong subsidence to create the space for sedimentation and significant water inflows into the basin. The Vistrenque Basin is controlled by the Nîmes fault that acted as a sinistral strike-slip fault within the NNE-SSW trending Languedoc faut belt during the Priabonian (Séranne et al., 2021). Furthermore, only an important basin structuration resulting from high subsidence rates and the absence of an outlet sill of the system allow to maintain profundal lake conditions where sedimentation does not take pace with the accommodation. Very steeply subsiding topographies commonly characterize strike-slip lake basins (e.g., Platt and Wright, 1992, Smit et al., 2008) and this is consistent with the strike-slip motion of the Nîmes fault during Priabonian and lower Rupelian(?) times as mentioned above although normal fault motions would have occurred in relation to the Western European rift extension. This basin configuration allows to account for the hectometre-scale monotonous succession of alternating FA2/FA3 facies associations in the slope and deepest areas of the lake system (**Fig. 5.16**). Periods of important extensive tectonic activity have favoured creation of a strong topography following the uplift of the footwall in the surroundings and consequently their erosion favoured by enhanced precipitations that promote the development of coarse-grained gravity-driven fluxes (FA3). Conversely, periods

of low water inflows lead to a decrease in terrigenous inputs and therefore favour carbonate production in the lake (FA2 facies association). FA2 and FA3 are formed in the deeper parts of the lake, the lateral evolution of facies is difficult to quantify in terms of changes in the depth of the depositional area.

A striking aspect of the Vistrenque Basin lake evolution is the development of deep gravity facies since the earliest stage of the sedimentation, as suggested by the turbidites of the base of the Série Grise in Pierrefeu 1, overlying the Mesozoic basement. This suggests that a deep topographic depression was already existing prior to its infill by water and prior lacustrine sedimentation. During the Priabonian to earliest Rupelian transgression/stillstand, some marginal areas of the Vistrenque Basin (at least around Butte Iouton to the North and Puech du Teil to the West: Semmani et al., *2022*, *see chapter 3 in this PhD manuscript*) were occupied by a shallow water lake margin with carbonate sedimentation showing high-frequency cycles of transgression and forced regression which suggest the occurrence of short episodes of negative inflow-evaporation balance in a period of mainly sub-humid climate. Finally, the high terrigenous fluxes, the persistence of a perennial deep-lake setting as well as the stable isotope signatures of deep-lake carbonates strongly suggest a relatively humid climate setting during the late Priabonian(?) and earliest Rupelian in the Vistrenque Basin (**Fig. 5.17**). This is consistent with palaeoclimatic reconstructions from sedimentologic and palaeobotanic data of the late Priabonian in the Alès and Saint-Chaptes basins (Tanrattana et al., 2020; Lettéron et al., 2021; Semmani et al., *under review, see chapter 4 in this PhD manuscript*).

The onset of the forced regressive hemicycle identified from the depositional and stable isotope records in Gallician 9, Vauvert 1 and Pierrefeu 1 wells is situated around 100 m above the occurrence of a pollinic association characterizing the Priabonian-Rupelian climatic deterioration in Vauvert 1 (3200m), and around 100 m above another pollinic association, earliest Rupelian in age, in Gallician 9 (2530m). The latter reflects a stage of major aridification during the earliest Rupelian times (Semmani et al., *under review, see chapter 4 in this PhD manuscript*). The present dataset suggests therefore that the Eocene-Oligocene transition (EOT) and the earliest Rupelian aridification evidenced from pollens held just prior to the effective reduction in lake volume and lacustrine forced regression. In Pierrefeu 1 well, located in the most subsiding profundal area of the lake, the stage of lacustrine forced regression starts with the deposition of organic-rich horizons (TOC>10%) associated with ^{13}C depleted isotope composition which suggests sulphate-reduction processes (**Fig. 5.12F**, **5.13A**, **5.14B**). Sulphate reduction processes are linked to enhanced water stratification likely resulting from increased salinity (e.g., Sonnenfeld, 1985). Vauvert 1 and Gallician 9 did not record such organic-matter enrichment and sulphate-reduction processes because of their shallower depositional settings and of prevailing more oxygenated waters. In Pierrefeu 1 well, the decrease in organic matter concentrations in lake bottom sediments in the later stages of forced regression is likely to be related to the decrease in terrestrial organic matter into the lake consequent to the continental aridification and the reduction of vegetation cover in the catchment area.

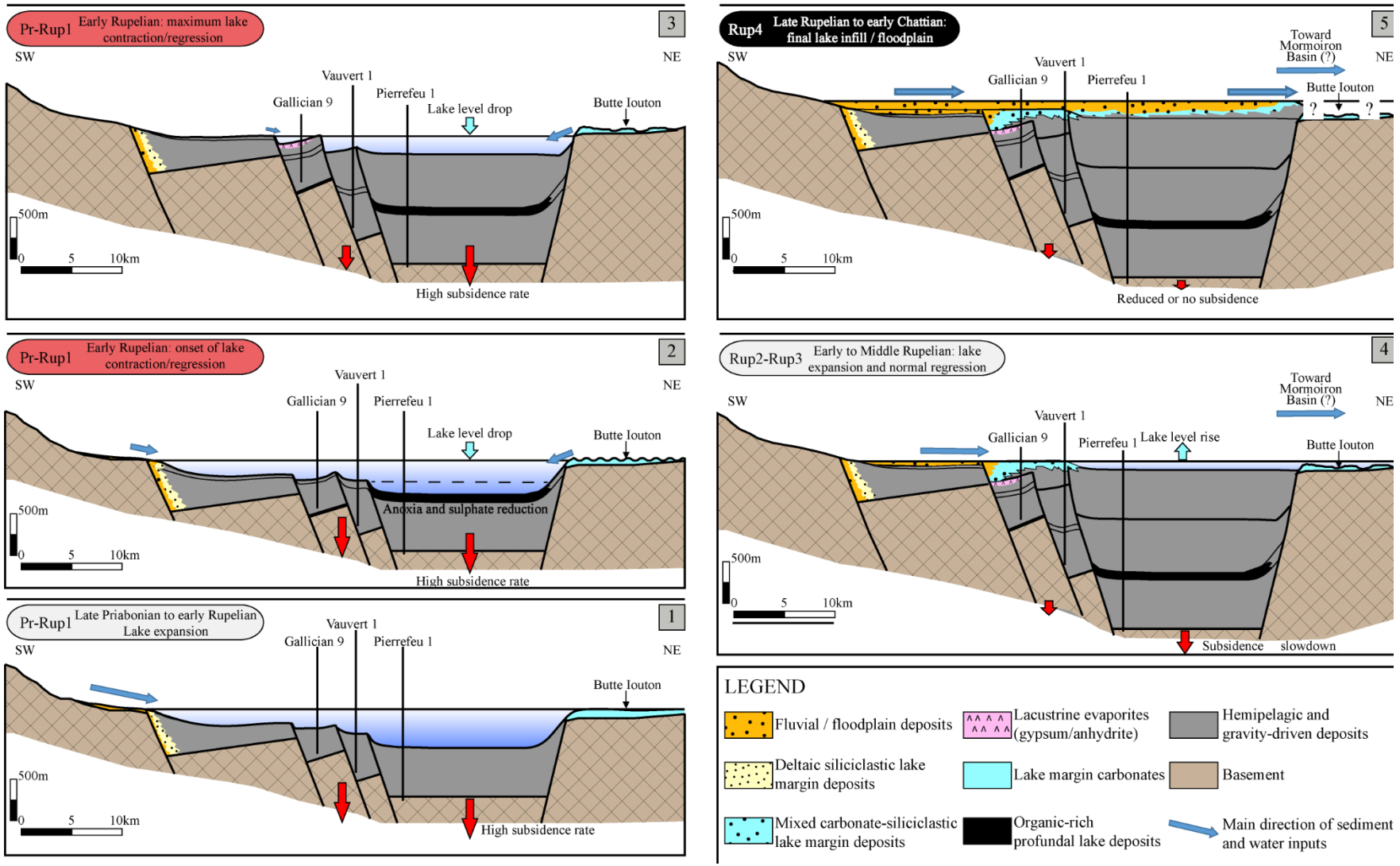

Figure 5.16: Conceptual model of the sedimentary infill of the Vistrenque lacustrine system from the Priabonian (?) to early Chattian as a function of palaeohydrological and tectonic setting. Sequences Pr-Rup1, Rup2, Rup3 and Rup4 are defined from the Gallician 9 well reference section.

The occurrence of evaporites in Gallician 9 and their absence in the more profundal settings of the Vauvert 1 and Pierrefeu 1 areas suggest transient disconnection of the depositional area of Gallician 9 from the main water body during the maximum of lake regression (**Fig. 5.16**). The combination of available palynological data, the depositional features identified in the studied wells and the chronostratigraphic constrains strongly suggest that a significant reduction of lake volume occurred during the early Rupelian and is associated with a stage of major aridification. Even though most studies regarding palaeoclimatic changes in European terrestrial environments during the EOT have shown a significant decrease in mean annual temperature around the Priabonian-Rupelian boundary (Mosbrugger et al., 2005; Erdei et al., 2012; Hren et al., 2013; Tanrattana et al., 2020), evidence for drastic changes in precipitations at a large geographic scale remain unclear. However, a southward gradient of drier conditions has been evidenced for Oligocene period from vegetation studies (Utescher et al., 2020). The present dataset represents therefore a robust, multiproxy evidence of aridification in terrestrial environment in Southeast France during the early Rupelian following the EOT transition. The link between global cooling and regional terrestrial aridification is not straightforward and requires detailed palaeo-relief and wind reconstructions to be established. However, the available palaeogeographic reconstructions for southeast France during the Paleogene (Joseph and Lomas, 2004; Semmani et al. *under review, see chapter 4 in this PhD manuscript*) suggest that decrease in lake volume during the early Rupelian results from decreased precipitations associated with global oceanic cooling and decreased regional moisture around the western Alpine Sea.

Gravity sedimentation in lakes downstream of an important hydrographic network carries significant water fluxes during the humid periods. The transgression of the lake system and its connection with neighbouring saline water bodies followed by an arid period explains the formation of the lacustrine basin evaporites. Compared to other continental basins in the Western European Rift system (e.g., Valence Basin, Bresse Basin, Upper Rhine Graben and in less extent the Manosque Basin; Rouchy, 1997) where evaporites records are significant during the Rupelian, evaporites are scarce in the southern part of the rift system constituted by the Camargue area and are limited to the early Rupelian stage of global cooling and associated continental aridification.

The overlying sequence Rup2 marks the end of evaporitic conditions in Gallician 9 well and a return to a terrigenous-rich, gravity driven sedimentation and to a long-term positive inflow-evaporation balance. Such an inversion in palaeohydrological balance is interpreted to be related to a potential continental humidification following the brief stage of cooling that occurred during the earliest Rupelian times (Westerhold et al., 2020) (**Fig. 5.17**).

The occurrence of deep-water gravity-driven sediments become less frequent toward the top of Rup2 sequence in Gallician 9 and shallow, marginal lacustrine sedimentation dominates in sequence Rup3 while sequence Rup4 is characterized by the development of floodplain environments in the studied wells from the Vistrenque Basin that intersect the Série Rouge and

Série Mixte formation (Gallician 1, 3, 7, 9, Vauvert 1, and Pierrefeu 1). Since the palaeohydrological balance remains positive during the middle to late Rupelian interval, such a palaeoenvironmental vertical evolution may suggest either an increase in terrigenous supplies or a decrease in subsidence rates. The latter interpretation is more likely since the vertical disappearance of gravity-driven sediments could be related to gentle basin topography following a slowing down of subsidence and fault activity. In addition, an increase in terrigenous supplies is unlikely since the southern Pyrenean reliefs which are believed to have sourced a large proportion of the sediment were probably less elevated during the Mid-late Rupelian compared to the late Priabonian to early late Rupelian. This elevation decrease is consistent with the collapse of this Pyrenean segment that started as early as the Priabonian south to the Languedoc area (Séranne et al., 2021). Moreover, available reconstructions of terrestrial precipitations (e.g., Tanrattana et al., 2020) suggest that the Mid-late Rupelian climate was not as humid as during the Priabonian.

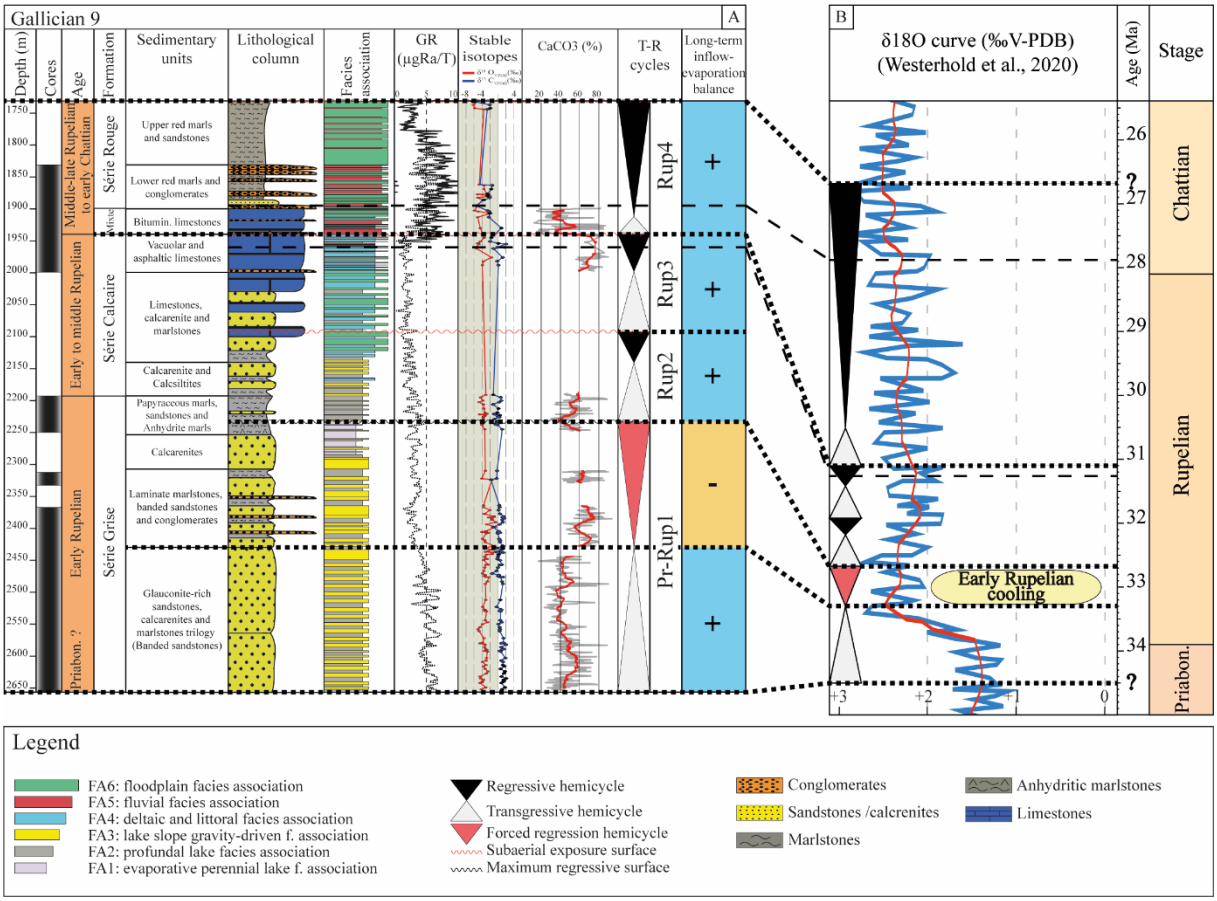

Figure 5.17: A) Reference section of Gallician 9 well showing the dominant depositional facies associations (FA), variations in $\delta^{13}C$ and $\delta^{18}O$ of bulk rock carbonates, $CaCO_3$ content, transgressive-regressive (T-R) cycles, and palaeohydrological cycles, correlated with B) benthic foraminiferal oxygen isotope curve (smoothed curve over 20ka in blue, smoothed curve over 1Ma in red; after Westerhold et al., 2020).

The Série Mixte and Série Rouge formations are characterised by metre-scale parasequences deposited in shallow lake to fluvial settings and suggest gentle lacustrine topography and

shallow waters. The widespread development of floodplain setting across the Vistrenque Basin is coherent with a stage of tectonic quiescence related to the cease of strike-slip motions of the Nîmes fault associated with the end of the Pyrenean compression (Séranne et al., 2021). Furthermore, this tectonic reconfiguration is consistent with the changes in the levels of the equilibrium profiles of the valleys on a 10-to-100-kilometre scale resulting in the involvement of crystalline sedimentary fluxes from distant sources, potentially the Pyrenean segment collapsed in the Gulf of Lion margin. Similar slowly subsiding shallow lake systems have been described as foreland basins in the Paleogene of Ebro Basin (Spain) at the front of the Pyrenean range by Platt and Wright (1992).

Finally, the overall shallowing upward trend recorded in sequences Rup2 to Rup4 combined with the upward decreasing trend in $\delta^{18}O$ and $\delta^{13}O$ which is indicative of long-term positive inflow-evaporation balance and therefore of an increase in connected lake volume, suggests that the Vistrenque Basin was likely connected to a neighbouring waterbody, and that the terminal fluvial plain system probably flowed into another lake located further north (Mormoiron and/or Apt-Manosque-Forcalquier basins).

5.6. Conclusion

Sedimentological and stratigraphic analysis of the Paleogene succession from the Vistrenque Basin (Camargue area) integrating carbon and oxygen isotope measurements on lacustrine carbonates and total organic carbon (TOC) data allowed to document a case of the record of changes in climate and tectonic setting around the Eocene-Oligocene transition in a continental basin from Southwestern Europe.

- Four depositional sequences (Pr-Rup1 to Rup4) have been defined within the Priabonian (?) to Early Chattian infill of the Vistrenque Basin. To account for the several hectometres thick stack of turbidites in the depocentre of the Vistrenque Basin, the sedimentary system consisted of a highly subsiding profundal freshwater to oligohaline lake which was fed with significant clastic fluxes and riverine inflows during the transgressive hemicycles of sequences Pr-Rup1 and Rup2 where the lake waterbody has recorded its maximum expansion.

- Local deposition of evaporites within the Vistrenque Basin during the Early Rupelian provides further evidence for the continental record of the brief aridification phase inferred from previous palynological studies. These evaporites occur at the top of the forced regressive stage of sequence Pr-Rup1 which is defined by the vertical evolution of facies and confirmed by a long-term increase in both $\delta^{18}O$ and $\delta^{13}O$ signatures of lacustrine carbonate matrices. Such a forced regression trend has been identified and correlated between three wells located in distinct tectonic blocks and is interpreted to result from a decrease in lake volume in response to decreased precipitations associated with global oceanic cooling and decreased regional moisture around the western Alpine Sea. This brief Early Rupelian continental aridification

stage is followed by a return to more humid conditions during the deposition of the transgressive hemicycle of sequence Rup2 from the Early-Middle Rupelian as indicated by an increase in terrigenous inputs resulting into the desalinization of the lake and long-term decrease of both $\delta^{18}O$ and $\delta^{13}O$ signatures.

- The regressive hemicycle of Sequence Rup2 and the following sequences Rup3 and Rup4 record an upward transition from deep-lacustrine lake settings to a gently steeping shallow lake characterized by important marginal lacustrine and palustrine environments and by an upward increase of floodplain and fluvial deposits reflecting an overall regressive trend of the lake system between the Early-Middle Rupelian and Early Chattian times.

- The thick succession (up to 2000 m) of Priabonian (?) to Early-Middle Rupelian deep-lacustrine gravity-driven deposits reflects sedimentation in a highly subsiding basin during a stage of strike-slip and transtension motions of the Nîmes fault. The overall regressive character of the marginal lacustrine and floodplain deposits within the upper part of the Paleogene Vistrenque basin infill corresponds to the stage of significant decrease in subsidence rates and reduced activity of the Nîmes fault. This period of tectonic quiescence in the Camargue area preceded the Chattian to Aquitanian extensional motions of the Nîmes fault related to the Gulf of Lion rifting.

5.7. Acknowledgements

This work was funded by the France's Ministry of Higher Education and Research and is part of the PhD of the first author (NS). This work also benefited from the financial supports of CEREGE (APIC 2018 RRH) and Carb3E TotalEnergies-AMIDEX Chair and we thank them profoundly for their support. We would like to thank TotalEnergies for providing in-house documents as a part of the data sharing agreement (Contract of cooperation and data exchange TotalEnergies - Aix-Marseille University FR00040451). The authors would also thank Gilles Graffin (STC core library, Boussens) who gave access to cores from the Camargue wells. The authors are grateful to Christophe Nussbaumer (TotalEnergies) for his review of the manuscript and for his suggestions and comments.

5.8. Supplementary data

Table S5.1: Carbon and oxygen isotopes ratios of the samples from Gallician 9, Vauvert 1 and Pierrefeu 1 wells, KB: kelly bushing (zero reference for driller's depth measurements).

Well	Lithostratigraphic unit	Core	Depth (m below KB)	$\delta^{13}C$ (‰ V-PDB)	$\delta^{18}O$ (‰ V-PDB)
Gallician 9	Série Mixte	K8	1902,6	-2,66	-5,92
Gallician 9	Série Mixte	K8	1904	-2,20	-4,98
Gallician 9	Série Mixte	K8	1907	-2,15	-1,81
Gallician 9	Série Mixte	K9	1913	-2,33	-5,09
Gallician 9	Série Calcaire	K12	1945	-1,70	-3,46
Gallician 9	Série Calcaire	K12	1951	-2,03	-4,42
Gallician 9	Série Calcaire	K13	1954	0,11	-4,94
Gallician 9	Série Calcaire	K13	1954	0,01	-5,11
Gallician 9	Série Calcaire	K13	1955	2,03	-4,79
Gallician 9	Série Calcaire	K13	1959,8	-0,13	-5,44
Gallician 9	Série Calcaire	K13	1960,1	1,75	-5,28
Gallician 9	Série Calcaire	K13	1960,1	1,55	-5,67
Gallician 9	Série Calcaire	K13	1962	-1,18	-5,38
Gallician 9	Série Calcaire	K14	1976	1,15	-1,64
Gallician 9	Série Calcaire	K15	1982	-0,24	-3,66
Gallician 9	Série Calcaire	K15	1988	0,07	-3,93
Gallician 9	Série Grise	K16	2191	-1,21	-3,06
Gallician 9	Série Grise	K16	2195	0,66	-4,40
Gallician 9	Série Grise	K17	2200	0,77	-3,80
Gallician 9	Série Grise	K17	2202,5	0,28	-4,74
Gallician 9	Série Grise	K18	2206	-1,26	-3,65
Gallician 9	Série Grise	K18	2212,5	0,08	-3,54
Gallician 9	Série Grise	K18	2219	-0,20	-3,29
Gallician 9	Série Grise	K19	2220,9	-1,06	-2,75
Gallician 9	Série Grise	K19	2221,6	-0,75	-4,59
Gallician 9	Série Grise	K19	2222,7	0,41	-3,26
Gallician 9	Série Grise	K19	2224	0,31	-3,32
Gallician 9	Série Grise	K19	2225	-0,04	-3,65
Gallician 9	Série Grise	K19	2226,1	0,32	-3,69
Gallician 9	Série Grise	K19	2229	-0,89	-3,70
Gallician 9	Série Grise	K20	2233,3	-0,37	-3,90
Gallician 9	Série Grise	K20	2237,3	-0,63	-3,99
Gallician 9	Série Grise	K20	2237,9	-0,19	-4,04
Gallician 9	Série Grise	K21	2245	1,03	-3,31
Gallician 9	Série Grise	K22	2310	-0,28	-3,18
Gallician 9	Série Grise	K23	2322	-0,39	-4,05
Gallician 9	Série Grise	K23	2324	-1,80	-1,54
Gallician 9	Série Grise	K24	2364	0,30	-3,64
Gallician 9	Série Grise	K24	2367	0,38	-3,62
Gallician 9	Série Grise	K24	2371,4	0,08	-2,03
Gallician 9	Série Grise	K24	2377,4	0,46	-3,42
Gallician 9	Série Grise	K24	2381,5	1,38	-0,93
Gallician 9	Série Grise	K25	2382	1,23	-0,97

Gallician 9	Série Grise	K25	2383	1,08	-2,35
Gallician 9	Série Grise	K25	2384,5	1,43	-1,54
Gallician 9	Série Grise	K26	2386,6	1,04	-1,45
Gallician 9	Série Grise	K26	2390,4	1,15	-0,54
Gallician 9	Série Grise	K26	2393,8	0,35	-2,85
Gallician 9	Série Grise	K26	2398	-1,23	-0,64
Gallician 9	Série Grise	K27	2404,7	0,17	-3,24
Gallician 9	Série Grise	K27	2405	0,27	-2,91
Gallician 9	Série Grise	K27	2406	-0,05	-4,04
Gallician 9	Série Grise	K27	2407	0,49	-2,37
Gallician 9	Série Grise	K27	2408	-0,08	-2,93
Gallician 9	Série Grise	K28	2416,6	0,28	-3,89
Gallician 9	Série Grise	K28	2418,7	0,48	-3,34
Gallician 9	Série Grise	K28	2421,6	0,47	-3,25
Gallician 9	Série Grise	K28	2427,4	1,19	-1,04
Gallician 9	Série Grise	K29	2431	-0,28	-3,35
Gallician 9	Série Grise	K29	2433,4	0,85	-1,21
Gallician 9	Série Grise	K29	2435,3	0,51	-2,36
Gallician 9	Série Grise	K29	2436,8	-0,53	-3,21
Gallician 9	Série Grise	K29	2438	1,30	-1,36
Gallician 9	Série Grise	K29	2440	0,27	-1,44
Gallician 9	Série Grise	K30	2441,3	0,07	-2,92
Gallician 9	Série Grise	K30	2444,5	0,00	-3,34
Gallician 9	Série Grise	K31	2448	-0,19	-2,70
Gallician 9	Série Grise	K31	2448	-0,15	-3,27
Gallician 9	Série Grise	K32	2450	0,47	-3,56
Gallician 9	Série Grise	K33	2456,9	0,95	-2,44
Gallician 9	Série Grise	K33	2457,2	0,37	-3,09
Gallician 9	Série Grise	K33	2461,5	-0,05	-3,35
Gallician 9	Série Grise	K33	2466,6	-0,38	-3,57
Gallician 9	Série Grise	K33	2470,7	-1,53	-3,90
Gallician 9	Série Grise	K34	2473,2	0,23	-3,17
Gallician 9	Série Grise	K34	2474,8	0,00	-3,46
Gallician 9	Série Grise	K34	2476,2	1,25	-3,02
Gallician 9	Série Grise	K34	2476,5	0,64	-2,30
Gallician 9	Série Grise	K34	2483,35	0,98	-2,68
Gallician 9	Série Grise	K35	2486,9	1,18	-3,16
Gallician 9	Série Grise	K37	2512	0,55	-3,09
Gallician 9	Série Grise	K39	2523	-0,37	-3,82
Gallician 9	Série Grise	K39	2527	0,72	-3,45
Gallician 9	Série Grise	K39	2528	0,77	-3,14
Gallician 9	Série Grise	K39	2529,5	0,36	-3,32
Gallician 9	Série Grise	K39	2530	0,62	-2,87
Gallician 9	Série Grise	K40	2544	0,55	-3,23
Gallician 9	Série Grise	K41	2547	0,90	-2,63
Gallician 9	Série Grise	K41	2550	0,07	-3,83
Gallician 9	Série Grise	K42	2555	0,39	-4,53
Gallician 9	Série Grise	K43	2558	0,46	-5,02
Gallician 9	Série Grise	K44	2561	0,36	-4,76
Gallician 9	Série Grise	K43	2572	1,37	-3,51

Gallician 9	Série Grise	K44	2579	1,31	-3,84
Gallician 9	Série Grise	K44	2580	0,77	-4,52
Gallician 9	Série Grise	K45	2582	1,97	-3,25
Gallician 9	Série Grise	K45	2586	0,76	-3,37
Gallician 9	Série Grise	K45	2589	1,43	-3,09
Gallician 9	Série Grise	K45	2590	0,97	-2,79
Gallician 9	Série Grise	K45	2592	0,35	-3,41
Gallician 9	Série Grise	K45	2593	0,65	-2,67
Gallician 9	Série Grise	K46	2603	1,81	-2,88
Gallician 9	Série Grise	K46	2607	0,76	-2,98
Gallician 9	Série Grise	K46	2609	1,23	-3,91
Gallician 9	Série Grise	K46	2614	1,20	-3,04
Gallician 9	Série Grise	K46	2616	1,54	-3,67
Gallician 9	Série Grise	K47	2620	0,62	-3,24
Gallician 9	Série Grise	K47	2624	1,74	-2,54
Gallician 9	Série Grise	K47	2627	1,44	-2,92
Gallician 9	Série Grise	K47	2632	0,82	-4,50
Gallician 9	Série Grise	K48	2635	2,05	-4,38
Gallician 9	Série Grise	K48	2637	1,38	-3,67
Gallician 9	Série Grise	K48	2639	1,40	-3,89
Gallician 9	Série Grise	K48	2641	1,12	-3,99
Gallician 9	Série Grise	K48	2642	0,82	-4,51
Gallician 9	Série Grise	K49	2649	1,72	-3,07
Gallician 9	Série Grise	K49	2652	1,00	-4,18
Pierrefeu 1	Série Grise	K15	2900	-0,10	-3,72
Pierrefeu 1	Série Grise	K15	2901	-0,41	-4,02
Pierrefeu 1	Série Grise	K15	2902	-0,07	-3,88
Pierrefeu 1	Série Grise	K15	2903	-0,34	-3,73
Pierrefeu 1	Série Grise	K16	2986	0,54	-4,17
Pierrefeu 1	Série Grise	K16	2987	0,14	-4,05
Pierrefeu 1	Série Grise	K17	3212	1,68	-2,62
Pierrefeu 1	Série Grise	K17	3213	-0,16	-3,90
Pierrefeu 1	Série Grise	K18	3442	1,71	-3,33
Pierrefeu 1	Série Grise	K18	3443	0,92	-3,17
Pierrefeu 1	Série Grise	K18	3444	1,73	-3,06
Pierrefeu 1	Série Grise	K18	3445	1,83	-3,32
Pierrefeu 1	Série Grise	K18	3446	0,83	-3,18
Pierrefeu 1	Série Grise	K18	3447	1,75	-3,25
Pierrefeu 1	Série Grise	K19	3525	3,66	-2,13
Pierrefeu 1	Série Grise	K19	3526	3,48	-2,29
Pierrefeu 1	Série Grise	K19	3527	1,34	-3,10
Pierrefeu 1	Série Grise	K19	3529	1,25	-2,98
Pierrefeu 1	Série Grise	K19	3530	3,06	-2,69
Pierrefeu 1	Série Grise	K19	3531	1,73	-2,97
Pierrefeu 1	Série Grise	K19	3532	1,46	-2,99
Pierrefeu 1	Série Grise	K19	3533	1,99	-2,34
Pierrefeu 1	Série Grise	K19	3534	2,00	-2,57
Pierrefeu 1	Série Grise	K19	3535	3,21	-1,66
Pierrefeu 1	Série Grise	K19	3536	3,13	-2,04
Pierrefeu 1	Série Grise	K19	3537	3,29	-1,67

Pierrefeu 1	Série Grise	K19	3538	3,24	-1,88
Pierrefeu 1	Série Grise	K19	3539	1,16	-2,95
Pierrefeu 1	Série Grise	K19	3540	1,28	-2,86
Pierrefeu 1	Série Grise	K19	3541	1,32	-2,88
Pierrefeu 1	Série Grise	K19	3542	2,44	-2,05
Pierrefeu 1	Série Grise	K20	3543	2,18	-2,82
Pierrefeu 1	Série Grise	K20	3544	2,31	-3,11
Pierrefeu 1	Série Grise	K20	3545	2,91	-2,09
Pierrefeu 1	Série Grise	K20	3546	2,61	-2,71
Pierrefeu 1	Série Grise	K20	3547	1,64	-3,55
Pierrefeu 1	Série Grise	K20	3548	3,02	-2,07
Pierrefeu 1	Série Grise	K20	3549	2,75	-2,18
Pierrefeu 1	Série Grise	K20	3551	2,60	-2,35
Pierrefeu 1	Série Grise	K20	3552	3,08	-2,50
Pierrefeu 1	Série Grise	K20	3553	3,01	-2,26
Pierrefeu 1	Série Grise	K20	3554	2,98	-2,17
Pierrefeu 1	Série Grise	K21	3555	1,33	-3,84
Pierrefeu 1	Série Grise	K21	3556	1,47	-3,87
Pierrefeu 1	Série Grise	K21	3557	2,86	-2,18
Pierrefeu 1	Série Grise	K21	3558	2,59	-2,50
Pierrefeu 1	Série Grise	K21	3559	2,79	-2,07
Pierrefeu 1	Série Grise	K21	3560	2,57	-2,09
Pierrefeu 1	Série Grise	K21	3561	3,05	-1,87
Pierrefeu 1	Série Grise	K21	3562	3,22	-1,47
Pierrefeu 1	Série Grise	K21	3563	3,26	-1,32
Pierrefeu 1	Série Grise	K21	3564	3,06	-1,85
Pierrefeu 1	Série Grise	K21	3565	1,84	-2,87
Pierrefeu 1	Série Grise	K21	3566	2,02	-2,63
Pierrefeu 1	Série Grise	K22	3666	1,23	-4,43
Pierrefeu 1	Série Grise	K22	3667	1,12	-4,51
Pierrefeu 1	Série Grise	K23	3738	1,42	-3,74
Pierrefeu 1	Série Grise	K23	3739	1,91	-3,82
Pierrefeu 1	Série Grise	K23	3740	1,13	-3,82
Pierrefeu 1	Série Grise	K24	3909	0,79	-4,92
Pierrefeu 1	Série Grise	K24	3910	0,81	-5,53
Pierrefeu 1	Série Grise	K24	3911	0,56	-4,94
Pierrefeu 1	Série Grise	K24	3912	1,80	-4,26
Pierrefeu 1	Série Grise	K25	3999	0,59	-5,12
Pierrefeu 1	Série Grise	K26	4080	-0,62	-3,71
Pierrefeu 1	Série Grise	K26	4081	-1,52	-5,71
Pierrefeu 1	Série Grise	K26	4082	-1,32	-5,87
Pierrefeu 1	Série Grise	K27	4115	-1,02	-6,76
Pierrefeu 1	Série Grise	K27	4116	-0,88	-6,06
Pierrefeu 1	Série Grise	K27	4120	-1,15	-6,21
Pierrefeu 1	Série Grise	K27	4121	-0,96	-6,14
Pierrefeu 1	Série Grise	K27	4126	-0,59	-6,19
Pierrefeu 1	Série Grise	K27	4127	-0,79	-6,23
Pierrefeu 1	Série Grise	K27	4128	-1,09	-6,14
Pierrefeu 1	Série Grise	K27	4129	-0,81	-6,56
Pierrefeu 1	Série Grise	K27	4130	-0,60	-6,85

Pierrefeu 1	Série Grise	K28	4196	-3,59	-6,58
Pierrefeu 1	Série Grise	K28	4197	-5,36	-7,08
Pierrefeu 1	Série Grise	K28	4198	-4,95	-6,90
Pierrefeu 1	Série Grise	K28	4199	-4,29	-6,73
Pierrefeu 1	Série Grise	K29	4296	-1,23	-7,31
Pierrefeu 1	Série Grise	K29	4297	-1,23	-6,94
Pierrefeu 1	Série Grise	K30	4824	-1,23	-7,21
Pierrefeu 1	Série Grise	K30	4825	-1,76	-7,59
Pierrefeu 1	Série Grise	K30	4826	-1,38	-7,37
Pierrefeu 1	Série Grise	K30	4827	-0,39	-6,40
Pierrefeu 1	Série Grise	K30	4828	-1,70	-7,40
Pierrefeu 1	Série Grise	K31	5012	0,91	-5,13
Pierrefeu 1	Série Grise	K31	5014	1,18	-4,88
Vauvert 1	Série Mixte	K32	2100	-0,37	-3,33
Vauvert 1	Série Grise	34	2548	0,31	-0,79
Vauvert 1	Série Grise	36	2640	2,23	-2,49
Vauvert 1	Série Grise	37	2899,5	0,10	-3,67
Vauvert 1	Série Grise	38	2904	2,50	-2,59
Vauvert 1	Série Grise	39	2906,8	0,80	-3,45
Vauvert 1	Série Grise	40	2910	0,27	-3,54
Vauvert 1	Série Grise	41	2915	2,70	-2,95
Vauvert 1	Série Grise	42	2916,85	0,83	-2,95
Vauvert 1	Série Grise	43	2931,1	2,91	-3,24
Vauvert 1	Série Grise	44	2943,2	1,27	-3,97
Vauvert 1	Série Grise	45	2949	2,87	-2,36
Vauvert 1	Série Grise	46	2951,75	0,92	-2,70
Vauvert 1	Série Grise	47	2966	0,69	-2,92
Vauvert 1	Série Grise	48	2969,02	0,04	-3,86
Vauvert 1	Série Grise	49	2976,9	2,32	-2,81
Vauvert 1	Série Grise	49	2983,66	2,09	-3,31
Vauvert 1	Série Grise	50	2987,8	3,05	-4,68
Vauvert 1	Série Grise	50	2995,25	2,67	-3,59
Vauvert 1	Série Grise	51	2996,5	0,02	-4,49
Vauvert 1	Série Grise	52	2999,3	0,55	-4,12
Vauvert 1	Série Grise	52	3006,6	1,45	-4,30
Vauvert 1	Série Grise	53	3020,78	0,14	-6,48
Vauvert 1	Série Grise	54	3024,97	-0,35	-6,01
Vauvert 1	Série Grise	55	3040	-0,40	-6,96
Vauvert 1	Série Grise	57	3061,7	-0,13	-5,97
Vauvert 1	Série Grise	57	3067,43	0,64	-4,89
Vauvert 1	Série Grise	58	3095,69	-0,87	-5,68
Vauvert 1	Série Grise	58	3099,2	0,92	-4,36
Vauvert 1	Série Grise	59	3200	-0,60	-6,87
Vauvert 1	Série Grise	60	3304,8	0,35	-5,63
Vauvert 1	Série Grise	61	3412	0,45	-5,31
Vauvert 1	Série Grise	61	3413,64	0,15	-6,23
Vauvert 1	Série Grise	62	3619,97	-0,70	-5,58
Vauvert 1	Série Grise	62	3621,97	-1,51	-6,35

Table S5.2: Total organic carbon (TOC) measurements from Pierrefeu 1 well. The TOC measurements have been performed in 1992 at the IFP (French Institute of Petroleum).

Nature	Lithostratigraphic unit	Depth (m)	TOC (%)
Core sample	Série Rouge	2645	0,96
Core sample	Série Rouge	2656	0,07
Core sample	Série Rouge	2760	0,22
Core sample	Série Rouge	2760,5	0,15
Core sample	Série Rouge	2761	0,54
Core sample	Série Rouge	2761,5	1,69
Core sample	Série Rouge	2762	0,17
Core sample	Série Grise	3213,8	0,12
Core sample	Série Grise	3443	0,29
Core sample	Série Grise	3525	0,48
Core sample	Série Grise	3528	0,37
Core sample	Série Grise	3542	0,36
Core sample	Série Grise	3545	0,38
Core sample	Série Grise	3545	0,43
Core sample	Série Grise	3546	0,29
Core sample	Série Grise	3551	0,49
Core sample	Série Grise	3563	1,07
Core sample	Série Grise	3640	0,44
Core sample	Série Grise	3664	0,39
Core sample	Série Grise	3740,6	0,27
Core sample	Série Grise	3745	0,43
Core sample	Série Grise	3775	0,46
Core sample	Série Grise	3880	0,36
Core sample	Série Grise	3885	0,28
Core sample	Série Grise	3975	0,36
Core sample	Série Grise	4070	0,19
Core sample	Série Grise	4090	0,64
Core sample	Série Grise	4150	3,1
Core sample	Série Grise	4195	12,81
Core sample	Série Grise	4270	12,76
Core sample	Série Grise	4284	13,96
Core sample	Série Grise	4311	1,71
Core sample	Série Grise	4395	1,51
Core sample	Série Grise	4439	2,02
Core sample	Série Grise	4491	0,72
Core sample	Série Grise	4573	1,02
Core sample	Série Grise	4743	0,74
Core sample	Série Grise	4859	1,27
Core sample	Série Grise	4897	0,51
Core sample	Série Grise	5049	0,84
Core sample	Série Grise	5106	0,48
Core sample	Série Grise	5129	0,16

Appendix A- Detailed log sections of some cored intervals from the Gallician wells.

a- Gallician 9 well (cores K22-K23)

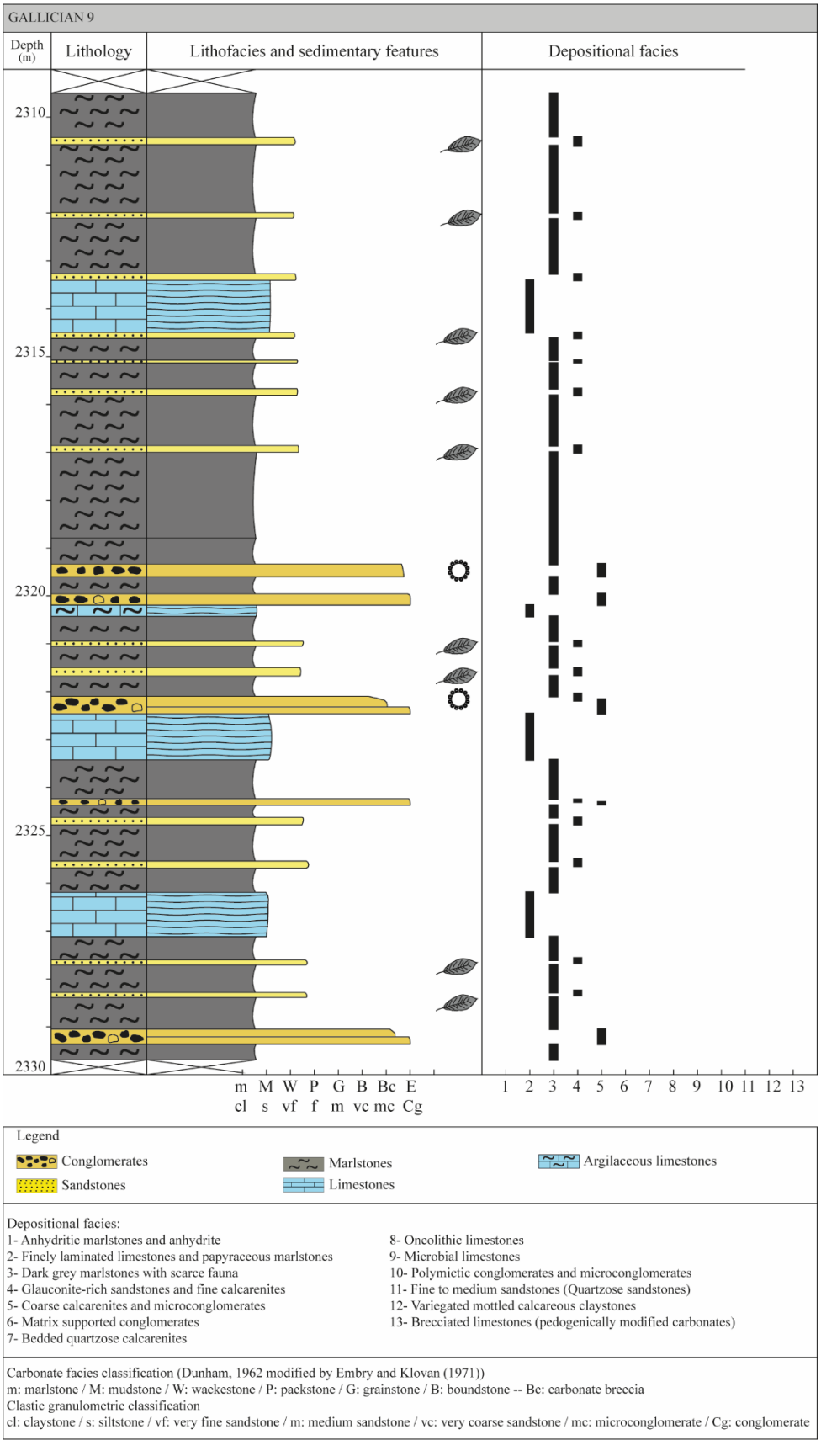

b- Gallician 9 well (cores K16-K21)

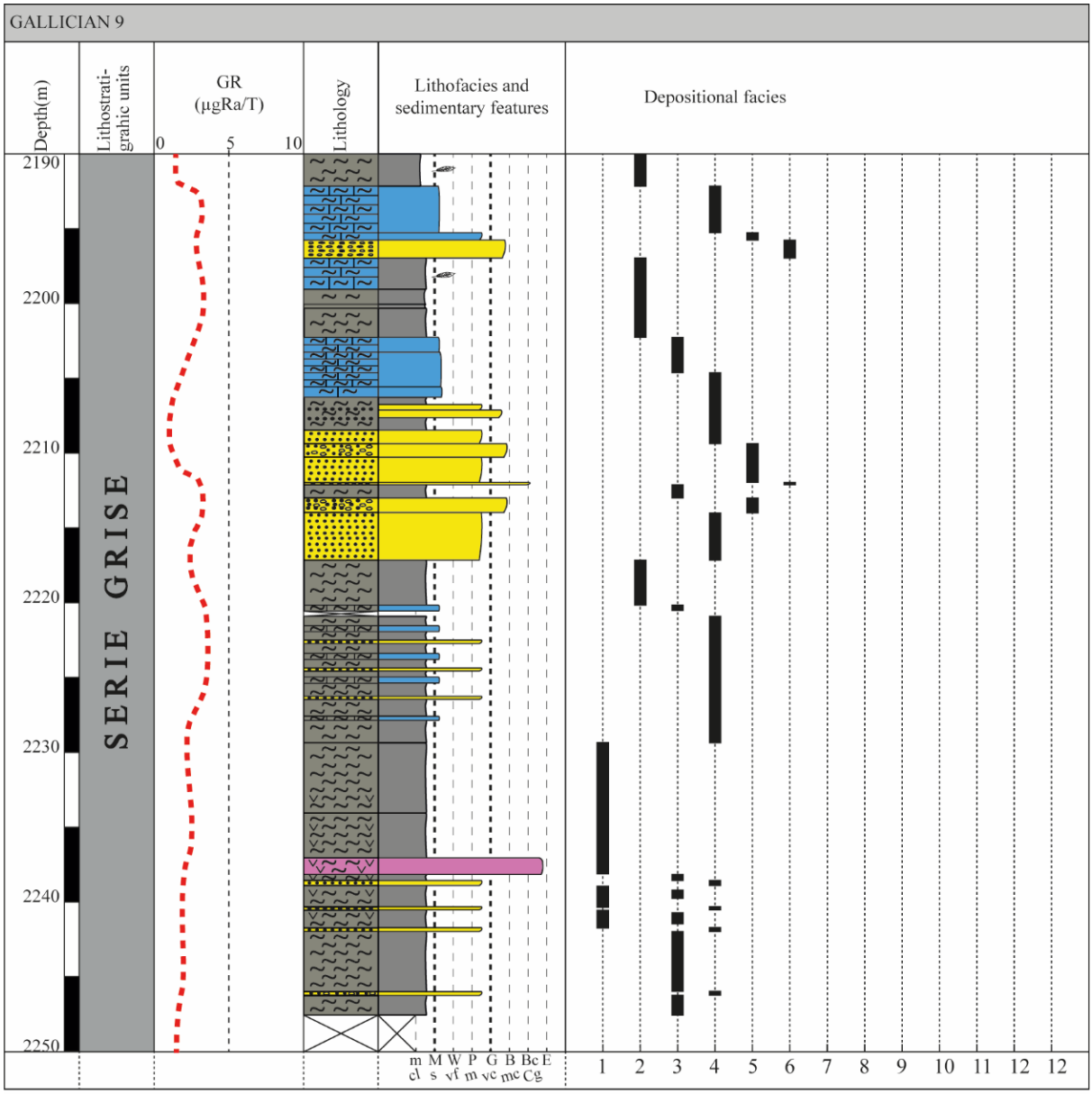

Depositional facies:

1- Anhydritic marlstones and anhydrite
2- Finely laminated limestones and papyraceous marlstones
3- Dark grey marlstones with scarce fauna
4- Glauconite-rich sandstones and fine calcarenites
5- Coarse calcarenites and microconglomerates
6- Matrix supported conglomerates
7- Bedded quartzose calcarenites
8- Oncolithic limestones
9- Microbial limestones
10- Polymictic conglomerates and microconglomerates
11- Fine to medium sandstones (Quartzose sandstones)
12- Variegated mottled calcareous claystones
13- Brecciated limestones (pedogenically modified carbonates)

Carbonate facies classification (Dunham, 1962 modified by Embry and Klovan (1971))
m: marlstone / M: mudstone / W: wackestone / P: packstone / G: grainstone / B: boundstone -- Bc: carbonate breccia
Clastic granulometric classification
cl: claystone / s: siltstone / vf: very fine sandstone / m: medium sandstone / vc: very coarse sandstone / mc: microconglomerate / Cg: conglomerate

c- Gallician 9 well (cores K4-K15) – cf. légende en b. Gallician 9 well (cores K16-K21)

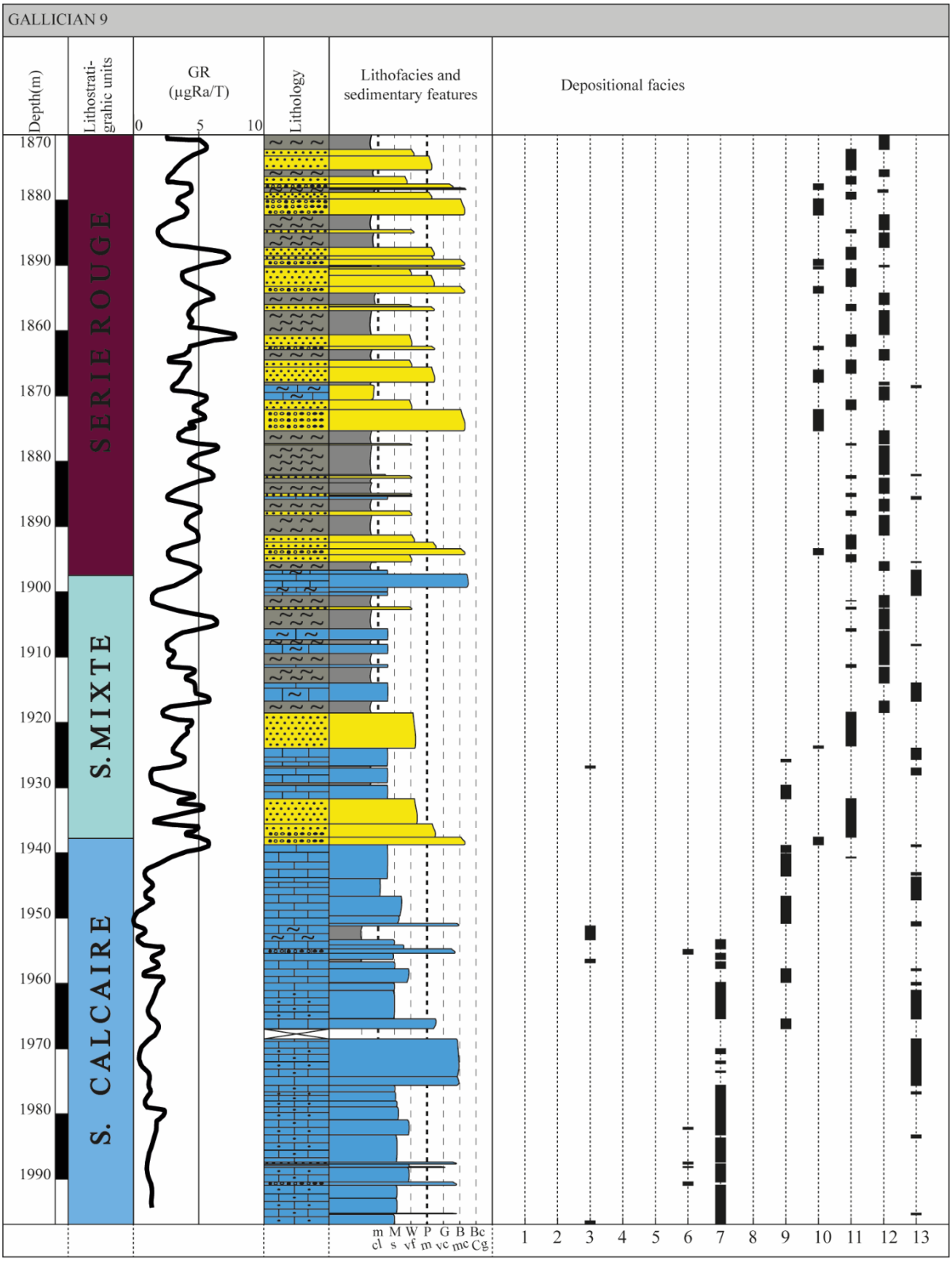

d- Gallician 3 well (K1-K45) – cf. légende en b. Gallician 9 well (cores K16-K21)

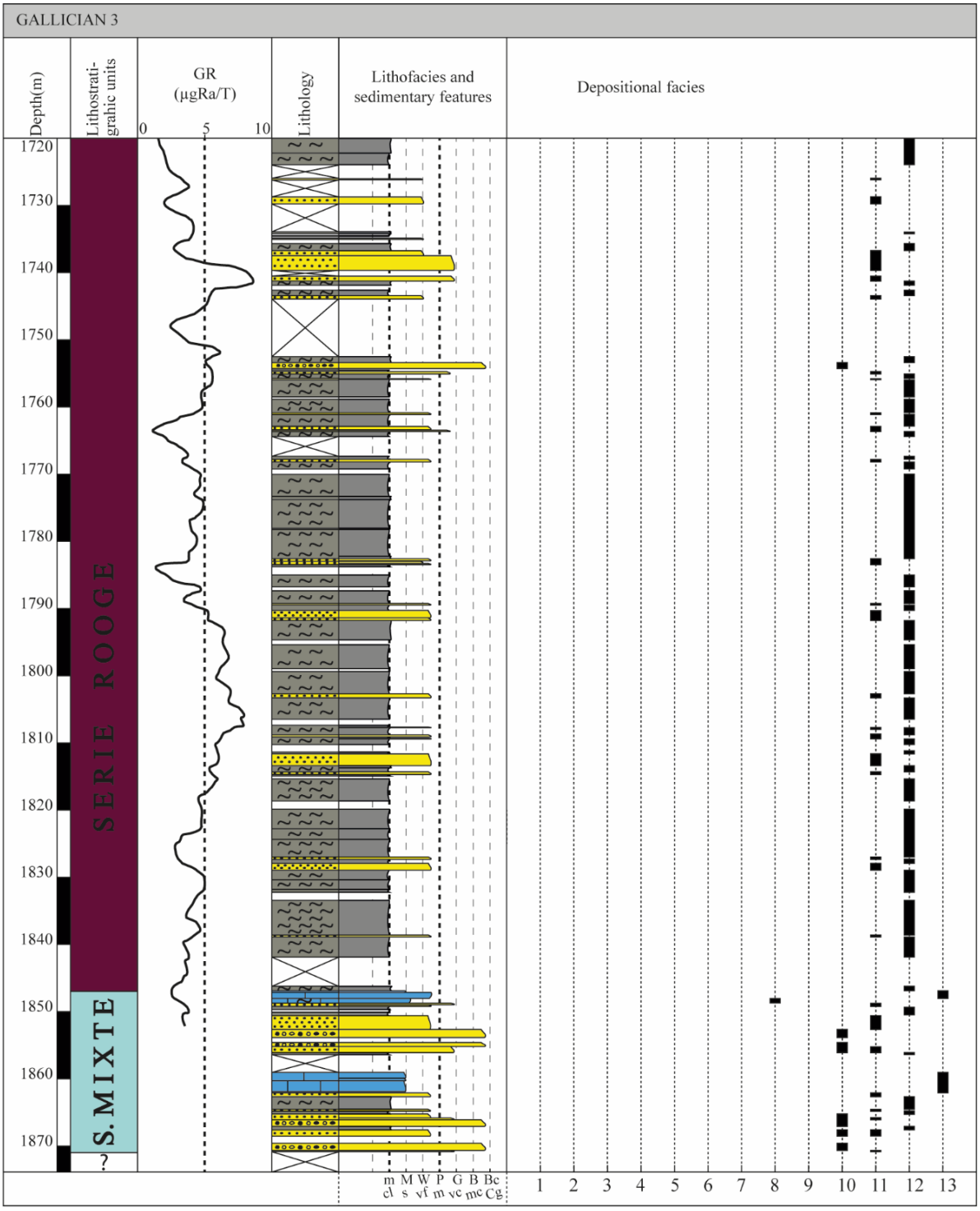

e- Gallician 7 well (K3-K35) – cf. légende en b. Gallician 9 well (cores K16-K21)

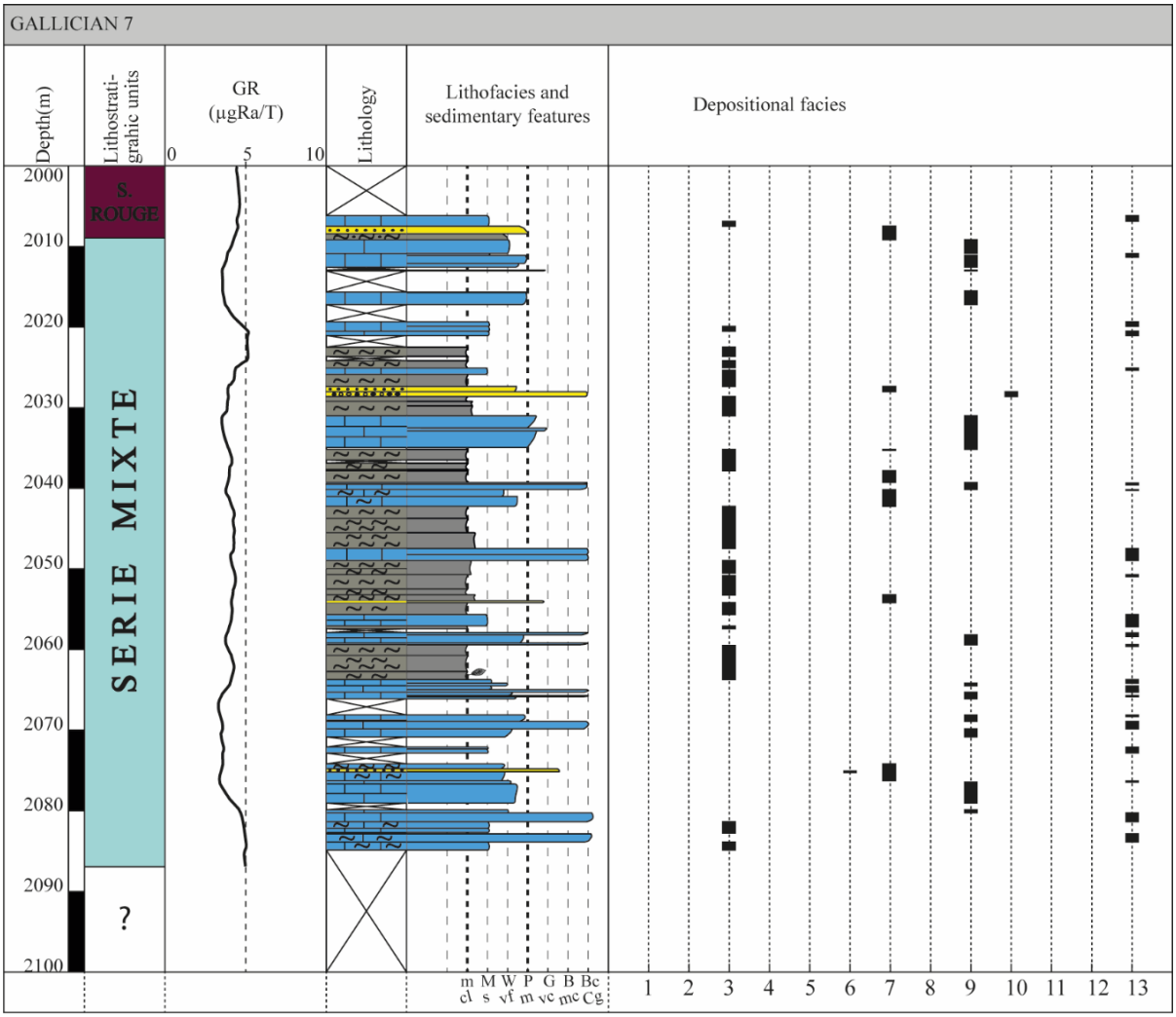

f- Vauvert 1 well (K37-K57) – cf. légende en b. Gallician 9 well (cores K16-K21)

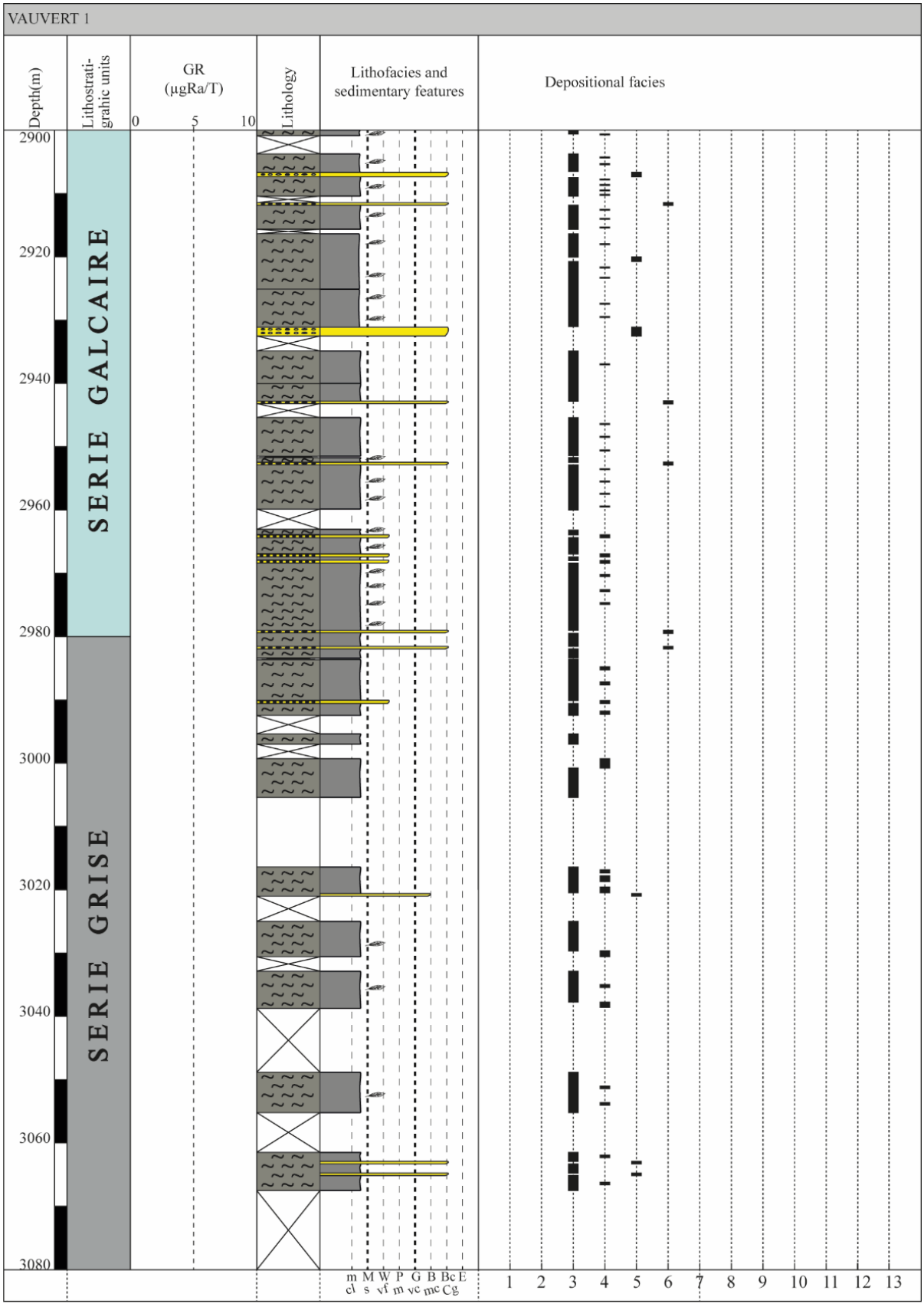

g- Vauvert 1 (K17-K30) – cf. légende en b. Gallician 9 well (cores K16-K21)

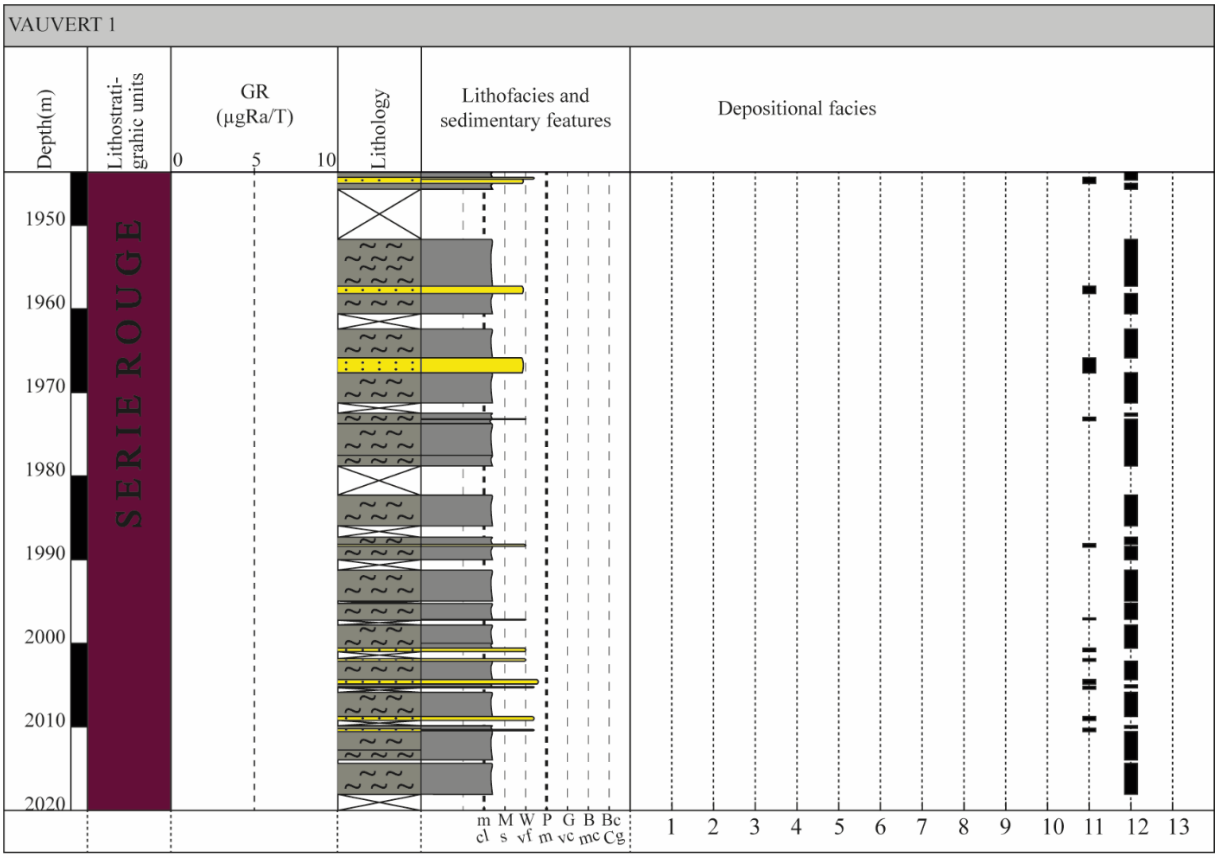

h- Gallician 1 well (K193-K225)

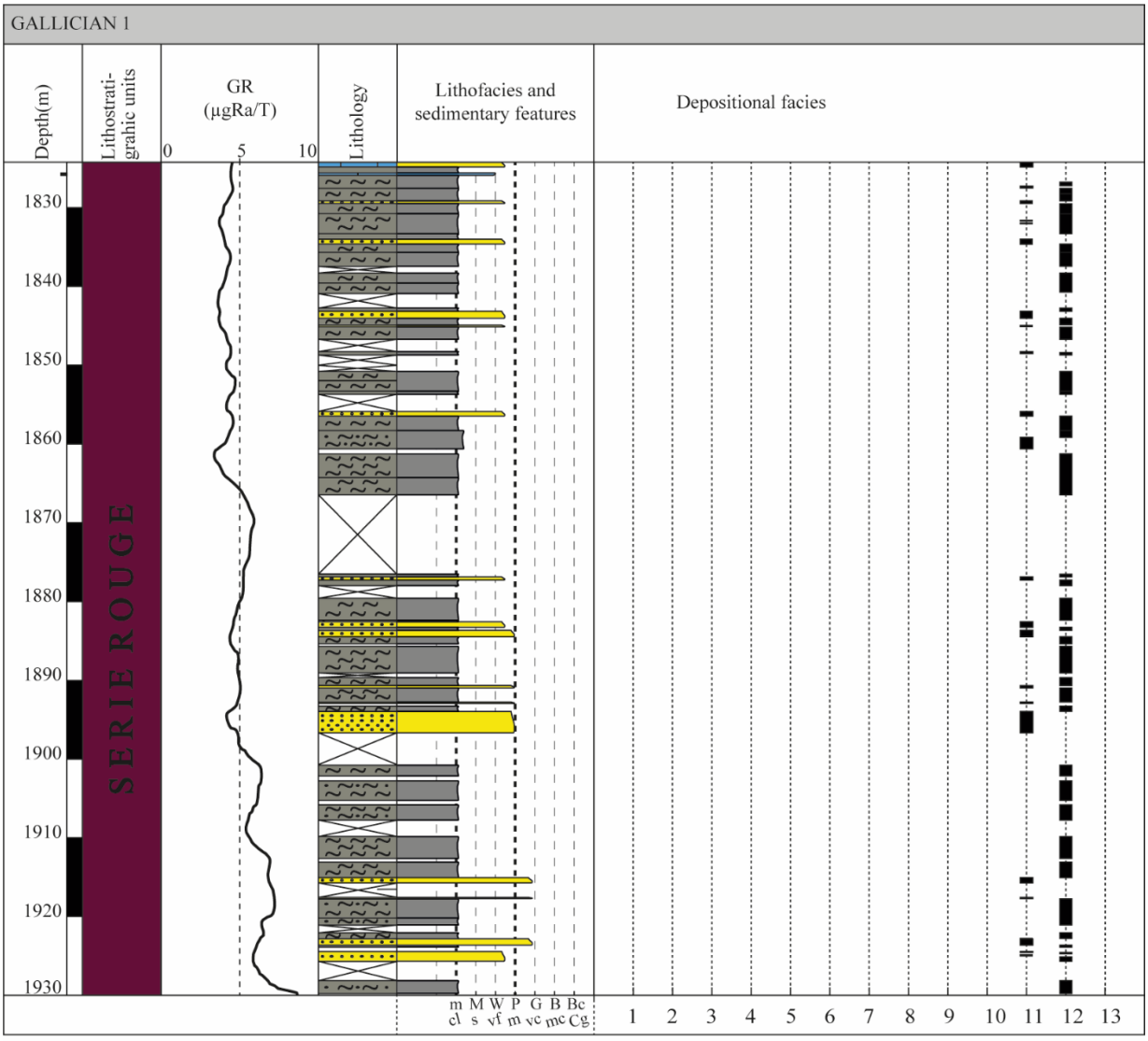

5.9. Références bibliographiques du chapitre 5

Alonso-Zarza A.M, Wright V.P. 2010. Chapter 5 Calcretes. *Developments in Sedimentology* 61 : 225-267.

Anderton R. 1985. Clastic facies models and facies analysis. In Brenchley P.J and Williams B.J.P, (eds.). Sedimentology: recent developments and applied aspects. *Geological Society, London, Special Publications*. Oxford, Blackwell Scientific Publications, pp 31-47.

Arenas C, Cabrera L, Ramos E. 2007. Sedimentology of tufa facies and continental microbialites from the Paleogene of Mallorca Island (Spain). *Sedimentary Geology* 197: 1-27.

Arenas C, Vazquez-Urbez M, Pardo-Tirapu G, Sancho-Marcen C. 2010. Chapter 3 Fluvial and associated Carbonate deposits. *Developments in Sedimentology* 61 :133-175.

Arthaud F, Laurent P. 1995. Contraintes, déformation et déplacement dans l'avant-pays Nord-pyrénéen du Languedoc méditerranéen. *Geodynamica Acta* 8: 142–157.

Ashley G.M, Renaut R.W. 2002. Rift sedimentation. In: R.W Renaut & G.M. Ashley (Eds.), Sedimentation in Continental Rifts, *SEPM Special Publication* 73: 3-10.

Bache F. 2008. Evolution Oligo Miocène des marges du micro océan Liguro-Provençal. Université de Bretagne-occidentale, Brest. Thèse de doctorat, 329 pp.

Basilici G. 1997. Sedimentary facies in an extensional and deep-lacustrine depositional system: the Pliocene Tiberino Basin, Central Italy. *Sedimentary Geology* 109(1-2) : 73-94.

Blanc-Valleron M.-M, Schuler M. 1997. Paleogene evaporitic basins of Alsace (Southern Rhine Graben). In G. Busson, & B. Schreiber, Sedimentary deposition in rift and foreland basins in France and Spain (pp. 85-135). New York: Columbia University Press.

Benedicto A. 1996. Modèles tectono-sédimentaires de bassins en extension et style structural de la marge passive du golfe du Lion (Partie Nord), Sud-est France. Université de Montpellier II. Thèse de doctorat, 249pp.

Benedicto A, Labaume P, Séguret M, Séranne M. 1996. Low-angle crustal ramp and basin geometry in the Gulf of Lion passive margin: the Oligocene-Aquitanian Vistrenque graben, SE France. *Tectonics* 15(6): 1192–1212.

Benedicto A, Séguret M, & Labaume P. 1999. Interaction between faulting, drainage and sedimentation in extensional hanging-wall syncline basins: Example of the Oligocene Matelles basin (Gulf of Lion rifted margin, SE France). *Geological Society*, London, Special Publications 156(1): 81-108.

Bestani L, Espurt N, Lamarche J, Floquet M, Philip J, Bellier O, et al. 2015. Structural style and evolution of the Pyrenean-Provence thrust belt, SE France. *Bulletin de la Société géologique de France* 186: 223–241.

Bouma A.H. 1962. Sedimentology of some Flysch deposits; A graphic approach to facies interpretation. *Elsevier*, 168 pp.

Carothers W W, Kharaka Yousif K. 1980. Stable carbon isotopes of HCO_3^- in oil-field waters---implications for the origin of CO_2. *Geochemica and Cosmochimica Acta* 44(2): 323-332.

Cavelier C, Alabouvette G, Amberger J.P, Cautru J.-P, Charollais J, Châteauneuf J.-J, et al. 1984. Paléogène. In : Debrand-Passard ed., Synthèse géologique du Sud-Est de la France. *Mémoire du BRGM* 125: 389-468.

Curial A, Moretto R. 1997. The Salt Basin of Bresse: Southern Saône Graben. In: Busson G, Schreiber B.C. eds., Sedimentary Deposition in Rift and Foreland Basins in France and Spain. Columbia Univ. Press, New York: pp. 136–194.

Dean W.E, Davies G.R, Anderson R.Y. 1975. Sedimentological significance of nodular and laminated anhydrite. *Geology* 3: 367-372.

Dromart G, Dumas D. 1997. The salt basin of Valence (France). In: Busson G, Schreiber B.C. eds., Sedimentary Deposition in Rift and Foreland Basins in France and Spain. Columbia Univ. Press, New York: pp. 195–239.

Dunham R.J. 1962. Classification of Carbonate Rocks According to Depositional Texture. In: Ham, W.E., Ed., Classification of Carbonate Rocks, AAPG, Tulsa, 108-121.

Eldrett J.S, Greenwood D.R, Harding I.C, Huber M. 2009. Increased seasonality through the Eocene to Oligocene transition in northern high latitudes. *Nature* 459: 969-973.

Embry A.F, Klovan J.E. 1971. A Late Devonian Reef Tract on Northeasterm Banks Island. *Canadian Petroleum Geology* 19: 730-781.

Erdei B, Utescher T, Hably L, Tamas J, Roth-Nebelsick A, Grein M. 2012. Early Oligocene Continental Climate of the Palaeogene Basin (Hungary and Slovenia) and the Surrounding Area. *Turkish Journal of Earth Sciences*: 21: 2(Article 1).

Espitalié J, Deroo G, Marquis F. 1985. La pyrolyse Rock-Eval et ses applications – Première partie. *Revue de l'Institut Français du Pétrole*: 40 (5) 563-579.

Fabre J, Mainguet M. 1991. Continental sedimentation and palaeoclimates in Africa during the Gondwanian Era (Cambrian to Lower Cretaceous): the importance of wind action. *Journal of African Earth Sciences* 12 (1-2): 107-115.

Freytet P. 1973. Petrography and paleoenvironments of continental carbonates deposits with a particular reference to Upper Cretaceous and Lower Eocene of Languedoc, Southern France. *Sedimentary Geology* 10 : 25-60.

Freytet P, Plaziat J.-C. 1982. Continental carbonate sedimentation and pedogenesis – Late Cretaceous and Early Tertiary of Southern France. In: Purser B. H. ed., *Contribution to Sedimentology*, *Schweizerbartsche Verlag*, Stuttgart, 12: 217 pp.

Gorini C. 1993. Géodynamique d'une marge passive: le Golfe du Lion (Méditerranée Occidentale). Thèse de doctorat, Université Paul Sabatier, Toulouse, 256 pp.

Gorini C, Le Marrec A, Mauffret A. 1993. Contribution to the structural and sedimentary history of the Gulf of Lions (western Mediterranean), from the ECORS profiles, industrial seismic profiles and well data. *Bulletin de la Société géologique de France* 164(3): 353–363.

Haughton P, Davis C, McCaffrey W, Barker S. 2009. Hybrid sediment gravity flow deposits – Classification, origin and significance. *Marine and Petroleum Geology* 26(10) : 1900-1918.

Hren M. T, Sheldon N. D, Grimes S. T, Collinson M. E, Hooker J. J, Bugler M, Lohmann K. C. 2013. — Terrestrial cooling in Northern Europe during the Eocene–Oligocene transition. *Proceedings of the National Academy of Sciences of the United States of America* 110: 7562-7567.

Joseph P, and Lomas S. 2004. Deep-water sedimentation in the Alpine Foreland Basin of SE France: new perspectives on the grès d'Annot and related systems - An introduction. Dans P. Joseph, & S. Lomas (Éds.), Deep-water sedimentation in the Alpine Foreland Basin of SE France: new perspectives on the grès d'Annot and related systems (Vol. 1, pp. 1-16). *The Geological Society of London, Special Publications*.

Kelts K, Talbot M. 1990. Lacustrine Carbonates as Geochemical Archives of Environmental change and Biotic/Abiotic Interactions. *In* Tilzer M, Colette S (eds). Large Lakes: Ecological Structure and Function, Springer, pp 288-315.

Lehn I, Fallgatter C, Kern H.P, Sergio Gomes Paim P. 2018. Co-genetic, cohesive and non-cohesive delta front facies: A case study of flow transformation in a lacustrine setting, Camaquã Basin, southernmost Brazil. *Journal of South American Earth Sciences* 86: 271-286.

Leng MJ, Marshall JD. 2004. Palaeoclimate interpretation of stable isotope data from lake sediment archives. Quaternary Science Reviews 23(7-8): 811-831.

Lesueur J.-L. 1991. Etude sédimentologique et stratigraphique du Bassin Paléogène d'Apt–Manosque–Forcalquier (Alpes de Haute Provence). Modalités de la transition Burdigalienne. Ph.D. thesis, University M. de Montaigne, Bordeaux III, France : 407 pp.

Lettéron A, Fournier F, Hamon Y, Villier L, Margerel J.-P, Bouche A, Feist M, Joseph P. 2017. Multi-proxy paleoenvironmental reconstruction of saline lake carbonates: Paleoclimatic and paleogeographic implications (Priabonian-Rupelian, Issirac Basin, SE France). *Sedimentary Geology* 358 : 97–120.

Lettéron A, Hamon Y, Fournier F, Séranne M, Pellenard P, Joseph P. 2018. Reconstruction of a saline, lacustrine carbonate system (Priabonian, St-Chaptes Basin, SE France): depositional models, paleogeographic and paleoclimatic implications. *Sedimentary Geology* 367: 20–47.

Lettéron A, Hamoun Y, Fournier F, Demory F, Séranne M, Joseph P. 2021. Stratigraphic architecture of a saline lake system: From lake depocenter (Alès Basin) to margins (Saint-

Chaptes and Issirac basins), Eocene-Oligocene transition, south-east France. *Sedimentology, Blackwell Publishing, in press,* ⟨DOI: 10.1111/sed.12920⟩, ⟨hal-03406458⟩.

Li H-C, Ku .-L. 1997. $\delta^{13}C$ - $\delta^{18}O$ covariance as a paleohydrological indicator for closed-basin lakes. *Palaeogeography, Palaeoclimatology, Palaeoecology* 133: 69 80.

Liu Z, Pagani M, Zinniker D, DeConto R, Huber M, Brinkhuis H, Shah S.R, Leckie R.M, Pearson A. 2009. Global cooling during the Eocene-Oligocene climate transition: *Science* 323 : 1187-1190.

Lowe D.R. 1982. Sediment gravity flows : II. Depositional models with special reference to the deposits of high-density turbidity currents. *Journal of Sedimentology, Society of Economic Paleontologists and Mineralogists* 52 : 279-297.

Lowe D.R, Guy M. 2000. Slurry-flow deposits in the Britannia Formation (Lower Cretaceous), North Sea: a new perspective on the turbidity current and debris flow problem. *Sedimentology* 47: 31-70.

Mascle A, Jacquart G, Deville E. 1994. The Corbières transverse zone of the Pyrenee-Provence thrust belt (south France) – Tectonic history and petroleum plays. *6th Conference, European Association of Petroleum Geoscientists & Engineers*, Extended Abstract, P556, Vienna, 1994.

Miall AD. 1985. Architectural-Element Analysis: A New Method of Facies Analysis Applied to Fluvial Deposits. Earth-Science Reviews 22, 261-308

Mosbrugger V, Utescher T, Dilcher D. L. 2005. Cenozoic continental climatic evolution of Central Europe. *Proceedings of the National Academy of Sciences* 102: 14964-14969.

Nutz A, Kwiecien O, Breitenbach S, Cai Y, Della Porta G, Danisch J, Kabiri L, Bodin S. 2019. Fluvio-lacustrine sedimentation in the Agadir-Tissint Feija (Anti-Atlas, Morocco): A promising palaeoclimate archive for the last glacial cycle in northwest Africa. *Depositional Record* 5(2): 362-387. ⟨10.1002/dep2.65⟩. ⟨hal-02468873⟩

Orti F, Salvany J.M. 2004. Coastal salina evaporites of the Triassic-Liassic boundary in the Iberian Peninsula: The Alaco´n borehole. *Geol. Acta* 2: 291–304.

Page M, Licht A, Dupont-Nivet G, Meijer N, Barbolini N, Hoorn C, Schauer A, Huntington K, Bajnai D, Fiebig J, Mulch A. 2019. Synchronous cooling and decline in monsoonal rainfall in northeastern Tibet during the fall into the Oligocene icehouse. *Geology* 47: 203-206.

Peckmann J, Paula J, Thiel V. 1999. Bacterially mediated formation of diagenetic aragonite and native sulfur in Zechstein carbonates (Upper Permian, Central Germany). *Sedimentary Geology* 126(1-4): 205-222.

Pellat E, Allard M. 1895. Dépôts lacustres de la Butte Iouton entre Comps et Beaucaire (Gard). *Bulletin de la Société Géologique de France* 23: 434-436.

Pentecost A. 2005. Travertine. Springer, 446 pp.

Platt N.H. 1989. Lacustrine carbonates and pedogenesis: sedimentology and origin of palustrine deposits from the Early Cretaceous Rupelo Formation, W Cameros Basin, N Spain : *Sedimentology* 36 :665-684.

Platt N.H, Wright V. 1991. Lacustrine carbonates : facies models, facies distribution and hydrocarbon aspects. *Spec. Publs Int. Ass. Sediment* 13 : 57-74.

Platt N.H, Wright V. 1992. Palustrine carbonates and the Florida Everglades; towards an exposure index for the fresh-water environment? *Journal of Sedimentary Petrology* 62 : 1058-1071.

Rémy J.A. 1985. Nouveaux gisements de mammifères et reptiles dans les grès de Célas (Éocène sup. du Gard). Etude des paléothériidés (Perissodactyla, Mammalia). *Palaeontographica, Abteilung A*, 189, 171-225.

Rémy J.A., Fournier F. 2003. Mammifères fossiles de Grès de Célas (Éocène supérieur du Gard) : Découvertes récentes. *Bulletin de la Société des Sciences Naturelles de Nîmes et du Gard*, Nîmes, 64 :18-30.

Rouchy J.-M. 1997. Paleogene continental rift system of Western Europe: locations of basins, paleogeographic and structural framework, and the distribution of evaporites. In: Busson, G., Schreiber, B.C. eds., Sedimentary Deposition in Rift and Foreland Basins in France and Spain. Columbia Univ. Press, New York: pp. 45–94.

Semmani N, Fournier F, Léonide P, Feist M, Boularand S, Borgomano J. 2022. Transgressive-regressive cycles in saline lake margin oolites: paleogeographic implications (Priabonian, Vistrenque Basin, SE France). *BSGF Earth Science Bulletin*: 193, 8.

Semmani N, Fournier F, Suc J-P, Fauquette S, Godeau N, Guihou A, Popescu S-M, Melinte-Dobrinescu M C, Thomazo C, Marié L, Borgomano J. The Paleogene continental basins from SE France: new geographic and climatic insights from an integrated approach, *under review*.

Séranne M, Benedicto A, Truffert C, Pascal G, Labaume P. 1995. Structural style and evolution of the Gulf of Lion Oligo-Miocene rifting: Role of the Pyrenean orogeny. *Marine and Petroleum Geology* 12: 809–820.

Séranne M, Couëffé R, Husson E, Baral C, Villard J. 2021. The transition from Pyrenean shortening to Gulf of Lion rifting in Languedoc (South France) –A tectonic-sedimentation analysis. *BSGF - Earth Sciences Bulletin* 192, 27.

Smit J, Brun J.-P, Cloetingh S, Ben Avraham Z. 2008. Pull-apart basin formation and development in narrow transform zones with application to the Dead Sea Basin. *Tectonics*: 27, TC6018.

Sonnenfeld P. 1985. Evaporites as oil and gas source rocks. *Journal of Petroleum Geology* 8(3): 253-271.

Tabor N.J, Myers T.S, Michel L.A. 2017. Sedimentologist's guide for recognition, description, and classification of Paleosols. *Terrestrial Depositional Systems* 165-208. http://dx.doi.org/10.1016/B978-0-12-803243-5.00004-2

Talbot MR. 1990. A review of the palaeohydrological interpretation of carbon and oxygen 1121 isotopic ratios in primary lacustrine carbonates. *Chemical Geology* 80: 261–279.

Talling P.J, Masson D.G, Sumner E.J, Malgesini G. 2012. Subaqueous sediment density flows: Depositional processes and deposit types. Sedimentology 59(7) : 1937-2003. https://doi.org/10.1111/j.1365-3091.2012.01353.x

Tanner L. 2010. Continental Carbonates as Indicators of Paleoclimate. *Developments in Sedimentology* 62: 179-214.

Tanrattana M, Boura A, Jacques F, Villier L, Fournier F, Enguehard A, Cardonnet S., Voland G, Garcia A, Chaouch S, De Franceschi D. 2020. Climatic evolution in Western Europe during the Cenozoic: insights from historical collections using leaf physiognomy. *Geodiversitas*: 42, 151–174.

Tinterri R, Magalhaes P.M, Tagliaferri A, Cunha R.S. 2016. Convolute laminations and load structures in turbidites as indicators of flow reflections and decelerations against bounding slopes. Examples from the Marnoso-arenacea Formation (northern Italy) and Annot Sandstones (south eastern France). Sedimentary Geology 344: 382-407.

Tinterri R, Civa A, Laporta M, Piazza A. 2020. Chapter 17 - Turbidites and turbidity currents. In Scarselli N, Adam J, Chiarella D, Roberts D. G, Bally A. W. ed. Regional Geology and Tectonics (Second Edition), Elsevier, 441-479.

Utescher T, Bruch A. A, Micheels A, Mosbrugger V, Popova S. 2011. Cenozoic climate gradients in Eurasia – a palaeo-perspective on future climate change?, *in* Utescher T, Böhme M, Mosbrugger V. (*eds*), The Neogene of Eurasia: Spatial gradients and temporal trends - The second synthesis of NECLIME. *Palaeogeography, Palaeoclimatology, Palaeoecology* 304: 351-358.

Valette M. 1991. Etude structurale du gisement salifère Oligocène de Vauvert (Gard), *Thèse de doctorat*, Univ. Montpellier II, 229 pp.

Valette M, Benedicto A. 1995. Chevauchements gravitaires halotectoniques dans le bassin distensif de Camargue (marge du golfe du Lion, SE de la France). *Bulletin de la Société Géologique de France* 166(2): 137-147.

Viles H.A, Taylor M.P, Nicoll K, Neumann S. 2007. Facies evidence of hydrodynamic regime shifts in tufa depositional sequences from the arid Naukluft Mountains, Namibia. *Sedimentary Geology* 195: 39-53.

Wade, B. S., Houben, A. J. P. Quaijtaal, W. Schouten, S. Rosenthal, Y. Miller, K. G., Katz, M. E., Wright, J. D. , Brinkhuis, H., 2012. Multiproxy record of abrupt sea-surface cooling across the Eocene-Oligocene transition in the Gulf of Mexico. Geology, 40, 2, 159-162.

Walker R.G. 1992. Facies, Facies Models and Modern Stratigraphic Concepts. In Walker R.G and James N.P, (eds.). Facies Models: Response to sea Level Change. *Geological Association of Canada*, pp 1-14.

Wentworth C. K. 1922. A scale for grade and class terms for clastic sediments. The Journal of Geology 30(5) : 377-392.

Westerhold T, Marwan N, Drury A.J, Liebrand D, Agnini C, Anagnostou E, Barnet J.S.K, Bohaty S.M, De Vleeschouwer D, Florin D, Lauretano V, Littler K, Lourens L.J, Lyle M, Pälike H, Röhl U, Tian J, Wilkens R.H, Wilson P.A, Zachos J.C. 2020. An astronomically dated record of Earth's climate and its predictability over the last 66 million years. *Science* 369: 1383–1387.

Yancey T.E, Elsik W.C, Sancay R.H, Prothero D.R, Ivany L.C, Nesbitt E.A. 2003. The palynological record of late Eocene climate change, northwest Gulf of Mexico: From Greenhouse to Icehouse-the marine Eocene-Oligocene transition, Columbia University Press, New York, New York, 252-268.

Zachos J, Pagani M, Sloan L, Thomas E, Billups K, 2001. Trends, rythms and aberrations in global climate 65 Ma to present. *Science* 292, 686-693.

Ziegler, P.A. 1992. European Cenozoic srift system. In: Ziegler, P.A. (Ed.), Geodynamics of Rifting, Volume I, Case History Studies on Rifts: Europe and Asia. *Tectonophysics* 208: 91–111.

6. CONCLUSIONS GÉNÉRALES ET PERSPECTIVES

6. Conclusions générales et perspectives

Le bassin cénozoïque de la Vistrenque (Camargue, SE France), le plus profond dépôt-centre du Sud-est de la France, a été étudié afin d'analyser la complexité de la réponse des bassins sédimentaires continentaux au forçages tectonique et climatique et aux changements paléohydrologiques. La question de l'origine de la salinité dans les systèmes lacustres et les modalités de connexion des masses d'eaux salées lacustres entre elles et avec le domaine marin dans le Sud-est de la France à l'Éocène supérieur et à l'Oligocène ainsi que les problèmes paléogéographiques qui en découlent ont été abordés dans cette thèse. La période étudiée (Priabonien à Chattien) couvre également la transition Éocène-Oligocène qui correspond à une crise climatique majeure du Cénozoïque, marquée par un refroidissement global du climat dont l'expression en milieu continental demeure encore peu documentée dans le Sud-est de la France.

Afin de replacer la Camargue au sein des systèmes de rifts cénozoïques du Sud-est de la France et documenter les voies potentielles d'incursions marines dans les bassins continentaux du Languedoc et de la Vallée du Rhône à la fin de l'Éocène et à l'Oligocène, ce travail a examiné les aspects sédimentologique, chronostratigraphique, géochimique et de stratigraphie séquentielle des séries paléogènes de la marge et du dépôt-centre du bassin de la Vistrenque.

Cette étude multidisciplinaire est basée sur l'étude de la succession carbonatée affleurant sur la marge septentrionale et des forages profonds réalisés dans le dépôt-centre du bassin. Elle a permis d'établir l'existence de connexions des masses d'eaux lacustres entre le bassin de la Vistrenque et les bassins voisins du Languedoc et de la Vallée du Rhône via la marge carbonatée du haut de Jonquières (butte Iouton) au Priabonien.

Pour restituer les contextes paléogéographiques, paléoclimatiques et paléohydrologiques du remplissage paléogène du bassin de la Vistrenque, l'établissement d'un cadre chronostratigraphique des séries de subsurface, jusqu'alors très mal contraint, a été entreprise. Le calendrier du remplissage documenté dans cette thèse a permis de considérer l'hypothèse d'un fonctionnement du bassin de la Vistrenque antérieurement à la phase de rifting Oligo-Aquitanien de la marge du golfe du Lion. Ce cadre chronostratigraphique et les nouvelles données micropaléontologiques et géochimiques ont permis 1) de réaliser de nouvelles reconstitutions paléogéographiques, 2) d'améliorer notre connaissance de l'évolution du bassin de la Vistrenque durant la période comprise entre la fin de l'Éocène et l'Oligocène supérieur, et 3) de caractériser l'expression de la dégradation climatique de la transition Éocène-Oligocène en milieu continental dans le Sud-est de la France.

6.1. Cadre chronostratigraphique

La révision biostratigraphique de la succession carbonatée oolithique affleurant à la butte Iouton sur la marge septentrionale du bassin de la Vistrenque inclut des données inédites de datation de gyrogonites de characées qui couplée à l'examen des assemblages malacologiques permet d'attribuer un âge Priabonien supérieur à la succession carbonatée oolithique.

La construction du cadre chronostratigraphique des séries sédimentaires paléogènes dilatées de subsurface utilise différentes approches : les datations absolues par la méthode U/Pb sur la calcite, les âges interprétés à l'aide de l'approche climatostratigraphique fondée sur les assemblages polliniques, les compositions isotopiques en soufre et strontium des évaporites (sulfates) prélevées sur les carottes couplées à la modélisation géochimique de ces compositions pour des mélanges de saumures d'origines différentes (marines et continentales). L'approche climatostratigraphique utilise des données de calibration biostratigraphiques (mammifères, charophytes) du bassin voisin d'Alès et apporte de nouvelles précisions sur les reconstitutions paléogéographiques dans le Sud-est de la France.

Les datations obtenues dans les séries de subsurface confirment le fonctionnement du bassin de la Vistrenque antérieurement à la phase du rifting Oligo-Aquitanien de la marge du golfe du Lion, au cours du Priabonien (?) et du Rupélien, potentiellement à la faveur des mouvements de décrochements senestres de la faille de Nîmes, dans le cadre de la phase tectonique décrochante du faisceau des failles cévénoles documentée dans le Languedoc voisin dès le Priabonien. Les séries paléogènes « anté-salifères » considérées dans ce travail se sont déposées pendant l'intervalle compris entre le Priabonien (?) – Rupélien basal et le Chattien inférieur : la Série Grise basale et la Série Calcaire sus-jacente sont d'âge Priabonien (?) à Rupélien inférieur tandis que les formations Série Mixte et Série Rouge susjacentes sont d'âge Rupélien moyen à Chattien inférieur. La Série Calcaréo-salifère du bassin de la Vistrenque est d'âge Chattien inférieur à Aquitanien qui correspond quant à lui à l'intervalle du rifting de la marge du Golfe du Lion.

6.2. Modèles de dépôt dans la marge et dans le dépôt-centre

L'analyse sédimentologique de la succession carbonatée de la marge a permis de reconstruire une marge carbonatée oolithique de lac salin. Un modèle de rampe carbonatée lacustre a été mis en évidence, présentant un domaine interne à sédimentation boueuse et un domaine externe à haute énergie où se forment les épaisses accumulations d'ooïdes et de péloïdes. Les isotopes du carbone et de l'oxygène montrent que la sédimentation carbonatée de bordure de lac se produit principalement pendant des phases de transgression lacustre contrôlées par la subsidence alors que les surfaces d'émersion marquent des périodes de bilan hydrique déficitaire et d'assèchement du lac (régression forcée). Les transgressions lacustres sont

expliquées par les connexions du bassin avec des masses d'eaux salées pendant les phases de transgression et d'expansion maximale des masses d'eaux salées régionales ; ceci est cohérent avec la dominance des associations de mollusques reflétant des eaux oligo-mésohalines durant l'intervalle considéré.

Le bassin de la Vistrenque comprend, à l'opposé de cette marge carbonatée septentrionale, une aire de sédimentation profonde au Sud à remplissage mixte mais essentiellement terrigène provenant des marges du bassin et des reliefs pyrénéens au Sud. L'analyse sédimentologique détaillée des carottes et les mesures de la composition isotopique du carbone et de l'oxygène des carbonates lacustres de cette succession dilatée dans le dépôt-centre permet de suggérer deux phases principales de fonctionnement du système lacustre. La partie inférieure du remplissage sédimentaire révèle un modèle paléoenvironnemental de lac profond fortement subsident à sédimentation gravitaire et alimenté par des flux terrigènes et des apports d'eau provenant essentiellement des reliefs Pyrénéens situés au Sud. Pour la partie supérieure du remplissage sédimentaire, un modèle de dépôt de lac peu profond avec un développement important d'une plaine d'inondation est proposé pour rendre compte de la sédimentation margino-lacustre carbonatée et fluviatile silicoclastique.

6.3. Origine de la salinité des systèmes lacustres

Dans la marge carbonatée, les signatures isotopiques (carbone et oxygène) des carbonates ainsi que les tendances d'évolution verticale de la salinité estimées par les assemblages de mollusques laissent envisager des connexions du système lacustre avec des masses d'eau salées adjacentes au Priabonien dans un contexte subsident. Les eaux salées qui alimentent les bassins continentaux du Sud-est de la France au Priabonien pourraient provenir du lessivage des évaporites triassiques et/ou de la connexion avec une eau marine.

Les nouvelles données micropaléontologiques et palynologiques ainsi que les compositions des eaux salées obtenues par la modélisation géochimique du $^{87}Sr/^{86}Sr$ et du $\delta^{34}S$ des sulfates dans les bassins de la Vistrenque et d'Alès apportent des preuves d'incursions marines, au moins épisodiques, dans le Sud-est de la France durant la période Priabonien inférieur-moyen à Chattien inférieur. Dans le bassin d'Alès, un mélange d'eau marine et d'eau lessivant les évaporites triassiques peut être envisagé pour la formation des évaporites priaboniennes. Dans le bassin de la Vistrenque, les compositions isotopiques du strontium et du soufre des anhydrites de la Série Calcaréo-salifère sont cohérentes avec la formation dans une eau composée d'un mélange d'eaux lessivant les évaporites triassiques et d'une eau d'origine marine. Le meilleur scénario de modélisation géochimique suggère que l'eau marine du mélange est d'âge Chattien supérieur à Aquitanien.

6.4. Reconstitutions paléogéographiques

La butte Iouton suggère que la succession carbonatée oolithique de lac peu profond s'est formée sur la marge d'un système de lacs salins interconnectés de grande dimension, occupant différents sous-bassins du Languedoc et de la Vallée du Rhône.

L'étude intégrée du bassin paléogène de la Vistrenque et des bassins priaboniens voisin d'Alès et de Saint-Chaptes apporte de nouvelles précisions pour le problème paléogéographique du Sud-est de la France. Nos reconstitutions paléogéographiques du Sud-est de la France pendant le Priabonien et le Rupélien supérieur suggèrent fortement des incursions marines depuis la mer alpine via deux voies potentielles : la haute vallée du Rhône via le seuil de Crest et la basse vallée du Rhône via les synclinaux pyrénéens du Haut-Var. D'autre part, les bassins évaporitiques de l'Oligocène supérieur en Camargue sont alimentés en solutés directement depuis la mer Méditerranée occidentale à la suite de l'effondrement du segment Pyrénéen ayant existé à l'emplacement de l'actuel Golfe du Lion pendant l'extension Oligocène-aquitanienne. Les reconstructions des végétations confirment l'existence d'un relief Pyrénéen au Sud de la Camargue, dans la continuité des Pyrénées franco-espagnoles et de la Provence, nos reconstitutions paléogéographiques n'envisagent pas d'incursions marines dans le Sud-est de la France par le Sud avant le Chattien.

6.5. Enregistrement de la transition climatique Éocène-Oligocène en milieu continental

Les reconstructions des végétations dans les bassins d'Alès (Priabonien) et de la Vistrenque (Rupélien basal) révèlent un changement floristique majeur entre l'Eocène et l'Oligocène dans le Sud-est de la France. L'analyse pollinique et la méthode d'amplitude climatique qui permet de restituer les estimations paléoclimatiques (températures et précipitations) indiquent une détérioration climatique soudaine et brève survenant au tout début de l'Oligocène. Cette détérioration climatique est caractérisée par une baisse des températures et une aridification climatique dans les basses altitudes. Cet événement climatique bref correspondrait à l'expression en milieu continental de la transition Eocène-Oligocène dans le Sud-est de la France et est suivi par le retour à des conditions plus humides et plus chaudes dès la fin du Rupélien inférieur-Rupélien moyen. Dans le bassin de la Vistrenque, le paroxysme de ce stade de refroidissement et d'aridification du climat est enregistré par la formation locale d'évaporites en réponse à un bilan précipitation-évaporation déficitaire marqué par la diminution des apports d'eau dans le bassin.

6.6. Evolution du bassin de la Vistrenque : contrôle climatique et tectonique

L'analyse sédimentologique, géochimique et stratigraphique du remplissage paléogène anté-salifère (Éocène supérieur (?) à Oligocène supérieur) dans les secteurs de Gallician et de Pierrefeu situés dans le centre du bassin de la Vistrenque révèle trois étapes principales de l'évolution du remplissage du bassin : 1) un bassin lacustre profond transgressif (Priabonien (?) - Rupélien basal) dans lequel la sédimentation était dominée par des dépôts terrigènes gravitaires sous climat humide dominant pendant une période marquée par des taux de subsidence élevés et une importante activité des failles ; 2) un bassin lacustre profond évaporitique et à régression forcée (Rupélien inférieur) caractérisé par une réduction drastique des apports terrigènes et par le dépôt d'évaporites dans des sous-bassins déconnectés de la masse d'eau lacustre ; 3) un stade de régression normale à long-terme (Rupélien moyen à supérieur / Chattien inférieur) et de remplissage du lac caractérisé par une augmentation des apports terrigènes et une transition verticale ascendante des dépôts gravitaires de lac profond vers une sédimentation en milieu lacustre marginal dans des plaines alluviales, interprétée comme résultant à la fois d'une humidification du climat et d'une diminution du taux de subsidence et de l'activité des failles.

La régression forcée du début du Rupélien du paléolac de la Vistrenque, interprétée comme le résultat du refroidissement et de l'aridification continentale soudaine et brève du Rupélien inférieur, est accompagnée par un changement floristique significatif qui pourrait s'insérer dans le cadre du refroidissement global à la transition Éocène-Oligocène (EOT : *Eocene-Oligocene Transition*). A la suite de cet épisode de refroidissement et d'aridification du Rupélien inférieur, le remplissage final du lac et la transition vers des dépôts de plaine d'inondation se sont produits dans un environnement plus humide, pendant une phase de diminution de l'activité de la faille de Nîmes ayant favorisé le comblement du bassin à la fin du Rupélien et au début du Chattien avant sa réouverture pendant le rifting du Golfe du Lion.

6.7. Perspectives

L'apport de cette thèse tant au niveau de la connaissance sur le bassin de la Vistrenque (chronstratigraphie, sédimentologie, modèles de remplissages, géochimie, stratigraphie séquentielle) qu'au niveau des problématiques scientifiques de la géologie du Sud-est de la France ouvre de nouvelles perspectives pour l'étude des bassins continentaux paléogènes du Sud-est de la France et de l'Europe de l'Ouest.

Dans le bassin de la Vistrenque, cette thèse est la première étude sédimentologique détaillée sur une sélection de forages représentative du dépôt-centre. Les reconstitutions paléoenvironnementales et paléohydrologiques pourraient être précisées à l'échelle temporelle et spatiale avec : 1) l'amélioration du pas d'échantillonnage des isotopes avec l'intégration des

cuttings dans les intervalles non carottés des forages étudiés (p.ex., Pierrefeu 1, Gallician 9, Vauvert 1) ; 2) la quantification de la fraction carbonatée détritique de la roche totale des sédiments lacustres du forage Gallician 9 afin d'extraire le signal géochimique lacustre primaire ; 3) l'intégration d'autres forages profonds des secteurs voisins (p.ex., Iscles 1, Charnier 1, Montcalm 2, Marette 1) pour mieux contraindre à l'échelle kilométrique les variations de faciès de dépôt.

Le cadre chronostratigraphique robuste construit dans cette thèse constitue un apport d'une grande valeur pour la révision des aspects structuraux du bassin de la Vistrenque. La réalisation de nouvelles datations dans les forages voisins précisera le calendrier du remplissage du bassin de la Vistrenque et les corrélations entre les secteurs de ce bassin fortement structuré. La prise en considération des nouveaux éléments d'âge obtenus dans ce travail permet par ailleurs des calages puits-sismique plus fiables, utiles pour entreprendre une révision de l'interprétation structurale du bassin à la lumière des apports de cette thèse sur le fonctionnement du bassin de la Vistrenque antérieurement à la phase du rifting Liguro-Provençal. A l'échelle de la Camargue, le bassin voisin de Vaccarès n'a pas été intégré dans ce travail mais il constitue un objet géologique intéressant à étudier puisqu'il pourrait constituer un jalon entre la Camargue et les bassins provençaux (Aix-en-Provence, Marseille, Haut-Var). L'utilisation de l'approche multidisciplinaire de cette thèse dans le forage de Vaccarès 1 apporterait ainsi de nouveaux éléments à la connaissance sur les bassins continentaux du Sud-est de la France et de leur Paléogéographie au Paléogène.

Les nouveaux résultats de cette thèse sur la salinisation des bassins continentaux et les éclairages apportés sur la paléogéographie du Sud-est de la France au Priabonien, Rupélien et Chattien constituent une contribution au débat scientifique sur ces questions. Par ailleurs, l'approche intégrée (assemblages polliniques, micropaléontologie, modélisation des mélanges des isotopes du soufre et du strontium) constitue une voie prometteuse pour réexaminer la question de l'origine de la salinité dans les dépôt-centres des bassins continentaux voisins (Mormoiron, Carpentras, Apt-Manosque-Forcalquier, Narbonne-Sigean, Valence ainsi que les bassins situés en offshore dans le golfe du Lion) et des autres segments du rift ouest européen qui ont enregistré la transition Eocène-Oligocène. La compréhension de l'expression de cet événement en milieu continental tant dans les aires proches des paléoreliefs pyrénéens que dans les zones proches du domaine marin alpin nécessite par ailleurs des analyses polliniques resserrées afin de capturer les différentes échelles de variabilité climatique.

- ANNEXES

Annexes

Annexe A : Liste des forages du bassin de la Vistrenque qui traversent les séries paléogènes (Série Rouge et unités sous-jacentes) étudiées dans ce travail (Z. sol = hauteur au-dessus du niveau de la mer). Les puits étudiés dans ce travail sont indiqués en gras.

Forage	Abréviation	Profondeur (m)	Z. sol (m)	Longitude	Latitude	Année	Référence BRGM
Albaron 6	ALB6	889,7	1,4	4,43246257	43,6584511	1950	BSS002GVGQ
Caissargues 1	CS1	1543	53	4,38039906	43,7792441	1950	BSS002EUWS
Milhaud 3	M3	902,5	20,5	4,33064935	43,7809563	1950	BSS002EUWV
Milhaud 4	M4	948,35	20,95	4,32397593	43,7802088	1950	BSS002EUWW
Vaccarès 1	V1	2174,95	1,04	4,49465985	43,5605511	1950	BSS002GVTR
Vistrengue 1	VI1	1494,89	23,04	4,33858785	43,7797723	1950	BSS002EUWT
Gallician 1	**G1**	**2004**	**3,93**	**4,27572123**	**43,636416**	**1951**	**BSS002GUWJ**
Gallician 3	**G3**	**1871**	**1,12**	**4,28219223**	**43,6367914**	**1951**	**BSS002GUWL**
Montcalm 1	M1	1413	2,51	4,27138062	43,5850159	1951	BSS002GUWU
Gallician 2	G2	2195	6,4	4,27048203	43,6357942	1952	BSS002GUWK
Gallican 4	**G4**	**2052**	**0,88**	**4,28527289**	**43,6369816**	**1952**	**BSS002GUWM**
Gallician 5	G5	2070	1,08	4,2822934	43,6368527	1952	BSS002GUWN
Gallician 6	G6	2456	23	4,26302345	43,6428541	1952	BSS002GUWP
Gallician 7	**G7**	**2087**	**0,79**	**4,27731525**	**43,6324361**	**1952**	**BSS002GUWQ**
Gallician 8	G8	2200	0,3	4,26333995	43,6257417	1952	BSS002GUWR
Vauvert 1	**V1**	**3626**	**27**	**4,27786436**	**43,6493537**	**1952**	**BSS002GUWW**
Aigues-mortes 1	AM1	1469	3,2	4,2463278	43,5315811	1953	BSS002JETG
Charnier 1	C1	2613	0,72	4,28950702	43,6071963	1953	BSS002GUWT
Montcalm 2	M2	2519	1,47	4,2926456	43,5894947	1953	BSS002GUWV
Gallician 9	**G9**	**2653**	**15**	**4,28327114**	**43,6440389**	**1956**	**BSS002GUWS**
Iscles 1	IS1	1787	1,5	4,35849936	43,6064365	1957	BSS002GVTF
Marette 1	MRT1	2504	0,84	4,17750925	43,5673848	1961	BSS002GUPB
Pierrefeu 1	**PF1**	**5137**	**67,4**	**4,30324273**	**43,6726144**	**1963**	**BSS002GTBV**
Baumelles 1	BAM1	1973	1,67	4,36618832	43,5171326	1988	BSS002JEVZ
Cros de Lagnon	CDL1	2092	18	4,28780828	43,6455366	1995	BSS002GVDA

Abstract

Sedimentary infills of continental basins constitute valuable archives of the evolution of environmental parameters at different time scales. These environmental parameters such as basin topography and salinity are influenced by tectonics and climate. In South-east France, several continental basins were formed during the Priabonian-Rupelian interval in a context of change from the compressive tectonic regime linked to the Pyreneo-Provençal orogeny to the extensive regime associated with the European Cenozoic Rift System and the fundamental climatic change at the end of the Eocene. The manifestation of this climatic deterioration in continental areas as well as the origin of the salinity of the lacustrine systems of South-east France are still poorly understood. The Vistrenque Basin located in the Camargue, the deepest Cenozoic depocentre in South-east France, is made up of more than 3200 m of Paleogene carbonate, siliciclastic and evaporite deposits. This highly expanded succession represents an exceptional archive to document the environmental impact of the climatic changes related to the Eocene-Oligocene transition and to reconstruct the palaeogeography of South-east France during the Paleogene. The methodology adopted in this work is based on the sedimentological, stratigraphic, micropalaeontological and geochemical analyses of outcrops and borehole data (cores, cuttings, logs).

The study of the outcrops located in the northern part of the basin allows to reconstruct a carbonate margin of a saline lake characterized by significant development of oolitic bodies during the Priabonian. Stratigraphic analysis reveals the existence of lake water connections with neighbouring saline waterbodies located in Languedoc and Rhône Valley during lacustrine transgressions. In the depocentre, the ages obtained in this work have allowed to construct a strong chronostratigraphic framework for the investigated sedimentary series, whose ages range from the Upper Eocene to the Upper Oligocene. This thesis provides evidence for, at least transient, incursions of sea-influenced waters into the Camargue and Languedoc continental troughs during the Priabonian, Lower Rupelian and Chattian. The salinization of these basins derived from the Alpine Sea during the Priabonian and Lower Rupelian times and two potential pathways can be considered: 1) the upper Rhône Valley via the Crest Sill, 2) the lower Rhône valley via the Pyrenean synclines of the Haut-Var area. During the Chattian, marine incursions into the Vistrenque derived from the south thanks to the opening of the western Mediterranean and the formation of the Gulf of Lion margin in place of the continuous Pyrenean reliefs that constituted a southern topographic barrier during the Priabonian and Lower Rupelian.

Four depositional sequences have been defined to document the evolution of the Vistrenque Basin during the Priabonian-Lowermost Rupelian to Early Chattian times. The first sequence consists of: 1) a transgressive hemicycle (Priabonian-earliest Rupelian) characterized by gravity-driven terrigenous sedimentation in deep lake setting in the centre of the basin and carbonate sedimentation on the northern margin; 2) a hemicycle of forced lake regression (early Rupelian) marked by a reduction in terrigenous fluxes and local formation of evaporites. The precipitation of evaporites is a consequence of the continental aridification associated with the global cooling at the Eocene-Oligocene transition. The following three sequences, which together show a long-term regressive trend (normal regression), reflect the evolution of the sedimentary system during the Rupelian from a deep lake to a shallow lake with deltaic and littoral sedimentation and the final development of a floodplain as early as the Chattian. This ultimate filling of the basin would be favoured by the end of the functioning of a strike-slip basin controlled by the Nîmes Fault.

Keywords: Continental basin, lacustrine sedimentation, palaeogeography, palaeoclimate, Eocene-Oligocene, Camargue

Résumé

Les remplissages sédimentaires des bassins continentaux constituent des archives précieuses de l'évolution des paramètres environnementaux à diverses échelles de temps. Ces paramètres environnementaux comme la topographie du bassin et la salinité sont influencés par la tectonique et le climat. Dans le Sud-est de la France, plusieurs bassins continentaux se sont formés durant l'intervalle Priabonien-Rupélien dans le contexte du changement du régime tectonique compressif lié à l'orogenèse pyrénéo-provençale au régime extensif associé au rift ouest-européen et de la dégradation climatique majeure de la fin de l'Éocène. L'expression de cette dégradation climatique en milieu continental ainsi que l'origine de la salinité des systèmes lacustres du Sud-est de la France sont encore mal comprises. Le bassin de la Vistrenque situé en Camargue, le plus profond dépôt-centre cénozoïque du Sud-est de la France, est constitué de plus de 3200 m de dépôts paléogènes carbonatés, silicoclastiques et évaporitiques. Cette succession très dilatée représente une archive exceptionnelle pour documenter les conséquences environnementales des changements climatiques liés à la transition Éocène-Oligocène et reconstituer la paléogéographie du Sud-est de la France au Paléogène. La méthodologie adoptée dans ce travail repose sur l'analyse sédimentologique, stratigraphique, micropaléontologique et géochimique des données d'affleurements et de forages (carottes, cuttings, diagraphies).

L'étude des affleurements situés au nord du bassin permet de reconstituer une marge carbonatée d'un lac salin caractérisée par un fort développement de corps oolithiques au Priabonien. L'analyse stratigraphique met en évidence des connexions avec les masses d'eaux salées voisines du Languedoc et de la Vallée du Rhône pendant les transgressions lacustres. Dans le dépôt-centre, les datations obtenues dans ce travail ont permis de construire un cadre chronostratigraphique robuste des séries étudiées qui s'échelonnent de l'Éocène supérieur à l'Oligocène supérieur. Cette thèse apporte des preuves d'incursions au moins épisodiques d'eaux influencées par la mer dans les fossés continentaux camarguais et languedociens durant le Priabonien, le Rupélien inférieur et le Chattien. La salinisation de ces bassins provient de la mer alpine au Priabonien et au Rupélien inférieur et deux couloirs d'incursion marine peuvent être envisagés : 1) la haute vallée du Rhône via le seuil de Crest, 2) la basse vallée du Rhône via les synclinaux pyrénéens du Haut-Var. Au Chattien, les incursions marines dans la Vistrenque proviennent du sud à la faveur de l'ouverture de la Méditerranée occidentale et la formation de la marge du golfe du Lion à la place des reliefs pyrénéens continus qui formaient une barrière topographique méridionale au Priabonien et au Rupélien inférieur.

Quatre séquences de dépôts ont été définies pour documenter l'évolution du bassin de la Vistrenque entre Priabonien - Rupélien basal et le Chattien inférieur. La première séquence est constituée de : 1) un hémicycle transgressif (Priabonien à Rupélien basal) marqué par une sédimentation lacustre profonde gravitaire terrigène dans le centre du bassin et une sédimentation carbonatée sur la marge nord ; 2) un hémicycle de régression forcée du lac (Rupélien inférieur) marqué par une réduction des flux terrigènes et la formation locale d'évaporites. La précipitation des évaporites est conséquente de l'aridification continentale en lien avec le refroidissement global à la transition Éocène-Oligocène. Les trois séquences suivantes dont l'ensemble présente une tendance régressive sur le long terme (régression normale) traduisent l'évolution pendant le Rupélien du système sédimentaire d'un lac profond à un lac peu profond à sédimentation deltaïque et littorale et le développement final d'une plaine d'inondation à partir du Chattien. Le comblement ultime du bassin serait favorisé par la fin de fonctionnement d'un bassin en décrochement contrôlé par la faille de Nîmes.

Mots-clés : Bassin continental, sédimentation lacustre, paléogéographie, paléoclimat, Éocène-Oligocène, Camargue.